ANNUAL REVIEW

INSTITUTE FOR MOLECULAR SCIENCE

1994

ANNUAL REVIEW

INSTITUTE FOR MOLECULAR SCIENCE

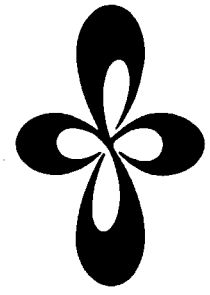

1994

Published by
Institute for Molecular Science
Okazaki National Research Institutes
Myodaiji, Okazaki 444, Japan
Phone 0564-55-7418 (Secretary room)
Telex 4537-475 KOKKEN J
Fax 0564-54-2254

IMS 1994

We present here the Annual Review for 1994 reporting the research activities of IMS during the past year.

Almost two decades have passed since the establishment of IMS in 1975, and I think now is the time for change and renewal. To do this, first of all we have to ask ourselves about the quality of the research work being carried out in IMS. Last year, the activities of all the research groups in IMS were critically reviewed by 18 distinguished molecular scientists, including 6 from overseas, who have served as external reviewers. Evaluations and comments by the individual external reviewers have been opened to the public in a report entitled −IMS Report, 93− published in March, 1994. The general level of the research groups was evaluated to be very high when measured by international standards. On the other hand, some severe and critical comments were expressed by several reviewers and these were also included in the report. The open publications of such critical comments prove the health of IMS, I believe. Through the critical review, many subjects and problems to be solved were clearly revealed. We are now making every effort to make a future plan for IMS based on thorough discussions of these subjects and problems by all the staff in IMS. The future plan will be included in IMS Report 94 appearing next year. The future of IMS depends on our ability to attract young molecular scientists full of vitality and creative power. As long as they feel that they can do something big in IMS, even under severe conditions such as a prohibition of internal promotion, IMS will continue as a center of excellence. Our future plan should be one to meet their expectations.

The turnover of personnel has been very high in the last year. Professor K. Nakasuji in the Department of Applied Molecular Science moved to Osaka University. There has been a high turnover especially among associate professors. Four associate professors, Drs. M. Watanabe, G. Isoyama, K. Shobatake and I. Ohmine moved as full professors to Tohoku University, Osaka University, Nagoya University (Faculty of Engineering) and Nagoya University (Faculty of Science), respectively. Professor S. Iwata of Keio University was appointed as Professor of the Department of Theoretical Studies to succeed Professor K. Morokuma who moved to Emory University, USA, last year. Professor Iwata also serves as the Director of the Computer Center. We have appointed Dr. Y. Tanimura and Mr. M. Watanabe as Associate Professors of the Department of Theoretical Studies and the Instrument Center, respectively. Professor Y. Yoshikawa and Associate Professor H. Nakazawa took positions in the Coordination Chemistry Laboratories by transfering from their positions at Okayama University and Hiroshima University, respectively. We also had a high turnover of Research Associates and Technical Associates. Overall replacement during the past year reached about one fifth of all the research positions in IMS.

Professor M. A. El-Sayed of Georgia Institute of Technology was assigned as a foreign Councillor to succeed Professor J. C. Polanyi. We are pleased that Professor H. Baba, Professor Emeritus of Hokkaido University, has agreed to serve as a Distinguished Research Consultant.

Finally, I would also like to congratulate Professor A. Nakamura for his Chemical Society of Japan Award, Professor K. Yoshihara for his DAIWA Award, Associate Professor T. Suzuki for his Chemical Society of Japan Award for a Young Scientist and Associated Professor N. Nemoto for his Progressive Award in Synthetic Organic Chemistry, Japan.

September, 1994

Mitsuo Ito

Mitsuo Ito
Director-General

CONTENTS

IMS 1994 ..... Mitsuo Ito iii

CONTENTS v

ORGANIZATION AND STAFF 1

COUNCIL 11

BUILDINGS AND CAMPUS 12

RESEARCH ACTIVITIES I
DEPARTMENT OF THEORETICAL STUDIES 15

A. Structures and Reactions of Group 2 and 3 Atoms and Their Ions with Water Clusters 15

1. Reactions of Singly Charged Alkaline-Earth Metal Ions with Water Clusters: Characteristic Size Distribution of Product Ions 15
2. Molecular Orbital Studies of Structures and Reactions of Singly Charged Magnesium Ion with Water Clusters, $Mg^+(H_2O)_n$ 15
3. The Theoretical Studies of the Boron-Water Cluster $B(H_2O)_n$ and their Ions $B^+(H_2O)_n$ with Comparing the Aluminum-Water Clusters 15
4. *Ab Initio* Studies on the Structures and Vertical Electron Detachment Energies of Copper-Water Negative Ion Clusters $Cu^-(H_2O)_n$ and $CuOH^-(H_2O)_{n-1}$ 15

B. Geometrical and Electronic Structures of Binary Clusters 16

1. Theoretical Study of Silicon-Sodium Binary Clusters. Geometrical and Electronic Structures of Si_nNa (n=1–7) 16
2. Photoelectron Spectroscopy of AIS^- Diatomic Anion 16

C. Oxonium and Ammonium Radicals in Water and Ammonia Clusters 16

1. *Ab initio* MO Study of Ammonium and Oxonium Radicals in Ammonia and Water Clusters 16

D. Structures and Reaction Dynamics in the Ground and Excited States of Argon Cluster ions Ar_n^+ 16

1. Theoretical Study of the Intra Cluster Reactions in Ar_4^+ 16

E. Excited States and Ionic States of Inner-valence and Inner Shell Regions of Simple Molecules 17

1. The Theoretical Analysis of the 2D Photoelectron Spectrum of HCl 17

F. Potential Energy Surfaces of Excited States and Dynamics of Some Diatomic and Triatomic Molecules 17

1. Potential Energy Surfaces of Some Low-Lying States of Fluoroformyl Radical FCO 17

G. Electronic Structure of Electron-Donor-Acceptor Complexes 17

1. Theoretical Studies of Ammonia-Halogen and Methylamine-Halogen Complexes: Geometries, Harmonic Vibrational Frequencies and Their Infra-Red Intensities, and Excited States of Ammonia-Chlorine Monofluoride Complex 17

H. Theoretical Studies of Molecular Conformations and Barriers to Internal Rotation and Inversion 17

1. Theoretical Studies of the Internal Rotation of the Methyl Group in o-, m-, and p-Fluorotoluenes and Their Cations 17

I. Development of New Theoretical and Numerical Techniques in the Study of Molecular Electronic Structures 18

1. On Some Approximation for Two-Electron Integrals 18
2. Irregular Order in Basicities of Methylamines in Aqueous Solution: A RISM-SCF Study 18

J. Structures and Reactions of Manybody Chemical Systems 18

1. Liquid Water Dynamics; Collective Motions, Fluctuation and Relaxation 18
2. Instantaneous Normal Mode Analysis of Liquid Water 18
3. Dynamics and Relaxation of an Intermediate Size Water Cluster $(H_2O)_{108}$ 19
4. Translational and Orientational Dynamics of a Water Cluster $(H_2O)_{108}$ and Liquid Water; Analysis of Neutron Scattering and Depolarized Light Scattering 19
5. Fluctuation, Relaxations and Hydration in Liquid Water; Hydrogen Bond Rearrangement Dynamics 19
6. The Origin of Many-body Effect in the Hydrated Proton Clusters 19
7. New Molecular Dynamics Method for Cooperative Proton Transfer Dynamics in Liquid Water 20
8. Topology and Dynamics in the Hydrogen Bond Network System 20
9. Ab initio MO Study for Photoisomerization of Octatetraene 20

K. Theoretical Studies of Chemical Reaction Dynamics 21

1. Constat Centrifugal Potential Approximation for Atom-Diatomic Chemical Reaction Dynamics 21
2. Effects of Potential Energy Surface Topography and Isotope Substitution in Atom-Diatom Chemical Reactions: The $Cl+H_2$ and $D+H_2$ Systems 21

3. Wentzel-Kramers-Brillouin Theory of Multidimensional Tunneling: General Theory for Energy Splitting ····· 21
4. WKB Theory of Tunneling between Tori ····· 21
5. Systematic of the Average Resonance Widths in Overlapping Resonance-Scattering and Its Connection with the RRKM Theory ····· 22
6. Decoupling Surface Analysis of $Cl+Cl_2$ Reaction Embedded in Ar_{52} Cluster ····· 22

L. Theory of Nonadiabatic Transition ····· 22
1. Two-State Linear Curve Crossing Problems Revisited. IV. The Best Analytical Formulas for Scattering Matrices ····· 22
2. Theory of Nonadiabatic Transition for General Two-State Curve Crossing Problems ····· 23

M. Theoretical Studies of Characteristics and Dynamics of Superexcited States of Molecules ····· 23
1. Characteristics and Dynamics of Doubly Excited States of Molecules ····· 23

N. Femtosecond Pump-Probe Spectroscopy of Molecules in the Condensed Phase ····· 23
1. Multistate Quantum Fokker-Planck Approach to Nonadiabatic Wave Packet Dynamics in Pump-Probe Spectroscopy ····· 23
2. Femtosecond Pump-Probe Spectroscopy of Intermolecular Vibrations in Molecular Dimers ····· 23
3. Effects of Anharmonicity in Pump-Probe Spectroscopy in the Condensed Phase ····· 23

O. Theoretical Studies of Organic Conductors and Superconductors ····· 24
1. Spin Fluctuations of Organic Conductors and Superconductors ····· 24

P. Intermolecular Potential for Molecular Simulations ····· 24
1. A Procedure to Generate Ab Initio Intermolecular Potential Function ····· 24

Q. Structure of Muonic Molecules ····· 24
1. Loosely Coupled Few-Body Systems ····· 24
2. Effect of the Finite Size of the Muonic Molecular Ion $(dd\mu)^+$ on the Energy Levels of the Atom $(dd\mu)e$ and Molecule $(dd\mu)dee$ ····· 24
3. Normalization of the Asymptotic Form of Three-Body $(dt\mu)^+$ and $(dd\mu)^+$ Wavefunctions ····· 24

RESEARCH ACTIVITIES II
DEPARTMENT OF MOLECULAR STRUCTURE ····· 26

A. Laboratory and Astronomical Spectroscopy of Transient Interstellar Molecules ····· 26
1. Submillimeter Wave Spectrum of the SiH_3^+ Ion. J=2−1, K=0 and 1 Transitions ····· 26
2. Microwave Spectrum of the NS Radical in the $^2\Pi_r$ Ground Electronic State ····· 26
3. Microwave Spectra of the $AlO(X^2\Sigma^+)$ Radical in the Vibrationally Excited States, v=1 and 2 ····· 26
4. Submillimeter-Wave Spectra of AlH and AlD ····· 27
5. Submillimeter-Wave Spectroscopy of the $CD_2(\tilde{X}^3B_1)$ Radical ····· 27
6. Microwave Spectrum of the HCCS Radical in the Rovibronic States ····· 27
7. Microwave Spectrum of the C_3S Molecule in the Vibrationally Excited States of Bending Modes, ν_4 and ν_5 ····· 27
8. Infrared Diode Laser Spectroscopy of the ν_1 Fundamental Mode of the C_3S Molecule ····· 27

B. Development of a Mt. Fuji Submillimeter-Wave Telescope ····· 28

C. Laser Investigation of Antiproton-Helium Compounds ····· 28
1. First Observation of Laser-Induced Resonant Annihilation in Metastable Antiprotonic Helium Atoms ····· 28
2. Laser Studies of the Decay Chain of Metastable Antiprotonic Helium Atoms ····· 29

D. Laser Cooling and Trapping of Neutral Atoms ····· 30
1. Laser Trapping of ^3He Atom ····· 30

E. Molecular Science of Biomolecules ····· 30
1. Resonance Raman Spectra of the Photointermediates in Phytochrome Phototransformation: Deprotonation of the Chromophore in the Bleached Intermediate ····· 30
2. Preparation and Characterization of Oxoiron(IV) Chlorin Complexes as the First Models for a Reaction Intermediate in the Catalytic Cycle of Cytochrome *d* ····· 31
3. A Multi-Reflection Raman Cell for Studying Dilute Aqueous Solutions ····· 31
4. Vibrational Assignments of the FeCO Unit of CO-Bound Heme Proteins Revisited: Observation of a New CO-Isotope-Sensitive Raman Band Assignable to the FeCO Bending Fundamental ····· 31
5. Observation of a New Oxygen-Isotope-Sensitive Raman Band for Oxyhemoproteins and Its Implications in Heme Pocket Structures ····· 32
6. Observation of Nonfundamental Fe-O_2 and Fe-CO Vibrations and Potential Anharmonicities for Oxy- and Carbonmonoxy-Hemoglobin; Evidence Supporting a New Assignment of the Fe-C-O Bending Fundamental ····· 32
7. Selective Resonance Raman Observation of the "607 nm" Form Generated in the Reaction of Oxidized Cytochrome *c* Oxidase with Hydrogen Peroxide ····· 32

8. Observation of the Fe-O_2 and Fe^{IV}=O Stretching Raman Bands for Dioxygen Reduction Intermediates of Cytochrome *bo* Isolated from *Escherichia coli* ····· 33
9. Ultraviolet Resonance Raman Studies of Quaternary Structure of Hemoglobin Using a Tryptophan β37 Mutant ····· 33
10. Presence of Two Fe^{IV}=O Heme Species in the Reaction of Cytochrome Oxidase with Oxygen Revealed by TR^3 Spectroscopy ····· 33
11. A Novel Spinning Cell System for UVRR Measurements of Powder- and Small Volume Solution Samples in Back-Scattering Geometry: Application to Solid Tryptophan and Mutant Hemoglobin Solution ····· 33

F. Vibrational Spectroscopy of Molecules in Transient States ····· 34
1. Recombination Intermediates of Photodissociated CO Myoglobin at Ambient Temperatures Detected by Time-Resolved Resonance Raman Spectroscopy ····· 34
2. Time-Resolved Resonance Raman Study of Porphyrins and Metalloporphyrins in the Electronic Excited States ····· 34
3. The Proximal Residue Largely Determines the CO Distortion in Carbonmonoxy Globin Proteins. An *ab initio* Study of a Haem Prosthetic Unit ····· 35
4. The Distal Residue-CO Interaction in Carbonmonoxy Myoglobins: a Molecular Dynamics Study of Two Distal Histidine Tautomers ····· 35
5. The distal-CO Interaction in Carbonmonoxy Myoglobins: the Molecular Dynamics of 3 Distal Mutants ····· 36

G. Molecular and Electronic Structures of Metallofullerenes and the Fullerene Radical Anions ····· 36
1. Laser Study on the Resonance-Enhanced Multiphoton Electron Detachment (REMPED) Processes for C_{60}^- and C_{70}^- ····· 36
2. ESR Study on Structures and Dynamics of $Sc_3@C_{82}$ ····· 36

RESEARCH ACTIVITIES III
DEPARTMENT OF ELECTRONIC STRUCTURE ····· 37

A. Ultrafast Intermolecular Electron Transfer Faster than Diffusive Solvent Relaxation ····· 37
1. Femtosecond Intermolecular Electron Transfer in Condensed Systems ····· 37
2. Temperature Dependence of Ultrafast Intermolecular Electron Transfer Faster than Solvation Process ····· 37
3. Chemical Substitution and Deuterium Isotope Effects on Ultrafast Intermolecular Electron Transfer: Possible Role of Molecular Vibrations ····· 38

B. Liquid Dynamics Studied by Higher Order Nonlinear Spectroscopies ····· 38
1. Ultrafast Raman Echo Study on the S-H Stretching of Liquid Ethanthiol ····· 38
2. Fifth Order Optical Response of Liquid CS_2 Observed by Ultrafast Non-Resonant Six-Wave Mixing ····· 39

C. Development of Ultrafast Spectroscopic Methods ····· 40
1. High Power Pico- and Femtosecond Laser Systems at kHz Repetition Rate ····· 40
2. Detection System for Five-Pulse Correlation Experiment ····· 41

D. Photodissociation Dynamics of Alkali Metal Dimers ····· 41
1. Complex Resonance in the Predissociation of Cs_2 ····· 41
2. Molecular Resonances in the Predissociation of Cs_2 ····· 42

E. Exciton Behavior of Dye J-Aggregates ····· 42
1. Temperature Dependence of Superradiant Emission of BIC J-Aggregates ····· 42
2. Two Exciton Emission of J-Aggregates ····· 43

F. Primary Processes in Photosystem I Reaction Center Complex ····· 43
1. The Primary Photochemical Processes in P700-Enriched Photosystem I Particles: Trap-Limited Excitation Decay and the Primary Charge Separation ····· 44
2. Rates of Primary Electron Transfer Reactions in Photosystem I Reaction Center Reconstituted with Different Quinones as the Secondary Acceptor ····· 44

G. Dynamic Behavior of Electronic Excited States ····· 45
1. Evidence for Quantization of the Transition State for cis-trans Isomerization ····· 45
2. Picosecond Transient Absorption of Aqueous Tryptophan ····· 46
3. Dual Fluorescence and Excited-State Intramolecular Proton Transfer in Jet-Cooled 3,4-Benzotropolone ····· 46
4. Picosecond Vibrational Relaxation in the Excited-State Proton-Transfer of 2-(3′-Hydroxy-2′-Naphthyl) Benzimidazole ····· 46

H. Photochemistry on Well-Defined Surfaces ····· 46
1. Adsorbed-State Specific Photodissociation Dynamics of N_2O on Si(100) ····· 47

I. Activation of Methane ····· 47
1. Photochemical C-H Bond Activation of Methane of a Pt(111) Surface ····· 47

J. Reactions of Coadsorbed Species on Well-Defined Surface 48
1. The Reactivity of Molecular and Atomic Oxygen in Oxygen-Exchange Reaction between NO and O_2 Coadsorbed on a Pt(111) Surface 48

K. Dynamic Processes in Electronically-and/or Vibrationally-Excited Molecules 49
1. Fragment Rotational Excitation due to the Parent Rotation in the Dissociation of Molecules 49
2. Photochemistry of $N_2O \cdot H_2O$ Complexes Produced in Supersonic Jets 49
3. Intermolecular Vibration and Dynamics of the Anisole-Benzene Complex Studied by Multi-Resonance Spectroscopy 49
4. Vibrational Energy Distribution in the Photofragment HCO Produced by the Photodissociation of Propionaldehyde in a Supersonic Jet 50
5. The C=O Stretching Frequency in the $S_1(\pi^*\text{-}n)$ State of Acetaldehyde and Its Deuterated Derivatives Determined with the Photofragment Excitation Spectroscopy 50
6. Photodissociation Dynamics of Acetaldehyde. Vibrational Energy Distribution in the Photofragment HCO 51
7. Applications of the Hole-Burning Spectroscopy in Molecular Beam Experiments 51
8. Vibrational and Rotational State Distributions of OH Produced in the Reaction $O(^1D)+H_2O$ 51

L. Self-Organization in Chemical Reactions 52
1. Photo-Response of Chemical Oscillators 52
2. Frequency Multiplying Bifurcations in the Oscillatory Belousov-Zhabotinskii Reaction Proceeding in Interacting Water Droplets of Reverse Microemulsion of Aerozol OT in Octane 52
3. Photoinduced pH Oscillations in the Hydrogen Peroxide-Sufite-Ferrocyanide System in the Presence of Bromocresol Purple in a Continuous-Flow Stirred Tank Reactor 53
4. A Simple Phenomenological Model for Nonequilibrium Interaction between Two Reactions in a Lorentz Gas 53
5. Photoinduction and Photoinhibition of Chemical Oscillations in the Tris(2,2′-bipyridine)ruthenium(II)-Catalyzed Minimal Bromate Oscillator 53
6. Photo-Induced Bifurcation between Steady and Oscillatory States in the $Fe(CN)_6^{4-}$-H_2O_2 Reaction in a Flow Reactor 54
7. Oscillatory Reaction in the Hydrogen Peroxide-Sulfite Ion-Hydrogen Ion-Hexacyanoferrate(II) Ion System in a Semibatch Reactor 54
8. Explanation of the Long-Lived Oscillations in the Chlorite Ion-Iodide Ion-Malonic Acid System 55
9. Light-Induced State Transitions in the Oscillatory ClO_2^--Cl^--Iodomalonic Acid System in a Semibatch Reactor 55
10. Photo-Induced Disproportionation of Iodomalonic Acid 56
11. Oxidation of Thiocyanate by Bromate Is not an Oscillatory Reaction in a Batch Reactor. A Comment 56
12. Mechanism of the Light-Sensitive Oscillatory Reaction between Hydrogen Peroxide and the Hexacyanoferrate(II) Ion 56
13. Photo-Induction and Inhibition of Chemical Oscillations in the Ferrocyanide-Bromate-Sulfite System in a CSTR 56
14. Photoresponse of the Briggs-Rauscher Reaction with Iodide Inflow 57

M. Laser Investigation of Photodissociation and Bimolecular Reactions 57
1. Photodissociation of *trans*-Dichloroethylene: State-Resolved Speed and Angular Distributions of Cl Atoms 57
2. Slicing Photofragment Spatial Distribution by Laser Sheet Ionization 58
3. Photodissociation of Acetylene in the A State: H-Atom Action Spectrum 58

N. External Magnetic Field Effects upon Chemical Reactions 59
1. Factors Controlling the Magnitude of Magnetic Field Effects on Photoredox Reaction Yields for Birfunctional Chain Molecules 59
2. Magnetic Field Effects on Photoinduced Substitution of 4-Methyl-2-quinolinecarbonitrile with Optcally Active (S)- or (R)-2-phenylpropionic Acid 60
3. Magnetic Field Effects on the $B^3\Pi_{0+}$ State of Gaseous Halogen and Interhalogen Molecules 60

RESEARCH ACTIVITIES IV
DEPARTMENT OF MOLECULAR ASSEMBLIES 61

A. Solid State Properties of Phthalocyanine Salts and Related Compounds 61
1. Pressure Dependence of the Infrared and Visible Spectra of Metallophthalocyanine Salts 61
2. X- and Q-band ESR Study of New Poly-CuPc Compounds Synthesized Under High Pressure: the Possibility of Two-dimensional Sheet Polymers 61

B. Structure and Properties of Organic Metals 62
1. Superconducting Properties of Na-Doped C_{60} Prepared from Sodium Azide 62

C. Far-infrared Properties of Organic Conductors 62
1. Construction of Far-infrared Reflectance Spectroscopic System 62
2. Far-infrared Reflectance of β''-$(BEDT\text{-}TTF)_2AuBr_2$ 63

D. NMR Study of Organic Conductors and Superconductors 63
1. ^{13}C-NMR Study on α-$(BEDT\text{-}TTF)_2MHg(SCN)_4$ 63
2. ^{13}C-NMR Study on κ-$(BEDT\text{-}TTF)_2X$ 63
3. Systematic Study of DCNQI-Cu Salts by NMR at Selective Nuclear Sites 64

E. Electron Transport and Magnetic Study of Organic Superconductors 64
1. Resistive Transition in an Extremely Two-Dimensional Superconductor α-$(BEDT\text{-}TTF)_2$-$NH_4Hg(SCN)_4$ 64
2. Construction of an ac Susceptibility Apparatus at Extremely Low-Temperature Region 64

F. Thermodynamic Study of Organic Conductors 65
1. Construction of Low-Temperature Specific Heat Apparatus 65
2. Specific Heat Study of α-$(BEDT\text{-}TTF)_2MHg(SCN)_4$ 65

G. Ultra-Thin Organic Film Systems Prepared by Molecular Beam Epitaxy (MBE) Technique 66
1. Epitaxial Growth of Chloroaluminum Phthalocyanine and Vanadyl Phthalocyanine Double-Layer Structure by the Molecular Beam Epitaxy 66
2. Spectral Dependence of the Anisotropy of $\chi^{(3)}$ of Epitaxially Grown Vanadyl Phthalocyanine Film 66

H. Novel Molecular System C_{60}: Fullerites and Fullerides 66
1. Evidence of Spontaneous Magnetic Order in the C_{60} Complex with Tetrakis (dimethylamino) ethlene 66
2. Preparation of Single Crystals of C_{60}-(TDAE) 66
3. Application of a Layer-by-Layer Deposition for the Preparation of Crystalline metal-doped C_{60} Thin Films 66
4. Disorder and Phonon Windows for Superconductivity in Fullerides 67

I. Electrochemical Properties of the Organofullerenes and Metallofullerenes 67
1. Redox Properties of Organofullerenes 67
2. Electrochemical Properties of $La@C_{82}$ 67
3. Characterization of the Isolated $Y@C_{82}$ 67

J. Phase Transitions and Dynamical Ordering in Liquid Crystals 68
1. ^1H and ^2H NMR Studies of Dynamic Orientational, Translational, and Dipolar Orders in Doubly Reentrant Liquid Crystal CBOBP and CBOBP-*d17* 68
2. Molecular Dynamics and Ordering Characteristics of the Hexatic Smectic B Liquid Crystal 68
3. ^{13}C-NMR Study of the Microscopic Ordering, Dynamics, and Intermolecular Interaction in the Discotic Liquid Crystalline 1,4,8,11,15,18,22,25-Octaoctylphthalocyanine 68
4. ^{31}P and ^{13}C NMR Studies on the Nature of New Liquid Crystalline Hexakis(alkylbiphenyl)cyclo-triphosphazenes 69

K. Conducting Molecular Systems 69
1. New Metallic Layered Compound of Titanium Disulfide Intercalated with Ethylenediamine 69
2. ^1H, ^{13}C, and ^{15}N NMR Studies of Titanium Disulfide-Ethylenediamine Intercalation Compound 69
3. Solid State High Resolution ^{13}C NMR Study of the Intermolecular Interaction in Organic Semi-conductors TTC_n-TTF 70
4. Transport Properties of C_{70} Single Crystals Doped with Alkali Metals 70

L. Photoelectron Spectroscopy of Organic Solids in Vacuum Ultraviolet Region 70
1. Intermolecular Energy-band Dispersion in Oriented Thin Films of Bis(1,2,5-thiadiazolo)-*p*-qui-nobis(1,3-dithiole) (BTQBT) by Angle-resolved Photoemission 70
2. Ultraviolet Photoelectron Spectra of C_{82} and K_xC_{82} 70
3. Electronic Structure of Metallofullerene, LaC_{82}: Electron Transfer from Lanthanum to C_{82} 71
4. Photoelectron Spectroscopy of Polysilanes, Polygermanes and Related Compounds 71
5. The Electronic Structure and Energy Level Alignment of Porphyrinmetal Interfaces Studied by Ultraviolet Photoelectron Spectroscopy 71
6. Electronic Structure of Doped C_{60}: Strong Correlation or Lattice Distortion? 72

M. Organic Metals 72
1. Ethylenedioxy Substituted 2,5-Bis(1′,3′-dithiol-2′-ylidene)-1,3,4,6-tetrathiapentalenes and Their Conducting Salts 72
2. Structure and Physical Properties of $(TMEO\text{-}TTP)_2Au(CN)_2$ 72
3. Crystal Structures of Highly Conducting Iodine Complexes of TTM-TTP 73

N. Electrical Conduction and its Related Properties of Organic Solids 73
1. Temperature Dependence of Hall Mobility in a Single Crystal of Organic Semiconductor BTQBT 73
2. Magnetic and Structural Characterization of Superconducting Sodium-Doped C_{60} Prepared with the Thermal Decomposition of Sodium Azide 73

O. Electronic Conduction and its Mechanism of Cytochromes 73

P. Preparation and Characterization of Semiconductor Thin Films by New Excitation Processes 74

1. Preparation and Characterizations of $CuIn_xGa_{1-x}Se_2$ Thin Films Crystallized by Annealing 74
2. Hydrogenated Amorphous Silicon Films Prepared from Trisilane by Windowless Hydrogen Discharge Lamp 74
3. Defect Creation in Hydrogenated Amorphous Silicon Films Induced by Vacuum Ultraviolet Light from Synchrotron and Undulator Radiation 74
4. Temperature Dependence of Band Gap Change in InN and AlN 74

Q. Molecular Beam Studies of Surface Reaction Dynamics 74

1. Translational-Vibrational Energy Transfer in Xe-Graphite Scattering 74
2. Velocity Distributions of Nascent $SiCl_n$ (n=2, 3, and 4) Products Formed from the Reaction of Si(111) with a Cl_2 Beam 75

R. Vacuum UV Photochemistry of Molecules and Clusters 76

1. Fluorescence Excitation Spectra and Quantum Yield in Vacuum Ultraviolet Photodissociation of CF_3CN 76
2. Absorption Spectrum of C_{60} in the Gas Phase: Formation and Recombination of Electron-Hole Pair 76
3. Photodissociative Excitation Processes in XeF_2 in the Vacuum UV Region of 105–165 nm 76

S. Surface and Interface Structures of Organic Molecules and Polymers Studied by Soft X-ray Absorption and Optical Second Harmonic Generation 77

1. Polarized XANES and Optical SHG Studies on the LC/polyimide Interfaces 77
2. Polarized XANES Studies on the Mechanical Rubbing Effect of Poly(tetrafluoroethylene) Oligomer and its Model Compounds 77

RESEARCH ACTIVITIES V
DEPARTMENT OF APPLIED MOLECULAR SCIENCE 78

A. New Multi-Stage Redox Systems 78

1. Charge-Transfer Complexes of Centrosymmetric DDQ (CDDQ) with TTF Type Donors 78
2. Crystal Structure of Centrosymmetric DDQ (CDDQ) 78

B. New Conjugated Electronic Systems 78

1. Oxidation Reaction of 2-(2-Quinolyl)-3-hydroxyphenalenone 79
2. Oxidation Reaction of 6-Hydroxyphenalenone 79
3. Synthesis and Physical Properties of New Charge-Transfer Complexes of Diazaphenalene Derivatives with TCNQ 79

C. New Cooperative Proton-Electron Transfer (PET) Systems 79

1. Physical Properties of Hydrogen-Bonded Charge-Transfer Complex of Ethylenediaminoglyoxime Transition Metal Complex with Tetracyanoquinodimethane 79
2. Metal-Pteridine Complexes Having Three-Dimensional Hydrogen-Bonded Network 80
3. *Ab-initio* Molecular Orbital Studies for the Dimer Model of Quinhydrone 80
4. *Ab-initio* Molecular Orbital Studies of the Alloxazines 81
5. 2,2′-Biimidazolate Transition Metal Complexes with One-dimensional Intermolecular H-bonding Chains 81
6. Crystal Structure of Nickel(II) Complex with Inter-molecular H-bondings of 2,2′-Biimidazolate Having Zigzag One-dimensional Chains 81
7. Crystal Structure of Nickel(II) Complex with Inter-molecular H-bondings of 2,2′-Biimidazolate Having Channel Structures: $([Ni(Hbim)_3](PTMA) \cdot 3MeOH)$ 81
8. Crystal Structure of Nickel(II) Complex with Inter-molecular H-bondings of 2,2′-Biimidazolate Having Double Interlocking Structures: $([Ni(Hbim)_3(NEt_4)]_2(H_2bim) \cdot MeOH)$ 82
9. Crystal Structure of One Dimensional Heterobimetallic Complex Bridged by 2,2′-Bibenzimidazolate ($bbim^{2-}$) Ligand: $([Cu(bbim)_2]Na(^nPr_4N) \cdot MeOH)$ 82

D. Transition Metal Oxide Clusters 83

1. Intramolecular Rearrangements of Cyclooctadiene-Rhodium(I) Fragments Supported on a Vanadium-Oxide Cluster as Evidenced by Dynamic ^{17}O NMR Spectroscopy 83
2. Vanadium-Oxide Clusters with Supported Bis(2-Phenylpyridine)rhodium(III) and -iridium(III) Fragments 84
3. Synthesis and Crystal Structure of $[(IrCp^*)_2(\mu\text{-}OH)_3]_2(Cr_2O_7) \cdot 8H_2O$ ($Cp^*=\eta^5\text{-}C_5Me_5$). A Novel Two-dimensional Hydrogen-Bonding Network 84
4. Synthesis and Molecular Structure of $[(IrCp^*)(\mu\text{-}S_2C_6H_4)]$ 84

E. Transition Metal Chalcogenide Clusters 85

1. Synthesis, Structure, and Property of Octanuclear Heterotrimetallic Sulfide Cluster; $[\{RhCp^*P(OEt)_3\}(\mu\text{-}WOS_3)(CuCl)Cu]_2(\mu\text{-}Cl)_2]$ Having a Linked Incomplete Cubane-Type Structure 85

2. Formation of Triangular Rhodium μ_3-Sulfido Complex, $[Rh_3Cp^*_3(\mu_3\text{-}(\eta^2\text{-}\parallel)\text{-}C_2H_2)(\mu_3\text{-}S)]$ ($Cp^*=\eta^5\text{-}C_5Me_5$), Containing Acetylene Ligand Generated from a Coupling of Two Bridging Methylene Units in Dirhodium Complex ····· 86
3. Influence of a Neutral Terminal Ligand on the Structure and Redox Potential of Hexamolybdemun(12+) Cluster Ion with Mixed Capping Ligand ····· 86
4. Oxidative Coupling of Coordinated SeH Group: Synthesis, Structure and Dynamic Behavior of Tetranuclear Rhodium Complex with μ_4-Se_2 Ligand, $[\{(RhCp^*)_2(\mu_2\text{-}CH_2)_2\}_2(\mu_4\text{-}Se_2)]^{2+}$ ($Cp^*=C_5Me_5$) ····· 86
5. Tetranuclear $[\{(RhCp^*)_2(\mu_2\text{-}CH_2)_2\}_2(\mu_4\text{-}Se_4)]^{2+}$ ($Cp^*=C_5Me_5$) Cationic Complex with a Rectangular $D2h$ Structure of a Se_4 Unit ····· 87
6. Synthesis and Property of Pentanuclear ($Cu^I\text{-}Rh^{III}_2\text{-}W^{VI}_2$) Heterometallic Sulfide Cluster Ion Predicted by Fast Atom Bombardment Mass Spectrometry ····· 87

F. Transition Metal Complexes with Di- or Tridentate Methyl-Substituted Phosphines ····· 88
1. Rhodium(III) Complexes with 1,1,1-Tris(dimethylphosphinomethyl)ethane (tmpme); Preparation and Structures ····· 88
2. Preparation and Structure of a Rhodium(III) Hydride Complex with 1,1,1-Tris(dimethylphosphinomethyl)ethane (tmpme) ····· 89
3. Reinvestigation of *cis*- and *trans*-$[RhCl_2(dmpe \text{ or } dmpp)_2]$ (dmpe=1,2-bis(dimethylphosphino)ethane; dmpp=1,3-bis(dimethylphosphino)propane) ····· 90

G. Modeling Reaction of Metalloenzyme Active Center ····· 90
1. Imidazolate-mediated Antiferromagnetic Coupling between Fe(III) Ions in Rigidly-linked Porphyrin Dimers and Trimers ····· 90
2. Oxygen Evolution by Water Oxidation with Manganese Porphyrin Dimers ····· 91
3. Modeling Reaction of Manganese Catalase with Dimanganese Complexes of Porphyrin Dimers ····· 91
4. Synthesis of an Active Center Model of Cytochrome P-450 for the Study on the Oxygen Activation Mechanism ····· 91

H. Design, Properties and Reactivity of New Organometallic Compounds ····· 92
1. Transition Metal Catalyzed Addition of Certain Nucleophiles to Imines ····· 92
2. Synthesis of a Water-soluble *o*-Carborane Bearing Uracil Moiety via Palladium Catalyzed Reaction under Essentially Neutral Condition ····· 92
3. A New Alkenyl Ether Giving Acetal with Stereospecific Manner ····· 92
4. Palladium Catalyzed Addition of Masked Formyl Cyanide $ROCH(CN)_2$ to Aldehydes ····· 92
5. Zinc Chloride as a Radical Initiator as well as Chelating Agent ····· 92
6. Intramolecular Michael Addition of γ-Alkylsulfonyloxy-α,β-Unsaturated Esters by Using Higher Order Cyano Copper or Silver Amides as a Base ····· 93
7. Palladium Catalyzed Addition of Activated Methylene and Methyne Compounds to Allenes ····· 93
8. Ytterbium Triflate Catalyzed Ring Opening of Aziridines with Amines ····· 93
9. Ytterbium Triflate and High Pressure Mediated Ring Opening of Epoxides with Amines ····· 93

I. Mechanistic Investigations of the Photosolvolyses Involving Carbocationic Intermediates ····· 94
1. Substituent Effects on the Photosolvolyses of 2-Chloropropiophenones in 2,2,2-Trifluoroethaol ····· 94
2. Solvent Effect on the Photosolvolysis of 2-Chloropropiophenone ····· 94
3. Effects of Nucleophiles on the Photosolvolysis of 2-Chloropropiophenone in Aqueous 2,2,2-Trifluoroethanol ····· 95

RESEARCH ACTIVITIES VI
DEPARTMENT OF VACUUM UV PHOTOSCIENCE ····· 96

A. Electronic Structure and Decay Mechanism of Inner-shell Excited Molecules ····· 96
1. Angular Distribution of Fragment Ions Following C 1s → π^* Photoexcitation of CS_2, OCS, and CO_2 ····· 96
2. Renner-Teller Effect and Rydberg-valence Mixing in the N K-edge Absorption Spectra of N_2O ····· 96
3. Vibronic Coupling in the C 1s (σ_g) → $3s\sigma_g$ Rydberg Excited State of CO_2 ····· 97
4. C 1s → π^* Triplet Excited State of CO: Momentum Transfer Dependence and Vibrational Structure ····· 97

B. Soft X-ray Photoelectron-Photoabsorption Spectroscopy and Electronic Structure of Transition Metal Compounds ····· 97
1. Construction of a New UHV Apparatus for Soft X-ray Photoelectron-Photoabsorption Spectroscopy ····· 97

C. Synchrotron Radiation Stimulated Surface Reactions ····· 98
1. Molecular Orientation and Photochemical Reaction of Organoaluminum Compounds Investigated by Buried Metal Layer Infrared Reflection Absorption Spectroscopy ····· 98

2. Development of Infrared Reflection Absorption Spectroscopy Using a Buried Metal Layer Substrate for *in-situ* Observation of Surface Photochemical Reactions Stimulated by Synchrotron Radiation ····· 98
3. Infrared Reflection Absorption Spectroscopy System for Study of Surface Photochemical Reactions Induced by Synchrotron Radiation ····· 98

D. Study of Ion-Pair Formation in the Vacuum Ultraviolet Region Using Positive Ion-Negative Ion Coincidence Spectroscopy (PINICO) ····· 100
1. Observation of Doubly Excited Rydberg States of N_2O by Positive Ion-Negative Ion Coincidence Spectroscopy ····· 100
2. Observation of Doubly Excited Rydberg States of CO_2 by Positive Ion-Negative Ion Coincidence Spectroscopy ····· 100

E. Photoionization Dynamics Studied by Electron Spectroscopy Combined with a Continuous Synchrotron Radiation Source ····· 100
1. Autoionization of an Excited Valence State of C_2H_2 ····· 101
2. Development of a Position-Sensitive Detection System for Photoelectron Spectroscopy ····· 101

F. Desorption Induced by Electronic Transitions on the Solid Surface of Condensed Gases ····· 102
1. Angular and Kinetic Energy Distributions for Desorption of Neon Metastable Atoms Induced by Excitons at the Surface of Solid Neon ····· 102

G. Identification of Defects in SiO_2 Related Materials and Their Photoresponse ····· 103
1. Precursor to Paramagnetic Centers in Gamma-Irradiated Doped Silica Glasses ····· 103
2. Formation Mechanism of Hydrogen-Associated Defect with an 11.9 mT Doublet in Electron Spin Resonance and Red Luminescence in $9SiO_2$:GeO_2 Fibers ····· 103
3. Study of Oxygen-Deficient Centers in SiO_2 Films Using Photoluminescence Spectra ····· 103
4. Preferred Concentration Enhancement of Photobleachable Defects Responsible for 5 eV Optical Absorption Band in SiO_2:GeO_2 Glass Preform by Heating in a H_2 Atmosphere ····· 103
5. Radiation-Induced Coloring and Paramagnetic Centers in Synthetic SiO_2:Al Glasses ····· 103
6. Characteristics of 5-eV Absorption Band in Sputter Deposited GeO_2-SiO_2 Thin Glass Films ····· 104

H. Effects of Substitution of Bi with Pb in $BaBi_{1-x}Pb_xO_3$ on Crystal Structure and Conduction Behavior ····· 104
1. Effect of Oxygen-Deficiency on the Structure and Conduction Behavior of $BaPb_{0.75}Bi_{0.25}O_{3-\delta}$ ····· 104
2. Effects of Substitution of Bi with Pb in $BaBi_{1-x}Pb_xO_3$ on Crystal Structure and Conduction Behavior ····· 104

I. Modulation of Electronic Structure of Complex Oxides of Transition Metallic Ions with Superstructure of Perovskite by Introduction of Excess Positive Holes or Electrons ····· 104
1. Preparation of Oxygen Excess $SrLaFeO_{4+\delta}$ and Its Electrical and Magnetic Properties ····· 104
2. Electrical and Magnetic Properties of Hole-Doped $Sr_{1+x}La_{1-x}FeO_4$ ····· 105
3. Electronic Structure of Hole-Doped $Sr_{1+x}La_{1-x}FeO_4$ Studied by UPS and XAS ····· 105

J. Electronic Structure Design of Wide Gap Conductors and Control of Their Conduction Behavior ···· 105
1. New Oxide Phase $Cd_{2(1-x)}Y_{2x}Sb_2O_7$ Pyrochlore with a Wide Band Gap and High Electrical Conductivity ····· 105
2. New Oxide Phase $Cd_{1-x}Y_2Sb_2O_6$ with a Wide Band Gap and High Electrical Conductivity ····· 105
3. New Ultraviolet-Transport Electroconductive Oxide, $ZnGa_2O_4$ Spinel ····· 106
4. Preparation of $Cd_{1-x}Y_xSb_2O_6$ Thin Film of Glass Substrate by Radio Frequency Sputtering ····· 106

K. Growth and Characterization of II-VI Compound Semiconductor Thin Film Using Metalorganic Sources ····· 106
1. Growth of Low-Resistivity n-Type ZnTe by Metalorganic Vapor Phase Epitaxy ····· 106
2. Low Temperature Growth of ZnTe by Synchrotron Radiation Using Metalorganic Sources ····· 106
3. Photoluminescence Properties of ZnTe Layers Grown by Photo-assisted Metalorganic Vapor Phase Epitaxy ····· 106
4. Synchrotron Radiation Excited Growth of ZnTe Using Metalorganic Sources ····· 107
5. Construction of the System for a Novel Low-temperature Growth of II-VI Compound Semiconductors Using Synchrotron Radiation ····· 107

RESEARCH ACTIVITIES VII
COORDINATION CHEMISTRY LABORATORIES ····· 108

A. Stereochemistry of Coordination Compounds and Adsorption Phonomena of Various Gases on Inorganic Solids ····· 108
1. Stereochemistry of Six-coordinated Silicon Complexes ····· 108
2. Force Field Calculation of Metal Complex Systems Including Antitumor Platinum(II) Complexes ····· 108
3. Steric Effect of Phenyl Substituents of Redox Potentials of Cobalt(II) Schiff Base Complexes ····· 108
4. Dielectric Behaviors in the Inorganic Solid-H_2O Systems ····· 109

5. Specific Feature of Copper-Ion-Exchanged Mordenite for Dinitrogen Adsorption at Room Temperature ····· 109

B. Creation of Complexes Containing New Types of Bonds between a Transition Metal and a Phosphorus ····· 109

1. Reaction of Iron Phosphonate Complexes Containing a Covalent Bond between Iron and Phosphorus and Their Reactivity ····· 109
2. Migratory Insertion of Phosphorus Ligand into a Transition Metal-Alkyl Bond ····· 110
3. Reactivity of Cationic Phosphenium Complexes toward Trivalent Phosphorus Compounds (L). Formation of $[(bpy)(CO)_2M\text{-}(phosphenium)L]^+$(M=Cr, Mo, W) by the CO/L Exchange Reaction, the Geometrical Isomerization, and the X-ray Structure Analyses ····· 110
4. A Valence Expansion Reaction on a Trivalent Phosphorus Atom in Iron Complexes ····· 110
5. Migration Reaction of a Transition-metal Fragment from a Transition Metal Having a Cp Ring to the Cp Ring ····· 110
6. Synthesis and Stereochemistry of Transition-metal Complexes with Tetraphosphamacrocycle ····· 110

C. Structures and Thermodynamics of Ionic and Molecular Ensembles in Solution ····· 111

1. Crystal and Molecular Structures of Pyridine Base Complexes of Cadmium(II) Chloride ····· 111
2. Preconcentration of Cadmium by Column Extraction with Trioctylmethylammonium Chloride and Determination by Graphite Furnace Atomic Absorption Spectroscopy ····· 111
3. Hydration of Poly(oxyethylene) Derivative Complexes of Alkali Metal Ions and Barium Ion in 1,2-Dichloroethane ····· 111
4. Thermal Stability of Substituted Pyridine Complexes of Cadmium Chloride ····· 112
5. Formation and Thermal Decomposition of Mixed-ligand Complexes of Transition Metal Chlorides Containing Substituted Pyridines ····· 112
6. Ion-pair of Tetraalkylammonium Picrates ····· 112
7. Partition and Dimerization of Ion-pair of Tetraalkylammonium Salts in Xylene ····· 112

D. Syntheses, Structures and Functions of Chromotropic Complexes ····· 113

1. Studies on Mixed Chelates. Five Coordinate Copper(II) Chelates with N,N,N′,N″,N″-Pentamethyldiethylenetriamine and β-Diketonates ····· 113
2. Synthesis and Properties of the Dinuclear Copper(II) Complexes Containing Dinucleating Ligands with Imidazole Nitrogen and Two Exogenous Bridging Ligands ····· 113

E. New Organometallic Catalysts ····· 113

1. Polymerization of Ethylene Catalyzed by the System, $Ta(C_5Me_5)(diene)(CH_3)_2$/MAO: An Isoelectronic Analogue for a Group 4 Metallocene Catalyst ····· 113

F. Straight Linear Metal-Metal Bonded Complexes ····· 113

1. New Synthetic Strategy for a Straight Linear Metal-Metal Bonded Tetranuclear Complex, the Pd-Mo-Mo-Pd System Supported by Four Tridentate 6-(Diphenylphosphine)-2-pyridonate Ligands ····· 113

G. Carbon Dioxide Activation on Metal Complexes and Chemical Simulation of Nitrogen Cycle ····· 114

1. Successive Reduction of CO_2 on a Ruthenium Complex ····· 114
2. Carbon-Carbon Bond Formation in Electrochemical Reduction of Carbon Dioxide by a Ruthenium Complex ····· 114
3. Catalytic Formation of Ketones by Double Alkylation of Carbon Monoxide Formed by Reductive Disproportionation of Carbon Dioxide on a Ruthenium Complex ····· 115
4. Molecular Structure of Copper Nitrito Complexes as the Reaction Intermediate of Dissimilatory Reduction of NO_2^- ····· 115
5. Structural Changes in Tris[(2-pyridyl)methyl]amine)-Copper(II) Derivatives by Successive Introduction of Methyl Substituent at the Ortho Position of the Pyridyl Moiety ····· 115
6. Oxalate Formation in Electrochemical CO_2 Reduction Catalyzed by a Rhodium-Sulfur Cluster ····· 115

H. Development of Highly Selective Reactions Using Early Transition Metal Complexes ····· 116

1. Zirconium Catalyzed C-C Bond Formation Reactions of Diynes with EtMgBr ····· 116
2. First Isolation and Characterization of a Zirconocene(methyl)-(ethylene) Complex ····· 116
3. Zirconium Catalyzed or Mediated Regioselective C-C Bond Formation Reactions of α,β-Unsaturated Acetals ····· 116
4. Reaction of 3-Zircona-1-cyclopentenes and Zirconacyclopentanes with Aldehydes. A Selective and Convenient Synthesis of 4-Penten-1-ols, (Z)-5-Iodo-4-penten-1-ols, and Related Alkanols ····· 116
5. A Reagent-Dependent Highly Chemoselective Halogenation Reaction of Zirconacyclopentenes ····· 117
6. Zirconium Catalyzed or Promoted Novel Type of Cyclization Reaction ····· 117
7. Chemoselective Functionalization of Zirconacyclopentenes ····· 117
8. Highly Regioselective Reaction of Zirconocene-alkene Complexes with Aldehydes or Ketones ····· 118
9. Novel Syntheses of Eight-five Fused Ring Compounds from Zirconacyclopentadienes ····· 118
10. Copper Catalyzed C-C Bond Formation Reaction of Allylzirconation Products of Alkynes ····· 118
11. Polar Paths for Reactions of Alkene-Zirconocene Complexes ····· 118

RESEARCH ACTIVITIES VIII
COMPUTER CENTER 120
A. Theoretical Studies of Highly Excited Vibrational States in Polyatomic Molecules 120
1. Semiclassical Study of Avoided Crossing 120
2. Rotation Induced Vibrational Mixing in Highly Excited Vibrational States of Formaldehyde II 120
3. Theoretical Study of the Potential Energy Surfaces and Dynamics of Low-Lying Electronic States of Formyl Radical HCO 120
4. Development of Parallel Direct SCF Program and Applications to Large Scale Molecular Orbital Calculations on Loosely Coupled Networks of Workstations 120
CHEMICAL MATERIALS CENTER 121
B. Preparation and Properties of Novel Heterocyclic Compounds 121
1. Interaction of Bis(1,2,6,7-tetracyano-3,5-dihydro-3,5-diiminopyrrolizinide) Metal Complexes with Phenazine and Derivatives. Crystal Structures of Addition Compounds of the Nickel(II) Complex with Phenazine and 5,10-Dimethyl-5,10-dihydrophenazine 121
2. Dithio-derivatives of p-Quinodimethanes Fused with 1,2,5-Thiadiazoles: a Novel Type of π-Donor-Acceptor System 121
3. Preparation and Properties of Novel Polythiophenes Containing 1,3-Dithiol-2-ylidene Moeties 121
4. Nonplanar Bis(1,3-dithiole) Donors Affording Novel Cation Radical Salts 122
5. An Absolute Asymmetric Synthesis of the [2+2] Cycloadduct via Single Crystal-to-Single Crystal Transformation by Charge-Transfer Excitation of Solid-State Molecular Complexes Composed of Vinylbenzenes and Bis[1,2,5]thiadiazolotetracyanoquinodimethane 122
6. Preparation and Properties of 7-(1,3-Dithiol-2-ylidene)-4-methyl-4,7-dihydro[1,2,5]thiadiazolo[3,4-b]pyridines: Novel Donor Molecules Containing a 1,2,5-Thiadiazole Unit 122
7. 2-(Thiopyran-4′-yliden)-1,3-dithioles Fused with Thiophene Units: Intramolecular S--S Interaction Affecting the Redox Properties and Molecular Geometries 123
8. Novel Heterocyclic π-Conjugated Polymers Possessing Dihydropyrazine-pyrazine Multistage Redox System 123
9. Sythesis, Structure, and Properties of Unsymmetrical Tetrathiafulvalene Derivatives Fused with 1,2,5-Thiadiazole Ring 123
INSTRUMENT CENTER 124
C. Studies of Solvated Metal Clusters 124
1. Photodissociation Process of $Ca^+(H_2O)_n$ (n=1–6) 124
2. Photoelectron Spectroscopy of Mass-Selected Copper-Water Cluster Negative Ions 125
3. Photoelectron Spectroscopy of Mass-Selected $Na^-(H_2O)_n$ Ions 126
D. Studies on Hypervalent Molecular Clusters 126
1. Electronic Structure and Stability of $NH_4(NH_3)_n$ Clusters 126
2. Photoionization Study of $NH_4(NH_3)_m(H_2O)_n$ 127
E. Collisional Relaxation and Chemical Reaction Dynamics of the Excited Group IIB Metal Atoms 127
1. Nascent Internal State Distributions of $ZnH(X^2\Sigma^+)$ Produced in the Reactions of $Zn(4^1P_1)$ with Simple Alkane Hydrocarbons 128
F. Studies of Ultrafine Particles 128
1. Properties of Crystalline CoS_2 Nanoparticles Produced by CO_2 Laser Pyrolysis 128
2. Investigation of the Intercalation of Rb into MoS_2 Nanoparticles 128
3. Correlation of the Reaction Pressure and Crystalline Phase of Fe-Carbides Produced by CO_2 Laser Pyrolysis 128
4. Relative Activity and Selectivity of Nanoscale Mo_2N, Mo_2C and MoS_2 Catalysts Prepared by Laser Pyrolysis 129
G. Studies of Nanoscale Carbons 129
1. Raman Scattering from Nanoscale Carbons Generated in a Co-Catalyzed Carbon Plasma 129
2. Interlayer Thermal Expansion of Carbon Nanotubes 129
3. Synthesis of $Sc_{15}C_{19}$ Crystallites Encapsulated in Carbon Nanocapsules by Arc Evaporation of Sc-C Composite 129
H. Solid State NMR Study of Inclusion Compound 130
1. ^{13}C Solid-State NMR Study on Populations, Conformations, and Molecular Motions of γ-Valerolactone Enantiomers Enclathrated in the Chiral Cholic Acid Host 130
EQUIPMENT DEVELOPMENT CENTER 130
I. Activities of Division of "IMS Machines" 130
1. Broad-Band Infra-Red Window for Ultra-High-Vacuum Apparatus 130
2. Time-of-Flight-Type Mass-Spectrometer for High-Mass Materials 131

J. Development of Experimental Devices 131
1. Fullerene Generator 131
K. Site-Selective Fluorescence Spectroscopy on Dye Molecules in Amorphous Matrices 132
1. Determination of Weighted Density of States of Vibrational Modes in Zn-substituted Myoglobin 132
2. Site-Selective Fluorescence Spectroscopy of Metal Porphyrins in Noncrystalline Materials 132
3. Glass Transition of Zn-substituted Myoglobin Probed by Absorption and Site-Selective Fluorescence Spectroscopies 133
ULTRAVIOLET SYNCHROTRON ORBITAL RADIATION FACILITY 134
L. Development of the UVSOR Light Source 134
1. Observation of Micro-Macro Temporal Structure and Saturation Mechanism on the UVSOR-FEL 134
M. Development of Beam Lines and Equipment for UVSOR 134
1. Construction of Constant-Length Spherical Grating Monochromator 134
N. Researches by the Use of UVSOR 135
1. Time Response of Photon-Stimulated Desorption of Excited-State Sodium Atoms from Sodium Halides 135
2. Accumulated Photon Echoes Generated by Synchrotron Radiation 135
3. Observation of Surface Core-Excitons in Alkali Chlorides 135
4. Optical Observation of the Interaction between Low Frequency Plasma and Magnetic Field in $La_{2-x}Sr_xCuO_4$ (x=0.1) 136
RESEARCH FACILITIES 137
Computer Center 137
Chemical Materials Center 137
Instrument Center 137
Low-Temperature Center 137
Equipment Development Center 137
Division of IMS Machines 138
Ultraviolet Synchrotron Orbital Radiation Facility 138
SPECIAL RESEARCH PROJECTS 139
1. Development and Evaluation of Molecular Synergistic Systems and Their Application to Chemical Energy Conversion 139
2. Materials Science on Molecular Devices 143
3. Material Control in Multi-Reaction Centers 145
OKAZAKI CONFERENCES 148
JOINT STUDIES PROGRAMS 151
1. Special Projects 151
2. Research Symposia 152
3. Cooperative Research 152
4. Use of Facilities 152
5. UVSOR 152
FOREIGN SCHOLARS 154
AWARDS 157
LIST OF PUBLICATIONS 159
AUTHOR INDEX-RESEARCH ACTIVITIES AND SPECIAL RESEARCH PROJECTS ... 169

ORGANIZATION AND STAFF

Organization

The Institute for Molecular Science compromises twenty two research laboratories-each staffed by a professor, an associate professor, two research associates and several technical associates-, two research laboratories with foreign visiting professors, and six research facilities. The laboratories are grouped into six departments and one facility for coordination chemistry:

Department of Theoretical Sciences	Theoretical Studies I
	Theoretical Studies II
	Theoretical Studies III[1)]
Department of Molecular Structure	Molecular Structure I
	Molecular Structure II[1)]
	Molecular Dynamics
Department of Electronic Structure	Excited State Chemistry
	Excited State Dynamics
	Electronic Structure[1)]
	Molecular Energy Conversion[2)]
Department of Molecular Assemblies	Solid State Chemistry
	Molecular Dynamics Assemblies
	Molecular Assemblies[1)]
Department of Applied Molecular Science	Applied Molecular Science I
	Applied Molecular Science II[1)]
	Physical Organic Chemistry[3)]
Department of Vacuum UV Photoscience	Photochemistry
	Chemical Dynamics
	Interface Molecular Science[3)]
	Synchrotron Radiation Research[2)]
Coordination Chemistry Laboratories	Synthetic Coordination Chemistry[3)]
	Complex Catalysis
	Fundamental Coordination Chemistry
	Coordination Bond[1)]
Research Facilities are:	Computer Center
	Chemical Materials Center
	Instrument Center
	Low-Temperature Center
	Equipment Development Center
	Ultraviolet Synchrotron Orbital Radiation (UVSOR) Facility

1) Professors and associate professors are adjunct professors from other universities.
2) Research Laboratories with foreign visiting professors.
3) Professors, associate professors, and research associates, along with their positions, are transferred from other universities.

Scientific Staff

Mitsuo ITO	**Professor, Director-General**

Emeritus Professors

Saburo NAGAKURA	President, The Graduate University for Advanced Studies
Eiji HIROTA	Vice-President, The Graduate University for Advanced Studies
Katsumi KIMURA	Professor, Japan Advanced Institute of Science and Technology
Keiji MOROKUMA	Professor, Emory University (USA)

Department of Theoretical Studies

Theoretical Studies I

Suehiro IWATA	Professor (January '94-)
Iwao OHMINE	Associate Professor (-March '94)[1)]
Tsutomu IKEGAMI	Research Associate (August '94-)
Akira SHUDO	Research Associate
Shinji SAITO	Technical Associate (-March '94)[1)]
Jean -F. RIEHL	JSPS Post-Doctoral Fellow (-December '93)[2)]
Feliu MASERAS	Research Fellow (-December '93)[3)]
Alexander MEBEL	Research Fellow (-October '93)[4)]
Satoru YOSHIDA	Visiting Research Fellow (-March '94)[1)]
Hidekazu WATANABE	Graduate Student (April '94-)
Tamiki KOMATSUZAKI	Graduate Student (-March '94)[5)]
Toshiaki FUJII	Graduate Student
Chizuru MUGURUMA	Graduate Student
Masakatsu ITO	Graduate Student (-March '94)[1)]
Masakazu MATSUMOTO	Graduate Student (-March '94)[1)]
Young Kee KANG	Visiting Scientist from Chungbuk National University (-February '94)[6)]

Theoretical Studies II

Hiroki NAKAMURA	Professor
Yoshitaka TANIMURA	Associate Professor (April '94-)
Chayugan ZHU	Graduate Student (-September '93), Research Associate (October '93-)
Shoji TAKADA	Technical Associate
Kengo MORIBAYASHI	JSPS Post-Doctoral Fellow
Itsuki BANNO	Research Fellow (-November '93)[7)]
Norikazu TOMITA	IMS Fellow (August '94-)
Kenichiro TSUDA	Graduate Student
Yuji MICHIHIRO	Graduate Student
Miyabi HIYAMA	Graduate Student

Theoretical Studies III

Kazuo KITAURA	Adjunct Professor from University of Osaka Prefecture (-March '94)
Yukikazu ICHIKAWA	Adjunct Professor from The Institute of Space Astronautical Science (April '94-)
Masayasu KAMIMURA	Adjunct Associate Professor from Kyushu University (-March '94)
Satoshi YABUSHITA	Adjunct Associate Professor from Chiba University (April '94-)
Seiichiro TENNO	Research Associate (June '94-)
Kiyohiko SOMEDA	Research Associate

Department of Molecular Structure

Molecular Structure I

Shuji SAITO	Professor
Norio MORITA	Associate Professor
Shuro TAKANO	Research Associate
Yoshiki MORIWAKI	Research Associate (April '94-)
Mitsutaka KUMAKURA	Technical Associate

Axel H. SALECK	JSPS Post-Doctoral Fellow (June '94-)
Andrej M. SOBOLEV	Research Student (-March '94)[8]
Jian TANG	Graduate Student
Tsuyoshi HIRAO	Graduate Student (April '94-)
Naomi INADA	Graduate Student (April '94-)
Keiichi NAMIKI	Graduate Student (April '94-)
Masahiro GOTO	Graduate Student from Nagoya Univ.*
Takeshi OKUBO	Research Fellow (April '94-)
Sang K. LEE	Visiting Professor from Pusan National University (December '93-February '94)
Timothy C. STEIMLE	Visiting Professor from Arizona State University (June '94-July '94)

Molecular Structure II

Tadaoki MITANI	Adjunct Professor from Japan Advanced Institute of Science and Technology
Kentaro KAWAGUCHI	Adjunct Associate Professor from National Astronomy Observatory (-March '94)
Masao KITANO	Adjunct Associate Professor from Kyoto University (April '94-)
Takashi OGURA	Research Associate
Hiroyuki OZEKI	Research Associate

Molecular Dynamics

Teizo KITAGAWA	Professor
Tatsuhisa KATO	Associate Professor
Michio MATSUSHITA	Research Associate
Yasuhisa MIZUTANI	JSPS Post-Doctoral Fellow (-December '93), Research Associate (January '94-)
Masahiro MUKAI	Research Associate (April '94-)
Shin-ichiro SATO	Technical Associate (-July '94)[9]
Naoki HAYASHI	Technical Associate (April '94-)
Satoru NAKASHIMA	IMS Fellow (-March '94)[10]
Philip JEWSBURY	JSPS Post-Doctoral Fellow (-February '94)[11]
Shun HIROTA	Graduate Student
Denis A. PROSHLYAKOV	Graduate Student
Ken KODAMA	Graduate Student
Tridibendra N. MISRA	Visiting Professor from Indian Association for the Cultivation and Science (October '93-November '93)
Anandi L. VERMA	Visiting Professor from North-Eastern Hill University (February '94-March '94)
Insook R. PAENG	Visiting Associate Professor from Seoul Woman's University (June '94-August '94)
Steven E. J. BELL	Visiting Scientist from The Queen's University of Belfast (June '94-September '94)

Department of Electronic Structure

Excited State Chemistry

Keitaro YOSHIHARA	Professor
Yoshiyasu MATSUMOTO	Associate Professor
Kyoichi SAWABE	Research Associate
Keisuke TOMINAGA	Research Associate
Shigeichi KUMAZAKI	Technical Associate
Kazuo WATANABE	Technical Associate
Bongsoo KIM	JSPS Post-Doctoral Fellow (-February '94),[12] Visiting Scientist from Kyungpook University, Korea (July-August '94)
Yukito NAITOH	JSPS Post-Doctoral Fellow
Yuri A. GRUZDKOV	JSPS Post-Doctroal Fellow (February '94-)
Yutaka NAGASAWA	Graduate Student (-March '94), Research Fellow (April '94)[13]
Hiroyuki KATO	Graduate Student
Ken-ichi SAITOW	Graduate Student (April '94-)

Tai Jong KANG	Visiting Scientist from Taegu University, Korea (January-Febrary 94')
Valey F. KAMALOV	JSPS Visiting Scientist from Institute of Chemical Physics, Russian Academy of Sciences, Russia (March '94-)
Gary P. KEOGH	Visiting Graduate Student from Imperial College of Science, Technology, and Medicine, UK (April '94-)
Haridas PAL	JSPS Visiting Scientist from Bhabha Atomic Research Centre, India (April '94-)
Biman BAGCHI	JSPS Visiting Scientist from Indian Institute of Science, India (May-June '94)
Stephen R. MEECH	Visiting Scientist from East Anglia University, UK (July-August '94)
B. H. KANG	Visiting Graduate Student from Kyungpook University, Korea (July-August '94)

Excited State Dynamics

Ichiro HANAZAKI	Professor
Toshinori SUZUKI	Associate Professor
Masao TAKAYANAGI	Research Associate
Kenichi TONOKURA	Research Associate
Hideki KATAYANAGI	Technical Associate (December '93-)
Akiko KAMINAGA	Technical Associate (April '94-)
Lizla S. BONTUYAN	Visiting Research Fellow (September '93-March '94), JSPS Post-Doctoral Fellow (April '94-)
Nobuaki YONEKURA	IMS Fellow (April '94-)
Suketu R. GANDHI	JSPS Fellow (July '94-)
Takumi KONO	Graduate Student (-September '93)[14]
Tetsuo SEKIGUCHI	Graduate Student (-March '94)[15]
Tatsuo GEJO	Graduate Student (-March '94), Visiting Research Fellow (April-May '94)[16]
Noriaki OKAZAKI	Graduate Student
Nobuhisa HASHIMOTO	Graduate Student
Yoshihiro NAKAMICHI	Graduate Student from Nara University of Education* (-March '94)
Vladmir K. VANAG	Visiting Scientist from N. N. Semenov Institute of Chemical Physics, the Russian Acd. of Sci., Russia (September '93-March '94)

Electronic Structure

Toru AZUMI	Adjunct Professor from Tohoku University (-March '94)
Hiroyasu SATO	Adjunct Professor from Mie University (April '94-)
Ryoichi NAKAGAKI	Adjunct Associate Professor from Kanazawa University
Yoshihito MORI	Research Associate
Takamichi KOBAYASHI	Research Associate

Molecular Energy Conversion

Gyula RÁBAI	Visiting Associate Professor from Kossuth Lajos University, Hungary (October '93-)
Fernando RULL PEREZ	Visiting Professor from University of Valladlid, Spain (March '94-)
Valery A. IVANOV	Visiting Professor from Bilkent University, Turkey (March '94-)

Department of Molecular Assemblies

Solid State Chemistry

Kyuya YAKUSHI	Professor
Kazushi KANODA	Associate Professor
Akito UGAWA	Research Associate
Yasuhiro NAKAZAWA	Research Associate
Ken-ichi IMAEDA	Technical Associate
Kazuya MIYAGAWA	Technical Associate
Mikihiro URUICHI	Technical Associate
Hirohiko SATO	IMS Fellow (-March '94)[17]
Illias I. KHAILULLIN	JSPS Post-Doctoral Fellow (-January '94)[18]
Takafumi MIYAZAKI	Visiting Research Fellow (-March '94), JSPS Post-Doctoral Fellow (April '94-)

Toshihiro HIEJIMA	Graduate Student
Jian DONG	Graduate Student
Hiromi TANIGUCHI	Graduate Student (April '94-)
Ko-ichi HIRAKI	Graduate Student (April '94-)
Akiko SHIMIZU	Graduate Student from Nagoya University* (April '94-)
Leonid S. GRIGORYAN	Visiting Scientist (September '93-June '94)[19]
Anvar A. ZAKHIDOV	Visiting Scientist (August-October '93)

Molecular Assemblies Dynamics

Yusei MARUYAMA	Professor
Seiichi MIYAJIMA	Associate Professor
Toshiyasu SUZUKI	Research Associate
Hironori OGATA	Research Associate
Osamu OHISHI	Technical Associate (April '94-)
Noriko YAMAMURO	IMS Fellow
Roger J. WHITEHEAD	JSPS Post-Doctoral Fellow (-March '94)
Takeshi ARAI	JSPS Post-Doctoral Fellow (July '94-)
Shaoli FANG	Graduate Student
Atsushi SUZUKI	Graduate Student
Toshifumi TERUI	Visiting Research Fellow (-September '93)[20]
Chikako NAKANO	Visiting Research Fellow
Keiichi KOHAMA	Visiting Research Fellow from Toyota Motor Corp. (-March '94)[21]
Yang fang LI	Visiting Scientist (January '94-April '94)
Zhu DAOBEN	Visiting Scientist (November-December '93)
Jan KALINOWSKI	Visiting Scientist (September-December '93)
Naomi MIYAJIMA	Visiting Scientist from Hokkaido Univ. (April '94-)

Molecular Assemblies

Akira YOSHIDA	Adjunct Professor from Toyohashi University of Technology (-March '94)
Kosuke SHOBATAKE	Adjunct Professor from Nagoya University (April '94-)
Yukio OUCHI	Adjunct Associate Professor from Nagoya University
Takehiko MORI	Research Associate (-March '94)[22]
Shinji HASEGAWA	Research Associate

Department of Applied Molecular Science

Applied Molecular Science I

Kazuhiro NAKASUJI	Professor (-March '94)[23]
Kiyoshi ISOBE	Associate Professor
Yasushi MORITA	Research Associate (-September '93)[23]
Makoto TADOKORO	Research Associate
Masaaki ABE	Research Associate
Takanori NISHIOKA	Technical Associate
Hiroshi SHIMOMURA	IMS Fellow
Yuichi KANEKO	Visiting Scientist from Kochi Univ. (May '94-)
Rimo XI	Graduate Student
Tetsuji ITOH	Graduate Student
Kunio HATANAKA	Graduate Student
Md. Badruz ZAMAN	Graduate Student
Minoru MITSUMI	Graduate Student
Koichi TAMAKI	Graduate Student
Seiji OGO	Graduate Student
Hee K. CHAE	Visiting Scientist from Hankuk Univ. of Foreign Studies (June '94-August '94)

Applied Molecular Science II

Yasuhiro AOYAMA	Adjunct Professor from Nagaoka University of Technology
Motokazu UEMURA	Adjunct Associate Professor from Osaka City University (-March '94)[24]
Takahiro HOSOKAWA	Adjunct Associate Professor from Osaka University (April '94-)[25]

Jiro TOYODA	Research Associate
Takayoshi SUZUKI	Research Associate

Physical Organic Chemistry

Yoshinori NARUTA	Associate Professor
Hisao NEMOTO	Associate Professor
Satoshi USUI	Research Associate
Naoki ASAO	Research Associate
Jianping CAI	Post-Doctoral Fellow (February '94-)
Masa-aki SASAYAMA	Graduate Student from Kyoto Univ.*
Mari ICHIMURA	Graduate Student from Kyoto Univ.*
Nobuyuki SAWADA	Graduate Student from Kyoto Univ.* (-March '94)
Hideki TANAKA	Graduate Student from Kyoto Univ.* (-March '94)
Kanako ICHIHARA	Graduate Student from Kyoto Univ.* (October '93-)
Masaoki GOTO	Graduate Student from Kyoto Univ.* (October '93-)
Takao SASAKI	Graduate Student from Kyoto Univ.* (October '93-)
Yukiyasu CHONAN	Graduate Student from Tohoku Univ.* (-August '93)[26]
Satoshi IWAMOTO	Graduate Student from Tohoku Univ.* (-March '94)
S. H. Razi ABDI	Visiting Scientist from Central Salt and Marine Chemicals Institute, India (July '94-)

Department of Vacuum UV Photoscience

Photochemistry

Nobuhiro KOSUGI	Professor
Kosuke SHOBATAKE	Associate Professor (-December '93)[27]
Katsuhiko OKUYAMA	Research Associate (-March '94)[28]
Yasutaka TAKATA	Research Associate (November '93-)
Haruhiko OHASHI	Technical Associate
Jun-ichi ADACHI	Technical Associate (April '94-)
Motohiko NAKAMURA	IMS Fellow (August '94-)
Hiroshi YOSHIKAWA	Graduate Student
Mitsuhiko KONO	Graduate Student
Koji ITO	Visiting Research Fellow (-March '94)

Chemical Dynamics

Tsuneo Urisu	Professor
Koichiro MITSUKE	Associate Professor
Kazuhiko MASE	Research Associate
Hiroaki YOSHIDA	Research Associate
Yoshiyuki TSUSAKA	Research Associate (July '94-)
Hideo HATTORI	Technical Associate
Mitsuru NAGASONO	Technical Associate
Yanping ZHANG	JSPS Post-Doctoral Fellow (-November '93)[29]
Hiroaki YOSHIGOE	Graduate Student
Minoru KANNO	Graduate Student
Yoshiaki IMAIZUMI	Graduate Student (April '94-)
Yasumasa HIKOSAKA	Graduate Student from Tokyo Institute of Technology* (April '94-)
Satoshi MINOURA	Graduate Student from Shinshu Univ.* (-March '94)

Interface Molecular Science

Hiroshi KAWAZOE	Professor
Mitsuhiro NISHIO	Associate Professor
Takuya HASHIMOTO	Research Associate (-September '93)[30]
Koji HAYASHI	Research Associate
Naoyuki UEDA	Research Associate (October '93-)
Makoto IKEJIRI	Graduate Student from Saga Univ.* (-September '94)
Toshihiro OGATA	Graduate Student from Saga Univ.*
Ghesyas S. IRFAN	Graduate Student from Saga Univ.*
Koichi NAKANOSE	Graduate Student from Saga Univ.* (-March '94)
Daisaku KATO	Graduate Student from Gifu Univ.* (October '93-September '94)

Hiroshi MIZOGUCHI	Graduate Student from Tokyo Institute of Technology* (April '94-)
Shinya HIRANO	Graduate Student from Saga Univ.* (April '94-)

Synchrotron Radiation Research

Valery A. IVANOV	Visiting Professor from Bilkent Univ. Ankara, Turky (March '94-)
Yuri A. BERLIN	Visiting Associate Professor from N.N.Semenov Institute of Chemical Physics of the Russian Academy of Sciences, Moscow, Russia (November '93-August '94)

Coordination Chemistry Laboratories

Akira NAKAMURA	Director

Synthetic Coordination Chemistry

Yutaka FUKUDA	Professor (-March '94)[31]
Yuzo YOSHIKAWA	Professor (April '94-)
Kiyoshi SAWADA	Associate Professor (-March '94)[32]
Hiroshi NAKAZAWA	Associate Professor (April '94-)
Hikaru ICHIDA	Research Associate (-March '94)[33]
Keiichi SATOH	Research Associate (-March '94)[32]
Yasushige KURODA	Research Associate (April '94-)
Tsutomu MIZUTA	Research Associate (April '94-)
Yasuharu OHMORI	Graduate Student from Okayama Univ.* (April '94-)
Koji YUTOH	Graduate Student from Okayama Univ.* (April '94-)
Yoshitaka YAMAGUCHI	Graduate Student from Hiroshima Univ.* (April '94-)
Masakazu HIROTSU	Graduate Student from Okayama Univ.* (April '94-)
Yuri MIZUNO	Graduate Student from Nara Women's Univ.* (April '94-)
Tomohide ICHIKAWA	Graduate Student from Niigata Univ.* (-March '94)
Haruko HOSOI	Graduate Student from Ochanomizu Univ.* (-March '94)
Etsuko KONDO	Graduate Student from Okayama Univ.* (April '94-)
Rei ITOH	Graduate Student from Hiroshima Univ.* (April '94-)
Michiyo KOKKA	Graduate Student from Hiroshima Univ.* (April '94-)
Tomoaki YAMASAKI	Graduate Student from Hiroshima Univ.* (April '94-)
Daisuke KATAOKA	Graduate Student from Okayama Univ.* (April '94-)
Motoyuki TASAKA	Graduate Student from Okayama Univ.* (April '94-)
Hong Ling LIU	Graduate Student from Okayama Univ.* (April '94-)
Koichiro TOYOTA	Graduate Student from Hiroshima Univ.* (April '94-)
Magnus SANDSTRÖM	Visiting Professor from Royal Inst. of Technology, Sweden (October '93-April '94)
Farideh JALILEHVAND	Visiting Research Fellow (October '93-March '94)

Complex Catalysis

Akira NAKAMURA	Professor (April '93-)
Hisanobu OGOSHI	Adjunct Professor from Kyoto Univ. (-March '94)[34]
Fumio KAWAIZUMI	Adjunct Associate Professor from Nagoya Univ. (-March '94)[35]
Yutaka FUKUDA	Adjunct Professor from Ochanomizu Women's Univ. (April '94-)
Junichiro SETSUNE	Adjunct Associate Professor from Kobe Univ. (April '94-)
Thomas DANIEL	Research Associate
Kenji WAIZUMI	Technical Associate (-September '93)[36]
Rainer HAHN	Visiting Research Fellow (April '94-)
Nathalie LAVAUD	Visiting Research Fellow (April '94-)

Functional Coordination Chemistry

Koji TANAKA	Professor
Tamotsu TAKAHASHI	Associate Professor
Hirotaka NAGAO	Research Associate
Noriyuki SUZUKI	Research Associate
Tetsunori MIZUKAWA	Technical Associate
Ryuichiro HARA	Technical Associate (April '94-)
Toyohisa ISHIDA	IMS Fellow (January '94-)
Martin KOTORA	JSPS Post-doctoral Fellow (-April '94), Visiting Research Fellow (May '94-)

Hide KAMBAYASHI	Graduate Student (-March '94), Visiting Research Fellow (April '94-)
Nobutoshi KOMEDA	Graduate Student from Osaka Univ.* (-March '94)
Koichiro AOYAGI	Graduate Student
Yoshinori KUSHI	Graduate Student
Hiroshi NAKAJIMA	Graduate Student
Kiyotsuna TOYOHARA	Graduate Student
Kayoko KASAI	Graduate Student
Zhenfeng XI	Graduate Student
Yasushi NISHIHARA	Graduate Student
Fernando RULL-PEREZ	Visiting Professor from Valladlid Univ., Spain (March '94-)
Douman JIN	Visiting Professor from Henan Inst. of Chemistry, China (September-December '93)
Denis Y. KONDAKOV	Visiting Research Fellow (-December '93)
Marina KONDAKOVA	Visiting Research Fellow (-December '93)

Coordination Bond

Kazuko MATSUMOTO	Adjunct Professor from Waseda Univ.
Akira NAGASAWA	Adjunct Associate Professor from Saitama Univ.

Research Facilities

Computer Center

Hiroki NAKAMURA	Director (-March '94)
Suehiro IWATA	Director (April '94-)
Mutsumi AOYAGI	Associate Professor
Shinkoh NANBU	Research Associate
Toshiya TAKAMI	Research Associate (February '94-)
Satoshi MINAMINO	Technical Associate

Chemical Materials Center

Ichiro HANAZAKI	Director
Yoshiro YAMASHITA	Associate Professor
Shoji TANAKA	Research Associate
Masaaki TOMURA	Technical Associate
Masatoshi KOZAKI	Graduate Student (-March '94)
Katsuhiko ONO	Graduate Student
Chitoshi KITAMURA	Graduate Student
Akira OHTA	Graduate Student

Instrument Center

Shuji SAITO	Director
Kiyokazu FUKE	Associate Professor
Shunji BANDOW	Research Associate
Fuminori MISAIZU	Research Associate
Daisuke KUWAHARA	Research Associate (January '94-)
Masaomi SANEKATA	Graduate Student
Ryozo TAKASU	Graduate Student (April '94-)

Low-Temperature Center

Yusei MARUYAMA	Director

Equipment Development Center

Teizo KITAGAWA	Director
Michio WATANABE	Associate Professor (April '94-)
Shuji ASAKA	Research Associate
Hiroshi KITAGAWA	Research Associate (-March '94)[37]
Jeung Sun AHN	Research Associate
Taro SEKIKAWA	Graduate Student from University of Tokyo* (-March '94)

Ultraviolet Synchrotron Orbital Radiation Facility

Kyuya YAKUSHI	Director (-March '94)
Nobuhiro KOSUGI	Director (April '94-)
Makoto WATANABE	Associate Professor (-September '93)[38]

Goro ISOYAMA	Associate Professor (-March '94)[39]
Masao KAMADA	Associate Professor
Kazumichi NAKAGAWA	Adjunct Associate Professor from Kobe Univ.
Atsunari HIRAYA	Research Associate
Shin-ichiro TANAKA	Research Associate
Hiroyuki HAMA	Research Associate
Shin-ichi KIMURA	Research Associate (October '93-)
Shigeo OHARA	IMS Fellow (-Nobember '93)[40]
Sayumi HIROSE	Graduate Student (-March '94), Research Fellow (April '94-)
Naoshi TAKAHASHI	Graduate Student (April '94-)
Kazuhiko KIMURA	Graduate Student (April '94-)

Technical Staff

Akira UCHIDA	Technical Division Head
Osamu MATSUDO	UVSOR Facility (Unit Chief) (-May '94) Technical Section Chief (June '94-)
Keiichi HAYASAKA	Technical Section Chief
Kiyonori KATO	Low-Temperature Center (Unit Chief) (-May '94) Technical Section Chief (June '94-)
Kusuo SAKAI	Technical Section Chief
Norio OKADA	Equipment Development Center (-September '93) Molecular Structure (Unit Chief) (October '93-March '94)[41]
Toshio KINOSHITA	UVSOR Facility (-May '94) Electronic Structure (Unit Chief) (June '94-)
Fumio NISHIMOTO	Computer Center (Unit Chief)
Kunihiko TANAKA	Computer Center
Fumitsuna TESHIMA	Computer Center
Masaaki NAGATA	Equipment Development Center (-May '94) Chemical Materials Center (Unit Chief) (June '94-)
Sachiyo NOMURA	Chemical Materials Center
Takaya YAMANAKA	Instrument Center
Masahiro SAKAI	Instrument Center
Hisashi YOSHIDA	Equipment Development Center (-May '94) Low-Temperature Center (Unit Chief) (June '94-)
Takashi TAKAYAMA	Low-Temperature Center
Toshio HORIGOME	Equipment Development Center (Unit Chief)
Mitsukazu SUZUI	Equipment Development Center
Shinji KATO	Equipment Development Center
Nobuo MIZUTANI	Equipment Development Center
Kouichi UCHIYAMA	Equipment Development Center
Tomonori TOYODA	Equipment Development Center
Masami HASUMOTO	UVSOR Facility
Jun-ichiro YAMAZAKI	UVSOR Facility
Eiken NAKAMURA	UVSOR Facility

* Carries out gradurate research of IMS on the Cooporative Education Program of IMS with graduate schools.

1) Present Address: Department of Chemistry, Nagoya University, Furo-cho, Chikusa-ku, Nagoya 464
2) Present Address: Lab. de Chimie Theorique, Batiment 490, Univ. Paris 11, 91405 Orsay, France
3) Present Address: Unitat Quimica Fisica, Universita Autonoma Barcelona, 08193 Bellateria, Barcelona, Spain
4) Present Address: Chernoglovka, Moskow Region Russia 142432
5) Present Address: Institute for Fundametal Chemistry, 34-4 Takano-Nishihiraki-cho, Sakyo-ku, Kyoto 606, Japan
6) Present Address: Department of Chemistry, Chungbuk National University, Cheongju, Chungbuk 360-763, Korea
7) Present Address: Faculty of Engineering, Yamanashi University, Takeda 4-4-37, Kohu-shi, Yamanashi
8) Present Address: Astronomical Observatory, Urals State University, Lenin Ave. 51, 620151 Ekaterinburgh, Russian Federation
9) Present Address: Japan Advanced Institute of Science and Technology, Tatsunokuchi, Ishikawa 923-12
10) Present Address: Dept. of Chemistry, Faculty of Engineering Science, Osaka Univ., Machikaneyama, Toyonaka 560

11) Present Address: The Protein Engineering Research Institute, Furuedai, Suita 565
12) Present Address: Department of Chemsitry Education, Kyungpook National University, Sankyuk-dong, Buk-gu, Taeku, 702-701, Korea
13) Present Address: Department of Chemistry, The University of Chicago, Chicago, Illinois 60637, USA
14) Present Address: Nippon Steel Corporation, 2-6-3, Otemachi, Chiyoda-ku, Tokyo, 100
15) Present Address: Kyushu National Agricultural Experiment Station, 2421, Suya, Nishigoushi-cho, Kikuchi-gun, Kumamoto, 861-11
16) Present Address: Physikalish-Chemishes Institut der Universitat Zurich Winterthurerstrasse 190, CH-8057 Zurich, Switzerland
17) Present Address: Dept. of Chemistry, Faculty of Science, Tokyo Institute of Technology, O-okayama, Meguro-ku, Tokyo 152
18) Present Address: Dept. of Thermophysics, Uzbek Academy of Science, 28 Katartal Str.Chilanzar C Tashkent 700135, Uzbekistan
19) Present Address: Electrotechnical Laboratory, Umezono 1-1-4 Tsukuba-shi, Ibaraki 305
20) Present Address: Communications Research Laboratory, 588-2, Iwaoka, Nishi-ku, Kobe 674
21) Present Address: Toyota motor corp. Higashi-fuji Technical Center, Mishuku 1200, Susono-shi, Shizuoka
22) Present Address: Dept. of Organic and Polymeric Materials, Tokyo Institute of Technology, O-okayama, Meguro-ku, Tokyo 152
23) Present Address: Department of Chemistry, Faculty of Science, Osaka Univ., Toyonaka, Osaka 560
24) Present Address: Department of Chemistry, Faculty of Science, Osaka City Univ., Sugimoto-3-3-138, Sumiyoshi, Osaka 558.
25) Present Address: Department of Chemistry, Faculty of Engineering Science, Osaka Univ., Toyonaka, Osaka 560
26) Present Address: Research Associate, Department of Chemistry Faculty of Science, Tohoku University, Aoba, Sendai, 980-77
27) Present Address: Dept. of Materials Chemistry, School of Engineering, Nagoya Univ., Furo-cho, Chikusa-ku, Nagoya 464-01
28) Present Address: Dept. of Industrial Chemistry, Faculty of Engineering, Nihon Univ., 1 Nakakawara Tokusada Tamura-cho, Kooriyama, Fukushima 963
29) Present Address: Sumitomo Heavy Industries, Ltd., 2-1-1 Yato-cho, Tanashi, Tokyo 188
30) Present Address: College of Arts and Science, Univ. of Tokyo, Komaba, Meguro-ku, Tokyo 153
31) Present Address: Dept. of Chem., Fac. of Science, Ochanomizu Women's Univ., 2-2-1 Otsuka, Bunkyo-ku, Tokyo 112.
32) Present Address: Dept. of Chem., Fac. of Science, Niigata Univ., 8050 Igarashi-Ninomachi, Niigata-shi, Niigata 950-21.
33) Present Address: Dept. of Chem., Fac. of Science, Univ. of Tokyo, 7-3-1 Hongo, Bunkyo-ku, Tokyo 113.
34) Present Address: Dept. of Chem., Fac. of Tech., Kyoto Univ., Yoshida-Honmachi, Sakyo-ku, Kyoto-shi, Kyoto 606-01.
35) Present Address: Fac. of Tech., Nagoya Univ., Furo-cho, Chikusa-ku, Nagoya-shi, Aichi 464-01.
36) Present Address: Fac. of Education, Yamaguchi Univ., 1677-1 Yoshida, Yamaguchi-shi, Yamaguchi 753.
37) Present Address: Dept. of Material Science, Japan Advanced Institute of Science and Technology, Tatsunokuchi, Ishikawa 923-12
38) Present Address: Research Institute for Scientific Measurements, Tohoku University, 2-1-1 Katahira, Aoba-ku, Sendai 980
39) Present Address: The Institute of Science and Industrial Research, Osaka University, 8-1 Mihogaoka, Ibaraki, Osaka 567
40) Present Address: Dept. of Physics, Nagoya Institute of Technology, Gokisho-cho, Showa-ku, Nagoya 466
41) Present Address: Astronomical Engineering Center, National Astronomical Observatory, 2-21-1, Ohsawa, Mitaka, Tokyo 181

COUNCIL

Mitsuo ITO	**Director-General**

Councilors

Chairman	Teijiro YONEZAWA	Professor Emeritus, Kyoto University
Vice-Chairman	Yukio HORI	Professor, Kanazawa Institute of Technology
	Hirotsugu AKAIKE	Professor Emeritus, The Institute of Statistical Mathematics
	Schunichi AKIMOTO	Professor Emeritus, The University of Tokyo
	Hideaki CHIHARA	Executive Director, Japan Association for International Chemical Information
	Yoshikazu ITO	Chairman of The Board, Toray Industries, Inc.
	Hiizu IWAMURA	Professor, The University of Tokyo
	Nobuo KATO	President, Nagoya University
	Kozo KUCHITSU	Professor, Josai University
	Haruo KURODA	Professor, Science University of Tokyo
	Yoshio MATSUNAGA	Professor, Kanagawa University
	Hidetake MORIMOTO	Adviser, Toyota Central Research & Development Loboratories, Inc.
	Toru MORIYA	Professor, Science University of Tokyo
	Kazuo SAITO	Professor Emeritus, Tohoku University
	Hideki SAKURAI	Professor, Tohoku University
	Shinichi SASAKI	President, Toyohashi University of Technology
	Hiroshi SHIONO	Professor, Seikei University
	Hisashi TANAKA	Former President, Kyoto Pharmaceutical University
	Peter DAY	Director, The Royal Institution of Great Britain
	Mostafa A. El-Sayed	Professor, Georgia Institute of Technology

The Council is the advisory board for the Director-General. Two of the councilors are selected among distinguished foreign scientists.

Distinguished Research Consultants

Hiroaki BABA	Professor Emeritus, Hokkaido University
Kenichi FUKUI	President, Institute for Fundamental Chemistry
Saburo NAGAKURA	President, The Graduate University of Advanced Studies
Kenji TAMARU	Professor, Science University of Tokyo
Ikuzo TANAKA	President, National Institute for Academic Degrees

Administration Bureau

Jiro SATO	Director-General, Administration Bureau (-June '94)
Mikio HASHIMOTO	Director-General, Administration Bureau (July '94-)
Nobuaki SHIMIZU	Director, General Affairs Department
Mutsuo MIYAZAKI	Director, Finance and Facilities Department
Isao FUJII	Head, Personnel Division
Ryouichi KUWABARA	Head, Personnel Division
Shigeaki AIHARA	Head, Research Cooperation an International Affairs Division
Yoshiji SHIMA	Head, Budget Division
Masayuki JINNO	Head, Accounts Division
Takashi SUZUKI	Head, Construation Division
Yoshiaki KAMACHI	Head, Equipment Division

BUILDINGS AND CAMPUS

The IMS campus covering 62,343 m^2 is located on a low hill in the middle of Okazaki City. The inequality in the surface of the hill and growing trees are preserved as much as possible, and low-storied buildings are adopted for conservation of the environment. The buildings of IMS are separated according to their functions as shown in the map. The Research Office Building and all Research Facilities except for the Computer Center are linked organically to the Main Laboratory Building by corridors. Computer Center, Library and Administration Buildings are situated between IMS and the neighboring National Institute for Basic Biology and National Institute for Physiological Sciences, because the latter two facilities are common to these three institutes.

The lodging facility of IMS called Yamate Lodge, located within ten minutes' walk, has sleeping accommodations for 19 guests and two families. Mishima Lodge, located within four minutes' walk east of IMS can accommodate 68 guests and ten families. Scientists who visit IMS as well as the two other institutes can make use of these facilities. Foreign visiting scientists can also live at these lodgings with their families during their stays.

The Institute for Molecular Science

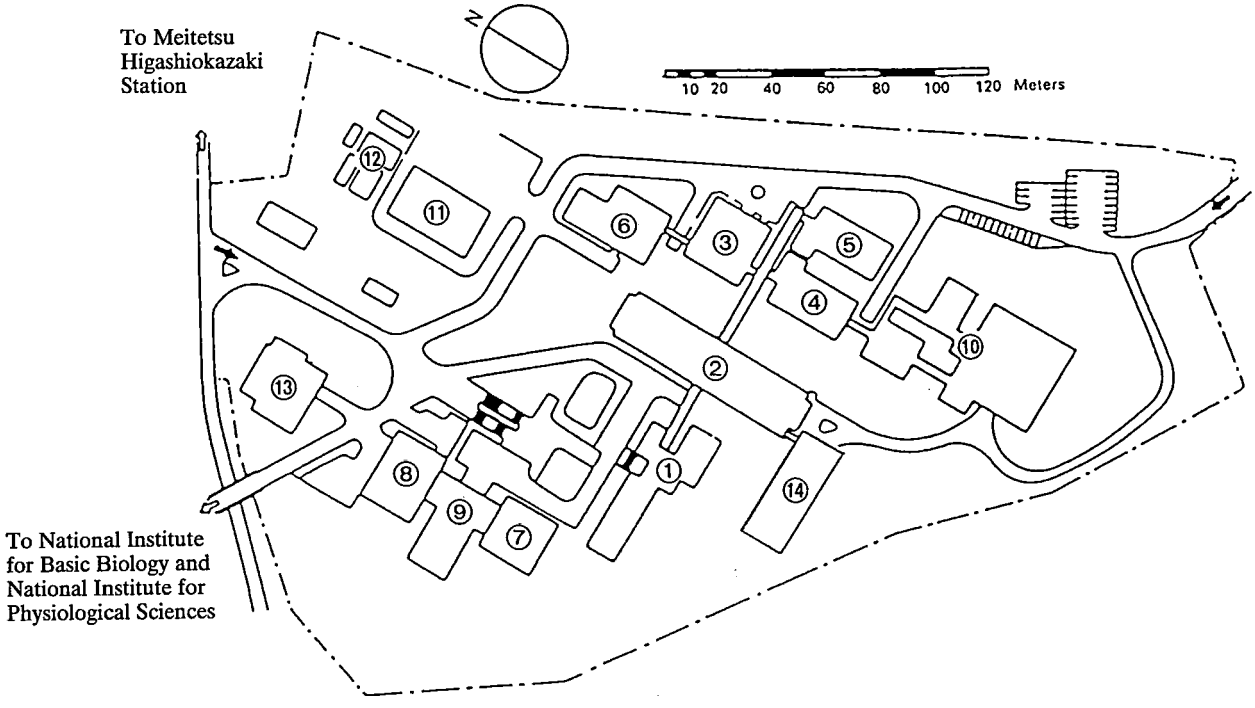

1. Research Office Building
2. Main Laboratory Building
3. Equipment Development Center
4. Instrument Center
5. Chemical Materials Center
6. Low-Temperature Center
7. Computer Center
8. Library
9. Central Administration
10. UVSOR Facility
11. Power Station
12. Waste-Water Disposition Facilities
13. Faculty Club
14. South Laboratory Building

Okazaki (population 300,000) is 260 km southwest of Tokyo, and can be reached by train in about 3 hours from Tokyo via New Tokaido Line (Shinkansen) and Meitetsu Line.
The nearest large city is Nagoya, about 40 km west of Okazaki.

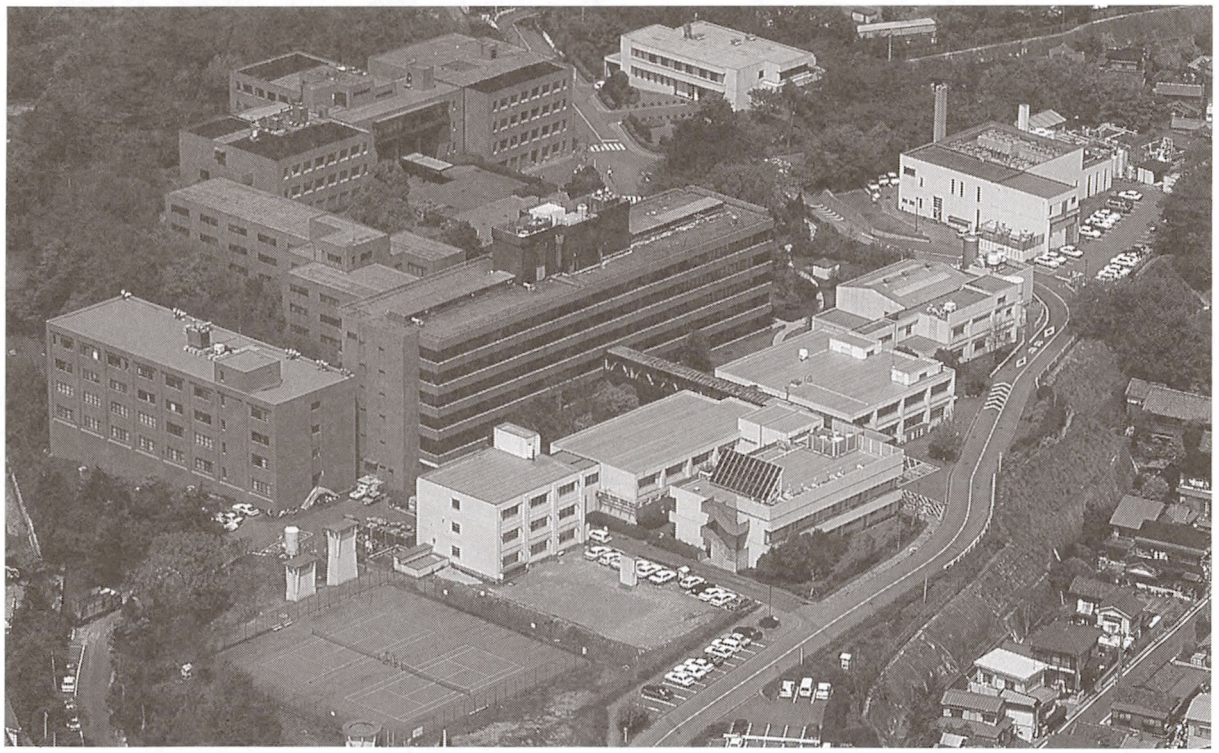

RESEARCH ACTIVITIES I
Department of Theoretical Studies

I—A Structures and Reactions of Group 2 and 3 Atoms and their Ions with Water Clusters

I-A-1 Reactions of Singly Charged Alkaline-Earth Metal Ions with Water Clusters: Characteristic Size Distribution of Product Ions

Masaomi SANEKATA *(The Graduate University for Advanced Studies)*, **Fuminori MISAIZU, Kiyokazu FUKE, Suehiro IWATA** *(Keio Univ. and IMS)*, **and Kenro HASHIMOTO** *(Tokyo Metropolitan Univ.)*

[*J. Am. Chem. Soc.*, in press]

The reactions of Mg^+ and Ca^+ ions with water clusters are examined using a reflectron time-of-flight mass spectrometer combined with a laser vaporization technique. Both the $M^+(H_2O)_n$ and $MOH^+(H_2O)_{n-1}$ (M=Mg and Ca) ions are found to form as the reaction products with characteristic size distributions: the latter ions are produced via an H-atom elimination reaction (oxidation of M^+). As for the Mg^+ ion, the $Mg^+(H_2O)_n$ ions are predominantly produced for $1 \leq n \leq 5$ and $n \geq 15$, while $MgOH^+(H_2O)_{n-1}$ are exclusively observed for $6 \leq n \leq 14$ in the mass spectrum. The similar product distributions are also observed for Mg^+-D_2O, Ca^+-H_2O, and Ca^+-D_2O systems, though they are found to be affected by deuterium and metal substitutions. On the basis of these results as well as those on the photoinduced reaction of $Mg^+(H_2O)_n$ reported previously, the first product switching at n=5 for Mg^+ (n=4 for Ca^+) is ascribed to the difference in the successive hydration energies of the M^+ and MOH^+ ions. As for the second product switching, two possible mechanisms are proposed such as the stabilization of a Rydberg-type ion-pair state and the involvement of a new product.

I-A-2 Molecular Orbital Studies of the Structures and Reactions of Singly Charged Magnesium Ion with Water Clusters, $Mg^+(H_2O)_n$

Hidekazu WATANABE *(Keio Univ. and The Graduate University for Advanced Studies)*, **Suehiro IWATA** *(Keio Univ. and IMS)*, **Kenro HASHIMOTO** *(Tokyo Metropolitan Univ.)*, **Fuminori MISAIZU, and Kiyokazu FUKE**

[*J. Am. Chem. Soc.*, in press]

With the *ab initio* molecular orbital calculations, the structures of the cation clusters $Mg^+(H_2O)_n$ and their hydrogen elimination products $(MgOH)^+(H_2O)_{n-1}$ are optimized. In $Mg^+(H_2O)_n$, the hydration number of the most stable isomers is three. In $(MgOH)^+(H_2O)_n$, all water molecules are directly bonded to Mg^+ for $n \leq 6$. The hydration energies of $(MgOH)^+$ is larger than that of Mg^+, because of strongly polarized $(MgOH)^+$molecular ion. The internal energy change of the hydrogen elimination of $Mg^+(H_2O)_n$ is positive for n=1–5, but become negative for n=6, which is in good agreement with the product switching in the TOF spectrum reported by Sanekata *et al.* The isotope effect and the n dependence of the equilibrium constants of hydrogen (deuterium) elimination reaction observed in their experiment can be explained qualitatively.

I-A-3 The Theoretical Studies of the Boron-Water Cluster $B(H_2O)_n$ and their Ions $B^+(H_2O)_n$ with Comparing the Aluminum-Water Clusters

Hidekazu WATANABE *(Keio Univ. and The Graduate University for Advanced Studies)*, **Hiroyuki NAKAMURA** *(Keio Univ.)*, **and Suehiro IWATA** *(Keio Univ. and IMS)*

With the *ab initio* molecular orbital calculations, the structures of the $B^+(H_2O)_n$ and $B(H_2O)_n$ are optimized. The most stable neutral $B(H_2O)_n$ are $[B(H_2O)](H_2O)_{n-1}$ type, which are similar to the neutral $[Al(H_2O)](H_2O)_{n-1}$, in which only one water molecule is directly bonded to the central metal and forms the chain structures. On the other hand, in the singly charged $B^+(H_2O)_n$, two kinds of the isomers are found. The one is $[B^+(H_2O)_2](H_2O)_{n-2}$ type of isomers, and is similar to $Al^+(H_2O)_n$. The other is $[B^+(H_2O)](H_2O)_{n-1}$ type, which has chain structures. But in the latter type of isomers, the clusters isomerize to $[BOH(H_3O^+)](H_2O)_{n-2}$ spontaneously. For $n \geq 3$, the structure $[BOH(H_3O^+)](H_2O)_{n-2}$ further isomerizes to $HBOH^+(H_2O)_{n-1}$; the boron atom extracts a hydrogen atom of the water molecule. Such isomerization reactions are not found in $[Al^+(H_2O)](H_2O)_{n-1}$. The isomers $HBOH^+(H_2O)_{n-1}$ or $[BOH(H_3O^+)](H_2O)_{n-2}$ are more stable than $[B^+(H_2O)_2](H_2O)_{n-2}$. On the other hand, in the Al-water clusters, the most stable isomers are $[Al^+(H_2O)_2](H_2O)_{n-2}$.

I-A-4 Ab Initio Studies on the Structures and Vertical Electron Detachment Energies of Copper-Water Negative Ion Clusters $Cu^-(H_2O)_n$ and $CuOH^-(H_2O)_{n-1}$

Chang-Guo ZHAN *(Central China Normal Univ. and IMS)* **and Suehiro IWATA**

[*Chem. Phys. Letters*, in press]

Equilibrium geometries of $Cu^-(H_2O)_n$ and $CuOH^-(H_2O)_{n-1}$ (n=1 and 2) negative ion clusters have been optimized by performing the *ab initio* calculations at the second-order Møller-Plesset (MP2) level with extended basis sets. To understand the nature of the interaction between Cu^- ion and water molecules, we have also optimized the geometries of $X^-(H_2O)_n$ (X=F, Cl, Br and I) at the same level. The calculated results show that all hydrogen atoms in the equilibrium geometries of $Cu^-(H_2O)_n$ (n=1 and 2) are equivalent to each other, which is contrasted to the geometries of $X^-(H_2O)_n$, where one of hydrogen atoms of H_2O is more strongly bonded to X^-. The detailed com-

parative study leads to understand easily the optimized geometries, and allows us to estimate the ionic radius of Cu^- ion as 1.86 Å. The MP4SDTQ procedure has been performed at the geometries optimized at the MP2 level to evaluate the vertical electron detachment energies as well as hydration energies, and all the calculated values are very close to the corresponding experimental data by Misaizu et al.

I—B Geometrical and Electronic Structures of Binary Clusters

I-B-1 Theoretical Study of Silicon-Sodium Binary Clusters, Geometrical and Electronic Structures of Si_nNa (n=1—7)

Reiko KISHI *(Keio Univ.)*, **Atsushi NAKAJIMA** *(Keio Univ.)*, **Suehiro IWATA** *(Keio Univ. and IMS)*, **and Koji KAYA** *(Keio Univ.)*

[*Chem.Phys.Letters*, **224**, 200—206 (1994)]

The geometries, ionization energies and adsorption energies of silicon-sodium binary clusters (Si_nNa, n=1-7) were studied with *ab initio* MO calculations. All the calculations were carried out at the restricted Hartree-Fock level of approximation for both closed and open shell system. The structure of the most stable isomer of Si_nNa keeps the frame of the corresponding Si cluster unchanged. The electronic structure of Si_nNa is similar to that of the corresponding negative ions Si_n^-. The ionization energies of Si_nNa were evaluated with the ΔSCF method, and they become smaller than that of the corresponding Si_n as was reported experimentally.

I-B-2 Photoelectron Spectroscopy of AlS^- Diatomic Anion

Atsushi NAKAJIMA *(Keio Univ.)*, **Tetsuya TAGUWA** *(Keio Univ.)*, **Kojiro NAKAO** *(Keio Univ.)*, **Kuniyoshi HOSHINO** *(Keio Univ.)*, **Suehiro IWATA** *(Keio Univ. and IMS)* **and Koji KAYA** *(Keio Univ.)*

[*Chem. Letters*, 1525-1528 (1994)]

Photoelectron spectra of AlS^- radical were measured using a magnetic bottle electron spectrometer. Electron affinity of AlS was determined to be 2.63eV. Besides, a new electronic excited state, $A'^2\Pi$, was found 0.4 eV above the ground state. The *ab initio* calculations were carried out for both anion and neutral molecules. The calculated energy difference between the anion ground state and the neutral states is in very good agreement with the experimental one.

I—C Oxonium and Ammonium Radicals in Water and Ammonia Clusters

I-C-1 *Ab initio* MO Study of Ammonium and Oxonium Radicals in Ammonia and Water Clusters

Seiichiro TEN-NO and Suehiro IWATA

The geometries and the electronic structures of a series of oxonium and ammonium radicals in ammonia and water clusters are investigated with *ab initio* molecular orbital methods. The structures of radical clusters and their cations are optimized with HF/6-31G* augumented with rydberg sp functions on N and O. In $NH_4(NH_3)_n$ (n=1—5), if the cationic structures, which qualitatively reproduce the experimental complexation energies, are assumed, the ionization energy (IP) monotonically decreases with the size of the clusters. For n>3, the rate of IP decrease in radical structures is much smaller than that in cationic structures. Rydberg spin densities at nucleus are strongly correlated with these quantities. Similar analysis is also implemented for ammonium and oxonium radicals in water clusters.

I—D Structures and Reaction Dynamics in the Ground and Excited States of Argon Cluster ions Ar_n^+

I-D-1 Theoretical Study of the Intra Cluster Reactions in Ar_4^+

Tsutomu IKEGAMI *(Keio Univ. and IMS)*, **Wataru SAKURAI** *(Keio Univ.)*, **and Suehiro IWATA** *(Keio Univ. and IMS)*

The intra-cluster reaction is an important field in the cluster study, as it is expected to connect the gas phase chemistry and the liquid phase chemistry. Probably, the argon cluster ion, Ar_n^+, is one of the simplest systems to display an intra-cluster reaction. It consists of a linear Ar_3^+ ion core and neutral Ar atoms. The ion core has two covalent bonds in it and acts as a solute, while the other Ar atoms behave like solvents. During the molecular dynamics calculation, a core switching reaction, $[Ar_3^+ + Ar]Ar_{n-4} \leftrightarrow [Ar + Ar_3^+]Ar_{n-4}$, was observed occasionally, in which one chemical bond is broken and a new chemical bond is formed. To study the basis of the reaction, a full-dimensional potential energy surface of Ar_4^+ was carefully surveyed.

The potential energy was calculated by using the diatomics-in-molecules (DIM) method. Two isomers were found: one is a distorted T-shape (**T**), and the other is a linear shape (**L**). The isomer **T** is more stable than **L** by 3.2 meV. Two reaction paths for the core switching reaction were obtained. One goes from **T** to **T**, whose transition state is located 116.2 meV higher in energy than **T**. Another goes from **L** to **L**, whose transition state is 3.5 meV higher than **L**. Since the transition state connecting **T** and **L**

is 22.0 meV higher than T, the direct path from T to T is negligible. Instead, the reaction is expected to proceed as T → L → L′ → T′. Isomerization reaction from T to T without core switching is also studied.

I—E Excited States and Ionic States of Inner-valence and Inner Shell Regions of Simple Molecules

I-E-1 The Theoretical Analysis of the 2D Photoelectron Spectrum of HCl

Suehiro IWATA *(Keio Univ. and IMS)*

The 2D photoelectron spectrum of HCl, which was recently reported by Comer's group in Manchester, is analyzed with the configuration interaction (CI) calculations. The observed spectrum above 22 eV shows three types of patterns; (a) parallel lines with a constant slope, (b) vertical lines, and (c) horizontal lines. Type (a) is the normal photoelectron bands. In this energy region, the bands are assigned to the simultaneous ionization and excitation. Some of the final states are the Rydberg states converging to the doubly charged ionic states. These bands become observable through the breakdown of the single determinant description either of the neutral ground state or of the final ionic states. The detailed analysis based on the CI potential energy curves reveals that some of the bands are assigned to the ionic states involving the excitation to 3d orbitals of Cl. This implies that the 3d orbitals of Cl contributes to the bonding of the neutral ground state HCl.

I—F Potential Energy Surfaces of Excited States and Dynamics of some Diatomic and Triatomic Molecules

I-F-1 Potential Energy Surfaces of Some Low-Lying States of Fluoroformyl radical FCO

Shinkoh NANBU *(Keio Univ. and IMS)*, **Masahiro GOMYO** *(Keio Univ.)*, **and Suehiro IWATA** *(Keio Univ. and IMS)*

[*Chem.Phys.*, **184**, 97-106 (1994)]

Potential Energy Surfaces for electronic ground and four excited states of the fluoroformyl radical, FCO, were calculated with the *ab initio* molecular orbital configuration interaction method. The electronic transition related with the progressions I and II in the photoabsorption spectra by Jacox [J.Mol.Spectry, **80**, 257 (1980)] was found to be the $1^2A''(1^2\Pi) \leftarrow 1^2A'$ transition. The pathway of the photodissociation, FCO $(1^2A') + h\nu \rightarrow CO\ (1^2\Sigma^+) + F(^2P)$, with a threshold near 280nm, was clarified.

I—G Electronic Structure of Electron-Donor-Acceptor Complexes

I-G-1 Theoretical Studies of Ammonia-Halogen and Methylamine-Halogen Complexes: Geometries, Harmonic Vibrational Frequencies and their Infra-Red Intensities, and Excited States of Ammonia-Chlorine Monofluoride Complex

Takao KOBAYASHI *(Keio Univ.)*, **Hidenori MATSUZAWA** *(Keio Univ. and Chiba Inst. Tech.)*, **and Suehiro IWATA** *(Keio Univ. and IMS)*

[*Bull.Chem.Soc.Jpn.*, in press]

The electronic correlation effects for the geometry and stability of the ammonia-halogen (NH_3-Cl_2 and NH_3-ClF) and the methylamine-halogen (CH_3NH_2-Cl_2 and CH_3NH_2-ClF) are examined with *ab initio* molecular orbital calculations. The intermolecular distance, r(N-Cl), with the second order Møller-Plesset (MP2) method are substantially shorten from the corresponding values with the SCF method. With the MP2 method the stabilization energies become large from those of the SCF calculations. Large high-frequency shifts for two intra CH_3-NH_2 coupled motions are found. The frequency shift and IR intensity change in the complex formation are very mode-specific. Besides, the potential energy surfaces of the ground and low-lying excited states of NH_3-ClF complex are calculated with the CI method. The first excited state is directly dissociated to $NH_3Cl + F$.

I—H Theoretical Studies of Molecular Conformations and Barriers to Internal Rotation and Inversion

I-H-1 Theoretical Studies of the Internal Rotation of the Methyl Group in o-, m-, and p-Fluorotoluenes and their Cations.

Yoko SONODA *(Keio Univ.)* **and Suehiro IWATA** *(Keio Univ. and IMS)*

Recently, Fujii, Takazawa and Ito determined experimentally the barrier heights of the methyl-group rotation in the ground state (S_0), the first excited state (S_1) and the cationic ground state (C_0) of three isomers of fluorotoluenes.

They are state-dependent as well as isomer-dependent.

To elucidate the state and isomer-dependency of the barrier height, the *ab initio* MO calculations were carried out for S_0 and C_0 of three isomers. Along the methyl rotation, most of the relevant geometrical parameters were optimized. The calculated barrier heights are well correlated with the experimental ones even quantitatively. The calculation indicates that the barrier height is not dependent on the bond length of carbons of methyl and benzene ring and that it is somewhat related to a small difference in electron distribution of "left" and "right" side of benzene ring.

I—I Development of New Theoretical and Numerical Techniques in the Study of Molecular Electronic Structures

I-I-1 On Some Approximation for Two-Electron Integrals

Seiichiro TEN-NO and Suehiro IWATA

A recently proposed approximation scheme for two-electron integral evaluation was examined within the LCAO-LDA method. In the approximation, before the integral evaluation an electron density over two atomic (or molecular) orbitals is expanded in terms of a linear combination of Gaussian type functions. Thus, any two-electron integrals are expressed by a linear combination of three-center integrals; in other words, the time-consuming four-center integral evaluations can be avoided.

To examine the accuracy of the approximation, the test calculations were carried out for ten-electron systems, Ne and water. The basis sets used were Dunning's [5s3p] for Ne and MCY's [4s3p2d/2s1p] for water. For the atomic case (Ne), an approximate energy within an accuracy of 10 μ hartree was attained by the uncontracted auxiliary functions of only double exponents and angular momentum indices (s and d) derived from the primitive basis function [5s3p]. For the molecular case, to reach the same accuracy, 11p on oxygen and 5p on hydrogen have to be added to the auxiliary functions derived similarly to the atomic case. This scheme requires only a tenth of the integral evaluation time in the traditional procedure.

This integral approximation can be easily extended to a variety of standard *ab initio* MO methods and scales as N^3 (where N is the number of basis functions), whereas the usual *ab initio* approaches scale as N^4. It is also very suited for the direct procedure in which the integrals are never kept on any auxiliary memory. The present results indicate that the approximation enables us to apply *ab initio* theory to very large molecules without much loss of accuracy.

I-I-2 Irregular Order in Basicities of Methylamines in Aqueous Solution: A RISM-SCF Study

Masaaki KAWATA *(Kyoto Univ.)*, **Seiichiro TEN-NO, Shigeki KATO** *(Kyoto Univ.)* **and Fumio HIRATA** *(Kyoto Univ.)*

[*J. Am. Chem. Soc.*, to be published]

Irregular order in basicities of a series of methylamines in aqueous solution is studied by means of *ab initio* quantum chemical calculation combined with extended version of reference interaction site model in statistical mechanics of molecular liquids (RISM-SCF). Free energy changes of solvent structure upon protonations are calculated in a hyper-netted chain (HNC) like approximation that is regarded superior to other approximations for polar solvent. By using HF/6-31G* with p function on hydrogen atoms directly attached to nitrogen atom, the irregularity in basicities is reproduced in qualitative agreement with well established experimental results. The method does not require a priori cavity assumption in solution, which introduces ambiguous parameters into the theories, and enable us to explain the physical origin of the basicity entirely from a microscopic point of view. Solvation structure around methylamine is also examined in terms of radial distribution functions. The result is an encouraging indication of the potential usefulness of the RISM-SCF approach to investigate a variety of quantum processes in solution.

I—J Structures and Reactions of Manybody Chemical Systems

Electronic structure and dynamical behavior of large systems such as liquid and polyenes are investigated theoretically. (a) Collective motion and fluctuation in liquid and clusters (b) Chemical reactions and relaxation in liquid and clusters, and (c) Electronic structure and dynamical behavior of polyenes, are analyzed.

I-J-1 Liquid Water Dynamics; Collective Motions, Fluctuation and Relaxation

Iwao OHMINE *(IMS and Nagoya Univ.)*

[to be published as Feature Article in *J. Phys. Chem.*]

Dynamics of liquid water in molecular scale was investigated theoretically. It has been shown that there exist local collective motions of water molecules and energy fluctuation associated with hydrogen bong rearrangement dynamics. The nature of the collective motions (time scale, spatial scale and energy scale of the collective motions) is analyzed by examining potential energy surfaces and trajectories. The dynamics of liquid water involves multi-relaxation processes and certain physical quantities yield so called 1/f spectra. These results of liquid water are compared with those of water clusters.

I-J-2 Instantaneous Normal Mode Analysis of Liquid Water

Minhaeng CHO*, Graham R. FLEMING* *(*Univ. of Chicago)*, **Shinji SAITO, Iwao OHMINE** *(IMS and Nagoya Univ.)*, **and Richard M. STRATT**** *(**Brown Univ.)*

[*J. Chem. Phys.*, **100**, 6672 (1994)]

We present an instantaneous-normal-mode analysis of liquid water at room temperature based on a computer simulated set of liquid configurations and we compare the results to analogous inherent-structure calculations. The separate translational and rotational contributions to each instantaneous normal mode are first obtained by computing the appropriate projectors from the eigenvectors. The extent of localizations of the different kinds of modes is then quantified with the aid of the inverse participation ratio roughly the reciprocal of the number of degrees of freedom involved in each mode. The instantaneous normal modes also carry along with them an implicit picture of how the topography of the potential surface changes as one moves from point to point in the very-high dimensional configuration space of a liquid. To help us understand this topography, we use the instantaneous normal modes to compute the predicted heights and locations of the nearest extrema of the potential. The net result is that in liquid water, at least, it is the low frequency modes that seem to reflect the largest-scale structure transitions. The detailed dynamics of such transitions are probably outside of the instantaneous-normal-mode formalism, but we do find that short-time dynamical quantities, such as the angular velocity autocorrelation functions, are described extraordinarily well by the instantaneous modes.

I-J-3 Dynamics and Relaxation of an Intermediate Size Water Cluster $(H_2O)_{108}$

Shinji SAITO* and Iwao OHMINE* *(IMS and Nagoya Univ.)*

[*J. Chem. Phys.*, in press]

The potential surface, melting, surface structure, and hydrogen bond network of an intermediate size water cluster $(H_2O)_{108}$ are investigated. The orientation relaxations of single and of collective molecules are analyzed and compared with those of liquid water. The collective orientation relaxation (COR) (i.e., dielectric relaxation) of the water cluster is found to be much faster than that of liquid water due to different boundary conditions. In both liquid and cluster, the cross correlation between individual molecular dipoles plays an important role in static and dynamic quantities. COR of the cluster yields a so-called 1/f fluctuation in contrast to the well-known Debye relaxation in liquid water. In order to understand these differences of COR between the water luster and liquid water, the wave vector dependence of the transverse and longitudinal components of COR is examined. A surface effect on hydrogen bond network and the correlation between structural change and coordination number are analyzed.

I-J-4 Translational and Orientational Dynamics of a Water Cluster $(H_2O)_{108}$ and Liquid Water; Analysis of Neutron Scattering and Depolarized Light Scattering

Shinji SAITO* and Iwao OHMINE* *(IMS and Nagoya Univ.)*

Molecular dynamics simulations were performed to analyze effects of the translational and orientational motions on the coherent and the incoherent neutron scattering and the depolarized light scattering (DLS) spectra of a water cluster $(H_2O)_{108}$ and liquid water. In the neutron scattering of the water cluster and liquid water, there exist two modes, the high and the low frequency modes, in the collective longitudinal current fluctuations for oxygen atoms. The low frequency mode is almost independent on wave number above 0.6 $Å^{-1}$, while the velocity of the high frequency mode is faster than 3000 m/s, as experimentally observed in liquid water. The nature of this high frequency mode is analyzed by changing the molecular interaction parameters characterizing the hydrogen bond structure of the system. It was found that the high mode is very sensitive to hydrogen bond structure and a three dimensional network structure of the hydrogen bonds is essential for its existence. We also analyzed the collective and individual longitudinal current fluctuations for hydrogen atoms. For the depolarized light scattering, the contribution of the cross correlation is examined and compared with those in the collective orientational relaxation in the far IR spectrum. The interaction-induced component plays a dominate role below 300 cm^{-1} while the permanent component does above 300 cm^{-1} in DLS of the cluster and liquid water. The induced component relaxes very slowly in the cluster and yields almost an identical relaxation to that of the dipole-dipole interaction tensors. It was found that the power spectrum of the DLS baseline of liquid water obtained from the MD calculation is in good agreement with experimentally observed spectrum by Walrafen et al.

I-J-5 Fluctuation, Relaxations and Hydration in Liquid Water; Hydrogen Bond Rearrangement Dynamics

Iwao OHMINE and Hideki TANAKA *(Kyoto Univ.)*

[*Chemical Reviews*, **93**, 2545-2566 (1993)]

Collective motions and fluctuations in liquid water dynamics and hydration mechanism is investigated. Ehhects of those collective motions on physical observables are analyzed.

I-J-6 The Origin of Many-body Effect in the Hydrated Proton Clusters

Tamiki KOMATSUZAKI *(Inst. Fund. Chem. and Grad. Univ. for Adv. Studies)* **and Iwao OHMINE** *(IMS and Nagoya Univ.)*

[*Chemical Physics*, **180**, 239 (1994)]

Energetics of proton transfer in liquid water is investigated by using ab initio calculation. Molecular electronic in-

teraction of hydrated proton clusters is classified into many body interaction elements by a new energy decomposition method. It is found that up to three-body molecular interaction is essential to describe the potential energy surface. The three-body effect mainly arises from the (non-classical) charge transfer and strongly depends on their configuration.

The basis-set dependency and correlation effect on the many-body interaction in hydrated proton clusters are analyzed in detail. The counterpoise corrected and uncorrected interactions with three different basis-sets (MIDI-4, MIDI-4**,6-311+G**) at SCF, MP2 and MP3 level calculations are investigated.

With respect to the total two-and higher-body interactions, the Basis Set Superposition Error (BSSE) of the two-body interaction is smaller at the SCF level than at the MP2-3 levels. This BSSE is not small even with 6-311+G**(1kcal/mol at SCF level and a few kcal/mol at MP levels). On the other hands, the correlation effect and BSSE of the higher-body interactions are negligible less than a half kcal/mol with all three basis sets. The BSSE corrected interaction energies at MP3 level with 6-311+G** are quite similar to the BSSE uncorrected those at SCF level with MIDI-4**. The basis-set dependence (MIDI-4 and MIDI-4**) of the two-body interaction energies are found to mainly arise from electrostatic component. The qualitative features of the two-and many-body interactions of the hydrated proton clusters can be,therefore, represented by the MIDI-4 energies at BSSE uncorrected SCF level calculation.

I-J-7 New Molecular Dynamics Method for Cooperative Proton Transfer Dynamics in Liquid Water

Tamiki KOMATSUZAKI *(Inst. Fund. Chem. and Grad. Univ. for Adv. Studies)* **and Iwao OHMINE** *(IMS and Nagoya Univ.)*

New molecular dynamics method has been developed on the basis of semi-empirical density functional theory in order to take into account the charge reorganization through proton transport in liquid water, which was clarified as the dominant role to the proton transfer potential surfaces by our previous research.

The switching algorism is developed for the blockage-method which defines the charge reorganization space dependent on the configuration of a system. The blockage should be applied on the basis of the amount of interactions among charge sites. It was found that the number of the blockage types must be more than two in order to describe the proton transfer potential surface smoothly. The tetrahedral site model for the water-oxygen is also examined, compared with the standard one-site model. It is concluded that the rigid many-site model on oxygen atom is not superior to the simple one-site model because the rigid-four site model must often have the singularity on the potential energy surfaces(for example, hydronium ion's inversion motion).

I-J-8 Topology and Dynamics in the Hydrogen Bond Network System

Masakazu MATSUMOTO and Iwao OHMINE* *(*IMS and Nagoya Univ.)*

To understand the hierarchical structure of the potential surface in the configurational space and the origin of collective dynamics, liquid water between intermediate temperature(300K) through supercooled region (80K) is investigated with molecular dynamics method. 64 water molecules are confined in a cell with periodic boundary and density is kept 0.997 at all temperature. Under 240K, the system is vitrified and the diffusion coefficient reaches to zero within 1 ns. No evidence for the transition to water II phase is observed.

Even in supercooled region around 240K, hydrogen bond rearrangements (HBR) seem to be held in the same manner as in the room temperature. Flip-flop type energy exchange and existance of cavities play important role in the large scale HBR. Active region, which means the region with frequent HBR, seems to distribute very inhomogeneously in time and space in the liquid water. Short ranged feature like local network topology of the HBN or rotability of water molecule may prevent such region from diffusion. Structure activity relationship(SAR) and enhanced isotope effect should be analyzed.

Vogel-Fultcher type critical slowing down approaching to 228K is observed. Slow dynamics and collective motion is well known phenomena in the system with simple repulsive interaction ("fragile glass" system), where potential surface is entirely flat. In other words, hierarchical structure of the potential surface is not necessary for such a critical phenomena. It should rather be studied why the hydrogen bond network(HBN) can morph without energetic barrier, or how the system finds the pathway to adjacent entropic vessel.

Quenching method, first introduced by Stillinger and Weber, is often used to clarify the "inherent structure" of the liquid. However, the method may often exaggerate "deeply-hidden" structure of the water when the hydrogen bond network has some bifurcated bonds. Alternative methods are now on study.

I-J-9 Ab initio MO Study for Photoisomerization of Octatetraene

Masakatsu ITO and Iwao OHMINE* *(*IMS and Nagoya Univ.)*

Three lowest singlets states($^1Bu^+$, 2^1Ag^-, Ground state) are involved in the photoisomerization process of polyenes. The potential energy surface of the three singlets states of octatetraene are calculated by using MCSCF and MRSDCI methods. We carried out MCSCF calculations using the CAS(complete active space) type configurations generated by occupying eight electrons in eight pi orbitals[1764CSF]. The basis set employed were STO-3G for geometry optimizations and DZ, DZ+P otherwise. Both trans-trans and cis-trans isomers are found to be planer in the 2^1Ag state and the vibrational frequencies of these two isomers are quite similar.

We then performed the MRSDCI calculations with DZ basis sets at the MCSCF optimized geometries to obtain more reliable energy surface in twisted conformations. We have chosen the reference configurations so that they comprise more than 90 percents of the MCSCF wave functions.

The potential energy surfaces were obtained as functions of the central C=C torsional angle. As twisting the C=C bond, the 1Bu and the ground states approach each other closely. In contrast, the potential curve of the 2Ag state is almost flat, while in the case of MCSCF calculation this state exhibits a enery maximum at the 90 degree twisting conformation. Further study of the potential energy surfaces in the more extended region of the conformation space is in progress.

I—K Theoretical Studies of Chemical Reaction Dynamics

Clarification of the reaction mechanisms and development of illuminating good approximate theories are our ultimate purposes.

I-K-1 Constat Centrifugal Potential Approximation for Atom-Diatom Chemical Reaction Dynamics

Kengo MORIBAYASHI, Shoji TAKADA, and Hiroki NAKAMURA

[*J. Chem. Phys.*, **100**, 4284 (1994)]

The constant centrifugal potential approximation (CCPA) is generalized so as to be applicable to the reactions of rotationally excited reactants. The accurate calculations of reaction probabilities are required only for $J \leq |\Omega_i|_{MAX}$ ($\leq j_i$), where J is the total angular momentum quantum number, j_i represents the initial rotational state of a reactant diatomic molecule, Ω_i is the z component of J in the body-fixed frame in the initial arrangement and $|\Omega_i|_{MAX}$ is the maximum of such $|\Omega_i|$'s that give significant contributions to the reaction. The method is applied of the D+H_2 (v_i=0, j_i) reaction with use of the hyperspherical coordinates, and is proved to be useful by comparing the results with those of the author's own accurate calculations. The reaction mechanisms are clarified with respect to the dependence on Ω_i and j_i

I-K-2 Effects of Potential Energy Surface Topography and Isotope Substitution in Atom-Diatom Chemical Reactions: The Cl+H_2 and D+H_2 Systems

Shoji TAKADA, Kenichiro TSUDA, Akihiko OHSAKI *(Miyazaki Univ.)* **and Hiroki NAKAMURA**

[*Adv. in Molecular Vibrations and Collision Dynamics*, vol. **2A** p.245 (1994)]

We report (1) the effects of potential energy surface (PES) topography on the reaction dynamics of D+H_2 → DH+H and Cl+XH → HCl+X, XCl+H (X=H, D) and (2) the kinetic isotope effects (KIE) in the latter reactions, on the basis of the exact 3D quantum mechanical calculations for J=0, where J is the total angular momentum quantum number. For the first subject, we employ the two PESs for each system. In the case of D+H_2, a large difference in the reaction probabilities is found for the two similar PESs with a small difference in the proper reaction zone. On the other hand, in the Cl+H_2 reactions, essentially the same probabilities are obtained for the two quite different PESs, which differ significantly in the H-Cl-H configuration improper for the relevant reaction. As for the KIE study, integral cross sections and thermal rate constants are calculated and compared for the three reactions, Cl+H_2, Cl+HD, and Cl+DH. We show, at first, that the quasiclassical trajectory results deviate from the present quantum mechanical ones not only at very low but also at quite high energies. The following three isotope effects are analyzed: (1) difference in zero-point energies, (2) quantum mechanical tunneling, and (3) initial rotational excitation. The constant centrifugal potential approximation (CCPA) based on the accurate results for J=0 is again proved to work well and applied extensively to investigate the KIE.

I-K-3 Wentzel-Kramers-Brillouin Theory of Multidimensional Tunneling: General Theory for Energy Splitting

Shoji TAKADA and Hiroki NAKAMURA

[*J. Chem. Phys.*, **100**, 98 (1994)]

A general Wentzel-Kramers-Brillouin (WKB) theory of multidimensional tunneling is formulated and an illuminating physical picture of the effects of multidimensionality is provided. Two basic problems are solved: (i) Maslov's semiclassical wave function in the classically accessible region is connected to the wave function in the classically inaccessible region and (ii) the latter is propagated into the deep tunneling region. It is found that there exist two distinct types of tunneling: pure tunneling and mixed tunneling. The former is the usual one in which the tunneling path can be defined by a certain classical trajectory on the inverted potential and its associated action is pure imaginary. In the latter case, no tunneling path can be defined and the Huygens-type wave propagation should be carried out. In this case, tunneling is always accompanied by classical motion in the transversal direction and the associated action is complex. A general procedure is presented for the evaluation of energy splitting ΔE in the double well. Moreover, under the locally separable linear approximation, a simple and convenient formula for ΔE is derived and is confirmed to work well by comparison with the exact numeral calculations.

I-K-4 WKB Theory of Tunneling between Tori

Shoji TAKADA and Hiroki NAKAMURA

[*Prog. Theor. Phys.* Supplement, No. 116 (1994)]

General WKB theory of multidimensional tunneling between tori is formulated and illuminating physical picture on the effects of multidimensionality is provided. On the basis of Wilkinson's work, (1) Maslov's semiclassical wavefunction in classically accessible region is connected to the wavefunction in classically inaccessible region and (2) the latter is propagated into deep tunneling region. It is found

that there exist two distinct regions of tunneling: a region where action is pure imaginary (I-region) and another region where action is complex (C-region). In I-region tunneling path can be defined by a certain classical trajectory on the inverted potential, while in C-region no tunneling path can be defined and the Huygens type wave propagation should be carried out. Moreover, wavefunction of a vibrationally excited state has nodal lines in C-region but not in I-region.

I-K-5 Systematics of the Average Resonance Widths in Overlapping Resonance-Scattering and Its Connection with the RRKM Theory

Kiyohiko SOMEDA, Hiroki NAKAMURA and Frederick H. MIES *(NIST)*

[*Chem. Phys.*, **187**, 195 (1994)]

Decay processes of densely distributed quasi-bound states are studied numerically by randomly generating the Hamiltonian matrices. The average decay rate obtained from the Feshbach theory of resonance scattering exhibits systematic behavior against the average density of states (ρ), the number of continua (K) and the average coupling strength to the continua (ν). The distribution of the decay rates bifurcates into *long-lived* and *short-lived branches* when ρ is larger than a certain critical value ρ_c, which is found to be roughly equal to the inverse of the 0-th order partial width $<\gamma_{\text{part.}}>$. Thus one can clearly distinguish the *isolated resonance regime* in the region $\rho<\rho_c$ and *overlapping resonance regime* in the region $\rho>\rho_c$. The states belonging to the short-lived branch exhibit a very broad energy spectrum and are recognized as background continua. They are not quasibound states in practice. The decay rates of the long-lived branch, on the other hand, systematically decrease with ρ at $\rho \gg \rho_c$. The average of these decay rates is proportional to $<\gamma_{\text{part.}}>^{-1} K\rho^{-2}$. When the short-lived branch is excluded, the average decay rate, $<\Gamma/\hbar>$, roughly agrees with that of RRKM rate in the region $\rho \approx \rho_c$, where the spectral profile becomes most diffuse. Outside the region $\rho \approx \rho_c$, $<\Gamma/\hbar>$ is always smaller than the RRKM rate. The above observation is confirmed also by a square-well potential model and ascertains the conventional belief that the RRKM theory holds only when resonances overlap and that it gives the upper bounds. It is noteworthy that this RRKM regime corresponds to the critical overalp, $\rho<\gamma_{\text{part.}}> \approx 1$.

I-K-6 Decoupling Surface Analysis of Cl + Cl_2 Reaction Embedded in Ar_{52} Cluster

Kiyohiko SOMEDA and Hiroki NAKAMURA

[*Bull. Chem. Soc. Japan*, **67**, 2659 (1994)]

A model triatomic reaction $Cl+Cl_2 \rightarrow Cl_2+Cl$ embedded in an Ar_{52} van der Waals cluster is analyzed classical mechanically by a novel theoretical method called "decoupling surface analysis". This method generates new reactive and vibrational variables in which the kinetic coupling as well as the potential coupling are minimized. An analysis of local frequencies of the vibrational variables along the reaction coordinate clarifies how the motions of ambient Ar atoms are coupled with the central Cl_3 system. When the local frequencies are plotted as a function of the reaction coordinate, avoided crossings among these curves are observed. Mixing of Cl motion and Ar motion is clearly detected by these avoided crossings. The vibrational mode having a character of the symmetric stretch of Cl_3 shows exclusively strong coupling with the reactive motion. This mode, however, very weakly couples with the ambient Ar motion. On the other hand, the bending and translation of Cl_3 are strongly mixed with the motions of ambient Ar atoms and produce unstable modes, which play the most significant role in energy exchange between the central reaction system and the ambient Ar atoms.

I—L Theory of Nonadiabatic Transition

Nonadiabatic transition is one of the very basic mechanisms of state (phase) change in various fields of physics and chemistry. Recently, we have succeeded in deriving good analytical new formulae for the Landau-Zener and nonadiabatic tunneling cases within the linear potential model. Especially, a simple and compact formula much better than the famous Landau-Zener formula was proposed. Generalizations to general curves potential are also successfully carried out. We can now present complete set of compact solutions for the general two-state curve crossing problems.

I-L-1 Two-State Linear Curve Crossing Problems Revisited. IV. The Best Analytical Formulas for Scattering Matrices

Chaoyuan ZHU and Hiroki NAKAMURA

[*J. Chem. Phys.*, **101**, 4855 (1994)]

Based on the achievements of the previous three papers of this series, the best working formulas for scattering matrix are obtained for both the Landau-Zener (LZ) and the nonadiabatic tunneling (NT) case: two formulas valid at $b^2 \geq 0$ and $b^2 \leq 0$ in the LZ case, and three formulas valid at $b^2 \leq -1$, $-1 \leq b^2 \leq 1$ and $b^2 \geq 1$ in the NT case, where b^2 represents the effective energy. Simple and compact formulas which work far better than the LZ formula are proposed for nonadiabatic transition probability by one passage of crossing point for both the LZ and NT cases. Furthermore, compact expressions are derived, for the first time for the nonadiabatic tunneling probability at $b^2 \leq 1$, i.e., at energies lower than the bottom of the upper adiabatic potential. All the formulas proposed here can be usefully utilized at any coupling strength, namely the validity range has been very much expanded compared to the previous formulas by employing certain empirical corrections. Besides, these formulas have convenience to enable to general curved potentials.

I-L-2 Theory of Nonadiabatic Transition for General Two-State Curve Crossing Problems

Chaoyuan ZHU and Hiroki NAKAMURA

Based on the achievements for the linear potential model, new accurate and compact formulas are established for general two-state curve crossing problems. These can cover practically the whole range of energy and coupling strength and can be directly applied to the various problems such as inelastic scattering, elastic scattering with resonance and perturbed bound state problem. All the basic potential parameters can be estimated directly from the adiabatic potentials and non-unique diabatization procedure is not required. Complex contour integrals are not necessary to evaluate the nonadiabatic transition probability and thus the whole theory is very convenient for various applications. The previously proposed simple and compact formula better than the famous Landau-Zener formula is shown to be applicable also to general curved potentials. The explicit expressions are derived also for the nonadiabatic tunneling (transmission) probability. Now, the present theory can present complete picture of the two-sate curve crossing problems.

I—M Theoretical Studies of Characteristics and Dynamics of Superexcited States of Molecules

Superexcited states show various intriguing properties and participate in a variety of dynamic processes. We believe that they will open a new challenging world of science. The ultimate purpose of our studies is to find new collective motions in these states and understand their participating dynamics.

I-M-1 Characteristics and Dynamics of Doubly Excited States of Molecules

Sungyul LEE *(Kunghee Univ.)*, **Masahiro IWAI and Hiroki NAKAMURA**

[*Molecules in Laser Fields*, ed. A. D. Bandrauk, (Marcel Dekker, New York), p.217 (1994)]

A variety of studies on the atomic doubly excited states are briefly summarized. The quantitative information on the potential energies E_r (R) and the autoionization widths $\Gamma(R)$ are presented for the doubly excited states of H_2. Electron correlation and autoionization mechanism in these molecular doubly excited states are analyzed in comparison with those of the corresponding atomic states. The dynamic processes involving SES studied so far are also briefly reviewed. The basic and powerful theoretical tool, that is, the multichannel quantum defect theory (MQDT) is also outlined there.

I—N Femtosecond Pump-Probe Spectroscopy of Molecules in the Condensed Phase

The nonlinear optical response of molecules in the condensed phase subjected to a femtosecond laser pulses is studied using various approaches developed in statistical physics.

I-N-1 Multistate Quantum Fokker-Planck Approach to Nonadiabatic Wave Packet Dynamics in Pump-Probe Spectroscopy

Yoshitaka TANIMURA and S. MUKAMEL *(University of Rochester)*

[*J. Chem. Phys.* **101**, 3049 (1994)]

The quantum Fokker-Planck equation of Caldeira and Leggett is generalized to a multi-state system with anharmonic potentials and a coordinate dependent nonadiabatic coupling. A rigorous procedure for calculating the dynamics of nonadiabatic transitions in condensed phases and their monitoring by femtosecond pump-probe spectroscopy is developed using this equation. Model calculations for a harmonic system with various nonadiabatic coupling strengths and damping rates are presented. Nuclear wavepackets in phase space related to electronic coherence are shown to provide an insight into the mechanism of nonadiabatic transitions.

I-N-2 Femtosecond Pump-Probe Spectroscopy of Intermolecular Vibrations in Molecular Dimers

Yoshitaka TANIMURA and S. MUKAMEL *(University of Rochester)*

We analyze the effects of an intermolecular vibration coupled to a bath on the optical response of a dimer. Using the third order response functions calculated by the path-integral approach we calculate the pump-probe spectrum, and show that the contribution from coherent transitions between the ground state and the doubly excited state dramatically affects the spectrum for off-resonant excitation.

I-N-3 Effects of Anharmonicity in Pump-Probe Spectroscopy in the Condensed Phase

Yoshitaka TANIMURA

Optical response functions for a two-level system with anharmonic potentials are calculated by performing functional integration. We analyze the difference probe absorption spectrum using the second order response function, and show the effects of anharmonicity in pump-probe spectroscopy in the condensed phase.

I—O Theoretical Studies of Organic Conductors and Superconductors

We study spin fluctuations of organic conductors and superconductors to explore the mechanism of organic superconductivity.

I-O-1 Spin Fluctuations of Organic Conductors and Superconductors

Norikazu TOMITA and Yoshitaka TANIMURA

We study electronic states of organic materials to explore microscopic mechanisms of their conductivity and superconductivity. We pay special attention to find a relation between spin fluctuations and superconductivity. This relation has been emphasized in high Tc superconductors and seems to have a key to study the mechanism of organic superconductivity, since antiferromagnetic spin fluctuations are experimentally observed in many high Tc super conductors as well as organic superconductors. We aim to disclose what is the (antiferromagnetic) spin fluctuation and how it causes the superconductivity (if it is the origin of the superconductivity).

I—P Intermolecular Potential for Molecular Simulations

I-P-1 A Procedure to Generate Ab Initio Intermolecular Potential Function

Kazuo KITAURA *(Univ. of Osaka Prefecture and IMS)*

[*Fluid Phase Equ.*, in press]

A procedure is presented for generating an intermolecular potential function from the ab initio MO calculations. Our potential function consists of the electrostatic, polarization, exchange and charge-transfer and dispersion potentials. According to the procedure, we derived the inter molecular potential function for ammonia dimer from the ab initio MO calculations with the DZP basis set at the MP2 level. The potential function well reproduced the optimized geometry and the binding energy of the dimer obtained from the ab initio calculations. The heat capacity calculated from the Monte Carlo simulation with the potential function agreed well with the experimental value, while the NN radial distribution function was in roughly accord with the experiment.

I—Q Structure of Muonic Molecules

I-Q-1 Loosely Coupled Few-Body Systems

Masayasu KAMIMURA *(Kyushu Univ. and IMS)*, **Yasushi KINO** *(RIKEN)* **and Emiko HIYAMA** *(Kyushu Univ.)*

[*Proc. Int. Symp. on Frontier in Nuclear Structure Physics,* Tokyo, 1994, in press]

Loosely coupled three-and four-body systems in atomic/molecular and nuclear physics were studied. For this aim, the Jacobian-coordinate coupled-rearrangement-channel Gaussian-basis variational method is very useful; short-range correlations and long-range tails are well described by the basis functions. Investigations were made of trimer and tetramer of ^{4}He atoms, muonic molecules, and three-nucleon bound states. Presice mechanism of radiative decay and particle decay of ($d^3He\mu$) and ($d^4He\mu$) was investigated with the use of Kohn-type variational calculation of scattering; recent experiment from KEK was beautifully explained. Further improvement of the calculational method was made by the discovery of 'infinitesimally shifted' Gaussian lobe basis functions which makes calculation of matrix elements of few-body Hamiltonian extremely simple. Application of the method to four-body systems is in progress.

I-Q-2 Effect of the Finite Size of the Muonic Molecular Ion $(dd\mu)^+$ on the Energy Levels of the Atom $(dd\mu)e$ and Molecule $(dd\mu)dee$

Masayasu KAMIMURA *(Kyushu Univ. and IMS)*

The energy shift due to the finite size of the pseudonucleus $(dd\mu)^+_{11}$ in the atom $(dd\mu)^+_{11}e$ and molecule $(dd\mu)^+_{11}dee$ is of importance in the theoretical estimation of the rate of d-d fusion catalyzed by negative muon[1]. The energy shift in the atom $(dd\mu)^+_{11}e$ is calculated using perturbation theory up to second order[2]. The finite-size shift is found to be 1.46 meV which gives a severe correction to the so-far observed energy of the muonic molecule ion $(dd\mu)^+_{11}$. First-order perturbation calculation of the finite-size energy shift in the molecule $(dd\mu)^+_{11}dee$ shows that contribution from the quadrupole component of the$(dd\mu)^+_{11}$ charge distribution, which is not taken into account by the conventional method, is found to be of the order of one meV. These suggest that the uncertainty in the current theoretical estimates of the binding energies of the states of the $(dd\mu)^+_{11}dee$ molecule should be significantly increased.

References

1)M. R. Harston, I. Shimamura and M. Kamimura, *Phys. Rev.* **A45**, 94 (1992).

2)M. R. Harston, S. Hara, Y. Kino, I. Shimamura and M. Kamimura, *Phys. Rev. A*, submitted.

I-Q-3 Normalization of the Asymptotic Form of Three-Body $(dt\mu)^+$ and $(dd\mu)^+$ Wavefunctions

Masayasu Kamimura *(Kyushu Univ. and IMS)*

In order to investigate a discrepancy between existing literature values for the normalization constant in the asymptotic form of three-body wavefunctions for$(dt\mu)^+$, we report the results of a new calculation of the normalization constants for this system as well as the related system $(dt\mu)^+$. These were obtained by fitting to accurate variational wavefunctions[1] with special care being taken to describe the long-range$(t\mu)$+d or $(d\mu)$+d behavior. The implications of this reevaluation[2] of the normalization constants are discussed in relation to the theoretical formation rates of molecules such as $(dt\mu)$dee and $(dd\mu)$dee which are key intermediates in the muon catalyzed fusion cycle.

References

1) M. Kamimura, *Phys. Rev.* **A38**, 621 (1988).
2) Y. Kino, M.R. Harston, I. Shimamura, E. Armour and M. Kamimura, *Phys. Rev. A*, submitted.

RESEARCH ACTIVITIES II
Department of Molecular Structure

II—A Laboratory and Astronomical Spectroscopy of Transient Interstellar Molecules

Vast, cold, and low-density space environment is a unique laboratory, whose physical and chemical conditions are rarely attained in the laboratory on Earth. The unique space laboratory is favorable to the existence of transient molecules such as molecular ions, free radicals, and unstable molecules, most of which are very exotic and non-terrestrial. These exotic transient molecules are generally difficult and challenging problems for laboratory spectroscopy. Laboratory spectroscopy may be enriched by astronomical studies on non-terrestrial transient species which represent new development in high-resolution molecular spectroscopy. On the other hand, detailed knowledge about new transient molecules obtained by laboratory spectroscopy is essential to a deeper understanding of physical and chemical processes in space. We develop a high-sensitivity submillimeter-wave and far-infrared spectrometers suitable for high-resolution spectroscopy of transient molecules of astronomical interest. We expect that our laboratory spectroscopy may accelerate the mutually beneficial aspect between laboratory spectroscopy, and astrochemistry and astrophysics.

II-A-1 Submillimeter Wave Spectrum of the SiH_3^+ Ion. J=2−1, K=0 and 1 Transitions

Sang K. LEE *(Pusan Natl. Univ. and IMS)*, **Hiroyuki OZEKI, Shuji SAITO, and Satoshi YAMAMOTO** *(Univ. of Tokyo)*

[*Chem. Phys. Letters*, **224**, 21 (1994)]

The observation of the rotational transitions of SH_3^+ has been extended[1] to the 600 GHz region. The SH_3^+ ion was generated by an electric discharge in the gas mixture of H_2S and H_2 in a hollow-cathode discharge cell. The J=2−1, K=0 and 1 transitions have been observed using a source-modulated submillimeter-wave spectrometer. The rotational constant B_0 and the centrifugal distortion constants D_J and D_{JK} are determined from the three observed rotational transitions. The molecular constants determined agree well with those reported by previous infrared studies[2,3].

References
1) S. Saito, S. Yamamoto, and T. Amano, *Astrophys. J.*, **314**, L27 (1987).
2) T. Nakanaga and T. Amano, *Chem. Phys. Letters*, **134**, 195 (1987).
3) T. Nakanaga and T. Amano, *J. Mol. Spectrosc.*, **133**, 201 (1989).

II-A-2 Microwave Spectrum of the NS Radical in the $^2\Pi_r$ Ground Electronic State

Sang K. LEE *(Pusan Natl. Univ. and IMS)*, **Hiroyuki OZEKI, and Shuji SAITO**

[*Astrophys. J. Suppl.*, in press]

The microwave spectrum of the NS radical in the ground electronic state has been remeasured in the frequency region of 69 to 350 GHz with the aim of making clear scattered LSR velocities determined by the NS lines from dark clouds[1]. Measurement errors for most of the observed lines were less than 20 kHz so that the observed laboratory frequencies are now sound standards as the rest frequencies of NS. The molecular constants including the rotational constant and its centrifugal distortion constant, the Λ-type doubling constants, and the hyperfine coupling constants of the nitrogen nucleus have been determined more precisely, when compared with those reported previously.

References
1) D. McGonagle, W. M. Irvine, and M. Ohishi, *Astrophys. J.*, **422**, 521 (1994).
2) J. R. Anacona, M. Bogey, P. B. Davies, C. Demuynck, and J. L. Destombes, *Mol. Phys.*, **59**, 81 (1986).

II-A-3 Microwave Spectra of the $AlO(X^2\Sigma^+)$ Radical in the Vibrationally Excited States, v=1 and 2

Masahiro GOTO *(Nagoya Univ. and IMS)*, **Shuro TAKANO, Satoshi YAMAMOTO** *(Univ. of Tokyo)*, **Haruhiko ITO** *(Nagaoka Univ. of Technology)*, **and Shuji SAITO**

[*Chem. Phys. Letters*, **227**, 287 (1994)]

The microwave spectra of the aluminum monoxide radical ($X^2\Sigma^+$) in the vibrationally excited states (v=1 and 2) have been observed by using a source modulated spectrometer combined with a free-space cell. The AlO radical was generated by discharge in pure N_2O or Ar gas with an aluminum hollow-cathode containing several pieces of alumina. The Al atom was mainly supplied from the alumina and partly from the inner surface of the aluminum electrode. Five rotational transitions were measured in the region of 180 to 380 GHz. The fine and hyperfine structure pattern of a certain rotational transition for the v=1 and v=2 states are completely different from that of a corresponding transition of the ground vibrational state. A detailed analysis of the patterns revealed that the spin-rotation coupling constant changes abnormally by the excitation of the vibrational mode[1].

References
1) H. Ito and M. Goto, *Chem. Phys. Letters*, **227**, 293 (1994).

II-A-4 Submillimeter-Wave Spectra of AlH and AlD

Masahiro GOTO *(Nagoya Univ. and IMS)* **and Shuji SAITO**

The J=1−0 transition of AlH and the J=2−1 transition of AlD were observed in 377 to 393 GHz by using a newly constructed high-temperature discharge cell made of an aluminum heat pipe (Figure 1). AlH or AlD were generated by the reaction of aluminum vapor with glow discharge products of H_2 or D_2, respectively. The electric quadrupole coupling constants for the Al nucleus were determined for the first time from the resolved hyperfine components: −36.72 (37) MHz for AlH and −34.3 (37) MHz for AlD, where the figures in parentheses represent three times the standard deviation.

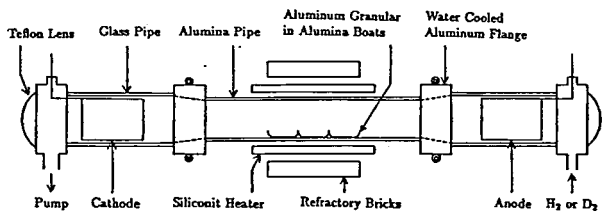

Figure 1. Alumina heat-pipe discharge cell

II-A-5 Submillimeter-Wave Spectroscopy of the $CD_2(\tilde{X}^3B_1)$ Radical

Hiroyuki OZEKI and Shuji SAITO

The simplest carbene, CH_2 radical, is one of essential intermediates in hydrocarbon chemistry. We reported the measurements of its submillimeter-wave spectral lines and discussed its astrophysical significance in the Annual Review of the last year. So far there has been no report on the measurements of pure rotational lines for CD_2, though several far infrared spectral lines were studied by the method of FIRLMR[1]. We measured 23 components of the four rotational lines of CD_2 in the frequency region of 250 to 530 GHz. The CD_2 radical was produced by discharging pure dideuterated ketene in a hollow-cathode cell. We found the 2_{12}−3_{03} and 5_{04}−4_{13} transitions in the 260 GHz region, deviated by 5 to 10 MHz, and by 10 to 20 MHz, respectively, from those predicted by the FIRLMR analysis. We redetermined 10 molecular constants of CD_2 from the observed 23 lines by the least squares method, though the number of the observed rotational lines is limited.

References

1) P. R. Bunker, T. J. Sears, A. R. W. McKellar, K. M. Evenson, and F. J. Lovas, *J. Chem. Phys.*, **79**, 1211 (1983).

II-A-6 Microwave Spectrum of the HCCS Radical in the Rovibronic States

Jian TANG *(Graduate Univ. for Advanced Studies)* **and Shuji SAITO**

The microwave spectrum of a linear carbon-chain radical, HCCS, was observed in the discharge mixture of CS_2 and C_2H_2, and searched for several astronomical sources without success[1]. We have measured its rotational spectra of both the bending vibrational states v_4=1 (HCC bending) and v_5=1 and 2 (CCS bending) up to 400 GHz. The spectral lines of $^2\Delta_{5/2}(v_5)$, $^2\Delta_{3/2}(v_5)$, $\mu^2\Sigma(v_5)$, $\kappa^2\Sigma(v_5)$, $^2\Pi_{3/2}(2v_5)$, $^2\Delta_{5/2}(v_4)$, and $\mu^2\Sigma(v_4)$ were assigned, and their effective molecular constants were determined. A large difference was found for γ_{eff} between the $\mu^2\Sigma(v_5)$ and $\kappa^2\Sigma(v_5)$ states. The difference could not be understood by Hougen's theory for the Renner-Teller effect[2], but be explained by taking into account a vibronic interaction between the $^2\Pi_{1/2}$(G.S.) and $\mu^2\Sigma(v_5)$ states. Furthermore, γ_{eff} of the $\mu^2\Sigma(v_4)$ state was found to have a value of about two times of B.

References

1) S. Saito, S. Takano, and S. Yamamoto, *Symp. on Mol. Struct.* (Fukuoka) 1C09 (1990).
2) J. T. Hougen, *J. Chem. Phys.*, **36**, 519 (1962).

II-A-7 Microwave Spectrum of the C_3S Molecule in the Vibrationally Excited States of Bending Modes, v_4 and v_5

Jian TANG *(Graduate Univ. for Advanced Studies)* **and Shuji SAITO**

[*J. Mol. Spectrosc.* in press]

Rotational spectra of the linear C_3S molecule in the excited bending vibrational states v_5=1, 2, 3, and 4 (CCS bending), and v_4=1 (CCC bending) have been observed in the frequency range of 116−383 GHz with a source-modulated microwave spectrometer. Molecular constants of vibration-rotation interaction terms up to higher orders were determined by the least-squares fitting of about 460 transition frequencies. The determined α_t, q_t, and q_t^J constants showed a good coincidence with those of ab initio calculation. The sign and magnitude of γ_{ll}, the dependence of the rotational constant B_v on the vibrational angular momentum, was explained by a symmetric-top-like molecular model. The constant q_t^K, the dependence of the l-type doubling and resonance constant q_t on the vibrational angular momentum, was determined experimentally for the first time. The obtained value of q_t^K was a thousand times greater than a theoretical estimate given by Watson's expression, but the order-of-magnitude of the experimental value can be understood by the analogy with a slightly asymmetric-top molecule.

II-A-8 Infrared Diode Laser Spectroscopy of the v_1 Fundamental Mode of the C_3S Molecule

Shuro TAKANO, Jian TANG *(Graduate Univ. for Advanced Studies)*, **and Shuji SAITO**

We rearranged the infrared diode laser spectromer of IMS[1]. A 2 m White-type glow-discharge cell was newly installed and the vacuum line was renewed. As a test of the infrared spectrometer system, we studied the v_1 fundamental mode of the C_3S molecule. The C_3S molecule is one of the important members of the sulfur-containing carbon-chain interstellar molecule[2]. C_3S was produced in the cell

kept at the room temperature by discharging a mixture of CS_2, C_2H_2, and He with the discharge current of 120 mA. The optimum pass length is 40 m. We observed about 50 lines in the region of 2046 to 2067 cm^{-1}, and analyzed them to determine molecular parameters by the least squares method.

References

1) C. Yamada, K. Nagai, and E. Hirota, *J. Mol. Spectrosc.*, **85**, 416 (1981).
2) S. Yamamoto, S. Saito, K. Kawaguchi, N. Kaifu, H. Suzuki, and M. Ohishi, *Astrophys. J.*, **317**, L119 (1987).

II—B Development of a Mt. Fuji Submillimeter-Wave Telescope

Shuji SAITO, Hiroyuki OZEKI, Satoshi YAMAMOTO *(Univ. of Tokyo)*, **Yutaro SEKIMOTO** *(Univ. of Tokyo)*, **Junji INATANI** *(National Astronomical Observatory)*, **Masatoshi OHISHI** *(National Astronomical Observatory)*, **and Norio KAIFU** *(National Astronomical Observatory)*

In these years the submillimeter-wave to far infrared region has attracted much attention in the field of astronomy, because the initial stage of star-forming activity or, in other words, the final stage of molecular cloud contraction shows various physical and chemical phenomena in the energy region of this wavelength. Several submillimeter-wave telescopes have now been developed to study astrophysics and astrochemistry of the star-forming region through atomic and molecular lines. Since atmospheric attenuation, mainly due to water vapor, becomes high in the submillimeter-wave to far infrared region, astronomical observations should be made at a high-altitude site with cold environment.

We plan to build a submillimeter-wave telescope at the summit of Mt. Fuji. The main scientific purpose of our project is (1) a survey of the neutral carbon (C_I) line at 492 GHz, and (2) a search for new simple and fundamental molecules, especially related to dust chemistry, which will make us to understand evolutional physical and chemical processes of the molecular cloud as a whole.

Mt. Fuji is the highest mountain in Japan, and has the altitude of 3776 m above the sea level. Weather data from Japan Meteorological Agency show that precipitable water vapor at the summit is expected to be less than 1.0 mm for about 40% of winter days (November 1990 to February 1991). This makes it possible to carry out good observations in the atmospheric window regions between 400 and 900 GHz.

The telescope planned has a 2 m diameter disk with surface accuarcy of 10 μm, enclosed with a radome transparent up to 1000 GHz. Since the weather conditions are very terrible in the winter, the temperature less than −30°C and the wind speed up to 100 m/s, and do not allow us to access to the summit, the radome building has to survive against strong winds and heavy snowing and icing, and data processing and telescope operation have to be made by remote control via satellite communication or microwave link.

In the end of October 1993 we measured atmospheric transmittance at the summit with a home made radio meter operated at 220 GHz, and found that the atmospheric optical depth was about 0.04 corresponding to about 50% transmittance at 500 GHz. This result suggests that we can expect better conditions of colder and dryer weather at the summit of Mt. Fuji in the mid winter. We plan to measure the optical depth in the coming winter under collaboration with the Mt. Fuji weather station of Japan Meteorological Agency.

This summer we sampled soil and rock from 3 m long cores obtained by a boring machine at the telescope site. It was found that scoria soil is frozen below about 85 cm in depth from the surface, and the frozen scoria is hard enough to support a heavy telescope building of 200 ton or more.

Detailed investigations are now in progress on the design of the telescope, telescope mounting, telescope base, radome, deicing and antisnow accumulation system, 500 GHz receivers, back-end acousto-optical spectrometer, data processing, and remote control.

II—C Laser Investigation of Antiproton-Helium Compounds

A recent discovery of anomalous survival of antiprotons in dense helium media suggested the production of an antiproton-helium compound ($\bar{p}$-He^+). If the formation of this unusual compound is true, it is the first long-lived exotic atom containing hadrons other than normal protons and neutrons. Moreover, from a viewpoint of atomic and molecular spectroscopy, this new compound is a very attractive object of study, because it has characters of both atoms and molecules; in other words, it is neither an atom nor a molecule, but a completely new entity. Therefore, we started the laser spectroscopic investigation of this compound in order, first, to get a definite evidence of the formation, second, to study its properties and dynamics, and finally to explore the possibility of its applications.

II-C-1 First Observation of Laser-Induced Resonant Annihilation in Metastable Antiprotonic Helium Atoms

N. MORITA, M. KUMAKURA, T. YAMAZAKI*, E. WIDMANN *(CERN)*, **H. MASUDA*, I. SUGAI*** *(*INS, Tokyo Univ.)*, **R.S. HAYANO**, F.E. MAAS**, H.A. TORII**** *(**Tokyo Univ.)*, **F.J. HARTMANN†, H. DANIEL†, T. von EGIDY†, B. KETZER†, W. MÜLLER†, W. SCHMID†** *(†München Tech. Univ.)*, **D. HORVATH** *(KFKI Inst.)*, **and J. EADES** *(CERN)*

[*Phys. Rev. Lett.*, **72**, 1180 (1994)]

Based on the observation scheme proposed in our

previous paper [*Nucl. Instrum. Methods*, **A330**, 439 (1993)], we have observed the first laser-induced resonant transition in antiprotonic helium atoms ($\bar{p}He^+$), using a low-energy antiproton beam ejected from LEAR (Low Energy Antiproton Ring) of CERN, Switzerland. The transition observed occurs between a metastable state and a short-lived state which proceeds to ionization through fast Auger transition. The former state is expected to have appreciable population, and a laser resonantly moves this population to the latter short-lived state, which is quickly autoionized. After the ionization, $\bar{p}He^{2+}$ immediately annihilates due to Stark effect caused by surrounding helium atoms, and consequently generates many high-energy elementary particles, such as pions. Detecting these particles, we have succeeded in observing the resonance effect of laser excitation. The observed transition with vacuum wavelength 597.259 ± 0.002 nm is assigned to (n=39, l=35) → (38, 34), and this wavelength is in quite good agreement with theoretical values predicted by several theoreticians through different calculation methods. This fact gives a definite evidence of the production of $\bar{p}He^+$, and shows that the anomalous longevity of antiprotons previously observed in helium media results from the formation of high-n high-l atomic states of $\bar{p}He^+$.

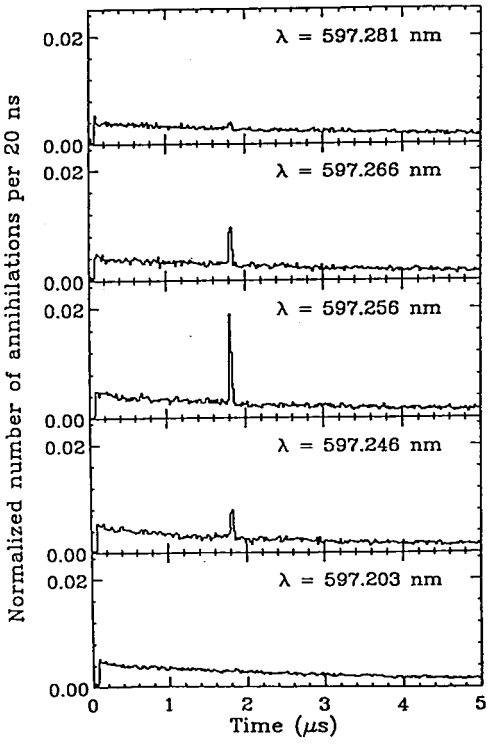

Figure 1. Wavelength-dependence of laser-induced annihilation signals of antiprotonic helium atoms. A sharp peak seen in each time-resolved annihilation spectrum is an annihilation signal induced by a laser pulse, which has a pulsewidth of 30 ns and enters the helium gas medium at 1.8 μs.

II-C-2 Laser Studies of the Decay Chain of Metastable Antiprotonic Helium Atoms

R.S. HAYANO*, F.E. MAAS*, H.A. TORII* *(*Tokyo Univ.)*, **N. MORITA, M. KUMAKURA, T. YAMAZAKI**, H. MASUDA**, I. SUGAI**** *(**INS, Tokyo Univ.)*, **F.J. HARTMANN†, H. DANIEL†, T. von EGIDY†, B. KETZER†, W. MÜLLER†, W. SCHMID†** *(†München Tech. Univ.)*, **D. HORVATH** *(KFKI Inst.)*, **J. EADES‡, and E. WIDMANN‡** *(‡CERN)*

Laser studies of metastable antiprotonic helium atoms, which we recently initiated by observing a sharp increase of antiproton annihilation rate induced by laser-stimulated resonant transitions, have been extended to obtain the nascent population and lifetime of the relevant levels. Varying the irradiation timing of a single laser pulse, which is tuned to the resonance already found at 597.26 nm, we can obtain the time dependence of the initial level population. Using two laser pulses with a variable time separation, we can also observe the feeding of the initial state from higher atomic levels. Making appropriate rate equations describing the population dynamics of the relevant levels and least-square-fitting these equations to the observed signals, we have determined the decay rates and initial populations of those levels. The decay rates thus obtained are in quite good agreement with theoretical values, and this fact further confirms the formation of this new exotic atom. We have also found that the initial level (n=39, l=35) of the laser-resonant transition has unexpectedly large population, which is as much as 7% of the total number of long-lived exotic atoms. This suggests that the nascent population distribution may, contrary to our expectation, be rather confined within a small number of long-lived states.

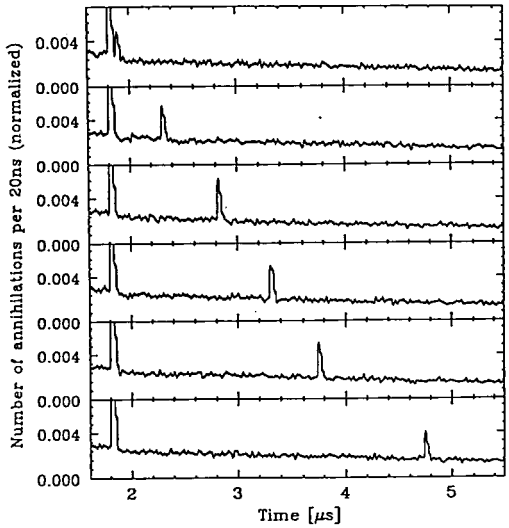

Figure 1. Time separation dependence of two-pulse laser-induced annihilation signals of antiprotonic helium atoms. Two sharp peaks in each spectrum are laser-induced annihilation signals and appear at the same time as the entrance of each laser pulse. The first laser pulse almost empties the initial level population, and the second pulse probes the subsequent recovery of the population.

II—D Laser Cooling and Trapping of Neutral Atoms

Atoms are accelerated or decelerated on absorption or emission of photons, since photons have momenta. On the other hand, a strong radiation field modifies the internal energy of atoms, so that atoms in an inhomogeneous radiation field receive a force from the field. Through these mechanisms, the translational motion of neutral atoms is not only be cooled to an extremely low temperature, but also easily controlled by laser radiation. As the translational temperature goes down to nano kelvin region, the atomic de Broglie wavelength becomes a macroscopic size. A macroscopic quantum-mechanical collective motion of an atomic assembly can then be expected to occur in a very thin gas. The long de Broglie wavelength also enables us to realize an atomic interferometry. On the other hand, easy control of atomic spatial position and velocity by laser radiation is expected to open the possibility of various applications. For this reason, we have been studying the laser cooling and trapping of neutral atoms.

II-D-1 Laser Trapping of ^{3}He atom

Mitsutaka KUMAKURA and Norio MORITA

Although laser trapping of neutral atoms has recently been applied to various isotope species, there have been no reports on the isotope of helium, ^{3}He. This may be partly because ^{3}He is very precious and its natural abundance is extremely small. However, helium is an important atom in the fundamental physics, and it must be interesting to investigate the difference between ^{4}He, which is a boson, and ^{3}He, a fermion, in "cold collision" processes and some other collective behaviors of translational motion. For this reason, we have attempted the laser trapping of ^{3}He atoms. Because of the lightness of helium atoms, the initial cooling process requires a long distance, so that the use of an atomic beam is unavoidable. This means that we have to circulate the ^{3}He gas without significant loss because it is too expensive to discard through vacuum pumping. Therefore, we have started with construction of a gas circulation system with purification mechanisms. The transition used for cooling and trapping is $2^3S_1(F=3/2) \rightarrow 2^3P_2(F=5/2)$, and four-beam-type magneto-optical trapping scheme is utilized. Metastable $2^3S_1(F=3/2)$ atoms are produced in a discharge cell cooled by liquid N_2 instead of the electron bombardment method so far used in our experiments. This improvement has brought about huge enhancement in the production of metastable atoms. As a result, we have successfully trapped 10^7 atoms in a spherical region with a diameter of 0.5 mm. Although additional lasers for repumping are, in general, necessary to trap atoms having hyperfine structures, we have achieved efficient trapping of ^{3}He without any additional lasers. This is because hyperfine splittings in ^{3}He are larger than in other atoms.

II—E Molecular Science of Biomolecules

Elucidation of a structure-function relationship of proteins is a current subject of this group. The primary technique used for this project is the stationary and time-resolved resonance Raman and absorption spectroscopies. The main themes that we want to explore are (1) mechanisms of oxygen activation by enzymes, (2) mechanisms of electron- and proton-transfers through proteins and their coupling in energy transducing membranes, (3) primary processes of photoreceptor proteins, (4) higher order protein structures and their dynamics. In category (1), we have examined stationary complexes of a variety of cytochrome oxidases, cytochrome P-450's, and peroxidases, and also treated their enzymatic reaction intermediates by using the mixed flow transient Raman apparatus and the Raman/absorption simultaneous measurement system. In addition, we recently observed nonfundamental bands of Fe-ligand vibrations and discussed anharmonicity of the potential functions. For (2) we have investigated bacteriorhodopsin and cytochrome c oxidase, while for (3) we treated a bacterial photosynthetic reaction center and a pigment for photomorphology. We found some structural differences between P_r and P_{fr} forms of native phytochrome as well as of large phytochrome. For (4), we developed a novel technique for UV Raman measurements based on the combined use of the first/second order dispersions of two gratings in an ordinary double monochromator and applied it successfully to 244-nm-excited RR spectra of several proteins including phytochrome, hemoglobin, and viruses. A new spinning cell system developed for UV Raman experiments requires a small amount of samples and therefore, it became possible to determine the UVRR spectra of mutant proteins. We applied this system to a β37 mutant of Hb and established the vibrational spectrum of β37 Trp of Hb A in the T and R quaternary structures.

II-E-1 Resonance Raman Spectra of the Photointermediates in Phytochrome Phototransformation: Deprotonation of the Chromophore in the Bleached Intermediate

Yasuhisa MIZUTANI, Satoru TOKUTOMI *(NIBB)*, and Teizo KITAGAWA

[*Biochemistry* **33**, 153–158 (1994)]

Resonance Raman (RR) scattering from a large pea phytochrome of type A was measured at cryogenic as well as ambient temperatures to study the chromophore structure of photointermediates. RR spectra excited with 364 nm at −120°C where the red absorbing form, P_r, and a photointermediate, I_{700}, are trapped, showed a strong band at 1625 cm^{-1} with a shoulder at 1648 cm^{-1} in the C=C stretching region. The shoulder disappeared and a new band appeared at 1597 cm^{-1} upon raising temperature to −80°C, where transformation from I_{700} to a bleached intermediate, I_{bl}, proceeds. At an ambient temperature, 16°C, a strong RR band was observed at 1625 cm^{-1} by the 364 nm

excitation under far-red illumination, whereas another RR band at 1599 cm^{-1} was intensified under red illumination. By comparison of these spectra with those of low temperatures, the 1625 and 1599 cm^{-1} bands were reasonably assigned to P_r and I_{bl} accumulated under red illumination, respectively. Chemically prepared bleached form, P_{bl}, also had a prominent band at 1599 cm^{-1}. The RR spectrum obtained by 407 nm excitation under red illumination showed two prominent bands at 1631 and 1591 cm^{-1}, which can be assigned to the far-red absorbing form, P_{fr}. The prominent 1625 cm^{-1} band of P_r in the C=C stretching region exhibited a downward frequency shift on deuteration, whereas those of I_{bl}, P_{fr} and also P_{bl} did not. This indicates distinct differences in protonation states between P_r and the other three species. Frequencies and relative intensities of RR bands in the region of I_{bl} resemble with P_{fr} but P_r, implying that chromophore configuration of I_{bl} and P_{fr} are similar to each other, however, they differ from that of P_r. These suggest that the configurational changes of the chromophore, such as E-Z photoisomerization, are involved in the primary process of the phototransformation, and that deprotonation of the chromophore follows it during a subsequent process yielding I_{bl}.

II-E-2 Preparation and Characterization of Oxoiron(IV) Chlorin Complexes as the First Models for a Reaction Intermediate in the Catalytic Cycle of Cytochrome *d*

Shinji OZAWA *(Kyoto Univ.)*, **Yoshihito WATANABE** *(Kyoto Univ.)*, **Satoru NAKASHIMA, Teizo KITAGAWA, and Isao MORISHIMA** *(Kyoto Univ.)*

[*J. Am. Chem. Soc.* **116**, 3439–3441 (1994)]

As models for a reaction intermediate in the catalytic cycle of cytochrome *d*, two types of oxoferryl chlorin complexes, (TPC)Fe^{IV}O(N-MeIm) and (TPC)Fe^{IV}O (TPC=tetraphenylchlorin, N-MeIm=N-methylimidazole), have been prepared for the first time by an autoxidation reaction of (TPC)Fe^{II} with O_2. Oxyiron(II)(TPC) and μ-peroxo-bridged iron(III) dimer, (TPC)Fe^{III}O OFe^{III}(TPC), are also detected in the course of the reaction. The six-coordinated (TPC)Fe^{IV}O(N-MeIm) complex is produced by adding N-methylimidazole to the μ-peroxo-bridged iron(III) chlorin dimer at −80°C. The μ-peroxo-bridged iron(III) dimer, the formation of which has been confirmed by paramagnetic NMR, undergoes homolytic cleavage of the O-O bond upon laser illumination to yield the five-coordinated (TPC)Fe^{IV}O complex. The absorption spectrum of (TPC)Fe^{IV}O(N-MeIm) shows a characteristic red-shifted band at 630 nm as observed in the case of the oxoferryl intermediate of cytochrome *d*. Proton NMR spectra of (TPC)Fe^{IV}O(N-MeIm) exhibit a small hyperfine shift of the pyrrole protons, consistent with the oxoferryl formulation. However, the paramagnetic NMR resonances of the saturated pyrrole (pyrroline) ring protons show unusual splitting into upfield and downfield region, suggesting deformation of the pyrroline ring of the chlorin complex. While the unusually high frequency of $\nu(Fe^{IV}=O)$(815 cm^{-1}) and large isotopic shift ($\Delta\nu$=46 cm^{-1}) observed for the oxoferryl intermediate of cytochrome *d* have been attributed to the chlorin macrocycle (heme *d*), the five- and six-coordinated oxoferryl chlorin complexes reported here exhibit $\nu(Fe^{IV}=O)$ frequencies and isotopic ($^{16}O/^{18}O$) frequency shifts nearly identical to those of the corresponding porphyrin complexes, respectively.

II-E-3 A Multi-Reflection Raman Cell for Studying Dilute Aqueous Solutions

Keiji KAMOGAWA, M. TAKAMURA *(Hiroshima Univ.)*, **H. MATSUURA** *(Hiroshima Univ.)*, **and Teizo KITAGAWA**

[*Spectrochim. Acta.* **50A**, 1513–1519 (1994)]

A cell for multi-reflection Raman measurements was constructed. This device consists of two rectangular prisms and, when applied to a rectangular sample cell, Raman signals were enhanced by seven to ten times compared with the single-pass measurement for a transparent solution. This system is readily applicable to studies of dilute aqueous solutions with low refractive indices. With this device, the C-H stretching Raman bands of benzene in water were observed with sufficiently high S/N ratios. Combination of the multi-pass cell with an optical-fiber light-collecting device enabled us to determine reproducibly the shifts of Raman bands from some reference state with an accuracy of 0.006 cm^{-1}.

II-E-4 Vibrational Assignments of the FeCO Unit of CO-Bound Heme Proteins Revisited: Observation of a New CO-Isotope-Sensitive Raman Band Assignable to the FeCO Bending Fundamental

Shun HIROTA, Takashi OGURA, Kyoko SHINZAWA-ITOH *(Himeji Inst. of Tech.)*, **Shinya YOSHIKAWA** *(Himeji Inst. of Tech.)*, **Masako NAGAI** *(Kanazawa Univ.)*, **and Teizo KITAGAWA**

[*J. Phys. Chem.* **98**, 6652–6660 (1994)]

In order to find the FeCO bending (δ_{FeCO}) fundamental, resonance Raman spectra in the 600–200 cm^{-1} region of CO adducts of hemoglobin (Hb), its isolated chains, myoglobin (Mb), cytochrome c oxidase (CcO), and cytochrome P-450 (P-450) were reexamined. A new CO-isotope-sensitive band was found around 365 cm^{-1} for all but MbCO. For HbCO this band was located at 367, 355, 363, and 353 cm^{-1} for $^{12}C^{16}O$, $^{13}C^{16}O$, $^{12}C^{18}O$, and $^{13}C^{18}O$ adducts, respectively, and thus exhibited a zigzag pattern against the increase of the total mass of CO, similar to the 575 cm^{-1} band which has been assigned to the δ_{FeCO} fundamental hitherto. Relative intensity of the ~365 cm^{-1} band to the 575 cm^{-1} band exhibited almost no change upon lowering of temperature from 20°C to −10°C, but since temperature dependent frequency shifts were appreciable, the present difference spectra could not determine if the intensity change by 11% expected for a difference combination band of a hot 210 cm^{-1} mode was involved or not. The maximum intensity enhancement of the 365 cm^{-1} band in the excitation profile within the Soret band occurred at longer wavelengths than that of the 575 cm^{-1} band. The frequency differences between the CO-isotope-sensitive

band around 575 cm^{-1} and one around 365 cm^{-1} were 208 ± 5, 213 ± 5, and 204 ± 3 cm^{-1} for all CO isotopes of HbCO, CcO · CO, and P-450 · CO, respectively. Despite that the Fe-CO and C-O stretching modes exhibited no deuteration shifts, the frequency of the 575 cm^{-1} band was higher in D_2O than in H_2O, and this feature was more prominent with MbCO than HbCO. The 575 cm^{-1} band of MbCO was remarkably strong upon excitation at 406.7 nm and this is distinct from other proteins examined. These observations suggest that the ~365 cm^{-1} band arises from the δ_{FeCO} fundamental and the 575 cm^{-1} band is its combination with a porphyrin vibration or possibly a Fe-C deformation mode. Normal coordinate calculations for the isolated FeCO unit reasonably reproduce the observed isotopic frequency shifts under these assignments.

II-E-5 Observation of a New Oxygen-Isotope-Sensitive Raman Band for Oxyhemoproteins and Its Implications in Heme Pocket Structures

Shun HIROTA, Takashi OGURA, Evan H. APPELMAN *(Argonne Natl. Lab.)*, **Kyoko SHINZAWA-ITOH** *(Himeji Inst. of Tech.)*, **Shinya YOSHIKAWA** *(Himeji Inst. of Tech.)*, **and Teizo KITAGAWA**

[*J. Am. Chem. Soc.*, in press]

A new oxygen-isotope-sensitive Raman band was found for oxyhemoglobin (HbO_2) and oxycytochrome c oxidase ($CcO \cdot O_2$) in the frequency region lower than the Fe-O_2 stretching mode ($\nu_{Fe\text{-}O_2}$). This band was located at 425 cm^{-1} for $Hb^{16}O_2$, shifted to 405 cm^{-1} with $Hb^{18}O_2$ and to ~423 cm^{-1} and ~407 cm^{-1} with $Hb^{16}O^{18}O$. The corresponding band appeared at 435 cm^{-1} for $CcO \cdot {}^{16}O_2$, shifted to 415 cm^{-1} with $CcO \cdot {}^{18}O_2$. Accordingly, the band has been assigned to the Fe-O-O bending mode (δ_{FeOO}). However, the corresponding band could not be identified for oxymyoglobin (MbO_2). The Fe-O_2 stretching mode ($\nu_{Fe\text{-}O_2}$) was observed at 568, 567, 544 and 544 cm^{-1} for $Hb^{16}O_2$, $Hb^{16}O^{18}O$, $Hb^{18}O^{16}O$, and $Hb^{18}O_2$, respectively, and the corresponding modes were observed at 571, 569, 547, and 545 cm^{-1} for MbO_2, and 571, 567, 548, and 544 cm^{-1} for $CcO \cdot O_2$. The $\nu_{Fe\text{-}O_2}$ bandwidths of HbO_2 and MbO_2 were alike and 1.5 times broader than that of $CcO \cdot O_2$, suggesting that the Fe-O-O geometry is more fixed in the latter. Despite the greatly different reactivities of bound O_2 in HbO_2 and $CcO \cdot O_2$, their $\nu_{Fe\text{-}O_2}$ and δ_{FeOO} frequencies and O_2-isotopic frequency shifts were alike, indicating similar Fe-O-O binding geometries. Normal coordinate calculations for an isolated three-atom molecule could reproduce the observed isotopic frequency shifts with the 115° bond angle reported for MbO_2, but not with the 155° angle reported for HbO_2.

II-E-6 Observation of Nonfundamental Fe-O_2 and Fe-CO Vibrations and Potential Anharmonicities for Oxy- and Carbonmonoxy-Hemoglobin; Evidence Supporting a New Assignment of the Fe-C-O Bending Fundamental

Shun HIROTA, Takashi OGURA, and Teizo KITAGAWA

[*J. Am. Chem. Soc.*, submitted]

The overtone and combination Raman bands of the Fe-ligand vibrations of heme proteins were investigated for the first time. The overtone of the Fe-O_2 stretching ($\nu_{Fe\text{-}O_2}$) of oxyhemoglobin (HbO_2) was found at 1136 cm^{-1} for $^{16}O_2$ (1088 cm^{-1} for $^{18}O_2$). Since the corresponding band for $^{16}O^{18}O$ adduct did not appear at an intermediate frequency, a possibility for assigning it to the O-O stretching was ruled out. For carbonmonoxyHb (HbCO), CO-isotope-sensitive bands were found at 738, 859–890, 1002, and 1183 cm^{-1} for $^{12}C^{16}O$ (718, 836, 971, and 1161 cm^{-1} for $^{13}C^{18}O$). The 738/718, 1002/971, and 859–890/836 cm^{-1} pairs for $^{12}C^{16}O/^{13}C^{18}O$ are reasonably interpreted as the overtones of the Fe-CO bending (δ_{FeCO}), Fe-CO stretching ($\nu_{Fe\text{-}CO}$), and their combination ($\nu_{Fe\text{-}CO} + \delta_{FeCO}$), respectively, when the difference peaks at 369/355 cm^{-1} was assigned to δ_{FeCO} fundamental while the 1183/1161 cm^{-1} pair is interpreted as a combination of ν_7 and $\nu_{Fe\text{-}CO}$. On the contrary, when the 577/558 cm^{-1} pair was assigned to the δ_{FeCO} fundamental, nonfundamental band was not recognized at the corresponding frequencies and interpretation of other bands was difficult. These observations strongly support the recently proposed new assignment of δ_{FeCO} fundamental (S. Hirota, T. Ogura, K. Shinzawa-Itoh, S. Yoshikawa, M. Nagai, and T. Kitagawa, J. Phys. Chem. **98**, 6652–6660 (1994)). The anharmonic constant for the Fe-CO stretching potential was calculated to be 0.010 but that for Fe-O_2 was much smaller (< 0.001).

II-E-7 Selective Resonance Raman Observation of the "607 nm" Form Generated in the Reaction of Oxidized Cytochrome *c* Oxidase with Hydrogen Peroxide

Denis A. PROSHLYAKOV, Takashi OGURA, Kyoko SHINZAWA-ITOH *(Himeji Inst. of Tech.)*, **Shinya YOSHIKAWA** *(Himeji Inst. of Tech.)*, **Evan H. APPELMAN** *(Argonne Natl. Lab.)*, **and Teizo KITAGAWA**

[*J. Biol. Chem.*, in press]

Resonance Raman (RR) spectra were measured selectively for the "607 nm" form, which has been assigned to a peroxy intermediate formed in the reaction of oxidized cytochrome *c* oxidase with hydrogen peroxide at ambient temperature. A single oxygen-isotope-sensitive band was found at 803 cm^{-1} for the reaction with $H_2^{16}O_2$ (at 769 cm^{-1} with $H_2^{18}O_2$) upon excitation at 607 nm, the wavelength of the difference absorption maximum characteristic of the "peroxy" intermediate. Upon excitation at shorter wavelengths (down to 580 nm), the Raman spectrum simply became weaker without yielding any new features. When $H_2^{16}O^{18}O$ was used, two bands were observed at 803 and 769 cm^{-1} (within an accuracy of 0.5 cm^{-1}), but with only half the intensity of those observed with $H_2^{16}O_2$ or $H_2^{18}O_2$, which ruled out the possibility that the 803-cm^{-1} band arose from the O-O or Fe-O_2 stretching of the $Fe^{III}(O^-O^-)$ heme. Conversely, the 34 cm^{-1} downshift with ^{18}O is in good agreement with the calculated $^{16}O/^{18}O$ shift (35 cm^{-1}) expected for the diatomic $Fe{=}^{16}O$ oscillator at 803 cm^{-1}. This band exhibited an upshift by 1.3 cm^{-1} in ^2H_2O, similar to the case of compound II of horseradish peroxidase (HRP) at neutral pH, and indicative of the presence of a

hydrogen bond to the Fe^{IV}=O oxygen. The 803/769 cm^{-1} pair of RR bands were also observed upon blue excitation, as is to the case for the bands found in the dioxygen cycle of this enzyme (Ogura, T., Takahashi, S., Hirota, S., Shinzawa-Ito, K., Yoshikawa, S., Appelman, E. H., and Kitagawa, T. (1993) J. Am. Chem. Soc. 115, 8527–8536). This observation provides the first direct characterization of the "607 nm" form of this enzyme in its reaction with H_2O_2.

II-E-8 Observation of the Fe-O_2 and Fe^{IV}=O stretching Raman bands for dioxygen reduction intermediates of cytochrome *bo* isolated from *Escherichia coli*

Shun HIROTA, Tatsushi MOGI *(Univ. of Tokyo)*, **Takashi OGURA, Tomoyasu HIRANO** *(Univ. of Tokyo)*, **Yasuhiro ANRAKU** *(Univ. of Tokyo)*, **and Teizo KITAGAWA**

[*FEBS Lett.*, **352**, 67–70 (1994)]

Reaction intermediates in dioxygen reduction by the *E. coli* cytochrome *bo*-type ubiquinol oxidase were studied by time-resolved resonance Raman spectroscopy using the artificial cardiovascular system. At 0 ~ 20 μs following photolysis of the enzyme-CO adduct in the presence of O_2, we observed the Fe-O_2 stretching Raman band at 568 cm^{-1} which shifted to 535 cm^{-1} with the $^{18}O_2$ derivative. These frequencies are remarkably close to those of other oxyhemoproteins including dioxygen-bound hemoglobin and aa_3-type cytochrome *c* oxidase. In the later time range (20 ~ 40 μs), other oxygen-isotope-sensitive Raman bands were observed at 788 and 361 cm^{-1}. Since the 781 cm^{-1} band exhibited a downshift by 37 cm^{-1} upon $^{18}O_2$ substitution, we assigned it to the Fe^{IV}=O stretching mode. This band is considered to arise from the ferryl intermediate, but its appearance was much earlier than the corresponding intermediate of bovine cytochrome *c* oxidase (> 100 μs). The 361 cm^{-1} band showed the $^{16}O/^{18}O$ isotopic frequency shifts of 14 cm^{-1} similar to the case of bovine cytochrome *c* oxidase reaction.

II-E-9 Ultraviolet Resonance Raman Studies of Quaternary Structure of Hemoglobin Using a Tryptophan β37 Mutant

Masako NAGAI *(Kanazawa Univ.)*, **Shoji KAMINAKA** *(Kurume Univ.)*, **Yuzo OHBA** *(Yamaguchi Univ. School of Medicine)*, **Yukifumi NAGAI** *(Fukui Medical School)*, **Yasuhisa MIZUTANI, and Teizo KITAGAWA**

[*J. Biol. Chem.*, in press]

Environmental changes of tyrosine (Tyr) and tryptophan (Trp) residues of hemoglobin (Hb) upon its T-to-R transition of quaternary structure was investigated with ultraviolet resonance Raman (UVRR) spectroscopy excited at 235 nm. DeoxyHb A (T-form) showed a UVRR spectrum distinctly different from those of the ligated Hbs (R-form) including oxy-, CO- and met-Hb A, while the ligated Hbs exhibited similar UVRR spectra irrespective of a ligand species and an oxidation state of the heme. To characterize the spectral change of Trp β37 at $\alpha_1\beta_2$ interface due to the quaternary structure transition, the UVRR spectra of Hb A were compared with the corresponding spectra of Hb Hirose in which Trp β37 is replaced by serine (Ser). The difference spectrum between deoxyHb A and deoxyHb Hirose gave rise to only Trp RR bands, which were reasonably ascribed to Trp β37 in deoxyHb A. RR bands at 873 cm^{-1} (W17) and at 1360/1343 cm^{-1} (W7 Fermi doublet) indicated that the indole ring of Trp β37 in deoxyHb A made a strong H-bonding at the N_1H site in hydrophobic environments. Tyr residues in deoxyHb Hirose seemed to be in the same environments as those of deoxyHb A. In contrast, the difference spectrum between Hb A and Hb Hirose in the ligated state displayed peaks for RR bands of both Trp and Tyr. The difference spectra were unaltered by addition of 5 mM IHP. This means that the differences were not caused by the tetramer to dimer dissociation but a conformation change within a tetramer. Comparison of the Hb A-Hb Hirose difference spectra in the oxy and deoxy states revealed that the oxygenation-induced changes of Trp RR bands arose mostly from Trp β37 and the remaining minor part from Trp β15, demonstrating that Trp β37 plays a pivotal role in the quaternary structural change in Hb A. The oxygenation-induced UVRR spectral changes of Trp and Tyr of Hb A are discussed in view of possible changes in interactions between Trp residues and near-by aromatic amino acids on the basis of X-ray crystallographic data.

II-E-10 Presence of Two Fe^{IV}=O Heme Species in the Reaction of Cytochrome Oxidase with Oxygen Revealed by TR^3 Spectroscopy

Takashi OGURA, Shun HIROTA, Kyoko SHINZAWA-ITOH *(Himeji Inst. of Tech.)*, **Shinya YOSHIKAWA** *(Himeji Inst. of Tech.)*, **and Teizo KITAGAWA**

The reaction of fully-reduced cytochrome oxidase with oxygen was carefully examined with time-resolved resonance Raman (TR^3) spectroscopy under improved experimental conditions at lower temperature. At Δt=540 μs following the start of reaction in H_2O there were two oxygen-isotope-sensitive bands at 804 and 785 cm^{-1}. At Δt=2.7 ms only the band at 785 cm^{-1} was observed. In D_2O, on the other hand, only the band at 804 cm^{-1} was observed at Δt=540 μs while two bands at 804 and 785cm^{-1} were observed at Δt=11 ms. These observations established that the species which gave the band at 804 cm^{-1} preceded the species giving the 785 cm^{-1} band. From these observations together with the results obtained for the reaction of oxidized enzyme with H_2O_2, we propose new assignments of these two Raman bands both to the Fe-O stretching modes of ferryloxo intermediates. The species which gave 804 cm^{-1} band was considered to be higher by one oxidative equivalent higher than that which gave 785 cm^{-1} band. However, the location of the extra oxidative equivalent remains to be determined.

II-E-11 A Novel Spinning Cell System for UVRR Measurements of Powder- and Small Volume Solution Samples in Back-Scattering Geometry: Application to Solid Tryptophan and Mutant Hemoglobin Solution

Shoji KAMINAKA *(Kurume Univ.)* **and Teizo KITAGAWA**

A novel spinning cell system practically useful in ultraviolet (UV) resonance Raman (RR) measurements of solid samples and small-volume solution samples was designed and constructed. The cell system, which resulted from special efforts to keep the on-axis spinning of a thin-wall sample tube and to make it possible to replace the inside gas, consists of a stepping motor (A), cell holder (H) and a synthetic quartz ESR tube as illustrated in Figure 1. Strict on-axis spinning of the cell in back-scattering geometry raised the S/N ratio more than three times than an ordinary spinning cell and the thin-wall of the ESR tube reduced the spectral background significantly. The advantage of this system was demonstrated by observing the CW 244-nm excited RR spectra of solid tryptophan and pulsed 235-nm excited RR spectrum of 50 μL aliquot of mutant hemoglobin solution.

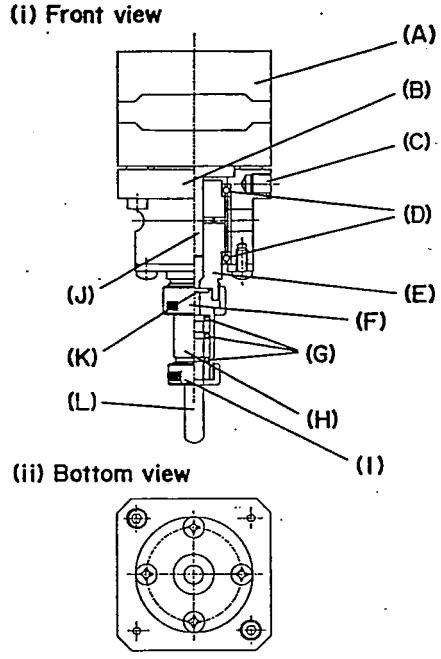

Figure 1.

II—F Vibrational Spectroscopy of Molecules in Transient States

Raman spectroscopy reveals the vibrational spectrum of a molecule, which is sensitive to geometrical as well as electronic structures. When a wavelength of the probe beam is tuned within the absorption band of the molecule in question, resonance enhancement of Raman intensity takes place and thus makes it possible to detect Raman scattering from an excited molecule or a reaction intermediate even if its population is considerably small. We have taken this advantage of resonance effects to explore the structures of metalloporphyrins and free-base porphyrins in the excited singlet and triplet states. By using various isotope-labeled porphyrins, we determined vibrational assignments of excited state porphyrins. We also investigated intermediates of photoreduction of iron-porphyrins. Recently we extended similar measurements to a ps time regime and succeeded in observing the RR spectra of vibrationally hot Ni-porphyrin in a dd electronic excited state and in determining the vibrational temperature from the intensity of Stokes/anti-Stokes Raman bands. The pump/probe time-resolved Raman system using two 7-ns visible lasers was applied to pursue the Fe-CO stretching Raman band of recombined species of photodissociated CO-myoglobin and their mutants. These experiments enables us to explore dynamical features of protein structures. In parallel with these experimental work, we theoretically treated dynamics of CO adduct of myoglobin and examined the effect of protonation and side-chain motions of distal histidine upon the Fe-CO structure. We extended these calculations to other mutants of Mb.

II-F-1 Recombination Intermediates of Photodissociated CO Myoglobin at Ambient Temperatures Detected by Time-Resolved Resonance Raman Spectroscopy

Satoru NAKASHIMA and Teizo KITAGAWA

[*J. Am. Chem. Soc.*, in press]

Time-resolved resonance Raman (TR^3) experiments were carried out for sperm whale carbonmonoxy myoglobin (COMb) using the pump-(7ns, 532nm, 4mJ) and probe (7ns, 416nm, 100μJ) pulses with various delay times (Δt=−20ns−1ms) at ambient temperature. The equilibrium Fe-CO stretching band, identified in the spectrum for Δt=−20ns (508 cm^{-1} for $^{12}C^{16}O$ and 497 cm^{-1} for $^{13}C^{18}O$) in the pump/probe measurements, was absent in the spectrum for Δt=0 ns and the TR^3 spectra for Δt=0 and 20 ns were different. A new band started to grow at 497 cm^{-1} from Δt=20 ns. This band did not exhibit the $^{13}C^{18}O$ isotopic frequency shift and accordingly is assigned to a mode of deoxy heme. The Fe-CO stretching band reappeared from Δt=100μs and was restored by 65% at 1 ms. The spectral difference of the deoxy heme between Δt=0 and Δt=20ns−100μs suggests that some conformational changes occur in the heme vicinity around 20 ns after photolysis but before the Fe-CO stretching band reappears, providing an evidence for the presence of a transient species, which is generated after CO migrates into the heme pocket but before binds to the heme.

II-F-2 Time-Resolved Resonance Raman Study of Porphyrins and Metalloporphyrins in the Electronic Excited States

Shin-ichiro SATO and Teizo KITAGAWA

[*Appl. Phys.*, **B59**, 415−431 (1994)]

Current developments of our Time-Resolved Resonance Raman (TR^3) studies on the ($\pi\pi^*$) excited state of free-base porphyrins and (*dd*) excited state of Ni-OctaEthyl-

Porphyrin (NiOEP) in solutions are described. A device for quasi-simultaneous measurements has been developed to obtain correct difference spectra for pump/probe spectra of various delay times and probe-only spectrum. This technique is practically powerful to obtain TR^3 spectra of porphyrins and metallo-porphyrins. An orbital-symmetry marker band (ν_2) exhibited upshifts along $S_0 \rightarrow S_1 \rightarrow T_1$ transitions for free-base octaethylporphyrin (H_2OEP), while downshifts along the same transitions for free-base Tetra-PhenylPorphyrin (H_2TPP). This is interpreted by the symmetry differences in the highest occupied molecular orbitals of H_2OEP (a_u-orbital) and H_2TPP(b_{1u}-orbital). An intensity-borrowing mode (ν_{19}) was enhanced by the Albrecht C-term in resonance with the $T_1 \rightarrow T_n$ transition, but not in resonance with the $T_1 \rightarrow T_n$ transition for H_2OEP. This fact can be considered to be due to different vibronic couplings between the singlet and triplet manifolds. For the (*dd*) exited state of NiOEP, our TR^3 study suggests that the excess energy upon the ($\pi\pi^*$) to (*dd*) transition was vibrationally cooled prior to the electronic relaxation from the (*dd*) state to the ground state with a relaxation time of ca. 300 ps. Comparison between Stokes and anti-Stokes resonance Raman spectra for the delay time of 0 ps indicated that the lower limit of vibrational temperature in 0—40 ps time range is 750 K.

II-F-3 The Proximal Residue Largely Determines the CO Distortion in Carbonmonoxy Globin Proteins. An *ab initio* Study of a Haem Prosthetic Unit

Philip JEWSBURY, Shigeyoshi YAMAMOTO *(Chukyo Univ.)*, **Tsutomu MINATO** *(Nara Univ.)*, **Minoru SAITO** *(Protein Engineering Research Inst.)*, **and Teizo KITAGAWA**

[*J. Am. Chem. Soc.*, in press]

The preliminary results of an *ab initio* investigation of a model haem prosthetic group show that the large off-perpendicular distortions of the Fe-C-O unit in the protein X-ray structures are mainly caused by the distorted orientation of the proximal residue. Inclusion of the distal residue in a supermolecule calculation has a smaller effect on the Fe-C-O geometry. Thus the large strain energies implied by the large off-perpendicular distortions of the Fe-C-O group in the X-ray structures are delivered by the protein tertiary structure, via the proximal residue, and not by the mobile distal side chain as had been previously proposed. The structure-function relationship, as revealed by the X-ray structure, can now be clarified. The Fe-C-O geometry is largely determined by the proximal residue, and so is non-perpendicular even in the His64Gly mutant. These distortions are expected to be present even under physiological conditions. The distal residue is *not* subject to a large repulsive interaction with the carbonyl ligand, thus its orientation in the solvated protein can be determined by weaker attractive electrostatic interactions, as inferred from recent experimental studies of distal residue mutant myoglobins. This result removes the need to invoke a large stabilisation of the distal side chain orientation by a rigid hydrogen bonding network, an interpretation of the physiological structure-function relationship that was at odds with the X-ray B-factors, and the mobility of the solvent molecules expected under physiological conditions.

II-F-4 The Distal Residue-CO Interaction in Carbonmonoxy Myoglobins: a Molecular Dynamics Study of Two Distal Histidine Tautomers

Philip JEWSBURY and Teizo KITAGAWA

[*Biophys. J.*, in press]

Four independent 90ps molecular dynamics simulations of sperm-whale wild type carbonmonoxy myoglobin (MbCO) have been performed using a new force field for the haem prosthetic group developed for the AMBER protein dynamics package from that already available with CHARMM. The protein primary structures of each trajectory differ only in the protonation site of the distal histidine nitrogen: two trajectories have the $64N_\delta$ nitrogen protonated, two the $64N_\varepsilon$ nitrogen protonated. All water molecules within 16Å of the carbonyl O are included (about 135 molecules), thus the haem pocket is considered solvated. In three trajectories the distal residue remains part of the haem pocket, with the protonated distal nitrogen pointing into the active site. This is in contrast with the neutron diffraction crystal structure which has the protonated $64N_\delta$ nitrogen pointing out of the active site, but is consistent with recent solution phase experiments measuring the CO stretching frequency (ν_{CO}) of MbCO and its various mutants. There are significant differences in the haem pocket structures found for each tautomer, resulting in different average electric fields at the ligand site. No significant difference in the Fe-C-O geometries is observed between any of the trajectories, supporting recent interpretations that the interaction between the haem pocket and Fe-bound CO is largely electrostatic rather than steric in nature. One trajectory (a $64N_\delta H$ tautomer) has the distal histidine moving out into the "solvent", leaving the pocket in an "open" structure with a significantly larger "entrance" to the active site than found in the "closed" conformations. The time averaged positions of the CO centres lie on, or close to, the haem normal in all four trajectories consistent with the small changes in Fe-C-O geometry oberved in a range of mutant MbCO crystal structures. The instantaneous orientations of the CO dipole lie around 20° to the haem normal, at angles similar to those observed in infrared polarization studies, thus explaining the apparent discrepancy between these experimental results. These trajectories suggest that the three ν_{CO} frequencies observed for wild type MbCO in solution, rather than representing significantly different Fe-C-O geometries as such, arise from three different haem pocket structures, each with electric fields at the ligand. Each pocket structure corresponds to a different distal histidine conformer: the A_3 band to the $64N_\varepsilon H$ tautomer, the $A_{1,2}$ band to the $64N_\delta H$ tautomer and the A_0 band to the absence of any significant interaction with the distal side chain.

II-F-5 The distal-CO Interaction in Carbonmonoxy Myoglobins: the Molecular Dynamics of 3 Distal Mutants

Philip JEWSBURY and Teizo KITAGAWA

Six 90ps molecular dynamics trajectories, two for each of three distal mutants of sperm whale carbonmonoxy myoglobin (MbCO), are reported. Solvent waters within 16Å of the active site have been included. In both His64Gln trajectories, the distal side chain remains part of the haem pocket forming a "closed" conformation similar to that of the wild type $64N_{\delta}H$ tautomer. Despite a connectivity more closely resembling the $N_{\varepsilon}H$ histidine tautomer, close interactions with the carbonyl ligand similar to those observed for the wild type $64N_{\varepsilon}H$ MbCO tautomer are prevented in the His64Gln mutant by repulsive interactions between the carbonyl O and the $64O_{\varepsilon}$. The aliphatic distal side chain of the His64Leu mutant shows little interaction with the carbonyl ligand in either of the His64Leu trajectories. Solvent water molecules move into and out of the active site in the His64Gly mutant trajectories; during all the other MbCO trajectories, including the wild type distal tautomers considered in an earlier work, solvent molecules rarely encroach closer than 6Å of the active site. These results are consistent with a recent structural interpretation of the wild type IR spectrum, and the current re-interpretation that the distal-ligand interaction in MbCO is largely electrostatic, not steric, in nature.

II—G Molecular and Electronic Structures of Metallofullerenes and the Fullerene Radical Anions

The continued interest in metallofullerenes and radical ions of fullerenes has resulted from the discovery of superconductivity in the CT complexes of alkali metals with fullerenes. Spectroscopic information concerning the electronic structure of C_{60}^- and C_{70}^- has been obtained by the resonance-enhanced multiphoton electron detachment (REMPED) measurements in the gass phase. Considering the metallofullerene as the endohedral (i.e. intramolecular) CT complex of a metal with the fullerene, the electronic structure of the mettalofullerne is expected to be very significant in explaining the possibility of the superconductivity or the ferromagnetism of the metallofullerene crystal.

II-G-1 Laser Study on the Resonance-Enhanced Multiphoton Electron Detachment (REMPED) Processes for C_{60}^- and C_{70}^-

Takeshi KODAMA, Tatsuhisa KATO, Taro MORIWAKI *(Tokyo Metropol. Univ.)*, **Haruo SHIROMARU** *(Tokyo Metropol. Univ.)*, **and Yohji ACHIBA** *(Tokyo Metropol. Univ.)*

[*J. Phys. Chem.*, **98** (42), 10671 (1994)]

The resonance-enhanced multiphoton electron detachment (REMPED) spectra for C_{60}^- and C_{70}^- have been obtained. They are regarded as the absorption spectra for these fullerene anions in the gas phase. The REMPED spectrum of a fragment anion produced in the fragmentation process of C_{70}^-, having a mass of 720, has been measured. This spectrum shows an identical threshold with C_{60}^- at ca. 8200cm^{-1}. Thus the fragment anion is assigned to C_{60}^- with the icosahedral structure. The REMPED spectrum of C_{70}^- shows a broad band in the near-infrared region. The nature of the appearance of this band is discussed in consideration of the ground electronic state for C_{70}^-.

II-G-2 ESR study on structures and dynamics of $Sc_3@C_{82}$

Tatsuhisa KATO, Shunji BANDOW, Masayasu INAKUMA *(Nagoya Univ.)*, **and Hisanori SHINOHARA** *(Nagoya Univ.)*

[*J. Phys. Chem.*, in press]

The ESR spectrum of $Sc_3@C_{82}$ in toluene and CS_2 solutions exhibits the symmetric hyperfine splitting of the 22 lines with a line width of 0.5 gauss at room temperature, which is consistent with the structure of $Sc_3@C_{82}$ having the C_{3v} symmetry. The line widths of the 22 lines are much broader than that for $Sc@C_{82}$, and show the unusual temperature dependence. The origin of the line widths can not be explained only by the line broadening effect originated in the hydrodynamic rotation of the whole molecule. We have found that the specific feature of the line widths reflects the intramolecular dynamics which averages between distinct scandium ion environment.

RESEARCH ACTIVITIES III
Department of Electronic Structure

III—A Ultrafast Intermolecular Electron Transfer Faster than Diffusive Solvent Relaxation

We have recently reported ultrafast fluorescence quenching of excited dye molecule (nile blue A perchlorate) in neat weakly polar electron-donating solvents and the picosecond transient absorption of reaction products. We attributed the fluorescence quenching to intermolecular electron transfer (ET). To understand the role of solvent dynamics and intramolecular motion in ET, it is important to study the time dependence of the reaction in detail. Accurate measurements of fluorescence decay were made with xanthenes and coumarins in aniline and *N,N*-dimethylaniline. We found ET rate constants in some cases determined directly by nuclear rearrangement and in the other cases by solvent relaxation dynamics. Most interestingly we found a substituent effect of ET in 7-aminocoumarins.

III-A-1 Femtosecond Intermolecular Electron Transfer in Condensed Systems

Keitaro YOSHIHARA, Yutaka NAGASAWA *(Graduate Univ. for Advanced Studies)*, **Arkadiy YARTSEV, Shigeichi KUMAZAKI, Hideki KANDORI, Alan E. JOHNSON, and Keisuke TOMINAGA**

[*J. Photochem. Photobiol. A* **80**, 167 (1994)]

We have investigated the ultrafast intermolecular electron transfer (ET) from an electron-donating solvent (aniline (AN) or *N,N*-dimethylaniline (DMA)) to an excited dye molecule (oxazines (Nile blue and oxazine 1) or coumarins). A non-exponential time dependence was observed in AN and can be explained by solvent reorientation and nuclear motion of the reactants. However, in DMA, a single exponential process was observed for Nile blue (160 fs) and oxazine 1 (280 fs), which can be explained by assuming that the rate of ET is limited mainly by ultrafast nuclear motion. A clear substituent effect on intermolecular ET was observed for the 7-aminocoumarins. When the alkyl chain on the 7-amino group is extended and a hexagonal ring with the benzene moiety is formed, the rate of ET is reduced by three orders of magnitude. This effect can be explained by a change in the free energy difference of the reaction and by the vibrational motion of the amino group.

III-A-2 Temperature Dependence of Ultrafast Intermolecular Electron Transfer Faster than Solvation Process

Yutaka NAGASAWA *(Graduate Univ. for Advanced Studies)*, **Arkadiy YARTSEV, Keisuke TOMINAGA, Alan E. JOHNSON, and Keitaro YOSHIHARA**

[*J. Chem. Phys.* **101**, 5717 (1994)]

Temperature dependence of intermolecular electron transfer (ET) between oxazine 1 (OX1) in the excited state and electron donor solvents such as aniline (AN) and N,N-dimethylaniline (DMA) was studies by observing fluorescence dynamics of OX1 (Figure 1). The fluorescence decay of OX1 in DMA showed a single exponential behavior with a time constant (280 fs) which was independent of temperature over the range of 280 to 353K. In AN, the ET caused non-exponential fluorescence decay whose time constants range from a few hundred femtoseconds to a few picoseconds depending on temperature. The time constants of these ET were smaller than the solvation times obtained by dynamic fluorescence Stokes shift of coumarin 102. This indicates the importance of vibrational nuclear motion in ET. The extended Sumi-Marcus two-dimensional reaction coordinate model which concerns the effect of high frequency mode was applied to explain the experimental observations. Good agreements were obtained between the experiments and calculations in terms of necessary parameters such as electronic matrix element and solvent reorganization energy. The difference between the ET of OX1 in DMA and AN can be mainly explained by the free energy difference between the reactant and the product.

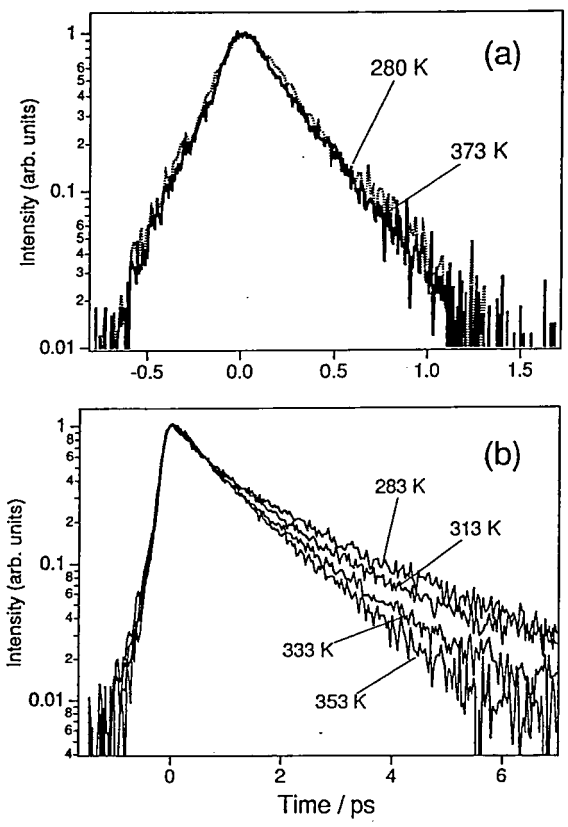

Figure 1. Temperature dependent fluorescence decays of OX1 (a) in DMA and (b) in AN.

III-A-3 Chemical Substitution and Deuterium Isotope Effects on Ultrafast Intermolecular Electron Transfer: Possible Role of Molecular Vibrations

Yutaka NAGASAWA *(Graduate Univ. for Advanced Studies)*, **Arkadiy YARTSEV, Keisuke TOMINAGA, and Keitaro YOSHIHARA**

[*Ultrafast Phenomena IX, Springer*, in press]

Deuterium isotope effect was observed, by means of femtosecond fluorescence up-conversion technique, for the ultrafast intermolecular electron transfer (ET) between coumarin 152 (C152) and aniline (AN) in the time region of 3 ~ 13 ps. The ET was ~10% slower for the deuterated AN compared to the normal one as shown in Figure 1. The deuteration of the amino hydrogens is more important than that of the phenyl hydrogens. Hindered rotation of the amino group may be contributing to the fast part of the solvation process. However, when the reaction becomes much faster (C151 in AN), the isotope effect becomes minor. This may indicate that much faster nuclear dynamics is also contributing to the ultrafast ET.

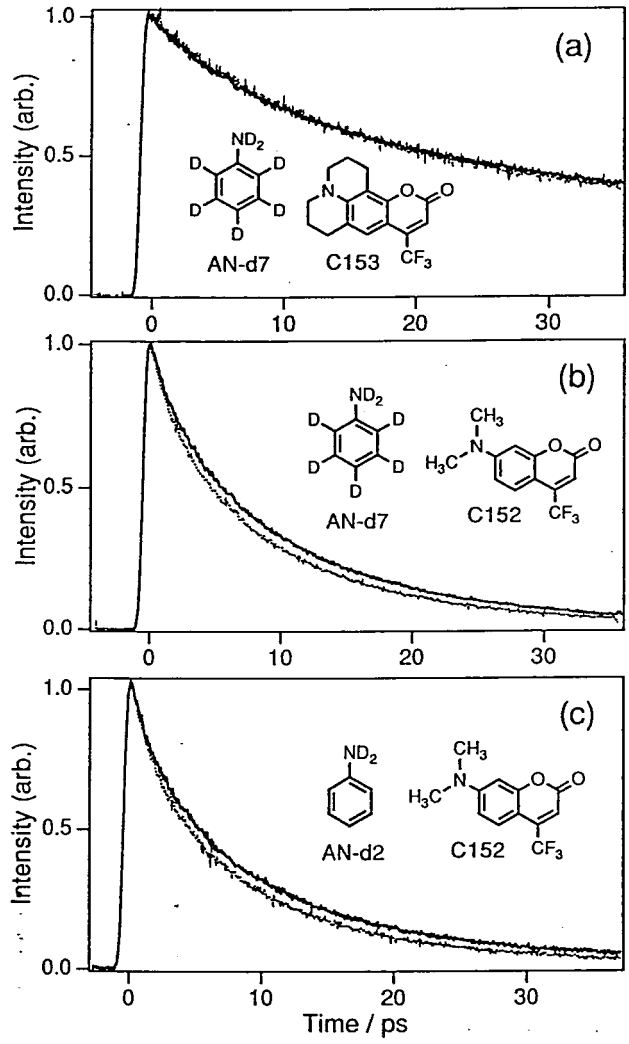

Figure 1. (a) Fluorescence decay of C153 in AN-h7 (broken line) and in AN-d7 (solid line). (b) Fluorescence decay of C152 in AN-h7 (broken line) and in AN-d7 (solid line). (c) Fluorescence decay of C152 in AN-h7 (broken line) and in AN-d2 (solid line).

III—B Liquid Dynamics Studied by Higher Order Nonlinear Spectroscopies

In the vibrational spectroscopies it is one of the key issues to distinguish homogeneous and inhomogeneous contributions to vibrational line broadening. Since the homogeneous and inhomogeneous contributions result from rapid perturbation to the oscillator and difference of the environment around the molecule of interest, respectively, it is possible to investigate microscopic liquid dynamics by distinguishing the two contributions. However, it is well known that frequency- or time-domain spectroscopies which are based on the third-order nonlinearlity are incapable of distinguishing the homogeneous and inhomogeneous contributions unambiguously. On the other hand, echo-type experiments, which make use of temporal two-dimentionality, have been proved to be a powerful technique to determine relative importance of inhomogeneity of dephasing process as demonstrated in magnetic resonance. We have been working on vibrational echo-type experiments on liquids in order to distinguish homogeneous and inhomogeneous contributions to the linewidths. This technique requires the application of the two excitations at different times, 0 and Δt_1, and each excitation consists of two short pulses to create vibrational coherent state by Raman transition. Vibratinal coherence is detected by observing anti-Stokes Raman scattering induced by a fifth pulse at $\Delta t_1+\Delta t_2$. Two different experiments, Raman echo and five-pulse correlation experiments, have been performed to study dephasing processes of high frequency intramolecualr and low frequency intermolecular vibrational modes, respectively.

III-B-1 Ultrafast Raman Echo Study on the S-H Stretching of Liquid Ethanthiol

Keisuke TOMINAGA, Ryoji INABA *(Univ. of Tokyo and IMS)*, **Tai Jong KANG** *(Taegu Univ. and IMS)*, **Yukito NAITOH, Keith A. NELSON** *(Massachusetts Institute of Technology and IMS)*, **Mitsuo TASUMI** *(Univ. of Tokyo)*, **and Keitaro YOSHIHARA**

[*in the Proceeding of XIV International Conference on Raman Spectroscopy*, p.444]

The Raman Echo is a phenomenon based on a seventh-order nonlinear process. This technique is capable of distinguishing the homogeneous and inhomogeneous contributions to the *high frequency vibrational* dephasing. In the Raman echo experiment two short pulses for the excitation have different wavelengths whose difference matches the vibratoinal frequency of interest. In Figure 1 Raman echo signals of the S-H stretching of ethanthiol are shown. In the measurements Δt_2 is scanned with fixed Δt_1. At first glance a large difference between the two signals is not observed, which suggests that there is no significant inhomogeneous contribution to the vibrational dephasing. However, since both the signals show non-exponential behavior and differ slightly, direct evidence of the existence of inhomogeneity may be obtained from the further Raman echo measurements and complete analyses on the data, which are currently under progress.

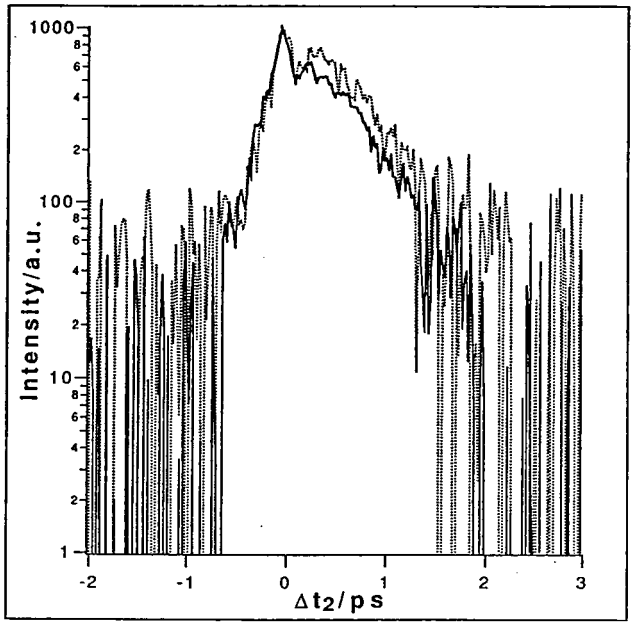

Figure 1. Raman echo signals of the S-H stretching of ethanthiol. Δt_1=0 and 3 ps for solid and dotted lines, respectively.

III-B-2 Fifth Order Optical Response of Liquid CS_2 Observed by Ultrafast Non-Resonant Six-Wave Mixing

Keisuke TOMINAGA, Yukito NAITOH, Tai Jong KANG *(Taegu Univ. and IMS)*, **Gary P. KEOGH** *(Imperial College of Science, Technology, and Medicine and IMS)*, **and Keitaro YOSHIHARA**

[*Ultrafast Phenomena IX*, in press]

The first observation of the fifth order optical response of liquid CS_2 was conducted by ultrafast non-resonant six-wave mixing with five different pulses. The technique allows us to unambiguously distinguish homogeneous and inhomogeneous contributions to *low frequency intermolecular* vibrational modes, and is similar to the Raman echo experiment except that the five pulses have same wavelength.

Figure 1 shows the fifth order signals from CS_2 as a function of Δt_2 with different fixed Δt_1. The dotted lines are the third order signals, which are identical to the fifth order signals within experimental error. The experimental results are consistent with the prediction by Tanimura and Mukamel[1] where a static inhomogeneous contribution is minor.

Reference

1) Y. Tanimura and S. Mukamel, *J. Chem. Phys.* **99**, 9496 (1993).

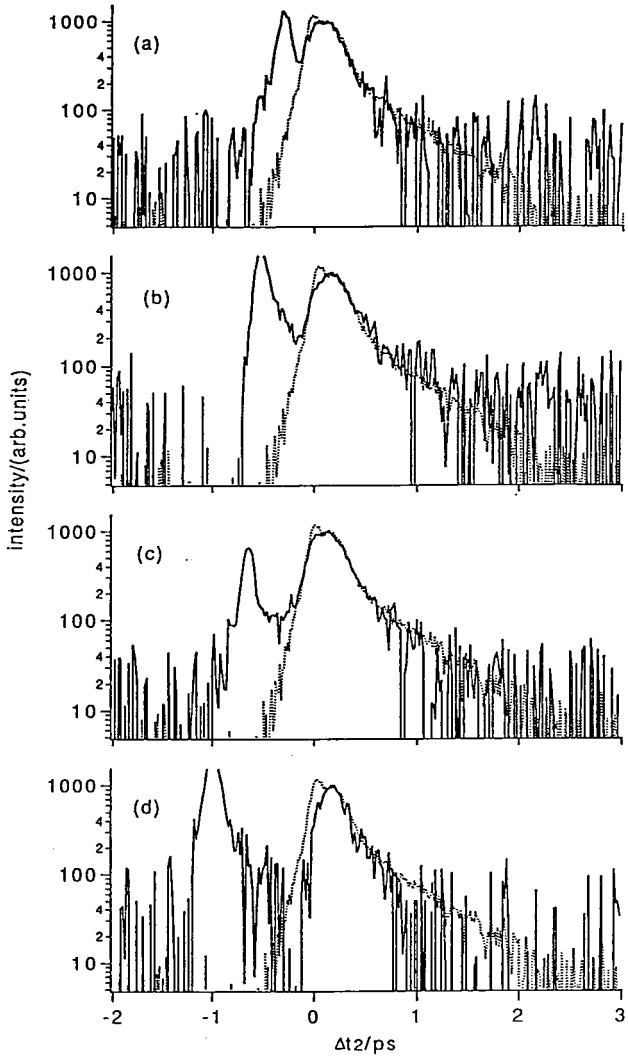

Figure 1. Solid lines; fifth order response signals from CS_2 as a function of Δt_2 with different Δt_1. Δt_1 is (a) 0.33 ps, (b) 0.50 ps, (c) 0.67 ps, and (d) 1.00 ps. Broken lines; the third order signals from CS_2.

III—C Development of Ultrafast Spectroscopic Methods

It is generally recognized that time scale of many elementary processes in chemical reactions and molecular dynamics fall into picosecond and femtosecond region. Development of ultrafast spectroscopic techniques enables us to observe these phenomena in real time. We have been developing suitable apparatuses for research subjects described in section III. This year we have constructed dye-laser-based high power pico- and femtosecond laser systems for multiple pulse scattering experiments.

III-C-1 High Power Pico- and Femtosecond Laser Systems at kHz Repetition Rate

Keisuke TOMINAGA, Yukito NAITOH, Tai Jong KANG *(Taegu Univ. and IMS)*, **and Keitaro YOSHIHARA**

[*in the Proceeding of XIV International Conference on Raman Spectroscopy*, p.444]

For the Raman echo and five-pulse correlation experiments, which are based on higher order nonlinear effects and require high energy pulses, we have developed high power (>10 μJ/pulse) pico-(~8 ps) and femtosecond (<100 fs) laser systems at kHz repetition rate. A home-made CW mode-locked Nd:YAG laser, pico-(~8 ps), and femtosecond (80 fs) dye lasers were used for the generation of the basic light pulses. Femtosecond laser pulses are amplified by a three-dye-stage dye laser pumped by a regenerative Nd:YAG amplifier operating at 3 kHz as shown in Figure 1(a). A thin color filter is placed between the first and second dye cells as a saturable absorber. A pair of the prisms made of BK7 is used to compensate the group velocity dispersion. By adjusting the position of the prism pair and selecting the filter, an amplified pulse as short as 90 fs is available. Without the filter the power of the short pulse goes up to 20 μJ/pulse. For the amplification of the picosecond pulse, preamplification is performed using a six-path bow-tie dye amplifier pumped by the second harmonics of the diode-laser-pumped Nd:YLF laser output (Figure 1(b)). The preamplified pulse with a power of about 1 μJ/pulse is power-amplified by using a dye cell, which is pumped by a part of the output of the YAG regenerative amplifier from the both sides. The final power is about ~10 μJ/pulse. These amplified pico- and femtosecond pulses are sent to the detection systems for the multi-pulse experiments.

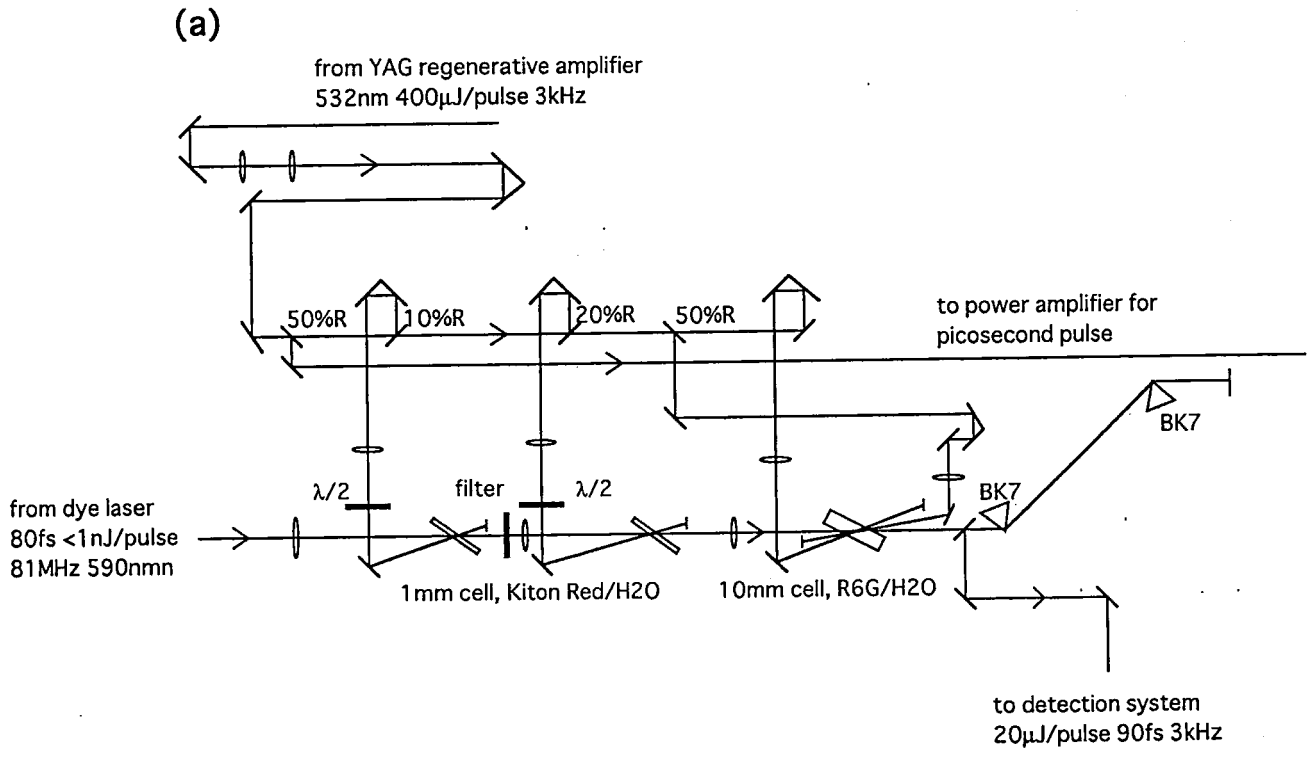

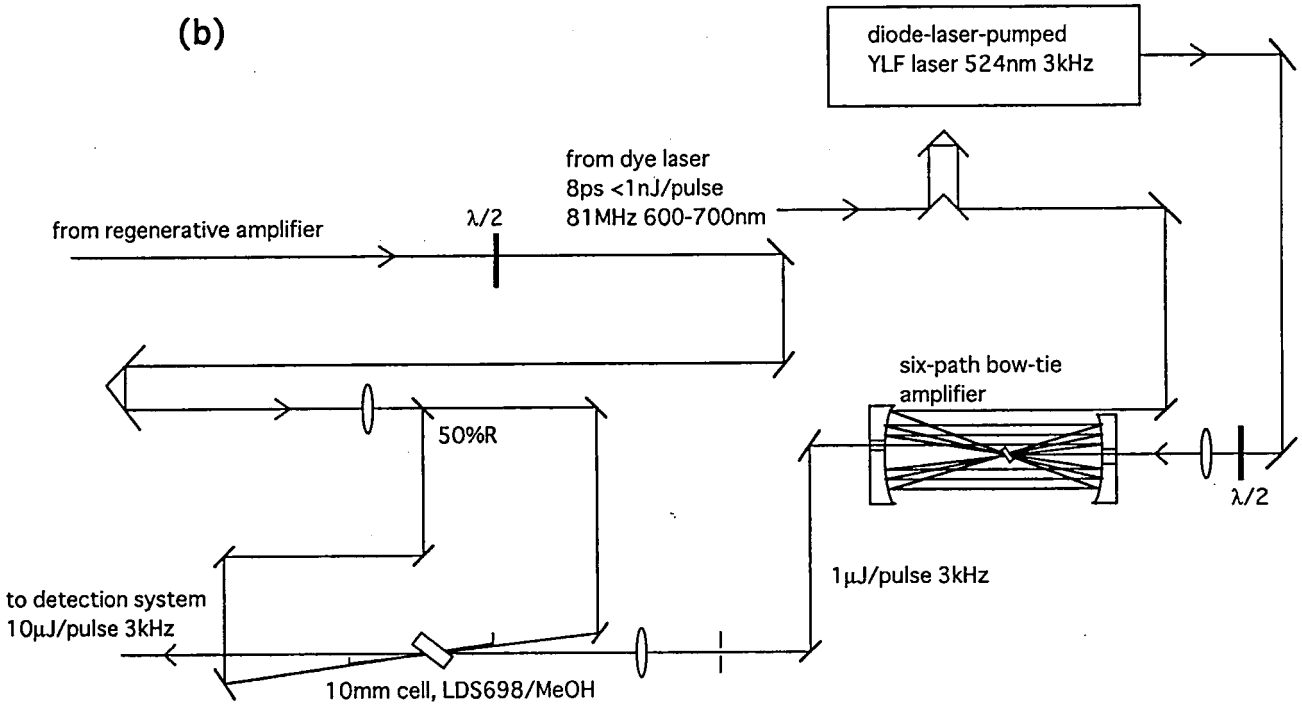

Figure 1. (a) An amplifier system for femtosecond pulse. 10%R, 20%R, and 50%R denote beam splitters with reflection of 10%, 20%, and 50%, respectively. $\lambda/2$ is a half-wave plate. The first and second dye cells contain a solution of Kiton Red in H_2O, and the third cell contains a solution of rhodamine 6G in H_2O. (b) An amplifier system for picosecond pulse. 50%R denotes a beam splitter with reflection of 50%, and $\lambda/2$ is a half-wave plate. A six-path bow-tie amplifier has a dye jet of a solution of LDS698 in ethylene glycol. In the power amplifier a solution of LDS698 in methanol is used.

III-C-2 Detection System for Five-Pulse Correlation Experiment

Keisuke TOMINAGA and Keitaro YOSHIHARA

Figure 1 shows an apparatus for detecting fifth order optical response by a six-wave mixing method. An amplified femtosecond pulse is split into five portions with an equal intensity by four beam splitters. These five pulses are focused by a spherical achromatic lens into the sample contained in a quartz cuvette with a glass thickness of 0.3 mm. The polarizations of the five pulses are controlled by half-wave plates and Glan-Laser prisms. The pulse configuration and polarization condition are shown in the inset in the figure. To eliminate third order signals from the fifth order signal, $\mathbf{k}_1$ and $\mathbf{k}_2$ are chopped at $6f$ (~ 840 Hz) and $\mathbf{k}_1'$ and $\mathbf{k}_2'$ are chopped at $5f$ (~ 700 Hz), and the signal is detected at the difference frequency f (~ 140 Hz) by a lock-in amplifier.

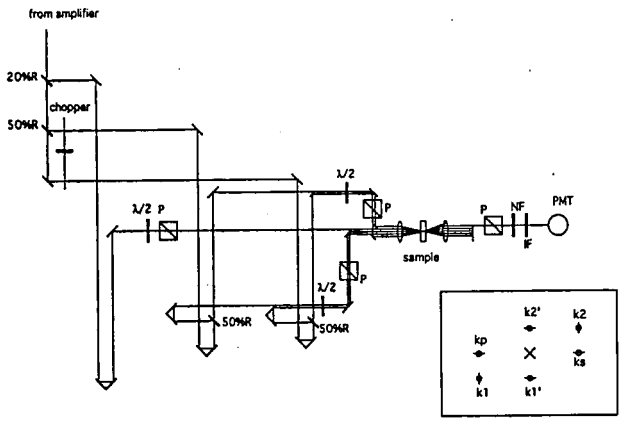

Figure 1. A detection system for fifth order optical response by a six-wave mixing method. 20%R and 50%R denote beam splitters with reflection of 20% and 50%, respectively. $\lambda/2$, P, NF, IF, and PMT are a half-wave plate, Glan-Laser polarizer, neutral density filter, interference filter, and photomultiplier tube. The inset; pulse configuration and polarization condition. A cross indicates the position of the center of the lens. Bars denote the polarizations of the pulses.

III—D Photodissociation Dynamics of Alkali Metal Dimers

Among alkali metal dimers, Cs_2 shows the most complex absorption bands which are due to very compact potential energy curves and large spin-orbit couplings. They are, therefore, suitable to study the predissociation occurring through multichannel interactions. When sufficient energy is provided, alkali dimers can dissociate into fragments that have nonzero angular momentum through many different channels. By applying the resonance enhanced two photon ionization (RE2PI) technique and mass spectrometry to a very cold molecular beam of alkali dimers, new information on the dissociation of the homonuclear and heteronuclear alkali dimers is obtained.

III-D-1 Complex Resonance in the Predissociation of Cs_2

Bongsoo KIM, Keitaro YOSHIHARA, and Sungyul LEE
(Kyunghee University)

[*Phys. Rev. Lett.* **73**, 418 (1994)]

We present detailed quantum mechanical analysis of the complex resonances observed in molecular predissociation. The complex features, which are shown in Figure 1 in the photodissociation spectrum of Cs_2, are reproduced well by the close-coupling calculation including three channels. A very narrow resonance with a linewidth of $\sim 2\times10^{-7}$ cm^{-1} is predicted. It is shown that q-reversal can occur in predissociation with only two channels involved. The calculated q-values under isolated resonance assumption are considerably different from the q-values obtained by 3-channel close-coupling calculations. This shows that the resonances are strongly overlapped.

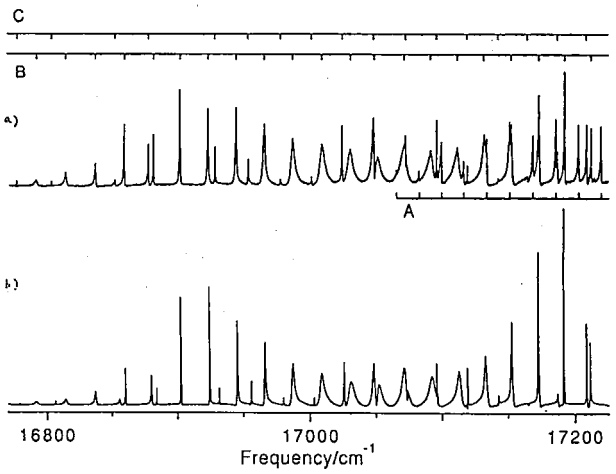

Figure 1. (a) Experimental photofragment yield spectrum obtained by selectively monitoring the Cs ($6^2P_{3/2}$) fragment. (b) Calculated spectrum convoluted by laser linewidth and the rotational state distribution of the initial state assuming a rotational temperature of 1K.

III-D-2 Molecular Resonances in the Predissociation of Cs_2

Bongsoo KIM and Keitaro YOSHIHARA

[*Laser Chemistry*, submitted]

The photodissociation of the orange band of Cs_2 is studied using pump and probe technique as in part shown in Figure 1. Very cold molecular beam of Cs_2 is produced using a high temperature pulsed nozzle. Cs_2^+ ions are produced by resonance enhanced two photon ionization method. A very broad absorption band, which has about 40 cm^{-1} linewidth, is observed near 17000 cm^{-1}. By changing the rotational temperature we showed that the asymmetric resonance lineshapes are not due to rotational structures.

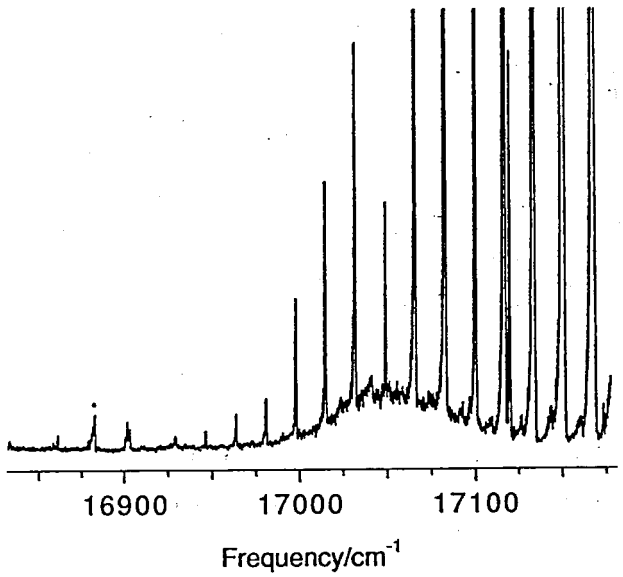

Figure 1. Expanded view of the Resonance-Enhanced-2-photon ionization spectrum of Cs_2.

III—E Exciton Behavior of Dye J-Aggregates

Strong intermolecular interaction in J-aggregate of cyanine dyes leads to enhancement of dipole moment and formation of the excitonic transition, characterized by narrow absorption and emission spectra. Exciton size as well as exciton dynamics in such molecular system can be measured by emission spectroscopy. This year we clarified exciton interaction with acoustical phonons indicated by temperature-dependent measurements and observed emission of two excitions which coexist in J-aggregate at room temperature for 30 ps at high pump intensities.

III-E-1 Temperature Dependence of Superradiant Emission of BIC J-Aggregates

Valey F. KAMALOV *(Inst. Chem. Phys., Russian Acad. and IMS)*, **Irina A. STRUGANOVA** *(Lasers for Photochem. and IMS)*, **Tadaaki TANI** *(Fuji Photo Film)*, **and Keitaro YOSHIHARA**

[*Chem. Phys. Lett.* **220**, 257 (1994)]

The emission lifetime of BIC J-aggregate decreases with increase of the temperature in the range 20—60K as shown in Figure 1(a). This shows the existance of a nonradiative relaxation channel in the BIC J-aggregate in glass. Both lifetime and intensity (shown in Figure 1(b)) were temperature dependent in different manner, indicating that the radiative rate constant is temperature dependence. The main changes of emission characteristics take place at around 40K, which can be attributed to the phonon with 30—40 cm^{-1}. This low frequency is typical for an acoustical phonon and the temperature dependence of emission characteristics can be explained in favor of exciton interaction with an acoustical phonon in the BIC J-aggregate rather than with optical phonon (as it takes place for the PIC J-aggregate[1]).

Reference

1) F. C. Spano, J. R. Kuklinski and S. Mukamel, *Phys. Rev. Lett.* **65**, 211 (1990).

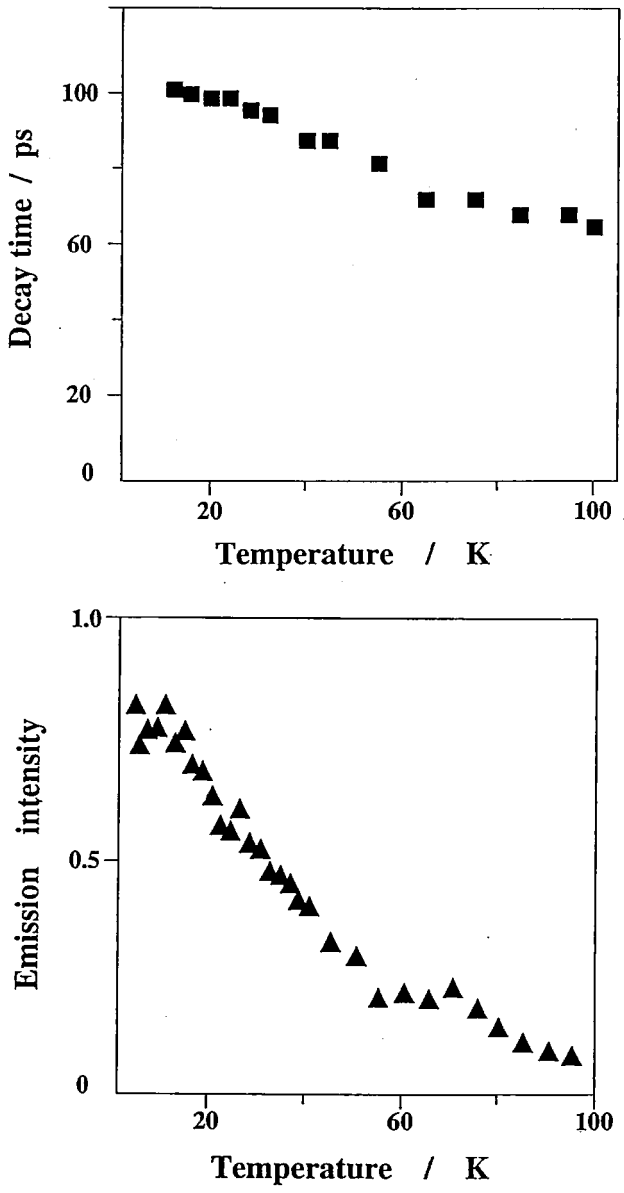

Figure 1. BIC J-aggregate emission decay time (a), emission intensity (b) temperature dependence. Excitation 582 nm.

III-E-2 Two Exciton Emission of J-Aggregates

Valey F. KAMALOV *(Inst. Chem. Phys., Russian Acad. Sci.)*, **Irina A. STRUGANOVA** *(Lasers for Photochem.)*, **Yasushi KOYAMA** *(Kwansei Gakuin Univ.)*, **and Keitaro YOSHIHARA**

[*Chem. Phys. Lett.* **226**, 132 (1994)]

A blue shift and narrowing of emission band of carbocyanine dye (BIC) J-aggregate in solution were observed at high excitation intensity as shown in Figure 1. This is explained by formation of a two-exciton state and efficient emission from the two-exciton state to one-exciton state. The lifetime of the two-exciton state of BIC J-aggregate in solution is 30 ps at room temperature. Repulsive interaction between excitons leads to the high energy (compare to one-exciton) shift of two-exciton transition.

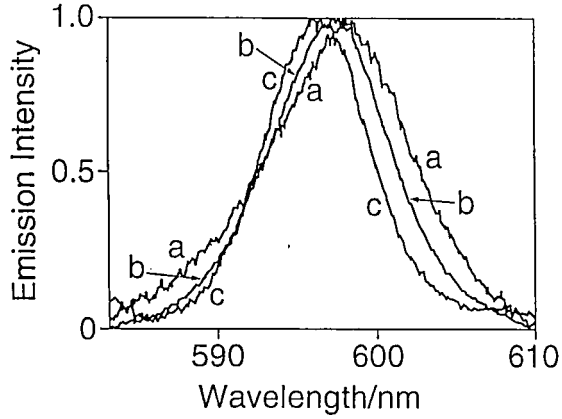

Figure 1. Emission spectra of BIC J-aggregate at different excitation intensities: curve (a) - low intensity $I=6.3\times10^3$ W/cm^2, curve (b) - intermediate intensity $I=3.6\times10^7$ W/cm^2, curve (c) - high excitation intensity $I=1.3\times10^9$ W/cm^2. Excitation wavelength is 527 nm.

III—F Primary Processes in Photosystem I Reaction Center Complex

The reaction center (RC) pigment-protein complexes of photosynthetic organisms undergo light-induced charge separation and convert light energy to the electrochemical potential. The most studied of the RC's are those isolated from the purple bacteria, which contain only six pigment molecules. This relative simplicity has enabled ones to observe the electronic excitation energy and primary electron transfer processes by selective photoexcitation of the pigments. Higher plant and cyanobacteria have two types of photochemical reaction systems which are functioning in series (photosystem I and II (PS I and PS II)). Primary processes in the RC's of PS I and II are scarcely understood for the following reasons. (1) The spectroscopic features of the RC isolated from PS I and II are more congested and overlapped to a higher degree than those of the purple bacterial RC's. (2) Isolation procedures have been less developed in PS I and II than in purple bacteria. The RC of PS II recently isolated seems to have electron carrier molecules and amino acid sequence of the polypeptides which are essentially similar to those of purple bacterial RC's. The RC in PS I, however, has little similarity to that of purple bacteria. The free energy gaps in the primary reaction steps and the electron carrier molecules in PS I RC are different from those in purple bacterial RC. In addition, the amino acid sequence of PS I polypeptides shows almost no homology to that of purple bacteria. We focused on the primary processes in PS I RC. It is interesting to compare the mechanisms in the different types of RCs to extract some essential features in the optimized systems for light energy collection and the following charge separation.

III-F-1 The Primary Photochemical Processes in P700-Enriched Photosystem I Particles: Trap-Limited Excitation Decay and the Primary Charge Separation.

Shigeichi KUMAZAKI, Hideki KANDORI, Hrvoje PETEK, Keitaro YOSHIHARA, and Isamu IKEGAMI *(Teikyo Univ.)*

[*J. Phys. Chem.* **98**, 10335 (1994)]

The energy transfer and primary charge separation in PS I RC particles with an antenna size of 12 chlorophylls (Chls)/P700 was studied by difference absorption spectroscopy. The transition from excited state of Chls to the charge-separated state of $P700^+A_0^-$ (P700; primary donor Chl, A_0; acceptor Chl *a*) proceeded with a time constant of 6.5 ps at ~278 K (Figure 1(a)). The distribution of excitation energy among the Chls seems to be equilibrated within 500 fs (Figure 1(b)). The decay rates of excited states of different Chl forms are almost constant ($t_{1/e}$=9.1 ps) in the region of 660–705 nm (Figure 1(b) and (c)). The decay time constant is almost comparable to the rise time constant of $P700^+A_0^-$ (6.5 ps). These results suggest that the transient signals at 500 fs consist mainly of the bleach of Chls which are rapidly exchanging excitation energy with P700 in subpicosecond time scale and that excitation is quenched at P700 in a few picoseconds. Comparison of the experimental distribution with simulated ones also suggests that excitation energy is distributed within 500 fs highly on P700 and also among other higher-energy Chl forms. On assuming a Boltzmann distribution of excitation energy among all the Chl forms at 278 K, the intrinsic time constant of the electron transfer from excited state of P700 to A_0 is estimated to be 3.0 ps. This reaction seems to be as fast as the primary charge separation in purple bacterial RCs (2.8–4.1 ps).[1)]

Reference

1) C. Kirmaier and D. Holten, *Photsynth. Res.* **13**, 225 (1987).

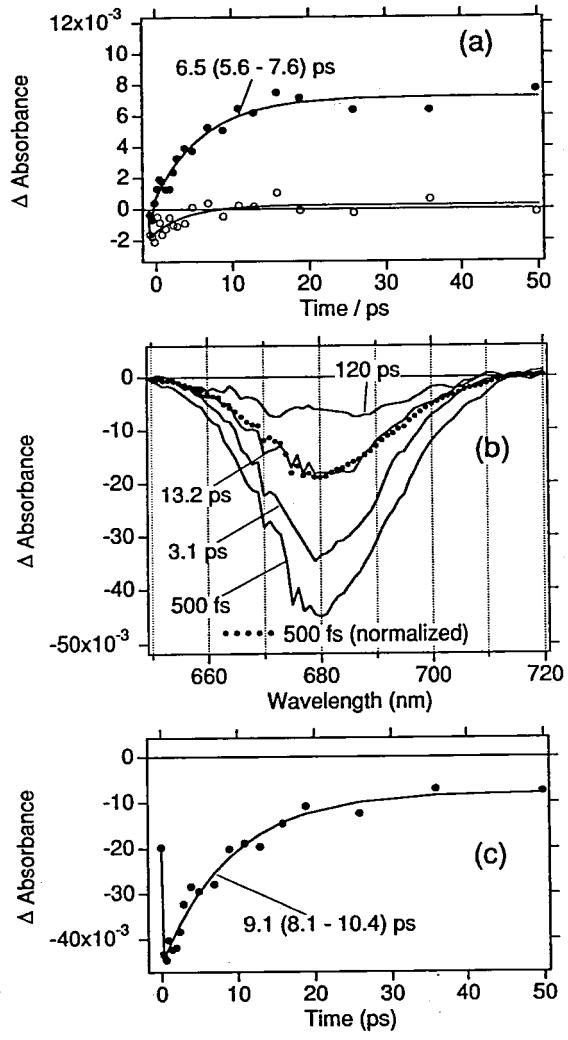

Figure 1. (a) Time dependence of averaged difference absorbance at 740(±10) nm. The open circles represent the data under the P700-preoxidized conditions and closed circles under the P700-neutral conditions. The absorption of the biradical state $P700^+A_0^-$ appears only under the latter conditions. (b) A series of transient absorption spectra only due to excited Chls under the P700-neutral conditions (solid lines). The absorbance changes due to the charge separation (the difference spectrum of $P700^+A_0^-/P700A_0$) were subtracted. The spectrum at 500 fs was reduced to that at 13.2 ps in order to compare the spectral shapes (dots). (c) The decay profile of excited Chls under the P700-neutral conditions. Closed circles are the averaged absorbance changes at 680(±2) nm in the series of spectra in (b).

III-F-2 Rates of Primary Electron Transfer Reactions in Photosystem I Reaction Center Reconstituted with Different Quinones as the Secondary Acceptor

Shigeichi KUMAZAKI, Masayo IWAKI *(NIBB)*, **Isamu IKEGAMI** *(Teikyo Univ.)*, **Hideki KANDORI, Keitaro YOSHIHARA, and Shigeru ITOH** *(NIBB)*

[*J. Phys. Chem.*, in press]

Rates of sequential electron transfer from excited states of Chls to A_0, and to the secondary acceptor quinone (Q_ϕ) were measured in spinach PS I particles. In the particles, 85–90% of antenna Chls are extracted and the intrinsic phylloquinone (Q_ϕ) is removed and replaced by different quinones.

(1) The formation of $P700^+A_0^-$ state occurred with a time constant of 8 ps (τ_1) in the particles with an antenna size of 30 Chls / P700. The $P700^+A_0^-$ state persisted more than 800 ps in the Q_ϕ-depleted particles. (2) After the reconstitution of menaquinone-4, phylloquinone or 2-methyl-1,4-naphthoquinone as Q_ϕ, the transition from $P700^+A_0^-Q_\phi$ to $P700^+A_0Q_\phi^-$ state occurred with time constants (τ_2) of 23, 23 or 34 ps. (3) In the PS I particles with an antenna size of 16 Chls / P700, a similar τ_1 of 11 ps and a τ_2 of 31 ps was observed when menaquinone was reconstituted as Q_ϕ. The main results are summarized in Table 1.

Studies of electron transfer rates between BH^- (bacteriopheophytin *a*) and a variety of reconstituted quinones which gives different $-\Delta G^\circ$ of the reaction in *Rb. sphaeroides* RC showed that reorganization energy for the reaction is 0.6 eV and that the time constant was never shorter than 220 ps in the range of $-\Delta G^\circ$ between 0.2 and 0.8 eV.[1] Based on Marcus electron transfer theory, there seem to be some difference in molecular geometry between PS I and purple bacterial RCs.

Reference

1) M. R. Gunner and P. L. Dutton, *J. Am. Chem. Soc.* **111**, 3400 (1989).

Table 1. Apparant time constants for the formation of $P700^+A_0^-$ (τ_1, time constant for the ground state depletion of A_0)[a] and for the transition from $P700^+A_0^-$ to $P700^+A_0Q_\phi^-$ state (τ_2, time constant for the ground state recovery of A_0)[a] obatined by the subpico- or picosecond difference absorpiton spectroscopy in various PS I preparations.

Preparations (Chl/P700 ratio)	Q_ϕ	τ_1 (ps)	τ_2 (ps)	excitation wavelength (nm)	Excitation intensity (photons/RC)
PS I particles					
Ether-extraction (30)	no added quinone	8±2	n.d.*	605	1.5
	MK	8±2	23±5		
	PhyQ	8±2	23±5		
	MNQ	8±2	34±7		
Ether-extraction (16)	no added quinone	11±3	n.d.*	605	0.8
	MK	11±3	31±6		
Ether-extraction[b] (12)	no added quinone	5.3±0.6 (6.5±1.1)[c]	n.d.*	638	0.4–1.3[d] 0.4–0.8[e]

n.d., not determined

(*) No substantial decay was observed until 800 ps.

a, τ_1, and τ_2 are obtained on the assumption that excitaton decay of Chls is independent of the redox state of P700.

b, This measurement was carried out in III-F-1.

c, Time constant for the rise of the absorption by $P700^+A_0^-$ state was obtained without interference of excitation decay of Chls.

d, τ_1 was almost constant in this excitation intensity range.

e. Excitation intensity range which gives 6.5 ps for the rise of absorption by $P700^+A_0^-$ state.

III—G Dynamic Behavior of Electronic Excited States

Optical excitation of molecules to electronically excited states causes a variety of dynamical behavior, depending upon the nature of electronic structures and environments, such as energy transfer, proton transfer, chemical reaction, radiationless transition, ionization, and others. Most of these processes fall into the nanosecond, picosecond and femtosecond times scales. In this chapter we firstly discuss our observation of the transition state of cis-trans isomerization. Secondly we report picosecond transient absorption of aqueous tryptophan. Thirdly we describe excited state intermolecular proton transfer of 3,4-benzotropolone and finally of 2-(3′-hydroxy-2′-naphthyl)benzimidazole.

III-G-1 Evidence for Quantization of the Transition State for cis-trans Isomerization

Young S. CHOI *(Inha Univ. and IMS)*, **Taek-Soo KIM** *(Inha Univ. and IMS)*, **Hrvoje PETEK, Keitaro YOSHIHARA, and Ronald L. CHRISTENSEN** *(Bowdoin College)*

[*J. Chem. Phys.* **100**, 9269 (1994)]

Cis-trans isomerization rates of trans, trans-1,3,5,7-octatetraene (OT) on the first excited singlet state (2^1Ag) potential surface have been obtained as a function of vibrational energy by measuring the fluorescence lifetimes as shown in Figure 1. A stepwise increase in the isomerization rate with increasing energy has been observed, which indicates quantization of the vibrational levels of the transition state for the cis-trans isomerization of a double bond. The energy spacing of 80 ± 10 cm^{-1} between the first two steps tentatively is assigned to an in-plane bending vibration of the transition state.

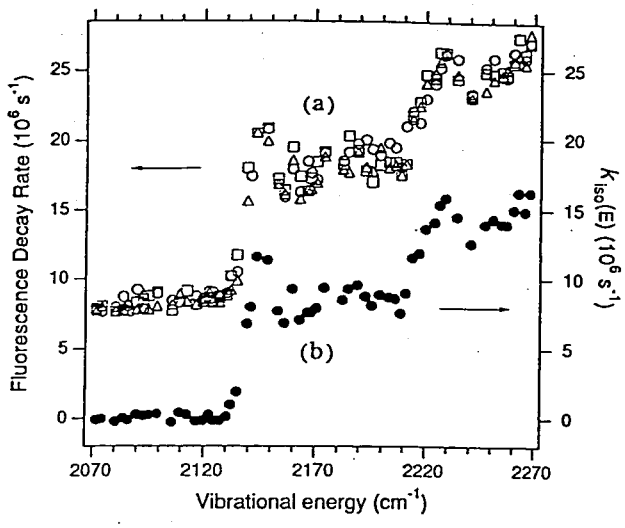

Figure 1. Curve (a): Fluorescence decay rates of trans,trans-1,3,5,7-octatetraene (OT) excited to its first excited singlet state (S_1) with vibrational energies from 2070 to 2270 cm^{-1}. The decay rate varies in a stepwise manner with energy. Curve (b): Isomerization rate constants OT (S_1) obtained by subtracting the contribution of other decay channels in the same vibrational energy range as for curve (a). Two steps, one around 2140 cm^{-1} and the other around 2220 cm^{-1}, indicating quantization of the transition state for cis-trans isomerization of double bond, are clearly noticeable.

III-G-2 Picosecond Transient Absorption of Aqueous Tryptophan

Hideki KANDORI, Raymond F. BORKMAN *(Georgia Institute of Technology and IMS)*, **and Keitaro YOSHIHARA**

[*J. Phys. Chem.* **97**, 9664 (1993)]

The primary photophysical and photochemical processes of aqueous tryptophan (Trp) are studied by picosecond transient absorption spectroscopy. Upon excitation of Trp at 292 nm, transient absorption appears within 1.5 ps in the whole visible region and remains for at least 400 ps. Under the present excitation conditions, the transient absorptions due to solvated electrons and the excited triplet state of Trp are relatively weaker, and the observed transient spectrum is predominantly due to excited singlet-state absorption $S_n \leftarrow S_1$.

III-G-3 Dual Fluorescence and Excited-State Intramolecular Proton Transfer in Jet-Cooled 3,4-Benzotropolone

Hiroshi SEKIYA *(Kyushu Univ.)*, **Mariko HABU** *(Kyushu Univ.)*, **Hiroki UJITA** *(Kyushu Univ.)*, **Takeshi TSUJI** *(Kyushu Univ.)*, **Akira MORI** *(Kyushu Univ.)*, **Hitoshi TAKESHITA** *(Kyushu Univ.)*, **Yukio NISHIMURA** *(Kyushu Univ.)*, **Hrvoje PETEK, and Keitaro YOSHIHARA**

[*Chem. Phys. Lett.* **215**, 641 (1993)]

The S_0-S_1 fluorescence excitation and dispersed fluorescence spectra of 3,4-benzotropolone have been measured in a supersonic free jet. The molecule shows dual fluorescence from the normal and tautomeric forms in the regions of 385–450 and 450–550 nm, respectively. The existence of a potential energy barrier to excited-state proton transfer has been suggested.

III-G-4 Picosecond Vibrational Relaxation in the Excited-State Proton-Transfer of 2-(3′-Hydroxy-2′-Naphthyl) Benzimidazole

Abderrazzak DOUHAL *(Institute de Quimica Fisica Rocasolano CSIC and IMS)*, **F. AMAT-GUERRI** *(Institute de Quimica Organica, CSIC)*, **A. U. ACUÑA** *(IQO, CSIC)*, **and Keitaro YOSHIHARA**

[*Chem. Phys. Lett.* **217**, 619 (1993)]

The fluorescence of 2-(3′-hydroxy-2′-naphthyl) benzimidazole in solution shows two bands at ≈400 and 600 nm, respectively assigned to the open-enol form bound to the solvent, and to the phototautomer produced from the closed-enol form. Both enol species coexist in the ground state. A fluorescence risetime of 16 ps has been attributed to the vibrational cooling-process of the excited phototautomer.

III—H Photochemistry on Well-Defined Surfaces

Recently, it has been found that upon the irradiation of light from visible to ultraviolet, a number of adsorbed molecules on metal surfaces reveal variety of photochemical processes, including photo-stimulated desorption, rearrangement of adsorbed states, photodissociation, and photo-initiated reactions with coadsorbates. Since photo-initiated reactions can be induced without any thermal activation of reactants, various combinations of coadsorbates can be prepared at sufficiently low surface temperatures. Thus, this provides a method for studying a new class of surface reactions which may not be induced thermally. In the last year, we studied photochemistry of adsorbates on well-defined metal surfaces mainly by temperature-programmed desorption (TPD) and time-of-flight (TOF) spectroscopy. In this year a couple of modifications in the UHV apparatus: (1) X-ray photoelectron spectroscopy (XPS) has been introduced. This reinforces our ability to clarify adsorbed states and is useful for the measurement of adsorbate coverage. (2) A closed-cycle He refrigerator is equipped with a sample manipulator. This improves our cooling capability; single crystals can be effectively cooled to ~40 K. In this year, we have focused on surface photochemistry and dynamics on semiconductor surfaces. These surfaces are more corrugated and have electronic structure quite different from metal surfaces. Therefore, the comparison with the measurements done with metal surfaces helps to understand a role of solid surfaces in surface photochemistry.

III-H-1 Adsorbed-State Specific Photodissociation Dynamics of N_2O on Si(100)

Hiroyuki KATO *(Graduate Univ. for Advanced Studies)*, **Yoshiyasu MATSUMOTO, Kyoichi SAWABE, and Jihwa LEE**

[submitted to *J. Chem. Phys.*]

Photodissociation dynamics (PDIS) of adsorbed molecules depends on adsorbed states involved. However, only a few studies have been conducted for elucidating PDIS dynamics of adsorbates on metal and semiconductor surfaces below one monolayer. In this paper, we report a remarkable dependence in the PDIS dynamics on the adsorbed state of N_2O on Si(100) at a submonolayer coverage. Photodissociation dynamics of N_2O on Si(100) at 193 nm has been studied by the measurement of time-of-flight (TOF) distributions of N_2 photofragments. Measurements of temperature-programmed desorption and X-ray photoelectron spectroscopy indicate that there are two adsorbed states of N_2O: weakly bound N_2O mainly on clean Si(100) and strongly bound N_2O on partially oxidized Si(100). Some of weakly bound N_2O are converted to a more strongly bound state when the surface is partially oxidized thermally and/or photochemically. N_2O in the two adsorbed states are dissociated with the irradiation of UV photons to produce an oxygen atom and N_2. The TOF distributions of N_2 photofragments show prominent two velocity components whose average translational energies are 0.80 ± 0.10 and 0.27 ± 0.02 eV, respectively. Controlled experiments on the adsorbed state of N_2O strongly indicate that the fast N_2 is originated in the strongly bound N_2O and the slow N_2 in the weakly bound N_2O.

III—I Activation of Methane

Since methane is the most abundant component of natural gas, converting methane to useful basic chemical products is one of the most important processes in industry. Since methane is the least reactive alkane, it is vital to develop new conversion methods directly transforming methane to products such as alcohols and higher hydrocarbons. Furthermore, it is very interesting to understand scientifically how methane is activated. Thus, the issue of "methane conversion" is a great challenge for chemists and now under intense study. Among catalytic processes in methane conversion, C-H bond cleavage on catalyst surfaces, i.e., "C-H bond activation", is generally considered to be the initial and most crucial step. While major efforts for C-H bond activation have been made to search catalysts on which methane dissociatively chemisorbed, we have taken photochemical approach in this study. It is well known that methane in the gas phase is transparent from visible to UV and has a continuous absorption band only in vacuum ultraviolet. Hence, methane dissociation through excitation of the band requires intense VUV photons that are not easily obtainable from conventional light sources and lasers. Thus, utilization of VUV photons for C-H bond activation is costly and not practical. However, we have found that methane physisorbed on Pt(111) can be effectively dissociated with the irradiation of 193 nm-photons, yielding a chemisorbed CH_3 radical and an adsorbed H atom as products. To our knowledge, this is the first observation of UV-photodissociation of methane on a well-defined surface. Furthermore, this study opens a new way to activate methane by the UV photons that can be readily obtained with a commercially available excimer laser.

III-I-1 Photochemical C-H Bond Activation of Methane on a Pt(111) Surface

Yuri A. GRUZDKOV, Kazuo WATANABE, Kyoichi SAWABE, and Yoshiyasu MATSUMOTO

[*Chem. Phys. Lett.* **227**, 243 (1994)]

Photodissociation of methane physisorbed on Pt(111) has been studied by post-irradiation temperature-programmed desorption (TPD). Figure 1(a) shows a typical TPD spectrum measured at m/e=13(CH^+) after the exposure of 1.6 L (1 L=10^{-6} Torr · s) of methane at 40 K. The TPD spectrum shows only a strong desorption peak denoted to α at 73 K. Fig. 1(b) shows a post-irradiation TPD spectrum of methane. The surface was first saturated with methane and then irradiated with the total of 5.6×10^{18} photons/cm^2 at 193 nm. The intensity of the desorption peak decreases and a new desorption peak of methane at ~260 K grows with the accumulated number of photons. This new desorption peak is attributed to recombination of CH_3 and H on Pt(111). This finding clearly indicates that methane on Pt(111) is dissociated to a chemisorbed CH_3 radical and an adsorbed H atom as products under the irradiation of 193-nm photons. This is markedly different from photodissociation in the gas phase, where vacuum ultraviolet photons are required to dissociate methane. The total cross section of photochemical processes is estimated to be 1.5×10^{-19} cm^2.

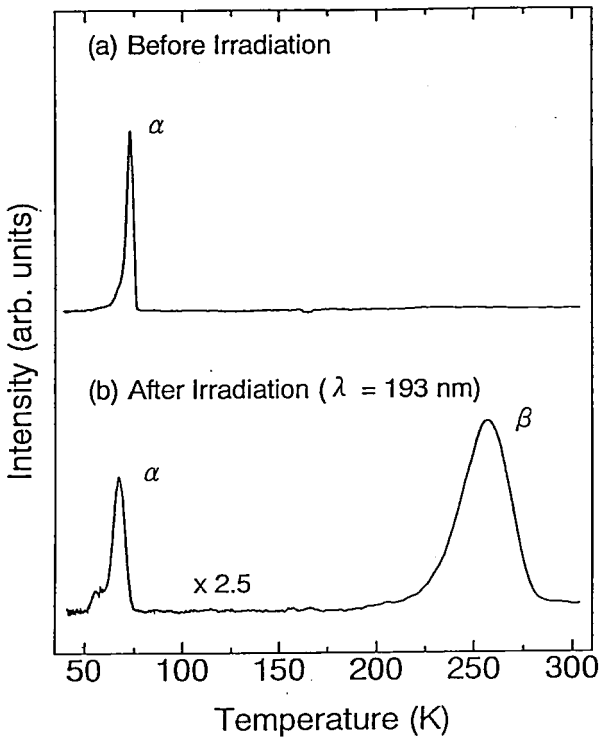

Figure 1. TPD spectra of methane (a) before and (b) after irradiation of 193-nm photons on the Pt(111) surface saturated with methane at 40 K. Signals are detected at m/e=13 (CH^+). The number of photons directed on the surface along the surface normal is 5.6×10^{18} cm^{-2}. The heating rates were 0.3 and 5.0 Ks^{-1}, below and above 164 K, respectively.

III—J Reactions of Coadsorbed Species on Well-Defined Surfaces

Vast majority of surface reactions studied so far has been interpreted in terms of a Langmuir-Hinshelwood mechanism; reactants are first adsorbed on a surface and a reaction takes place between two chemisorbed species. Therefore, it is very important to investigate how reactions occur among coadsorbed species on a well-defined surface. For this purpose, coadsorbed species are prepared at sufficiently low surface temperatures and reactions are induced by annealing the surface. Here, we mainly focus on an important class of surface reactions, i.e. oxidation on metal surfaces. Although the reactivity of atomic oxygen has been thoroughly investigated, the role of molecular oxygen in oxidation reactions has been hardly known. In the last year, we showed that molecular oxygen of Pt(111) reveals high reactivity in oxygen-exchange reaction with coadsorbed NO by temperature-programmed desorption. In order to clarify reaction mechanisms, we have further carried out infrared reflection absorption spectroscopy (IRAS) experiments on the coadsorbed system.

III-J-1 The Reactivity of Molecular and Atomic Oxygen in Oxygen-Exchange Reaction between NO and O_2 Coadsorbed on a Pt(111) Surface

Kyoichi SAWABE, Yoshiyasu MATSUMOTO, Jun YOSHINOBU *(RIKEN)*, **and Maki KAWAI** *(RIKEN)*

[submitted to *Surf. Sci.*]

The oxygen exchange reaction between $N^{16}O$ and $^{18}O_2$ coadsorbed on Pt(111) has been studied by temperature-programmed desorption, low energy electron diffraction (LEED) and Fourier transform infrared reflection absorption spectroscopy (IRAS). While the reaction product of $^{18}O^{16}O$ desorbs at 155K, $N^{18}O$ desorbs 145, 310 and 340 K. Reaction schemes are quite different in two different temperature regimes. At ~145K molecularly adsorbed oxygen is responsible for the exchange reaction. Since IRAS spectra show no signature of complex formation between NO and oxygen, it is likely that the exchange reaction proceeds via a transient complex between NO and molecular oxygen. Only above 270 K an absorption band of $N^{18}O$ is observed. This indicates that the exchange reaction takes place with atomic oxygen above this temperature. The oxygen-exchange reaction is greatly suppressed when NO is coadsorbed on the surface with p(2×2) well-ordered oxygen. Evolution of LEED patterns obtained from the coadsorbed surfaces as a function of annealing temperature indicates that coadsorbed NO disturbs the diffusion of oxygen adatoms. Therefore, the meta-stable oxygen adatoms that do not posses a long-range order are mainly responsible for the exchange reaction above 270 K.

III—K Dynamic Processes in Electronically-and/or Vibrationally-Excited Molecules

Fundamental molecular aspects of chemical reactions and energy transfer processes in the electronically or vibrationally excited states have been studied. Particular interests have been directed to the study of the photochemical reaction dynamics of carbonyl compounds, to the dynamics of vibrationally-excited van der Waals complexes using the stimulated-emission-pumping-laser-induced-fluorescence spectroscopy and the hole-burning spectroscopy, and to the photochemical reaction dynamics of the weakly-coupled complexes such as van der Waals and hydrogen-bonded complexes. Some applications of the stimulated-emission-pumping-laser-induced-fluorescence spectroscopy and the hole-burning spectroscopy are also presented to determine the molecular geometries and the vibronic structures in the excited electronic states.

III-K-1 Fragment Rotational Excitation due to the Parent Rotation in the Dissociation of Molecules

Ichiro HANAZAKI

[*Chem. Phys. Lett.* **218**, 151 (1994)]

An analytical expression is derived to estimate how much parent rotational energy is carried over to the fragment rotation when a molecule is dissociated. The model is based on the classical treatment of rotational motion, by which the effect can be estimated separately from other sources of rotational excitation. It can readily be applied to the parent and fragment molecules of any size and of any type. Some illustrative examples of its application are given to demonstrate the relative importance of the parent rotation in exciting the fragment rotation.

III-K-2 Photochemistry of $N_2O \cdot H_2O$ Complexes Produced in Supersonic Jets

Hong-Lae KIM, Masao TAKAYANAGI, and Ichiro HANAZAKI

[*Chem. Phys. Lett.* **222**, 431 (1994)]

We have studied the 193 nm photodissociation of $N_2O \cdot H_2O$ complexes produced in a supersonic jet resulting in the reactant pair reaction, $N_2O \cdot H_2O + h\nu \rightarrow 2OH + N_2$. The internal energy in the product OH radicals and the relative populations over the spin-orbit and Λ-doublet sublevels have been determined by the laser-induced fluorescence technique, suggesting a reaction scheme much different from the corresponding bimolecular reaction, $O(^1D) + H_2O \rightarrow 2OH$, observed in bulb experiments. The bimolecular reaction gives distinctly different rotational and vibrational distributions for OH produced by the abstraction by $O(^1D)$ and that left after the abstraction; the former carries much higher internal energy than the latter. This result seems to suggest the direct abstraction reaction in the case of the bimolecular reaction. On the other hand, there is little difference between the rotational or vibrational distributions for two OH groups formed in the reactant-pair reaction. The total internal energy is also much lower than that for the bimolecular reaction. These results indicate that the reactant-pair reaction should proceed nearly adiabatically through the $O(^1D) \rightarrow O(^3P_2)$ curve crossing and a relatively long-lived reaction intermediate.

References

1) P. Andresen and E.W. Rothe, *J. Chem. Phys.* **82**, 3634 (1985).

2) I. Hanazaki, *Chem. Phys. Lett.*, **201**, 301 (1993).

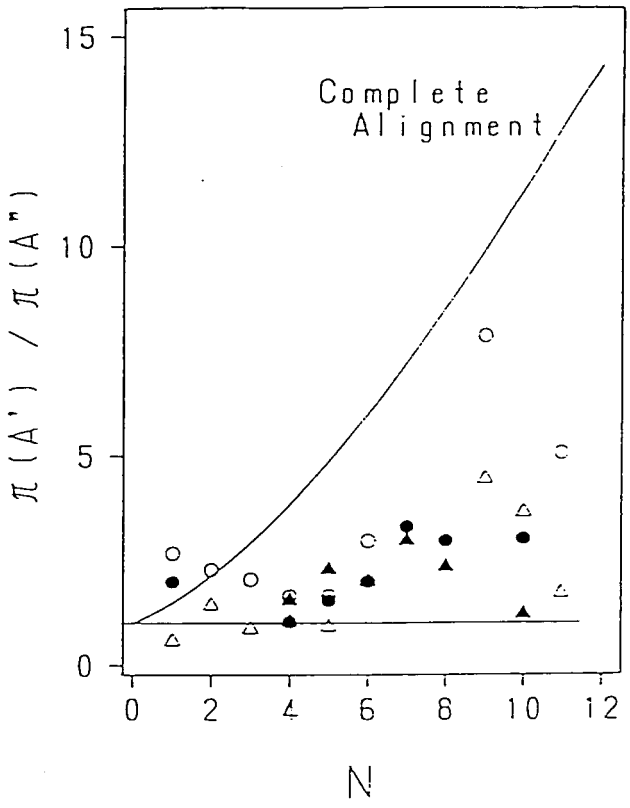

Figure 1. Population distibution in the two Λ-doublet states of OH measured from the R_1/Q_1 (○), R_2/Q_2 (●), P_1/Q_1 (△) and P_2/Q_2 (▲) transitions. Solid curves are calculated from Andresen and Rothe for the complete alignment[1] and from Hanazaki[2] for unconstrained dynamics, respectively.

III-K-3 Intermolecular Vibration and Dynamics of the Anisole-Benzene Complex Studied by Multi-Resonance Spectroscopy

Masao TAKAYANAGI and Ichiro HANAZAKI

[*Spectrochim. Acta* **50A**, 1435 (1994)]

The intermolecular vibrations of the anisole-benzene complex in the ground and excited electronic states have been observed by the LIF (laser-induced fluorescence) and fluorescence-dip techniques. Short progressions due to the intermolecular vibrations suggest a small structure change of the complex upon electronic excitation. The LIF excitation spectrum shows predominant progressions with the spacing of 27 cm^{-1}, which is tentatively assigned to one of the intermolecular bending modes in the excited electronic

state. On the other hand, the fluorescence-dip spectrum shows only a series of bands with irregular intervals due to the intermolecular modes in the ground electronic state. The decay rates of the vibrationally excited complex in the ground electronic state have also been measured with the SEP-LIF (stimulated emission pumping-laser induced fluorescence) technique, where the complex vibrationally excited by SEP is probed by the delayed LIF measurements (Figure 1). The complex excited to its purely intermolecular mode stays in the initially prepared state after a delay time of 1 μs. On the other hand, the complex excited to the intramolecular vibrational states above 500 cm^{-1} does not seem to stay in the prepared states. Neither the relaxed complex nor the dissociated monomer was detected. A possible reason for this observation is discussed.

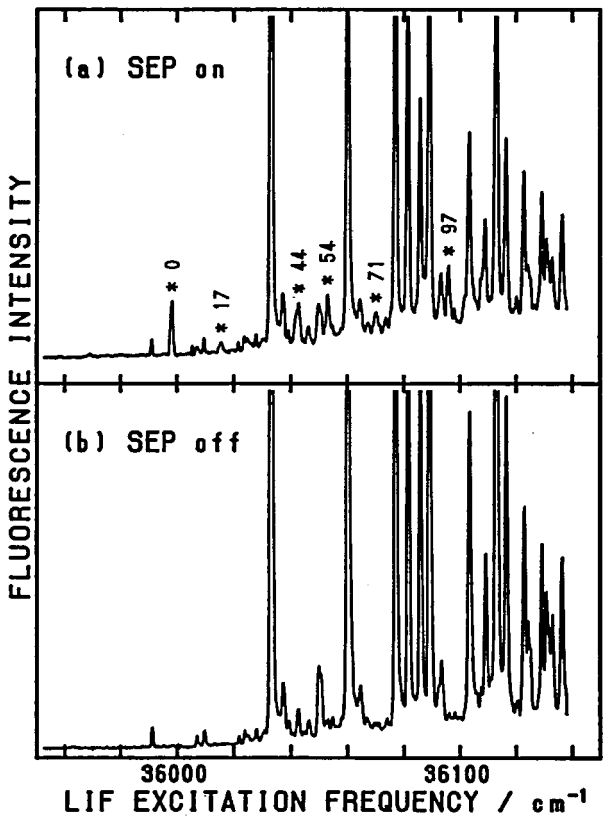

Figure 1. LIF-excitation spectrum measured with (a) and without (b) the SEP excitation of the anisole-benzene complex to the 35 cm^{-1} vibrational state. In (a), bands appearing upon SEP excitation are marked with asterisks, together with the frequency shifts from the band due to the transition from the initially excited vibrational state to $v'=0$ at 35999 cm^{-1}.

III-K-4 Vibrational Energy Distribution in the Photofragment HCO Produced by the Photodissociation of Propionaldehyde in a Supersonic Jet

Tatsuo GEJO *(Grad. Univ. Adv. Studies)*, **Masao TAKAYANAGI, and Ichiro HANAZAKI**

The nascent vibrational energy distribution in HCO produced by the photodissociation of propionaldehyde was measured under the supersonic-jet condition with the pump-probe technique. The pump wavelength was varied between 330 and 277.5 nm. The threshold wavelength for the production of the ground state HCO was found to be 328.5 nm, while those for the bending and CO-stretching excitations of the fragment were 317.5 and 310 nm, respectively. The excess energy above the reaction barrier was found to be distributed statistically among the fragments' degrees of freedom. The result is similar to that for acetaldehyde reported previously.

III-K-5 The C=O Stretching Frequency in the S_1 (π^*-n) State of Acetaldehyde and Its Deuterated Derivatives Determined with the Photofragment Excitation Spectroscopy

Takumi KONO *(Grad. Univ. Adv. Studies)*, **Masao TAKAYANAGI, and Ichiro HANAZAKI**

[*Laser Chem.*, in press]

The vibrational structure was recorded for the S_1 (π^*-n) state of acetaldehyde (CH_3CHO) and its deuterated derivatives (CH_3CDO, CD_3CHO and CD_3CDO) up to ~3500 cm^{-1} above the 0–0 bands with the LIF (laser-induced fluorescence) and PHOFEX (photofragment excitation) techniques (Figure 1). In the PHOFEX spectroscopy, the yield of the formyl radical, $HCO(\tilde{X})$ or $DCO(\tilde{X})$, produced in the photodissociation of acetaldehyde is measured against the excitation frequency. The yield was determined by monitoring one of the rotational lines in the $\tilde{B} \leftarrow \tilde{X}$ transition of the formyl radical by the LIF technique. This is the first measurement of the vibronic structure of acetaldehydes in supersonic jets above the dissociation threshold where they are non-fluorescent. The results have made it possible to locate ν_4 (the C=O stretching) and $2\nu_4$ bands unequivocally; the ν_4 fundamentals appear at 1217, 1189, 1210 and 1178 cm^{-1} above the 0–0 band for CH_3CHO, CH_3CDO, CD_3CHO and CD_3CDO, respectively. The corresponding overtone ($2\nu_4$) bands are observed, respectively, at 2414, 2350, 2399 and 2334 cm^{-1}. All the vibronic bands newly observed in the PHOFEX spectra are found to be interpreted as the combinations of ν_4 and $2\nu_4$ with the modes appearing in the lower frequency (< 1200 cm^{-1}) region, which consist of ν_{10} (the C-C-O in-plane bending), ν_{14} (the C=O out-of-plane wagging) and ν_{15} (the methyl torsion).

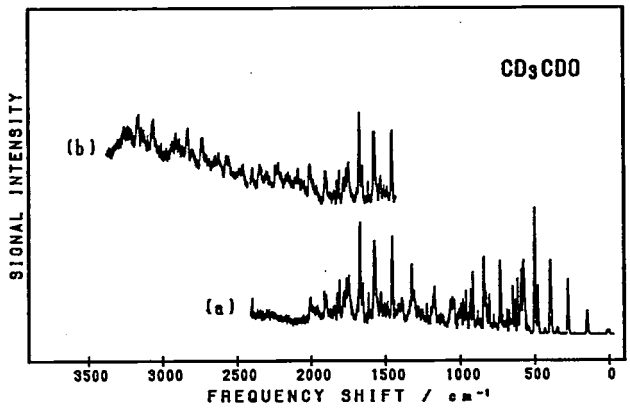

Figure 1. (a) LIF-excitation and (b) PHOFEX spectra of CD_3CDO in a supersonic jet. The ordinate shows the frequency shift from the 0–0 band at 29810 cm^{-1}.

III-K-6 Photodissociation Dynamics of Acetaldehyde. Vibrational Energy Distribution in the Photofragment HCO

Tatsuo GEJO*, Masao TAKAYANAGI, Takumi KONO*, and Ichiro HANAZAKI *(*Grad. Univ. Adv. Studies)*

[*Chem. Phys. Lett.* **218**, 151 (1994)]

Vibrationally excited HCO radicals have been observed in the photodissociation of acetaldehyde in a supersonic jet with the pump-probe technique. The threshold wavelength for the bending and CO-stretching excitations was 308.7 and 302.6 nm, respectively. The nascent vibrational distribution relative to the ground state has been determined as a function of the excitation wavelength in the 280–330 nm region. The observed vibrational distribution of HCO is found to be consistent with the model in which the excess energy above the reaction barrier is statistically distributed among the fragments' degrees of freedom (Figure 1).

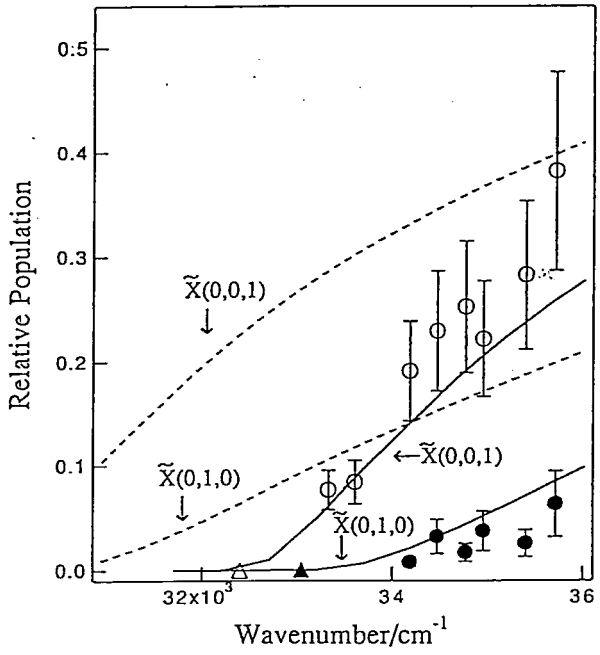

Figure 1. Relative population in the HCO, $\tilde{X}$ (0,0,1) (○) and $\tilde{X}$ (0,1,0) (●) levels to that in the $\tilde{X}$ (0,0,0) level. The curves are the results of the calculation based on the statistical model. (—) The available energy is taken to be the excess energy above the barrier height. (---) The available energy is taken to be the total energy released. The triangles shows the threshold energies.

III-K-7 Applications of the Hole-Burning Spectroscopy in Molecular Beam Experiments

Masao TAKAYANAGI and Ichiro HANAZAKI

[*J. Spectrosc. Soc. Jpn., in press*]

The hole-burning technique was applied to some molecules and van der Waals complexes in molecular beams. The advantage of applying this technique is in that (1) the electronic spectrum of a single species among several in a molecular beam can be measured selectively, and in that (2) the short-lived vibronic state which cannot be detected with the fluorescence or ionization technique can be probed. The electronic transitions of a molecule and its van der Waals complexes usually appear in the same energy region and it is rather difficult to distinguish the transitions of a specific species from those of others in the LIF-excitation spectra. The hole-burning technique enables the measurements of the spectra of a single species selectively; e.g., the excitation spectra of anisole monomer, anisole · Ar, and anisole · Ar_2 are measured selectively. Similarly, the transitions of the isomers or the species in the different vibrational states can be measured selectively with this technique. The spectra of *m*-cresole isomers, each of which stays in the ground vibrational and torsionally excited vibrational states, can be also separated (Figure 1). As the demonstration of the second advantage of the hole-burning technique, the spectrum of vinoxy radical is shown, where non-fluorescent vibronic states are observed. The preferable measuring conditions and the limitation of the applicability are discussed. The possible applications of this technique in the future are also discussed.

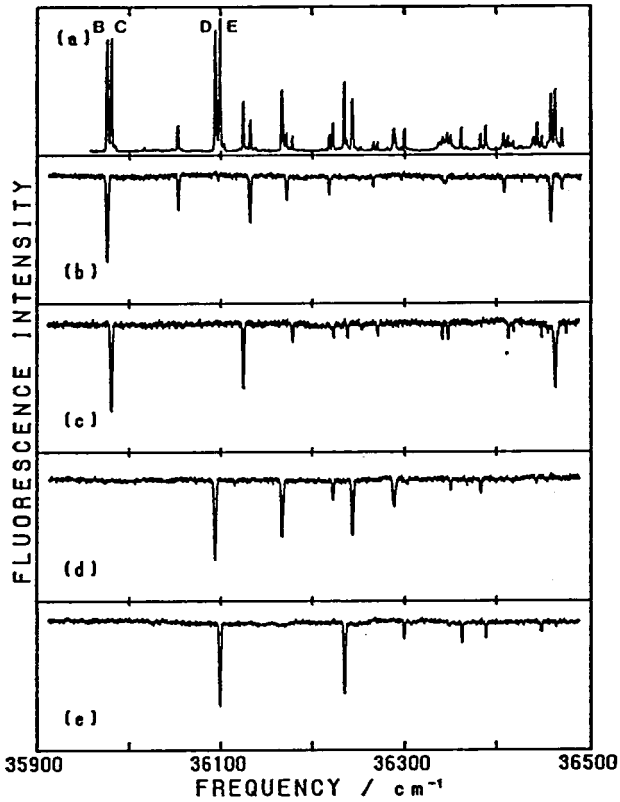

Figure 1. (a) LIF-excitation spectrum of *m*-cresole in a supersonic jet, where the transitions of four species (two isomers in the ground and low-lying excited vibrational states) are observed. (b)–(e) Hole-burning spectra measured with the probe frequencies set, respectively, at the band B–E observed in (a). Spectrum of each species is selectively observed.

III-K-8 Vibrational and Rotational State Distributions of OH Produced in the Reaction $O(^1D)+H_2O$

Masao TAKAYANAGI, Hong-Lae KIM *(Kangweon National Univ.)*, **and Ichiro HANAZAKI**

Vibrational and rotational state distributions of OH produced in the reaction $O(^1D)+H_2O$ were measured, and compared with that produced in the 193 nm photolysis of

the $N_2O \cdot H_2O$ complex. Upon the 193 nm irradiation to the mixture of N_2O (70 mTorr) and H_2O (10 mTorr) flowed in a cell, N_2O dissociates to N_2 and $O(^1D)$, the latter of which reacts with H_2O to produce two $OH(X^2\Pi)$'s. The state distributions were probed with the delayed LIF measurement. The OH produced in the bimolecular reaction was found to be rotationally and vibrationally much hotter than that produced from the complex. The rotational temperatures of OH produced in the bimolecular and complex reactions are about 3000 and 2000 K, respectively. About 45 and 12% of OH was found in $v''=1$ for the bimolecular and complex reactions, respectively. These results are similar to those for the reaction of the $O_3 \cdot H_2O$ complex and the corresponding bimolecular reaction.[1] The bimolecular reaction, $O(^1D)+H_2O$, seems to proceed via the direct abstraction-type mechanism.

Reference

1) D. G. Sauder, J. C. Stephenson, D. S. King, and M. P. Casassa, *J. Chem. Phys.* **97** 952 (1992); D. S. King, D. G. Sauder, and M. P. Casassa, *J. Chem. Phys.* **100** 4200 (1994).

III—L Self-Organization in Chemical Reactions

The self-organizing process in chemical systems is known to occur as a result of nonlinear chemical processses. This kind of chemical systems exhibit sustained temporal chemical oscillations and spatial pattern formation. Moreover, they sometimes exhibit more complicated nonlinear phenomena such as bistability, excitability, multi-frequency oscillations, and the chaotic behavior. They have received attention for thier close relation to the activity of living systems in the spontaneously-organized dynamic behavior. Possible applications of such phenomena to the sensing- and image storage devices have also been interested in. We have paid a special attention to the response of chemical oscillator systems to photo-illumination, which is very important in view of the above-mentioned interests but have not been studied so far in any systematic manner. Here we present some results of the studies on bifurcation structures in the chemical oscillators under the stationary light illumination.

III-L-1 Photo-Response of Chemical Oscillators

Ichiro HANAZAKI, Yoshihito MORI, Tetsuo SEKIGUCHI, and Gyula RÁBAI

The method proposed earlier by one of the authors to analyze quantitatively the wavelength- and intensity-dependence of the light illumination effect on chemical oscillators is critically reexamined. Its application to the analysis of the effect of stationary light illumination on the Belousov-Zhabotinsky and related minimal oscillator systems is discussed in detail to explore the primary photochemical precess and subsequent reactions of the key intermediates responsible for the photo-response. In particular, the bifurcation structure in the BZ minimal oscillator system is established as a function of the illumination light intensity and the bromide-ion concentration $[Br^-]_0$ externally supplied to the flow system. The most important finding here is that the bromide ion concentration $[Br^-]$ in the reactor decreases in the photoinhibition of oscillations as well as the photoinduction of oscillations. This is in clear contrast to the previously proposed scheme for the photoinhibition in the full BZ oscillators that the photoillumination causes an increase of $[Br^-]$ in the reactor, which results in the inhibition of oscillation. A possible reaction scheme under the light illumination is proposed. Some hints are given for possible future developments of the photo-control of chemical oscillators.

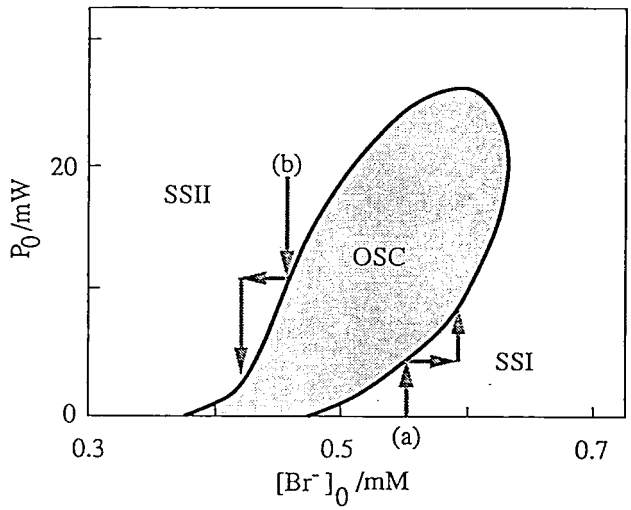

Figure 1. State diagram for the photoilluminated minimal bromate oscillator in a continuously-flowed stirred tank reactor $[Ru(bpy)_3^{2+}]_0$=0.26 mM, $[BrO_3^-]_0$=0.2 M, $[H_2SO_4]_0$=0.38 M, residense time=150 sec and temperature=25.0±0.1°C.

III-L-2 Frequency Multiplying Bifurcations in the Oscillatory Belousov-Zhabotinskii Reaction Proceeding in Interacting Water Droplets of Reverse Microemulsion of Aerozol OT in Octane.

Vladimir K. VANAG and Ichiro HANAZAKI

It has been found experimentally that the ferroin-catalyzed Belousov-Zhabotinskii (BZ) oscillatory reaction proceeding in water-in-oil microemulsion with anionic surfactant (AOT) exhibits frequency-multiplying bifurcations including frequency-doubling, -tripling and quadrupling. This bifurcation occurs only when the water fraction in the microemulsion is reasonably large (5—11%) and the flow rate of the emulsion through the reactor is very low (or in

the batch condition). The bubbling of oxygen-free nitrogen gas through the reactor is found to prohibit the bifurcations. On the basis of these observations, it is assumed that some volatile species controls the bifurcation. It is suggested that the bromine molecules produced during the oscillatory reaction in the aqueous phase is released into the organic phase and play an important role in governing the bifurcation structure. It is also suggested that the bifurcation is not simply due to the supply of bromine into the aqueous phase but communications between microdroplets should be enhanced when the bromine concentration in the organic phase exceeds a certain critical value, since the frequency changes by an integral factor, which is characteristics of the behavior in the coupled oscillators.

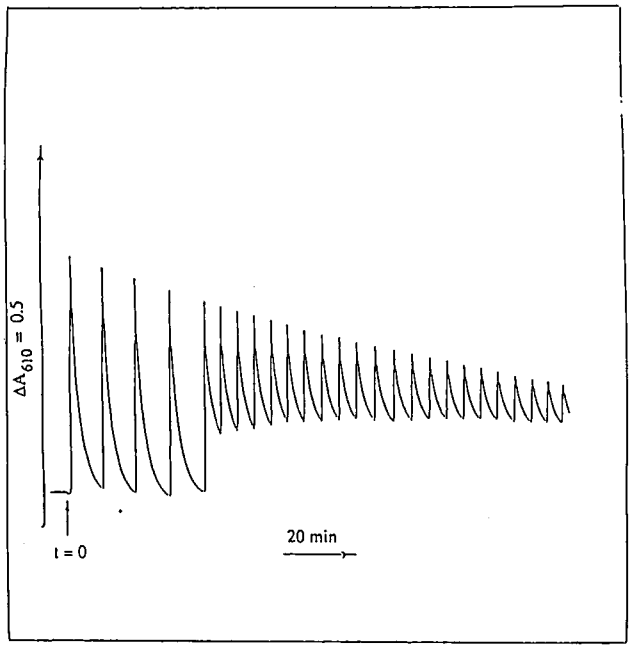

Figure 1. Kinetics of the ferroin-catalyzed BZ reaction in AOT reverse micelles in octane with ω=8.03, k_0=0.013 mL/min, ϕ_w=0.11, and the stirring rate is 720 rpm. The initial concentrations of the reagents in the aqueous phase: $[H_2SO_4]_{0w}$=0.3 M, $[BrO_3^-]_{0w}$=0.1 M, $[MA]_{0w}$=0.25 M, [ferroin]$_{0w}$=2.24 mM. No bubbling through the reactor was performed.

III-L-3 Photoinduced pH Oscillations in the Hydrogen Peroxide-Sufite-Ferrocyanide System in the Presence of Bromocresol Purple in a Continuous-Flow Stirred Tank Reactor

Vladimir K. VANAG , Yoshihito MORI and Ichiro HANAZAKI

[*J. Phys. Chem.* **98**, 8392 (1994)]

The H_2O_2-SO_3^{2-}-$Fe(CN)_6^{4-}$ system, one of the pH oscillators, is shown to be sensitive to visible light. Addition of a pH indicator, bromocrezol purple (BCP), to this system is found not only to show a sharp change of color along with the oscillation but also to acquire new nonlinear interactions due to the screening effect of the indicator. The state diagram spanned by the flow rate and the illumination light power is determined for this system. It is shown that the oscillatory region in the state diagram extends to higher light intensty by the addition of indicator. This behavior is also confirmed by a simulation calculation. In the experiments on wave propagation and spatial patterns in thin films, it is often difficult to detect spatial inhomogenieties because of extremely low extinction of light. The high absorption coefficient of the added indicator at 590 nm is expected to make the system color change visible even for solution films of 1mm thickness or less.

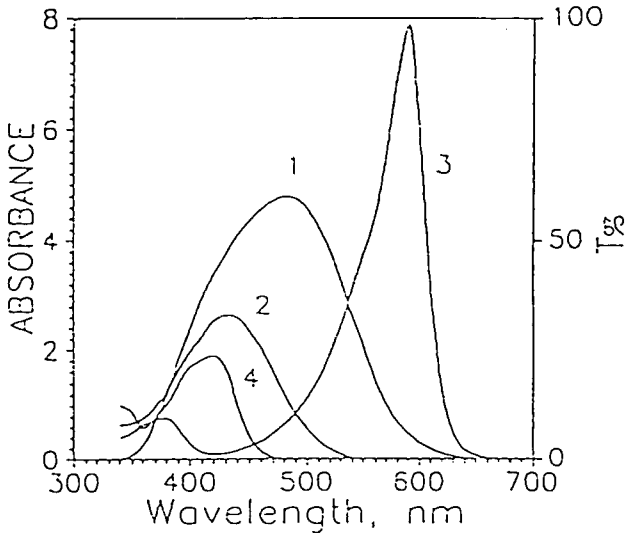

Figure 1. Optical spectra of (1) B480 filter (transperency on the right aixis), (2) protonated form of bromocresol purple, (3) deprotonated form of bromocresol purple, and (4) ferricyanide; [BCP]=1.85×10^{-4} M, $[Fe(CN)_6^{3-}]$=2 mM in 0.3 M H_2SO_4. Curves 2 – 4 are for a cell with optical pathlength of 2 cm.

III-L-4 A Simple Phenomenological Model for Nonequilibrium Interaction between Two Reactions in a Lorentz Gas

Jerzy GORECKI and Ichiro HANAZAKI

[*Chem. Phys.* **181**, 39 (1994)]

A simple phenomenological model, which assumes that different reagents in a chemical system may be characterized by different temperatures, is applied to calculate the nonequilibrium effects in a system with two competing reactions. The results are compared with molecular dynamics simulations of a model thermally activated reaction and good agreement between both methods is observed. The limiting case of a large mass ratio between different reactants (Lorentz gas) is discussed.

III-L-5 Photoinduction and Photoinhibition of Chemical Oscillations in the Tris(2,2′-bipyridine)ruthenium(II)-Catalyzed Minimal Bromate Oscillator

Tetsuo SEKIGUCHI*, Yoshihito MORI, Noriaki OKAZAKI*, and Ichiro HANAZAKI *(*Grad. Univ. Adv. Studies)*

[*Chem. Phys. Lett.* **219**, 81 (1994)]

The tris(2,2′-bipyridine)ruthenium(II)-catalyzed minimal bromate oscillator is shown to exhibit the chemical oscillation similar to the system with other catalysts. The photoresponse of the minimal oscillator has been investigated for

the first time to show both induction and inhibition of sustained oscillations. Figure 1 shows time profiles of redox and Br^--selective electrode potentials. When the illumination light power is increased, the system bifurcates from a reduced steady state (SSI) to an oscillatory state and from the oscillatory state to an oxidized steady state (SSII). It has been found that $[Br^-]$ in the reactor tends to decrease not only in the photoinduction but also in the photoinhibiton of chemical oscillations, in contrast to the previous view for the photoinduced pattern formation in the full Belousov-Zhabotinsky system. This result may require a more detailed investigation for the latter system.

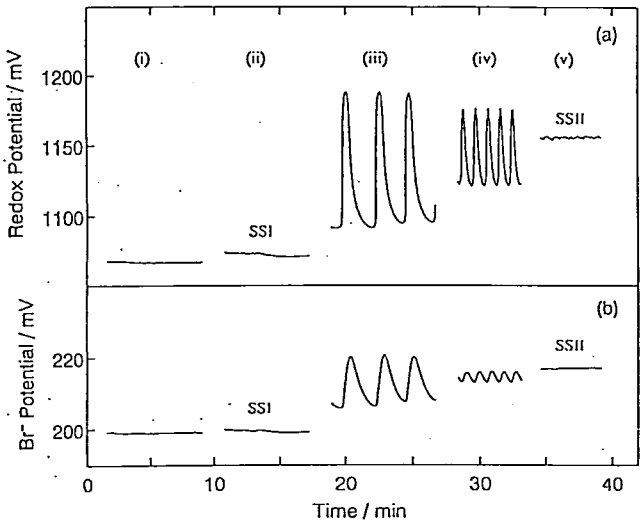

Figure 1. Photoinduction and photoinhibition of oscillations. (a) the redox potential and (b) the Br^--selective electrode potential. The irradiation power (P_0) is (i) dark, (ii) 0.3 mW, (iii) 2.0 mW, (iv) 6.9 mW and (v) 19 mW. Initial concentrations are $[Br^-]_0$=0.500 mM, $[Ru(II)]_0$=0.256 mM, $[BrO_3^-]_0$=200 mM and $[H_2SO_4]_0$=0.375 M. The residence time is 150 sec and the temperature is 24.8 ± 0.2°C.

III-L-6 Photo-Induced Bifurcation between Steady and Oscillatory States in the $Fe(CN)_6^{4-}$-H_2O_2 Reaction in a Flow Reactor

Yoshihito MORI, Gyula RÁBAI, and Ichiro HANAZAKI

The photo-induced bifurcation structure in the $Fe(CN)_6^{4-}$-H_2O_2-H_2SO_4 system in a continuous-flow stirred tank reactor has been determined. The photo-induced transition between the low pH steady state and the oscillatory state shows a hysteresis, similarly to the dark reaction reported previously.[1] The action spectrum for the photo-inhibition of oscillations suggests that the primary light absorber in the visible region is $Fe(CN)_6^{3-}$, similarly to the photo-induction of oscillations reported previously,[2] while in the UV region $Fe(CN)_6^{4-}$ is also active. The primary photochemical processes are shown to be

$$Fe(CN)_6^{4-} + H_2O + h\nu \rightarrow Fe(CN)_5H_2O^{3-} + CN^-$$

and

$$Fe(CN)_6^{3-} + H_2O + h\nu \rightarrow Fe(CN)_5H_2O^{2-} + CN^-$$

The state diagram spanned by the irradiation light power and the flow rate as external control parameters is shown in Figure 1, on the basis of which the mechanism of oscillations is discussed qualitatively.

References

1) Y. Mori and I. Hanazaki, *J. Phys. Chem.* **97**, 7375 (1993).
2) Y. Mori and I. Hanazaki, *J. Phys. Chem.* **96**, 9083 (1992).

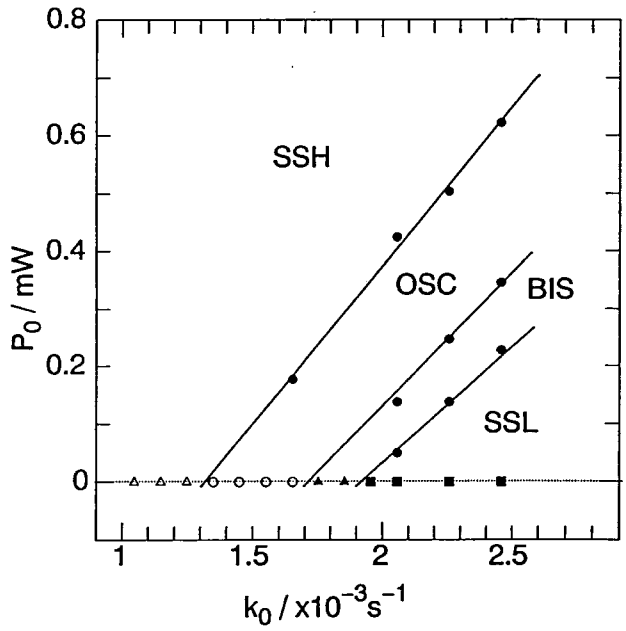

Figure 1. State diagram spanned by the 420 nm-illumination light power (P_0) and the flow rate (k_0). Closed circles represent the bifurcation points measured in the present work. Open triangles, open circles, closed rectangles and closed triangles represent a high pH steady state (SSH), an oscillatory state (OSC), a low pH steady state (SSL) and a bistable state between SSL and OSC, respectively, in the dark.[1] The initial concentrations are $[Fe(CN)_6^{4-}]_0$=3.30 mM, $[H_2O_2]_0$=50.0 mM and $[H_2SO_4]_0$=0.900 mM. The temperature is 25.0 ± 0.1°C.

III-L-7 Oscillatory Reaction in the Hydrogen Peroxide-Sulfite Ion-Hydrogen Ion-Hexacyanoferrate (II) Ion System in a Semibatch Reactor

Gyula RÁBAI and Ichiro HANAZAKI

[*J. Phys. Chem.* **98**, 2592 (1994)]

In addition to the study of chemical reactions in a closed and continuous-flow stirred tank reactor (CSTR), experiments in the intermediate configuration, dubbed semibatch reactor, can also be of practical and theoretical importance. A commonly used procedure consists of the controlled continuous admission of one or more reactants to a reaction vessel in which the other reactants are already present. In contrast to the CSTR and batch reactors, there has been no systematic exploitation of semibatch reactors in the study of exotic reactions. We suggest that the semibatch reactor is a potentially powerful tool for the experimental study of oscillatory reactions, because it can provide valuable information for better understanding of these reactions.

As shown in Figure 1, damped pH oscillations have been measured in the unbuffered reaction mixture of H_2O_2-HSO^{3-}-$Fe(CN)_6^{4-}$ in a semibatch reactor when all the reagents were simultaneously flowed, at a constant controlled rate, into the reactor containing pure water in the

beginning. Oscillations occurred within a limited range of the ratio of incoming reagent concentrations: $1.1 < [H_2O_2]_o/[SO_3^{2-}]_o < 1.3$; $[Fe(CN)_6^{4-}]_o/[H^+]_o > 1.0$; $[SO_3^{2-}]_o/[H^+]_o > 2$. The known simple model, consisting of the empirical rate laws of the component reactions, has successfully been used to simulate the dynamical behavior.

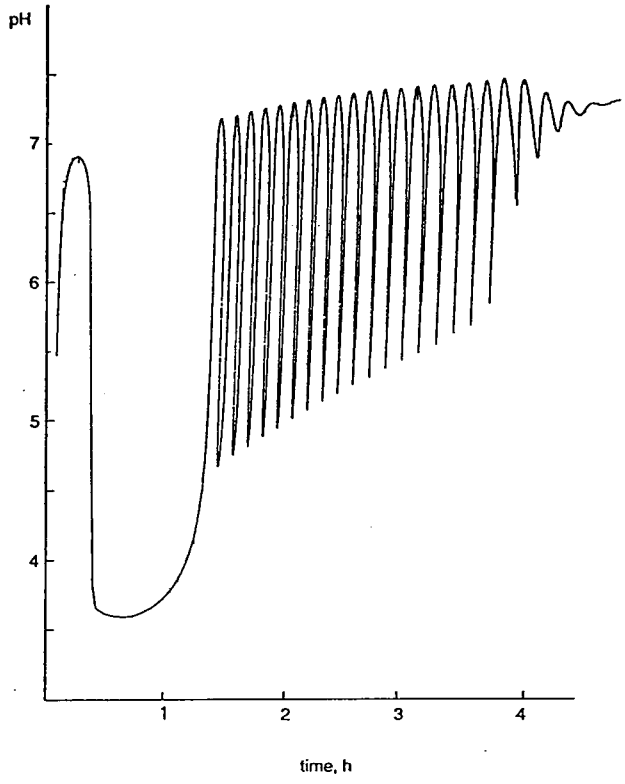

Figure 1. Measured oscillatory pH - time curve in a semibatch reactor. Initial volume of the reaction mixture is 250 ml, and the flow rate is 18 ml/hour. $[H_2O_2]_o$=0.06 M, $[SO_3^{2-}]_o$=0.05 M, $[Fe(CN)_6^{4-}]_o$=0.02 M, $[H^+]_o$=0.014 M, T=25°C.

III-L-8 Explanation of the Long-Lived Oscillations in the Chlorite Ion-Iodide Ion-Malonic Acid System

Gyula RÁBAI

[*J. Phys. Chem.* **98**, 5920, (1994)]

Long-lived redox potential oscillations in the chlorite ion-iodide ion-malonic acid system and in its derivatives, ClO_2-I_2-malonic acid and ClO_2-Cl^--iodomalonic acid systems, were shown to proceed according to a general type chlorite-controlled mechanism. First the chlorite ion disproportionates to Cl^- and chlorine dioxide in a rather fast reaction. Then a slow reduction of chlorine dioxide by malonic acid or iodomalonic acid takes place that serves as a continuous source of the chlorite ion. A moderately fast equilibrium between iodomalonic acid and a reactive intermediate (R) maintains a steady concentration of R at around 10^{-6} M during a significant part of the oscillatory cycle. Autocatalytic oxidation of R with ClO_2^- takes place according to the general model of chlorite based oscillators. The key to the oscillations is that, at a critical value of $[ClO_2^-]$, the autocatalytic oxidation becomes faster than the equilibrium and both R and ClO_2^- are used up. Model calculations as well as experiments in a semibatch reactor have verified this explanation. In a typical semibatch experiments we introduced diluted chlorite solution into a reaction mixture containing iodomalonic acid and chloride ion. Long-lived oscillations were observed. Dual effect (inhibition-induction) of Cl^- on oscillations suggests that iodine monochloride or I_2 can be the crucial intermediate (R) of this oscillatory reaction.

III-L-9 Light-Induced State Transitions in the Oscillatory ClO_2^--Cl^--Iodomalonic Acid System in a Semibatch Reactor

Gyula RÁBAI and Ichiro HANAZAKI

[*J. Phys. Chem.* **98**, 10550 (1994)]

We have discovered that the dynamical behavior of the oscillatory ClO_2^--Cl^--iodomalonic acid reaction in a semibatch reactor is extremely sensitive to the UV light, while the light above 420 nm does not affect the kinetics. We studied the peculiar photo-responses of this oscillator system in order to obtain additional mechanistic insights. We found that continuous illumination increased the amplitude and the period. Oscillations were completely abolished beyond a critical light power. Shown in Figure 1 are light-induced transitions from nonoscillatory to oscillatory state and bursting-like responses upon periodic perturbations with 370 nm light. The light-accelerated formation of a reactive iodine species from iodomalonic acid and its subsequent reaction with the chlorite ion is assumed to be responsible for the light sensitivity of the dynamical behavior. Addition of small amount of diluted iodine solution to the reaction mixture initiates state transitions similar to the light-induced ones. In addition to leading to this mechanistic information, our finding calls for an investigation of the light effect on the symmetry-breaking, reaction-diffusion spatial structures found recently in the chlorite-iodide-malonic acid system.

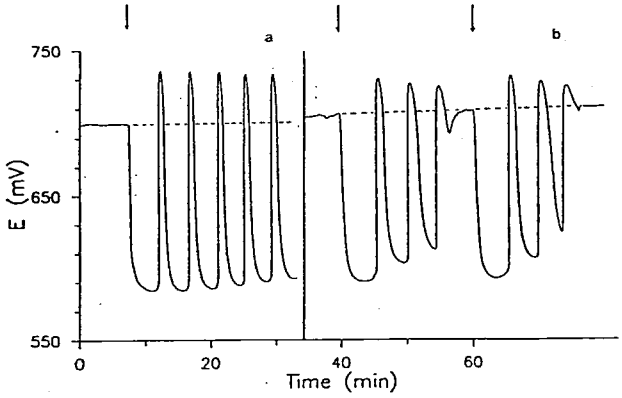

Figure 1. (a) light-induced transition from nonoscillatory to oscillatory state. 10 s illumination with P_0=5.3 μW/mL was applied at the arrow. (b) bursting-like photo-responses. The arrows indicate 1 min illuminations with P_0=5.3 μW. $[H_2SO_4]$=0.0050 M, $[NaHSO_4]$=0.015 M, [NaCl]=0.0033 M, [IMA]=5.0×10^{-4} M, $[NaClO_2]_{input}$=0.0010 M, inflow rates (a) 0.12 mL/min, and (b) 0.16 mL/min. Dashed lines show the trace of the reaction without perturbation.

III-L-10 Photo-Induced Disproportionation of Iodomalonic Acid

Gyula RÁBAI and Ichiro HANAZAKI

[*Int. J. Chem. Kin.*, in press]

The light-sensitive decomposition of iodomalonic acid is of importance because it is a major component reaction of several chemical oscillator systems. The stoichiometry, equilibrium, and kinetics of the photo-induced disproportionation of iodomalonic acid to I^-, I_2, and tartronic acid have been studied by means of spectrophotometry and iodide selective electrode at 20.0±0.2°C, pH 2.0–4.0. At pH > 2.9, only I^- and $HOCH(COOH)_2$ are detected as major products and the reaction reaches 100% conversion. At pH < 2.9, I_2 and malonic acid are also formed and the reaction stops at a conversion rate less than 100%. Both UV (band with a peak at 360 nm) and visible light (480 nm) have been found to be effective. Two primary photochemical processes are identified:

$$\text{(M1)} \quad ICH(COOH)_2 + h\nu \rightarrow I\cdot + \cdot CH(COOH)_2$$
$$\text{(M2)} \quad I_2 + h\nu \rightarrow 2I\cdot$$

While both reactions are sensitive to UV light, only (M2) can be affected by visible light. (M1) and (M2) are considered to initiate a chain reaction sequence in which I· radicals oxidize iodomalonic acid. Dual effects of reaction products on the reaction rate have been observed: while iodine increases the efficiency of visible light and accelerates the reaction, malonic acid inhibits the photo-decomposition by mediating the recombination of I· radicals to I_2.

III-L-11 Oxidation of Thiocyanate by Bromate is not an Oscillatory Reaction in a Batch Reactor. A Comment

Gyula RÁBAI and Ichiro HANAZAKI

[Submitted to *J. Phys. Chem.*]

In contrast to a previous report,[1] we have found no irregular oscillatory responses in a Landolt-type reaction between $NaBrO_3$ and NaSCN in diluted $HClO_4$. The redox potential of the reaction mixture changes monotonously. On the basis of independent kinetics studies we concluded that this reaction is too fast to support any long-lived chemical oscillations in a batch reactor and the irregular potentiometric traces reported in reference 1) are probably resulted from poorly controlled experimental conditions rather than chemical reactions.

Reference

1) Valent, I.; Adamcikova, L. *J. Phys. Chem.* **98**, 4304 (1994).

III-L-12 Mechanism of the Light-Sensitive Oscillatory Reaction between Hydrogen Peroxide and the Hexacyanoferrate(II) Ion

Gyula RÁBAI, Yoshihito MORI, and Ichiro HANAZAKI

We have developed a detailed mechanism consisting of 20 steps and 16 variable species for the title reaction. Most of the component reactions considered in the model are known and their kinetics data are available in the literature. The key steps of the mechanism responsible for the light sensitivity of oscillations are the light-induced dissociation of the hexacyanoferrate(II)/(III) complexes to the pentacyanomonoaquo complexes and the cyanide ions. An autocatalytic reaction sequence between the pentacyanomonoaquo ferrate(II) complex and the hydroperoxide radical is considered which provides the feedback necessary for oscillations. Computer simulations show that the proposed model is capable of describing both the observed complex kinetics in a batch reactor and the light-induced(inhibited) oscillations in a continuous-flow stirred tank reactor (CSTR). The mechanism is yet to be refined in order to describe the experimental bifurcation structure of the dynamical behavior found in a CSTR.

III-L-13 Photo-Induction and Inhibition of Chemical Oscillations in the Ferrocyanide-Bromate-Sulfite System in a CSTR

Akiko KAMINAGA, Gyula RÁBAI, and Ichiro HANAZAKI

The simultaneous oxidation of sulfite and ferrocyanide by bromate is known to show, depending on experimental conditions, pH oscillation, high pH and low pH steady states when it is run in a continuous flow-stirred tank reactor (CSTR). Our systematic experiments have revealed that this dynamical behavior is sensitive to light illumination. Photo-induced oscillations were observed under the experimental conditions which support low pH steady state in the dark. As shown in the figure 1, when the system in the low pH steady state is irradiated with a light band around 390 nm, it bifurcates into the oscillatory state at a critical value of the light power. In other instances light can suppress oscillations that exist in its absence; the illuminated system bifurcates into high pH steady state.

We suggest that illumination enhances the rate of the oxidation of ferrocyanide, which is the H^+ consuming component reaction of the system.

$$BrO_3^- + 6Fe(CN)_6^{4-} + 6H^+ \rightarrow 6Fe(CN)_6^{3-} + 3H_2O + Br^-$$

The primary photochemical process is thought to be the photoaquation of $Fe(CN)_6^{4-}$ producing $Fe(CN)_5(H_2O)^{3-}$ which reacts relatively fast with bromate.

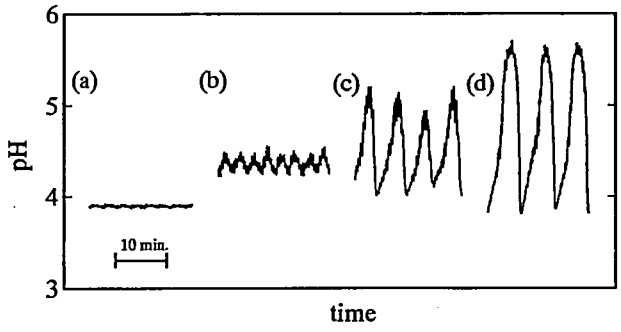

Figure 1. Time profile of pH of the reaction mixture under illumination. The initial concentrations are $[Fe(CN)_6^{4-}]_0$=15 mM, $[BrO_3^-]_0$=75 mM, $[SO_3^{2-}]_0$=89 mM, and $[H_2SO_4]_0$=7.5 mM. The residence time is 44 minutes. The illumination light source is a 500 W Hg lamp with a band pass filter (B390) and appropriate ND filters. (a) dark, (b) 74 mW, (c) 80 mW, and (d) 100 mW.

III-L-14 Photoresponse of the Briggs-Rauscher Reaction with Iodide Inflow

Noriaki OKAZAKI *(Grad. Univ. Adv. Studies)*, **Yoshihito MORI, and Ichiro HANAZAKI**

The Briggs-Rauscher (BR) reaction is known to show an inhibition of oscillation and a synchronization oscillation under the light irradiation[1]. In order to examine the effect of iodide production caused by light irradiation, we have studied the photoresponse of BR-system by varying the initial concentration of iodide ion systematically.

Figure 1 shows a state diagram spanned by the initial concentration of iodide ($[I^-]_0$) and irradiation power (P_0). It was found that the increase in P_0 has the tendency of stabilizing an oxidized steady state (SS1), whereas increase in $[I^-]_0$ stabilizes a reduced steady state (SS2). The bifurcation lines (γ_O and γ_R) intersect at point P, manifesting a typical cross-shaped phase diagram (XPD). The result indicates that the effect of light irradiation is not simply parallel to the effect of iodide inflow. The iodide production is not likely to play a dominant roll in the photoresponse of BR-system.

An oscillatory state (OSC) exists in the region where both the steady states are unstable. However, it extends over the stable region of SS1 and/or SS2. Thus, we have observed a tristability consisting of OSC, SS1 and SS2 in a considerably wide control-parameter range (□PQRS). The observations provide a novel possibility of controlling chemical oscillators by the photo-irradiation.

Reference

1) E. Dulos and P. De Kepper, *Biophys. Chem.*, **18**, 211 (1983).

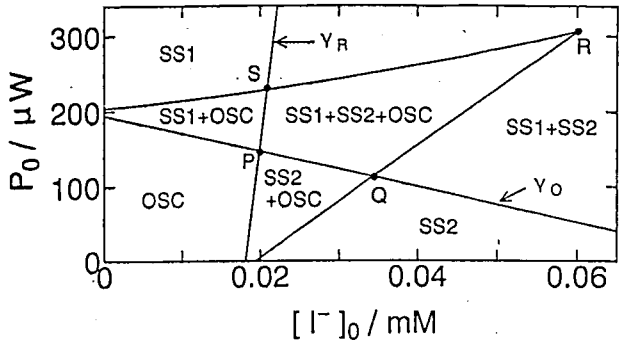

Figure 1. State diagram spanned by the initial concentration of iodide ($[I^-]_0$) and 460nm monochromatic light intensity (P_0). Experimental conditions are: $[H_2SO_4]_0$=16mM, $[MnSO_4]_0$=3mM, $[KIO_3]_0$=15mM, $[H_2O_2]_0$=200mM, $[CH_2(COOH)_2]_0$=2mM, residence time=3.5min, temperature=24.5±0.1°C.

III—M Laser Investigation of Photodissociation and Bimolecular Reactions

The reactions encountered in atmospheric and interstellar chemistry involve systems that are generally larger than the triatomic system (A+BC) which has been extensively studied as a model for chemical reactions. The elucidation of such complicated (realistic) dynamics is currently a major theoretical and experimental challenge. Lasers with high intensity, good monochromaticity, and well-defined polarization provide extremely sensitive detection methods of atoms and molecules with the capability of examining scalar (e.g. energy) and vector (e.g. linear and angular momentum) quantities in great detail. The goal of this project is to perform reactive scattering experiments with laser spectroscopic detection methods, and to elucidate the detailed dynamics of important atmospheric and interstellar reactions. Major effort is currently directed to the development of the two-dimensional imaging technique to visualize the scattering of atoms and molecules in reactions. During the period of 1993—1994, an imaging apparatus was constructed, and critical tests were made using photodissociation experiments.

III-M-1 Photodissociation of *trans*-Dichloroethylene: State-Resolved Speed and Angular Distributions of Cl Atoms

Toshinori SUZUKI, Kenichi TONOKURA, Lizla S. BONTUYAN, and Nobuhisa HASHIMOTO *(Graduate Univ. for Advanced Studies)*

[*J. Phys. Chem., in press*]

The elimination of atomic chlorine in the ultraviolet photodissociation of *trans*-dichloroethylene (*trans*-DCE) was studied by two-dimensional ion imaging. *Trans*-DCE was photodissociated at 193, 210, and 235 nm and speed and angular distributions of Cl (^2P_J; J=1/2, 3/2) photofragments were measured. Two components were observed in the translational energy distributions, similar to those observed by Umemoto *et al.* using photofragment translational spectroscopy.[1] One component has a strong anisotropy and a Gaussian-shaped translational energy distribution, while the other has a weak anisotropy and a Boltzmann-like distribution. The former is ascribed to rapid C-Cl bond rupture due to surface crossing between the (π, π^*) and (n, σ^*) or (π, σ^*) states, while the latter is to thermal

decomposition via internal conversion to the ground electronic state. The wavelength dependence and Cl*/Cl branching ratios of the two dissociation channels were also investigated.

Reference

1) M. Umemoto *et al.*, *J. Chem. Phys.* **83**, 1657 (1985).

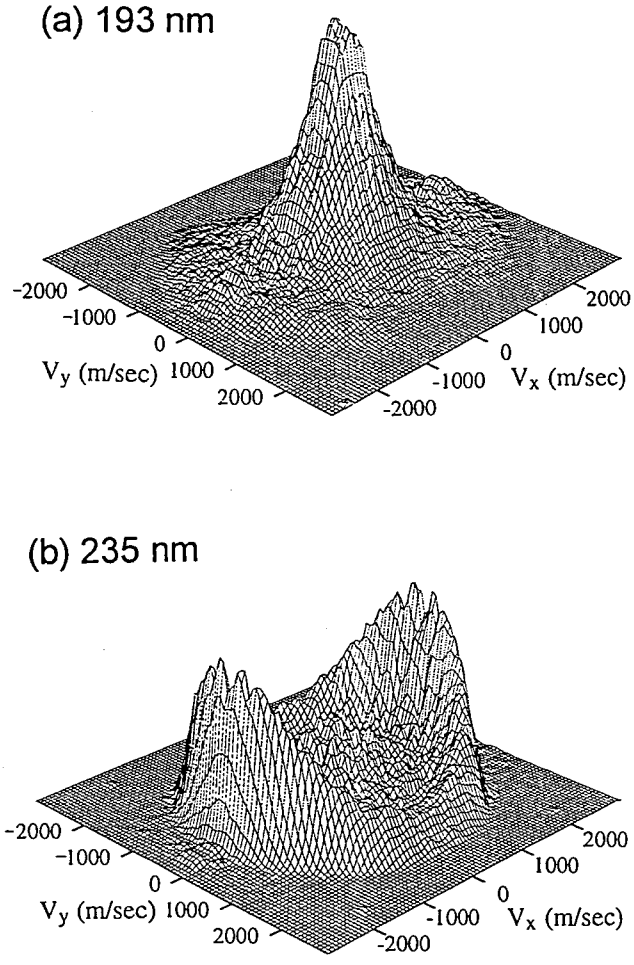

Figure 1. The product velocity contour maps for the $Cl(^2P_{3/2})$ photofragment produced by the photodissociation of *trans*-DCE at 193 (a) and 235 nm (b).

III-M-2 Slicing Photofragment Spatial Distribution by Laser Sheet Ionization

Kenichi TONOKURA and Toshinori SUZUKI

[*Chem. Phys. Lett.* **224**, 1 (1994)]

Sections of the three dimensional distribution of products in photodissociation were observed by ion imaging with a sheet-shaped laser beam. Images of sections which contain the center-of-mass directly provide the differential cross sections and obviate the need for the noise-sensitive mathematical transformation. The [1+1] REMPI detection of NO and [2+1] REMPI of $O(^3P_2)$ produced by the 355 nm photolysis of NO_2 were tested. The results are compared with the images of sections reconstructed from the two-dimensional projections of the entire three dimensional distribution using the inverse Abel transform.

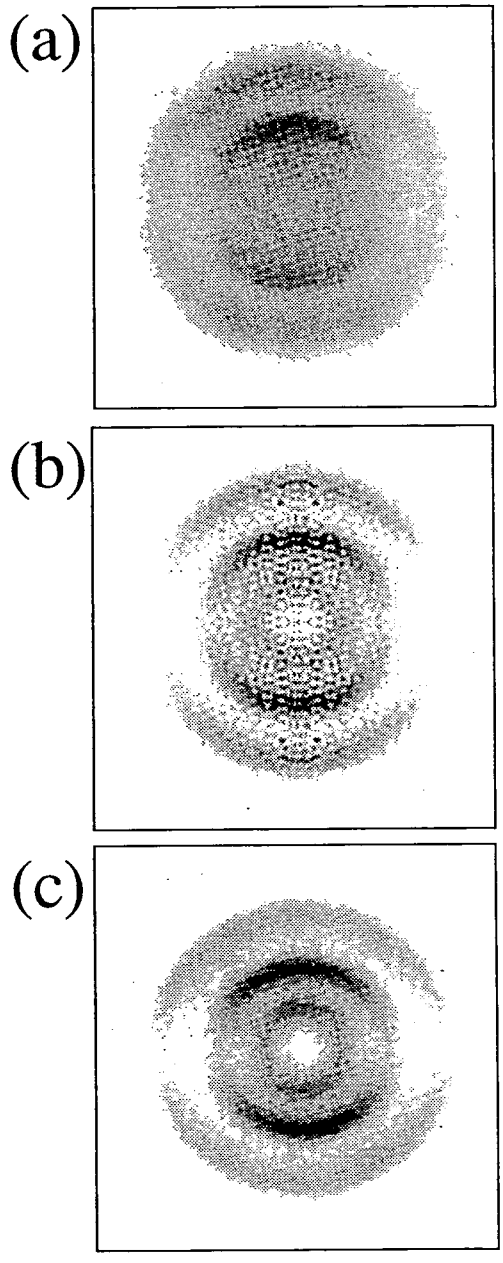

Figure 1. The ion images of $O(^3P_2)$ atoms produced by the 355 nm photodissociation of NO_2; (a) the projection of the entire 3D distribution (raw image), (b) the reconstructed image of (a) by inverse Able transform, and (c) the raw image of the ions observed by laser sheet ionization. The probe laser beam was positioned 0.85 mm downstream from the photolysis beam.

III-M-3 Predissociation of Acetylene in the A state: H-Atom Action Spectrum

Nobuhisa HASHIMOTO *(Graduate Univ. for Advanced Studies)* **and Toshinori SUZUKI**

The $\tilde{A}(^1A_u) \leftarrow \tilde{X}(^1\Sigma_g)$ spectrum of jet-cooled acetylene was measured by monitoring the $H(^2S)$ photofragment by [2+1] REMPI. The formation of H atom was found to start at Evib ~4475 cm^{-1} in the A state, which is in good agreement with the sudden decrease of fluorescence quantum yield at this energy reported by Haijima *et al.*[1] The energy threshold for the dissociation, C_2H_2 $(\tilde{A}^1A_u) \rightarrow C_2H$ $(\tilde{X}^2\Sigma^+)$ + $H(^2S)$, was determined to be 133.0±0.4 kcal/mol.

Kinetic energy measurements of the H atom by one-dimensional Doppler spectroscopy yielded a C-H bond energy (D_0) of 130.6±0.8 kcal/mol. Rotational state dependence of the predissociation rate was found to be very similar between the V^4K^1 and V^5K^1 vibrational states, in contrast to the result of Haijima *et al.*

Reference

1) A. Haijima *et al.*, *J. Chem. Phys.* **92**, 959 (1990).

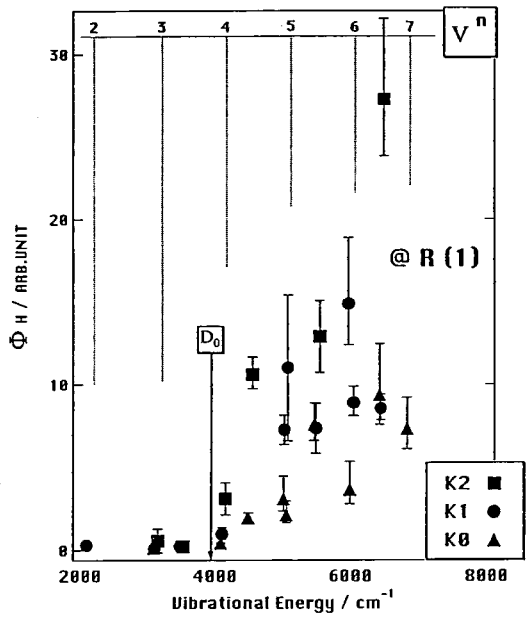

Figure 1. The excess energy dependence of the yield of hydrogen atoms.

III—N External Magnetic Field Effects upon Chemical Reactions

Magnetic field effects upon chemical reactions provide us with useful methods for elucidating reaction mechanism and technique for controlling reaction rates, product yields, and concentration of a certain isotope. In the recent decade, the magnetic field effects upon photochemical reactions have been studied for a variety of organic molecules. Special attention has been paid to the hyperfine interaction between the electronic spin and nuclear magnetic moments within radical pair intermediates. In particular, intramolecular photoredox reactions in the solution phase have been extensively investigated for a series of aromatic carbonyl and nitro-aromatic species. In most cases the photoreactions involving triplet biradicals have been examined in some detail. The formation yield for the cage product decreases in the presence of external magnetic fields, whereas that for the escape product correspondingly increases. Application of the magnetic field may cause an appreciable change in the relative yield of cage and escape products, i.e. the branching ratio of competitive processes. This means that the magnetic field effects have some potential for application, e.g. control of reaction yields or selection of reaction pathways.

In addition, we have also studied the magnetic field effects on gaseous molecules. One of the largest external magnetic field effects were observed for the β band of NO in the gaseous state. More recently, it has been found that some halogen and interhalogen molecules exhibit magnetic quenching.

III-N-1 Factors Controlling the Magnitude of Magnetic Field Effects on Photoredox Reaction Yields for Bifunctional Chain Molecules

Ryoichi NAKAGAKI *(Kanazawa Univ. and IMS)*, **Yasuhiro TSUJIMOTO** *(Kanazawa Univ.)*, **and Kiyoshi MUTAI** *(Univ. of Tokyo)*

We have studied magnetic field effects on photoredox reactions involving biradical reaction intermediates for a series of methylene-linked bichromophoric molecules consisting of nitroaromatic chromophore and reductant moiety. A bimolecular escape process which can compete with the intersystem crossing is necessary for observing magnetic field effects on the end product yields when the photoreaction involves triplet biradicals. Appreciable magnetic field effects on the photoredox reaction yields were observed for bifunctional species containing nitroaromatic and arylamino moieties, while no magnetic field effects were detected for the end product yield of α,α-diphenylated cycloalkanone (13-membered ring). These findings indicate that the bimolecular escape process is efficient for the biradical containing strong oxidant and reductant moieties. We can conclude that the following factors may control the escape process reactivity or the magnitude of magnetic field effects on the end product yield: (1) the electron affinity of the oxidant moiety, (2) the electron-donating ability of the reductant radical, (3) the delocalization of unpaired electron in the reductant radical, (4) steric factors in the reductant radical.

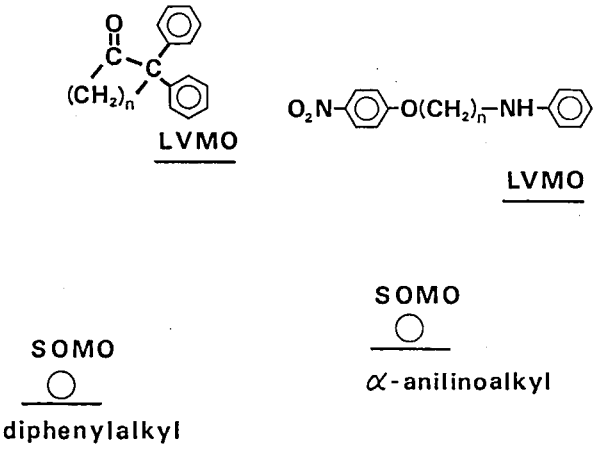

Figure 1. Schematic description of energy levels for the oxidant and reductant: LVMO (the lowest vacant orbital of the starting species which act as oxidant) and SOMO (singly occupied orbital of the reductant site of a biradical). Two extreme examples of intramolecular photoreactions involving biradical intermediates produced on photolysis. Photochemical ring cleavage of the cyclic ketone yields a biradical intermediate containing acyl and diphenylalkyl. Photoinduced hydrogen abstraction by the nitro group takes place at the methylene group adjacent to the anilino nitrogen.

III-N-2 Magnetic Field Effects on Photoinduced Substitution of 4-Methyl-2-quinolinecarbonitrile with Optically Active (S)- or (R)-2-phenylpropionic Acid

Ryoichi NAKAGAKI *(Kanazawa Univ. and IMS)*

[*Chem. Phys.* **185**, 405 (1994)]

According to a recent paper by Hata[1]; S-(+)- and R-(-)-2-phenylpropionic acids exhibit inequivalent reactivity toward the excited state of 4-methyl-2-quinolinecarbonitrile and magnetic field effects are observed on the reaction yields for photoproduct obtained after photolysis of the reactant quinoline with the R-type acid in benzene. Although this work is of significance in connection with the magnetic field effects on asymmetric synthesis of biological molecules, the author has attributed the inequivalent reactivity to an unidentified type of chiral symmetry breaking. We have repeated the photosubstitution reaction under similar experimental conditions. It was found that the optically active acids show equivalent reactivity toward the excited state of the reactant quinoline. No significant magnetic field effects were detected upon the relative quantum yield for the photosubstitution product in benzene. No unusual phenomena were observed under well controlled conditions with sufficient repetitions.

Reference

1) N. Hata, *Chem. Phys.* **162**, 47 (1992).

III-N-3 Magnetic Field Effects on the $B^3\Pi_{0+}$ State of Gaseous Halogen and Interhalogen Molecules

Takamichi KOBAYASHI and Saburo NAGAKURA *(Grad. Univ. for Adv. Studies)*

Although magnetic quenching (decrease of emission intensity by external magnetic field) has been observed in many gaseous polyatomic molecules, only a few diatomic molecules have been known to exhibit magnetic quenching. In order to fully understand the mechanism of the external magnetic field effects on the gaseous molecules it is important to study smaller molecules systematically since their electronic structures are better understood than those of larger molecules.

In the present study, the $B^3\Pi_{0+}$ state of Br_2, Cl_2, IBr and ICl has been investigated by fluorescence excitation spectroscopy and many vibrational states of Br_2 and the $v'=2$ state of IBr have been found to exhibit magnetic quenching, whereas Cl_2 and ICl do not exhibit magnetic quenching. These results are discussed in terms of internal perturbations such as predissociation and the Zeeman perturbation between the $B^3\Pi_{0+}$ state and the excited electronic states nearby.

The observed magnetic quenching (caused by magnetic predissociation) of Br_2 is rotationally-dependent which should be compared with the reported rotationally-dependent lifetimes, i.e. the degree of magnetic quenching becomes larger as the lifetime becomes longer. This suggests that the magnetic quenching decreases as the rate of non-radiative transitions (natural predissociation in this case) increases.

RESEARCH ACTIVITIES IV
Department of Molecular Assemblies

IV—A Solid State Properties of Phthalocyanine Salts and Related Compounds

Some phthalocyanine molecules contain unpaired d-electrons in the conjugated π-electron system. Owing to this special nature, the itinerant π-electrons and localized unpaired d-electrons coexist in solid phthalocyanine salts, in which a one-dimensional double-chain system is formed. The exchange interaction of itinerant π-electrons with localized magnetic moments is a new aspect in the field of organic metals. For the basic understanding of these materials and to search for a new phenomenon, where a magnetic interaction takes an important role, we prepared and characterized solid phthalocyanine salts and related compounds.

IV-A-1 Pressure Dependence of the Infrared and Visible Spectra of Metallophthalocyanine Salts

Toshihiro HIEJIMA *(Grad. Univ. Adv. Studies)* **and Kyuya YAKUSHI**

[*Synthetic Metals*, in press]

We have characterized the isostructural organic conductors, $NiPc(AsF_6)_{0.5}$ and $CoPc(AsF_6)_{0.5}$, to elucidate the role of the magnetic moment on the transition metal by comparing the compounds with non-magnetic metal (Ni^{2+}) and magnetic metal (Co^{2+}). The unusual property of $CoPc(AsF_6)_{0.5}$ was described in this Annual Reviews of 1993. The pressure dependence of the electronic states of $(NiPc(AsF_6)_{0.5}$ and $(CoPc(AsF_6)_{0.5})$. was examined by measuring the optical spectra of these highly conductive phthalocyanine salts. In both compounds, we found remarkable changes in the spectra of infrared, near-infrared, and visible regions, in which the molecular vibration, charge-transfer transition, and intra-molecular electronic transition appear, respectively. All of these observations can be interpreted as the pressure-induced charge transfer above 2 GPa from the 1D d-band comprising the central metal chain to the 1D π-band of the macrocyclic-ligand chain. Most importantly this is a reversible change against the pressure. This means that the concentration of the charge carriers is controlled by the pressure in these compounds.

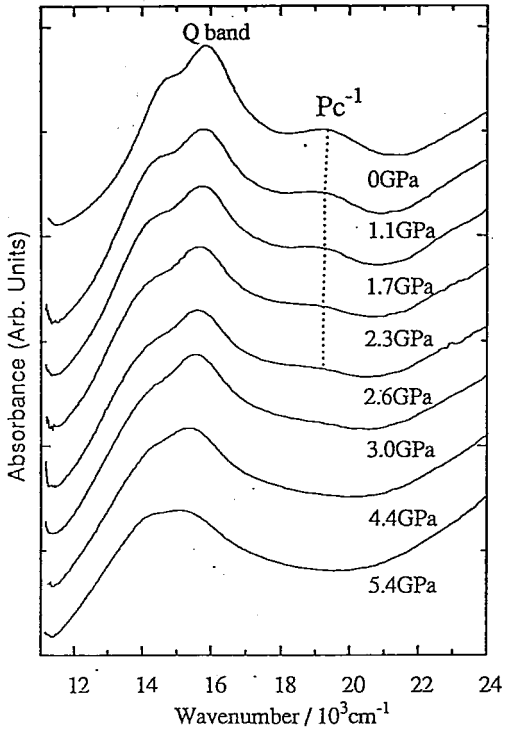

Figure 1. Pressure dependence of the absorption spectrum of $CoPc(AsF_6)_{0.5}$. in the region of Q-band. Note that the absorption band characteristic of the ring-oxidized pthalocyanine (denoted by Pc^{-1}) continuously decreases upon applying the hydrostatic pressure.

IV-A-2 X- and Q-band ESR Study of New Poly-CuPc Compounds Synthesized Under High Pressure: the Possibility of Two-dimensional Sheet Polymers

Ilias I. KHAIRULLIN, Ichimin SHIROTANI *(Muroran Ins. Tech.)*, **and Kyuya YAKUSHI**

[*Synthetic Metals* **64**, 217 (1994)]

We have tried to prepare the metallophthalocyanine sheet polymer (poly-MPc) by applying high pressure and temperature. The poly-CuPc and poly-NiPc compounds synthesized under 5 GPa at 400-780°C are systematically studied here with the use of X- and Q-band ESR spectroscopy. In addition to the broad ESR signal derived from the local spins on Cu^{2+}, new paramagnetic species appear which exhibit an anisotropic spectrum with an axial symmetry having linewidth ΔH=1—1.2 G. The principal values of the **g** tensor of this new signal are 2.0024 in the parallel component and 2.0030 in the perpendicular one. Spin concentration of these new species is estimated to be $(7—9)\times10^{19}$ spins g^{-1} which is approximately two orders of magnitude greater than that of the CuPc sheet oligomer which was synthesized under ambient pressure. The substitution of the central metal does not strongly influence the ESR properties of the narrow signal. We suppose that the new signal comes from the delocalized π-electrons of the sheet polymer. On the other hand, in the samples synthesized at temperatures higher than 650°C, the broad and narrow signals merge into a single symmetric signal. We explain the ESR properties of these compounds from the viewpoint of the sheet polymer model.

IV—B Structure and Properties of Organic Metals

The study of organic metals rapidly developed when the dimensionality of an intermolecular charge-transfer interaction is expanded. This expansion of dimensionality has been brought about by the discovery of new molecules such as BEDT-TTF or C_{60}. In this project we treat one-, two-, and three-dimensional organic metals and superconductors to know what is most important for stabilizing a metallic state and for designing new superconducting materials.

IV-B-1 Superconducting Properties of Na-Doped C_{60} Prepared from Sodium Azide

Ilias I. KHAIRULLIN, Kenichi IMAEDA, Kyuya YAKUSHI, and Hiroo INOKUCHI

[*Physica C*, in press]

We started the alkali-metal doping of C_{60} and other higher fullerene since 1991, and demonstrated that the combination of the microwave absorption spectroscopy (LFS) and ESR is very efficient to search for new superconducting materials especially in air-sensitive materials like doped C_{60}. In 1993, we found a new superconducting C_{60} compound prepared from NaN_3, and already described briefly about the structure and properties in the Annual Review of 1993. Subsequently, we have systematically studied this new Na-doped C_{60} superconductor. First we established the preparation method of this compound and then characterized the superconducting properties by the experiment of magnetization. The volume fraction of superconducting phase of the best sample is 38%. The critical temperature, T_c, of the superconductivity is 13 K, the critical magnetic fields are $H_{c1}(0)=3.9\pm2$ mT and $H_{c2}(0)=10\pm1$ T from the SQUID magnetometry. The coherence length and penetration depth are calculated as ξ=57 Å and λ=4200 Å, respectively. The superconducting phase have a f.c.c. lattice with a=14.33 Å.

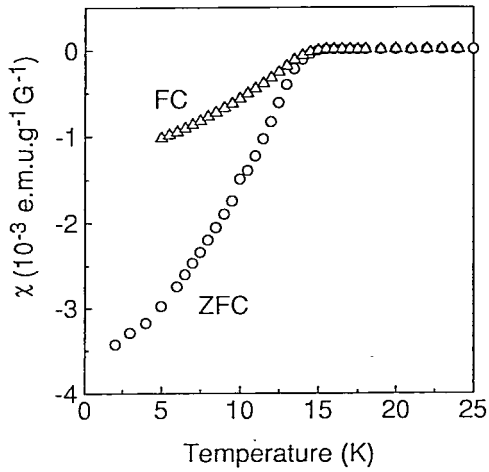

Figure 1. Temperature dependence of the magnetic susceptibility of Na-doped C_{60} prepared from NaN_3. From the zero-field cooling (ZFC) curve, the superconducting volume fraction is estimated to be *ca.* 38%.

IV—C Far-infrared Properties of Organic Conductors

A number of organic conductors exhibit interesting behaviors such as CDW, SDW, or superconducting transitions at low temperatures. These phenomena are characterized by the presence of energy gap with a small excitation energy, which typically lies in far-infrared regions. The far-infrared study should then yield valuable information about the one-electron band structure as well as the transport dynamics of collective modes. For the purpose of quantitative investigations the optical spectra are usually measured by a reflectance technique because of a opaque nature of the sample crystals. However, the reflectivity measurement on a small sample is often suffered by diffraction and/or interference effect, which make it difficult to obtain an absolute reflectivity. We have successfully constructed a high-precision, far-infrared reflectance spectroscopic system equipped with a LHe cryostat. The electronic structures of some $(BEDT\text{-}TTF)_2X$ salts have been investigated.

IV-C-1 Construction of Far-infrared Reflectance Spectroscopic System

Akito UGAWA and Kyuya YAKUSHI

We have constructed a reflectance spectroscopic system to measure the reflectivity of small single crystals over the range of 20—700 cm^{-1} at temperatures between 5—300 K. Figure 1 shows the reflectance unit equipped with LHe flow-type cryostat. Both a sample crystal and an Au reference mirror are mounted on OFC blocks, which are held at the opposite side of a heat exchanger to each other. The measurement object can be interchangeable by rotating the heat exchanger rod, which is doubly-sealed with O-rings to a vacuum shroud. The thermal contraction during cooling operations can be eliminated by a remote z-stage so that the sample is at the same height of an incident light. This unit is inserted into a sample compartment of a Bruker IFS-113v Fourier-transform interferometer.

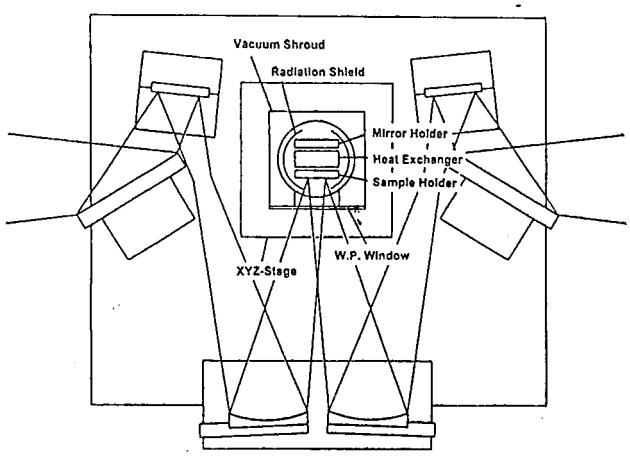

Figure 1. Reflectance unit with LHe cryostat for far-infrared reflectance measurement.

IV-C-2 Far-infrared Reflectance of β″- (BEDT-TTF)$_2$AuBr$_2$

Akito UGAWA, David B. TANNER *(Univ. of Florida)*, **and Kyuya YAKUSHI**

[*Synth. Met.*, to be published]

We have measured the temperature dependence of far-infrared reflectance of β″-(BEDT-TTF)$_2$AuBr$_2$ to investigate the possibility of SDW transition. The polarized reflectance in the two-dimensional BEDT-TTF layers shows a highly anisotropic feature of conduction band. Both the E∥c and E⊥c reflectance line shapes, which are Drude-like at room temperature, demonstrate a clear dip below 100 cm^{-1} even at 40 K. The frequency dependent conductivity at 7 K indicates the presence of a single-particle gap at 2Δ=130 cm^{-1} assignable to the SDW nesting along c. The nesting fluctuation exists already at room temperature because of a strongly one-dimensional nature of the band dispersion.

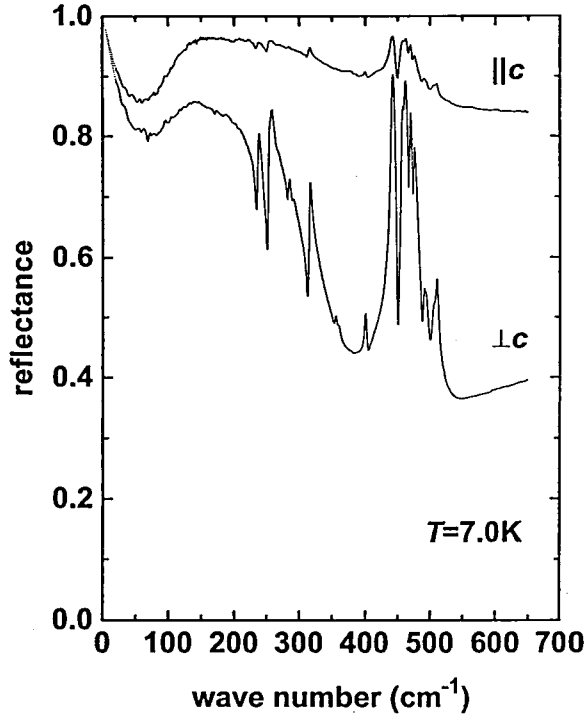

Figure 1. Polarized Reflectance of β″-(BEDT-TTF)$_2$AuBr$_2$ measured at 7.0 K.

IV—D NMR Study of Organic Conductors and Superconductors

The nuclear magnetic resonance (NMR) is a powerful method to examine electronic state of condensed matters. With this microscopic method, one can get further insight into nature of the metallic, superconducting and magnetic states than with other macroscopic measurements. This project aimes at understanding the unsolved problems concerning the peculiar electronic structure in several organic materials.

IV-D-1 ^{13}C-NMR Study on α-(BEDT-TTF)$_2$MHg-(SCN)$_4$

Kazushi KANODA, Atsushi KAWAMOTO *(Ochanomizu Univ.)*, **Kazuya MIYAGAWA, and Yasuhiro NAKAZAWA**

[Submitted to *Synth. Metals*]

NMR experiments of organic conductors have so far been performed extensively at the proton site. However, the protons are located at edges of the molecule and, in many cases, have so small spin density of the molecular orbital responsible for conduction electrons. Therefore, the proton is not the best nuclear probe to see the electronic structure of these materials. Selective substitution of ^{13}C isotope to the carbon sites where spin density is richer is a useful method for NMR study. In this study, we attack a problem encountered in a series of compounds, α-(BEDT-TTF)$_2$-MHg(SCN)$_4$ [M=K, Rb] by ^{13}C-NMR; these compound undergoes some phase transition from metallic state to another metallic state, which is discussed in context of spin density wave state in many literatures but is not yet clear. We introduced ^{13}C isotope into the central carbon sites of BEDT-TTF molecule and performed ^{13}C-NMR measurements at these sites for α-(BEDT-TTF)$_2$MHg(SCN)$_4$ in the temperature range between 2 and 300 K. We observed anomalies in the nuclear spin-lattice relaxation rate, T_1, and shift of the NMR line below 8 K for the K salt and below 12 K for the Rb salt. These indicate some phase transition surely exists at these temperatures. However, absence of critical fluctuation near the transition temperature and absense of splitting or broadening of the NMR line is against the static magnetic ordering as found in usual SDW systems such as the TMTSF compounds. Even if SDW ordering is involved in this transition, the moment of the magnetic order turns out to be of the order of 0.1% of μ_B or less. The present results imply that the electronic density of states decreases to a half below the transition.

IV-D-2 ^{13}C-NMR Study on κ-(BEDT-TTF)$_2$X

Kazuya MIYAGAWA, Atsushi KAWAMOTO *(Ochanomizu Univ.)*, **Yasuhiro NAKAZAWA, and Kazushi KANODA**

[Submitted to *Synth. Metals*]

The electronic state of the κ phase family of BEDT-TTF compounds, κ-(BEDT-TTF)$_2$X [X=Cu(NCS)$_2$, and Cu[N(CN)$_2$]Br], has been investigated by ^{13}C-NMR. The ^{13}C isotope was substituted selectively into the central double bonded carbon sites of BEDT-TTF. The ^{13}C nuclear spin-lattice relaxation rate and line spectra have been measured for the Cu(NCS)$_2$ and Cu[N(CN)$_2$]Br salts. The Knight shift evaluated from the width of the spectra of the powdered samples is temperature-insensitive and scaled to the uniform susceptibility. However, the relaxation rate,

T_1^{-1}, does not obey the Korringa law but exhibits anomalous temperature dependence with a peak formation around 50 K. The absolute value of T_1^{-1} is in excess of the Korringa relation. These behaviors are considered to come from strong antiferromagnetic spin fluctuations with finite wave vector, which is suppressed below 50 K. The κ phase family, situated in the vicinity of metal-insulator and magnetic transitions, is characterized by strong electron correlations.

IV-D-3 Systematic Study of DCNQI-Cu Salts by NMR at Selective Nuclear Sites

Atsushi KAWAMOTO *(Ochanomizu Univ.)*, **Kazuya MIYAGAWA, Yasuhiro NAKAZAWA, and Kazushi KANODA**

[Submitted to *Synth. Metals*]

DCNQI-Cu systems have given frontiers for electronic states in charge transfer complexes containing organic molecules and metallic ions. $(DMe\text{-}DCNQI)_2Cu$ is a representative among these systems because the topical problems in this family such as the metallic state, the re-entrant transition, the insulating state and the magnetic transition, appear with pressure applied or by partial substitution of deuterium. To examine the electronic state in detail and get a unified picture on the variety of the states of these systems, we have performed ^{13}C-NMR experiments on partially and non-deuterated $(DMe\text{-}DCNQI)_2Cu$. For this purpose, the carbon site in =N-CN in the DMe-DCNQI molecule was substituted to ^{13}C isotope. From the measurements of the nuclear spin lattice relaxation rate, T_1^{-1}, we obtained the following conclusions. (1) In the metallic state of non-deuterated $(DMe\text{-}DCNQI)_2Cu$, a relation of T_1TK_s= a constant holds, where T is temperature and K_s is the Knight shift. (2) The relaxation rate is enhanced up to four or five times larger value than that expected by the uncorrelated Korringa relation. (3) The low temperature re-entrant metallic state in $d_2\text{-}(DMe\text{-}DCNQI)_2Cu$ shows the same shift and relaxation rate as the non-deuterated metallic state. Therefore, the present results are against the electron-mass enhancement suggested by specific heat measurements. We also synthesized DCNQI molecules of which nitrogen sites are selectively substituted by ^{15}N. The ^{15}N-NMR measurements are now underway.

IV—E Electron Transport and Magnetic Study of Organic Superconductors

Several organic charge transfer salts which show superconductivity have a layered structure in which conducting donor molecule layers are separated by thick insulating anion layers. Therefore, extremely two-dimensional character is expected in both transport and magnetic properties. In this project, we try to study unique characters of the low-dimensional superconductors such as low-dimensional fluctuations around the transition and the vortex dynamics in the mixed state of type-II superconductors.

IV-E-1 Resistive Transition in an Extremely Two-Dimensional Superconductor α-$(BEDT\text{-}TTF)_2NH_4Hg(SCN)_4$

Hirohiko SATO, Hiromi TANIGUCHI, Yasuhiro NAKAZAWA, Atsushi KAWAMOTO *(Ochanomizu Univ.)*, **Kiyonori KATO, and Kazushi KANODA**

[Submitted to *Synth. Metals*]

The superconductive properties of the title compound has been investigated precisely in terms of extremely two-dimensional model system. The in-plane resistance shows very broad resistive transition between 0.8K and 2.3K, whereas the out-of-plane resistance exhibits rather sharp transition around 0.9K. Although temperature dependences of normal state resistance above the transition temperature show large sample dependences, this anisotropic behavior is reproducible in all samples. The *I-V* characteristics around the transition in both configurations also show interesting behaviors. In the in-plane configuration, it shows non-linear dependence and the data were fitted to the formula of $V \propto I^{\alpha}$. The exponent value of α shows an temperature dependence and it increases from 1.0 at 0.9K to 2.5 at 0.68K, suggesting the existence of *Kosteritz-Thouless* transition in this system. The out-of-plane *I-V* characteristics, on the other hand, show linear dependence around zero current. Below 0.85K clear voltage jumps are visible at the critical currents of this superconductor. The data were tentatively analized in terms of a thermally fluctuated Josephson junction model, assuming that the coupling between conducting layers is very weak. In order to further investigate a possibility of the Josephson characters, we constructed a simultaneous measurement system of in-plane susceptibility and out-of-plane resistance. Our preliminary results show that the diamagnetic component observed in suscptibility abruptly disappear when the applied current crosses the critical current mentioned above. We are now trying to understand the relation between *I-V* characteristics and ac susceptibility in the superconductivity in question.

IV-E-2 Construction of an ac Susceptibility Apparatus at Extremely Low-Temperature Region

Yasuhiro NAKAZAWA, Hiromi TANIGUCHI, Kiyonori KATO, and Kazushi KANODA

There are some organic materials which show exotic conducting and magnetic behavior below 1K and it is important to expand experiments necessary for sample characterization down to the mK region. For this purpose, we have constructed a low-temperature ac susceptibility apparatus of mutual-inductance method for about 1~100mg of samples. The apparatus was mounted on the sample stage of the dilution refrigerator (KELVINOX-25 36115

in the Low-Temperature Center) and measureable temperature ranges between 50mK and 2K. We made two identical coils with 10mm long, 5.5mm inner diameter, and 10.5mm outer diameter which serve as a sample coil and a cancellation coil, respectively. Thin copper wire of 0.1mmϕ is wound 800 turns for primary excitation and 1400 turns for signal detection. Typical excitation current applied for the sample during measurements is 50μA~1mA, which corresponds to the ac field of 2mOe~100mOe. The unique point of this apparatus is an introduction of cancellation unit in addition to the usual excitation unit as shown in Fig.1. By adjusting the amplitude and the phase of ac current in the cancellation unit, it is possible to cancel out the background signal usually originated from residual unbalance between two coils. Using the two-channel function generator (*YOKOGAWA FG120*), we can simultaneously operate the excitation unit and the cancellation unit at exactly the same frequency. We have got a remarkable improvement of signal to noise ratio both in the real part and the imaginary part of the ac susceptibility.

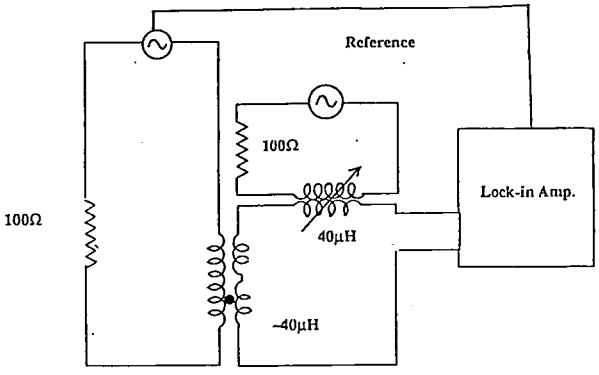

Figure 1.

IV—F Thermodynamic Study of Organic Conductors

In order to get reliable information on the absolute value of electronic density of states and on the entropy distribution around the phase transition, the specific heat study is inevitable. In a line of our systematic studies of BEDT-TTF based charge transfer salts, we have recently started specific heat experiments at low-temperature region.

IV-F-1 Construction of Low-Temperature Specific Heat Apparatus

Yasuhiro NAKAZAWA, Atsushi KAWAMOTO *(Ochanomizu Univ.)*, **and Kazushi KANODA**

Specific heat is an important physical quantity to characterize bulk nature of material. It provides with important information on the low-temperature electronic structure of conducting and magnetic material and on the low-energy phonon structure. Furthermore, by studying temperature dependences of entropy, we can quantitatively discuss the nature of phase transition. In order to establish an overall picture on electronic structure of various organic conductors, we constructed a low-temperature specific heat apparatus. Since the absolute precision is very important for this purpose, we adopted the adiabatic heat pulse method. The calorimeter is composed of a small tungusten sample holder (0.1mm t, 10mm ϕ) and three copper radiation shields surrunding it. The temperatures of radiation shields can be controlled independently to follow the sample temperature. The system is equipped with ^{3}He type refrigeration system and the measureable temperature ranges from 0.6K to 30K. The heat capacity of addenda is 6×10^{-7}J/K at 0.6K which corresponds to that of approximately 100mg of copper. Typical $\Delta T/T$ is about 1~3% depending on the temperature range. The calorimeter can be used in the 10T superconducting magnet and magnetic field dependences are also measureable.

IV-F-2 Specific Heat Study of α-(BEDT-TTF)$_2$MHg(SCN)$_4$

Yasuhiro NAKAZAWA, Atsushi KAWAMOTO *(Ochanomizu Univ.)*, **and Kazushi KANODA**

[Submitted to *Synth. Metals*]

The α-phase of (BEDT-TTF)$_2$MHg(SCN)$_4$ exhibits several interesting physical properties at low temperatures. M=K, Rb and Tl salts show an anomalous phase transition at 8.5K, 12K and 10K, respectively both in transport and magnetic susceptibility. On the other hand, M=NH$_4$ salt does not have such a phase transition. In order to clarify the origin and nature of this phase transition and to discuss the differnce of electronic structure from a thermodynamic viewpoint, we performed a systematic study of low-tempearture specific heat for M=K, Rb and NH$_4$ salts in a temperature range of 1~20K. The low-temperature data below 2.3K obey a simple formula of $C_p/T=\gamma+\beta T^2$. The obtained values are γ=5.29mJ/molK^2, β=16.3mJ/molK^4 for K-salt, γ=10.4mJ/molK^2, β=15.4mJ/molK^4 for Rb-salts and γ=28.8mJ/molK^2, β=15.2mJ/molK^4 for NH$_4$-salt. The Debye temperature (Θ_D) is estimated to be 202K, 199K and 208K, respectively. In the case of NH$_4$ salt, the γ value coincides well with the electron density of states estimated from Pauli paramagnetic susceptibility at 50K. On the other hand, in the case of K and Rb salts γ value reaches only to 35.3% and 55.9%, respectively. These results mean that in the low-temperature phase of latter two salts, electronic density of states is depressed below the expected value from the high-temperature phase. Concerning the specific heat behavior around the phase transition temperature, we could not see distinct anomally at the transition temperatures both in K- and Rb-salts, implying that this transition occurs with a gradual change of electronic structure.

IV—G Ultra-Thin Organic Film Systems Prepared by Molecular Beam Epitaxy (MBE) Technique

As a strategy for a development of new molecular systems of organic materials, we have undertaken the fabrication of ultra-thin organic multi-layer systems with the use of an MBE technique. We are expecting the preparation of such novel 2-dimensional materials as molecutar superlattice systems or intercalation compounds in which special electronic states in the bulk and/or new charge-transfer states in the interfaces could be realized.

We have prepared ultra-thin epitaxially grown phthalocyanine films on alkali halide single crystal substrates. On the basis of this single crystalline film, we are now fabricating double-layer systems of phthalocyanines.

Nonlinear optical effects are found to be significantly correlated with the film structure. The spectral responses of the non-linear susceptibilities are now going to be studied for the phthalocyanine thin film systems.

IV-G-1 Epitaxial Growth of Chloroaluminum Phthalocyanine and Vanadyl Phthalocyanine Double-Layer Structure by the Molecular Beam Epitaxy

Shaoli FANG, Keiichi KOHAMA *(Toyota Motor Corp. and IMS)*, **Hajime HOSHI** *(Tokyo Institute of Technology)*, **and Yusei MARUYAMA**

[*Synth. Met.* **64**, 167 (1994)]

The epitaxial growth of chloroaluminium phthalocyanine on vanadyl phthalocyanine single-crystalline film on KBr substrate is realized using the highly controlled technique of molecular beam epitaxy. Scanning electron microscopy studies indicate that the chloroaluminum pohthaloceyanine layer exhibits unidirectional epitaxy and the epitaxial growth is further confirmed by the low temperature spectral studies of the chloroaluminium phthalocyanine and vanadyl phthalocyanine double-layer structure.

IV-G-2 Spectral Dependence of the Anisotropy of $\chi^{(3)}$ of Epitaxially Grown Vanadyl Phthalocyanine Film

Shaoli FANG, Keiichi KOHAMA *(Toyota Motor Corp. and IMS)*, **Hajime Hoshi** *(Tokyo Institute of Technology)*, **Yusei MARUYAMA**

[Submitted to *J. Appl. Phys.*]

Spectral dependence of the anisotropy of $\chi^{(3)}$ of epitaxially grown vanadyl phthalocyanine has been studied through the technique of third harmonic generation. It is found that the variation of the anisotropy of $\chi^{(3)}$ is a result of the dispersion of the complex ratio $3\chi_{1221}/\chi_{1111}$. There is a sharp two-photon resonance in $\chi^{(3)}$ that may be attributed to the presence of the state 1.88eV above the ground state. Enhancement of $\chi^{(3)}$ is achieved in the unidirectionally oriented vanadyl phthalocyanine film by one order of magnitude.

IV—H Novel Molecular System C_{60}: Fullerites and Fullerides

In the early stage of the research of C_{60} solids we used single crystals which were grown from CS_2 solution. Now we succeeded in the vapor-phase growth of C_{60} and C_{70} single crystals which are free from solvent inclusion. We have studied transport properties of C_{60} single crystals without or with doping of some electron donors.

IV-H-1 Evidence of Spontaneous Magnetic Order in the C_{60} Complex with Tetrakis (dimethylamino) ethlene

Atsushi SUZUKI, Toshiyasu SUZUKI, Roger J. WHITEHEAD, and Yusei MARUYAMA

[*Chem. Phys. Lett.* **223**, 517 (1994)]

Precise measurements on the magnetism of the C_{60}-tetrakis (dimethylamino) ethylene (TDAE) complex provide the first direct observation of spontaneous magnetization and hysteresis curves (remanent magnatization 1.7251×10^{-2} emu g^{-1} and 1.6G at 5K, respectively) with the use of a SQUID magnetometer at zero or low field (resolution 0.4 G). Observed results on the thermo-remanent magnetization, zero-field magnetization and the real and imaginary parts (m′, m″) of the ac magnetic moment all support the existence of spontaneous magnetization and hysteresis below 15K.

IV-H-2 Preparation of Single Crystals of C_{60}-(TDAE)

Atsushi SUZUKI, Toshiyasu SUZUKI and Yusei MARUYAMA

In order to investigate the nature of the magnetic properties of C_{60}-TDAE, we have tried to prepare single crystals of C_{60}-TDAE with applying a diffusion method for the solution of C_{60} and TDAE.

IV-H-3 Application of a Layer-by-Layer Deposition for the Preparation of Crystalline metal-doped C_{60} Thin Films

Takeshi ARAI, Toshifumi TERUI *(Communications Research Laboratory, Kobe)* **and Yusei MARUYAMA**

Preparation of crystalline metal-doped C_{60} films have been tried by a layer-by-layer deposition method. La_xC_{60} systems are the first target for this strategy.

IV-H-4 Disorder and Phonon Windows for Superconductivity in Fullerides

Valery IVANOV *(Kurnakov Institute and IMS)* **and Yusei Maruyama**

[To be submitted to *Physica C*]

The fullerides A_xC_{60} are classified as isotropic "dirty" superconductors of the second kind with phonon mediated electron-electron pairing. In suggested oversimplified model the A_xC_{60} is characterized by windows of low-frequency intermolecular phonons, high-frequency intramolecular ones and Coulomb energy ranges with cutoffs ω_{er}, ω_{ra} and ω_c, respectively. On the reason of the inherent imperfections of fullerides the extremely short collision lifetime of electrons force to assume the "impurity representation" and to impose the $\omega_{er,\ ra,\ c}$ in initial superconducting equations in accordance with the Anderson theorem for potential scattering. The different interaction radii, $r_{e\text{-}e} < r_{e\text{-}ra} < r_{e\text{-}er}$ lead to renormalization of the calculated coupling strength constant and to abandonment of intermolecular phonons for superconducting pairing in A_xC_{60} due to log's of the Tolmachev-Bogolubov-Fyablikov kind. To illustrate the usefulness of suggested three square-well model of A_xC_{60} the isotope effect exponent and pressure effect for T_c are calculated.

IV—I Electrochemical Properties of the Organofullerenes and Metallofullerenes

Buckminsterfullerene, C_{60} is an electronegative molecule which can accept up to six electrons in the solid state and solution. Because of this property, superconducting and ferromagnetic materials have been produced by doping with alkali metals and organic donors. We are interested in the electronic structures of fullerene derivatives, such as organofullerenes and metallofullerenes, and performed electrochemical measurements.

IV-I-1 Redox Properties of Organofullerenes

Toshiyasu SUZUKI, Yusei MARUYAMA, Takeshi AKASAKA *(Tsukuba Univ.)*, **Wataru ANDO** *(Tsukuba Univ.)*, **Kaoru KOBAYASHI** *(Yokohama National Univ.)*, **and Shigeru NAGASE** *(Yokohama National Univ.)*

[*J. Am. Chem. Soc.*, **116**, 1359 (1994)]

A comparative study using cyclic, differential pulse and Osteryoung square wave voltammetry is presented on organofullerenes derivatized with oxygen-, carbon-, and silicon-containing groups. Electron affinities of the organofullerenes increase with increasing electronegativities of the attached atoms. $C_{60}O$ is a stronger electron acceptor than C_{60}, although its electroreductions are CV irreversible. In the carbon-derivatized C_{60}, hybridization of the attached carbon atoms and electron-withdrawing groups also affect their reduction potentials. As previously described for C_{60}, no CV reversible electrooxidation waves were observed for all organofullerenes studied. Electron-donating groups, such as alkyl and silyl, significantly lower the oxidation potentials of the organofullerenes. The AM 1 molecular orbital calculations were performed on C_{60} and selected organofullerenes. The first and second reduction potentials correlate well with the LUMO energy levels, while the third reduction potentials correlate better with the LUMO + 1 energy levels. The peak oxidation potentials also show a good linear correlation with the HOMO energy levels.

IV-I-2 Electrochemical Properties of La@C_{82}

Toshiyasu SUZUKI, Yusei MARUYAMA, Tatsuhisa KATO, Koichi KIKUCHI *(Tokyo Metropol. Univ.)*, **and Yohji ACHIBA** *(Tokyo Metropol. Univ.)*

[*J. Am. Chem. Soc.*, **115**, 11006 (1993)]

Electrochemical measurements have been done on the pure metallofullerene La@C_{82} for the first time. Five reversible reduction and one reversible oxidation processes were observed by cyclic voltammetry, differential pulse voltammetry, and Osteryoung square wave voltammetry. Our results indicate that La@C_{82} is a moderate electron donor as well as a stronger electron acceptor than any empty fullerenes.

IV-I-3 Characterization of the Isolated Y@C_{82}

Koichi KIKUCHI *(Tokyo Metropol. Univ.)*, **Yasuhiko NAKAO** *(Tokyo Metropol. Univ.)*, **Shinzo SUZUKI** *(Tokyo Metropol. Univ.)*, **Yohji ACHIBA** *(Tokyo Metropol. Univ.)*, **Toshiyasu SUZUKI, and Yusei MARUYAMA**

[*J. Am. Chem. Soc.*, **116**, 9367 (1994)]

The major Y@C_{82} isomer (Y@C_{82}-A) has been isolated in pure form and characterized for the first time. Its UV-vis-near-IR absorption spectrum is strikingly similar to that of the major La@C_{82} isomer (La@C_{82}-A). Two characteristic peaks (990 and 1405 nm) are slightly shifted to the short wavelengths relative to those of La@C_{82}-A (1000 and 1420 nm). The cyclic voltammogram of Y@C_{82}-A shows one reversible oxidation and four reversible reductions. The first oxidation and reduction potentials of Y@C_{82}-A are anodically shifted by 30 and 80 mV, respectively, relative to those of La@C_{82}-A. These relatively small shifts are in agreement with the ab initio calculations which predict that the ionization potential and the electron affinity of Y@C_{82} are almost the same as those of La@C_{82}.

IV—J Phase Transitions and Dynamical Ordering in Liquid Crystals

Nuclear magnetic resonance (NMR) methods have been applied to the study of dynamical ordering in liquid crystal systems of recent interest. Our studies contain reentrant mesogens, hexatic phase, discotic columnar mesophases, and newly developed liquid crystals of cyclotriphosphazene derivatives.

IV-J-1 ^{1}H and ^{2}H NMR Studies of Dynamic Orientational, Translational, and Dipolar Orders in Doubly Reentrant Liquid Crystal CBOBP and CBOBP-*d17*

Seiichi MIYAJIMA and Takamasa HOSOKAWA

[Magnetic Resonance and Related Phenomena vol. 2, pp. 631, ed. K. M. Salikhov, 1994, Zavoisky Physical-Technical Institute of the Russian Academy of Sciences, Kazan]

One of the peculiar phenomena in the liquid crystal world is a reentrant nematic phase transition, in which one-dimensional periodic lattice *melts* as the temperature is *lowered.* Here we present determination of the microscopic nature of the doubly reentrant phase transition sequence, Isotropic (I)-Nematic (N)-Smectic Ad (S_{Ad})-Reentrant Nematic (RN)-Smectic A1 (S_{A1}), in 4-cyanobenzoyloxy-[4-octylbenzoyloxy]-*p*-phenylene (CBOBP) and its chain-deuterated homologue CBOBP-*d17.*

It has been revealed from the technique of director realignment in the magnetic field that the rotational viscosity changes drastically at the S_{A1}-RN-S_{Ad}-N phase transitions, while the orientational order parameter S_0 of the molecular core was nearly continuous at the RN-S_{Ad}-N transitions. The S_0 exhibited a first order jump at the S_{A1}-RN transition. ^{1}H NMR line shape in CBOBP-*d17* showed that intermolecular aromatic ^{1}H-^{1}H dipolar interaction is larger in the S_{Ad} phase than in the S_{A1} phase although the average intermolecular distance is larger in S_{Ad}. This provides an evidence that antiparallel association occurs predominantly in the S_{Ad} phase.

^{2}H NMR study revealed that each of the segmental order parameters S_i (i=1—8) of the octyl chain increased on going from S_{Ad} to RN phase, showing that the octyl chain is in a more restricted environment in the RN phase despite the more fluid macroscopic properties.

Unusually large isotope effect (—5 K) was observed for the temperature of the reentrant phase transition (RN-S_{Ad}) showing that this transition is closely related to the dynamical nature of the octyl chain.

The present ^{1}H and ^{2}H NMR studies revealed that the S_{A1} and S_{Ad} phases are stabilized by competing mechanisms: Electrostatic gain due to the antiferroelectric intermolecular correlation stabilizes the S_{Ad} structure which guarantees high alkyl disorder. When the temperature is lowered, the energetic gain caused by more stretched alkyl chain favors the S_{A1} structure. The RN phase appears as a *frustrated* state due to these competing interactions. This phase is characterized by the *coexistence of low viscosity and fairly high orientational orders.*

IV-J-2 Molecular Dynamics and Ordering Characteristics of the Hexatic Smectic B Liquid Crystal

Noriko YAMAMURO and Seiichi MIYAJIMA

In their theory of two-dimensional melting, Halperin and Nelson predicted possible existence of *hexatic* phase in between two-dimensional liquid and solid, and is characterized by the existence of quasi long range *bond orientational order.* One of the existing prototypes for this phase is the hexatic smectic B [S_B(hex)] phase in liquid crystal. To analyze the structural and dynamical nature of this mesophase, ^{1}H and ^{13}C NMR studies were undertaken for 4-propyonyl-(4-heptanoyloxy)azobenzene (PHOAB), the only existing compound having S_A-S_B(hex)-S_B(cryst) phase sequence, corresponding to 2-D liquid-hexatic-solid phases.

The orientational order for the azobenzene core was revealed to be nearly saturated ($\geq$0.9) in S_B(hex) and S_B(cryst) phases so that no appreciable change was observed at the phase transition. However, the dynamical characteristics of the hexatic phase was revealed by the magnetic relaxation measurement. The predominant relaxation mechanism was self-diffusion in the S_B(hex) phase, the correlation time for this motion being 5×10^{-9} s. On entering the S_A phase the correlation time becomes shorter by about 0.66, while on entering the S_B(cryst), the diffusional motion nearly stops and the rotational motion predominates. Our NMR observation revealed that two-dimensional quasi long range bond orientational order in the S_B(hex) phase is realized by rapid rotation and high orientational order about the long molecular axis, and translational diffusion of an intermediate rate.

IV-J-3 ^{13}C-NMR Study of the Microscopic Ordering, Dynamics, and Intermolecular Interaction in the Discotic Liquid Crystalline 1, 4, 8, 11, 15, 18, 22, 25-Octaoctylphthalocyanine

Noriko YAMAMURO, Seiichi MIYAJIMA and M. J. COOK* *(*Univ. East Anglia)*

From the viewpoint of developing disordered material with novel electronic properties, alkyl-substituted phthalocyanines are of interest since they condense in discotic columnar mesophase in which the phthalocyanine (Pc) rings are stacked face-to-face so that intermolecular π-π overlap may be expected. By using the title compound recently synthesized in the University of East Anglia, we performed ^{13}C and ^{1}H NMR experiments to study the microscopic ordering, dynamics, and intermolecular interaction in the D_{hd} (discotic hexagonal disordered) and D_{rd} (discotic rectangular disordered) mesophases.

Co-facial intermolecular interaction was evidenced by the intermolecular diamagnetic effect in the magic-angle-sample-spinning experiment. It has also been revealed, from the NMR spectra for the magnetic-field-aligned specimen of the D_{hd} phase, that the molecules are aligned so that the Pc plane normal is perpendicular to the external field, and the ring rotates rapidly enough (> 6 kHz) so that the chemical shift anisotropy within the plane is averaged

out. The order parameter of the Pc ring normal about the director was revealed to be very small. By using the molecular-frame-fixed shielding tensor of the known aromatic carbons, S=0.16 was obtained. The symmetry change at the D_{rd}-D_{hd} phase transition was accompanied by significant broadening and downfield shift of the aromatic carbon lines, which is due to tilting of the director from the external field.

The disordered nature of the D_{hd} phase is consistent with the long interplanar separation (4.4 Å), and should be due to the position of the alkyl substitution which incorporates high steric hindrance. Weakness of the interplanar interaction and the highly disordered nature of the Pc ring suggest that the alkyl chains play an important role in sustaining the columnnar architecture.

IV-J-4 ^{31}P and ^{13}C NMR Studies on the Nature of New Liquid Crystalline Hexakis(alkylbiphenyl)cyclotriphosphazenes

Seiichi MIYAJIMA, Toshiya SUZUKI*, Keiichi MORIYA*, and Shinichi YANO* *(*Gifu Univ.)*

New liquid crystalline compounds, Hexakis(alkylbiphenoxy)cyclotriphosphazene have been synthesized, and their structural and dynamical natures were studied by ^{31}P and ^{13}C NMR spectroscopies. Novel mesomorphic features were expected due to uniqueness of the molecular structure such as containing twelve phenylene rings and the central cyclotriphosphazene (CTP) ring. In the high temperature liquid crystalline (S_A) phase of the dodecyl derivative, the ^{31}P NMR exhibited a line shape characteristic of rotating triangular three spin system. It has been revealed, from the angular dependence study, that the molecules are ordered so that the C_3 axis of the cyclotriphosphazene (CTP) ring preferentially points along the external magnetic field, the orientational order being 0.44 which is very small for S_A liquid crystal. From the combined studies of chemical shielding and the dipolar splittings, the chemical shielding tensor was determined: The shielding tensor was nearly axially symmetric having its most shielded axis within the CTP plane. The components are (32.7, 32.7, −35.4), the isotropic value and the anisotropy being 10.0 and 68.1, respectively (in ppm units relative to phosphoric acid). ^{13}C NMR study revealed a higher orientational order at the phenylene sites. These results show a unique nature of the CTP liquid crystal: The six substituents are bundled together in a cylindrical shape. The terminal dodecyl and the central CTP are highly disordered, while the twelve phenylene rings maintain the overall cylindrical shape, and play major role in sustaining the ordered structure.

IV—K Conducting Molecular Systems

New metallic layered compound, titanium disulfide intercalated with ethylenediamine, highly conducting organic semiconductors, TTC$_n$-TTF, and alkali metal-doped fullerenes have been studied by the technique of solid state NMR.

IV-K-1 New Metallic Layered Compound of Titanium Disulfide Intercalated with Ethylenediamine

Seiichi MIYAJIMA, Hironori OGATA, Hiroki FUJIMORI*, Kazuhisa KOBASHI*, Takehiko CHIBA*, and Kazuhiro ENDO** *(*Nihon Univ and **ETL)*

To investigate the effect of molecular motion on the electronic properties of solids, a new metallic layered compound was synthesized. Titanium disulfide (TiS_2) has nearly zero electronic density of states at the Fermi energy in its pristine form. If a guest molecule is incorporated into the van der Waals gap of TiS_2, the electronic states will be modified by charge transfer and hydrogen bonding, and these interaction can possibly be modulated by the motion of the guest molecule.

By the reaction of TiS_2 with an electron donor, ethylenediamine (en), nonstoichiometric compound, $Ti_{1.1-1.4}S_2(en)_{0.3-0.4}$, was formed. X-Ray analysis showed cell doubling along a, while lattice expansion took place along c by 3.92 Å. The compound was stable at ambient atmosphere. The metallic nature was proved by the Pauli paramagnetism and conduction ESR. The ESR relaxation was dominated by Elliot mechanism. The temperature-dependence of the resistivity was represented by $\rho=a+bT+cT^2$, where b was 2.6×10^{-6} Ω cm K^{-1} while this term was absent in the pristine TiS_2, verifying the increase in intrapocket electron-phonon scattering due to increased $N(E_F)$.

IV-K-2 ^{1}H, ^{13}C, and ^{15}N NMR Studies of Titanium Disulfide-Ethylenediamine Intercalation Compound

Seiichi MIYAJIMA, Hironori OGATA, Hiroki FUJIMORI*, Kazuhisa KOBASHI*, Takehiko CHIBA*, Kazuhiro ENDO, and R. E. TAYLOR***** *(*Nihon Univ, **ETL, and ***Bruker Japan)*

Guest-host interaction and dynamics of the guest molecule were studied by the technique of solid state high resolution and broadband NMR. ^{13}C and ^{15}N CP/MAS spectra suggest charge transfer shifts. High resolution ^{1}H NMR was performed by applying Brum-Rhim 24 pulse sequence with magic angle sample rotation. In addition to the main peak at 2.5 ppm which is near the peak position, 1.1 and 2.7 ppm, for solution ethylenediamine, extra peak appeared at 7.0 ppm with significant intensity, suggesting hydrogen bonding between amino proton and the host sulfur atom. Structural inhomogeneity was also evidenced. Spin-lattice relaxation rates were measured by broadline NMR. Motionally induced relaxation was observed above 50 K. Assuming a rotational jump of the guest molecule among three sites, the activation energy of 15.5 kJ mol^{-1} and the rotational correlation time of *ca.* 1×10^{-8} s were estimated at room temperature. This low potential barrier and the rapid rotation is consistent with the absence of dipolar multiplet due to ^{13}C-^{14}N residual dipolar interaction in the ^{13}C CP/MAS spectrum. Coexistence of charge transfer, hydrogen bonding, and molecular motion are thus proved, however, no anomaly was observed for the electrical

conduction which is attributable to the dynamics of the guest molecule.

IV-K-3 Solid State High Resolution ^{13}C NMR Study of the Intermolecular Interaction in Organic Semiconductors TTC_n-TTF

Seiichi MIYAJIMA, Takehiko CHIBA*, Gunzi SAITO, and Hiroo INOKUCHI***** *(*Nihon Univ., **Kyoto Univ., and ***Okazaki Natl. Res. Inst.)*

[*J. Phys. Chem.* submitted]

The derivatives of tetrathiafulvalene (TTF) with four long alkylthio chains, tetrakis(alkylthio)-tetrathiafulvalenes, TTC_n-TTF, are known to be ones of the known most conducting single component organic compounds. Mechanism of this high conductivity has been studied by the technique of solid state high resolution ^{13}C NMR. In the solid state of the long-chain compounds, significant downfield shifts, 3–4 ppm from those in the molten states, were observed for the alkyl carbon lines, and it was shown that the energy difference between the *trans/gauche* rotational isomeric states are more than ten times larger in the solid state than that in the molten state. This provides an evidence of highly closely packed nature of the alkylthio chains in the solid state. It was also found that the solid state chemical shieldings for both of the alkyl and the ethylene carbons gradually decreased as the chain length increased, suggesting that the electronic excitation enegy gradually decreases due to the increasing intermolecular π-π overlap. Only the inner ethylene carbons exhibited upfield shift on crystallization, which has been interpreted as an enhancement of the π-electron density in the central area of the TTF moiety. These findings provide evidences that the one-dimensional electrical conduction is enhanced by the intermolecular π-π overlap caused by the extremely closely packed nature of the long alkylthio chains, and therefore the electronic states of the organic semiconductors can be controlled by the length of the alkyl chains.

IV-K-4 Transport Properties of C_{70} Single Crystals Doped with Alkali Metals

Hironori OGATA, Seiichi MIYAJIMA, and Yusei MARUYAMA

To investigate the existence of metallic phase, various kinds of alkali metal(Na, K, Rb or Cs) doped C_{70} compounds were synthesized by using C_{70} single crystals grown from the vapor phase as a starting material, and temperature dependences of electrical resistivity and thermoelectric power were measured. Amounts of alkali metal doping were optimized by monitoring the resistivity *in situ*. Table 1 shows the electrical resistivity at room temperature, activation energy, and thermoelectric power at room temperature for each sample. The room temperature resistivity decreases from Na-complex to Cs-complex. This fact may be explained by assuming that the formation of over-doped phase is hindered for large dopants. No metallic behaviors were observed.

Table 1. Values of electrical resistivities at room temperature, activation energies, and thermoelectric powers at room temperature for alkali-metal doped C_{70} single crystrals.

	$\rho(\Omega \cdot cm)$(r.t.)	E_a(eV)	S(μV/K)(r.t.)
Na_xC_{70}	$\sim 10^6$	0.5	—
K_xC_{70}	$\sim 10^4$	0.5	−70
Rb_xC_{70}	$\sim 10^3$	0.3	+80
Cs_xC_{70}	$\sim 10^2$	0.18	+20

IV—L Photoelectron Spectroscopy of Organic Solids in Vacuum Ultraviolet Region

The works of ultraviolet photoelectron spectroscopy (UPS) and also of UPS with synchrotron radiation lightsource (UVSOR-UPS) of organic materials, especially BTQBT and C_{60} series, have been proceeded to find their quantitative electronic structures.

IV-L-1 Intermolecular Energy-band Dispersion in Oriented Thin Films of Bis(1,2,5-thiadiazolo)-*p*-quinobis(1,3-dithiole) (BTQBT) by Angle-resolved Photoemission

Shinji HASEGAWA, Takehiko MORI, Kenichi IMAEDA, Shoji TANAKA, Yoshiro YAMASHITA, Hiroo INOKUCHI, Hitoshi FUJIMOTO *(Kumamoto Univ.)*, **Kazuhiko SEKI** *(Nagoya Univ.)*, **and Nobuo UENO** *(Chiba Univ.)*

[*J. Chem. Phys.* **100**, 6969 (1994)]

Angle-resolved ultraviolet photoemission spectra using synchrotron radiation were measured for oriented thin films of Bis(1,2,5-thiadiazolo)-*p*-quinobis(1,3-dithiole) (BTQBT) on graphite. From the photon energy dependence of normal emission spectra, the energy-band dispersion of π-bands were observed for the highest (HOMO) and next highest (NHOMO) bands. This is the first observation of intermolecular dispersion in a single-component organic molecular crystal. The results demonstrate that the BTQBT molecules have a strong intermolecular interaction, which can be derived from the introduction of a covalent interaction between sulfur atoms in addition to the usual intermolecular interaction by van der Waals forces.

IV-L-2 Ultraviolet Photoelectron Spectra of C_{82} and K_xC_{82}

Shojun HINO*, Kazuo MATSUMOTO*, Shinji HASEGAWA, Kentaro IWASAKI, Kyuya YAKUSHI, Takashi MORIKAWA, Takashi TAKAHASHI**, Kazuhiko SEKI***, Koichi KIKUCHI****, Shinzo SUZUKI****, Isao IKEMOTO****, and Yohji ACHIBA****** *(*Chiba Univ., **Tohoku Univ., ***Nagoya Univ., ****Tokyo Metropolitan Univ.)*

[*Phys. Rev.* **B48**, 8418 (1993)]

Photoelectron spectra of C_{82}, one of the newly isolated fullerene compounds, are measured with a synchrotron radiation light source. The spectra resemble those of C_{84}, and their spectral onset is at 1.1_5 eV below the Fermi level (E_f). The first band is a broad band and consists of two peaks located at 2.2 eV and 3.3 eV. A slight structure is observed at the low binding energy side of the first band. The intensity of the two peaks of the band oscillates with the incident photon energy change, as are observed in C_{60}, C_{70} and C_{84}. The second band located between 4 and 6.2 eV with a peak at 5.3 eV and an accompanying shoulder at the low binding energy side. The third band locates between 6.2 and 9 eV and consists of a peak at 7.8 eV and a distinct shoulder at 6.5 eV. Potassium dosing brings a new band between the E_f and the first band and its intensity grows as the potassium dosage increases. The spectral onset approaches toward the E_f in accordance with increase of potassium dosage but it does not cross the E_f, which indicates a semi-conductive nature of the potassium dosed C_{82} complex. The spectra of low or high potassium dosage can be understood by the rigid band model, but the spectral change at medium potassium dosage seems to support a non rigid band filling of the electron from the potassium atoms.

IV-L-3 Electronic Structure of Metallofullerene, LaC_{82}: Electron Transfer from Lanthanum to C_{82}

Shojun HINO*, Hiroaki TAKAHASHI*, Kentaro IWASAKI*, Kazuo MATSUMOTO*, Takafumi MIYAZAKI, Shinji HASEGAWA, Koichi KIKUCHI, and Yohji ACHIBA**** *(*Chiba Univ., **Tokyo Metropolitan Univ.)*

[*Phys. Rev. Lett.* **71**, 4261 (1993)]

Ultraviolet photoelectron spectra (UPS) of LaC_{82} that is in question whether the lanthanum atom is inside the carbon cage or not are measured for the first time. The UPS of LaC_{82} is analogous to those of C_{82}, but there is a critical difference in the region just below the Fermi level. Comparison of both LaC_{82} and C_{82} spectra reveals that two new peak components are formed in LaC_{82}. They locate at 0.9 and 1.6 eV below the Fermi level, and their intensity ratio is 1 : 2. This indicates that three electrons are transferred from the lanthanum atom to the lowest unoccupied molecular orbital (LUMO) and second LUMO of the C_{82} molecule, that is, $La^{+3}C_{82}^{-3}$. Theoretical calculations on LaC_{82} suggest that an oxidation state of the lanthanum atom depends on its position in the LaC_{82} molecule; it is +2 when the lanthanum atom is outside the cage, but it is +3 when it is inside the cage. Our UPS results support an encapsulation of the lanthanum atom inside the carbon cage.

IV-L-4 Photoelectron Spectroscopy of Polysilanes, Polygermanes and Related Compounds

Hisao ISHII*, Akira YUYAMA*, Satoru NARIOKA*, Kazuhiko SEKI*, Shinji HASEGAWA, Masaie FUJINO, Hiroaki ISAKA**, Michiya FUJIKI**, and Nobuo MATSUMOTO**** *(*Nagoya Univ., **Nippon Telegraph and Telephone Corporation)*

[*Synthetic Metals*, in press]

Ultraviolet photoelectron spectra were measured for five polysilanes, two polygermanes, three Si-Ge copolymers and tert-butyloctasilacubane. The UPS spectra of the polyalkylsilanes and polyalkylgermanes indicate that the valence electronic structure can be regarded as an overlap of those of the backbone and substituents. On the other hand, the spectra of polyarylsilanes imply that the uppermost part of the valence band structure is slightly different from the superposition of those of the Si backbone and substituents due to σ-π interaction. The results of copolymers and tert-butyloctasilacubane are also discussed.

IV-L-5 The Electronic Structure and Energy Level Alignment of Porphyrinmetal Interfaces Studied by Ultraviolet Photoelectron Spectroscopy

Hisao ISHII*, Satoru NARIOKA*, Daisuke YOSHIMURA*, Masaki SEI*, Yukio OUCHI, Shinji HASEGAWA, Takafumi MIYAZAKI, Yutaka HARIMA, Kazuo YAMASHITA**, and Kazuhiko SEKI*** *(*Nagoya Univ., **Hiroshima Univ.)*

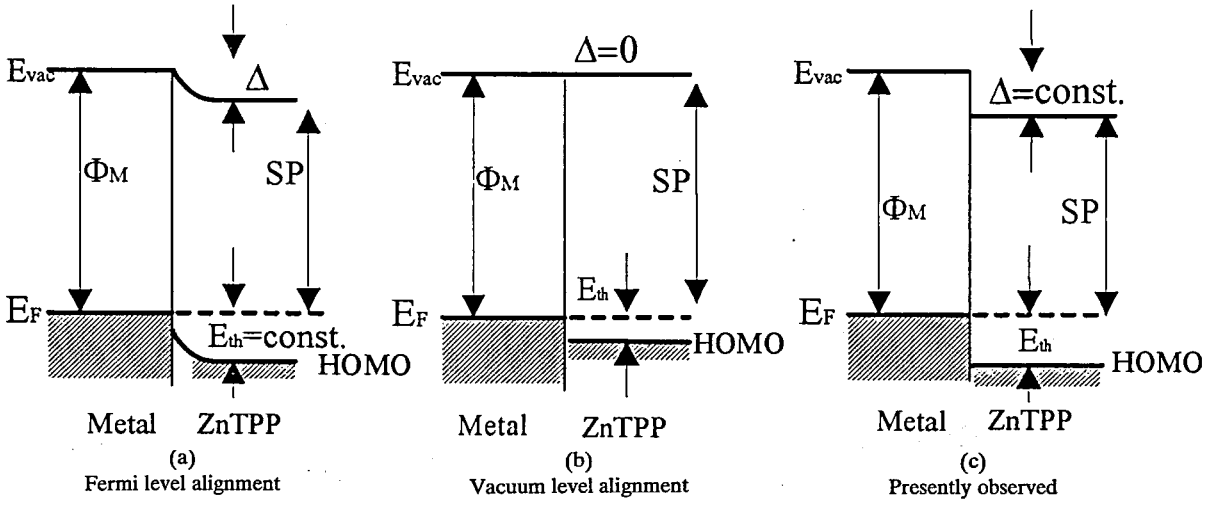

Figure 1.

Recently the applications of various organic semiconductors to electric devices have been extensively studied. The electronic structure of organic compound/metal interface is indispensable for understanding and refining the performance of organic devices. However there have been few studies even about the details of band lineup at organic/metal interface and this basic problem for organic devices is not yet well understood. In this study, we investigated the electronic structure of metal/5, 10, 15, 20-tetraphenylporphyrin (ZnTPP) interfaces known as solar cell systems using ultraviolet photoelectron spectroscopy (UPS), including the effect of samples exposure to oxygen. Figure 1(c) shows the energy diagram of the interface obtained from our results. We found that the electronic energy levels of ZnTPP align with the vacuum level of the substrate metal with a constant energy shift of the vacuum levels across the interface. These findings cannot be explained by the concept of Fermi level alignment (Fig.1(a)) or vacuum level alignment (Fig.1(b)). We also found that sample exposure to oxygen induces energy level shift in close relation with change of substrate work function at oxygen exposure. The observed interfacial electronic structure is consistent with the electric characteristics of Al/ZnTPP/Au solar cell.

IV-L-6 Electronic Structure of Doped C_{60}: Strong Correlation or Lattice Distortion?

Takashi TAKAHASHI, Takashi MORIKAWA, Hiroshi KATAYAMA-YOSHIDA *(Tohoku Univ)*, **Shinji HASEGAWA, Hiroo INOKUCHI, Kazuhiko SEKI** *(Nagoya Univ.)*, **Shojun HINO** *(Chiba Univ.)*, **Kouichi KIKUCHI, Sinzo SUZUKI, Isao IKEMOTO, and Yohji ACHIBA** *(Tokyo Metropolitan Univ.)*

[*Physica* **B186-188**,1068 (1993)]

It was found by photoemission and inverse photoemission that an energy gap with a finite density of state at the bottom (a pseudo-gap) opens at the Fermi level for alkali-doped solid C_{60} at the composition A_3C_{60} (A=alkali metal). Strong electron correlation and lattice distortion (Jahn-Teller effect) are discussed as possible origins for pseudo-gap.

IV—M Organic Metals

In an attempt to develop new organic superconductors and to explore the related phenomena, new organic conductors have been prepared and the physical properties have been investigated. In this year, the structural and physical properties of cation-radical salts of bis-fused TTF donors are investigated. Among them, $(EOET\text{-}TTP)_3AsF_6$ is a new κ-type salt with 3:1 composition. The donor TMEO-TTP makes many salts metallic down to He temperatures with linear and octahedral anions. TTM-TTP gives three different phases of the iodine salts, one of which, $(TTM\text{-}TTP)I_3$, shows metallic conductivity, 700 Scm^{-1} at room temperature, in spite of its 1:1 composition.

IV-M-1 Ethylenedioxy Substituted 2,5-Bis(1',3'-dithiol-2'-ylidene)-1,3,4,6-tetrathiapentalenes and Their Conducting Salts

Yohji MISAKI,* Hiroyuki NISHIKAWA,* Kazuya KAWAKAMI,* Tokio YAMABE,* Takehiko MORI, Hiroo INOKUCHI, Hatsumi MORI, and Shoji TANAKA**** *(*Kyoto Univ., **ISTEC)*

[*Chem. Lett.* **1993**, 2073]

Several radical-cation salts of the title electron donor (see Scheme) showed metallic conductivity down to 0.6 K. The X-ray crystal structure of the AsF_6 salt, $(EOET\text{-}TTP)_3AsF_6$ revealed that the donors have "κ-type" arrangement in the conducting sheet. This is the second example of the κ-type salt having a composition other than 2:1. This salt exhibits metallic conductivity down to 0.6 K as well.

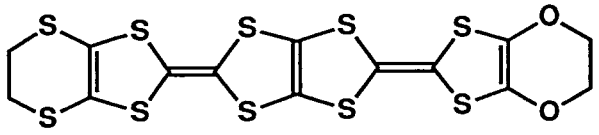

EOET-TTP

IV-M-2 Structure and Physical Properties of $(TMEO\text{-}TTP)_2Au(CN)_2$

Takehiko MORI, Hiroo INOKUCHI, Yohji MISAKI,* Hiroyuki NISHIKAWA,* Tokio YAMABE,* Hatsumi MORI, and Shoji TANAKA**** *(*Kyoto Univ., **ISTEC)*

[*Chem. Lett.* **1993**, 2085]

Radical-cation salts of TMEO-TTP with linear and octahedral anions exhibit metallic conductivity down to 0.6 K. The title salt has two-dimensional donor arrangement (Fig. 1), and the measurements of electrical conductivity, thermoelectric power, and ESR show a characteristic metal-to-metal transition.

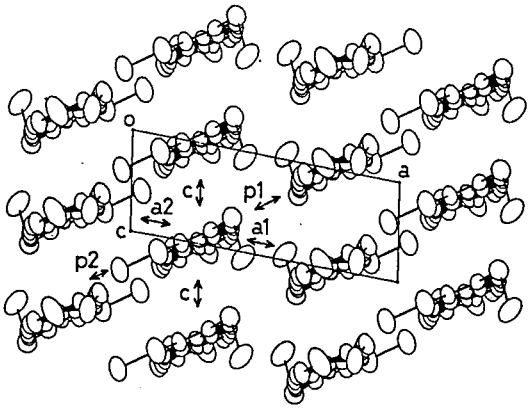

Fig. 1 Donor arrangement of $(TMEO\text{-}TTP)_2Au(CN)_2$.

IV-M-3 Crystal Structures of Highly Conducting Iodine Complexes of TTM-TTP

Takehiko MORI, Hiroo INOKUCHI, Yohji MISAKI,* Tokio YAMABE,* Hatsumi MORI, and Shoji TANAKA**** *(*Kyoto Univ., **ISTEC)*

[*Bull. Chem. Soc. Jpn.* **67**, 661 (1993)]

Methylthio substituted bis-fused tetrathiafulvelene, TTM-TTP (2,5-bis[4,5-bis(methylthio)-1,3-dithiol-2-ylidene]-1,3,4,6-tetrathiapentalene) makes three phases of iodine complexes: (TTM-TTP)I_3, α-(TTM-TTP)$_2I_3$, and β-(TTM-TTP)$_2I_3$. The 1:1 complex exhibits high conductivity, 700 Scm^{-1} at room temperature, and is metallic down to about T_{MI}=160 K (Fig. 1). This complex has uniform columns of the donor molecules. In the semiconducting α-(TTM-TTP)$_2I_3$, one quarter of the donors is incorporated in the anion sheet, and the sides of the other trimeric donors are blocked by the anion sheets. β-(TTM-TTP)$_2I_3$ shows metallic conductivity down to T_{MI}=20 K.

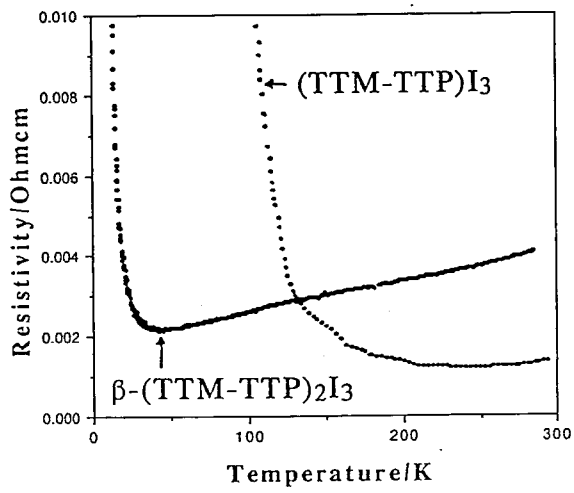

Fig. 1. Electrical conductivity of (TTM-TTP)I_3 (//c) and β-(TTM-TTP)$_2I_3$ (//c).

IV—N Electrical Conduction and its Related Properties of Organic Solids

The electronic properties of single component organic semiconductors, BTQBT and its related compounds, and C_{60} complexes have been observed.

IV-N-1 Temperature Dependence of Hall Mobility in a Single Crystal of Organic Semiconductor BTQBT

Kenichi IMAEDA, Yongfang LI *(Inst. of Chem., Beijing)* **Yoshiro YAMASHITA, Hiroo INOKUCHI, and Mizuka SANO** *(International Christian Univ.)*

The Hall mobility of a BTQBT (bis(1,2,5-thiadiazolo)-*p*-quinobis(1,3-dithiole)) single crystal was found to be 2.4 $cm^2V^{-1}s^{-1}$ at 330 K and 6.3 $cm^2V^{-1}s^{-1}$ at 175 K. It changed with temperature as $T^{-1.6}$ in the range 175 to 330 K, which corresponds to the $T^{-1.5}$ temperature dependence theoretically predicted for the mobility determined by lattice scattering. The sign of carrier was determined to be positive over the whole temperature range, which indicates an electrical conduction dominated by hole carriers.

IV-N-2 Magnetic and Structural Characterization of Superconducting Sodium-Doped C_{60} Prepared with the Thermal Decomposition of Sodium Azide

Kenichi IMAEDA, Ilias I. KHAIRULLIN *(Uzbek Acad. of Sci.)*, **Kyuya YAKUSHI, and Hiroo INOKUCHI**

[*Synthetic Metals, to be published in Proceedings of ICSM '94*]

We have prepared Na_4C_{60} samples by the different ways of the thermal decomposition of sodium azide NaN_3. The superconducting (SC) samples were obtained by the decomposition under the dynamic vacuum, while the non-SC samples by the decomposition in the sealed tube. The SC sample was composed of two fcc phases with a lattice constant a=14.207(5) Å (phase A) and a=14.339(4) Å (phase B). On the contrary, the non-SC sample had single fcc phase which can be assigned to phase A. This result strongly suggests that phase B is the SC phase.

IV—O Electronic Conduction and its Mechanism of Cytochromes

Hiroo INOKUCHI, Kenichi IMAEDA, Yusuke NAKAHARA *(Tech. Coll. of Miyakonojo)*, **Kenji ICHIMURA** *(Kumamoto Univ.)*, **Yongfang LI** *(Inst. Chem. Academia Sinica)*

Using x-ray photoelectron spectroscopy (XPS) and Langmuir-Blodgett film preparation technique, the electronic conduction and its mechanism of cytochrome *c* series has been analyzed.

IV—P Preparation and Characterization of Semiconductor Thin Films by New Excitation Processes

Semiconductor thin films of high quality, especially prepared at low temperatures, are required for the development of VLSI(Very Large-Scale Integration) and new functional devices in the near future. Synchrotron radiation-assisted, plasma-enhanced, and photo-excited CVD (Chemical Vapor Deposition) are promising. We have been developing new semiconducting thin films and new devices by these excitation methods.

IV-P-1 Preparation and Characterizations of $CuIn_XGa_{1-X}Se_2$ Thin Films Crystallized by Annealing

Toshiyuki YAMAGUCHI, Masayoshi SUZUKI *(Wakayama College of Tech.)*, **and Akira YOSHIDA** *(Toyohashi Univ. of Tech. and IMS)*

[*Jpn. J. Appl. Phys.* **32** Suppl. **32-3**, 62 (1993)]

A new approach for fabrication of polycrystalline $CuIn_XGa_{1-X}Se_2$ ($0 \leqq X \leqq 1$)thin films by annealing of evaporated Cu-In-Ga-Se alloy films has been presented. X-ray diffraction analyses showed that these thin films had chalcopyrite structure and the lattice parameters were varied linearly with X in the films. The thin films had optical absorption coefficients in the high 10^4 cm^{-1} range and the band gaps were changed from 0.99 to 1.68 eV with decreasing X. The variation of band gaps yielded the bowing parameter of 0.156 eV.

IV-P-2 Hydrogenated Amorphous Silicon Films Prepared from Trisilane by Windowless Hydrogen Discharge Lamp

Akira YOSHIDA *(Toyohashi Univ. of Tech. and IMS)*, **Shinji IKEDA, and Hiroshi TSUCHIMOTO** *(Toyohashi Univ. of Tech.)*

[*J. Non-Cryst. Solids* **164—166**, 95 (1993)]

High quality hydrogenated amorphous silicon (a-Si:H) films have been successfully deposited through the direct photolysis of trisilane using microwave-excited hydrogen discharge tube. The electrical and optical properties of the films have been investigated. The deposition rate decreases with increasing the substrate temperature, indicating that an adsorption-controlled process is dominant during the deposition. High quality films with the photosensitivity (σ_p/σ_d) of about 10^7 were obtained, when the substrate temperature was kept at 300°C.

IV-P-3 Defect Creation in Hydrogenated Amorphous Silicon Films Induced by Vacuum Ultraviolet Light from Synchrotron and Undulator Radiation

Yoji SAITO *(Seikei Univ.)* **and Akira YOSHIDA** *(Toyohashi Univ. of Tech. and IMS)*

[*Philos. Mag.* **B 70**, 133 (1994)]

Vacuum ultraviolet light from synchrotron and undulator radiation sources creates defects in hydrogenated amorphous silicon films. The dependence of the defect creation kinetics on photon energy has been investigated.The concentration of the defects induced by photons having an energy above 24 eV is proportional to the irradiation time. The rapid defect creation is due to the breaking of silicon-silicon bonds by the photo-induced plasmons.

IV-P-4 Temperature Dependence of Band Gap Change in InN and AlN

Q.X. Guo *(Toyohashi Univ. of Tech.)* **and Akira YOSHIDA** *(Toyohashi Univ. of Tech. and IMS)*

[*Jpn. J. Appl. Phys.* **33**, 2453 (1994)]

The optical band gap of InN and AlN single crystal films was measured through absorption spectra in the temperature range of 4.2 to 300 K. The samples were grown on (0001) α-Al_2O_3 substrates by metalorganic vapor phase epitaxy. The Varshni equation and the Bose-Einstein expression have been compared with the experimental results. The nitride III-V compound semiconductors have smaller temperature dependence of band gap change. In III—V compound semiconductors, the variation of the band gap change increases in the order of N, P and As.

IV—Q Molecular Beam Studies of Surface Reaction Dynamics

In the present project we investigate dynamics of surface reactions using molecular beam-surface scattering techniques. Experimental data obtained in this project are angular and velocity distributions of the scattered species detected by a rotatory quadrupole mass spectrometer using a TOF technique as a function of reactant collision energy and surface conditions such as the substrate temperature, incident angle, and surface structure and coverage. We are interested in obtaining information on molecule-surface interaction potential energies for reactive and non-reactive systems in order to find the ways of controlling surface reactions.

IV-Q-1 Translational-Vibrational Energy Transfer in Xe-Graphite Scattering

Koji ITO*, Hiroshi YOSHIKAWA *(Grad. Univ. Advanced Studies)*, **Kosuke SHOBATAKE, and Tetsuo FUJIMOTO*** *(* Nagoya Univ.)*

The translational-vibrational energy transfer in the Xe-graphite scattering has been studied using a newly constructed molecule-surface scattering apparatus with a rotatable mass spectrometer detector. The time-of-flight (TOF) distributions of scattered Xe atoms are measured at three

collision energies of 0.45, 0.17, and 0.070 eV, at two incident angles of 35 and 60 degrees from normal, and at two surface temperatures of 300 K and 500 K. Figure 1 shows typical TOF spectra of Xe atoms detected at three scattering angles of (d) θ_f=0°, (c) θ_f=50°, and (b) θ_f=60°C for the Xe beam incident angle, θ_i=60°, along with (a) that of incident Xe beam from which the Xe collision energy of 0.45 eV has been determined. The Xe TOF spectrum scattered at θ_f=0° is fitted to a Maxwell-Boltzmann (MB) distribution with a translational temperature close to the surface temperature. The spectrum at θ_f=50° clearly shows that it consists of three components. The fastest component is fitted to a shifted MB distribution which is sharper than a MB distribution obeys a hard cube model which assumes that the parallel velocity component does not change after collision for all the scattering conditions studied. The slowest component can be fitted to a MB distribution close to that with the surface temperature. The medium velocity component which can be also fitted to a shifted MB distribution may be assigned to a directly but more inelastically scattered species than the fast component on a softer potential surface. The TOF spectra were analyzed assuming that it consists of three components. The angular distribution of the scattered atoms is sharply distributed at higher scattering angles than the specular angle for the collision energies, E_i=0.45 and 0.17 eV but at lower scattering angle at E_i=0.070 eV.

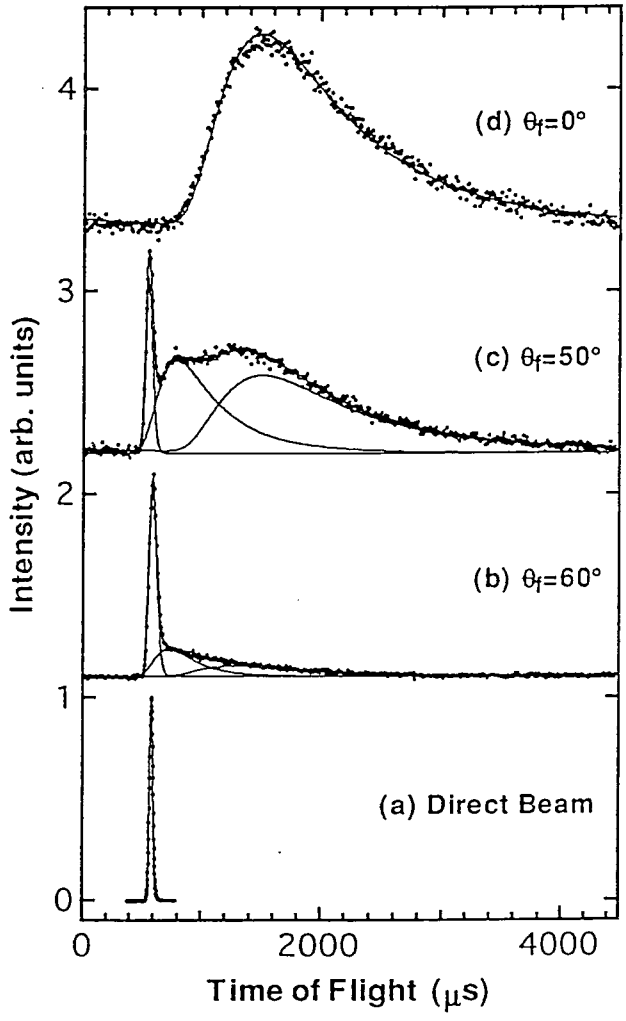

Figure 1. TOF spectra of (a) the direct incident Xe beam and Xe atoms scattered from the graphite surface kept at room temperature measured at the scattering angles (b) θ_f=60°, (c) θ_f=50°, and (d) θ_f=0°C for the incident angle of the Xe beam at θ_i=60° and collision energy of 0.45 eV. The solid curves are the calculated best-fit distributions.

IV-Q-2 Velocity Distributions of Nascent $SiCl_n$ (n = 2, 3, and 4) Products Formed from the Reaction of Si(111) with a Cl_2 Beam

Hiroshi YOSHIKAWA *(Grad. Univ. Advanced Studies)* **and Kosuke SHOBATAKE**

[*Chem. Phys. Lett.*, **223**, 341 (1994)]

The velocity distributions of desorbed nascent species formed from the etching reaction of Si(111) bombarded with a Cl_2 beam were measured using a time-of-flight (TOF) technique, detecting the products at masses, $SiCl_n^+$ (n = 1, 2, 3 and 4) on a molecule-surface scattering apparatus with a rotatable mass spectrometer detector. Fig. 1 illustrates the typical TOF spectra of the products detected at the four masses. The TOF spectra were fitted to Maxwell-Boltzmann distributions with translational temperatures close to or slightly higher than the surface temperatures, which means that the products are desorbed after well accommodating to the surface. The detected products were identified as neutral $SiCl_n$ (n = 2, 3, and 4) molecules. We find that the $SiCl_2$ radical is the major product in the surface temperature region between 700 and 1000 K.

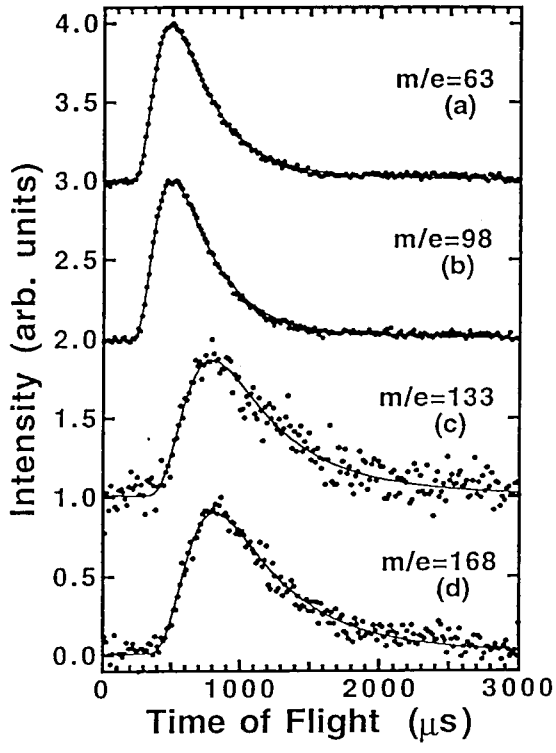

Figure 1. Time-of-flight distributions of desorbed products detected at masses, m/e=(a) 63 ($SiCl^+$), (b) 98 ($SiCl_2^+$), (c) 133 ($SiCl_3^+$), and (d) 168 ($SiCl_4^+$). Spectra of (a) and (b) were measured at surface temperature T_s=870 K, and those of (c) and (d) at T_s=570 K. The solid lines were calculated best-fit Maxwell-Boltzmann distributions.

IV—R Vacuum UV Photochemistry of Molecules and Clusters

In the present project we seek to obtain detailed information about, 1) photodissociative excitation processes from highly excited molecules and 2) photochemistry of excited van der Waals (vdW) molecules and clusters formed in a supersonic expansion. The techniques applied are absorption and fluorescence spectroscopies of gaseous molecules and vdw molecules on an apparatus constructed on the beam line BL2A of UVSOR facility. In particular we use fluorescence excitation, fluorescence polarization, and dispersed fluorescence spectroscopies to identify product species and obtain information on the dynamics of photochemical reactions.

IV-R-1 Fluorescence Excitation Spectra and Quantum Yield in Vacuum Ultraviolet Photodissociation of CF_3CN

Dock-Chil CHE*, Toshio KASAI*, Hiroshi OHYAMA*, Keiji KUWATA* *(*Osaka Univ.)*, **Mitsuhiko KONO, Kiyohiko TABAYASHI, and Kosuke SHOBATAKE**

[*Chemistry Letters*, **1994**, 133]

The fluorescence excitation spectra of CN(A,B→X) and $CF_3(2A'_1 \rightarrow 1A''_2)$ and quantum yield for the CN(B) radical formation were measured in the photodissociation of CF_3CN in 105—135 nm. The quantum yield for the CN(B) radical formation was found to be only a few percent. The similarity in the excitation energy dependence of CN(B→X) and of CN(A→X) indicated a common dissociation mechanism via the 3s Rydberg state of CF_3CN for both states.

IV-R-2 Absorption Spectrum of C_{60} in the Gas Phase: Formation and Recombination of Electron-Hole Pair

Hisato YASUMATSU*, Tamotsu KONDOW* *(*Univ. of Tokyo)*, **Hiroshi Kitagawa** *(Equipment Development Center)*, **Kiyohiko TABAYASHI, and Kosuke SHOBATAKE**

The absorption spectra of gaseous C_{60} at temperatures 830—870 K was measured in the energy range of 3.5—11.4 eV. The peaks at 7.9 and 9.2 eV, and a dip at 8.5 eV were assigned as Feshbach resonance with superexcited states. The photoionization quantum yield was explained in terms of formation and recombination of an electron-hole pair.

The absorption spectrum was measured on an apparatus constructed on Beamline BL2A of UVSOR. The C_{60} sample in a windowless absorption cell was resistively heated to temperatures of 830—870 K in a vacuum chamber pumped down to 1×10^{-6} Torr so that the vapor pressure of C_{60} is kept at 5—10 Torr. Figure 1 shows the spectrum of C_{60} vapor in the absolute cross section, the uncertainty of which is estimated to be about 25 % and most of which is due to the uncertainty of temperature reading.

In the low energy range three broad bands peaked at 3.8, 4.9, and 6.0 eV are observed. Two distinct bands peaked at 7.9 and 9.2 eV and a dip at 8.5 eV appear in the energy range higher than the ionization energy of 7.61 eV. They are assigned to Feshbach resonances involving superexcited states which originate from core-excited Rydberg states of C_{60}.

IV-R-3 Photodissociative Excitation Processes in XeF_2 in the Vacuum UV Region of 105—165 nm

Mitsuhiko KONO *(Grad. Univ. Advanced Studies)* **and Kosuke SHOBATAKE**

Photodissociative excitation processes of XeF_2 for $XeF_2+h\nu \rightarrow XeF^*(B, C \text{ and } D)+F$ are studied by absorption and fluorescence spectroscopies in the vacuum UV region of 105—165 nm. The quantum yields and polarization anisotropy are measured along with the dispersed fluorescence spectra for emissions from XeF(*B*, *C* and *D*) excimers formed from XeF_2 excited by linearly polarized, monochromatized synchrotron radiation on an apparatus at

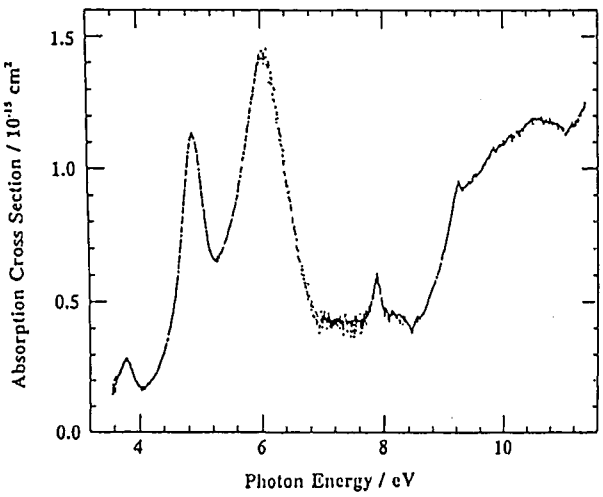

Figure 1. Absorption spectrum of C_{60} in the gas phase in the temperature range 830—870 K.
The ordinate represents absolute cross section whose uncertainty is estimated as 25 %.

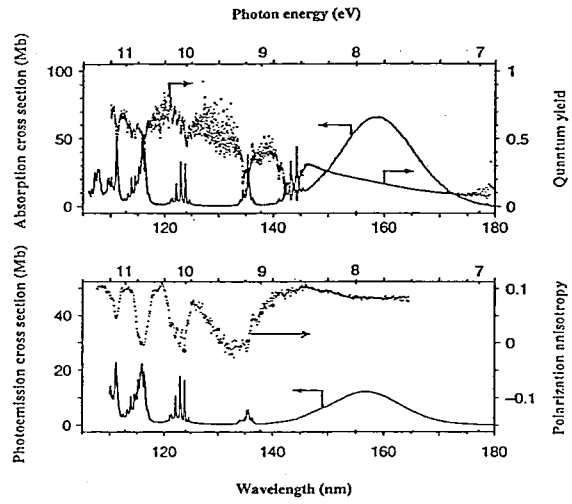

Figure 1. a) Absorption spectrum and quantum yield for XeF* formation in dissociative excitation of XeF_2. b) Polarization anisotropy for total fluorescence and fluorescence excitation spectrum.

the Beamline BL2A of UVSOR. The absorption and the fluorescence excitation spectra are measured to determine the quantum yield for the XeF* excimer formation from XeF_2 as shown in Figure 1. The latter has been determined by comparing the fluorescence intensity to that of OH(A→X) formed from photodissociative excitation of H_2O.[1)]

Figure 1a shows the absorption spectrum (solid line) of XeF_2 along with the quantum yield for total emission (dots) in the excitation wavelength (λ_{exc}) region 105—165 nm at a resolution of 0.10 nm. Most of the bands have been assigned by Nielsen and Schwarz.[2)] However some of the bands are reassigned in light of the results of fluorescence polarization anisotropy measured for formed XeF* shown in Figure 1b which also illustrates the fluorescence excitation spectrum obtained by monitoring the total emission at a resolution of 0.5 nm for the excitation light. It is noted that the quantum yield for XeF* excimer formation is found to be very high, especially at 110 nm it reaches about 0.75.

References
1) L. C. Lee, *J. Chem. Phys.* **72**, 4334 (1980)
2) U. Nielsen and W.H.E. Schwarz, *Chem. Phys.* **13**, 195 (1976)

IV—S Surface and Interface Structures of Organic Molecules and Polymers Studied by Soft X-ray Absorption and Optical Second Harmonic Generation

Study on the surface and interface structure of organic molecules and polymers have been of great interest because of the potential to be used as the key information to the molecular device application. We have performed a series of experiments with use of X-ray Absorption Near Edge Structure (XANES) and Optical Second Harmonic Generation (Optical SHG) which provide highly-surface-sensitive structural information. Our first experiments have been focused mainly on the structural study on the functional polymer surface and its interface with liquid crystal molecules. We have found that the surface structure of liquid crystal is strongly affected by the local structure of polymers.

IV-S-1 Polarized XANES and Optical SHG Studies on the LC/polyimide Interfaces

Yukio OUCHI *(Nagoya Univ. and IMS)*, **Masaki SEI***, **Kazuhiko SEKI*** *(Nagoya Univ.)* **and Yoshiyasu MATSUMOTO**

It is well known that a rubbed polymer surface may align a liquid crystal (LC) film, whose optical axis makes a pre-tilt angle from the polymer substrate. As for the mechanism of the alignment, it is widely believed that the mechanically rubbed polymer is subjected to the local structure change, such as a realignment of the polymer chain and hence the elongated chain induces the uniaxial alignment of the LC film. Although many surface analytical techniques have been applied to reveal the mechanisms of the alignment, its microscopic understanding is still lacking.

In this study, we have performed a series of experiments with use of (1) C K-edge and N K-edge X-ray absorption near edge structure (XANES) spectroscopy for the first time in order to investigate the local structure of polymer surface, and of (2) optical second harmonic generation (SHG) so as to estimate the orientational distribution function of the LC monolayer on the polymer substrate.

Sample compounds were BPDA (biphenyl—3,3',4,4'—tetracarboxylic dianhydride) type polyimides; BPDA type polyimides with *even* number alkylene chain induce a large LC pre-tilt angle and those with odd number alkylene chain does almost 0 degree LC pre-tilt angle. XANES spectra have successfully revealed the structure difference between the *odd* and *even* number BPDA polyimides. For example, we have found that the biphenyl part of C8-BPDA is selectively tilted form the substrate by 15°.

In SHG experiments, we have measured an 8CB (4'-n-octyl-4-cyanobiphenyl) monolayer evaporated on the rubbed BPDA substrate. The results indicate that the alignment of the 8CB monolayer is strongly affected by the structure of the substrate polymers. We will discuss the surface structures of rubbed BPDA and the alignment mechanisms of the 8CB molecules on the BPDA substrate.

IV-S-2 Polarized XANES Studies on the Mechanical Rubbing Effect of Poly(tetrafluoroethylene) Oligomer and its Model Compounds

Yukio OUCHI *(Nagoya Univ. and IMS)*, **Kouhei NAGAYAMA*, Kazuhiko SEKI*** *(Nagoya Univ.)*

Poly(tetrafluoroethylene)(PTFE) is of great interest lately for their applications to the aligning-layers for various organic-functional molecules. However, the mechanisms responsible for the alignment in relation to the mechanical rubbing process are hardly understood. In this study, we have performed a series of experiments with use of F K-edge and C K-edge CANES (X-ray absorption near-edge structure) spectroscopy in order to determine (1) the initial alignment of the poly(tetrafluoroethylene) oligomer (TFO; carbon number n=100~400 with the peak at 172) and its model compound (n-$C_{24}F_{50}$) by vacuum evaporation and (2) the possible structure change of these compounds subjected to the mechanical rubbing process.

We have found that in the evaporated TFO film the fluorocarbon chains were almost parallel to the surface and were uniaxially realigned along the rubbing direction by the mechanical rubbing process, while in the evaporated PFT film the fluorocarbon chains were oriented normal to the surface and hardly changed its structure by the mechanical rubbing process. This is probably due to the fact that TFO has lower crystalinity than PFT and hence the realignment of the chains were induced by the mechanical rubbing.

We have demonstrated that the evaporated TFO films subjected to the rubbing may be used as the substrate for an epitaxial growth. As an example, PFT films evaporated on the rubbed TFO films perfectly align along the rubbing direction of TFO.

RESEARCH ACTIVITIES V
Department of Applied Molecular Science

V—A New Multi-Stage Redox Systems

Interdisciplinary cooperation between synthetic chemistry, physical chemistry, and solid state physics has opened a new field of science which forcuses on the development and study of molecular materials having interesting electrical, magnetic, and optical properties in the solid state. In general, molecular level correlation of molecular solid state micro structure and bulk material properties is essential to construct new molecular materials. Such consideration regarding highly electrically conducting behavior reveals the importance of conjugated electronic systems having multi-stage redox nature, which can transfer electrons smoothly by multi-stage manners. We have designed and synthesized two classes of new multi-stage redox systems, such as peri-condensed Weitz type donors, and amphoteric multi-stage redox systems. The peri-condensed Weitz type redox systems are designed by replacing two of the sp^2 carbon atoms in a polycyclic arene by two sulfur atoms. Such heterocycles have produced new organic molecular metals which contain non-TTF and non-TCNQ type components. The amphoteric multi-stage redox systems are designed so as to decrease the difference between the oxidation and the reduction potentials of a molecule. We have already reported the synthesis and properties of conjugated hydrocarbons with the highest amphotericity. Design and synthesis of new types of multi-stage redox systems, and investigations of their physical and solid state properties are actively continued.

V-A-1 Charge-Transfer Complexes of Centrosymmetric DDQ (CDDQ) with TTF Type Donors

Badruz ZAMAN, Yasushi MORITA *(IMS and Osaka Univ.)*, **Jiro TOYODA, and Kazuhiro NAKASUJI** *(IMS and Osaka Univ.)*

The solid state properties of molecular materials depend on the molecular packing. One of the factors to determine the molecular packing is molecular shape or symmetry. One of the most important acceptors in the solid state chemistry and physics is 2,3-dichloro-5,6-dicyano-1,4-benzoquinone (DDQ) whose mlecular symmetry is C_{2v}. The positional isomer of DDQ, 2,5-dichloro-3,6-dicyano-1,4-benzoquinone, possesses C_{2h} molecular symmetry, that is centrosymmetric DDQ (CDDQ). This acceptor is known compound. We studied the molecular properties, the crystal structure, and its charge-transfer complexes in order to clarify the difference of the molecular packing and solid state properties compared with DDQ, and to obtain new molecular materials. The charge-transfer complexes of CDDQ with TTF type donors were prepared by diffusion method in H-shape tube. The electronic absorption spectra for CT complexes with TTF, TMTSF, and BEDT-TTF in the solid state showed a band at the longer wavelength region than 2600 nm, and therefore, IR spectra showed the broad bands around 3000 cm^{-1}. These results suggest that the complexes might have partial CT state and high-electrical conductivities.

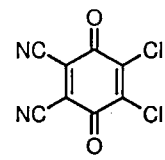

DDQ

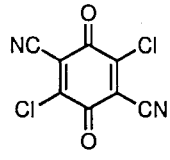

CDDQ

V-A-2 Crystal Structure of Centrosymmetric DDQ (CDDQ)

Jiro TOYODA, Badruz ZAMAN, Yasushi MORITA *(IMS and Osaka Univ.)*, **and Kazuhiro NAKASUJI** *(IMS and Osaka Univ.)*

The single crystals of CDDQ itself suitable for X-ray crystal structure analysis were obtained by recrystallization from dichloromethane.

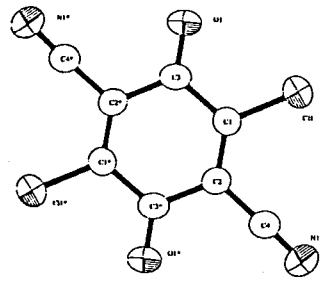

Formula	$C_8Cl_2N_2O_2$
MW	227.01
Crystal System	monoclinic
Space Group	$P2_1/n$ (#14)
Z value	2
Lattice Parameters	a = 8.298(3) Å
	b = 6.129(3) Å
	c = 8.881(2) Å
	b = 106.00(2)°
	V = 434.2(3)Å^3

V—B New Conjugated Electronic Systems

Design and synthesis of novel conjugated electronic systems are continuing in the exploration of new molecular materials which might have interesting chemical reactivities and physical properties. In this research project, new electronic systems having closed shell and open shell electronics are actively searched for. Chemical modifications of known electronic systems are also important. An example is as follows. Stable, conjugated, neutral radicals have attracted much attention as new materials having potentially interesting solid state properties, as single component conductors, and magnetically interesting materials. We have utilized odd alternant hydrocarbon, phenalenyl, as the basic skeleton for neutral radicals, and modified the phenalenyl skeleton by introducing donor and acceptor substituents to suppress the thermodynamic and kinetic instability. Such modification is one of the typical procedure in physical organic chemistry to stabilized unstable electronic systems.

V-B-1 Oxidation Reaction of 2-(2-Quinolyl)-3-hydroxyphenalenone

Kunio HATANAKA, Yasushi MORITA *(IMS and Osaka Univ.)*, **and Kazuhiro NAKASUJI** *(IMS and Osaka Univ.)*

In order to explore stable neutral radicals based on phenalenyl systems, we designed 3- and 6-oxophenalenoxyl radicals, **1** and **2**.

So far the result of oxidation reactions of 3-hydroxyphenalenone derivatives and the MO calculations have suggested that the spin density at 2-position of **1** is very large. To clarify the steric and electronic effect of the substituent of **1**, we performed oxidation of 2-(2-quinolyl)-3-hydroxyphenalenone **3** with $K_3[Fe(CN)_6]$, PbO_2, or Ag_2CO_3. In the case of Ag_2CO_3, the product obtained was determined as the C-C dimer **4** at 2-position of the phenalenyl moiety of the desired radical species from the anlysis of the spectroscopic data. In other cases, no reactions were occured and **3** was recovered. Such a low reactivity is due to the electon withdrawing group at 2-position of **3** or N ··· HO intramolecular hydrogen bond.

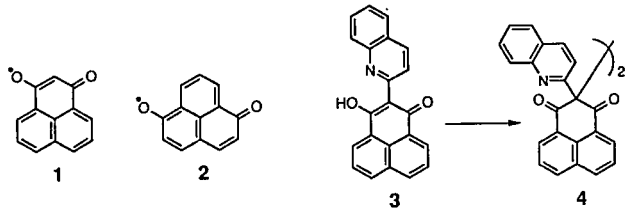

V-B-2 Oxidation Reaction of 6-Hydroxyphenalenone

Kunio HATANAKA, Yasushi MORITA *(IMS and Osaka Univ.)*, **and Kazuhiro NAKASUJI** *(IMS and Osaka Univ.)*

As a basic study to clarify the chemical reactivities of 6-oxophenalenoxyl radical **1**, we performed oxidation of 2,5-dimethyl-6-hydroxyphenalenone **2** with three different conditions. The compound **3** was obtained as a major oxidation product with PbO_2 or Ag_2CO_3 in chloroform. The reaction with PbO_2 in acetone gave **4** mainly. These reactions are considered C-O bond formation at 2-position of the phenalenyl moiety of desired 6-oxophenalenoxyl radical and C-C bond formation of CH_2 radical formed at methyl group of **2**.

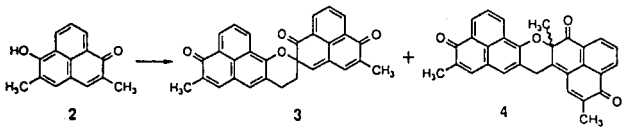

V-B-3 Synthesis and Physical Properties of New Charge-Transfer Complexes of Diazaphenalene Derivatives with TCNQ

Koichi TAMAKI, Yasushi MORITA *(IMS and Osaka Univ.)*, **and Kazuhiro NAKASUJI** *(IMS and Osaka Univ.)*

Heterocyclic analog of an odd alternant hydrocarbon phenalenyl, diazaphenelene, **1** and **2**, possesses characteristic features in the redox properties, the hydrogen bonding ability and the coordination ability of the nitrogen atoms. In this study, we have synthesized 1,6-diazaphenalene **2** and its new three derivatives **3**—**5**. The compound **3** showed tautomerism behavior in NMR measurement. IR spectra showed that the compound **2** contains H-bonding and the compounds **3**—**5** no H-bonding in the solid state. We prepared charge-transfer complexes of the diazaphenalene derivatives with TCNQ. The complexes showed low energy of charge-tarnsfer transition around 3000 cm^{-1}. The degree of CT was estimated as 0.55—0.98 from the CN stretching frequencies. The conductivity measurements for the compressed pellets showed that the CT complexes of **3**—**5** possess relatively high-conductivity, 0.2—0.02 Scm^{-1}.

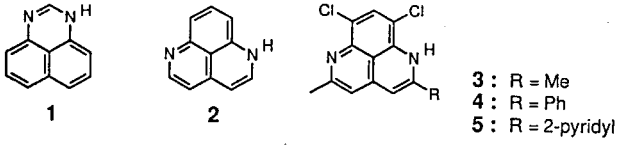

V—C New Cooperative Proton-Electron Transfer (PET) Systems

From the viewpoint of synthetic chemistry, we have begun exploration of molecular materials having interesting chemical reactivities and physical properties, while constructing an interdisciplinary strategy for interesting materials. Our particular attention in this research project is paid to the hydrogen-bonded charge-transfer (HBCT) systems which exhibit cooperative proton-electron interactions in the solid state. If a cooperative proton-electron transfer (PET) occurs inter-molecularly in such systems, a state which can be characterized as a molecular assembly of *H-bonded neutral radicals* might be produced. The type and strength of the proton-electron cooperativity can control the solid state properties in an interesting way. A stepwise consideration on the PET phenomenon leads to two reasonable molecular design strategies to realize such a PET state under milder conditions: (1) the exploration of new electronic systems having a smaller intermolecular CT gap and (2) an electronic modification to stabilize H-bonded neutral radicals. Our current fundamental efforts are concentrated on the design and synthesis of a wide range of HBCT systems having the cooperative interaction between H-bonding and electron transfer process, in both organic materials and transition metal complexes.

V-C-1 Physical Properties of Hydrogen-Bonded Charge-Transfer Complex of Ethylenediaminoglyoxime Transition Metal Complex with Tetracyanoquinodimethane

Tetsuji Itoh, Jiro Toyoda, Makoto Tadokoro, Hiroshi Kitagawa, Tadaoki MITANI, and Kazuhiro NAKASUJI *(IMS and Osaka Univ.)*

The hydrogen-bonded charge-transfer complex containing a transition metal, (ethylenediaminoglyoximato) (ethylenediaminoglyoxime) palladium (II), with tetracyanoquinodimethane, Pd(Hdag)(H_2dag) · TCNQ, was prepared. The complex showed a segregated stacking mode of crystal structure and contained hydrogen-bonds between the anionic and cationic columns and between the cationic columns. We estimated the degree of CT for Pd(Hdag)-(H_2dag) · TCNQ to be 0.70 and 0.67 by using the nitrile stretching frequency and by the bond length ratio procedure of TCNQ skeleton, respectively. The formal charge of the TCNQ skeleton for the Pd(Hdag)(H_2dag) · TCNQ is one. The reason of the discrepancy between the estimated values and the formal charge is not clear at this stage, but the H-bonding interaction between NH of the amino group and N of the nitrile group might reduce the ionicity to a some extent. We observed a broad absorption band around 3300 cm^{-1}, which can be assigned to the intra band CT transition in the TCNQ column with a partial ionicity. The preliminary measurement of the electrical conductivity for a single crystal of the Pd(Hdag)(H_2dag) · TCNQ gave 90 Scm^{-1} with metallic behavior around room temperature and semi-conducting behavior below 200 K with the activation energy of 79 meV. Such highly conducting behavior is consistent with the partial ionicity estimated and the existence of the intra-band CT transition.

V-C-2 Metal-Pteridine Complexes Having Three-Dimensional Hydrogen-Bonded Network

Minoru MITUMI, Jiro TOYODA, and Kazuhiro NAKASUJI *(IMS and Osaka Univ.)*

Control of the cooperative interaction between electron-transfer and proton-transfer in the hydrogen-bonded charge-transfer systems (HBCT) is a new way to regulate the electronic properties in the solid state. In principle, the CT interaction can be replaced to the redox properties of the transition metal atoms. In order to study the basic chemistry of such systems, we have planed to construct the molecular systems containing the H-bonded networks of metal complexes in which a ligand is connected by the intermolecular H-bonds. As a basic skeleton of the ligands, we have utilized the pteridine derivatives, such as lumazine (HLM) and pterin (HPR), which have chelating ability to metal atom and H-bonding sites of NH···O and NH···N types in the solid state. We have obtained the crystal structures of [Cu(LM)$_2$(H_2O)$_2$] (**1**), [Cu(PR)$_2$(H2O)$_2$] (**2**), and [Zn(PR)$_2$(H_2O)$_2$] · 2H_2O (**3**), which were prepared by slow diffusion of the deprotonated ligands (LM and PR) and metal source in water. The characteristic features in the crystal structure of the H-bonded transition metal complexes studied here are as follows: 1) the two pteridine ligands chelate to metal ion through O(4) and N(5) donor atoms of pteridines, 2) the molecular units are connected to two-dimensional H-bonded molecular sheet by the coordinated water molecules, 3) in two-dimensional H-bonded molecular sheet, there are the stacking structures of the pteridine skeleton, 4) the sheets are further connected to three-dimensional H-bonded networks via the H-bonded sites of the pteridines ligands, and 5) almost all H-bonding sites existing in the molecule participate in intermolecular H-bonding interactions.

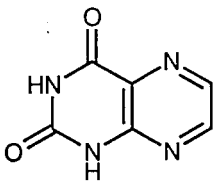

Lumazine (HLM)

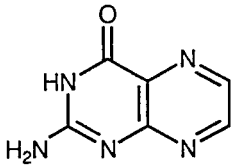

Pterin (HPR)

V-C-3 *Ab-initio* Molecular Orbital Studies for the Dimer Model of Quinhydrone

Jiro TOYODA, Kazuhiro NAKASUJI *(IMS and Osaka Univ.)* **Satoshi MINAMINO, and Kazuo KITAURA** *(University of Osaka Prefecture)*

The benzoquinone-hydrobenzoquinone complex (quinhidron) is a DA-type CT-complex which exists as one-dimensional hydrogen bonded networks. Vibrational spectra suggest that in this complex, a proton and an electron are cooperatively transferred (PET) to give semiquinone radicals under conditions of high pressure. To better understand this PET type phase transition at the molecular level, we have undertaken *ab-initio* molecular orbital calculations of this system using the UHF/3-21G* basis set. Semi qualitative basic properties, such as optimized molecular geometries, electronic structures, and molecular energies were calculated for relevant quinone related model species (hydroquinone, quinone, hydroquinone cation radical, quinone anion radical, semiquinone anion, semiquinone cation semiquinone radical, semiquinone dimer, hydrogen bonded hydroquinone-quinone complex, etc.). The energies of both hydrogen bonded hydroquinone-quinone complexes and semiquinone dimer are more stable than the sum of energies of the corresponding components by about 12 kcal mol^{-1}. The stability can be attributed to the intermolecular H-bonding.

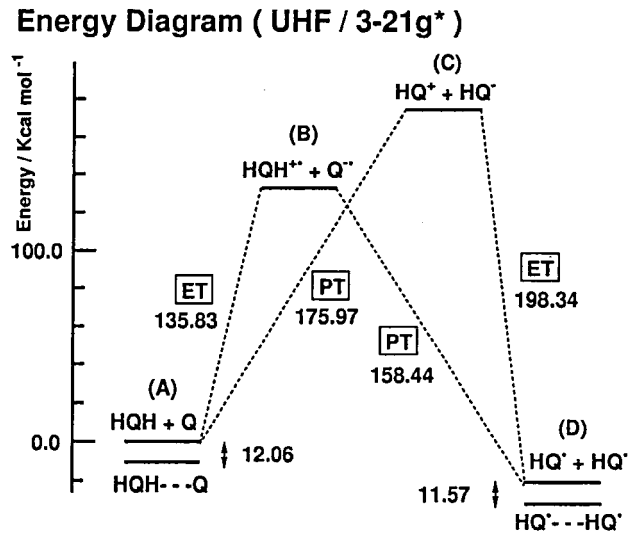

V-C-4 *Ab-initio* Molecular Orbital Studies of the Alloxazines

Jiro TOYODA, and Kazuhiro NAKASUJI *(IMS and Osaka Univ.)*

The biochemical importance of Alloxazine is well known. The structure and energies for the cooperative PET type phase transition have been studied by using an *ab-initio* molecular orbital (MO) method at the UHF and the UHF/3-21G* basis set for relevant alloxazines related model species; 1H-alloxazines and 10H-iso-alloxazines, and oxidized forms, the reduced form, and the radicals. The energies of 10H-isoalloxazine is thermodinamically much more favourable at 1-H protonated than 5-H protonated on total energy.

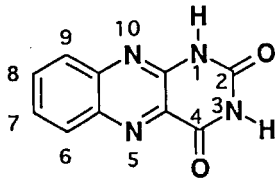

Alloxazine

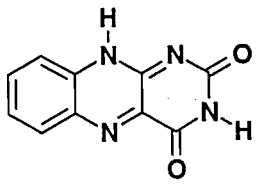

Iso-alloxazine

V-C-5 2,2′-Biimidazolate Transition Metal Complexes with One-dimensional Intermolecular H-bonding Chains

Makoto TADOKORO, Akira MIYAZAKI*, Jiro TOYODA, Kiyoshi ISOBE, Toshiaki ENOKI* *(*Tokyo Inst. Tech.)*, **and Kazuhiro NAKASUJI** *(IMS and Osaka Univ.)*

In order to realize HBCT systems by using transition metal complexes it is requirement that metal complexes have not only the cojugated ligand systems but also an ability to construct one, two or three-dimensional network systems with intermolecular H-bonds. We have already demonstrated that the Cu(II) complex ($[Cu(salenNMe_2)(Hbim)]_2$) with one deprotonated 2,2′-biimidazolate ligand ($Hbim^-$) can form the intermolecular H-bonding dimer which has NH-N bond between the $Hbim^-$ ligands, as the first step. Mono-transition metal complexes with two $Hbim^-$ ligands are possible to form one-dimensional chain structures with intermolecular H-bonds between $Hbim^-$ ligands.

In fact, we have synthesized the Cu(II) complex ($[Cu(Hbim)_2]_n$) with two $Hbim^-$ ligands. IR spectral data (ν(NH)= 2525 cm^{-1} and 2γ(NH)= 1899 cm^{-1}) may support that the complex has a relatively strong intermolecular H-bond of the NH-N type between ligands to form one-dimensinal chain structures as shown in Figure **1**. In the case of the Ni(II) complex ($[Ni(Hbim)_2(pyr)]_n$) of *trans*-isomer having two $Hbim^-$ ligands and pyrazines, IR spectral data (ν(NH)= 2517 cm^{-1} and 2γ(NH)= 1881 cm^{-1}) support the existence of one-dimensional chain structure of intermolecular H-bonds. This complex showed a weak antiferromagnetic behavior, which suggests the interaction between Ni(II) through the pyrazine and the existence of the two-dimensinal molecular system (Figure **2**).

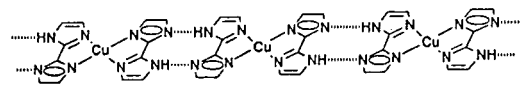

Figure 1. $[Cu(Hbim)_2]_n$

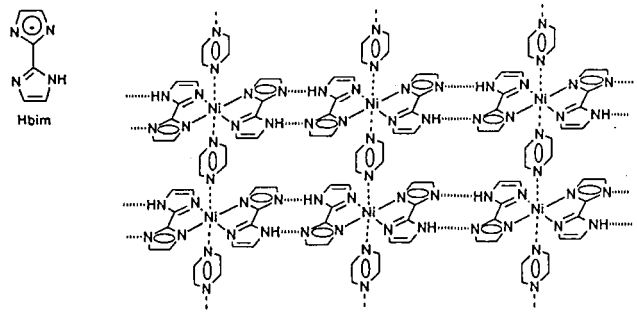

Figure 2. $\{[Ni(Hbim)_2](Pyr)\}_n$

V-C-6 Crystal Structure of Nickel(II) Complex with Inter-molecular H-bondings of 2,2′-Biimidazolate Having Zigzag One-dimensinal Chains

Makoto TADOKORO, Jiro TOYODA, Kiyoshi ISOBE, and Kazuhiro NAKASUJI *(IMS and Osaka Univ.)*

The transition metal complexes with three $Hbim^-$ ligands have an ability to form a three-dimesional H-bonding networks. We have found that the Ni(II) complexes having three 2,2′-biimidazolate ligands ($[Ni(Hbim)_3]^-$) form a variety of crystal structure of the complex with intermolecular H-bonding networks depending on the kinds of the cations.

We studied the crystal structures of three Ni complexes ($[Ni(Hbim)_3]^-$) with mono cations, $^nPr_4N^+$ (tetra-n-propyl-ammonium), $ETPY^+$ (ethylpyridinium), and $BTEA^+$ (Benzyltriethyl-ammonium). All the three complexes possess intermolecular H-bonding structures of the zigzag one-dimensional chains in which two of the three $Hbim^-$ ligands connect the metal complex units. The zigzag chain structures are made up of an alternate arrangement of enamtiomers of Δ and Λ configurations on the Ni(II) anions. The other remaining $Hbim^-$ ligand does not participate in the H-bonding chains and has an H-bonding interaction with MeOH from recrystallization solvent.

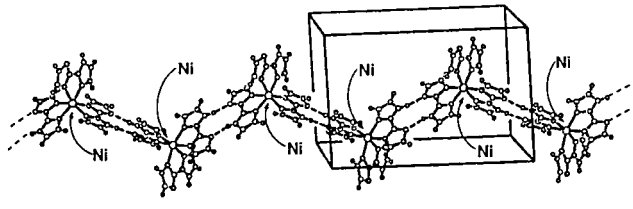

Figure 1. Crystal Packing with Zigzag One-dimensional Chain of $[Ni(Hbim)_3](ETPY)$

V-C-7 Crystal Structure of Nickel(II) Complex with Inter-molecular H-bondings of 2,2′-Biimidazolate Having Channel Structures: $([Ni(Hbim)_3]\cdot(PTMA)\cdot 3MeOH)$

Makoto TADOKORO, Jiro TOYODA, Kiyoshi ISOBE, and Kazuhiro NAKASUJI *(IMS and Osaka Univ.)*

A nickel(II) complex of ([Ni(Hbim)$_3$](PTMA)) with the PTMA$^+$ (phenyltrimethylammonium) cation forms channel structures having the hole about ~9 Å along the c axis as shown in Figure **1**. These channel structures are built by an alternate stacking of Δ and Λ sheets. These sheets consist of both PTMA$^+$ cations and intermolecular H-bonding dimers of the [Ni(Hbim)$_3$]$^-$ anions, and are made up of only one enamtiomer of tris-bi-imidazolate nickel complexes ether Δ or Λ types, respectively. The internal channel structures of this compound are hydrophilic and filled with H-bonded MeOH. The columns of MeOH molecules exist in the channel structures.

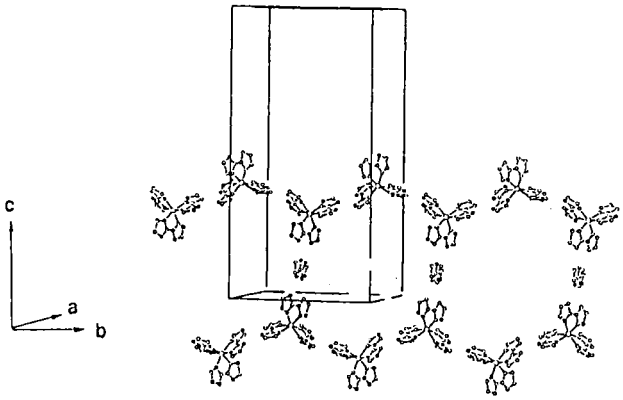

Figure 1. Honeycomb Sheet Structure in [Ni(Hbim)$_3$(NEt$_4$)]$_2$-(H$_2$bim) with Double Interlocking Structure

V-C-8 Crystal Structure of Nickel(II) Complex with Inter-molecular H-bondings of 2,2′-Biimidazolate Having Double Interlocking Structures: ([Ni(Hbim)$_3$(NEt$_4$)]$_2$(H$_2$bim) · MeOH)

Makoto TADOKORO, Jiro TOYODA, Hidehiro UEKUSA*, Kiyoshi ISOBE, Yuji Ohashi* *(*Tokyo Inst. Tech.),* **and Kazuhiro NAKASUJI** *(IMS and Osaka Univ.)*

The [Ni(Hbim)$_3$(NEt$_4$)]$_2$(H$_2$bim) complex with the NEt$_4^+$ cation showed a complicated unique crystal structure. First, this complex has a zigzag one-dimensional chain structure with intermolecular H-bonds similar to the structure described in **V-C-6**. The chain structure is comprised of alternate arrangements of enamtiomers of Δ and Λ configrations on the tris-biimidazolate nickel(II) anions. Second, free biimidazole ligands (H$_2$bim) connect the zigzag one-dimensional chains to give a honeycomb sheet structure by intermolecular H-bonds, as shown in Figure **1**. Third, the two pairs of the honey-comb sheets with perpendicular arrangement form a double interlocking structure. The orientation of the intermolecular H-bonding and the conformation around the nickel center play an important role for formation of the double interlocking structure. Finary, the unit of the interlocking double honeycomb sheets arrnage in three dimensionally to form the infinite interlocking structure of the double honeycomb sheets.

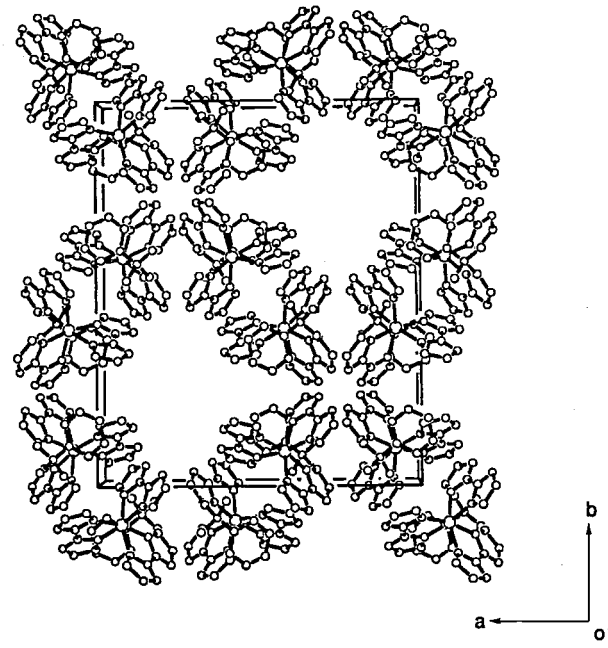

Figure 1. Crystal Packing with Channel Structure of [Ni(Hbim)$_3$]-(PTMA) Along *c* Axis

V-C-9 Crystal Structure of One Dimensional Heterobimetallic Complex Bridged by 2,2′-Bibenzimidazolate (bbim^{2-}) Ligand: ([Cu(bbim)$_2$]Na(^{n}Pr$_4$N)-· MeOH)

Makoto TADOKORO, Jiro Toyoda, Kiyoshi ISOBE, and Kazuhiro NAKASUJI *(IMS and Osaka Univ.)*

Since 2,2′-biimidazole (H$_2$bim) is a bidentate ligand with a multi-proton donor property, it can coordinate to transition metal ions as three types: neutral (H$_2$bim), mono-deprotonated (Hbim$^-$), and di-deprotonated (bim^{2-}) forms. It was reported that 2,2′-bibenzimidazole (H$_2$bbim) has the same function toward transition metal ions as does 2,2′-biimidazole. We have studied the crystal structure of a Cu(II) complex ([Cu(bbim)$_2$]-(^{n}Pr$_4$N)Na) with two bbim^{2-} as a di-deprotonated ligand. The X-ray crystal analysis shows that this Cu(II) complex consists of one-dimensional infinite chains with an alternate bonding sequence of Cu(II) and Na(I) bridged by the bbim^{2-} ligand (Figure **1**). Interestingly, Cu(II) ion in this complex has the tetrahedral coordination structure. The interaction between these infinite chains is separated by ^{n}Pr$_4$N$^+$ cations.

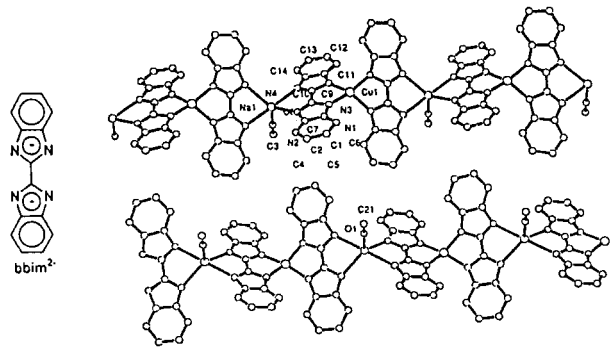

Figure 1. Crystal Packing with One-Dimensional Structure of [Cu(bbim)$_2$](^{n}Pr$_4$N)Na bridged by bbim^{2-}

V—D Transition Metal Oxide Clusters

Molecules of organometallic oxide clusters consist of metal oxides and organometallic groups that differ with each other in chemical properties. To date we have mainly focused on finding the method to assemble cluster frameworks and synthesized several new types of clusters such as the integrated cubane-type and planar-type clusters. Our current efforts have been concentrated on elucidation of the chemical properties of the oxide parts and the M—O bond functionality. Now we move on to the subject to see the reactivity of organometallic parts as well as the M—C bond functionality in the oxide clusters.

V-D-1 Intramolecular Rearrangements of Cyclooctadiene-Rhodium(I) Fragments Supported on a Vanadium-Oxide Cluster as Evidenced by Dynamic ^{17}O NMR Spectroscopy

Masaaki ABE, Kiyoshi ISOBE, Katsuhiko KIDA *(Kwansei Gakuin Univ.),* **Akira NAGASAWA** *(Saitama Univ. and IMS),* **and Atsushi YAGASAKI** *(Kwansei Gakuin Univ.)*

Polyoxoanion-supported organometallic compounds are structural and functional models toward catalytic metal-oxide surfaces. Dynamic behavior of the organometallic groups plays a vital role in surface reactions, however, the mechanistic studies have been limited to date. We approached the subject by using newly prepared surface modeling vanadate clusters having one or two organorhodium(I) fragments, $[\{Rh(COD)\}_2(V_4O_{12})]^{2-}$ (**1**) and $[\{Rh(COD)\}(V_4O_{12})]^{3-}$ (**2**) (COD: 1,5-cyclooctadiene). Complex **1** was characterized by a single-crystal X-ray diffraction (Figure 1).

Variable-temperature ^{17}O NMR spectra of the ^{17}O-enriched sample of **1** (Figure 2) reveal that the complex is fluxional in solution. Four resonances at low temperature (labelled as A, B, C, and D) coalesce (C and D) or extremely broaden (A and B) with increasing temperature. This dynamic process clearly indicates that two cyclooctadienerhodium(I) fragments in **1** are mobile intramolecularly on vanadium-oxide surfaces. A single resonance in ^{51}V (δ −479) and in ^{103}Rh (δ +2933) NMR spectra is also in accord with the scheme. Complex **2** displays three ^{17}O-resonances in CH_3CN at 25°C, indicating the intramolecular rearrangements of a Rh fragment in **2** are in the fast-exchange limit even at room temperature.

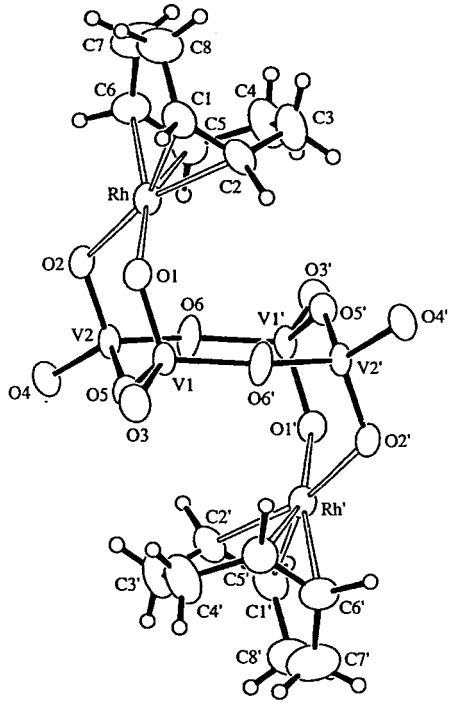

Figure 1. An ORTEP diagram (50% ellipsoids) of the anionic part of $[(n\text{-}C_4H_9)_4N]_2[\{Rh(COD)\}_2(V_4O_{12})] \cdot DMF$ with atomic labeling scheme. Selected bond distances (Å) and angles (deg): Rh-O1=2.060(5), Rh-O2=2.070(5), Rh-C1=2.102(9), Rh-C2=2.102(8), Rh-C5=2.101(9), Rh-C6=2.091(9), V1-O1=1.678(5), V1-O3=1.606(5), V1-O5=1.790(5), V1-O6'=1.793(5), V2-O2=1.667(5), O1-Rh-O2=89.7(2), Rh-O1-V1=122.3(3), Rh-O2-V2=119.3(2).

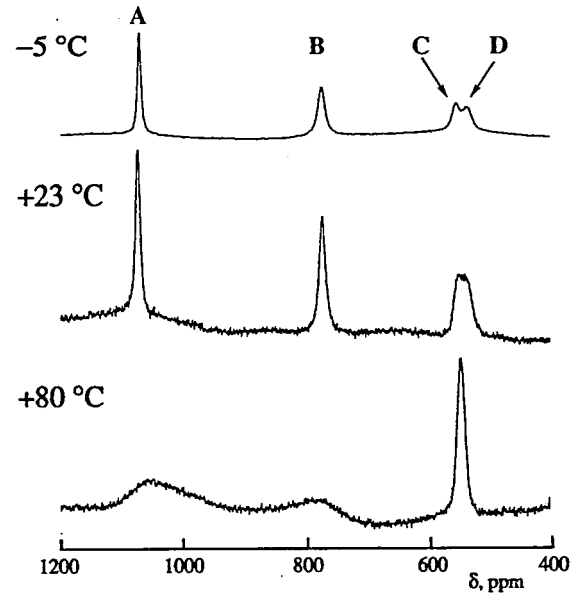

Figure 2. Variable-temperature ^{17}O NMR spectra of ^{17}O-enriched $(PPN)_2 \cdot$ **1** in 1,2-dichloroethane.

V-D-2 Vanadium-Oxide Clusters with Supported Bis(2-Phenylpyridine)rhodium(III) and -iridium(III) Fragments

Masaaki ABE and Kiyoshi ISOBE

Vanadium-oxide supported organometallic compounds usually display dynamic behavior in solution due to intramolecular rearrangements of organometallic moieties on vanadium-oxide surfaces as well as fluxional processes occuring in the organometallic fragment itself. Therefore, the dynamic processes sometimes seem to be complicated and compounds with structurally rigid organometallic fragments will be helpful to elucidate the fluxional processes. In this study, we selected cyclometalated Rh^{III} and Ir^{III} fragments and successfully isolated the vanadate-supported clusters, $[\{(ppy)_2M\}_2(V_4O_{12})]^{2-}$ (ppyH=2-phenylpyridine; M=Rh^{III} (**1**), Ir^{III} (**2**)).

A reaction between $[(ppy)_2M(\mu\text{-Cl})]_2$ and $(n\text{-}C_4H_9)_4NVO_3$ in 1:4 molar ratio in CH_3CN produced $\{(n\text{-}C_4H_9)_4N\}_2[\{(ppy)_2M\}_2(V_4O_{12})]$ (M=Rh and Ir) in ca. 70% yield. A crystallographic study of $(PPN)_2[\{(ppy)_2Rh\}_2(V_4O_{12})]\cdot 3CH_3CN\cdot 2H_2O$ (Figure 1) reveals that the two $(ppy)_2Rh^+$ fragments coordinate to a vanadium-oxide ring through Rh—O bonds (2.169(5)-2.185(4) Å) in both sides of the ring, which takes a twist-chair type conformation as seen in $[\{\beta\text{-methallyl})_2Rh^{III}\}_2(V_4O_{12})]^{2-}$. In solution, complex **1** seems to be rather rigid as judged from variable-temperature ^1H and ^{51}V NMR spectroscopies, suggesting the sterically bulky organometallic fragments may have a great influence on its intramolecular motions on surfaces. Further studies on dynamic behaviors of complex **1** and **2** are in progress.

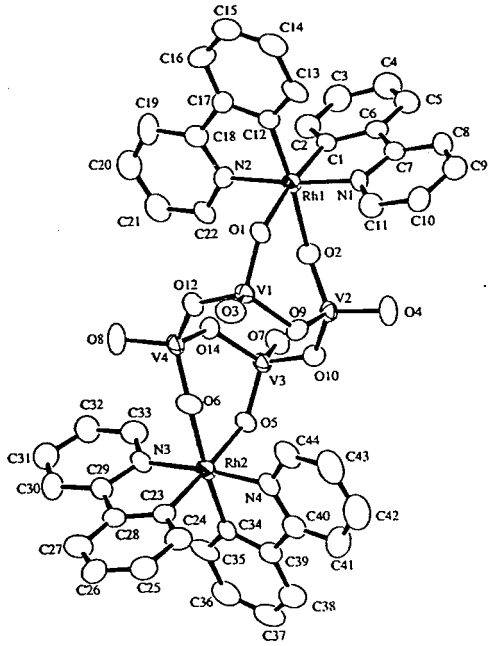

Figure 1. An ORTEP diagram (40% ellipsoids) of the anionic part of $(PPN)_2[\{(ppy)_2Rh\}_2(V_4O_{12})]\cdot 3CH_3CN\cdot 2H_2O$ with atomic labeling scheme. Selected bond distances (Å) and angles (deg): Rh1-O1=2.185(4), Rh1-O2=2.179(5), Rh1-C1=1.967(6), Rh1-C12=1.989(7), Rh1-N1=2.022(5), Rh1-N2=2.033(6), V1-O1=1.675(5), V2-O2=1.663(5), O1-Rh1-O2=82.7(2), Rh1-O1-V1=132.1(3), Rh1-O2-V2=139.8(3).

V-D-3 Synthesis and Crystal Structure of $[(IrCp^*)_2(\mu\text{-}OH)_3]_2(Cr_2O_7)\cdot 8H_2O$ ($Cp^*=\eta^5\text{-}C_5Me_5$). A Novel Two-Dimensional Hydrogen-Bonding Network

Joon T. PARK *(KAIST and IMS)*, **Takanori NISHIOKA, Takayoshi SUZUKI, and Kiyoshi ISOBE**

[*Bull. Chem. Soc. Jpn.*, **67**, 1968 (1994)]

The title complex has been prepared from a reaction of $[(IrCp^*Cl)_2(\mu\text{-}Cl)_2]$ with K_2CrO_4 in water. It has been characterized via a single-crystal X-ray diffraction study. In the solid state the tri-μ-hydroxo-diiridium complex cations, the dichromates having the staggered conformation, and the water molecules of crystallization are entirely connected by hydrogen bonds forming a novel two-dimensional layer structure as shown in Figure 1.

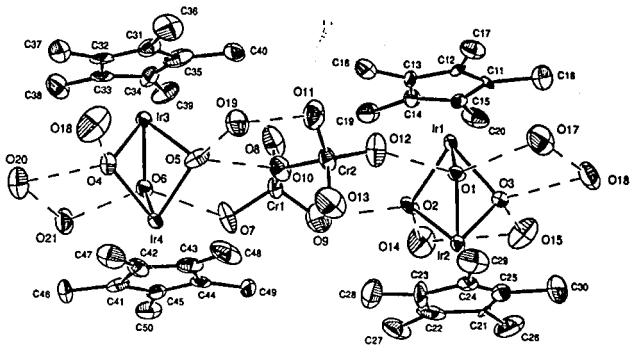

Figure 1. ORTEP drawing of $[(IrCp^*)_2(\mu\text{-}OH)_3]_2(Cr_2O_7)\cdot 8H_2O$ with atom numbering scheme. Bond lengths (l/ Å) and angles (ϕ/ °) are Ir-O=2.09(2)–2.15(2), Ir-C^R=2.09(3)–2.16(3), Cr-O^T=1.56(2)–1.62(2), Cr-O^B=1.76(2) and 1.80(2), O-Ir-O=70.5(6)–75.7(6), Ir-O-Ir=91.8(7)–94.1(6), O^T-Cr-O^T=108(1)–113(1), O^T-Cr-O^B=106.8(9)–112(1), and Cr-O^B-Cr=136(1), where C^R, O, O^T, and O^B denote ring carbon of Cp*, hydroxy oxygen bridged two iridium atoms, terminal oxygen of dichromate, and bridging oxygen of dichromate, respectively.

V-D-4 Synthesis and Molecular Structure of $[(IrCp^*)(\mu\text{-}S_2C_6H_4)]$

Xi RIMO *(Grad. Univ. for Adv. Studies and IMS)*, **Takayoshi SUZUKI, and Kiyoshi ISOBE**

As a part of our efforts to develop chemistry of the triple cubane-type oxide cluster $[RhCp^*MoO_4]_4$ with mercaptans, the benzenedithiolato dimer $[(RhCp^*)_2(\mu\text{-}S_2C_6H_4)_2]$ (**1**) as well as the corresponding oxidized product $[(RhCp^*)_2(\mu\text{-}SC_6H_4(O))_2]$ (**2**) were synthesized and characterized. Complex **1** shows an interconversion with monomer in CD_2Cl_2, but only the dimer form was isolated from solution. Hence we synthesized the corresponding iridium complex in the same method, and found that only a monomer form $[(IrCp^*)(\mu\text{-}S_2C_6H_4)]$ (**3**) can be obtained from solution. The molecular structure of **3** is shown in Figure 1. Crystallographic data for **3**: monoclinic, $P\,2_1/n$, a=8.453 (8) Å, b=13.838 (8) Å, c=13.829 (4) Å, β=90.93 (8)°, V=1618 (2) Å^3, and Z=4. The ^1H and ^{13}C NMR as well as IR spectroscopy of **3** did not give any resonance relative to the dimer form. Comparing the bond lengths of Ir-S (mean 2.250 Å) in **3** with Rh-S (mean 2.363 Å) in **1** it can be

seen that the sulfur atom forms a strong bond with the iridium atom and hence the electronic density of the sulfur in **3** is decreased, which may leads to no bonding interaction between the lone pair of sulfur and the d orbital of iridium in another molecule to form a dimer.

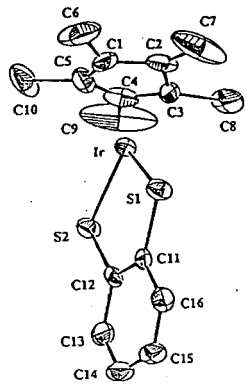

Figure 1. Perspective view of $[(IrCp^*)(\mu\text{-}S_2C_6H_4)]$.

V—E Transition Metal Chalcogenide Clusters

M–S bond functionality in high nuclearity compounds plays an important role in redox reactions as seen in biological and industry processes due to its covalency in bonding. We have been developing the methodology for the rational synthesis of sulfide clusters by using the μ-SH dinuclear complex and WS_4^{2-} as starting materials, because a variety of reactions such as addition, oxidation, (de)protonation, and partial desulfurization can be applied to both starting materials to build the cluster frameworks. We are also synthesizing selenide clusters to compare with the chemistry of sulfide cluster and will show unique structure and properties of these clusters.

V-E-1 Synthesis, Structure, and Property of Octanuclear Heterotrimetallic Sulfide Cluster; $[\{RhCp^*P(OEt)_3(\mu\text{-}WOS_3)(CuCl)Cu\}_2(\mu\text{-}Cl)_2]$ Having a Linked Incomplete Cubane-Type Structure

Seiji OGO *(Grad. Univ. for Adv. Studies and IMS),* **Takayoshi SUZUKI, and Kiyoshi ISOBE**

The chemistry of heterometallic sulfide clusters has been developed rapidly in recent years because of interests of the geometrical structures, especially relevance to the core structure of nitrogenase, and the catalytic ability for hydrodesulfurization (HDS) reaction. However, it is still difficult to control of the framework formation of a desired sulfide cluster. We have tried to find a controlled synthetic method by introduction of an organometallic group into the cluster framework and have synthesized the octanuclear heterometallic sulfide cluster, $[\{RhCp^*P(OEt)_3(\mu\text{-}WS4)(CuCl)Cu\}_2(\mu\text{-}Cl)_2]$ (**2**) (see *Annual Review*, **1993**, p.79). We are elucidating the reactivities of **2** and the related compounds.

Compound **2** reacted slowly with H_2O dissolved in CH_2Cl_2(0.12 mol/l) at room temperature to form $[\{RhCp^*P(OEt)_3(\mu\text{-}WOS_3)(CuCl)Cu\}_2(\mu\text{-}Cl)_2]$ (**3**) (51% yield for 60-day reaction, eq. 1) (Scheme 1).

$$[\{RhCp^*P(OEt)_3(\mu\text{-}WS_4)(CuCl)Cu\}_2(\mu\text{-}Cl)_2] + 2H_2O \rightarrow [\{RhCp^*P(OEt)_3(\mu\text{-}WOS_3)(CuCl)Cu\}_2(\mu\text{-}Cl)_2] + 2H^+ + S^{2-} \quad \text{(eq. 1)}$$

Although the decrease in amount of H_2O in the reaction system with the progress of the reaction was confirmed by ^1H NMR measurement of a sealed reaction tube, the formation of H_2S was not detected by ^1H NMR and an H_2S gas detector tube. Recrystallization from DMF/diethyl ether (DMF=dimethylformamide) gave purple crystals of **3** · DMF. Molecular structure of **3** determined by the X-ray analysis is shown in Scheme 1. All metal ions and sulfur atoms in **3** form an incomplete cubane-type framework. The W atom forms distorted tetrahedral coordination geometry by one O and three S atoms. The Cu2 has a trigonal planar geometry with two S and one terminal Cl atoms, but Cu1 strongly distorted tetrahedrally coordinates to two S and two Cl atoms. The Cu1 atom is 0.3229 Å above from the plane formed by S1, S3, and Cl1 atoms (Cu2 is 0.0916 Å above from the corresponding plane).

The reaction of **3** and H_2S immediately took place in CH_2Cl_2 at room temperature to form compound **1** (yield 91%, eq. 2).

$$1/2[\{RhCp^*P(OEt)_3(\mu\text{-}WOS_3)(CuCl)Cu\}_2(\mu\text{-}Cl)_2] + 3/2H_2S \rightarrow [RhCp^*P(OEt)_3(\mu\text{-}WS_4)CuCl] + 1/2Cu_2S + H^+ + Cl^- + H_2O \quad \text{(eq. 2)}$$

In this reaction H_2S reacts with one of the CuCl groups in **3**, that is, it shows that CuCl in **1** is inert for H_2S.

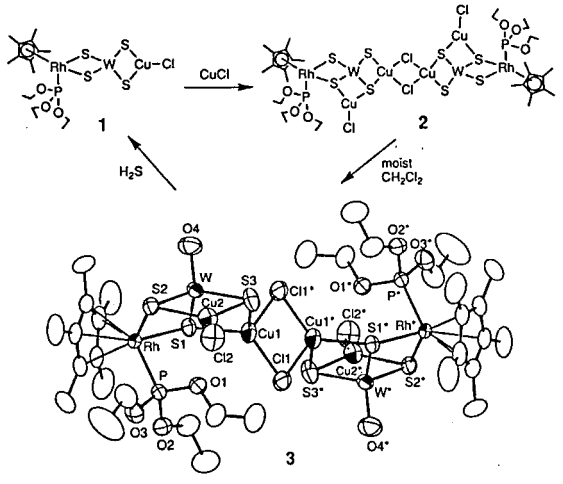

Scheme 1. Synthesis and structure of $[\{RhCp^*P(OEt)_3(\mu\text{-}WOS_3)(CuCl)Cu\}_2(\mu\text{-}Cl)_2]$ (**3**).

V-E-2 Formation of Triangular Rhodium μ_3-Sulfido Complex, $[Rh_3Cp^*_3(\mu_3\text{-}(\eta^2\text{-}\text{II})\text{-}C_2H_2)(\mu_3\text{-}S)]$ ($Cp^*=\eta^5\text{-}C_5Me_5$), Containing Acetylene Ligand Generated from a Coupling of Two Bridging Methylene Units in Dirhodium Complex

Takanori NISHIOKA, Kiyoshi ISOBE, Yoshiki OZAWA *(Himeji Institute of Technology and IMS)*, **and Amelio VAZQUEZ DE MIGUEL** *(University of Alcala de Henares and IMS)*

In order to synthesize a cluster containing the μ_3-S ligand, we performed a reaction of the $M(\mu_2\text{-}SH)M$ with $M(\mu_2\text{-}OH)M$ groups. For these groups a labile μ_2-methylene rhodium complex with hydrosulfide bridging a Rh–Rh single bond and the basic hydroxide rhodium complex were used. A reaction of $[Rh_2Cp^*_2(\mu_2\text{-}CH_2)_2(\mu_2\text{-}SH)](BPh_4)$ (**1**) with $[Rh_2Cp^*_2(\mu_2\text{-}OH)_3](BPh_4)$ (**2**) in acetone led to the formation of trirhodium μ_3-sulfido complex with acetylene ligand $[Rh_3Cp^*_3(\mu_3;\eta^2(\text{II})\text{-}C_2H_2)(\mu_3\text{-}S)]X_2$ (X=BPh_4 (**2a**); X=BF_4 (**2b**)). This reaction transforms not only the μ_2-SH ligand to the μ_3-S ligand but also the two μ_2-CH_2 ligands to the acetylene. The $M(\mu_2\text{-}OH)M$ group induces a deprotonation and a carbon-carbon coupling.

The yield of **2a** in this reaction was not so high (30% based on Rh) and the reaction gives messy product: reaction mixture shows many CH_3 signals from the pentamethylcyclopentadienyl groups in the ^1H NMR spectra between δ=1.5–2.3. Isolation of **2a**, however, was made easily due to its less solubility in the dichloromethane and methanol as compared with many other unknown products. **2a** is soluble in polar organic solvent such as acetonitrile, acetone, and nitromethane. On the other hand **2b** is amphiphilic, and is soluble in water and in organic solvents such as dichloromethane and acetone. Recrystallization of **2b** from dichloromathane-benzene yielded dark red crystals.

The structure of **2b** was confirmed by X-ray analysis. The cationic moiety contains a triangle of rhodium atoms that are bridged by the triply bridged sulfido ligand on one side of the cluster and by the acetylene ligand with μ_3-η^2(II)- fashion on the other side as shown in Figure 1.

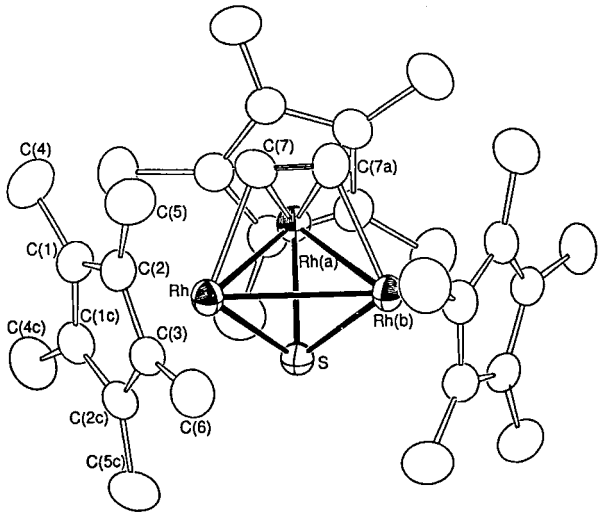

Figure 1. ORTEP drawing of $[Rh_3Cp^*_3(\mu_3;\eta^2(\text{II})\text{-}C_2H_2)(\mu_3\text{-}S)]^{2+}$ with atom numbering scheme.

V-E-3 Influence of a Neutral Terminal Ligand on the Structure and Redox Potential of Hexamolybdemun(12+) Cluster Ion with Mixed Capping Ligand

Masahiro EBIHARA *(Gifu. Univ.)*, **Takashi KAWAMURA** *(Gifu. Univ.)*, **Kiyoshi ISOBE, and Kazuo SAITO**

[*Bull. Chem. Soc. Jpn.*, in press]

$(n\text{-}Bu_4N)_2[(Mo_6Br_7S)Cl_5(CH_3CN)]$ was synthesized, and its crystal structure was determined. The Mo-Mo distance (2.637(7) Å) is similar to that of $(Et_4N)_3[(Mo_6Br_7S)Cl_6]$. The structure of the cluster anion $[(Mo_6Br_7S)Cl_5(CH_3CN)]^{2-}$ is shown in Figure 1. The oxidation potential is higher than that of $[(Mo_6Br_7S)Cl_6]^{3-}$ by 0.21 V. The shift of potential may be caused by change of net charge of the cluster anion.

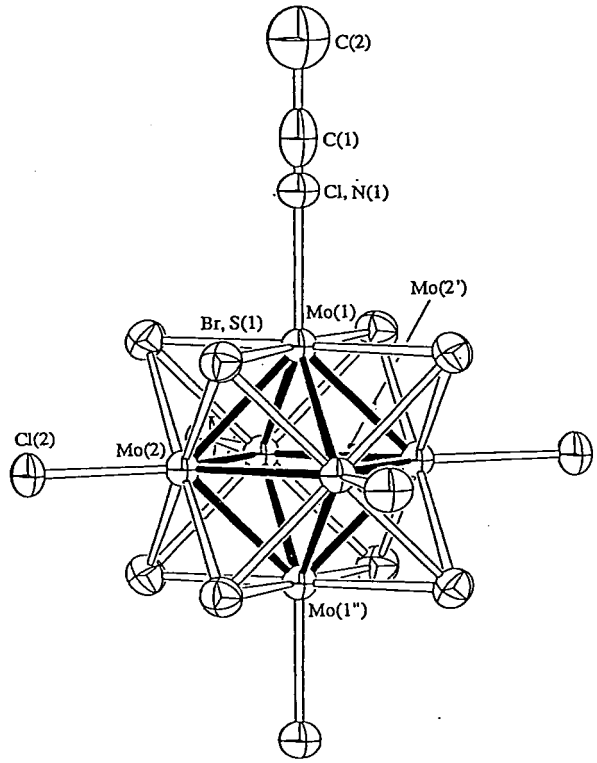

Figure 1. The structure of the cluster anion $[(Mo_6Br_7S)Cl_5(CH_3CN)]^{2-}$. The C atom of CH_3CN ligand at one of the disordered sites are omitted. The crystallographically equivalent atoms are marked as follows; 'y, x, z; "x, y, -z.

V-E-4 Oxidative Coupling of Coordinated SeH Group: Synthesis, Structure and Dynamic Behavior of Tetranuclear Rhodium Complex with μ_4-Se_2 Ligand, $[\{(RhCp^*)_2(\mu_2\text{-}CH_2)_2\}_2(\mu_4\text{-}Se_2)]^{2+}$ ($Cp^*=C_5Me_5$)

Hiroshi SHIMOMURA, Takanori NISHIOKA, Masaaki ABE, and Kiyoshi ISOBE

A reaction of $[\{RhCp^*(\mu_2\text{-}CH_2)Cl\}_2]$ with H_2Se in MeOH formed a μ_2-SeH complex, and was isolated as a BPh_4 salt $[\{RhCp^*(\mu_2\text{-}CH_2)\}_2(\mu_2\text{-}SeH)](BPh_4)$ (**1**; $Cp^*=C_5Me_5$). In CH_3CN, complex **1** was oxidized by molecular oxygen giving a tetranuclear complex $[\{(RhCp^*)_2(\mu_2\text{-}CH_2)_2\}_2(\mu_4\text{-}Se_2)](BPh_4)_2$ (**2**) as an oxidative coupling product. Complex **2** crystallized in space group *C*2/*c*,

a=25.599(3), b=12.296(4), c=31.933(4) Å, β=110.870(9)° and Z=4. The ORTEP drawing of the cationic part of **1** is shown in Figure 1. The structure involves the Se_2 bridging two Rh-Rh bonds (Rh-Rh=2.539(1) Å) in a side-on fashion (Rh1-Se=2.622(1), Rh2-Se'=2.530(1) Å). The Se-Se distance is 2.306(6) Å, which is corresponding to a nearly single Se-Se bond. Complex **2** showed an intriguing dynamic behavior of "synchronous double-site atomic inversion" in CD_3CN. The line shape analyses of the temperature dependent ^1H NMR spectra for the μ_2-CH_2 groups elucidated the mechanism of the dynamic behavior and provided activation parameters, $\Delta G^{\ddagger}$=66±1 kJmol^{-1} (at 298.15 K), $\Delta H^{\ddagger}$=70±1 kJmol^{-1} and $\Delta S^{\ddagger}$=15±1 Jmol^{-1}K^{-1}.

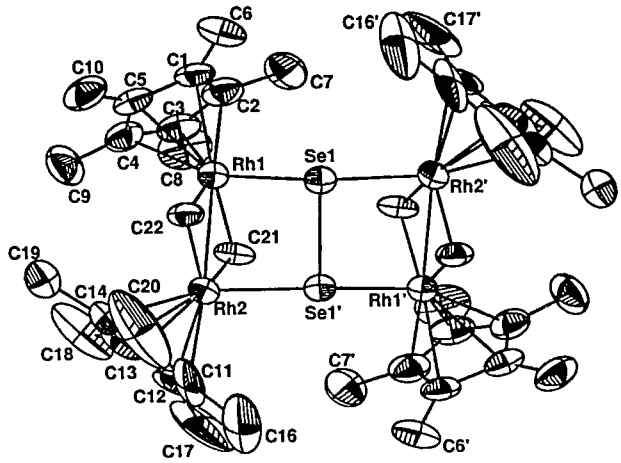

Figure 1. The ORTEP drawing of cationic part of [{(RhCp*)$_2$(μ_2-CH_2)$_2$}$_2$(μ_4-Se_2)](BPh$_4$)$_2$.

V-E-5 Tetranuclear [{(RhCp*)$_2$(μ_2-CH_2)$_2$}$_2$(μ_4-Se_4)]$^{2+}$ (Cp*=C_5Me_5) Cationic Complex with a Rectangular *D*2h Structure of a Se_4 Unit

Hiroshi SHIMOMURA and Kiyoshi ISOBE

In V-E-3 we described the formation of [{(RhCp*)$_2$(μ_2-CH_2)$_2$}$_2$(μ_4-Se_2)](BPh$_4$)$_2$ (**1**) from the oxidation of [[RhCp*(μ_2-CH_2)]$_2$(μ_2-SeH)](BPh$_4$) in CH_3CN. The oxidation in the presence of an excess amount of H_2Se gave another new tetranuclear complex [{(RhCp*)$_2$(μ_2-CH_2)$_2$}$_2$-(μ_4-Se_4)](BPh$_4$)$_2$ (**2**), quantitatively. The reaction probably involves a three electron process in which the μ_2-SeH complex is oxidized to **2**, yielding water as the conjugate reduced product (eq. 1).

$$2[[RhCp^*(\mu_2\text{-}CH_2)]_2(\mu_2\text{-}SeH)]^+ + 2H_2Se + 3/2O_2 \rightarrow [\{(RhCp^*)_2(\mu_2\text{-}CH_2)_2\}_2(\mu_4\text{-}Se_4)]^{2+} + 3H_2O$$

The use of excess H_2Se may play an important role in formation of the Rh(SeH_2) species containing a framework such as [Rh(SeH)-Rh(SeH_2)]$^+$, in which the H_2Se function attached to the cationic complex is most likely oxidized at first.

Complex **2** crystallized in space group $P2_1/a$ (monoclinic) a=15.544(4), b=17.371(7), c=15.922(3) Å, β=104.82(2)°, V=4156.2(20) Å^3, and Z=2. The ORTEP drawing of the cationic part of **1** is shown in Figure 1. The framework of complex **2** involves a rectangular *D*2h structure of a Se_4 unit bridging two Rh-Rh bonds (Rh-Rh=2.648(2) Å). Two of the four Se-Se distances (Se1-Se2 and Se1'-Se2'; 2.558(3) Å) are substantially shorter than the other two distances (Se1-Se2' and Se1'-Se2; 2.716(3) Å). The bond orders of these bonds are less than 1, but the lengths are significantly shorter than the sum of the van der Walls radii of these atoms (4.00 Å).[1)]

Reference

1) *Lange's Handbook of Chemistry*, 13th ed.; Dean, J. A., Ed.,; McGraw-hill: New York, 1985; pp.3–125.

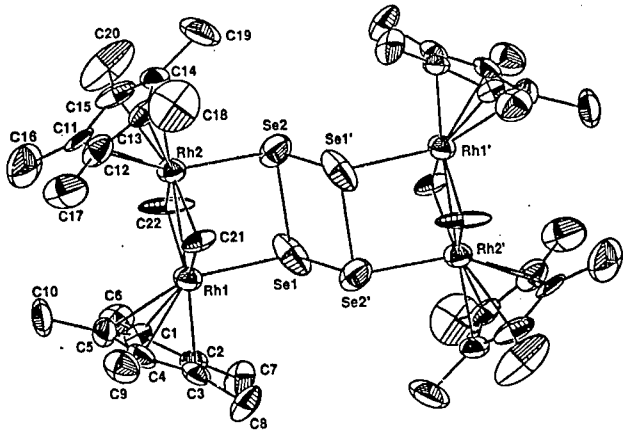

Figure 1. The ORTEP drawing of cationic part of [{(RhCp*)$_2$(μ_2-CH_2)$_2$}$_2$(μ_4-Se_4)](BPh$_4$)$_2$.

V-E-6 Synthesis and Property of Pentanuclear (Cu^I-Rh^{III}_2-W^{VI}_2) Heterometallic Sulfide Cluster Ion Predicted by Fast Atom Bombardment Mass Spectrometry

Seiji OGO *(Grad. Univ. for Adv. Studies and IMS)*, **Sachiyo NOMURA, Takayoshi SUZUKI, and Kiyoshi ISOBE**

While the analysis of a single-crystal X-ray diffraction method provides structural information in detail, the technique is limited when a suitable crystal for the analysis can be isolated. For non-crystalline compounds fast atom bombardment (FAB) mass spectrometry (MS) can take the place of it by analyzing the fragmentation patterns. However, it should be remarkable that in FAB MS spectra some peaks at higher mass numbers than the molecular ion are often observed under certain conditions because of recombination of fragment ions in FAB MS chamber. We are investigating whether the FAB MS can predict the actual synthesis in the case of transition metal sulfide cluster compounds.

A FAB MS spectrum of a neutral compound, [RhCp*P(OEt)$_3$(μ-WS_4)CuCl] (**2**), showed many isotopic distribution patterns at the higher mass region than at that of the isotopic molecular ion peaks of **2** (the most abundant peak: 816) as shown in Figure. 1. Fortunately, All of their distribution patterns are assigned to certain ions. One of them corresponds to an isotopic pattern (the most abundant peak: 1497) of a pentanuclear cluster formulated by $C_{32}H_{60}CuO_6P_2Rh_2S_8W_2$ (**3**). We tried to prepare **3** by the reaction between [RhCp*P(OEt)$_3$$WS_4$] (**1**) and

$[Cu(CH_3CN)_4][PF_6]$ in acetonitrile at room temperature (Scheme 1). The reaction gave small red needle crystals which have the same composition as that of **3** and show the most abundant peak at 1497 in the highest *m/z* value region. The isotopic distribution pattern is also close to that observed in **2**. Hence these are the same species with each other. In order to obtain a crystal suitable for a single-crystal X-ray analysis, an acetonitrile solution of **3** and $Na[BPh_4]$ was kept in a few weeks at room temperature. Red crystals were obtained, however, the highest mass ion of the compound in the FAB MS spectrum agrees with the molecular ion of divalent complex, $[\{RhCp^*P(OEt)_3\}_2(\mu\text{-}WS_4)]^{2+}$ (**4**), and the structure of the complex is confirmed by X-ray analysis (Scheme 1).

Now we are going to perform EXAFS analysis to establish the metal ion sequence in compound **3**.

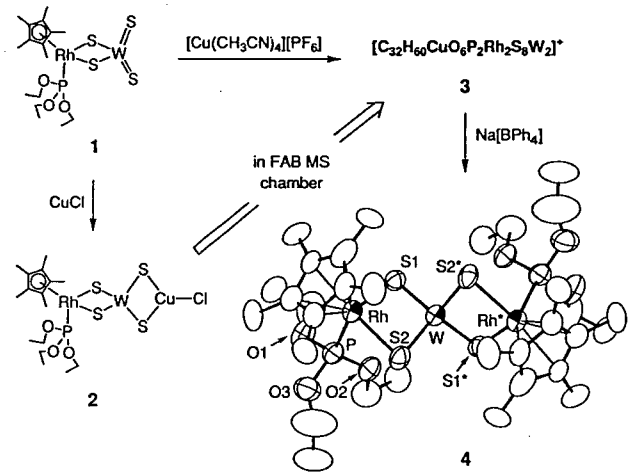

Scheme 1. Synthesis of $[C_{32}H_{60}CuO_6P_2Rh_2S_8W_2]^+$ (**3**) and structure of $[\{RhCp^*P(OEt)_3\}_2(\mu\text{-}WS_4)]^{2+}$ (**4**).

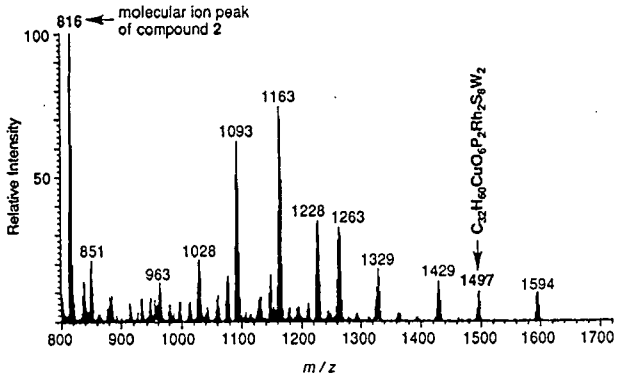

Figure 1. FAB MS spectrum of **2**.
Analysis conditions; The Mass spectrum was obtained with a Shimadzu / Kratos CONCEPT 1S mass spectrometer operating at an accelerating potential of 8 kV. Xenon was used to generate the primary ionizing beam. The FAB gun was operated at 7–8 kV and a current of 1mA. The metal complex was dissolved in *m*-nitrobenzylalcohol (NBA) and placed on a stainless steel FAB probe tip. The analytical mass range was generally from *m/z* 100 to 1700 with a scan time of 3 s/decade. The MS system was tuned and calibrated with perfluoroalkyl phosphazine (Ultramark).

V—F Transition Metal Complexes with Di- or Tridentate Methyl-Substituted Phosphines

Phosphine complexes of transition metals have been studied extensively, because some of the complexes, for example the Wilkinson's complex, the binap-Ru complexes and so on, have important catalytic abilities for organic syntheses and activation of small inactive molecules. Further, since the electronic and steric properties of tertiary phosphines (PR_3) can be altered in a systematic and predictable way over a wide range by varying R, the phosphines are suitable for the detailed investigation of the molecular and electronic structure and the reactivity of the complexes in terms of the properties of the ligands contained. A methyl group on the phosphorus atom makes the phosphine ligand less steric bulky and highly electro-donating, and therefore, compared to the well-studied phenyl-substituted phosphines, the methyl derivatives are expected to give the complexes having highly reactive metal centers. However, owing to the difficulties of preparation and handlings of the methyl-substituted phosphines, the transition metal complexes with those are not well-studied yet.

We have prepared several rhodium(III) complexes with di- or tridentate methyl-substituted phosphines, and are now investigating the structures and reactivities of the complexes. The reason why multidentate phosphine ligands are used in our study is that the ligands can give restrictions for the geometrical structure of the complexes obtained.

V-F-1 Rhodium(III) Complexes with 1,1,1-Tris(dimethylphosphinomethyl)ethane (tmpme); Preparation and Structures

Takayoshi SUZUKI, Kiyoshi ISOBE, Kazuo KASHIWABARA *(Nagoya Univ.)*, **and Junnosuke FUJITA** *(ICU)*

The tripod-type ligand, 1,1,1-tris(dimethylphosphinomethyl)ethane (tmpme) can coordinate three sites at an

octahedral metal center in a *facial* fashion, and the strong *trans influence* of the dimethylphosphino group makes other ligands at the *trans* positions labile. Therefore, the transition metal complexes of tmpme are expected as highly reactive catalysts, in which the reaction site can be controlled by the multidentate ligand. Although a large number of transition metal complexes with the diphenylphosphino derivative, 1,1,1-tris(diphenylphosphinomethyl)ethane (tppme), have been reported previously, the tmpme complexes are limited in the first-row transition metals, for example Cr, Fe and Co. In this study we have prepared and characterized the tmpme complexes of rhodium(III), which are interesting in the reactivity and the catalytic abilities.

The molecular structure of $[RhCl_3(tmpme)]$, which was obtained by a reaction of *trans*-$[RhCl_2(py)_4]Cl$ and tmpme in pyridine, is depicted in Figure 1. The complex is very soluble in water, but the UV-vis and NMR spectra of an aqueous solution of the complex show a concentration dependence. From the analysis of the ^{31}P NMR spectrum the dependence are caused by release of chloride ligands from the Rh centers and dimerization of the coordinatively unsaturated species. On addition of HBF_4 aq. or $HClO_4$ aq. to the aqueous solution, white crystals of $[\{Rh(tmpme)\}_2(\mu\text{-}Cl)_3]$ (BF_4 or ClO_4)$_3$ was obtained (Figure 2). The bridging chloride ligands of the dimeric complex are difficult to remove in an acidic or neutral solution, but in a reaction of $[RhCl_3(tmpme)]$ and Ag_2O in water all chloride ligands are removed as a precipitate of AgCl and $[\{Rh(tmpme)\}_2(\mu\text{-}OH)_3]^{3+}$ is obtained, which was crystallized and analyzed by X-ray as BF_4 salt (Figure 3). Moreover, acidification of the aqueous solution with HBF_4 aq. gives an aqueous solution containing $[Rh(tmpme)(H_2O)_3]^{3+}$, which could be a good starting material for the further studies of the related complexes.

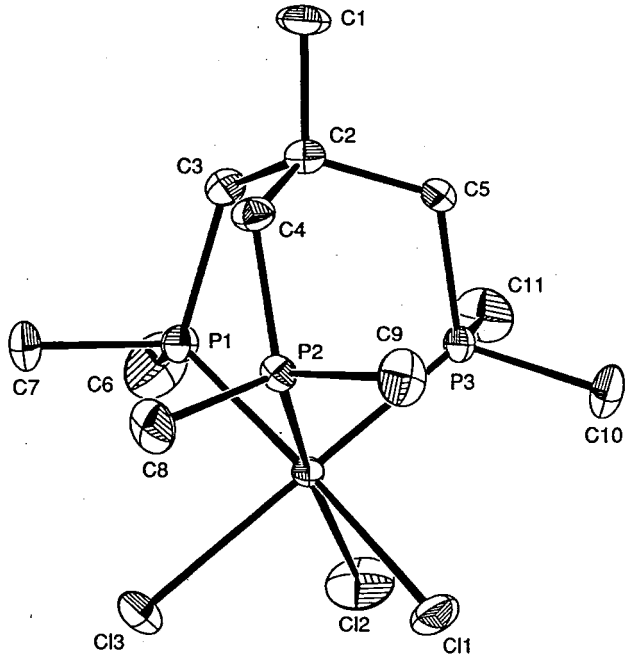

Figure 1. Molecular structure of $[RhCl_3(tmpme)]$.

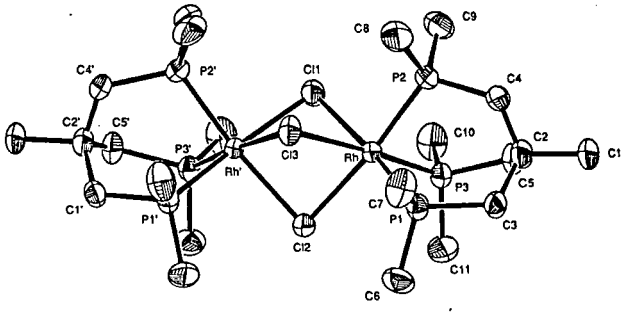

Figure 2. Perspective view of the complex cation in $[\{Rh(tmpme)\}_2(\mu\text{-}Cl)_3](BF_4)_3$.

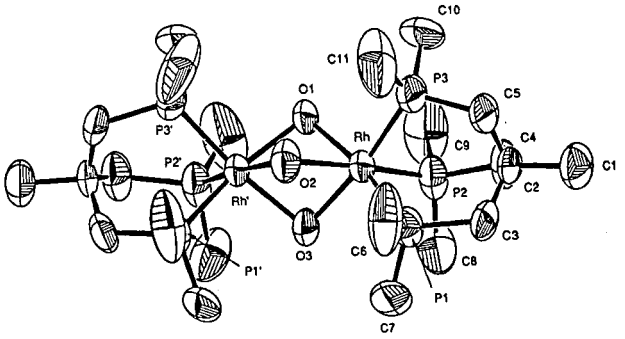

Figure 3. Perspective view of the cationic part of $[\{Rh(tmpme)\}_2(\mu\text{-}OH)_3](BF_4)_3$.

V-F-2 Preparation and Structure of a Rhodium(III) Hydride Complex with 1,1,1-Tris(dimethylphosphinomethyl)ethane (tmpme)

Takayoshi SUZUKI and Kiyoshi ISOBE

A number of rhodium hydride complexes have been reported previously, since they are of interest in not only their various geometrical structures but also their reactivity as the intermediate of complex catalyst. As we mentioned above that the tmpme complexes are expected to be highly reactive, the hydride complexes are one of the most attractive species to investigate the structure and reactivity. Here, we will make a brief report of preparation and structure of the rhodium(III) hydride complex, in which the tridentate ligand, tmpme, binds to an octahedral rhodium(III) ion in a *facial* configuration.

Addition of $NaBH_4$ to the suspension of $[RhCl_3(tmpme)]$ in methanol gave an orange solution, from which orange crystals were obtained by addition of a saturated methanol solution of NH_4BF_4 (or NH_4PF_6). The crystal structure of the complexes is confirmed by X-ray analysis (Figure 1) to be a *syn*-type dimeric structure with two bridging hydride ligands and two terminal ones. It is noteworthy that the rhodium centers are not reduced in this reaction, although in the tppme case one of rhodium centers is reduced to form $[\{Rh^{III}(tppme)\}(\mu\text{-}H)_3\{Rh^{II}(tppme)\}]^{2+}$. In solution, there is a dynamic behavior due to rapid exchange of the bridging and terminal hydrides at room temperature, which is observed by the ^1H and ^{31}P NMR spectra. This exchange process suggests that further reactions of this hydride complex are possible.

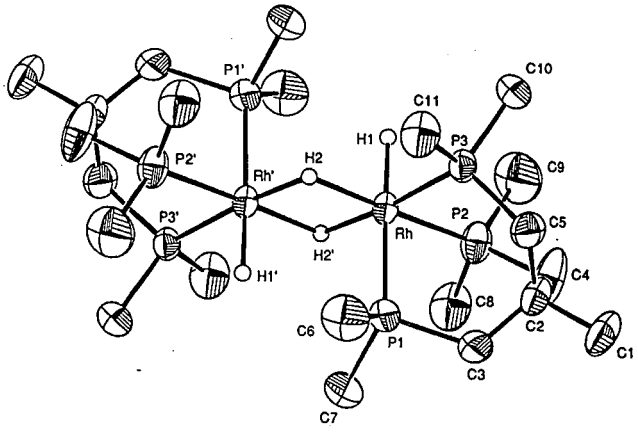

Figure 1. Perspective view of the cationic part of [{Rh(tmpme)H}$_2$(μ-H)$_2$](BF$_4$)$_2$.

V-F-3 Reinvestigation of *cis*- and *trans*-[RhCl$_2$(dmpe or dmpp)$_2$] (dmpe=1,2-bis(dimethylphosphino)ethane; dmpp=1,3-bis(dimethylphosphino)propane)

Takayoshi SUZUKI, Kiyoshi ISOBE, and Kazuo KASHIWABARA *(Nagoya Univ.)*

A pair of geometrical isomers, *cis*- and *trans*-[RhCl$_2$(dmpe)$_2$]$^+$, is one of the most fundamental complexes in rhodium(III)-phosphine complexes, of which many derivatives are now utilizing as complex catalysts. The pair of complexes was first prepared by Butter and Chatt in 1970, and their work is quoted in many papers and reviews. However, they did not give the structural and spectrochemical properties of the complexes in detail, moreover, we can not follow their experiments to prepare the *cis*-isomer. Here, we describe a new method to prepare the title complexes and their properties.

A reaction of *trans*-[RhCl$_2$(py)$_4$]Cl and dmpe or dmpp in acetonitrile formed a white precipitation of *cis*-[RhCl$_2$(dmpe or dmpp)$_2$]Cl and a yellow filtrate containing the *trans*-isomer mainly. Both isomers are possible to isolate and purify as PF$_6^-$ salts and characterized by elemental analyses, ^{1}H, ^{13}C, and ^{31}P NMR spectra, and X-ray crystallographic analyses for the dmpp complexes (Figure 1). From measurements of the UV-vis spectra of these complexes, it is found that *cis*-[RhCl$_2$(dmpe)$_2$]$^+$ is isomerized to the *trans*-isomer by radiation of UV-light, but the other complex is stable thermodynamically and photochemically. This isomerization process may be the reason why the spectral data of *cis*-[RhCl$_2$(dmpe)$_2$]$^+$ reported by Butter and Chatt are incorrect and the purification of the complex is rather difficult.

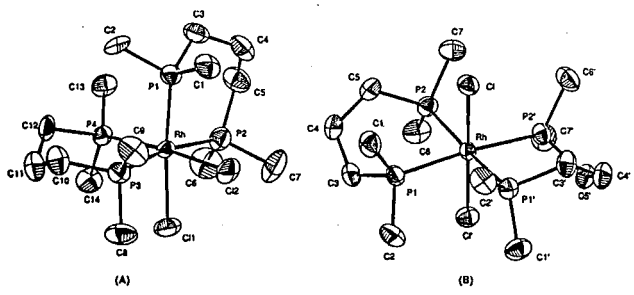

Figure 1. Perspective views of the complex cations in *cis*-[RhCl$_2$(dmpp)$_2$]PF$_6$ (A) and *trans*-[RhCl$_2$(dmpp)$_2$]PF$_6$ (B).

V—G Modeling Reaction of Metalloenzyme Active Center

Metalloenzymes play key roles in various chemical conversions in biological systems. Most of them have not been well characterized structurally and/or mechanistically due to their instability. To build new reaction systems and to obtain further insight into the natural systems, artificial models of several important metalloenzyme active centers were prepared and were used to simulate the natural enzymatic reactions. In this research project, four metalloenzymes were studied by means of the construction of the corresponding artificial models. Cytochrome c_3 has an array of four hemes, which mediate efficient electron transport through membranes. We prepared iron(III) porphyrin dimers linked by a suitable linker molecule and found their imidazole/imidazolate complexes have relatively large interaction between two metals. In the functional modeling of water oxidation enzymes, we found manganese porphyrin dimers with a suitable Mn-Mn separation could oxidize water and evolve oxygen. The relating manganese porphyrin dimers can mediate disproportionation of hydrogen peroxide and they are new models of Mn catalases. We determined the reaction mechanism of by kinetic study with use of the high valent manganese complex. Finally, we attained the synthesis of the active center model of cytochrome P-450, which will be used for the study of oxygen activation mechanism.

V-G-1 Imidazolate-mediated Antiferromagnetic Coupling between Fe(III) Ions in Rigidly-linked Porphyrin Dimers and Trimers

Yoshinori NARUTA, Nobuyuki SAWADA[a], and Makoto TADOKORO *([a]Kyoto University)*

[*Chem. Lett.*, 1713 (1994)]

Electronic and magnetic interactions between transition metal ions have been interesting from theoretical and experimental stand points to design high conducting or paramagnetic materials. 1,8-Anthracene- and *o*-phenylene-linked iron(III) porphyrin dimers and the trimer were synthesized to determine the electronic and magnetic interactions between metal ions through an imidazolate ligand. Their Fe(III) ions were ligated by imidazolate(s) in their molecular cleft to form the corresponding low-spin complexes. From the X-ray crystallographic analysis of the anthracene-linked dimer (Figure 1), the Fe-N$_{ax}$(im) distance (im=imidazolate) and the Fe-N$_{ax}$(Him) (Him=imidazole) were determined to be 1.95—1.96 and 2.01—2.02 Å, respectively. The former separation is very small in comparison with the analogous complex (2.18 Å). In these iron complexes, relatively large imidazolate-mediated antiferro-

magnetic exchange coupling ($-J$=15.3–29.4 cm^{-1}) between the Fe(III) ions is observed by means of their esr and magnetic susceptibility measurements. These complexes are considered to be good functional models of cytochrome c_3, a biologial electron carrier.

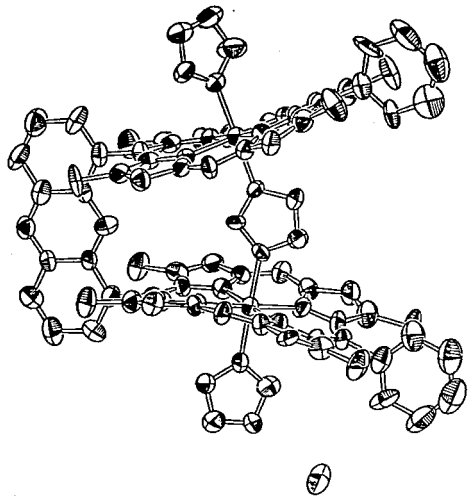

Figure 1. ORTEP drawing for the $(Him)_2(im)$ complex of anthracene-linked iron(III) porphyrin dimer.

V-G-2 Oxygen Evolution by Water Oxidation with Manganese Porphyrin Dimers

Y. NARUTA, M. SASAYAMA[a], and T. SASAKI[a] *([a]Kyoto University)*

[*Angew. Chem.*, **106**, 1964 (1994)]

Photosystem II in plant RC contains a tetranuclear manganese complex, which catalyzes evolution of oxygen by oxidation of water. We found that manganese porphyrin dimers linked by an *o*-phenylene bridge were good functional model compounds and evolved oxygen in an aqueous media by means of anodic oxidation. We prepared other manganese porphyrin dimers bearing various linker molecules. Their Mn-Mn separations were estimated to be 4.5–10.0 Å by MM+. Catalytic oxidation of these complexes under the same conditions showed that they were less effective than the *o*-phenylene-linked ones. We concluded that the separation required for efficient oxidation of water was around 4 Å.

V-G-3 Modeling Reaction of Manganese Catalase with Dimanganese Complexes of Porphyrin Dimers

Y. NARUTA and M. SASAYAMA[a] *([a]Kyoto University)*

[*J. Chem. Soc., Chem. Commun.*, in press]
[*J. Am. Chem. Soc.*, submitted]

Manganese catalases contain dimanganese complexes in their active center and they mediate the disproportionation of hydrogen peroxide to oxygen and water. In the modeling reaction, we showed manganese porphyrin dimers having appropriate metal-metal separations were good functional models. These Mn porphyrin dimers also exhibit high catalase activity in the presence of a nitrogen base. Two roles of this bases in the development of catalase activity have been separately estimated by their kinetic study. In this reaction, the corresponding Mn(IV)-Mn(IV) complex is supposed to be a reactive intermediate, which could form by the reaction with the initial H_2O_2 molecule and can oxidize the second H_2O_2 to evolve oxygen. The first stage of this reaction is considered to be the rate determining step from the mechanistic study. Thus, we prepared the Mn(IV)-Mn(IV) complex by chemical oxidation at low temperature and determined the reaction rate with H_2O_2 and its activation parameters. The rate of the disappearance of the high valent complex was much larger than the overall rate of the oxygen evolution and this evidence support our proposed mechanism.

V-G-4 Synthesis of an Active Center Model of Cytochrome P-450 for the Study on the Oxygen Activation Mechanism

Yoshinori NARUTA, Mari ICHIMURA[a], and Fumito TANI[a] *([a]Kyoto University)*

The detailed reaction mechanism of oxygen activation in cytochrome P-450 is not fully clarified. Especially, the dioxygen complex of a heme in the presence of a thiolate ligand has never been observed in model complexes, because of the easy reductive dissociation of O_2 by the single-electron transfer from a thiolate ligand, an extremely strong base. In cyt. $P\text{-}450_{cam}$, Thr-259 is supposed to stabilize the coordinated oxygen atom and to assist the protonation to the terminal oxygen through a proton relay system. We designed an accurate reaction center model complex, which have a thiolate residue and hydroxyl groups at the appropriate position in the different cavities over the central metal (Figure 2). The synthesis of this complex has attained in 5 steps from the corresponding 'twin-coronet' porphyrin, whose synthesis we have already established. The formation of the corresponding oxy compound and its characterization is now under way.

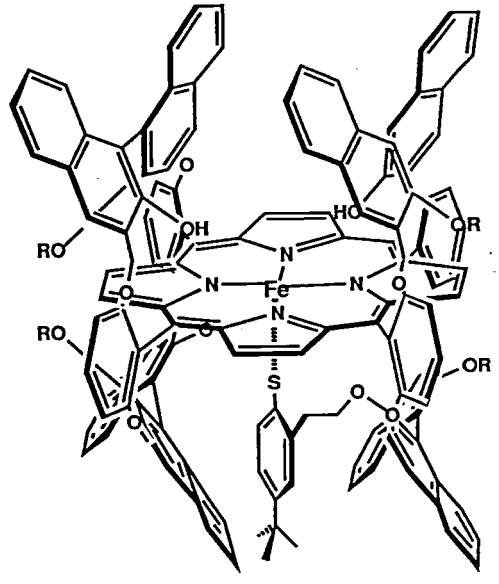

Figure 2. Structure of the synthesized model complex of cytochrome P-450 active center.

V—H Design, Properties and Reactivity of New Organometallic Compounds

A variety of carbon-metal bonds can produce unconventional reactivities and properties of the organometallic compounds. At present, development of new organometallic reagents for organic chemical transformations especially asymmetric reactions is one of our important projects. The other is synthesis of new organometallic compounds, especially organoboron compounds having strong affinity to cancer cells for Neutron Capture Therapy.

V-H-1 Transition Metal Catalyzed Addition of Certain Nucleophiles to Imines

Yoshinori YAMAMOTO[a], Yasufumi KUBOTA[a], Yoshihiro HONDA[a], Hiroyuki FUKUI[a], Naoki ASAO, and Hisao NEMOTO *([a]Tohoku Univ.)*

[*J. Am. Chem. Soc.*, **116**, 3161 (1994)]

Transition metal catalyzed nucleophilic addition to activated imines (**1**) with active methyne compounds bearing cyano group (**2**) has been accomplished.

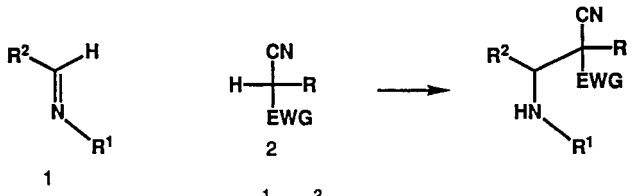

Figure 1.

V-H-2 Synthesis of a Water-soluble o-Carborane Bearing Uracil Moiety via Palladium Catalyzed Reaction under Essentially Neutral Condition

Hisao NEMOTO, Jianping CAI, and Yoshinori YAMAMOTO[a] *([a]Tohoku Univ.)*

[*J. Chem. Soc., Chem. Commun.*, 577 (1994)]

A water-soluble o-carborane bearing a uracil moiety **3** has been synthesized via a palladium-catalysed reaction under essentially neutral conditions.

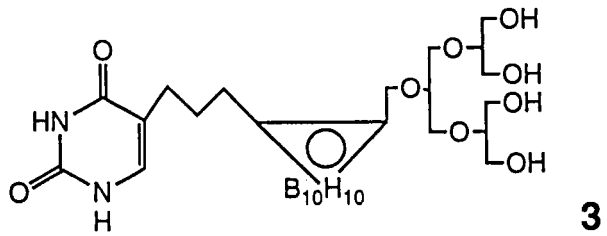

Figure 2.

V-H-3 A New Alkenyl Ether Giving Acetal with Stereospecific Manner

Hisao NEMOTO

[*Tetrahedron Lett.*, in press]

A new alkenyl ether, bicyclo[3.3.0]-2-oxa-5-(2-propenyl)-1-octene, (**4**) can stereospecifically produce cis-fused bicyclo[3.3.0]-2-oxa-(2-pentenyl)-1-alkoxyoctane (**5**) and the stereochemistry was proved by X-ray analysis.

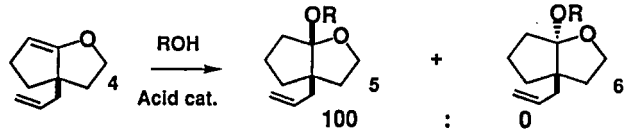

Figure 3.

V-H-4 Palladium Catalyzed Addition of Masked Formyl Cyanide ROCH(CN)$_2$ to Aldehydes

Hisao NEMOTO, Yasufumi KUBOTA[a], and Yoshinori YAMAMOTO[a] *([a]Tohoku Univ.)*

[*J. Chem. Soc., Chem. Commun.*, 1665 (1994)]

The palladium catalysed reactions of masked formyl cyanides **7** with aldehydes **8**, followed by treatment with either diketene or acetic anhydride-pyridine, afford the addition products protected with acetylacetate **9** or acetyl group **10**, respectively.

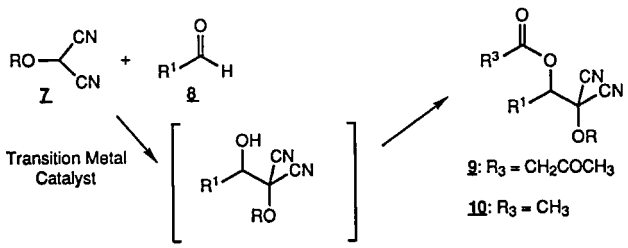

Figure 4.

V-H-5 Zinc Chloride as a Radical Initiator as well as Chelating Agent

Yoshinori YAMAMOTO[a], Setsuko ONUKI[a], Masatoshi YUMOTO[a], and Naoki ASAO *([a]Tohoku Univ.)*

[*J. Am. Chem. Soc.*, **116**, 421 (1994)]

The reaction of allyltributyltin with methyl 2-[N-((4S)-4-(1-methylethyl)-2-oxazolidinone-3-carbamoyl)amino]-2-bromoacetate **12** was accelerated at −50°C in the presence of AIBN and stopped in the presence of galvinoxyl, indicating that the reaction proceeds through radical mechanism. The reaction was accelerated dramatically at −78°C in the presence of $ZnCl_2 \cdot OEt_2$, and the $ZnCl_2$-mediated reaction was stopped in the presence of galvinoxyl. In the presence of 2 equiv $ZnCl_2 \cdot OEt_2$, the reaction afforded methyl (2R)-2-[N-((4S)-4-(1-methylethyl)-2-oxazolidinone-3-carbamoyl)amino]-4-pentenoate **13(R)** with high diastereoselectivity (93:7). Taken together, $ZnCl_2 \cdot OEt_2$ works as a

radical initiator as well as chelating agent. The $ZnCl_2 \cdot OEt_2$ mediated reaction of 1,1-diphenylmethyl bromide with allyltributyltin gave 4,4-diphenyl-but-1-ene in high yield. On the other hand, no reaction took place between 1,1-diphenylmethyl bromide and $BF_3 \cdot OEt_2$. The $ZnCl_2$ mediated allylation proceeded in high yields in cases of tertiary-, allylic-, α-alkoxy, and sec-benzyl-halides, whereas the reaction did not occur with primary and secondary halides. It is proved that the $ZnCl_2$ mediated allylation of bromomalonate and related compounds proceeds via a radical pathway.

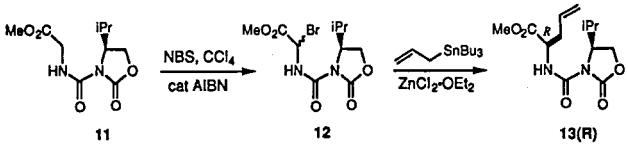

Figure 5.

V-H-6 Intramolecular Michael Addition of γ-Alkylsulfonyloxy-α,β-Unsaturated Esters by Using Higher Order Cyano Copper or Silver Amides as a Base

Naoki ASAO, Masaki MEGURO[a], and Yoshinori YAMAMOTO[a] *([a]Tohoku Univ.)*

[*Synlett*, 185 (1994)]

Treatment of γ-alkylsulfonyloxy-α,β-unsaturated esters **14** with higher order cyano copper or silver amides gave γ-sultones **15** stereoselectively in good to high yields. Furthermore, the ring cleavage of sultones produces a carbon chain **16** having a new chiral center adjacent to the original asymmetric carbon, and this 1,2-asymmetric induction takes place in nearly 100%de.

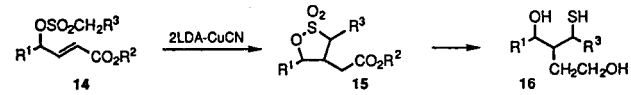

Figure 6.

V-H-7 Palladium Catalyzed Addition of Activated Methylene and Methyne Compounds to Allenes

Yoshinori YAMAMOTO[a], Mohammad Al-MASUM[a], and Naoki ASAO *([a]Tohoku Univ.)*

[*J. Am. Chem. Soc.*, **116**, 6019 (1994)]

The addition of activated methylene and methyne compounds **17** to allenes **18** takes place in the presence of catalytic amounts of $Pd_2(dba)_3 \cdot CHCl_3$ in THF under reflux, giving the internal alkenes **19** and **20**. The nucleophile always attacks the terminal carbon of allenes. With monosubstituted allenes **18a-c**, the trans alkenes **20** are normally produced with high stereoselectivity. With disubstituted allenes **18d-g**, a mixture of the trans and cis alkenes (**19** and **20**) is afforded in general.

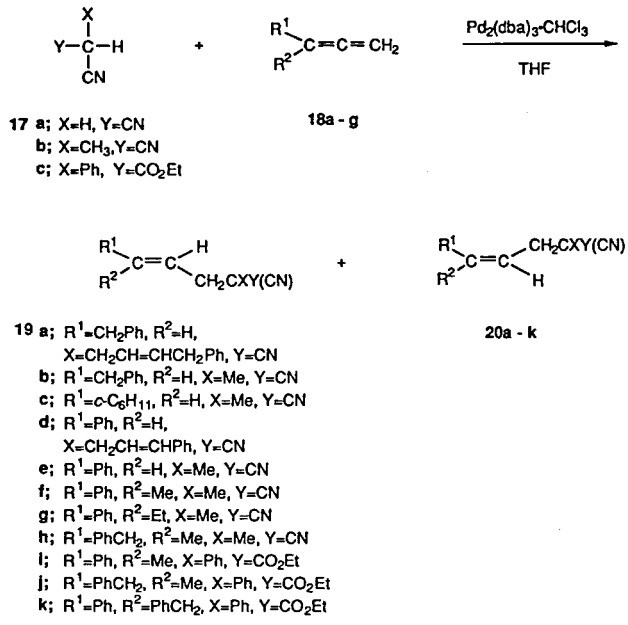

Figure 7.

V-H-8 Ytterbium Triflate Catalyzed Ring Opening of Aziridines with Amines

Masaki MEGURO[a], Naoki ASAO, Yoshinori YAMAMOTO[a] *([a]Tohoku Univ.)*

[*Tetrahedron Lett.*, **35**, 7395 (1994)]

Ring Opening of azirizines with amines takes place readily in the presence of catalytic amount of ytterbium triflate, giving the corresponding 1,2-diamines in good to high yields.

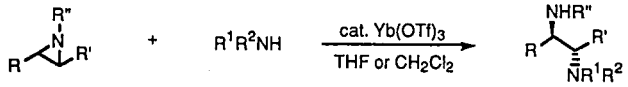

Figure 8.

V-H-9 Ytterbium Triflate and High Pressure Mediated Ring Opening of Epoxides with Amines

Masaki MEGURO[a], Naoki ASAO, and Yoshinori YAMAMOTO[a] *([a]Tohoku Univ.)*

[*J. Chem. Soc., Perkin Trans. I*, 2597 (1994)]

Ring opening of epoxides with amines in THF takes place very readily in the presence of catalytic amounts of ytterbium triflate, giving the corresponding β-amino alcohols in good to high yields. With mono- and di-substituted epoxides, the use of an equivalent amount of amines is enough to obtain the desired amino alcohols in high yields. With tri- and tetra-substituted epoxides, the use of excess amounts (2~3 equiv) of amines is needed. The $Yb(OTf)_3$ catalyzed reaction of epoxides with amines in CH_2Cl_2 is rather complicated; the yield of amino alcohols is generally lower and depends upon the addition order of the catalyst, amine, and epoxide. The ring opening is accomplished also under high pressures in the absence of $Yb(OTf)_3$. The ring opening via the combination of $Yb(OTf)_3$ and high pressures in CH_2Cl_2 is more effective than the independent use

of the $Yb(OTf)_3$ or high pressure method itself. Oxetane and a β-lactone undergo the ring opening reaction in the presence of $Yb(OTf)_3$.

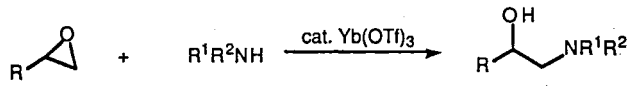

Figure 9.

V—I Mechanistic Investigations of the Photosolvolyses Involving Carbocationic Intermediates

The mechanistic investigations of photosolvolyses are of great interest because photosolvolysis has proven to be a convenient method for the generation of carbocations that are not readily available in the thermal solvolyses. Ketones possessing a heteroatom substituent (X) at the α-carbons are known to undergo photochemical C-X bond heterolysis with the formations of unstable α-ketocarbonium ions through the interaction between the π^*-orbital of carbonyl double bond and the σ^*-orbital of the C-X bond. This project focuses on the photoinduced bond heterolysis of 2-chloropropiophenone that exhibits competing phenyl-rearrangement and nucleophilic substitution reactions (Scheme 1). The photosolvolysis mechanisms in aqueous 2,2,2-trifluoroethanol were investigated by the aid of substituent effect, solvent effect, and effect of nucleophiles on the product distributions.

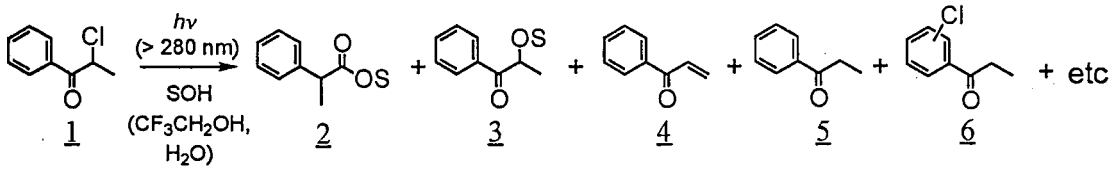

Scheme 1.

V-I-1 Substituent Effects on the Photosolvolyses of 2-Chloropropiophenones in 2,2,2-Trifluoroethanol

Satoshi USUI, Jyunji NISHIMOTO[a], and Katsutoshi OHKUBO[b] *([a]Kumamoto University, [b]Kyushu University)*

Substituent effects on the product distributions of the photosolvolyses of 2-chloropropiophenones (1) were investigated in 2,2,2-trifluoroethanol (TFE). The photosolvolysis of 1 in TFE afforded five products without the thermal solvolysis of 1 (Scheme 1). According to the product distributions in Table 1, the photosolvolyses of all substituted derivatives showed excellent material balances of over 95%, and the photosolvolyses products were mainly C-Cl bond heterolysis ones (2—4); the *m*-OMe and *m*-Me derivatives resulted in the considerable amount of the C-Cl bond homolysis products (5 and 6). Among the heterolysis products (2, to 4), the product distribution between a phenyl-rearrangement product (2) and nucleophilic substitution ones (3 and 4) apparently suffered from the substituent effect of 1. The increase in the electron-donating ability of the substituent resulted in the decrease in the product distributions of 2, that is contrary to the substituent effects observed for the thermal acetolysis.[1] It is also apparent from Table 1 that strong π-donating methoxy substituents facilitated the nucleophilic substitution pathway. The methoxy substituent at the *p*-position resulted in the almot same amount of 2 and 3, and notably, the *m*-OMe derivative appreciably exalted the nucleophilic substitution pathway. This novel substituent effect may be reflected to the *meta* electron transmission effect.[2]

References

1) H. C. Brown, C. J. Kim, C. J. Lancelot, and P. v. R. Schelyer, *J. Am. Chem. Soc.*, **92**, 5244 (1970).

2) H. E. Zimmerman and V. R. Sandel, *J. Am. Chem. Soc.*, **85**, 915 (1963).

Table 1. Substituent Dependencies of the Product Distributions (%) of the Photosolvolysis 1 in TFE-d_3[a)]

Substituent	1	2	3	4	5 and 6
p-OMe	66.4	14.0	12.9	5.2	1.0
p-OMe-*m*-Cl	57.2	12.4	16.9	12.1	1.4
p-OMe-*m*-Br	39.7	16.2	20.3	20.9	2.4
p-OMe-*m*-CN	62.9	12.7	11.4	10.6	0.2
m-OMe[b)]	30.0	1.8	21.3	11.9	29.8
p-Me	67.3	22.6	7.3	2.8	0.0
m-Me	49.7	26.8	5.8	5.0	11.1
H	54.7	36.1	3.3	4.2	1.7
p-Cl	45.6	42.1	5.8	6.5	0.0
m-Cl	45.1	49.6	3.6	4.1	2.0
m-CN	51.2	27.6	1.8	12.7	3.3
m-CF_3	49.1	35.2	0.0	10.9	2.2

a) After 1 h irradiation, unless otherwise noted. b) After 0.5 h irradiation.

V-I-2 Solvent Effect on the Photosolvolysis of 2-Chloropropiophenone

Satoshi USUI, Jyunji NISHIMOTO[a], and Katsutoshi OHKUBO[b] *([a]Kumamoto University, [b]Kyushu University)*

Solvent effect on the product distributions of the photosolvolysis of 2-chloropropiophenone (1) was investigated in aqueous 2,2,2-trifluoroethanol (TFE). The photosolvolysis of 1 in 50% (w/w) aqueous TFE (50T) mainly gave bond heterolysis products similar to the photosolvolysis in absolute TFE. Among the heterolysis products, a phenyl-rearranged (2) and a nucleophilically substituted ones (3), were obtained as H_2O adducts (S=OH in Scheme 1), and no TFE adducts were obtained. The product distributions of

the 2 and 3, were suffered from solvent effect, and the increase of the water content decreased the product distribution of 2 while that of 3 increased (Table 2). Furthermore, the product distribution of elimination product 4, showed a similar solvent dependency to that of 3. These results suggest that increase of the solvent polarity prevails the α-ketocarbocation formation over the phenyl-rearrangement pathway. It is also noticeable in Table 2 that the rate of photosolvolysis, which was given in first-order rate constant, was less influenced by the solvent polarity. The current solvent effect examination concludes that the present photosolvolysis proceeds via rate-determining intermediate formation (either radical or carbocationic) followed by product formation through carbocationic intermediate.

Table 2. Product Distributions[a)] and Observed First-Order Rate Constants ($k_{Obs}/10^{-5}$ s^{-1}) of the Photo-solvolysis of 1 in Aqueous 2,2,2-Trifuloroethanol

Solvent[b)]	2	3	4	5 and 6	k_{Obs}
100T	79.7%	7.3%	9.1%	3.8%	23.5
50T	36.0%	10.5%	14.1%	5.5%	25.9

a) 1h after irradiation. b) Figures denote the weight % of 2,2,2-trifluoroethanol.

V-I-3 Effects of Nucleophiles on the Photosolvolysis of 2-Chloropropiophenone in Aqueous 2,2,2-Trifluoroethanol

Satoshi USUI, Jyunji NISHIMOTO[a], and Katsutoshi OHKUBO[b] *([a]Kumamoto University, [b]Kyushu University)*

The effects of nucleophiles (Nu) on the photosolvolysis of 2-chloropropiophenone (1) were investigated in aqueous 2,2,2-trifluoroethanol (TFE). As summarized in Table 3, the addition of weak nucleophiles such as Cl^- or Br^- had little effects on the product distributions of the photosolvolysis. The addition of N_3^- or SO_3^{2-}, on the other hand, decreased the distribution of the bond-heterolysis product 2, 3, and 4; instead, corresponding nucleophilically substituted products (2, S=Nu) were obtained. Although the effects of the tow nucleophiles are seemingly interpreted as the trapping of α-ketocarbocation by the N_3^- or SO_3^{2-}, they were differentiated by the fact that addition of SO_3^{2-} apparently increased the observed photosolvolysis rates (k_{Obs}) while that of N_3^- did not. Furthermore, a characteristic feature of the effect of SO_3^{2-} was the suppression of every other by-products including 5 and 6. These results suggest that the present photosolvolysis proceeds through plural intermediates, and N_3^- or SO_3^{2-} reacts with different one.

Table 3. Effects of Nucleophiles on the Product Distributions and Observed First-Order Rate Constants ($k_{Obs}/10^{-5}$ s^{-1}) of the Photosolvolysis of 1 in 50% (w/w) Aqueous 2,2,2-Trifluoroethanol

Nu	Conc./M	2	3	4	k_{Obs}
None		36.0%	10.5%	14.1%	25.9
Cl^-	0.01	39.4%	11.7%	15.0%	25.2
	0.1	29.7%	9.8%	13.4%	25.4
Br^-	0.1	27.6%	8.8%	17.2%	24.1
N_3^-	0.01	14.0%	8.5%	9.7%	27.9
	0.1	6.9%	4.9%	4.4%	25.6
SO_3^{2-}	0.01	23.1%	7.6%	1.0%	42.4

RESEARCH ACTIVITIES VI
Department of Vacuum UV Photoscience

VI—A Electronic Structure and Decay Mechanism of Inner-shell Excited Molecules

This project is being carried out in collaboration with Photon Factory, National Laboratory for High-Energy Physics (KEK-PF) and with McMaster University, Canada. We observed vibrational enhancement through Rydberg-valence mixings in the high-resolution O K-edge spectra of O_2, and discussed potential energy curves, avoided curve crossings, and atomic Auger decay [See, A. Yagishita, E. Shigemasa, N. Kosugi, *Phys. Rev. Lett.* **72**, 3961 (1994)]. This year we have extended our approaches to some linear triatomic molecules and spin-forbidden inner-shell excited molecules. Mr. Jun-ichi Adachi from KEK-PF has joined the Kosugi group in April 1994 as a technical associate in this field.

VI-A-1 Angular Distribution of Fragment Ions Following C 1s → π^* Photoexcitation of CS_2, OCS, and CO_2

Jun-ichi ADACHI, Nobuhiro KOSUGI, Eiji SHIGEMASA* and Akira YAGISHITA* *(*KEK-PF)*

The angle-resolved ion-yield spectra following the C 1s → π^* photoexcitation of CS_2, OCS, and CO_2 have been measured using linearly polarized soft x-ray, as shown in figure 1. The widths of the π^* resonance peaks of CS_2, OCS, and CO_2 are 170 meV, 390 meV, and 630 meV in FWHM, respectively. In contrast to the case for diatomic molecules, the fragment ions following the C 1s → π^* photoexcitation of these molecules are emitted not only in the perpendicular direction (I_{90}) to the electric vector of the incident light but also in the parallel direction (I_0). It is also found that the amount of the fragments emitted in the parallel direction (I_0) depends on the widths of the π^* resonance peaks. These present observation is investigated in terms of the Renner-Teller effect.

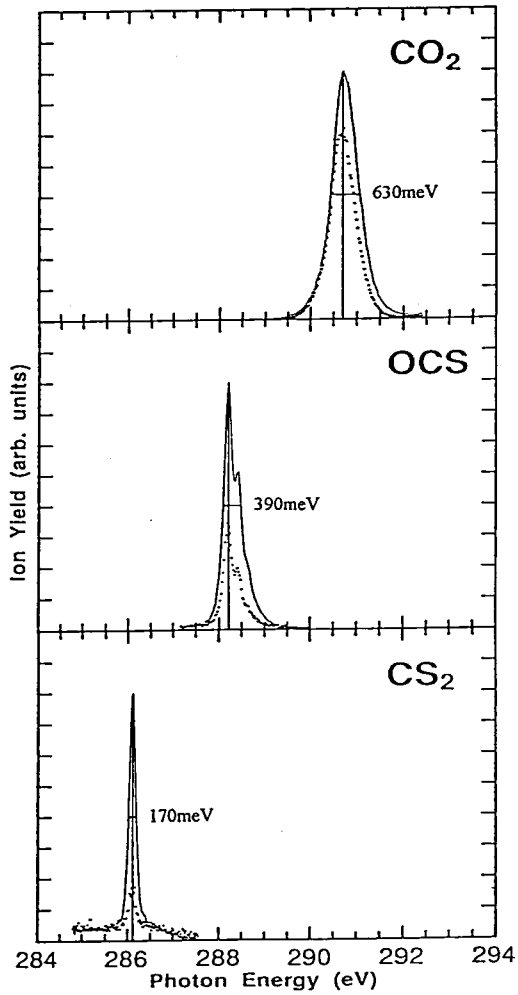

Figure 1. C K-edge ion-yield spectra of CS_2, OCS, and CO_2. The solid line shows the ion-yield in the 90° to the electric vector of the incident light and dotted line shows one in the 0°.

VI-A-2 Renner-Teller Effect and Rydberg-valence Mixing in the N K-edge Absorption Spectra of N_2O

Jun-ichi ADACHI, Nobuhiro KOSUGI, Eiji SHIGEMASA* and Akira YAGISHITA* *(*KEK-PF)*

Figure 1 shows the N K-shell high-resolution angle-resolved ion-yield spectrum of N_2O (N_t-N_c-O). The FWHM of the N_c 1s → π^* peak (1.05 eV) is larger than that of the N_t 1s → π^* peak (0.74 eV). A preliminary result of the SCF calculation shows that the N_c and N_t 1s → π^* excited states have bent equilibrium structures with N_t-N_c-O angles of about 126° and 136°, respectively, due to the Renner-Teller effect. The N_c 1s → π^* excited state has a stronger bending mode excitation than in the N_t 1s → π^* resonance state. It is also found that the peak intensities of the N_t 1s → nsσ Rydberg series are anomalous; the 4sσ Rydberg peak is more intense than 3sσ and 5sσ. This is because the N_2O molecule has a vacant σ^* orbital below the ionization threshold and the σ^*-Rydberg mixing takes place near the 4sσ Rydberg state.

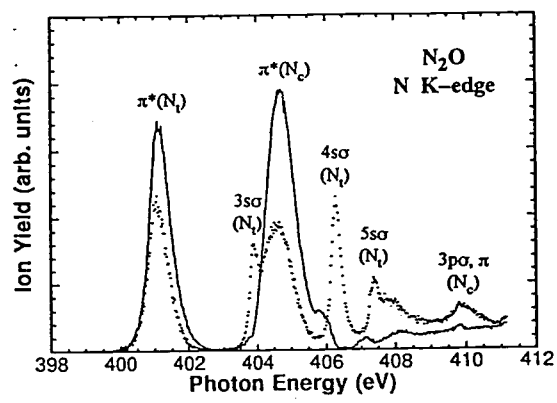

Figure 1. N K-edge ion-yield spectrum of N_2O. The solid line shows the ion-yield in the 90° to the electric vector of the incident light and dotted line shows one in the 0°.

VI-A-3 Vibronic Coupling in the C 1s (σ_g) → 3sσ_g Rydberg Excited State of CO_2

Jun-ichi ADACHI, Nobuhiro KOSUGI, Eiji SHIGEMASA* and Akira YAGISHITA* *(*KEK-PF)*

The C K-shell excited Rydberg states of CO_2 molecules have been investigated with the high-resolution angle-resolved ion-yield spectroscopy. It is found that the fragment ions emitted following the C 1s (σ_g) → 3sσ_g Rydberg excitation are mainly observed in the 90° direction to the electric vector of the incident light. This is because the 3sσ_g Rydberg state is mainly coupled with the bending mode. It is also found that the 3pσ_u and the 3pπ_u Rydberg states have different vibrational spacings and can be differenciated though these electronic states are almost degenerate.

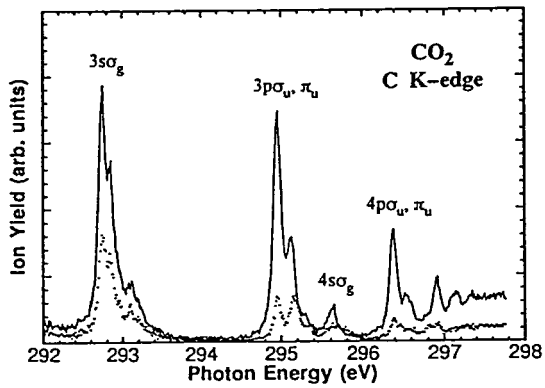

Figure 1. C K-edge ion-yield spectrum of CO_2. The solid line shows the ion-yield in the 90° to the electric vector of the incident light and dotted line shows one in the 0°.

VI-A-4 C 1s → π^* Triplet Excited State of CO: Momentum Transfer Dependence and Vibrational Structure

James T. FRANCIS*, Nobuhiro KOSUGI, and Adam P. HITCHCOCK* *(*McMaster Univ.)*

[*J. Chem. Phys.*, in press]

The intensity of the C 1s → π^* (X $^1\Sigma^+$ → $^3\Pi$) spin-forbidden inner-shell excitation of CO has been measured by electron energy loss spectroscopy using a range of scattering angles (0—45°) and impact energies (376 to 1806 eV) in order to investigate the momentum transfer dependence. Based on experimental and theoretical Franck-Condon analysis of the vibrational structure we have qualified differences in the potential energy curves of the singlet and triplet C 1s → π^* excited states and the doublet C 1s ionized state.

VI—B Soft X-ray Photoelectron-Photoabsorption Spectroscopy and Electronic Structure of Transition Metal Compounds

This is a new project we just started in November 1993, when Dr. Yasutaka Takata from KEK-PF joined the Kosugi group as research associate. In addition to him, Dr. Motohiko Nakamura has joined as an IMS fellow from Science University of Tokyo in August 1994. The experiments are done using a high-performance electron energy analyzer connected to the soft X-ray double crystal monochromator of the beamline BL1A at the UVSOR facility.

VI-B-1 Construction of a New UHV Apparatus for Soft X-ray Photoelectron-Photoabsorption Spectroscopy

Yasutaka TAKATA, Motohiko NAKAMURA, and Nobuhiro KOSUGI

In order to investigate the electronic structure of transition metal compounds by soft x-ray photoelectron-photoabsorption spectroscopy, we have constructed a new UHV apparatus. It consists of three vacuum chambers; an analysis chamber, a preparation chamber, and an air-lock chamber. Top view of the whole system is shown in Figure 1. The main component of the analysis chamber is an electron energy analyzer (SES-200) manufactured by SCIENTA, Uppsala, Sweden. It features high energy resolution and high detection efficiency by use of a large 200 mm hemispherical analyzer and an electron lens, respectively. The typical reolving power ($E_P/\Delta E$) is more than 1300 and the ultimate resolution (ΔE) is 5 meV. Absorption spectra can be measured in Auger electron yield. The ultimate base pressure of the system will be less than 5 $\times 10^{-11}$ Torr.

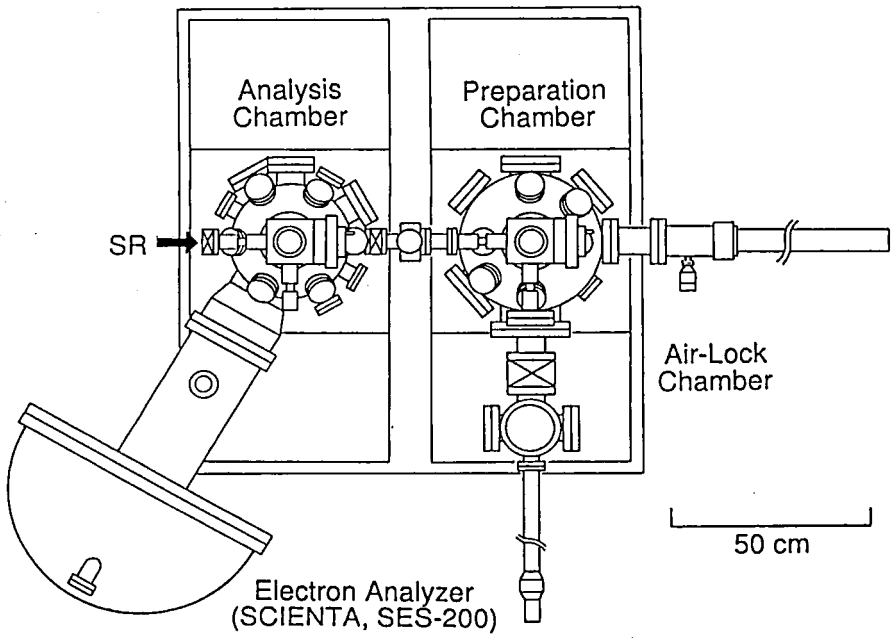

Figure 1. Top view of a newly constructed UHV apprataus for soft x-ray photoelectron-photoabsorption spectroscopy.

VI—C Synchrotron Radiation Stimulated Surface Reactions

Study of synchrotron radiation (SR) stimulated surface reaction is attractive for fundamental scientists, because dynamical processes induced by photostimulated electron excitations on surfaces are scarcely explored so far. This field is important also in applied science, since fundamental study is expected to develop new techniques for semiconductor processing such as SR stimulated etching and SR stimulated epitaxial growth.

VI-C-1 Molecular Orientation and Photochemical Reaction of Organoaluminum Compounds Investigated by Buried Metal Layer Infrared Reflection Absorption Spectroscopy

Tsuneo URISU, Yanping ZHANG *(Sumitomo Heavy Industries, Ltd.)*, **Mitsuru NAGASONO, Akitaka YOSHIGOE, Yoshiaki IMAIZUMI, and Shinri SATO** *(Hokkaido University)*

The structure and synchrotron radiation (SR) irradiation effects for the low temperature condensed layer of several organoaluminum compounds on the SiO_2 surface were investigated by infrared reflection absorption spectroscopy using the buried metal layer substrate (BML-IRAS). Trimethylaluminum is a dimer at less than 180 K, and a photoproduct having the methyl group is produced by SR irradiations. The condensed layer of dimethylethylamine alane (DMEAA) as deposited at temperatures less than 140 K is consisted of randomly oriented dimer molecules, and it changes to more orderly orientation of monomer molecules by increasing temperatures higher than 140 K. Concerning the SR irradiations, the results are different between different molecular orientations. By SR irradiations to the orderly orientation layer, a new broad vibration band possibly assigned to the gathering of inhomogeneous AlH stretching vibrations appears. On the other hand, in the case of the random orientations of the dimer molecules, such the new broad band does not appear, and only intensity decrease is observed for all bands.

VI-C-2 Development of Infrared Reflection Absorption Spectroscopy Using a Buried Metal Layer Substrate for *in-situ* Observation of Surface Photochemical Reactions Stimulated by Synchrotron Radiation

Akitaka YOSHIGOE, Mitsuru NAGASONO, Kazuhiko MASE, and Tsuneo URISU

Infrared reflection absorption spectroscopy (IRAS) is usually used to evaluate metal surfaces, but can also be applied for semiconductor or insulator surfaces by using buried metal layer (BML) substrates, in which a metal thin film is buried under a semiconductor or an insulator film (buffer layer). In this work, IRAS sensitivity was quantitatively evaluated for Langmuir-Blodgett films on a BML substrate of SiO_2/Al/Si(100). The root mean square value of the surface roughness of the BML substrate was estimated to be 1 nm with atomic force microscopy (AFM). The measured IRAS signal intensity is consistent with the value calculated assuming the ideal multilayer structure for the BML substrate.

VI-C-3 Infrared Reflection Absorption Spectroscopy System for Study of Surface Photochemical Reactions Induced by Synchrotron Radiation

Mitsuru NAGASONO, Akitaka YOSHIGOE, Kazuhiko MASE, and Tsuneo URISU

The aim of the present study is to measure the change of the adsorbed species and/or the adsorption states under

reactions induced by synchrotron radiation (SR) using infrared reflection absorption spectroscopy (IRAS), and to clarify the reaction mechanisms. An advantage of IRAS is high resolution as compared with electron energy loss spectroscopy, and feasibility to measure under presence of gas in a reaction chamber, i.e., *in situ*.

The IRAS system shown in figure 1 is composed of a Fourier transform infrared spectrometer (FTIR: JEOL JIR-7000), three mirror systems, and a mercury cadmium telluride (MCT) detector, and can measure the reactions in an etching and an epitaxial growth chamber. Optical paths are purged with dry air without CO_2. For measurements in the etching chamber, a collimated parallel infrared beam interfered by the FTIR is focused on the sample at an incident angle of 85° by an off-axis paraboloidal mirror M2 (diameter, D = 50 mm, effective focal length, F = 320 mm, diverting angle, α = 65°) through a ZnSe window. A reflected beam is collimated again by a mirror M5 (D = 50 mm, F = 320 mm, α = 65°), and is focused on the MCT detector by mirror M6 (D = 50 mm, F = 45 mm, α = 90°). For measurements in the epitaxial growth chamber, the IR beam is focused at incident angle of 82.5° by a mirror M4 (D = 50 mm, F = 320 mm, α = 90°) through a ZnSe window. The reflected beam is collimated by a mirror M7 (D = 50 mm, F = 320 mm, α = 90°), and is focused on the MCT detector by mirror M8 (D = 50 mm, F = 45 mm, α = 90°). The signals from the MCT detector are amplified, and give IR spectra after fast FT calculation.

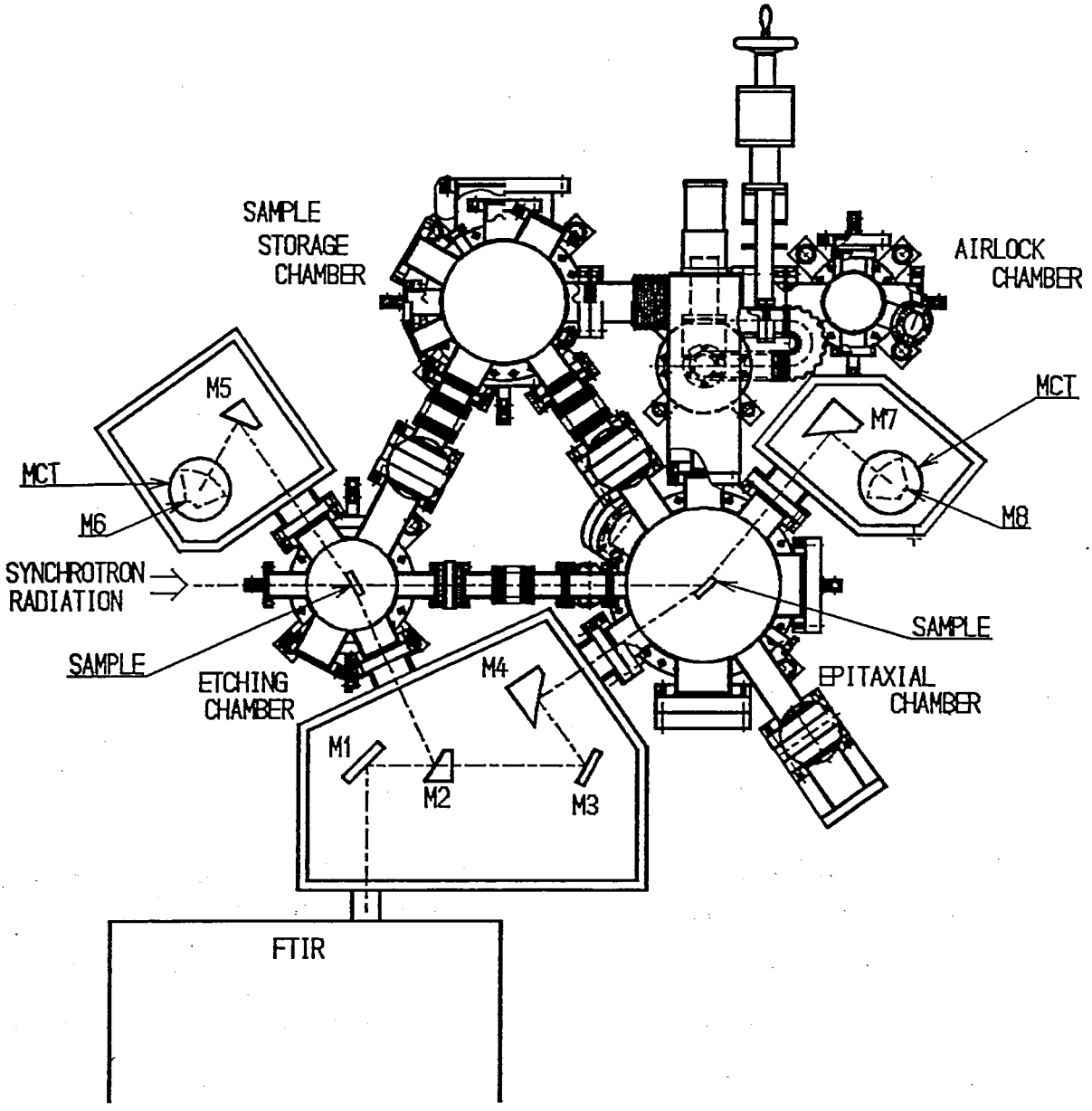

Figure 1. Reaction chambers and an IRAS system for study of SR excited surface photochemical reactions. For measurements in the etching chamber, IR beam passes through M1, M2, Sample, M5, and M6. For measurements in the epitaxial growth chamber, IR beam passes through M1, M3, M4, Sample, M7, and M8.

VI—D Study of Ion-Pair Formation in the Vacuum Ultraviolet Region Using Positive Ion-Negative Ion Coincidence Spectroscopy (PINICO)

Photoexcitation of molecules to highly excited states is often accompanied by dissociation into a pair of positive and negative ions in the photon energy range of 10—50 eV. Detecting the negative ions thus formed provides a sensitive probe to investigate the properties of superexcited states lying in the vacuum ultraviolet. For full understanding of the ion-pair formation, we recently developed a novel coincidence technique, PINICO, utilizing the flight-time correlation of a pair of positive and negative ions produced by single photon excitation. This year PINICO method is applied to the studies of the ion-pair formation from N_2O^{**} and CO_2^{**} in doubly excited Rydberg states lying above 20 eV.

VI-D-1 Observation of Doubly Excited Rydberg States of N_2O by Positive Ion-Negative Ion Coincidence Spectroscopy

Hiroaki YOSHIDA and Koichiro MITSUKE

[*J. Chem. Phys.* **100**, 8817 (1994)]

Ion-pair formation processes of N_2O are studied in detail using synchrotron radiation in the 24—34 eV photon energy range. Positive ion-negative ion coincidence (PINICO) spectroscopy makes it possible to distinguish dissociation into three bodies, O^-+N^++N, from dissociation into two bodies, $O^-+N_2^+$. The photodissociation efficiency curves for the two processes are measured. The three-body dissociation is found to be dominant over the two-body dissociation above 25.3 eV. An analysis of the shape of coincidence signals shows that the three-body dissociation results from photoexcitations to superexcited states with $^1\Sigma^+$ symmetry followed by conversion to ion-pair states correlating with $O^-(^2P_u)+N^+(^3P_g)+N(^4S_u)$. The positive charge in the ion-pair states is considered to reside in the central N atom. Several resonance-like peaks observed in the efficiency curves are assigned to doubly excited Rydberg states $N_2O^{**}(^1\Sigma^+)$ lying in the energy range of 24—34 eV.

VI-D-2 Observation of Doubly Excited Rydberg States of CO_2 by Positive Ion-Negative Ion Coincidence Spectroscopy

Hiroaki YOSHIDA and Koichiro MITSUKE

Doubly excited Rydberg states of CO_2 lying in the energy range of 25—36 eV are investigated by PINICO spectroscopy. Photodissociation efficiency curves are measured for dissociation into three bodies, O^-+C^++O, and that into two bodies, O^-+CO^+. Figure 1 shows the curve for the three-body dissociation. Several resonance-like peaks in the curve are assigned to doubly excited Rydberg states $CO_2^{**}(^1\Sigma_u^+)$ converging to satellite states of CO_2^+. The shape of time-of-flight coincidence signals is interpreted in terms of the kinematics in predissociation and the angular distribution of fragment ions with respect to the electric vector direction of the incident light.

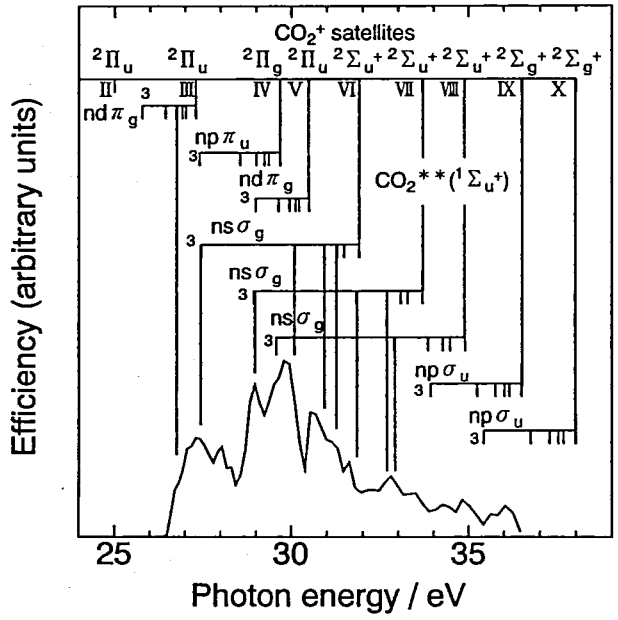

Figure 1. Photodissociation efficiency curve for the ion-pair formation $CO_2+h\nu \rightarrow O^-+C^++O$, as a function of the photon energy. Several peaks are assigned to doubly excited Rydberg states $CO_2^{**}(^1\Sigma_u^+)$ converging to satellite states of CO_2^+.

VI—E Photoionization Dynamics Studied by Electron Spectroscopy Combined with a Continuous Synchrotron Radiation Source

Molecular photoionization is a major phenomenon in vacuum UV excitation and provides a large amount of information on fundamental electron-core interactions in molecules. Especially, autoionizing and shape resonances become of main interest, since they often give rise to conspicuous behaviors in photoionization cross section, vibrational branching ratio, and photoelectron angular distributions. In order to elucidate dynamical aspects of photoionization, we have constructed a versatile machine for photoelectron spectroscopy. This year, autoionizing resonance in photoionization from the $1\pi_u$ level of acetylene is discussed in terms of strong excitation in a single vibrational mode which is by no means excited through direct ionization.

We modify the experimental setup in several points to get a higher electron count rate and better spectral resolution. Great improvement in detection efficiency has been realized by introducing a position-sensitive detector.

VI-E-1 Autoionization of an Excited Valence State of C_2H_2

Hideo HATTORI and Koichiro MITSUKE

Autoionization process of C_2H_2 is studied by photoelectron spectroscopy using synchrotron radiation in the energy region from 12.5 to 14.4 eV.

Figure 1 shows photoelectron spectra of C_2H_2 measured at several excitation energies. All features in the spectra can be assigned to vibrational states of the electronic ground state of $C_2H_2^+$. Asterisks denote peaks due to a vibrational ground state and v_2=1 and 2 states of the C-C stretching mode ν_2 (the vibrational spacing = 0.22 eV), which peaks are also observed in a HeI photoelectron spectrum. In addition, we can observe a progression with average spacings of 0.37 eV in an entire photon energy region from 12.8 to 14.1 eV. This pronounced vibrational excitation is considered to arise from autoionizing resonance which contributes to an anomalously broad maximum over the same energy region in the photoionization cross section curve of C_2H_2.[1] We assign this progression to a C-H stretching mode ν_1 by comparing average spacings between C_2H_2 and C_2D_2. Undoubtedly, autoionization occurs via a super-excited state with equilibrium C-H distances much different from those of the ground state C_2H_2 and $C_2H_2^+$. Thus, the maximum in the photoionization cross section curve is attributed to an excited valence state $3\sigma_g \rightarrow 3\sigma_u$, since this state is expected from calculation of Hayashi *et al.*[1] to lie at about 14 eV and to have longer C-H bond length. Our results indicate that C_2H_2 in this excited valence state has a lifetime long enough to change the geometry before autoionization.

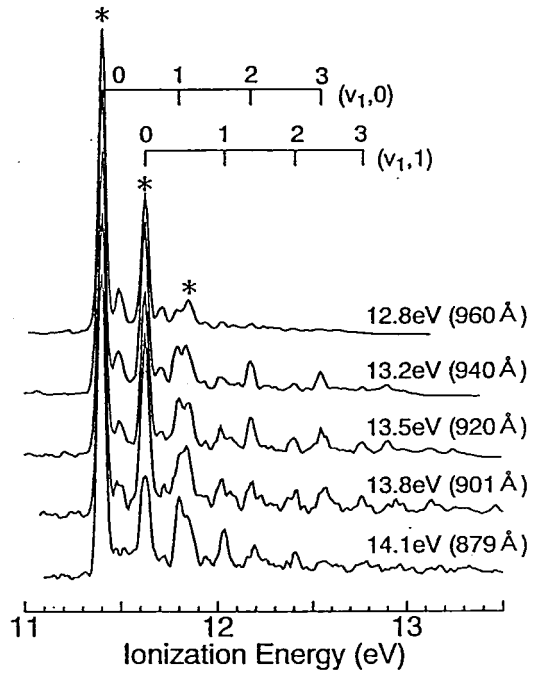

Figure 1. Photoelectron spectra of C_2H_2 at the excitation energy from 12.8 eV to 14.1 eV. Two progressions of the C-H stretching mode are observed. The (v_1,v_2) mark denotes the vibrational state in which v_1 and v_2 quanta of the C-H and C-C stretching modes, respectively, are simultaneously excited. The asterisk indicates the peaks observed by HeI photoelectron spectroscopy. The overall resolution is 60 meV (FWHM).

Reference

1) T. Hayaishi, S. Iwata, M. Sasanuma, E. Ishiguro, Y. Morioka, Y. Iida, and M. Nakamura, *J. Phys. B* **15**, 79 (1982).

VI-E-2 Development of a Position-Sensitive Detection System for Photoelectron Spectroscopy

Yasumasa HIKOSAKA*, Hideo HATTORI, Takumi HIKIDA*, and Koichiro MITSUKE *(*Tokyo Inst. of Tech.)*

A new detection system for photoelectron spectroscopy has been developed on the beamline BL3B at UVSOR. The crux of this system is a position-sensitive detector (PSD) composed of dual microchannel plates and a resistive anode encoder. We first removed an exit slit and a single channel detector from a spherical electron energy analyzer and then fitted PSD on the end of the analyzer. Great improvement in detection efficiency has been realized by this alteration as described below.

The former single channel detector collects the electrons whose kinetic energy falls within a narrow energy range determined from the size of the exit slit. In contrast, PSD can simultaneously detect all of the energy-dispersed electrons that can pass through between the two spherical sector surfaces; the range of the electron kinetic energy is

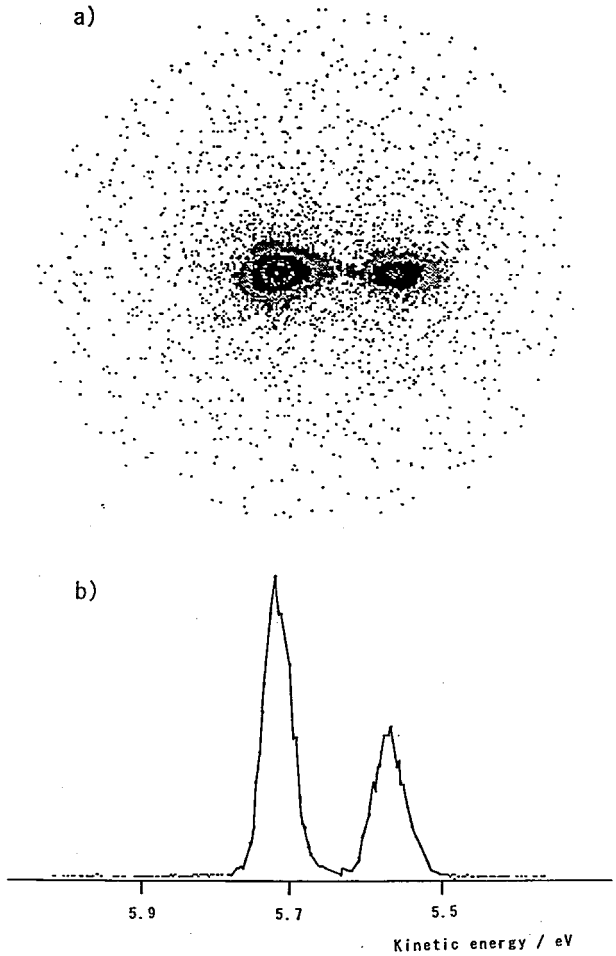

Figure 1. Photoelectron spectrum for $Ar^+(^2P_{3/2}, ^2P_{1/2})$ at the energy resolution of 40 meV FWHM. a) Image on the position-sensitive detector, and b) a one-dimensional spectrum obtained by conversion of the image data.

about 10% of a transmission energy for the analyzer. Moreover, the spatial resolution of PSD is 10 times as high as that of the single channel detector. Consequently, a photoelectron spectrum with much better resolution can be obtained in a short period by using the new detection system. At the energy resolution of 70 meV FWHM, for example, the accumulation time is reduced to 1/50 of that required in a previous measurement, as far as other conditions are the same. When the energy resolution of the incident light is set to about 28 meV, the highest overall resolution is estimated to be 30 meV. The photoelectron spectrum obtained at the resolution of 40 meV is shown in Figure 1a). The electron energy is dispersed in the horizontal direction of this image. Summing all signal counts at a given horizontal position over a range of vertical axis leads to a one-dimensional spectrum in Figure 1b). We are now studying autoionizing and shape resonances in molecular photoionization processes and the properties of involved superexcited states.

VI—F Desorption Induced by Electronic Transitions on the Solid Surface of Condensed Gases

Photon-stimulated desorption (PSD) of molecules or ions from condensed gases is a direct probe of surface reactions induced by electronic excitation of adsorbed molecules and diverse relaxation processes which subsequently occur. It is proposed by several authors that surface and bulk excitons play important roles in PSD of rare gas solids. In this study, we measure angular and kinetic energy distributions of desorbed Ne metastable atoms from a Ne surface. Using monochromatized synchrotron radiation allows us to discuss the detailed mechanism of excitation and decay of excitons.

VI-F-1 Angular and Kinetic Energy Distributions for Desorption of Neon Metastable Atoms Induced by Excitons at the Surface of Solid Neon

Daniel E. WEIBEL*, Toshiki NAGAI*, Takato HIRAYAMA*, Ichiro ARAKAWA*, Minoru KANNO, Koichiro MITSUKE, and Makoto SAKURAI** *(*Gakushuin Univ., **Kobe Univ.)*

Photon-stimulated desorption of neon metastable atoms Ne* from the surface of a solid Ne is studied using monochromatized synchrotron radiation at the beam line BL5B of UVSOR. The sample is prepared by gas deposition on a Pt(111) substrate at a temperature of 6 K. The thickness of the sample is a few hundreds atomic layers. The experiments are performed in an ultrahigh vacuum chamber with a base pressure of 1×10^{-8} Pa. Desorbed Ne* atoms are detected by a microchannel plate detector equipped with a two-dimensional position sensitive anode. Electron charge pulses from 4 corner collection electrodes of the anode are sent to a position analyzer which performs a fast computation of the incident position of Ne* using the sums and ratios of the four charges. A time-of-flight (TOF) technique is utilized to measure the kinetic energy distribution. Moreover, applying a time gate to the position analyzer enables us to obtain the angular distribution of Ne* at a specific kinetic energy.

Two mechanisms are widely accepeted for Ne* desorption induced directly by excitons: cavity ejection (CE) and excimer dissociation (ED). In a TOF spectrum, pronounced peaks at kinetic energies of ca. 0.18 and 1.4 eV are attributed to CE and ED, respectively. When the first-order surface exciton (S1) is excited at the photon energy $E_{h\nu}$ of 17.2 eV, Ne* desorption through the CE mechanism results in a very sharp angular distribution along the surface normal (see Figure 1). This distribution is found to be fitted into a function form of $(\cos\theta)^{15}$, where θ is a polar angle. This remarkable sharpness is consistent with the CE mechanism in which an excited atom is ejected by repulsion between a self-trapped exciton and surrounding atoms. On the other hand, a much broader angular distribution is obtained for Ne* desorption through the ED mechanism at $E_{h\nu}$=19.0 eV (excitation of the second-order exciton S′). This observation may be explained as that an excited dimer ejected by the CE mechanism dissociates into Ne*+Ne in vacuum rather than on the surface.

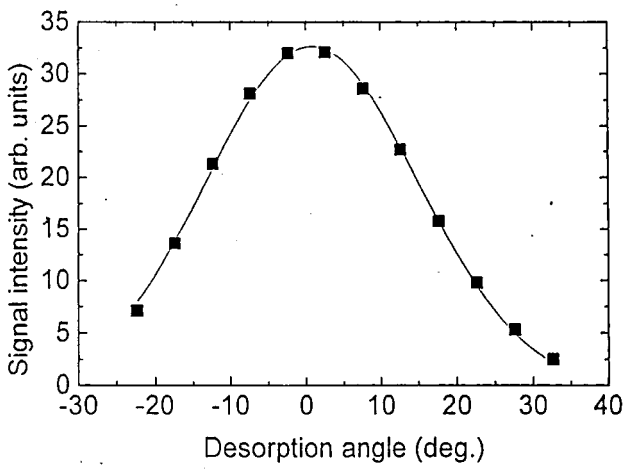

Figure 1. The angular distribution for desorption of Ne* atoms through the cavity ejection mechanism induced by the first-order surface exciton. Data points are fitted with a Lorentzian function.

VI—G Identification of Defects in SiO_2 Related Materials and Their Photoresponse

Pure and doped silica glasses are widely used as an optical material. A wide variety of defect species are formed during the preparation processes. The concentration of the defects is less than 10ppm, but they affect strongly the optoelectronic functions. In this Project, identification of the defect species, elucidation of their formation mechanism, and their optoelectronic properties are studied.

VI-G-1 Precursor to Paramagnetic Centers in Gamma-Irradiated Doped Silica Glasses

Koichi AWAZU* *(*Electrotech. Lab.)*, **Hiroshi KAWAZOE, Koushi HARADA**** *(**Tokyo Inst. Tech.)*, **Kazuhiro KIDO***** *(***Nikon Corp.)*, **and Satoru INOUE******** *(****Nat'l. Inst. Res. Inorg. Mat.)*

[*J. Appl. Phys.* **73**, 1644 (1993)]

Silica glasses having various concentrations of chlorine, fluorine, hydrogen(SiO_{2-x}), and oxygen(SiO_{2+x}) were prepared to examine the precursors of paramagnetic centers induced by γ rays. In the case of glasses sintered under chlorine and hydrogen ambients, the concentration of the E'center induced by γ-ray irradiation scaled with the partial pressure of chlorine and hydrogen. In contrast, the E'center was suppressed in glasses doped with fluorine. Stress in the glasses was also found to enhance formation of the E'center. Planar ring structures in the glass are influenced by stress and are proposed as precursors to the E'center.

VI-G-2 Formation Mechanism of Hydrogen-Associated Defect with an 11.9 mT Doublet in Electron Spin Resonance and Red Luminescence in $9SiO_2$:GeO_2 Fibers

Koichi AWAZU* *(*Electrotech. Lab.)*, **Ken-ichi MUTA**** *(**Showa Electric Wire & Cable Co.)*, **and Hiroshi KAWAZOE**

[*J. Appl. Phys.* **74**, 2237 (1993)]

The nature and the origin of the 11.9mT hyperfine doublets in electron spin resonance spectrum observed in $9SiO_2$:GeO_2 fibers were examined. When fibers were heated in hydrogen atmosphere at 100°C, the intensity of the doublet increased. When gamma-ray irradiated, the intensity drastically increased. The photoluminescence bands peaking at 1.91eV (650nm) and 1.83eV (680nm) excited with Ar ion laser operated at 488nm were also observed in the treated fibers with the doublets. The relation between the photoluminescence and the doublets was found. The intensities of the photoluminescence peaking at 1.91eV was tentatively proposed as the small silicon particles with hydrogen impurities generated in the fibers.

VI-G-3 Study of Oxygen-Deficient Centers in SiO_2 Films Using Photoluminescence Spectra

Koichi AWAZU* *(*Electrotech. Lab.)*, **Kikuo WATANABE**** *(**Hitachi Ltd.)*, **and Hiroshi KAWAZOE**

[*Jpn. J. Appl. Phys.* **32**, 2746 (1993)]

Amorphous silicon dioxide(a-SiO_2) films prepared with thermal oxidation of silicon substrates are studied using photoluminescence. Two luminescence bands at 4.2eV (290nm) and 2.14eV (582nm) are observed in a-SiO_2 film. Peak positions of both the photoluminescence bands are the same as for the $B_{2\alpha}$ band in bulk silica.

VI-G-4 Preferred Concentration Enhancement of Photobleachable Defects Responsible for 5eV Optical Absorption Band in SiO_2:GeO_2 Glass Preform by Heating in a H_2 Atmosphere

Hideo HOSONO* *(*Tokyo Inst. Tech.)*, **Hiroshi KAWAZOE, and Ken-ichi MUTA**** *(**Showa Electric Wire & Cable Co. Ltd.)*

[*Appl. Phys. Lett.* **63**, 479 (1993)]

Heat treatment of a $5GeO_2$-$95SiO_2$ glass preform in a H_2 atmosphere at 500° for 70h increased intensities of an absorption band centered at 5eV by a factor of ~3. Intensities of photobleachable component, which is the precursor of UV-induced Ge E'centers and assigned to a neutral oxygen monovacancy, of the 5-eV band were enhanced by a factor of ~8 by heating. This increment is ~3 times as large as that of UV-unbleachable component, which is assigned to Ge^{2+} centers coordinated by two oxygens (neutral oxygen divacancy).

VI-G-5 Radiation-Induced Coloring and Paramagnetic Centers in Synthetic SiO_2:Al Glasses

Hideo HOSONO* *(*Tokyo Inst. Tech.)* **and Hiroshi KAWAZOE**

[*Nucl. Instr. Meth. Phys. Res.* **B91**, 395 (1994)]

Optical absorption bands and paramagnetic centers induced with γ-rays or excimer laser light were examined in high purity synthetic SiO_2:Al glasses prepared by VAD method. Gamma-induced absorptions ranging 1.5—6.2eV were deconvoluted into 5-Gaussian components peaking at 2.3, 3.2, 4.1, 4.9 and 5.8eV. Two paramagnetic EPR centers associated with an Al ion were observed, Al-OHC and Al E'center and both centers are close to each other. These results indicate that a hole and an electron generated by irradiation are predominantly trapped at an oxygen bridging an Al and a Si and an Al coordinated with only three oxygens, respectively. A close correlation between 5-optical bands except the 5.8-eV band and Al-OHC/Al E'center was obtained. It was assigned from a consideration of the nature of these Al-related centers that a band peaking at 2.3eV-band are due to Al-OHC and Al E'centers give a band peaking at 4.1eV. Oscillator strength was evaluated to be 0.06 for the 2.3eV-band or 0.2 for the 4.1eV-band. Although no coloring and paramagnetic centers were noted for XeCl laser light (304nm), the results for ArF laser light

(193nm) were almost the same as the case of γ-irradiation. This difference suggests that a pair generation of Al-OHC and Al E'-center occurs via two photon process.

VI-G-6 Characteristics of 5-eV Absorption Band in Sputter Deposited GeO_2-SiO_2 Thin Glass Films

Junji NISHII* *(*Osaka Nat'l. Res. Inst.)*, **Hideo HOSONO**** *(**Tokyo Inst. Tech.)*, **and Hiroshi KAWAZOE**

[*Appl. Phys. Lett.* **64**, 282 (1994)]

Thin films (4.6 μm thick) of $5GeO_2$-$95SiO_2$ and $55GeO_2$-$45SiO_2$ (mol %) glasses were prepared by rf sputtering method in an Ar-O_2 atmosphere. An intense absorption band at around 5eV was distinctly observed in both films after the as-deposited films were annealed at 350° for 30min in a vacuum. A part of this 5-eV band was gradually decreased by UV irradiation. Saturated absorptivity changes ($-\Delta\alpha_\infty$) of the UV bleached component, which is considered to be the origin of Hill gratings [K.O. Hill, Y. Fujii, and B.S. Kawasaki, *Appl. Phys. Lett.* **32**, 647 (1978)] and second harmonic generation in SiO_2 glass fibers doped with GeO_2, after a prolonged irradiation were $50cm^{-1}$ for $5GeO_2$-$95SiO_2$ films and $400cm^{-1}$ for $55GeO_2$-$45SiO_2$ films. These values are greater by one or two orders of magnitude than those ($\sim 2cm^{-1}$) of bulk germanosilicate glasses prepared by the vapor axial deposition method.

VI—H Effects of Substitution of Bi with Pb in $BaBi_{1-x}Pb_xO_3$ on Crystal Structure and Conduction Behavior

$BaBi_{1-x}Pb_xO_3$ system has been known to show superconductivity in $0.65 < x < 0.9$. Crystal structures are modulated upon the substitution due to the twisting of $Bi(Pb)O_6$ octahedra. The modulation in crystal structure gives rise to a marked changes in electronic structures of the materials. In this project, effects of the substitution on the chemical state of Bi and on the electrical conduction behavior are studied.

VI-H-1 Effect of Oxygen-Deficiency on the Structure and Conduction Behavior of $BaPb_{0.75}Bi_{0.25}O_{3-\delta}$

Takuya HASHIMOTO and Hiroshi KAWAZOE

[*Solid State Commun.* **87**, 251 (1993)]

Oxygen-deficiency (δ) and its effect on the structure and electrical properties of $BaPb_{0.75}Bi_{0.25}O_{3-\delta}$ were studied. δ could be controlled from 0.00 to 0.15. It was observed that the crystal symmetry varied with increasing δ from orthorhombic ($\delta = 0.00 \pm 0.005$) through tetragonal ($\delta = 0.09 \pm 0.005$, 0.11 ± 0.005) and to cubic ($\delta = 0.15 \pm 0.005$). Electrical resistivity increased by increasing δ. The superconducting transition was observed at 13K and 10K in the specimens of $\delta = 0.00 \pm 0.005$ and $\delta = 0.09 \pm 0.005$, respectively. In the specimens of $\delta = 0.11 \pm 0.005$ and 0.15 ± 0.005, superconductivity was not observed.

VI-H-2 Effects of Substitution of Bi with Pb in $BaBi_{1-x}Pb_xO_3$ on Crystal Structure and Conduction Behavior

Takuya HASHIMOTO, Hiroshi KAWAZOE, and Harunari SHIMAMURA* *(*Tokyo Inst. Tech.)*

[*Physica* **C 223**, 131 (1994)]

The crystal structure of $BaBi_{1-x}Pb_xO_3$ was investigated by X-ray diffraction. In the range $0.0 < x < 0.5$, monoclinic symmetry containing two Bi sites was clearly observed. This suggests that Bi exhibits disproportionation to two different chemical states, 3+ and 5+, supplying no electron carrier in the range $0.0 < x < 0.5$. As x increases above 0.5, a continuous phase variation from monoclinic to orthorhombic was observed, which showed good agreement with a continuous variation of the temperature dependence of resistivity and a qualitatively similar X-ray absorption near-edge structure on composition x. This continuous effect of the substitution of Bi with Pb in $BaBi_{1-x}Pb_xO_3$ contrasted with the case of the substitution of Ba with K in $Ba_{1-x}K_xBiO_3$, which shows a distinct phase transition involving electron carrier generation at $x \sim 0.35$.

VI—I Modulation of Electronic Structure of Complex Oxides of Transition Metallic Ions with Superstructure of Perovskite by Introduction of Excess Positive Holes or Electrons

All of the first transition metallic ions constitute the identical superstructure of perovskite. Number of the filled d electrons on the respective cations changes according to a kind of the cations, and the electronic structure and electrical properties are greatly modulated on going from Sc to Cu. Some of the perovskites are known to show a metal-insulator transition. In this project, studied are changes in electronic structures and electromagnetic properties of complex oxides of the transition metallic cations upon the introduction of excess positive holes or electrons.

VI-I-1 Preparation of Oxygen Excess $SrLaFeO_{4+\delta}$ and Its Electrical and Magnetic Properties

Takahisa OMATA* *(*Tokyo Inst. Tech.)*, **Kazushige UEDA*, Naoyuki UEDA, Motomi KATADA**** *(**Tokyo Metro. Univ.)*, **Satoru FUJITSU***** *(***Shonan Inst. Tech.)*, **Takuya HASHIMOTO, and Hiroshi KAWAZOE**

[*Solid State Commun.* **88**, 807 (1993)]

Oxygen excess $SrLaFeO_{4+\delta}$ was prepared and the electrical and magnetic properties were measured. Electrical resistivities at room temperature were 3×10^3 and 5×10^1 Ω-cm for the N_2-annealed sample and the sample annealed under oxygen pressure of 20 bar, respectively. The antiferromagnetic Neel Temperature decreased from 355K for the N_2-annealed sample to 334K for the sample annealed under oxygen pressure of 20 bar. Fe Mossbauer spectra showed that iron is in the high spin and trivalent state even in the strongly oxidized $SrLaFeO_{4+\delta}$. Discussed arethe characteristics of the positive holes introduced by excess oxygens and the effects of the holes on resistivities.

VI-I-2 Electrical and Magnetic Properties of Hole-Doped $Sr_{1+x}La_{1-x}FeO_4$

Takahisa OMATA* *(*Tokyo Inst. Tech.)*, **Kazushige UEDA*, Hideo HOSONO*, Motomi KATADA**** *(**Tokyo Metro. Univ.)*, **Naoyuki UEDA, and Hiroshi KAWAZOE**

[*Phys. Rev.* **B 49**, 10194 (1994)]

Hole-doped $Sr_{1+x}La_{1-x}FeO_4$ ($0<x<0.3$) samples were prepared, and electrical transport, magnetic properties and ^{57}Fe Mossbauer spectra of the resulting materials were measured. The results were compared with those of hole-doped charge-transfer (CT) insulators. The antiferromagnetic Neel temperature decreased from ~350 to ~150K on going from $x=0.3$, and dc electrical resisitivity at room temperature decreased from $\sim 10^3$ Ωcm for $x=0$ to $\sim 10^0$ Ωcm for $x=0.3$. The heavily doped samples showed semiconducting behavior even for $x = 0.3$. Seebeck voltage measurements demonstrated that all the samples were p-type semiconductors. Although the changes in the magnetic properties upon doping were qualitatively similar to the CT insulators such as $(La,Sr)_2CuO_4$ and $(La,Sr)_2NiO_4$, the changes in the electrical-transport properties upon doping differed from those in the CT insulators. The origin of these differences is discussed with reference to the changes in the electronic structure upon doping.

VI-I-3 Electronic Structure of Hole-Doped $Sr_{1+x}La_{1-x}FeO_4$ Studied by UPS and XAS

Takahisa OMATA* *(*Tokyo Inst. Tech.)*, **Kazushige UEDA*, Hideo HOSONO*, Takafumi MIYAZAKI, Shinji HASEGAWA, Naoyuki UEDA, and Hiroshi KAWAZOE**

[*Phys. Rev.* **B 49**, 10200 (1994)]

The electronic structure of K_2NiF_4-type $Sr_{1+x}La_{1-x}FeO_4$ compounds ($0<x<0.3$) was studied by ultraviolet-photoemission and X-ray absorption spectroscopies. Resonant photoemission measurements demonstrated that although the satellite feature of $Sr_{1-x}La_{1-x}FeO_4$ was attributed to d^4 final states, the whole valence band was constructed from well mixed Fe 3d and O 2p states. It was suggested that the parent $Sr_{1+x}La_{1-x}FeO_4$ compound is intermediate between Mott-Hubbard and charge-transfer insulators. O K-edge and Fe K-edge X-ray-absorption measurements showed that hole bands composed of O 2p and Fe 3d character were formed in the original conduction-band edge upon hole doping, while the valence-band structure obtained by nonresonant photoemission measurements did not change. Changes in the electrical and magnetic properties were correlated with those in electronic structure.

VI—J Electronic Structure Design of Wide Gap Conductors and Control of Their Conduction Behavior

Wide gap conductors are interesting materials from scientific viewpoint: the conductivity of the material reaches $1\times10_4$ $S \cdot cm^{-1}$ irrespective of their wide band gap (>3.1eV). These are also technologically important as transparent electrodes, gas sensors and semiconductor-catalysts. In the present study it is aimed to give a firm basis of the materials design of wide gap conductors. The ongoing study includes proposition of a working hypothesis for searching new materials, preparation of materials, estimation of physical properties, characterization of electronic structures by spectroscopic methods using synchrotron radiation and energy band calculations.

VI-J-1 New Oxide Phase $Cd_{2(1-x)}Y_{2x}Sb_2O_7$ Pyrochlore with a Wide Band Gap and High Electrical Conductivity

Kazuhiko YANAGAWA* *(*Waseda Univ.)*, **Yoshimichi OHKI*, Takahisa OMATA**** *(**Tokyo Inst. Tech.)*, **Hideo HOSONO**, Naoyuki UEDA, and Hiroshi KAWAZOE**

[*Jpn. J. Appl. Phys.* **33**, L238 (1994)]

It was found for the first time that the electrical conductivity of Y-substituted $Cd_2Sb_2O_7$, $Cd_{2(1-x)}Y_{2x}Sb_2O_7$, with the pyrochlore structure, is larger than at least $3.3\times10^0 Scm^{-1}$ and the optical band gap of the sample is wider than 3.5eV. These values indicate that $Cd_{2(1-x)}Y_{2x}Sb_2O_7$ pyrochlore has a characteristic of a transparent conductor.

VI-J-2 New Oxide Phase $Cd_{1-x}Y_2Sb_2O_6$ with a Wide Band Gap and High Electrical Conductivity

Kazuhiko YANAGAWA* *(*Waseda Univ.)*, **Yoshimichi OHKI*, Naoyuki UEDA, Takahisa OMATA**** *(**Tokyo Inst. Tech.)*, **Takuya HASHIMOTO, and Hiroshi KAWAZOE**

[*Appl. Phys. Lett.* **63**, 3335 (1993)]

It was initially found that $CdSb_2O_6$, in which a small part of the Cd ions was substituted with Y ions, has characteristics of a transparent conductor. The electrical conductivity

at room temperature of the Y-substituted $CdSb_2O_6$ ceramic was larger, by at least $1\times10^0 Scm^{-1}$, while that of the non-substituted $CdSb_2O_6$ was smaller than $10^{-5}Scm^{-1}$. The optical band gap of $CdSb_2O_6$ was found to be larger than 4.1eV by the measurements of diffuse reflectance spectra.

VI-J-3 New Ultraviolet-Transport Electroconductive Oxide, $ZnGa_2O_4$ Spinel

Takahisa OMATA* *(*Tokyo Inst. Tech.)*, **Naoyuki UEDA, Kazushige UEDA*, and Hiroshi KAWAZOE**

[*Appl. Phys. Lett.* **64**, 1077 (1994)]

$ZnGa_2O_4$ having the spinel structure was prepared, and optical and electrical properties of the material were measured. By the measurements of diffuse reflectance spectra, $ZnGa_2O_4$ was found to have a wider band gap (~ 5eV) than ITO (indium tin oxide). Electrical conductivity of the H_2-annealed ceramic of $ZnGa_2O_4$ was $3\times10^1 Scm^{-1}$. Thus the $ZnGa_2O_4$ spinel was found to be a new UV-transparent electronic conductor.

VI-J-4 Preparation of $Cd_{1-x}Y_xSb_2O_6$ Thin Film of Glass Substrate by Radio Frequency Sputtering

Kazuhiko YANAGAWA* *(*Waseda Univ.)*, **Yoshimichi OHKI*, Takahisa OMATA**** *(**Tokyo Inst. Tech.)*, **Hideo HOSONO****, **Naoyuki UEDA, and Hiroshi KAWAZOE**

[*Appl. Phys. Lett.* **65**, 406 (1994)]

$Cd_{1-x}Y_xSb_2O_6$ thin films were deposited onto a silica glass substrate by rf sputtering method. The highest conductivity observed for $Cd_{0.95}Y_{0.05}Sb_2O_6$ thin films was $4.1\times10 Scm^{-1}$, with a carrier concentration of $1.3\times10^{20}\,cm^{-3}$ and a Hall mobility of $1.9\,cm^2V^{-1}S^{-1}$. No distinct optical absorption band was observed from the visible to the infrared region. These observations show that $Cd_{1-x}Y_xSb_2O_6$ thin films have characteristics of a transparent conductor, whose transparent wavelength region covers the near infrared.

VI—K Growth and Characterization of II-VI Compound Semiconductor Thin Film Using Metalorganic Sources

Epitaxial growth at low temperature is essential to control the electrical and optical properties of the layer in the fields of II-VI materials. We believe that photon-assisted growth using metalorganic sources is useful as a low temperature growth technique of these materials. Especially, we consider that a use of synchrotron radiation as a light source for the growth is valuable for the low temperature growth. We have investigated the growth characteristics and the characterization of the grown layer in order to clarify the growth process in the photon-assisted growth.

VI-K-1 Growth of Low-Resistivity n-Type ZnTe by Metalorganic Vapor Phase Epitaxity

Hiroshi OGAWA*, Syed Irfan GHEYAS*, Hitoshi NAKAYAMA*, Mitsuhiro NISHIO, and Akira YOSHIDA** *(*Saga University, **Toyahashi Univ. of Tech.)*

[*Jpn. J. Appl. Phys.* **33**, L980 (1994)]

Doping of ZnTe has been carried out by metalorganic vapor phase epitaxity using triethylaluminum as the dopant source. N-type ZnTe layers with a carrier concentration of $(1-4)\times10^{17}cm^{-3}$ and a resistivity as low as 0.1—0.3 Ωcm have been obtained. It has been indicated by the photoluminescence measurement that Al is incorporated effectively into the epitaxial layer.

VI-K-2 Low Temperature Growth of ZnTe by Synchrotron Radiation Using Metalorganic Sources

Makoto IKEJIRI*, Toshihiro OGATA*, Hiroshi OGAWA*, Mitsuhiro NISHIO, and Akira YOSHIDA**
*(*Saga University, **Toyahashi Univ. of Tech.)*

[*J. Vac. Sci. & Technol.* **A12**, 278 (1994)]

The use of synchrotron radiation to convert diethylzinc and diethyltelluride molecules into ZnTe has been employed for ZnTe growth. The formation of ZnTe epitaxial layer on (100) oriented GaAs substrate at room temperature is experimentally demonstrated. It is shown by x-ray photoelectron spectroscopy that no carbon is included in the film.

VI-K-3 Photoluminescence Properties of ZnTe Layers Grown by Photo-assisted Metalorganic Vapor Phase Epitaxy

Syed Irfan GHEYAS*, Makoto IKEJIRI*, Toshihiro OGATA*, Hiroshi OGAWA*, and Mitsuhiro NISHIO
*(*Saga University)*

[*J. Crystal Growth*, in press]

Previous studies on metalorganic vapor phase epitaxy have already demonstrated that lowering the growth temperature unilaterally without facilitating the efficient pyrolysis of source materials only deteriorates the crystal quality and enhances residual impurity inclusion. Photo-assisted metalorganic vapor phase epitaxy allows smoother decomposition of the precursor sources at a relatively low temperature. It is thus expected that this growth procedure has a large effect on the crystalline quality of the epitaxial layers. In this study, effects of light illumination on the photoluminescence properties of ZnTe has been investigated by using epitaxial layers grown with different carrier gases, transport rate of source materials and light sources or by introducing triethyaluminum as a dopant. Free exciton emission can be observed in only the epitaxial layers grown with illumination under H_2 atmosphere, implying that the illumination is effective for the growth of good quality

ZnTe layers. The illumination strengthens the transition due to exciton bound to donor impurities, namely Cl which is substituted into Te lattice site, at low temperature. These effects are closely related to the use of photons having an energy higher than the bandgap of ZnTe. It seems that the photo-assisted metalorganic vapor phase epitaxy technique also brings about the effective formation of Al donor by suppressing the generation of the complex of Al and Zn-vacancy in the ZnTe epitaxial layer.

VI-K-4 Synchrotron Radiation Excited Growth of ZnTe Using Metalorganic Sources

Toshihiro OGATA*, Syed Irfan GHEYAS*, Makoto IKEJIRI*, Hiroshi OGAWA*, and Mitsuhiro NISHIO
*(*Saga University)*

[*J. Crystal Growth*, in press]

Photons contained in the synchrotron radiation beam have enough energy for the excitation of virtually any metalorganic molecules to valence or even core electronic excitation level. Furthermore, the photon irradiation is expected to enhance the surface migration of adsorbed species and lead to epitaxial growth at low temperature. In this study, the photon-excited growth of ZnTe on the (100) GaAs substrate has been studied at very low pressure of $\sim 10^{-5}$Torr using synchrotron radiation as a light source. Diethylzinc and diethyltelluride were used as source materials, while hydrogen was employed as a carrier gas. The epitaxial layer of ZnTe can be obtained even at room temperature. It is expected that the surface excitation plays an important role in the growth, whereas thermal or gas phase excitation does not contribute. The quantum yield for forming ZnTe molecules by photons is estimated to be higher than 0.7%.

VI-K-5 Construction of the System for a Novel Low-temperature Growth of II-VI Compound Semiconductors Using Synchrotron Radiation

Toshihiro OGATA*, Makoto IKEJIRI*, Syed Irfan GHEYAS*, Hiroshi OGAWA*, and Mitsuhiro NISHIO
*(*Saga University)*

[*Rev. Sci. Instrum.*, in press]

We have demonstrated for the first time the possibility of achieving epitaxial growth of ZnTe even at room temperature using metalorganic reagents. There have been only a few reports on the synchrotron radiation excited growth using metalorganic sources. Thus, it is very valuable to design and build the growth system that allows the systematic investigation of the synchrotron radiation excited growth using metalorganic sources. As a novel application of synchrotron radiation, in this study, we investigate a growth technique for the II-VI compound semiconductors. The growth system suitable for synchrotron radiation excited deposition has been designed and constructed in the beam line, BL4A, at the UVSOR facility. It has been confirmed by using the constructed growth system that this method is useful as a low-temperature growth technique of II-VI compounds.

RESEARCH ACTIVITIES VII
Coordination Chemistry Laboratories

Prof. Yutaka Fukuda and Prof. Kiyoshi Sawada and Drs. Hikaru Ichida and Keiichi Sato finished their term in March 1994 in the Laboratory of Synthetic Coordination Chemistry and returned to Ochanomizu Women's University, Niigata University, University of Tokyo, and Niigata University respectively. Their effort during their term is gratefully acknowledged. Prof. Yuzo Yoshikawa and Prof. Hiroshi Nakazawa and Drs. Yasushige Kuroda and Tamotsu Mizuta took the position of Synthetic Coordination Chemistry from April 1994. Prof. Kazuko Matsumoto and Prof. Akira Nagasawa continued their position as Adjunct Prof. of the Laboratory of Coordination Bond. Prof. Yutaka Fukuda and Prof. Jun-ichiro Setsune took the position of Adjunct Prof. of the Laboratory of Complex Catalysis from April 1994.

VII—A Stereochemistry of Coordination Compounds and Adsorption Phenomena of Various Gases on Inorganic Solids

VII-A-1 Stereochemistry of Six-coordinated Silicon Complexes

Yasuharu OHMORI, Yasushige KURODA, Masaaki KOJIMA*, Hong Ling LIU, Motoyuki TASAKA, and Yuzo YOSHIKAWA *(*Okayama Univ.)*

Six-coordinated complexes of silicon(IV) are not very familiar as compared to four-coordinated tetrahedral compounds, a huge amount of which have been already synthesized and investigated in inorganic-, organic-, and industrial-chemistry fields.

We reported the complete optical resolution of $[Si(phen)_3]^{4+}$. The optical resolution of $[Si(bpy)_3]^{4+}$ is currently in progress in our laboratory.

The resolution of $[Si(phen)_3]^{4+}$ was performed by a chromatographic method using an SP-Sephadex C-25 column. Each enantiomer is so stable in an aqueous solution that the absorption spectrum and optical rotation were unchanged after a month at room temperature. This is the first example of stable (in water) enantiomers of six-coordinated octahedral silicon(IV) complexes. The circular dichroism (CD) spectra were measured. According to exciton theory, the absolute configuration of the faster-moving $(+)_{589}$ isomer can be assigned to Λ. Though we have already attempted the resolution of $[Si(bpy)_3]^{4+}$ by a chromatographic method, the effective resolution was not attained under the same conditions.

The elution order (Λ moves faster than Δ) of the enantiomers for both the bpy and phen complexes is the same as that observed for the corresponding cobalt(III) complexes.

In general, the chromatographic elution of ionic species largely depends on the degree of electric neutralization, such as the formation of ion pairs. In the present case, it is considered that the formation of the higher ion pairs may play a dominant role in the electric neutralization. Now we are carrying out the force-field calculation of these ion-pair systems in order to elucidate the chromatographic elution mechanism.

This section will be developed to syntheses and stereochemistry of higher-coordinated (5 and/or 6) silicon compounds.

VII-A-2 Force Field Calculation of Metal Complex Systems Including Antitumor Platinum(II) Complexes

Toshihito YOSHII*, Masaaki KOJIMA*, Koji YUTO, Yuri MIZUNO, and Yuzo YOSHIKAWA *(*Okayama Univ.)*

Strain-energy minimization of adducts of the platinum(II) complexes containing 1,2-cyclohexanediamine (DACH) with the sequence d(pCpGpAp) · d(pGpCpTp) of a synthetic B-DNA were carried out by using a modification of the MM2 program. (C,G,A,T, and p denote cytidine, guanosine, adenosine, thymidine, and phosphate, respectively.) In result, the *trans*-DACH complex adducts are about 8 kcal/mol more stable than the *cis* one in their total energies.

Platinum complex adducts of 2-(aminomethyl)cyclohexylamine abbreviated as AMCHA were also estimated. In calculations, their *trans*-AMCHA complex adducts are about 3 to 6 kcal/mol more stable than the *cis* ones. The differences are less than that between the DACH ones. In addition, this relaxation of strain was made by the six-membered ring in view of strain energies.

This strain-energy minimization technique will be developed to a series of propeller-type complexes (*trans*-dihalogenotetrakis(substituted pyridine)metal(III) ion), photochemical products of tris(L-cysteinesulfinato)cobaltate(III) ion, and dinuclear chromium(III) complexes containing amino acids.

VII-A-3 Steric Effect of Phenyl Substituents of Redox Potentials of Cobalt(II) Schiff Base Complexes

Masakazu HIROTSU, Kiyohiko NAKAJIMA, Masaaki KOJIMA*, Setsuo KASHINO*, and Yuzo YOSHIKAWA** *(*Okayama Univ., **Aichi Univ. of Educ.)*

Cobalt(II) complexes containing tetradentate Schiff base ligands with phenyl substituents were prepared, and the steric effect of the phenyl substituents on the redox potentials was studied. The structure of [Co{7-Phsal-(rac)-stien}] ($H_2$7-Phsal-(rac)-stien was derived from 2-hydroxybenzophenone and *rac*-1,2-diphenylethylenedimine) was determined by the X-ray method to show that the phenyl groups

in the N-N chelate moiety are in axial positions. The redox potential of the cobalt(II/III) couple in CH_3CN for the complex is changed to a more positive value by *ca.* 300 mV than that for [Co(salen)]. The shift is ascribed to the steric effect of the axial phenyl groups.

VII-A-4 Dielectric Behaviors in the Inorganic Solid-H_2O Systems

Yasushige KURODA, Daisuke KATAOKA, Yuzo YOSHIKAWA, Setsuo MORIMOTO, and Mahiko NAGAO*** *(*Okayama Univ., **Okayama Univ. Science)*

Dielectric properties, permittivities, and losses, of the SrF_2-H_2O system in which the two dimensional condensation of water occurs were investigated as a function of surface coverage at 298, 273, and 230 K and in the frequency range from 0.1 Hz to 5 MHz. In this system large dielectric dispersions were observed at 298 K, near 0.3 and 15 Hz and in the coverages of 0.13 and 1.26, respectively. Some experiments were planned to elucidate these relaxations. As a result, it is concluded from a heterogeneity of the system, *i.e.*, Maxwell-Wagner type, and not to the orientational polarization of the adsorbed water, namely Debye type. The former polarization is explained by the two-layer model based on the difference in conductances between the electrode-particle and the particle-particle. The conductance varies with the amounts of adsorbed water, and the mechanism of conduction in the adsorbed layer is interpreted in terms of Grotthus' mechanism for the adsorbed water. Moreover, it is found that the two-dimensionally condensed water causes a small change in the conductance. The adsorbed state of water on the SrF_2 surface is discussed on the basis of experimental data.

Similar measurements were also performed at low temperatures (77 to 298 K). The analysis of the dielectric loss curves suggests that the rotation of the water molecules condensed two-dimensionally is expected to be more hindered than that of bulk ligand water, though not so much as in ice.

Such dielectric behavior is also observed in the Cu_2O-H_2O and Ag_2O-H_2O systems.

VII-A-5 Specific Feature of Copper-Ion-Exchanged Mordenite for Dinitrogen Adsorption at Room Temperature

Yasushige KURODA, Yuzo YOSHIKAWA, Shin-ichi KONNO*, Hideaki HAMANO*, Hironobu MAEDA*, Ryotaro KUMASHIRO*, and Mahiko NAGAO* *(*Okayama Univ.)*

Adsorption properties of copper-ion-exchanged mordenite (CuM) for dinitrogen molecules (N_2) were examined at 298 K. The intensive IR absorption band observed at 2299 cm^{-1} was attributed to the N_2 species strongly adsorbed on CuM. The interaction of N_2 with CuM is explored using adsorption calorimetry, X-ray absorption fine structure (XAFS), and photoemission spectroscopy. The differential heat and entropy of adsorption for N_2 on CuM were 60 $kJmol^{-1}$ and 60 $JK^{-1}mol^{-1}$ at the initial stage of adsorption, respectively, and those for N_2 on NaM (non-copper-mordenite) gave the values of 32 $kJmol^{-1}$ and 130 JK^{-1} mol^{-1}, which revealed that the N_2 molecules interact strongly with CuM to rest in the localized state. The monolayer capacity is estimated to be 4.12 cm^3g^{-1} for N_2 on CuM-150 that gives a value of 0.22 for the N_2/Cu ratio. XAFS and emission data for CuM degassed at 873 K exhibit a couple of bands at 8.983 and 8.994 keV, and 18700 and 20800 cm^{-1}, respectively. The former bands are assigned to the $1s$-$4p$ transition and the latter bands to the $3d^94s^1$-$3d^{10}$ transition. These spectral data are reasonably explained by assuming the presence of Cu(I) species in mordenite. It is proved from the emission data that the adsorption site including Cu(I) species easily formed by heat treatment at 873 K *in vacuo* is effective for N_2 adsorption. Such easy conversion of Cu(II) to Cu(I) may be due to the spatial distribution of ion-exchanged sites on mordenite. The appearance of IR and at 2299 cm^{-1} is due to the adsorption of N_2 on the Cu(I) species and to the induction of a transition moment by the strong field of this site. Although a rather high value of heat of adsorption might suggest a chemisorption, it is made plausible that this type of N_2 adsorption is physisorption.

VII—B Creation of Complexes Containing New Types of Bonds between a Transition Metal and a Phosphorus

The most typical bond fashion between a transition metal and a phosphorus is a dative bond, where the lone-pair electrons on a phosphorus atom are donated to a vacant d orbital of a transition metal. We focus on rather new types of bond fashion between a transition metal and a phosphorus, such as a covalent bond, a multiple bond, and a hypervalent bond. New preparative methods of complexes containing such bonds have been developed and the reactivities of these complexes have been examined.

VII-B-1 Reaction of Iron Phosphonate Complexes Containing a Covalent Bond between Iron and Phosphorus and Their Reactivity

Hiroshi NAKAZAWA and Katsuhiko MIYOSHI* *(*Hiroshima University)*

[*Council Sci. Inform.*, in press (1994)]

Reaction of iron and ruthenium chloride complexes with amino-substituted phosphites are described. $Cp(CO)_2MCl$ ($Cp=\eta^5$-C_5H_5; M=Fe, Ru) reacts with a series of $P(NR_2)_n(OR)_{3-n}$ in benzene at room temperature to give $[Cp(CO)_2M\{P(NR_2)_n(OR)_{3-n}\}]Cl$, which is converted into $Cp(CO)_2M\{P(O)(NR_2)_n(OR)_{2-n}\}$ by a thermal reaction. The isolation of the cationic complexes corresponding to the intermediate in the ionic mechanism of the Arbuzov-like dealkylation reaction is achieved by introduction of amino

group(s) on a phosphorus atom. A comparison of spectroscopic data reveals that $Ru^{\delta+}$-$P^{\delta-}$ polarization is greater than $Fe^{\delta+}$-$P^{\delta-}$ polarization for both M-P(phosphite) and M-P(phosphonate) bonds.

Reaction of $[CpL_2Fe\{P(NC_4H_8)_n(OMe)_{3-n}\}]^+$ with KOH gives a phosphonate complex, $CpL_2Fe\{P(O)(NC_4H_8)_{n-1}(OMe)_{3-n}\}$, with selective deamination. The mechanism proposed is that an OH^- nucleophilically attacks the phosphite phosphorus to form a metallaphosphorane complex, followed by the formation of a phosphoryl group with releasing an amino group.

Electronic and steric effect on the Arbuzov-like dealkylation reaction is discussed. Reactivity of iron phosphonate complexes is also described.

VII-B-2 Migratory Insertion of Phosphorus Ligand into a Transition Metal-Alkyl Bond

Hiroshi NAKAZAWA, Yoshitaka YAMAGUCHI, Tsutomu MIZUTA, Satoshi ICHIMURA*, and Katsuhiko MIYOSHI* *(*Hiroshima University)*

Treatment of $Cp(CO)(R^1)Fe\{PN(Me)CH_2CH_2NMe(OR^2)\}$ (R^1=Me, CH_2Ph; R^2=Me, Et) with $BF_3 \cdot OEt_2$ and then PPh_3 yields $[Cp(CO)(PPh_3)Fe\{PN(Me)CH_2CH_2NMe(R^1)\}]^+$. The reaction proceeds via the formation of cationic phosphenium complex $[Cp(CO)(R^1)Fe\{PN(Me)CH_2CH_2NMe\}]^+$, then a migratory insertion of the phosphenium ligand into the iron-alkyl bond. The reaction of $Cp(CO)(CH_2OMe)Fe\{PN(Me)CH_2CH_2NMe(OR)\}$ (R= Me, Et) with $BF_3 \cdot OEt_2$ proves that the OMe on the CH_2OMe ligand is selectively abstracted to give the methylidene complex. The complex is trapped with PPh_3 to give a phosphine ylide complex $[Cp(CO)(CH_2PPh_3)Fe\{PN(Me)CH_2CH_2NMe(OR)\}]^+$ which is characterized by X-ray analysis.

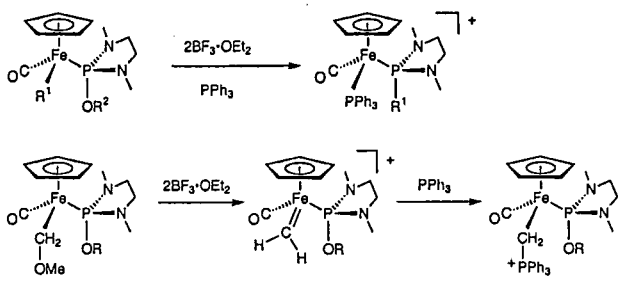

VII-B-3 Reactivity of Cationic Phosphenium Complexes toward Trivalent Phosphorus Compounds (L). Formation of $[(bpy)(CO)_2M(phosphenium)L]^+$ (M=Cr, Mo, W) by the CO/L Exchange Reaction, the Geometrical Isomerization, and the X-ray Structure Analyses

Hiroshi NAKAZAWA, Yoshitaka YAMAGUCHI, Tsutomu MIZUTA, and Katsuhiko MIYOSHI* *(*Hiroshima University)*

Cationic phosphenium complexes of group 6 transition metals (**1**) react with trivalent phosphorus compounds (L), such as diamino-substituted phosphite ($PN(Me)CH_2CH_2NMe(OR)$) or phosphine (PPh_3) to afford two geometrical isomers **2** and **3**. The cis isomer (**2**) is an electronically stable complex and the trans isomer (**3**) is a sterically stable complex. The X-ray analysis of trans-$[(bpy)(CO)_2\{PN(Me)CH_2CH_2NMe(OMe)\}Mo\{PN(Me)CH_2CH_2NMe\}] \cdot OTf$ showed the existence of double bond character between Mo and the phosphenium phosphorus.

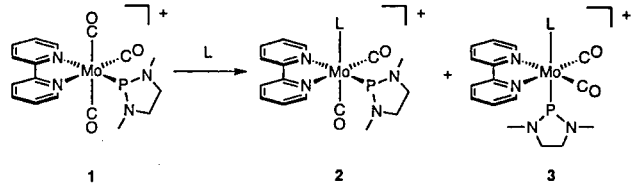

VII-B-4 A Valence Expansion Reaction on a Trivalent Phosphorus Atom in Iron Complexes

Hiroshi NAKAZAWA, Kazuyuki KUBO*, and Katsuhiko MIYOSHI* *(*Hiroshima University)*

A novel synthetic route for metallaphosphoranes was developed; $[Cp(CO)_2Fe\{P(OPh)_3\}]PF_6$ was allowed to react with $Li(o\text{-}OC_6H_4NH_2)$ to give $Cp(CO)_2FeP(OC_6H_4NH)_2\}$ in good yield (69%). This reaction involves nucleophilic attack of ^-OR and NH_2R groups in $Li(o\text{-}OC_6H_4NH_2)$ on the phosphorus atom followed by release of ^-OPh groups. Some other ironphosphoranes are prepared in the similar manner. Berry pseudorotation around the metallaphosphorane phosphorus is discussed.

VII-B-5 Migration Reaction of a Transition-metal Fragment from a Transition Metal Having a Cp Ring to the Cp Ring

Hiroshi NAKAZAWA, Michiyo KOKKA, and Katsuhiko MIYOSHI* *(*Hiroshima University)*

Treatment of dinuclear transition-metal complexes $[Cp_2M_2(CO)_{2n}]$(M=Fe, Ru, n=2; M=Mo, W, n=3) with $LiN(i\text{-}Pr)_2$ and then MeI in THF afforded (η^5-$C_5H_4\{M(CO)_nCp\}M(CO)_nMe$. The reaction indicates that an $M(CO)_nCp$ fragment migrates from a transition metal to the Cp ring on the metal. The migration reaction was observed not only for homodinuclear complexes but also for heterodinuclear complexes; $[Cp(CO)Fe(\mu\text{-}CO)_2Ru(CO)Cp]$, $[Cp(CO)_2Fe\text{-}Mo(CO)_3Cp]$, and $[Cp(CO)_nMMn(CO)_5]$ (M=Fe, n=2; M=Mo, W, n=3). For $Cp(CO)_2Fe\text{-}Mo(CO)_3Cp$, the selective migration of the $Mo(CO)_3Cp$ fragment was observed.

VII-B-6 Synthesis and Stereochemistry of Transition-metal Complexes with Tetraphosphamacrocycle

Tsutomu MIZUTA, Tsutomu SASAKI*, Tomoaki YAMASAKI, Hiroshi NAKAZAWA, and Katsuhiko MIYOSHI* *(*Hiroshima University)*

The chemistry of transition-metal complexes with

phosphamacrocycle still remains to be exploited compared with that of azamacrocycle metal complexes. We recently secceeded to obtain the complex **1** where R=Me, Et, and M=Ni, Pd, Pt, in the reaction of $[M(PHR\text{-}PHR)_2]^{2+}$(PHR-PHR=1,2-bis(alkylphosphino)ethane) with 1,3-dibromopropane in the presence of weak base, K_2HPO_4. The employment of the transition-metal template reaction resulted in the selective formation of 2 isomers out of 5 diastereomers. The isomers thus obtained were estimated to have cis (**2**) and trans (**3**) geometry.

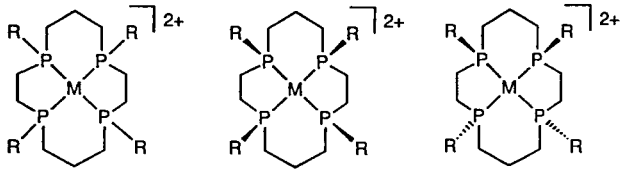

1 **2** **3**

VII—C Structures and Thermodynamics of Ionic and Molecular Ensembles in Solution

The interaction of ion-ion and ion-molecule in solution has been studied for various kinds of systems of complex formation and solvents. The weak interactions such as ion-pair, intermolecular, and solvation, play an important role to determine the general feature of thermodynamics and structures of complexes in solution. The studies of transfer phenomena between two phases are also important to understand the reactions in homogeneous solution.

VII-C-1 Crystal and Molecular Structures of Pyridine Base Complexes of Cadmium(II) Chloride

Keiichi SATOH, Toshio SUZUKI*, and Kiyoshi SAWADA *(*Niigata Univ.)*

[*Inorg. Chim. Acta*, in press]

Crystal and molecular structures of dichlorobis(pyridine)cadmium(II) (**1**), dichlorobis(3-methylpyridine)cadmium(II) (**2**), dichlorobis(4-methylpyridine)cadmium(II) (**3**) , and dichloromono(4-methylpyridine)cadmium(II) (**4**) were determined by means of single-crystal X-ray diffraction method. All crystal were monoclinic. Cadmium atoms of **1**, **2**, and **3** are octahedrally coordinated with four chloride ions in di-μ-chloro polymeric linear chain and two nitrogen atoms of pyridine base in trans configuration. In **4** cadmium atom is coordinated with five chloride ions in which four chloride ions form di-μ-chloro polymeric chain and one belongs another polymeric chain and with one nitrogen atom of 4-methylpyridine. The crystal structures indicate the absence of peculiar interaction between polymeric chains such as hydrogen bond.

VII-C-2 Preconcentration of Cadmium by Column Extraction with Trioctylmethylammonium Chloride and Determination by Graphite Furnace Atomic Absorption Spectroscopy

Kiyoshi SAWADA, Satoshi OHGAKE*, Michiko KOBAYASHI,* and Toshio SUZUKI* *(*Niigata Univ.)*

[*Bunseki Kagaku*, **42**, 741 (1993)]

The solvent-extraction system of cadmium with trioctylmethylammonium chloride (TOMA · Cl) from a chloride solution was applied to the column-extraction preconcentration of cadmium. After elution from the column, the cadmium ion was determined by atomic absorption spectroscopy. The optimum conditions for column extraction were investigated.

One percent of a TOMA · Cl xylene solution was supported on an inorganic resin, the surface of which was coated by lipophilic silicone. The cadmium ion was collected on the resin supporting the organic phase from sea water, or a 0.5 M NaCl solution acidified by 0.1 M HCl. The cadmium ion was quantitatively collected on one gram of resin from 200 ml of sample solution at a flow rate of 6 ml min^{-1}. Most of the diverse ions were separated by this procedure. The loaded cadmium ion was eluted by 1 ml of 0.1 M $HClO_4$. The concentration of cadmium was determined by graphite furnace atomic absorption spectroscopy. A two-hundred-fold concentration of cadmium and separation from diverse ions were achieved much more conveniently compared with batch extraction or by using a chelating resin column. The detection limit of cadmium was obtained as 5 ppt. The method was applied to sea-water samples.

VII-C-3 Hydration of Poly(oxyethylene) Derivative Complexes of Alkali Metal Ions and Barium Ion in 1,2-Dichloroethane

Yoichi KIKUCHI,* Mitsuru KUBOTA, Toshio SUZUKI,** and Kiyoshi SAWADA** *(*Iwate Univ., **Niigata Univ.)*

[*Bull. Chem. Soc. Jpn*, in press]

The water molecules were coextracted into 1,2-dichloroethane (1,2-DCE) with the ion pairs of various poly(oxyethylene) derivative (POE compound) complexes of alkali metal ions and barium ion with picrate ion. The mean number of water attached to POE compounds, $X_{H2O,S}$, and its complex, $X_{H2O,comp}$, in water saturated 1,2-DCE was determined by means of aquametry. The value of $X_{H2O,S}$ increases with the increase in the number of the oxyethylene unit (EO unit) of the POE compound. The value of $X_{H2O,comp}$, decreases in the order $Li^+ > Na^+ > K^+ = Rb^+ = Cs^+$ in any POE compound systems, and increases with the increase in the number of EO units of the POE compounds for a given metal ion. The water molecules attached to the complex are interpreted by the hydration of the central metal ion, and the hydrated metal ion is surrounded by the EO chain in the complex. The large

number of water molecules are coordinating to the lithium ion complexes and bring about a serious distortion in the structure.

VII-C-4 Thermal Stability of Substituted Pyridine Complexes of Cadmium Chloride

Kiyoshi SAWADA, Keiichi SATOH, Yoshio MASUDA*, Yasuhiro SHIRAKURA*, and Toshio SUZUKI*
*(*Niigata Univ.)*

The heats of decomposition, ΔH_{dec} of a series of pyridine base (R-py) complexes of cadmium chloride were determined by means of differential scanning calorimetry, where the complexes were bis(pyridine base) complexes, $CdCl_2(R\text{-}py)_2$, for pyridine and 4-methyl-, 3-methyl-, 4-acetyl- and 4-cyano-pyridines and mono(pyridine base) complexes, $CdCl_2(R\text{-}py)$, for 2-methyl- and 2-ethylpyridine. The heats of dissolution of the complexes $CdCl_2(R\text{-}py)_2$, cadmium chloride $CdCl_2$, and pyridine bases R-py in non-polar aprotic solvent 1,2-dichloroethane containing tetrabutyl ammonium were determined by a calorimetry. The stability of the crystalline complexes was interpreted by using the heat of dissolution and reaction of the complexes in solution. The increase in the stability of the complexes, i.e., ΔH_{dec} of the complex, is predominantly attributed to the intermolecular interaction of complex or pyridine base.

VII-C-5 Formation and Thermal Decomposition of Mixed-ligand Complexes of Transition Metal Chlorides Containing Substituted Pyridines

Kiyoshi SAWADA, Chikako HONDA, and Keiichi SATOH

The formation of mixed-ligand complexes of divalent first row transition metal chlorides with substituted pyridines has been investigated by the methods of spectrophotometry and solvent extraction in 1,2-dichloroethane as solvent at 25.0°C. The substitution equilibria of tetrahedral metal chlorides with pyridine bases are written as follows:

$$MCl_2Y_2 + Rpy \overset{K_1}{\rightleftharpoons} MCl_2Y(R\text{-}py) + Y \quad (1)$$

$$MCl_2Y(R\text{-}py) + R\text{-}py \overset{K_2}{\rightleftharpoons} MCl_2(R\text{-}py)_2 + Y \quad (2)$$

where M is Co^{2+}, Cu^{2+}, Zn^{2+}, or Cd^{2+} and R-py is the substituted Pyridine (4-methyl-, 3-methyl-, 2-methyl-, 2-ethyl-, 4-acetyl- and 4-cyanopyridines and pyridine). Y refers to the chloride ion or neutral ligand (TOPO: trioctylphosphine oxide). The values of log K_1 and log K_2 show linear correlations with the pKa of the conjugate acids of the substituted pyridines.

Thermal decomposition of the crystals of the substituted pyridine adducts of cadmium chloride, $CdCl_2(R\text{-}py)_n$, has been investigated by the methods of TG, DTA, DSC and XRD. The decomposition reaction is written as: $CdCl_2(R\text{-}py)_4 \rightarrow CdCl_2(R\text{-}py)_2 \rightarrow CdCl_2(R\text{-}py) \rightarrow CdCl_2(R\text{-}py)_{2/3} \rightarrow CdCl_2$.
This scheme was confirmed by the elementally analysis of the compounds decomposed at constant temperatures. The XRD profiles of the complexes thermally decomposed are essentially same as those of the complexes crystallized from ethanolic solution. The patterns of TG and DTA curves of former complexes is almost the same as those of latter one. Because of the decomposition of the pyridine bases, the copper(II) complexes, $CuCl_2(R\text{-}py)_n$, show very complicated thermal decomposition reactions.

VII-C-6 Ion-pair of Tetraalkylammonium Picrates

Kiyoshi SAWADA, Fumie CHIGIRA,* and Keiichi SATOH *(*Niigata Univ.)*

Tetraalkylammonium salts have been used as the most common electrolytes for the non-aqueous solvents. The thermodynamic properties of the salts such as partition equilibria, solubility, ion-pair formation etc. have been studied in a variety of solvents. The detailed equilibria or structure of ion-pair, however, are not fully elucidated. The ion-pair formation of symmetric ($TAAn^+$; $(C_nH_{2n+1})^4N^+$, n=5–8) and asymmetric ($TOMA^+$; $(C_8H_{17})_3(CH_3)N^+$, CTMA; $(C_{16}H_{33})(CH_3)_3N^+$,) tetraalkylammonium ions, R^+, with picrate ion (Pic^-) in 1,2-dichloroethane was studied at 25°C by means of conductivity method. Limiting molar conductivity of ions, Λ_0, and ion-pair formation constants, K_{ip} were obtained by the analysis of the conductometric data with Fuoss-Justice Equation. Stokes radius, r_S, of the tetraalkylammonium ions was estimated from the limiting molar conductivity. The value of r_S almost linearly correlates with the number of carbon atoms of R^+, $N_C \cdot r_S$ estimated for asymmetric R^+ is comparable to that of symmetric R^+ having a corresponding number of carbon atoms. The closest approach, a, between the cation and anion of the ion-pair was estimated from the ion-pair formation constant. a increases steeply by the increase in the number of carbon atoms until $(C_3H_7)_4N^+$. The value of a of higher R^+ scarcely increases by the increase in the number N_C. The closest approach of the asymmetric R^+ is much smaller than that predicted from the number of carbon atoms. By taking into consideration the results of partition equilibria and electronic spectra, the structures of ions and ion-pairs were discussed.

VII-C-7 Partition and Dimerization of Ion-pair of Tetraalkylammonium Salts in Xylene

Kiyoshi SAWADA, Tsuyoshi SOHARA,* and Yoichi KIKUCHI** *(*Niigata Univ., **Iwate Univ.)*

The partition equilibria of symmetric ($TAAn^+$; $(C_nH_{2n+1})_4N^+$, n=5–8) and asymmetric ($TOMA^+$; $(C_8H_{17})_3(CH_3)N^+$) tetraalkylammonium ions, R^+, with inorganic anions X^- (=Cl^-, Br^-, BF_4^-, ClO_4^-, NO_3^-, SCN^-,) into xylene was studied at 25.0°C. The tetraalkylammonium ion in xylene presents in a form of ion-pair, $R^+ \cdot X^-$, and the ion-pair is partially dimerized as $(R^+ \cdot X^-)_2$. The distribution constants, K_{dist}, and dimerization constants, K_{dim}, of the ion-pairs in xylene were determined. By taking into consideration the ion-pair formation constant in organic solvent, $K_{ip,org}$, the distribution constant of ion-pair was interpreted by the partition of dissociated ions of cation and anion. The logarithmic distribution constants corrected for

ion-pair formation, log K_{dist}-log $K_{ip,org}$, of each tetraalkylammonium ion linearly correlate to a reciprocal of ionic radius of anion except for NO_3^- and SCN^-. The values of log K_{dist}-log $K_{ip,org}$ of symmetric cation $TAAn^+$ show good linear correlations with the number of carbon atoms of $TAAn^+$ except for $TOMA^+$ system. The distribution constants of asymmetric ion $TOMA^+$ system show considerably large values compared with those of $TAAn^+$ having a comparable number of carbon atoms. On the other hand, the dimerization constants of ion-pairs of $TOMA^+$ system are considerably smaller than those of $TAAn^+$. These peculiar behaviors of ion-pair of asymmetric cation $TOMA^+$ were explained by the relatively large ion-pair formation constant caused by the shorter closest approach between $TOMA^+$ and anion.

VII—D Syntheses, Structures and Functions of Chromotropic Complexes

VII-D-1 Studies on Mixed Chelates. Five Coordinate Cooper(II) Chelates with N,N,N′N″,N″-Pentamethyldiethylenetriamine and β-Diketonates

Noriko SHINTANI, Etsuko NUKUI, Kozo SONE *(Ochanomizu Univ.)*, **Hiroshi MIYAMAE** *(Josai Univ.)*, **and Yutaka FUKUDA** *(Ochanomizu Univ. and IMS)*

[*Bull. Chem. Soc. Jpn.*, **67**, 1828 (1994)]

Mixed Cu(II) chelates with the titled ligand(pmdt) and five β-diketonat(dike) ligands, i.e., dipivaloylmethanate(dipm), acetylacetonate(acac), pivaloyltrifluoroacetonate(pfac), trifluoro- and hexafluoroacetylacetonate (tfac and hfac, respectively), were prepared and studied. Thier general formula, $[Cu(dike)(pmdt)]ClO_4$, suggests that they are five coordinated; X-ray crystal analyses confirmed that the chelates with acac and tfac are distorted square pyramidal, with the axial site occupied by one of the O atoms of dike. Similar structures are presumed for the remaining chelates on the bases of spepctral similarities. In solutions, these five-coordinated chelates are solvated to various extents, showing a characteristic solvatochromism.

VII-D-2 Synthesis and Properties of the Dinuclear Copper(II) Complexes Containing Dinucleating Ligands with Imidazole Nitrogen and Two Exogenous Bridging Ligands

Yasuko NAKAO, Makoto OONISHI, Tomoko UZU, Hiroko KASHIHARA *(Okayama Univ.)*, **Shinichiro SUZUKI** *(Osaka Univ.)*, **Masahiro SAKAI, and Yutaka FUKUDA** *(IMS)*

[*Bull. Chem. Soc. Jpn.*, **67**, 2586 (1994)]

Dinuclear copper(II) complexes, $[Cu_2(nR)X_2](ClO_4)_2$ (X=N_3^-, NCS^-, and OAc^-) have been synthesized and characterized, where nR=N,N,N′N′-tetrakis[1(1-ethyl-2-benzimidazolyl)methyl]-1,3-diaminopropane(3Me), N,N,N′N′-tetrakis[(1-ethyl-2-benzimidazolyl)methyl]-1,3-diaminopropane(3Et), N,N,N′N′-tetrakis[1-methyl-2-benzimidazolyl)methyl]-1,4-diaminobutane (4Me), and N,N,N′N′-tetrakis[1-ethyl-2-benzimidazolyl)-methyl]-1,4-diaminobutane(4Et). Weak antiferromagnetic interactions were found for $[Cu_2(3Me)(NCS)_2](ClO_4)_2 \cdot 3H_2O$ (coupling constant J=−2.1 cm^{-1}, H=$-2JS_1 \cdot S_2$) and $[Cu_2(3Me)(OAc)_2](ClO_4)_2 \cdot H_2O$ (J=−2.0 cm^{-1}), but no exchange interaction has been observed to 4.2 K for $[Cu_2(3Me)(N_3)_2](ClO_4)_2 \cdot H_2O$. The electrochemistry of these complexes in N,N-dimethylformamide showed two electron reductions at +210 — −30 mV vs Ag-AgCl (Cu^{2+}-Cu^{2+} → Cu^+-Cu^+).

VII—E New Organometallic Catalysts

VII-E-1 Polymerization of Ethylene Catalyzed by the System, $Ta(C_5Me_5)(diene)(CH_3)_2$/MAO: An Isoelectronic Analogue for a Group 4 Metallocene Catalyst

Kazushi MASHIMA*, Shinjiro FUJIKAWA*, and Akira NAKAMURA *(*Osaka Univ.)*

[*J. Am. Chem. Soc.*, **115**, 10990 (1993)]

Utilyzing the concept of 14-electron isolobal analogy, novel olefin polymerization catalyst systems involving Group 5 transition metals were found. The basic strategy here is to generate a 14-electron species from the organometallic complexes containing a cyclopentadienyl and a l, 3-diene ligands, e.g. $Cp(diene)MX_2$, M=Nb, Ta. These complexes are 16-electron species which can generate the 14-electron species by abstraction of the anionic ligand X by suitable means. Actually, living polymerization of ethylene was realized for the first time by the catalysis of a system, $(C_5Me_5)(C_4H_6)TaCl_2$/Methylaluminoxane in toluene at −20°C to give a polymer with very narrow molecular weight distribution, M_w/M_n=1.08 with M_n=2.55×10^4.

VII—F Straight Linear Metal-Metal Bonded Compexes

VII-F-1 New Synthetic Strategy for a Straight Linear Metal-Metal Bonded Tetranuclear Complex, the Pd-Mo-Mo-Pd System Supported by Four Tridentate 6-(Diphenylphosphine)-2-pyridonate

Ligands

Kazushi MASHIMA*, Hiroshi NAKANO*, and Akira NAKAMURA *(*Osaka Univ.)*

[*J. Am. Chem. Soc.*, **115**, 11632 (1993)]

Simultaneous addition of later transition metal atoms such as Pt and Pd at the both terminal axial sites of the Mo=Mo quadruply-bonded complex, $Mo_2(pyphos)_4$, **1**, was found to give completely straight linear heterometal complexes. Reduction of the metal-metal bond order at the Mo-Mo part is evidenced by the elongation of the Mo-Mo bond by 0.03Å upon the addition of two Pt atoms. In contrast to the observed simultaneous addition, an addition of one equivalent of Pd(II) ion on one of the axial site resulted in formation of a trinuclear complex without Mo-Pd bonding.

VII—G Carbon Dioxide Activation on Metal Complexes and Chemical Simulation of Nitrogen Cycle

Reduction of carbon dioxide has been extensively studied. Although a variety of metal complexes have proven to catalyze electro- and photochemical CO_2 reductions, the products in those reductions are limited to formic acid and carbon monoxide. Development of multi-electron reduction of CO_2 accompanied by carbon-carbon bond formation by homogeneous catalysts is expected to contribute for the utilization of CO_2 as a possible Cl resources for preparations of various chemicals. Assimilatory and dissimilatory reductions of NO_3^- and NO_2^- are the key reactions in the nitrogen cycle, which regulates the amounts of inorganic nitrogen compounds on earth. There are long-standing arguments for the precursors to NO evolution during the turnover and N_2O in the pathway from NO_2^- to N_2 by nitrite reductases containing iron heme or copper proteins. Nitrite coordinates on Cu with either oxygen (nitrito) or nitrogen (nitro). The catalytic reduction of NO_2^- via nitrito and nitro-copper complexes may, therefore, afford an foundamental information on enzymatic nitrite reductases. The purpose of this project is to elucidate the mechanisms for the dissimilatory reduction of NO_2^- and to develop a new catalytic system for the multi-electron reduction of CO_2.

VII-G-1 Succesive Reduction of CO_2 on a Ruthenium Complex

Kiyotuna TOYOHARA, Hirotaka NAGAO, and Koji TANAKA

Reduction of CO_2 on electrodes takes place at potentials more negative than −2.0 V vs SCE. The redox potential of CO_2, on the other hand, undergoes anodic shift when protons participate in the CO_2 reduction. The more electrons and protons are involved in the CO_2 reduction, the more the redox potential shift to positive potentials. Thus, the multi-electron reduction of CO_2 is much more favorable thermodynamically compared with two-electron reduction of CO_2. The multi-electron reduction of CO_2 on metal complexes would composes of several reaction steps. The possible precursors for HCOOH, CO, HCHO,CH_3OH and CH_4 as the 2, 4, 6, and 8 electron reduction of CO_2 are M-C(O)OH, M-CO, M-CHO, M-CH_2OH, and M-CH_3 complexes. The molecular structures of the series of metal complexes responsible for those highly reduced products may afford the information on the metal-carbon bonds strength for each step. Along this line, we have determined the molecular structures and ν(Ru-C) bands of a series of Ru metal complexes (Figure 1).

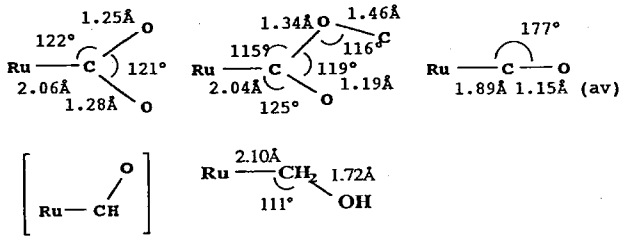

Figure 1. Successive reduction of CO_2 to CH_2OH on the $[Ru(bpy)_2(CO)]^{n+}$ (n=0, 1) moiety.

VII-G-2 Carbon-Carbon Bond Formation in Electrochemical Reduction of Carbon Dioxide by a Ruthenium Complex

Hirotaka NAGAO, Tetsunori MIZUKAWA, and Koji TANAKA

[*Inorg. Chem.*, **33**, 3415 (1944)]

A carbonyl ligand of $[Ru(bpy)_2(CO)_2](PF_6)_2$ (**1**) (bpy=2,2′-bipyridine) and $[Ru(bpy)(trpy)(CO)](PF_6)_2$ (**2**) (trpy=2,2″:6′2″-terpyridine) is reversibly converted to hydroxycarbonyl and η^1-CO_2 moieties by treatment with OH^-. **1** and **2** also react with $NaBH_4$ to afford CH_3OH *via* formyl and hydroxymethyl complexes, and the molecular structure of $[Ru(bpy)_2(CO)(CH_2OH)]PF_6$ (**3**) was determined by X-ray structure analysis. Crystal Data for **3**, monoclinic, space group C2/c, a=34.683(3)Å, b=124.68(1)°, V=4736(1)Å^3, Z=8, and R=0.059 (R_w=0.070) for 2880 data with $F_0 > 3\sigma(F_0)$. The controlled potential electrolysis of **2** at −1.75 V *vs.* Ag|Ag$^+$ in CO_2-saturated C_2H_5OH/H_2O (8:2 v/v) at −20°C produced HC(O)H, CH_3OH, H(O)CCOOH, and $HOCH_2COOH$ together with CO and HCOOH, while the similar electrochemical CO_2 reduction in the presence of **1** gave only CO and HCOOH. The achievement of multi-electron reduction of CO_2 by **2** is ascribed to $[Ru(bpy)(trpy)(CHO)]^+$ formed by the two-electron reduction of **2** is protic media.

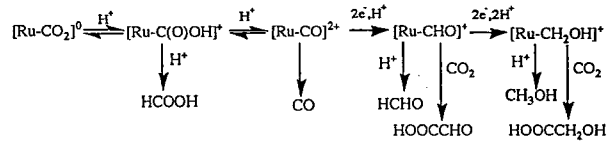

VII-G-3 Catalytic Formation of Ketones by Double Alkylation of Carbon Monoxide Formed by Reductive Disproportionation of Carbon Dioxide on a Ruthenium Complex

Hiroshi NAKAJIMA, Hirotaka NAGAO, Tetsunori MIZUKAWA, and Koji TANAKA

Electrochemical CO_2 reduction by $[Ru(bpy)_2(L)(CO)]^{2+}$ (L=quinoline derivatives) produces CO and HCOOH in protic conditions. On the other hand, reductive disproportionation reaction of CO_2 affording CO and CO_3^{2-} smoothly takes place in the absence of proton source under similar electrochemical CO_2 reduction. (eq 1). Further-

$$2CO_2 + 2e^- \rightarrow CO + CO_3^{2-} \quad (1)$$

more, the similar electrolysis in the presence of methyliodide results in the formation of ketones and β-keto acids together with concomitant evolution of ethane. The formation of ketones results from double alkylation of CO formed in the reductive disproportionation of CO_2 (eq 1). The reaction (2) is explained by an acyl intermediate in the catalytic cycle of the CO_2 reduction.

$$2CO_2 + 2CH_3I + 4e^- \rightarrow CH_3C(O)CH_3 + CO_3^{2-} + 2I^- \quad (2)$$

VII-G-4 Molecular Structure of Copper Nitrito Complexes as the Reaction Intermediate of Dissimilatory Reduction of NO_2^-

Nobutoshi KOMEDA*, Hirotaka NAGAO, Gin-ya ADACHI*, Masatatsu SUZUKI, Akira UEHARA**, and Koji TANAKA** *(*Osaka Univ. **Kanazawa Univ.)*

[*Chem. Lett.*, 1521 (1933)]

A controlled potential electrolysis of an aqueous solution (pH 7.0) containing $[Cu(tpa)(H_2O)](ClO_4)_2$ (tpa=tris[2-pyridyl)methyl]amine) and $NaNO_2$ at −0.40 V (*vs.* Ag/AgCl) catalytically produced NO and N_2O. The fact that $[Cu(tpa)(ONO)]^+$ and $[Cu(tpa)(NO_2)]^+$ exist as equilibrium mixtures in solutions indicates that electrochemical reduction of NO_2^- proceeds via $[Cu(tpa)(ONO)]^+$ and $[Cu(tpa)(NO_2)]^+$. Removal of the bound- or terminal-oxygen from the Cu-ONO moiety by irreversible protonation upon the electrochemical reduction of the complex probably result in NO dissociation due to the Cu-O bond cleavage or the labile Cu-ON bond. Free NO thus formed will form a nitrogen-bound nitrosyl adduct, $[Cu(tpa)(NO)]^+$, which also may be formed in the reduction of $[Cu(tpa)(NO_2)]^+$ in H_2O without the Cu-NO bond cleavage because of the removal of the terminal-oxygen of the nitro ligand. Thus, dissimilatory reduction of NO_2^- via $[Cu(tpa)(ONO)]^+$ reasonably explains NO evolution (Scheme 1).

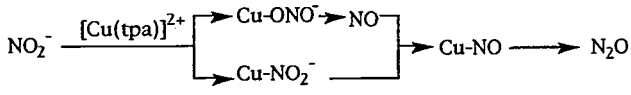

VII-G-5 Structural Changes in Tris[(2-pyridyl)methyl]amine)-Copper(II) Derivatives by Successive Introduction of Methyl Substituent at the Ortho Position of the Pyridyl Moiety

Nobutoshi KOMEDA*, Hirotaka NAGAO, Gin-ya ADACHI*, Masatatsu SUZUKI, Akira UEHARA**, and Koji TANAKA** *(*Osaka Univ., **Kanazawa Univl.)*

The reaction of $[Cu(tpa)Cl]^+$ (tpa=tris[2-pyridyl)methyl]amine) with NO_2^- produces $[Cu(tpa)(ONO)]^+$ and $[Cu(tpa)(NO_2)]^+$, and $[Cu(tpa)Cl]^+$ (tpa=tris[2-pyridyl)methyl]amine effectively catalyzes the reduction of NO_2^- to N_2O under the controlled potential electrolysis at −0.40 V (vs Ag/AgCl) in H_2O (pH 7.0). Successive introduction of methyl group at the ortho position of pyridyl moiety of $[Cu(tpa)Cl]^+$ causes about by 100 mV positive potential shifts of the redox potentials of the complexes. Such an anodic shift of the redox potentials of the $[Cu(Me_ntpa)Cl]^{+/0}$ couple (n=0−3) results in the decrease in the catalytic activity of the reduction of NO_2^- in the following order: $[Cu(tpa)Cl]^+ > [Cu(Me_1tpa)Cl]^+ > [Cu(Me_2tpa)Cl]^+ \gg [Cu(Me_3tpa)Cl]^+ \approx 0$. Unexpected anodic shift caused by the introduction of electron donating methyl group into the pyridyl ligand of $[Cu(tpa)Cl]^+$ may be associated with the changes in the binding modes of the Me_ntpa ligand in those complexes. Crystal structures of $[Cu(tpa)Cl]^+$ and $[Cu(Me_ntpa)Cl]^+$ (n=1, 2, 3) showed trigonal bipyramidal and square pyramidal structures, respectively. The gradual anodic shift of the redox potentials of square planar $[Cu(Me_ntpa)Cl]^+$ (n=1, 2, 3) may correlate with lengthening the bond distances between equatorial N(1−3) and Cu rather than shortening the bond distances between axial N4 and Cu (Figure 1).

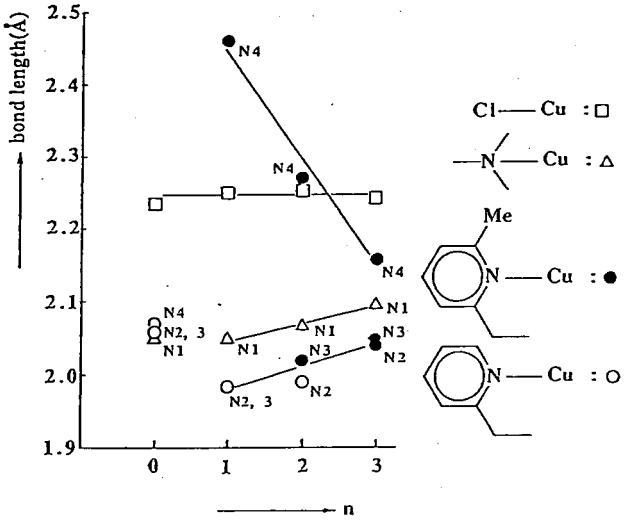

Figure 1. Relevant bond length of $[Cu(Me_ntpa)Cl]^+$ (n=0−3)

VII-G-6 Oxalate Formation in Electrochemical CO_2 Reduction Catalyzed by a Rhodium-Sulfur Cluster

Yoshinori KUSHI, Hirotaka NAGAO, Takanori NISHIOKA, Kiyoshi ISOBE, and Koji TANAKA

A variety of transition metal complexes have been

shown to catalyze electrochemical CO_2 reduction affording CO and/or HCOOH, where metal-η^1-CO_2 intermediates are generally believed as the precursors for those products. In this connection, molecular structures of Rh-, Co-, and Ru-η^1-CO_2 complexes have been elucidated so far. On the other hand, a CO_2 adduct bonded on bridging sulfur of $[Mo_2Fe_6S_8(SEt)_9]^{5-}$ is proposed as a reaction intermediate in CO_2 fixation to thioesters affording α-keto-acids. Thus, not only low valent metals but also electron rich sulfur ligands are the possible sites for the activation of CO_2 by metal complexes. We have found the first successful oxalate generation in a high yield in electrochemical CO_2 reduction catalyzed by $[(Cp^*Rh)_3(\mu^3\text{-}S)_2](BPh_4)_2$ as a homogenous catalyst. A solution IR spectrum evidenced formation of the 1:2 adduct of $[(RhCp^*)_2(\mu^3\text{-}S)_2]^0$ with CO_2 as the possible precursor for the oxalate formation.

VII—H Development of Highly Selective Reactions Using Early Transition Metal Complexes

Highly selective bond formation reactions have been investigated using early transition metal complexes, especially zirconium complexes. Zirconocene alkene or alkyne complexes, zirconacyclopentane, zirconacyclopentene, zirconacyclopentadienes could be used for selective C-C bond formation or selective functionalization.

VII-H-1 Zirconium Catalyzed C-C Bond Formation Reactions of Diynes with EtMgBr

Tamotsu TAKAHASHI, Koichiro AOYAGI, Victor DENISOV, Noriyuki SUZUKI, Danièle CHOUEIRI*, and Ei-ichi NEGISHI* *(*Purdue Univ.)*

[*Tetrahedron Lett.*, **34**, 8301 (1993)]

Carbon-carbon bond formation reactions of diynes with EtMgBr were catalyzed by Cp_2ZrCl_2. Caron-carbon bond formation occurred at C1 carbon of diynes and megnesium-carbon bond was formed at C2 carbon of diynes. This is in sharp contrast to the carbometalation reaction using the Me_3Al/Cat. Cp_2ZrCl_2 system which provided carbon-carbon bond at C2 carbon and carbon-aluminum bond at C1 carbon of diynes. The final products, magnesiated enynes easily stereochemically isomerize to give a mixture of (E) and (Z) isomers.

Stoichiometric reactions of diynes with zirconium-ethylene complex gave zirconacyclopentenes with alkynyl substituents at a position with very high regioselectivity. Diynes did not dimerize on "zirconocene equivalent" even at higher temperature in the presence of an excess of diynes. Transmetallation reaction of the zirconacyclopentene compounds with EtMgBr selectively proceeded at alkenyl carbon bonded to zirconium.

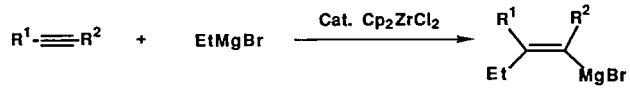

VII-H-2 First Isolation and Characterization of a Zirconocene(methyl)-(ethylene) Complex

Tamotsu TAKAHASHI, Kayoko KASAI, Noriyuki SUZUKI, and Kiyohiko NAKAJIMA* *(*Aichi Univ. of Education)* **Ei-ichi NEGISHI**** *(**Purdue Univ.)*

[*Organometallics*, **13**, 3413 (1994)]

The first example of a zirconocene(alkyl)(olefin) complex, i.e., $(Cp_2ZrMe)_2(CH_2CH_2)$, was prepared by the reaction of Cp_2ZrMe_2 with a zirconocene-ethylene complex, $[Cp_2ZrEt(CH_2{=}CH_2)]MgBr$, and the structure of this complex was determined by single-crystal X-ray diffraction study. The structure of this complex showed one methyl group on each zirconium and an ethylene ligand simultaneously coordinating to the two zirconocene moieties.

VII-H-3 Zirconium Catalyzed or Mediated Regioselective C-C Bond Formation Reactions of α,β-Unsaturated Acetals

Tamotsu TAKAHASHI, Denis Y. KONDAKOV, and Noriyuki SUZUKI

[*Chem. Lett.*, 259 (1994)]

Zirconium-alkyne complexes or zirconacyclopentenes, which were easily prepared in situ from alkynes, reacted with acrolein diethylacetal to afford vinyl ether derivatives. The C-C bond formation proceeded exclusively at β-position of the α,β-unsaturated acetal. Zirconium catalyzed C-C bond formation reactions of α,β-unsaturated acetals with EtMgBr also proceeded at β-position exclusively.

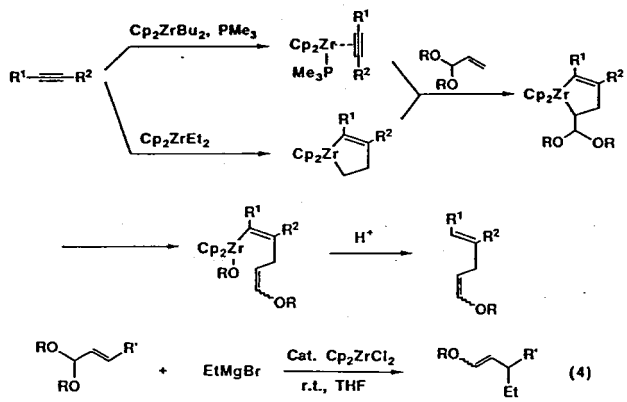

VII-H-4 Reaction of 3-Zircona-1-cyclopentenes and Zirconacyclopentanes with Aldehydes. A Selective and Convenient Synthesis of 4-Penten-1-ols, (Z)-5-Iodo-4-penten-1-ols, and Related Alkanols

Christophe COPERET*, Eiichi NEGISHI*, Zhenfeng XI, and Tamotsu TAKAHASHI *(*Purdue Univ.)*

[*Tetrahedron Lett.*, **35**, 695 (1994)]

3-Zircona-1-cyclopentenes and zirconacyclopentanes

react with aldehydes at or below 25°C to give the corresponding carbonyl addition products, i.e., 7-membered oxazirconacycles, which can be readily converted to the corresponding alcohols via protonolysis and 5-iodoalcohols via iodinolysis; the latter product can be further converted to 7-membered lactones via Pd-catalyzed carbonylation.

VII-H-5 A Reagent-Dependent Highly Chemoselective Halogenation Reaction of Zirconacyclopentens

Tamotsu TAKAHASHI*, Koichiro AOYAGI, and Denis Y. KONDAKOV

[*J. Chem. Soc., Commun.*, 747 (1994)]

Recently we have reported that the chemoselectivity of a monohalogenation reaction of zirconacyclopentene compounds **1** with I_2 was selective but dependent on their substituents. To the contrary, an excess of MeOH/I_2 method was not dependent on the substituents. This method always afforded trisubstituted alkenyl iodides **2** with a high isomerical purity. Especially the use of an excess of methanol was important to avoid the formation of diiodide as a by-product.

As shown in Scheme 1, when R is aryl group, alkenyl halides **2** are provided by MeOH/X_2 (X_2=I_2 or Br_2) and homoallyl halides **3** are obtained by treatment with X_2. However, when R is alkyl group, both methods, X_2 and MeOH/X_2 give alkenyl halides **2** selectively. Therefore there is no method to prepare homoallylic halides **3** from zirconacyclopentene **1** when R is alkyl. This situation prompted us to develop a new halogenation reagent with an opposite chemoselectivity to X_2.

In this paper we reported that CCl_3Br or CBr_4 is a new bromination reagent for some organozirconocene compounds and that this reagent gave a highly chemoselective monobromination product of zirconacyclopentenes (R=alkyl) with an opposite chemoselectivity to NBS or Br_2 which are the usual bromination reagent of organozirconium compounds.

Chemoselective monobromination reactions of 2,3-dialkylzirconacyclopentenes were highly dependent on the reagents; NBS or Br_2 gave alkenyl halides selectively, whereas CCl_3Br or CBr_4 gave homoallylic halides with a high chemoselectivity.

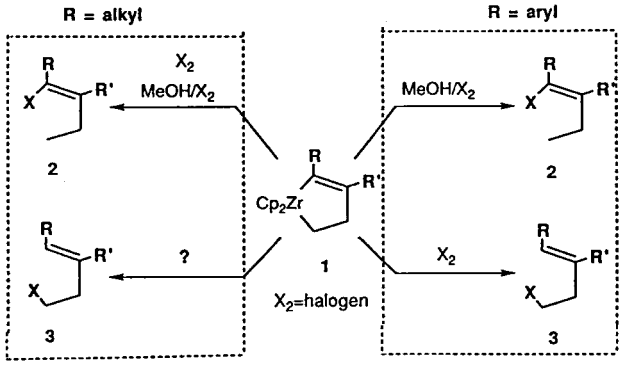

Scheme 1.

VII-H-6 Zirconium Catalyzed or Promoted Novel Type of Cyclization Reaction

Tamotsu TAKAHASHI, Denis Y. KONDAKOV, and Noriyuki SUZUKI

[*Organometallics*, **13**, 3411 (1994)]

Intramolecular cyclization reactions of YCH_2CH=$CHCH_2XCH_2CH$=CH_2, (X=CH_2, NPr or NPh; Y=PhO or MeO), which have a terminal double bond and allylic ether moiety, were catalyzed by zirconocene dichloride (10—20 mol%) in the presence of n-BuMgCl. Cyclization products, 2-methyl-1-vinylcyclopentane, 4-methyl-1-propyl-3-vinylpyrrolidine and 4-methyl-1-phenyl-3-vinylpyrrolidine were obtained in 60—80% yields. Stoichiometric cyclization with Cp_2ZrBu_2 or $(C_5H_3Me_2)_2ZrBu_2$ at room temperature gave the same products in high yields after hydrolysis. When an excess of Cp_2ZrBu_2 was used, the stereoisomerization of cis product to trans isomer was observed.

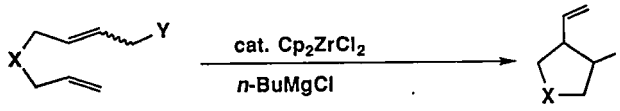

VII-H-7 Chemoselective Functionalization of Zirconacyclopentenes

Koichiro AOYAGI, Kayoko KASAI, Denis Y. KONDAKOV, Ryuichiro HARA, Noriyuki SUZUKI, and Tamotsu TAKAHASHI

[*Inorg. Chim. Acta.*, **220**, 319 (1994)]

Zirconacyclopentenes, which were readily prepared by the reaction of Cp_2ZrEt_2 with alkynes or by the reaction of vinylsilane with alkynes in the presence of Cp_2ZrBu_2 (Negishi reagent), reacted with iodine to give either stereodefined alkenyl iodides or homoallylic iodides selectively after hydrolysis. The chemoselectivity of this reaction was strongly dependent on the substituent R group of C2-carbon attached to zirconium. When R was phenyl group, homoallylic iodides were selectively formed. On the other hand, alkyl substituted zirconacyclopetenes reacted with iodine to afford alkenyl iodides selectively. A small amount of diiodides were produced as by-products.

Reactions of zirconacyclopentenes with an excess of MeOH and iodine in this order gave only alkenyl iodides with an excellent selectivities. The formation of diiodides was not detected. This monohalogenation procedure using an excess of MeOH/I_2 was not substituent-dependent in the system used here.

Treatment of alkylsubstituted zirconacyclopentenes with CBr_4 or CCl_3Br yielded only homoallylic bromides, after hydrolysis, with >99% chemoselectivity. It is in sharp contrast to the reaction with usual bromination reagents such as Br_2 and NBS which led to the selective formation of alkenyl bromides. A sequential treatment of zirconacyclopentenes with CBr_4 and I_2 in this order, a mixed dihalogenation product was selectively formed. Reaction with Me_3SnCl was not substituent-dependent. The sp^3 carbon attached to Zr selectively reacted with Me_3SnCl to give homoallyltin

compounds.

Insertion reaction of isonitrile in the Zr-carbon bond of zirconacyclopentenes were chemoselective but neither substituent-dependent nor reagent-dependent in the system used here.

VII-H-8 Highly Regioselective Reaction of Zirconocene-alkene Complexes with Aldehydes or Ketones

Noriyuki SUZUKI, Christophe J. ROUSSET, Koichiro AOYAGI, Martin KOTORA, Tamotsu TAKAHASHI, Maki HASEGAWA, Yu NITTO, and Masahiko SABURI

[*J. Organomet. Chem.*, **473**, 117 (1994)]

Reactions of zirconocene-alkene complexes $Cp_2Zr(RCH{=}CH_2)(PR'_3)$ (R=H, alkyl, silyl or aryl) with aldehydes or ketones were investigated. Zirconocene-ethylene, -propylene or 1-butene complexes reacted with aldehydes or ketones at terminal carbons of alkenes to give the corresponding alcohols after hydrolysis with a high regioselectivities. Similar type of reaction product was also obtained by a reaction of a zirconacyclopentane with aldehyde. This reaction proceeded via β-β' carbon-carbon bond cleavage of zirconacyclopentanes. Zirconocene-vinylsilane complexes reacted with ketones to give 2,2-di(cyclopentadienyl)-1-oxa-2- zirconacyclopentanes **1** with an excellent regioselectivity. Carbon-carbon bond formation occurred exclusively at terminal carbons of vinylsilanes. Corresponding γ-silylalcohols were obtained after hydrolysis of **1**. Products showed that vinylsilanes reacted with carbonyl compounds at the β-carbon to silyl group. It is in sharp contrast to the conventional reactions of vinylsilanes which normally attacked electrophile at the α-carbon. The reactions of styrene and its derivatives with pentan-3-one on zirconium gave a mixture of two regioisomers. Substituents of alkenes tend to be in α-position to Zr in **1**. This orientation showed a different aspect of the formation of **1** from the alkene-alkene coupling reaction on zirconium. The regioselectivity of the reaction with carbonyl compounds decreases in this order; R=alkyl > silyl > aryl. Factors which governed regioselectivities were discussed. These reactions proceeded via β-β' carbon-carbon bond cleavage of zirconacyclopentanes.

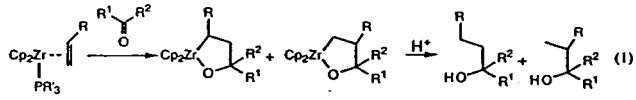

VII-H-9 Novel Syntheses of Eight-five Fused Ring Compounds from Zirconacyclopentadienes

Tamotsu TAKAHASHI, Martin KOTORA, Kayoko KASAI, Noriyuki SUZUKI, and Kiyohiko NAKAJIMA*
*(*Aichi Univ. of Education)*

[*Organoemtallics*, in press]

Zirconacyclopentadienes reacted with 2 equiv of allyl chloride in the presence of either catalytic or stoichiometric amount of CuCl and LiCl salt (2 eq) to give stereodefined 1,4,6,9-decatetraenes in 66–96% yields. Reaction of 1,4,6,9-decatetraenes obtained here such as 4,5,6,7-tetraethyldeca-1,4,6,9-tetraene with 1 equiv of Negishi reagent (Cp_2ZrCl_2+2 n-BuLi) in THF at room temperature for 3 h and the subsequent carbonylation at 0°C gave eight-five fused ketones such as 3,4,5,6-tetraethylbicyclo[6.3.0]undeca-3,5-dien-10-one in 76% yield.

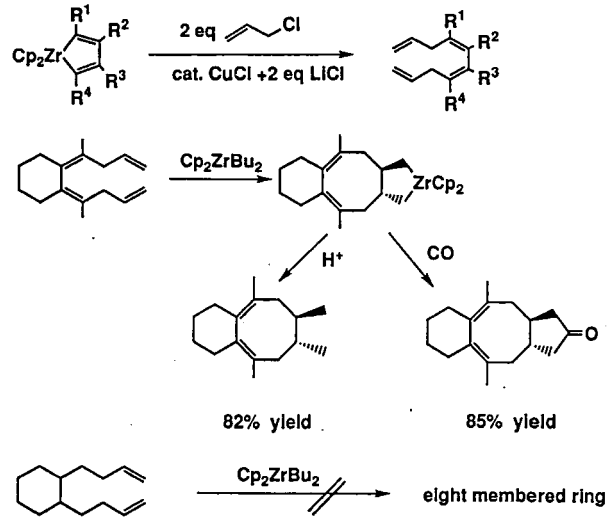

VII-H-10 Copper Catalyzed C-C Bond Formation Reaction of Allylzirconation Products of Alkynes

Tamotsu TAKAHASHI, Martin KOTORA, Kayoko KASAI, and Noriyuki SUZUKI

[*Tetrahedron Lett.*, **35**, 5685 (1994)]

Reaction of allylzirconation products of alkynes with allyl chloride was catalyzed by copper salts to give stereodefined 1,4,7-trienes.

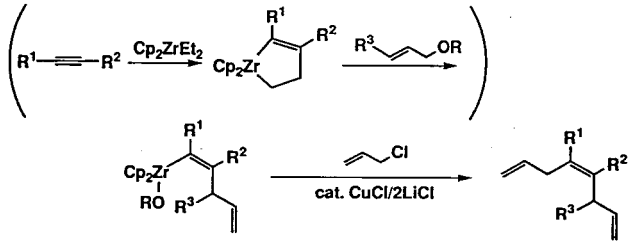

VII-H-11 Polar Paths for Reactions of Alkene-Zirconocene Complexes

Ei-ichi NEGISHI*, Danièle CHOUEIRY*, Thinh B. NGUYEN*, Douglas R. SWANSON*, Noriyuki SUZUKI, and Tamotsu TAKAHASHI *(*Purdue Univ.)*

[*J. Am. Chem. Soc.*, **116**, 9751 (1994)]

Although the reactions of alkene-zirconocene derivatives can, in some cases, proceed stereospecifically, they can also undergo stereoisomerization leading to nonstereospecific but highly stereoselective processes, which most likely proceeds via novel dipolar zirconate species. Specifically, (E)- and (Z)-1-phenyl-1,6-heptadienes react with $(n\text{-}Bu)_2ZrCp_2$ in a stereospecific manner to give the corresponding trans-fused 3-zirconacyclo[3.3.0]octanes. Upon

standing, however, the more stable isomer in which the benzylic H and the adjacent bridgehead H are trans to each other dominates. A much faster stereoisomerization process was observed in the reaction of (Z)-β-methylstyrene with Et_2ZrCp_2 to give trans-1,1-bis(cyclopentadienyl)-2-phenyl-3-methylzirconacyclopentane. Furthermore, various (Z)-stilbenes, (Z)-β-methylstyrene, (Z)-β-silylstyrene, and (E)-cyclooctene undergo stereoisomerization catalyzed by n-Bu_2ZrCp_2. This isomerization reaction is an associative process, which is first order in alkenes and second order in alkene-zirconocene complexes which act as catalysts. Those zirconocene derivatives that cannot be readily converted to alkene-zirconocenes, e.g. Me_2ZrCp_2, do not serve as catalysts. Isomerization of (Z)-PhCD=CHMe gives only its E isomer indicating that the reaction simply involves cleavage of the π-bond. Electron-withdrawing para substituents in stilbenes retard the stereoisomerization process, indicating the involvement of benzyl cationic species and zirconate anions. These polar processes represent yet another novel reaction pattern that $ZrCp_2$ derivatives display.

RESEARCH ACTIVITIES VIII
Computer Center

VIII—A Theoretical Studies of Highly Excited Vibrational States in Polyatomic Molecules

Research activities of this year include : (a) semiclassical study of avoided crossing for nonintegrable systems, (b) electronic structure and dynamics of small polyatomic molecules, and (c) development of parallel computational environment for large scale electronic structure calculations. Dr. Takami joined as research associate in Feb. 1993.

VIII-A-1 Semiclassical Study of Avoided Crossing

Toshiya TAKAMI

[*Phys. Rev. E*, submitted]

The origin of avoided crossings in nonintegrable systems is investigated in detail by semiclassical methods. It is well known that avoided crossings in nearly integrable systems occur around resonances between tori, i.e., the origin of them is the tunneling trajectory with imaginary action. In the nonintegrable systems like highly excited molecules, however, the origin will be due to real trajectories rather than imaginary ones because the existence of the real one is always guaranteed by the ergodicity.

In order to study the relation between avoided crossings and real trajectories in nonintegrable systems, the trace formula for the stadium billiard system is analyzed quantitatively through Fourier analysis. We introduce a diabatic transformation around avoided crossings and show that the spectral density after the transformation become higher for several short periodic orbits. Further, we carry out the periodic-orbit quantization to study semiclassical reproduction of avoided crossings. From these analysis, we conclude that the origin of avoided crossings in nonintegrable systems is the long and complicated periodic orbits around short and simple ones.

VIII-A-2 Rotation Induced Vibrational Mixing in Highly Excited Vibrational States of Formaldehyde II

Mutsumi AOYAGI

The effects of both anharmonic and Coriolis interactions on the intramolecular dynamics in Formaldehyde are investigated quantum mechanically. Variational calculations including all of the vibrational modes, and the rotational modes are performed using the ab initio SDCI potential energy surface. Both time-dependent and time-independent analyses are made on the calculated eigenstates (up to 12000 cm^{-1}) to elucidate the role of Coriolis interaction in highly excited vibrational states. We also carried out the analyses of curvature distribution with respect to Hamiltonian parameters both on H_2CO and model Hamiltonian systems; the stadium billiard and the kicked rotator systems. We found that the anharmonic couplings assisted by b- and c-type Coriolis interactions and extensive K-mixings play a crucial role in the intramolecular dynamics at high energy region($E > 7500$ cm^{-1}). We also found that curvature distribution obtained from the H_2CO results shows similar characteristics with one from the stadium billiard system.

VIII-A-3 Theoretical Study of the Potential Energy Surfaces and Dynamics of Low-Lying Electronic States of Formyl Radical HCO

Shinkoh NANBU and Mutsumi AOYAGI

Multireference configuration-interaction(MR-CI) calculation for numerous geometrical configurations of HCO and COH are carried out to obtain the global potential energy surfaces for electronic ground and excited states including Rydberg s and p states. The Franck-Condon factors for several electronic transitions are obtained by solving the Schrodinger equation describing the motion of nuclei on the full dimensional potential energy surfaces. Furthermore, theoretical analyses of hightly excited vibrational states of HCO and COH are also made by using 3-dimensional DVR method.

VIII-A-4 Development of Parallel Direct SCF Program and Applications to Large Scale Molecular Orbital Calculations on Loosely Coupled Networks of Workstations

Satoshi MINAMINO, Shinkoh NANBU, and Mutsumi AOYAGI

We are developing a parallel code of a direct SCF program on loosely coupled networks of workstations, and are applying it to large scale molecular orbital calculations. This program system can be used on several distributed computing tools, including PVM and TCGMSG. Benchmark calculations using 10 CPU of HP9000/735 workstations are carried out to investigae the scalability of this problem. we observed that almost linear scalability was obtained for this problem, and that the load unbalance appeared when some of CPU nodes were used for other jobs. To enhance the total throughput, we are now improving our code by using algorithm called "spool of tasks".

Chemical Materials Center

VIII—B Preparation and Properties of Novel Heterocyclic Compounds

Heterocycles containing sulfur or nitrogen atoms are useful as components of organic conductors since heteroatoms in their rings are helpful to stabilize ions or ion-radical species, and extended π-conjugation reduces Coulombic repulsion. In addition, intermolecular interactions caused by heteroatom contacts can be expected to form unique molecular assemblies. In this project novel electron acceptors and donors based on heterocycles such as 1,2,5-thiadiazole and 1,3-dithiole were synthesized and their properties including those of the charge-transfer complexes or ion-radical salts were investigated. Thiophene derivatives were also prepared and led to new types of polythiophenes by electrochemical oxidation.

VIII-B-1 Interaction of Bis(1,2,6,7-tetracyano-3,5-dihydro-3,5-diiminopyrrolizinide) Metal Complexes with Phenazine and Derivatives. Crystal Structures of Addition Compounds of the Nickel(II) Complex with Phenazine and 5,10-Dimethyl-5,10-dihydrophenazine

Mario BONAMICO*, Vincenzo FARES*, Alberto FLAMINI*, Nicola POLI*, Yoshiro YAMASHITA, and Kenichi IMAEDA *(*CNR, Italy)*

[*J. Chem. Soc., Dalton Trans.*, 3463 (1993)]

The charge-transfer compounds of the electron-acceptor moiety $[NiL_2]$ (L=1,2,6,7-tetracyano-3,5-dihydro-3,5-diiminopyrrolizinide) and the electron-donating phenazine derivatives [phenazine (phz), 5,10-dimethyl-5,10-dihydrophenazine (dmphz) and N-methylphenazinium cation (mphz)] have been synthesized and characterized. The X-ray crystal structures of $[NiL_2] \cdot 2phz \cdot 2MeCN$ and $[NiL_2] \cdot dmphz \cdot 2MeCN$ have been determined. Both compounds are monoclinic, mixed-stacked compounds with planar acceptor and donor moieties. The latter compound showed a semiconductive behavior (σ=3×10^{-4} S cm^{-1}, Ea=0.28 eV). The cobalt derivative $[CoL_2] \cdot dmphz \cdot 2MeCN$ has also been synthesized and characterized, which is isomorphous and isostructural with the nickel analogue.

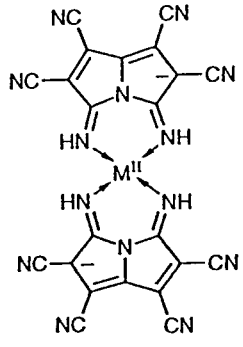

$[ML_2]$

VIII-B-2 Dithio-derivatives of p-Quinodimethanes Fused with 1,2,5-Thiadiazoles: a Novel Type of π-Donor-Acceptor System

Yoshiro YAMASHITA, Katsuhiko ONO, Shoji TANAKA, Kenichi IMAEDA, Hiroo INOKUCHI, and Mizuka SANO* *(*International Christian Univ.)*

[*J. Chem. Soc., Chem. Commun.*, 1803 (1993)]

4H,8H-(1,3-Dithiol-2-ylidene)benzo[1,2-c:4,5-c']bis[1,2,5]thiadiazole-4-one (BTQT) was prepared by a Wittig-Horner reaction of the corresponding dione. The longest absorption maximum was observed at 620 nm (sh) in a KBr disk. The X-ray analysis revealed that the planar molecules are uniformly stacked and the overlap mode is in accord with an effective interaction between the HOMO and LUMO, suggesting that an intermolecular charge-transfer interaction is possible in the crystal. Short interheteroatom contacts result in a novel three-dimensional structure. BTQT showed unusual behavior on measurement of the resistivity of single crystals. The correlation of the current with voltage *(E)* fails to obey Ohm's law. The current increases approximately in proportion to E^3.

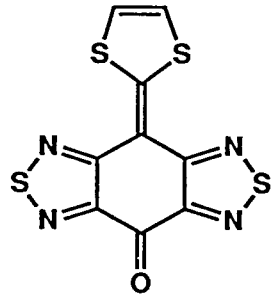

BTQT

VIII-B-3 Preparation and Properties of Novel Polythiophenes Containing 1,3-Dithiol-2-ylidene Moieties

Masatoshi KOZAKI, Shoji TANAKA, and Yoshiro YAMASHITA

[*J. Org. Chem.*, **59**, 442 (1994)]

Novel polythiophenes **1** and **2** were prepared by electrochemical oxidation of the corresponding monomers which were obtained using Wittig-Horner or Wittig reactions. Electrochemically dedoped films of **1** and **2** have interband absoptions at 610—690 nm and 420—590 nm, respectively. Some films exhibited high electrical conductivities with doping, for instance, **1c** $\cdot (PF_6^-)_x$; 33 S cm^{-1}, **1e** $\cdot (BF_4^-)_x$; 52 S cm^{-1}. Derivatives **1f-h**, containing linear alkyl chains, were found to be somewhat soluble in THF and chloroform. MNDO-PM3 calculations showed that the torsion angles between the neighbor monomer fragments in the dimers and trimers are about 30°.

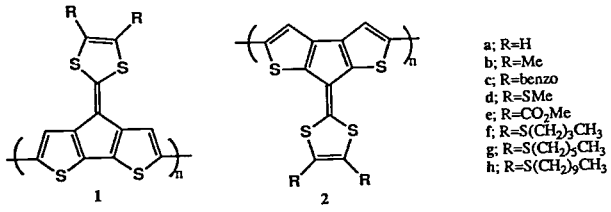

1 2

VIII-B-4 Nonplanar Bis(1,3-dithiole) Donors Affording Novel Cation Radical Salts

Yoshiro YAMASHITA, Katsuhiko ONO, Shoji TANAKA, Kenichi IMAEDA, and Hiroo INOKUCHI

[*Adv. Materials*, **4**, 295 (1994)]

Although a lot of donors and acceptors giving organic conductors are known, most of them are planar molecules. In contrast, bis(1,3-dithiole) compounds **1** are butterfly-shaped molecules owing to steric interactions between the peri-hydrogens and the S atoms. The X-ray structural analysis of the neutral molecule **1d** revealed that the deformed molecules are uniformly stacked with the good overlap between molecules. The cyclic voltammogram of **1** showed one-stage two-electron oxidation waves. This fact indicates that the cation radicals are thermodynamically unstable and undergo disproportionation very easily in solution. The dibenzo derivative **1d** gave the PF_6 and ClO_4 salts of the cation radical as single crystals on electrochemical oxidation. The electrical conductivity of the PF_6 salt at room temperature was fairly high (8.3 S cm^{-1}).

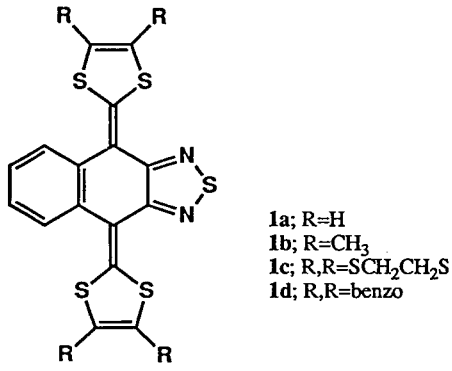

VIII-B-5 An Absolute Asymmetric Synthesis of the [2+2] Cycloadduct via Single Crystal-to-Single Crystal Transformation by Charge-Transfer Excitation of Solid-State Molecular Complexes Composed of Vinylbenzenes and Bis[1,2,5]thiadiazolotetracyanoquinodimethane

Takanori SUZUKI*, Takanori FUKUSHIMA*, Yoshiro YAMASHITA, and Tsutomu MIYASHI* *(*Tohoku Univ.)*

[*J. Amer. Chem. Soc.*, **116**, 2793 (1994)]

The title electron acceptor, BTDA, formed weak electron donor-acceptor (EDA) complexes with aryl olefins such as styrene (ST) and divinylbenzenes(DVs). Upon charge-transfer (CT) excitation of these complexes in MeCN, the [2+2]-type cycloadducts **1** were formed via a single electron transfer. Similar cycloaddition reactions were efficiently induced when the solid-state molecular complexes of BTDA and aryl olefins were irradiated. The reactivity of the o-DV · BTDA crystal was much higher than that in solution and the adduct was formed via the single crystal-to-single crystal transformation. Because of the asymmetric crystal structure of the complex, the optically pure product with 95% ee was obtained from the achiral components without any external chiral source.

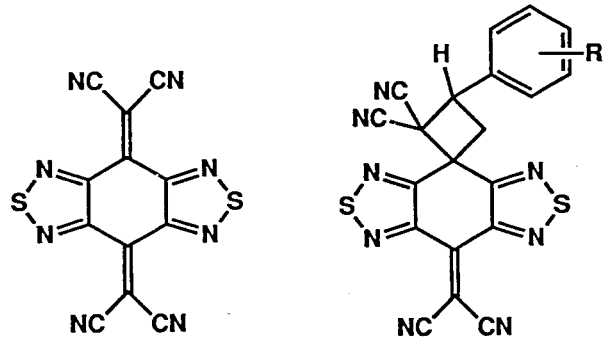

BTDA 1

VIII-B-6 Preparation and Properties of 7-(1,3-Dithiol-2-ylidene)-4-methyl-4,7-dihydro[1,2,5]thiadiazolo[3,4-b]pyridines: Novel Donor Molecules Containing a 1,2,5-Thiadiazole Unit

Katsuhiko ONO, Shoji TANAKA, Kenichi IMAEDA, and Yoshiro YAMASHITA

[*J. Chem. Soc., Chem. Commun.*, 899 (1994)]

A pyridone derivative **1** was obtained by methylation of the corresponding chloropyridine followed by hydrolysis. New donors **2** were prepared by using a Wittig-Horner reaction in 27—55% yields. The absorption maxima were observed around 510 and 490 nm, which are regarded as intramolecular CT bands. The parent compound **2a** was sublimed to give a single crystals as red needles. X-Ray structure analysis reveals that the crystal structure is constructed of a set of four columns which interact with each other by S---S contacts. The oxidation potentials of the donors are lower than that of TTF and they formed highly conducting complexes with TCNQ.

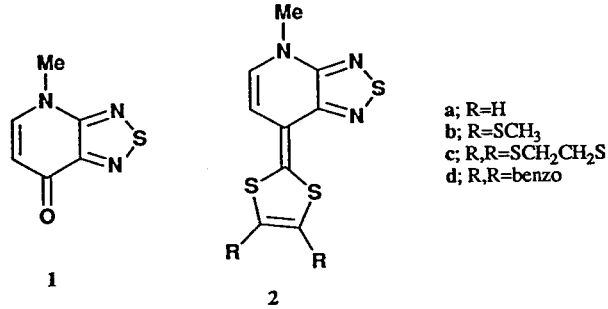

1 2

VIII-B-7 2-(Thiopyran-4'-yliden)-1,3-dithioles Fused with Thiophene Units: Intramolecular S---S Interaction Affecting the Redox Properties and Molecular Geometries

Takanori SUZUKI*, Tomoo SAKIMURA*, Shoji TANAKA, Yoshiro YAMASHITA, Hiroaki SHIOHARA*, and Tsutomu MIYASHI* *(*Tohoku Univ.)*

[*J. Chem. Soc., Chem. Commun.* 1431 (1994)]

Cyclic voltammograms of the title compounds **1a,b** showed two pairs of reversible waves corresponding to the two-stage one-electron oxidation. Although the first oxidation potential is almost the same as that of TTF, the difference between the first and second oxidation potentials is very small, indicating the reduced Coulombic repulsion. The X-ray structure analysis of **1b** shows the nonplanar geometry due to the repulsive contacts between S atoms (av. 3.06 Å). In contrast, the cation radical is endowed with the molecular planarity in spite of the shorter S---S contacts (av. 2.87 Å). Ab initio calculations indicate a considerable increase in atomic charge on thiophene S atoms in the cation radical state, suggesting that the positive charge is delocalized through the short S---S contacts.

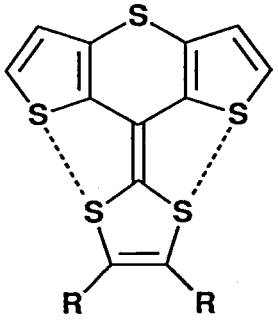

1a; R=H
1b; R,R=benzo

VIII-B-8 Novel Heterocyclic π-Conjugated Polymers Possessing Dihydropyrazine-pyrazine Multistage Redox System

Shoji TANAKA, Masaaki TOMURA, and Yoshiro YAMASHITA

Heterocyclic π-conjugated polymers changing band structure upon redox reactions have a large potential for application as molecular electric wire with switching function. As a model of such 'switching' polymers, we have synthesized novel mixed oligomers **1ox, 1red** and their polymers possessing dihydropyrazine/pyrazine redox center. In order to clarify the switching behavior of this system, the electronic properties of the oxidized and reduced forms have been investigated. The AM1 calculations for the oligomers suggested that the oxidized form **1ox** has a remarkably small HOMO-LUMO gap compared to the reduced form **1red** due to the more efficient π-electron delocalization over the ring system. The spectral and electrochemical data support this prediction. The lowest energy absorption maxima of **1ox** and **1red** appear at 990 nm and 350 nm, respectively. The cyclic voltammograms revealed that the oligomer **1ox** has a highly amphoteric redox property ($E_{p,a}$ of +0.87 V and $E_{p,c}$ of −0.19 V *vs.* SCE), while **1red** exhibits only oxidation peaks ($E_{p,a}$ of +0.80 V *vs.* SCE). As in the case of the oligomers, the electronic features of the corresponding polymers strongly depend on the redox states of the pyrazine part. The electronic spectrum of **poly-1ox** in the dedoped state exhibits an interband absorption in near IR region and the onset is below ~0.5 eV (the absorption edge can not be determined clearly because of the intense absorption of the ITO electrode itself), making it one of the lowest bandgap polymers reported to date. The cyclic voltammograms of **poly-1ox** show both oxidation and reduction waves; the electrochemical band gap determined from the thresholds for p-type and n-type doping is about 0.3 eV. In contrast **poly-1red** was electrochemically active only in the p-doping region. These findings suggest that this system can be a promising candidate for redox switching materials.

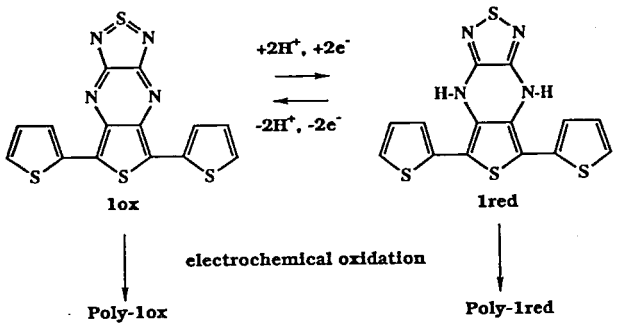

VIII-B-9 Synthesis, Structure, and Properties of Unsymmetrical Tetrathiafulvalene Derivatives Fused with 1,2,5-Thiadiazole Ring

Masaaki TOMURA, Shoji TANAKA, and Yoshiro YAMASHITA

In order to enhance intermolecular interactions in organic conducting solid by S•••N and S•••S heteroatom contacts, unsymmetrical tetrathiafulvalene (TTF) derivatives fused with a 1,2,5-thiadiazole ring were synthesized by a reaction of a 1,3-dithiol-2-one derivative fused with a 1,2,5-thiadiazole ring with various 1,3-dithiole-2-thione derivatives in the presence of trimethyl phosphite in toluene. The first oxidation potentials of TDA-TTF, DMTTDA-TTF, and EDTTDA-TTF (vs. SCE, in acetonitrile) were +0.69, +0.73, and +0.74 V, respectively. Electrolytic oxidation of EDTTDA-TTF with n-Bu_4NClO_4 as an electrolyte in tetrahydrofuran gave (EDTTDA-TTF)ClO_4 as a black crystal. Electrical conductivity of the salt at room temperature was 1.6×10^{-3} S cm^{-1}. The X-ray crystallographic analysis of DMTTDA-TTF indicated that a coplanar two-dimensional network was formed by short S•••N and S•••S contacts in the crystal, as shown in Figure 1. Crystal data for DMTTDA-TTF are: monoclinic, $P2_1/n$, a=7.923(5), b=12.690(3), c=13.366(3) Å, β=93.86(3)°, V=1340.8(8) Å^3, and Z=4.

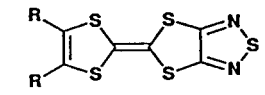

R	
H	TDA-TTF
SCH_3	DMTTDA-TTF
$-SCH_2S-$	MDTTDA-TTF
$-SCH_2CH_2S-$	EDTTDA-TTF

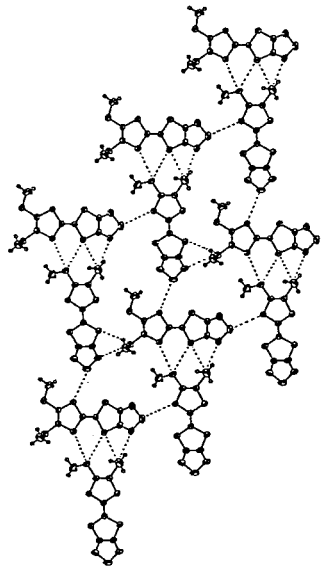

Figure 1. The two-dimensional network in the crystal of DMTTDA-TTF. The dotted lines show short intermolecular S•••N and S•••S contacts.

Instrument Center

VIII—C Studies of Solvated Metal Clusters

Solvated metal ions and metal cluster ions afford a particularly interesting collection of systems for study because they bridge the gap between bare, isolated ions and ionic solids and electrolyte solutions. From the point of view of cluster chemistry, the questions of charge delocalization, the formation of solvation shells, and the interaction of solvent with metal surfaces appear especially attractive.

In this project we investigate the photodissociation and photoelectron spectroscopies of various kinds of solvated metal atom (ion) clusters to unveil the microscopic aspect of solvation.

VIII-C-1 Photodissociation Process of $Ca^+(H_2O)_n$ (n=1–6)

Masaomi SANEKATA, Fuminori MISAIZU, and Kiyokazu FUKE

Photodissociation processes of size-selected $Ca^+(H_2O)_n$ (n=1–6) were examined in the wavelength region from 335 nm to 1440 nm using a reflectron mass spectrometer. The dissociation process of $Ca^+(H_2O)_n$ was found to be not only the simple evaporation of water molecules but also the photoinduced intracluster reaction including the hydrogen atom elimination. The dissociation spectra obtained by plotting the total yield of fragment ions as a function of wavelength exhibit large redshift as large as 18000 cm^{-1} for n=6. The spectra are assigned to the ^2P-^2S transition mainly localized on the metal ion. In contrast to $Mg^+(H_2O)_n$, [1] the amount of redshifts increases monotonically in the range from n=1 to 6. These results seem to consistent with the prediction of the Monte Carlo calculations, which suggests that the first shell around the Ca^+ ion closes with five and/or six water molecules.[2] Figure 1 shows the branching ratio of the $Ca^+(H_2O)_n$ (n=1–3) photodissociation as a function of the photolysis energy. As for n=1, the evaporation process is predominant in the lower excited states (Π-type), while the reactive fraction becomes substantially large in the higher excited state (Σ-type). These features in reactivity are marked contrast with those for $Mg^+(H_2O)$; in the latter case, the reaction to produce $MgOH^+$ is the dominant process exhibiting no excitation energy dependence. For n=2 and larger clusters, the reaction becomes the predominant process in the whole energy region examined. The large difference in the photodissociation processes of hydrated Mg^+ and Ca^+ ions are ascribed to the difference in the electronic structures of these ions; the ^2D state of Ca^+ lies between the

^2P and ^2S states and is deeply involved in the photodissociation process.

References

1) F. Misaizu, M. Sanekata, K. Fuke, and S. Iwata, *J. Chem. Phys.* **100**, 1161 (1994).
2) E. Kochanski and E. Constantin, *J. Chem. Phys.* **87**, 1661 (1987).

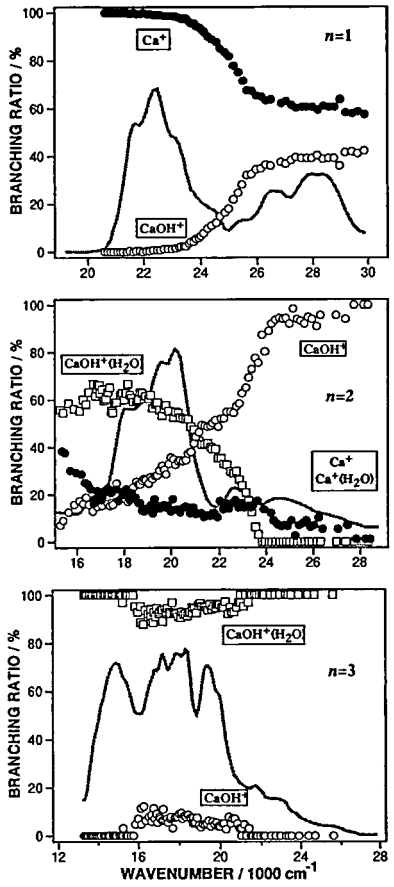

Figure 1. Branching ratios of the evaporation and reaction products in the photodissociation of $Ca^+(H_2O)_n$ (n=1–3) plotted as a function of photon energy. No evaporation product is detected for the n=3 photodissociation. The solid lines show the photodissociation spectra of each clusters obtained by plotting the total yield of the fragment ions.

VIII-C-2 Photoelectron Spectroscopy of Mass-Selected Copper-Water Cluster Negative Ions

Fuminori MISAIZU, Keizo TSUKAMOTO, Masaomi SANEKATA, and Kiyokazu FUKE

[*Laser Chem.*, in press]

Negative-ion photoelectron spectroscopy has been applied in order to obtain size dependent information about the electronic structures of clusters of metal atoms solvated with polar molecules. In the present work we have investigated the photoelectron spectra of $Cu^-(H_2O)_n$ cluster ions with n=0–4 and also those of $Cu_2^-(H_2O)_n$ with n=0 and 1. Cluster negative ions were directly produced by laser vaporization and were mass selected in a time-of-flight (TOF) mass spectrometer. After decelerating the ions by a potential switching method, the negative ions were irradiated with a detachment laser: the fourth harmonic of a Nd:YAG laser, 266 nm, was used for the detachment. Detached electrons were collected by a magnetic bottle photoelectron spectrometer and the photoelectron spectra were obtained by the TOF measurement of the electrons. Figure 1 shows the photoelectron spectra of $Cu^-(H_2O)_n$ and $Cu_2^-(H_2O)_n$. The ground state of the Cu^- ion is in the $^1S(3d^{10}4s^2)$ state and thus the s and d electron detachments to produce $^2S(3d^{10}4s^1)$ and $^2D(3d^94s^2)$ states of the Cu atom were observed at 1.23 and 2.7 eV in the photoelectron spectrum, respectively. In the spectra of $Cu^-(H_2O)_n$, the lowest energy bands were assigned to the electron detachment from the $CuOH^-(H_2O)_{n-1}$ which were produced in the source together with the above cluster ions. The observed bands for $Cu^-(H_2O)_n$ were all assigned to the transitions to the states originating in the ground ^2S and first excited ^2D states of the Cu atom. From the peak positions observed in the photoelectron spectra we have determined the hydration energies for the $Cu^-(H_2O)_n$ ions. The hydration energies were found to be almost constant at 0.5–0.6 eV for n=1–4. These values are almost consistent with those of hydrated halide negative ions by considering the electrostatic interaction between the atomic negative ion and the permanent dipole of water. As for the hydrated Cu_2^- ion, we have found that the hydration energy (ca. 0.4 eV) is slightly larger than that for $Cu^-(H_2O)$ (0.35 eV). This difference is considered to be mainly due to the stabilization of the dimer negative ions as a result of polarization.

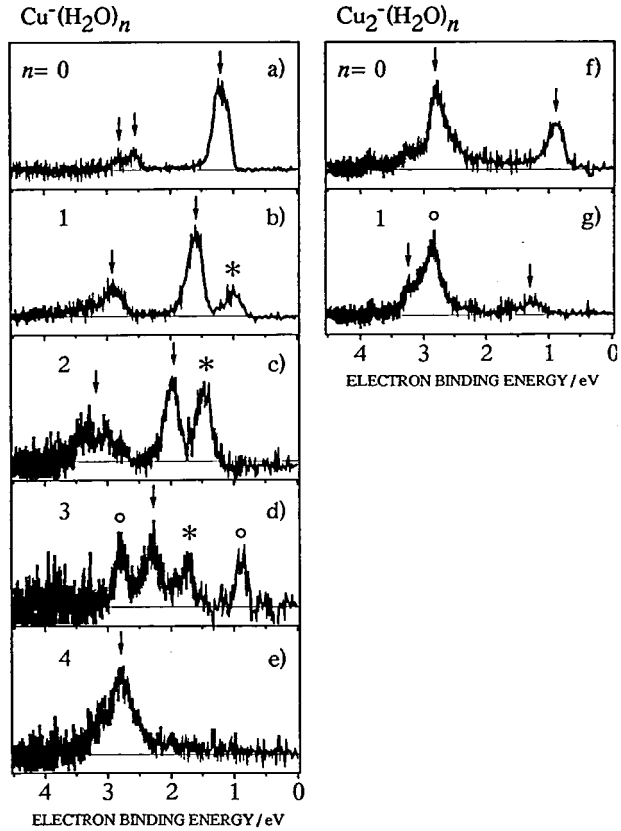

Figure 1. Photoelectron spectra of $Cu^-(H_2O)_n$ (n=0–4) and $Cu_2^-(H_2O)_n$ (n=0 and 1) with detachment wavelength at 266 nm (4.66 eV). Asterisks in b)–d) show the bands from the $CuOH^-(H_2O)_n$ ions. For the spectra of $Cu^-(H_2O)_3$ (d) and $Cu_2^-(H_2O)$ (g), the bands from coexisting ions which were not discriminated by pulsed mass gate are shown by circles.

VIII-C-3 Photoelectron Spectroscopy of Mass-Selected $Na^-(H_2O)_n$ Ions

Fuminori MISAIZU, Keizo TSUKAMOTO, Masaomi SANEKATA, and Kiyokazu FUKE

[*Surface Rev. and Lett.*, in press]

The clusters consisting of an alkali metal atom solvated by polar molecules are considered as a model of bulk solvated electron systems. Recently, Hertel et al. and our group were measured the ionization potentials of such clusters and obtained the results indicating that the ion-pair state which is a counterpart to the bulk hydrated electrons may be stabilized at fairly small number of solvent molecules for the $Na(H_2O)_n$ and $Cs(H_2O)_n$ clusters.[1,2] In order to examine the electronic structure of the clusters more directly and explicitly, photoelectron spectroscopy of the $Na^-(H_2O)_n$ ions is investigated in the present study.

Figure 1 shows photoelectron spectra of $Na^-(H_2O)_n$ cluster ions obtained with detachment wavelength at 355 nm for n=0 and 1, and at 266 nm for $2 \leq n \leq 7$. The spectrum of Na^- (Fig.1(a)) consists of two bands peaked at 0.55 and 2.65 eV. These bands correspond to the transitions of Na (^2S)←Na^- (^1S) and Na (^2P)←Na^- (^1S), respectively. The photoelectron spectra of $Na^-(H_2O)_n$ with n up to 7 all exhibit two-band features analogous to that of Na^-, though the electron binding energies at the peaks, i.e., vertical detachment energies (VDEs), increase gradually with increasing n. This observation implies that the valence electron of the sodium atom in the clusters is still localized on the atom and that the detachment energy simply increases as a result of hydration. As for the electronic states of the neutral $Na(H_2O)_n$, we detected the excited states which originate from Na(^2P) and no other state assignable to the ion-pair state like $Na^+(H_2O)_n^-$, which is expected to correspond to the solvated electron in the bulk solution. In contrast, the VDEs plot vs. $(n+1)^{-1/3}$ (the variable is inversely proportional to the cluster radius) shows that the VDEs linearly increase with decreasing $(n+1)^{-1/3}$ and can be extrapolated to the value of 3.2 eV at $(n+1)^{-1/3}=0$, i.e., $n=\infty$. This value corresponds to the photoelectric threshold for bulk hydrated electrons. This observation implies that ground electronic states of the $Na^-(H_2O)_n$ negative ion clusters with n more than a few water molecules may already have a nature of bulk hydrated electrons.

References

1) I. V. Hertel , C. Huglin, C. Nitsch and C. P. Schulz, *Phys. Rev. Lett.*, **67**, 1767 (1991).
2) F. Misaizu, K. Tsukamoto, M. Sanekata and K. Fuke. *Chem. Phys. Lett.*, **188**, 241 (1992).

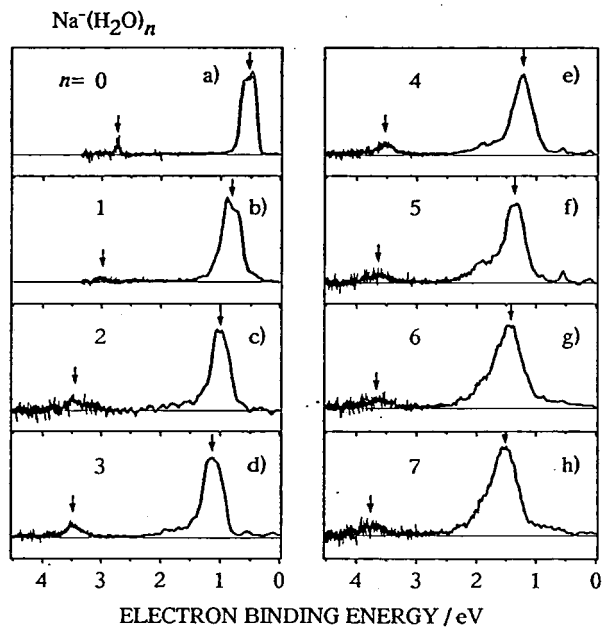

Figure 1. Photoelectron Spectra of $Na^-(H_2O)_n$ obtained with detachment wavelengths at 355 nm (3.49 eV) for n=0 and 1 and at 266 nm (4.66 eV) for n=2–7. Peak positions of the lower energy band in each spectrum for $n \geq 2$ are reproduced within an error of 0.10 eV in the spectra obtained with detachment wavelength at 355nm.

VIII—D Studies on Hypervalent Molecular Clusters

Electron delocalization in finite clusters has been the subject of intensive studies. Various clusters such as negatively-charged cluster ions, clusters containing neutral alkali atoms, etc., have been investigated in relation to this topic. Recently, we extended these studies to the clusters containing a Rydberg radical such as NH_4. This radical is isoelectronic with an alkali atom, and thus its solvated clusters may serve as a new model to get further insight into the fundamental interaction of electrons with polar solvent molecules.

VIII-D-1 Electronic Structure and Stability of $NH_4(NH_3)_n$ Clusters

Kiyokazu FUKE, Ryozo TAKASU, and Fuminori MISAIZU

[*Chem. Phys. Lett.*, **229**, 597 (1994)]

In the present work, the electronic structure and stability of $NH_4(NH_3)_n$ were studied by one-photon ionization and time-of-flight (TOF) mass spectroscopy. $NH_4(NH_3)_n$ were formed by the photolysis of jet-cooled ammonia clusters with an ArF excimer laser at 193 nm. Clusters were photoionized by a dye laser and mass-analyzed by a reflectron TOF mass spectrometer. The lifetimes of these clusters were estimated by measuring the intensity of $NH_4^+(NH_3)_n$ as a function of the pump-probe time delay. The photoionization thresholds for $NH_4(NH_3)_n$ (n=0–35) were determined by recording the mass spectra produced with various photon energies; 4.76–2.07 eV (260–600 nm). The results of IPs are summarized in Figure 1. From the results on IP as well as the successive binding energies of $NH_4^+(NH_3)_n$ determined by high-pressure mass spectroscopy,[1] we estimated the binding energies of $NH_4(NH_3)_n$ for n up to 6. These results show that the clusters have much larger binding energies than that for ammonia itself and their bonding

character is to some extent ionic. The lifetime (τ) of NH_4 is reported to be on the order of 10 ps, but those for clusters are found to be elongated extensively; 1 $\mu s < \tau < 10$ μs for $n \leq 4$ and $\tau > 130$ μs for $n \geq 5$. The enhanced stability for the large clusters may be ascribed to the increasing ionic character in the ground state. As seen in Fig. 1, the IPs for $NH_4(NH_3)_n$ decrease more or less monotonically with decreasing $(n+1)^{-1/3}$ to a limit coincides with the estimated IP of an excess electron solvated in bulk ammonia (ca. 1.4 eV). This trend in IPs is similar to that found previously for the Cs-ammonia system.[2] These resuts are discussed in relation to the electron localization modes in these clusters.

References

1) M. Meot-Ner (Mautner) and C. V. Speller, *J. Phys. Chem.* **90**, 6616 (1986).
2) F. Misaizu, K. Tsukamoto, M. Sanekata and K. Fuke, *Chem. Phys. Lett.* **188**, 241 (1992).

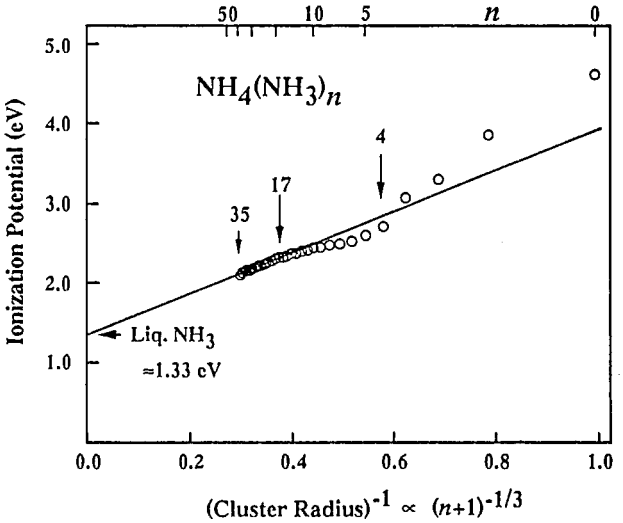

Figure 1. Ionization potentials of $NH_4(NH_3)_n$ (n=0–35) plotted versus $(n+1)^{-1/3}$. The estimated errors for the present IPs are ±0.03 eV. The result of the least-squares fitting for n=15–35 is also shown. The extrapolated value to $(n+1)^{-1/3}=0$ ($n \to \infty$) is 1.33 eV. The correlation coefficient of the fitted line, r, is 0.987.

VIII-D-2 Photoionization Study of $NH_4(NH_3)_m(H_2O)_n$

Ryozo TAKASU, Kiyokazu FUKE, and Fuminori MISAIZU

[*Surface Rev. and Lett.*, in press]

$NH_4(NH_3)_m(H_2O)_n$ was studied by one-photon ionization and time-of-flight (TOF) mass spectroscopy. The clusters were produced by an ArF excimer laser photolysis of ammonia-water binary clusters formed by expanding the He gas bubbled through a heated liquid ammonia-water. Figure 1a shows the photoionization mass spectrum of $NH_4(NH_3)_m(H_2O)_n$ produced by the sequential absorption of two 193-nm photons. On the other hand, Fig. 1b shows the mass spectrum obtained with the 280-nm photon as the ionization light source; the delay time between the photolysis and ionization lasers is 500 ns. These results indicate that NH_4 radical is also stabilized in the ammonia-water binary clusters. The IPs of these clusters were determined by measuring the photoionization efficiency curves. As for NH_4-H_2O, the IP is estimated to be 4.07 eV and is higher than that for NH_4-NH_3 (3.88 eV). Using the binding energy of NH_4^+-H_2O determined by high-pressure mass spectroscopy (0.89 eV[1]) as well as the IP of NH_4, the binding energy of NH_4-H_2O is estimated to be 0.34 eV. The IPs of $NH_4(NH_3)_m(H_2O)_n$ show a clear trend; the clusters with the same solvation number k ($k=m+n$), the IPs decrease monotonically with increasing number of NH_3 molecules. This trend is ascribed to the large binding energy of NH_4^+–NH_3 (1.08 eV[1]) comparing with that for NH_4^+–H_2O. The trend in IPs within the same k seems to indicate that NH_3 binds directly to NH_4.

Reference

1) M. Meot-Ner (Mautner) and C. V. Speller, *J. Phys. Chem.* **90**, 6616 (1986).

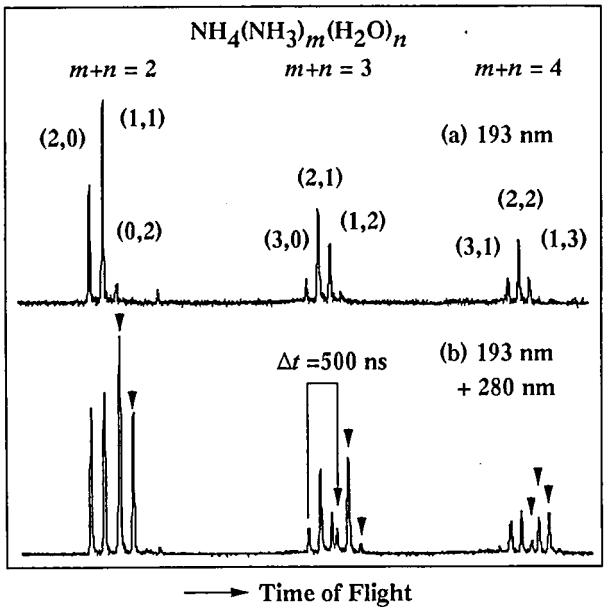

Figure 1. (a) Typical TOF mass spectrum of protonated ammonia-water binary clusters obtained by two-photons of ArF excimer laser at 193 nm. (b) TOF mass spectrum at delay time of 500 ns between the pump (193 nm) and the probe (280 nm) lasers.

VIII—E Collisional Relaxation and Chemical Reaction Dynamics of the Excited Group IIB Metal Atoms

The collisional quenching and chemical reaction of electronically excited metal atoms have been the subject of extensive studies because of its importance in photophysics and photochemistry. In the present project we seek to obtain more detailed information about the reaction dynamics of the excited group IIB metal atoms.

VIII-E-1 Nascent Internal State Distributions of ZnH($X^2\Sigma^+$) Produced in the Reactions of Zn(4^1P_1) with Simple Alkane Hydrocarbons

Hironobu UMEMOTO, Shigeru TSUNASHIMA, Hiroyuki IKEDA, Kazuto TAKANO, Kazuya KUWAHARA, Kei SATO *(Tokyo Inst. of Tech.)*, **Keiichi YOKOYAMA** *(J. Atomic Energy Res. Inst.)*, **Fuminori MISAIZU, and Kiyokazu FUKE**

[*J. Chem. Phys*, **101**, 4803 (1994)]

The reactions of Zn(4^1P_1) with CH_4, C_2H_6, C_3H_8, and $C(CH_3)_4$ were studied by employing a laser pump and probe technique. The nascent rotational and vibrational state distributions of ZnH($X^2\Sigma^+$) produced in the reaction of Zn(4^1P_1) and alkane hydrocarbons were determined. The rotational distributions of ZnH ($X^2\Sigma^+$, v'=0) could be approximated by Boltzmann distributions. The corresponding Boltzmann temperatures decreases with the size of the hydrocarbons. ZnH($X^2\Sigma^+$) was also vibrationally excited. As sumarized in Table 1, the distributions for the complex alkanes such as $C(CH_3)_4$ resembled to the statistical ones, while those for simple alkanes such as CH_4 were a little hotter than the statistical ones. These results suggest that the reaction proceeds via relatively long-lived insertive complexes. The quantum yield of ZnH was the largest for CH_4. This suggests the presence of C-C bond cleavage for heavier alkanes.

Table 1. Vibrational state distributions of ZnH($X^2\Sigma^+$) produced in the reactions of Zn(4^1P_1) with alkanes

Alkane		v'=0	v'=1	v'=2	v'=3
CH_4	experimental	1.0	0.8	0.4	0.12
	prior	1.00	0.57	0.32	0.17
	RRKM	1.00	0.53	0.27	0.13
C_2H_6	experimental	1.0	0.6	0.3	0.10
	prior	1.00	0.38	0.14	0.05
	RRKM	1.00	0.39	0.15	0.05
C_3H_8	experimental	1.0	0.5	0.2	0.07
	prior	1.00	0.3	0.08	0.02
	RRKM	1.00	0.31	0.09	0.02
$C(CH_3)_4$	experimental	1.0	0.3	0.1	0.03
	prior	1.00	0.22	0.05	0.01
	RRKM	1.00	0.19	0.03	0.01

VIII—F Studies of Ultrafine Particles

To study the size effect of electron spin ordering and transportation properties, various kinds of ultrafine particles are produced by a newly developed Laser pyrolysis technique. Furthermore, the synthesis mechanism of ultrafine particles by the Laser pyrolysis and the catalytic activity of Mo-based nanoparticles are studied.

VIII-F-1 Properties of Crystalline CoS_2 Nanoparticles Produced by CO_2 Laser Pyrolysis

S. BANDOW, W.-T. LEE*, R. OCHOA*, M. HOLDEN*, Xiang-Xin BI, Y. MARUYAMA and P. C. EKLUND*** *(*Center for Applied Energy Research, University of Kentucky, **Massachusetts Institute of Technology)*

CoS_2 nanoparticles were produced by the laser driven pyrolysis of $C_5H_5Co(CO)_2$ with H_2S. The production rate was only 50 mg/hr, because of the low vapor pressure of this precursor. Other Co-carbonyl precursors were found to be too reactive, spontaneously reacting with the H_2S without laser assistance. X-ray diffraction indicated the particles were primarily CoS_2 with a very small admixture of β-Co. Transmission electron microscopy showed that the particles were indeed single crystals with an average diameter of 5 nm. Bulk CoS_2 is ferromagnetic with a Curie temperature of 122 K. To study the magnetism in these nanoparticles, we have measured the heat capacity by an adiabatic method between 60 and 180 K, and no sign of the magnetic transition was detected.

VIII-F-2 Investigation of the Intercalation of Rb into MoS_2 Nanoparticles

S. BANDOW, W.-T. LEE*, R. OCHOA*, M. HOLDEN*, Y. MARUYAMA and P. C. EKLUND* *(*Center for Applied Energy Research, University of Kentucky)*

MoS_2 nanoparticles (*ca.* 8 nm in diameter) were first produced by the laser driven pyrolysis of vapors of $Mo(CO)_6$ with H_2S. C_2H_4 was admixed with these reactants for use as a passive power absorbing gas to couple the CO_2 laser radiation into the reactant gas stream. The as-synthesized MoS_2 nanopowder was then intercalated with Rb by placing these components in opposite ends of a sealed and evacuated glass ampoule which was then heated in a furnace. X-ray diffraction and TEM showed that the host MoS_2 was indeed single crystal nanoparticles, although many particles exhibited stacking faults along the *c*-axis. Raman scattering and conduction electron spin resonance CESR were used ex situ to monitor particle sintering and the Rb-intercalation process. The latter proceeds rapidly at low temperatures (*ca.* 140 C) due to the high crystallinity and nanoscale size of the host particles. Superconductivity has been observed in bulk $Rb_{0.3}MoS_2$ at 9K. Experiments to determine the superconducting properties of our material are in progress.

VIII-F-3 Correlation of the Reaction Pressure and Crystalline Phase of Fe-Carbides Produced by CO_2 Laser Pyrolysis

S. BANDOW, W.-T. LEE*, Xiang-Xin BI, Y. MARUYAMA and P. C. EKLUND*** *(*Center for Applied Energy Research, University of Kentucky, **Massachusetts*

Institute of Technology)

FeC_x nanoparticles were produced by the CO_2 laser driven pyrolysis of $Fe(CO)_5$ with C_2H_4. Maintaining all other process parameters fixed (e.g., nozzle dia. 1mm, laser power 100 W, C_2H_4 flow at 80 sccm), the chamber pressure was increased systematically from 200 to 500 Torr. Under these conditions, the nanoparticles so produced were observed to evolve from α-Fe at low pressure to Fe_3C at intermediate pressures, and finally to Fe_7C_3 at the highest pressures. These results can be explained in terms of the Fe-C phase diagram and the relative rates of diffusion of the Fe-carbonyl and ethylene out of the reaction zone.

VIII-F-4 Relative Activity and Selectivity of Nanoscale Mo_2N, Mo_2C and MoS_2 Catalysts Prepared by Laser Pyrolysis

R. OCHOA*, G.T. HAGER*, W.-T. LEE*, S. BANDOW, Y. MARUYAMA, P.C. EKLUND*, F. DERBYSHIRE* and E. GIVENS* *(*Center for Applied Energy Research, University of Kentucky)*

Nanocrystalline Mo_2N, Mo_2C and MoS_2 catalysts with relatively high surface area (63, 75 and 84 m^2/g, respectively) have been synthesized by Laser Pyrolysis from the reaction of an organometallic precursor ($Mo(Co)_6$) with a gaseous reactant (NH_3, H_2S and C_2H_4). Characterization of these particles by X-ray diffraction and transmission electron microscopy showed them to be monophasic with a narrow particle size distribution (average particle size is 4 nm). The crystalline phases have been identified as 2H-MoS_2, cubic Mo_2C and γ-Mo_2N.

The catalytic activity of these nanoparticles has been investigated for various model compound reactions representative of the main reaction processes occuring during coal liquefaction: aromatic hydrogenation, bond cleavage and heteroatom removal (O, S, N). The results of the activity and selectivity of these catalysts compared to those from the reactions over a molybdenum-promoted sulfated hematite, indicate that the ultrafine particles posses high activity for heteroatom removal with selectivity toward production of aromatics and poor activity for bond cleavage.

VIII—G Studies of Nanoscale Carbons

Arc-derived nanoscale carbons, single- and multi-wall carbon nanotubes, are synthesized and characterized by Raman spectroscopy and powder X-ray diffraction. Carbon nanocapsules including Sc-carbide are also studied by transmission electron microscopy and powder X-ray diffraction.

VIII-G-1 Raman Scattering from Nanoscale Carbons Generated in a Co-Catalyzed Carbon Plasma

J.M. HOLDEN*, Ping ZHOU*, Xiang-Xin BI*, P.C. EKLUND*, Shunji BANDOW, R.A. JISHI, K.Das CHOWDHURY***, G. DRESSELHAUSE* and M.S. DRESSELHAUSE**** *(*University of Kentucky, Center for Applied Energy Research, **California State University, ***Massachusetts Institute of Technology)*

[*Chem. Phys. Lett.*, **220**, 186 (1994)]

Carbonaceous material including nanoscale soot, carbon-coated nanoscale Co Particles and nanotubes have been generated from a dc arc discharge between carbon electrodes. Sharp first- and second-order lines are observed in the Raman scattering spectra of the arc-derived carbons only when Co metal is present in the core of the anode. The sharp lines in the Raman spectrum of the Co-catalyzed, arc-derived carbons have not been observed previously in carbonaceous materials and are tentatively assigned to carbon nanotubes on the basis of a zone-folded model for the vibrational spectra of armchair tubules.

VIII-G-2 Interlayer Thermal Expansion of Carbon Nanotubes

Shunji BANDOW

The morphological properties of arc derived carbon nanotubes are studied by powder X-ray diffraction. Small interlayer thermal expansion coefficient α_c compared with that of HOPG (highly oriented pyrolytic graphite) is obtained for carbon nanotubes. The values of α_c for carbon nanotube, turbostratic graphite and HOPG at 220 K are $1.71 \pm 0.04 \times 10^{-5}$, $2.04 \pm 0.06 \times 10^{-5}$ and 2.58×10^{-5} K^{-1}, respectively. These values and temperature dependence of α_c for carbon nanotubes are explained by the turbostratic nature of graphite: Multi-wall carbon nanotubes do not have concentric cylindrical structure but have highly defective rolled paper structure.

VIII-G-3 Synthesis of $Sc_{15}C_{19}$ Crystallites Encapsulated in Carbon Nanocapsules by Arc Evaporation of Sc-C Composite

Yahachi SAITO*, Mitsumasa OKUDA*, Tadanobu YOSHIKAWA*, Shunji BANDOW, Saeki YAMAMURO, Kimio WAKOH**, Kenji SUMIYAMA** and Kenji SUZUKI**** *(Mi'e University, **Tohoku University)*

[*Jpn. J. Appl. Phys.*, **33**, L186 (1994)]

Crystalline of scandium carbides nesting in multilayered, polyhedral graphitic cages (nanocapsules) were produced by evaporating a scandium-graphite composite rod by electric arc discharge in helium gas. The composite particles were characterized by analytical electron microscopy and X-ray diffraction. The encapsulated scandium carbide was identified to be $Sc_{15}C_{19}$, instead of dicarbide RC_2 (R represents rare-earth elements) which was the form of carbide commonly found for other rare-earth elements entrapped in nanocapsules. The size of the capsules ranged from about 10 to 100 nm. Morphological features of the other graphitic carbon, multilayered and polyhedral, were quite similar to those previously discovered for the capsules protecting RC_2 (R = Y, La, Ce, ..., Lu).

VIII—H Solid State NMR Study of Inclusion Compound

VIII-H-1 ^{13}C Solid-state NMR Study on Populations, Conformations, and Molecular Motions of γ-Valerolactone Enantiomers Enclathrated in the Chiral Cholic Acid Host

Fumio Imashiro*, Daisuke Kuwahara and Takehiko Terao* *(*Kyoto Univ.)*

[*J. Chem. Soc. Perkin Trans.* 2, 1759 (1993)]

^{13}C Solid-state NMR were measured for γ-valerolactone in the cholic-acid host which exhibits efficient optical resolution. Both the more-favored (S)-(-)-enantiomer [(S)-1] and the less-favored (R)-(+)-enantiomer [(R)-1] of γ-valerolactone were found to coexist microscopically in the cholic-acid channels by two-dimensional exchange NMR. Their populations were non-destructively determined from the intensities of their methyl-carbon signals. The principle values of the ^{13}C chemical-shift tensors for the methyl carbons were determined by the one dimensional switching-angle sample spinning(1D-SASS) NMR method. By comparing the ^{13}C chemical-shift tensors with those calculated by the ab initio GIAO method, the conformation of each enantiomer was determined as follows: (S)-1 has the methyl group in the equatorial direction to the five-membered ring of γ-valerolactone, while (R)-1 has it in the axial direction. The optical resolution of γ-valerolactone by the inclusion method using the cholic-acid host mainly ascribed to the energy difference in the conformations of γ-valerolactone. Temperature variation of the ^{13}C chemical-shift power pattern for the methyl carbons of both enantiomers revealed the presence of an overall reorientation among a finite number of isotropically distributed sites accompanying slow rotational diffusion. The rate of the reorientation for (S)-1 is higher than that for (R)-1; moreover, the corresponding barrier for (S)-1 is notably lower than that for (R)-1.

Equipment Development Center

VIII—I Activities of Division of "IMS Machines"

Equipment Development Center has the division for construction of so-called "IMS Machines", which are designed on the basis of ideas and/or proposals from the members of the Institute for Molecular Science. New technologies required for their construction are developed by the staff of this division with an introduction of recently developed engineering and in collaboration with researchers of other institutes, universities and facilities of industries. The main aim of these activities is to expand technical capability of this center, intending a development of future technology of the molecular science.

In this fiscal year, 1993, the project themes listed below were adopted as IMS Machines. Their construction is now under way.

1. Broad-Band Infra-Red Window for Ultra-High-Vacuum Apparatus
(Tsuneo URISU and Norio OKADA, cooperated by Takao NANBA (Kobe University) and Sumitomo Electric Industries)
2. Time-of-Flight-Type Mass-Spectrometer for High-Mass Materials
(Mitsukazu SUZUI, Hisashi YOSHIDA, Tadaoki MITANI(JAIST), and Shimadzu Corporation).

For fiscal year of 1994, three themes listed below were newly selected as IMS Machines, and one theme as survey project.
1. High Precision Slit Driver for Ultra-High-Vacuum Monochromator
(proposed by Masao KAMATA)
2. Electron-Stimulated-Desorption-Ion-Angular-Distribution Detector with Time-of-Flight Type Mass Separator
(proposed by Kyoichi SAWABE)
3. Light Beam Path Stabilizer
(proposed by Shuji ASAKA)
4. ESR Resonator for High-Pressure and Low-Temperature Sample (survey project)
(proposed by Kyuya YAKUSHI)

Application of patents is promoted in this division. For fiscal year of 1993, two titles listed below were applied.
1. Valve Driver for Low Temperature Liquid Transfer Tube
2. Time-of-Flight Type Mass-Spectrometer

VIII-I-1 Broad-Band Infra-Red Window for Ultra-High-Vacuum Apparatus

The aim of this project is the development of an infra-red window for ultra-high-vacuum apparatus by utilizing a diamond plate. High purity diamond has the following advantages as an optical window material: a wide optical transmission range extending from ultra-violet to sub-millimeter region except the intrinsic absorption around 2000 cm^{-1}, no deliquescence, and a high mechanical strength. The recently developed diamond synthesis by a vapor phase deposition has enabled us to obtain a diamond plate with a very high purity and a large area.

We have tested our method of fixing the window

material to a metal frame on a sample supplied by Sumitomo Electric Industries, and found that the adhesion strength is sufficient. Optical transmission property has also been investigated under a cooperation of Prof. Namba (Kobe University). As seen in Figure 1, it showed a good transmission characteristics.

Manufacturing of diamond plates for this project is now under way.

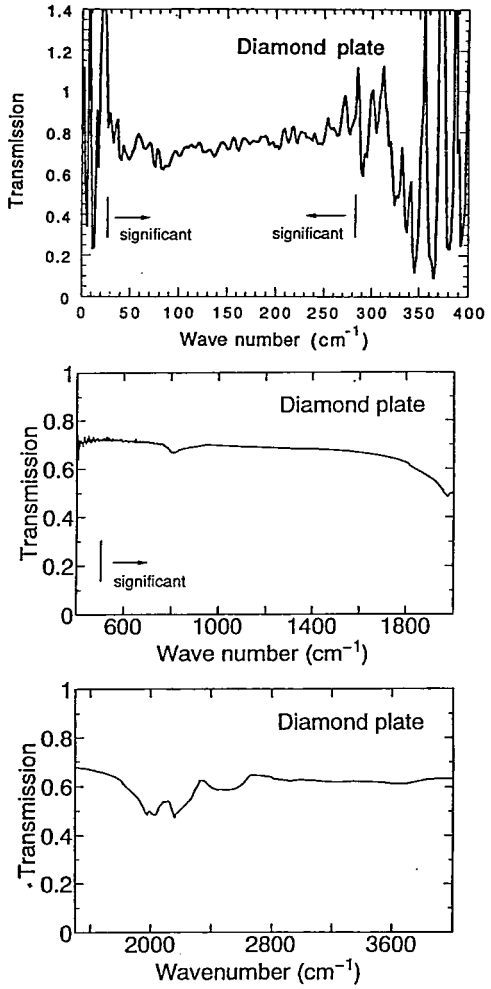

Figure 1. Optical transmission of CVD diamond plate of thickness 0.25mm

VIII-I-2 Time-of-Flight-Type Mass-Spectrometer for High-Mass Materials

This project is aimed at developing a mass spectrometer for analyzing fullerenes with carbon atoms over 100. The project "mass spectrometer for separating fullerenes" was selected as IMS machine survey theme in 1992, and after one year of feasibility survey the project in the title has been selected as a subgoal to the final target.

The under-development mass spectrometer is a time-of-flight type analyzer with an ion stream chopper (Figure 1). We have designed it to obtain a mass resolution of 200, and to be usable in negative CI and laser ionization modes. After a detailed ion trajectory analysis under a cooperation of Shimadzu Corporation a new design has been adopted, which enables a high resolution relatively easily. A prototype of the analyzer is now under construction.

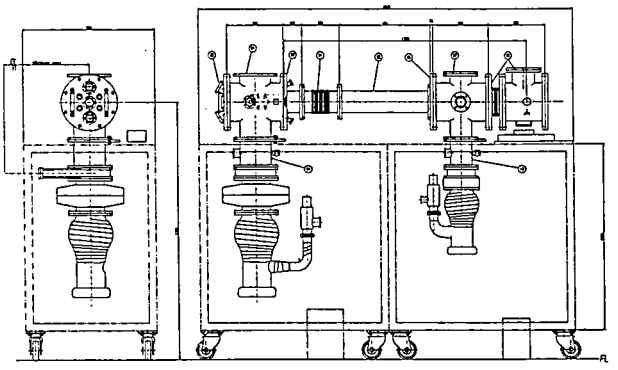

Figure 1. Outline design of time-of-flight-type mass-spectrometer for high-mass materials

VIII—J Development of Experimental Devices

VIII-J-1 Fullerene Generator

Masaaki NAGATA, Shinji KATO, Koichi UCHIYAMA, and Tadaoki MITANI *(JAIST)*

A fullerene generator has been newly developed aiming at the investigation of fullerene generation process (Figure 1). Improvements in design compared to the last developed one (IMS Annual Review, 141 (1992)) are as the following. Carbon electrode feeders have been designed so that they can be electrically motor-driven. Water cooling of the whole generator device has been enabled. Thus the device has become quite compact, and its operation and maintenance procedure has been simplified. Under planning now is the connected operation of the present generator and the TOF mass spectrometer, which is being constructed as an IMS machine.

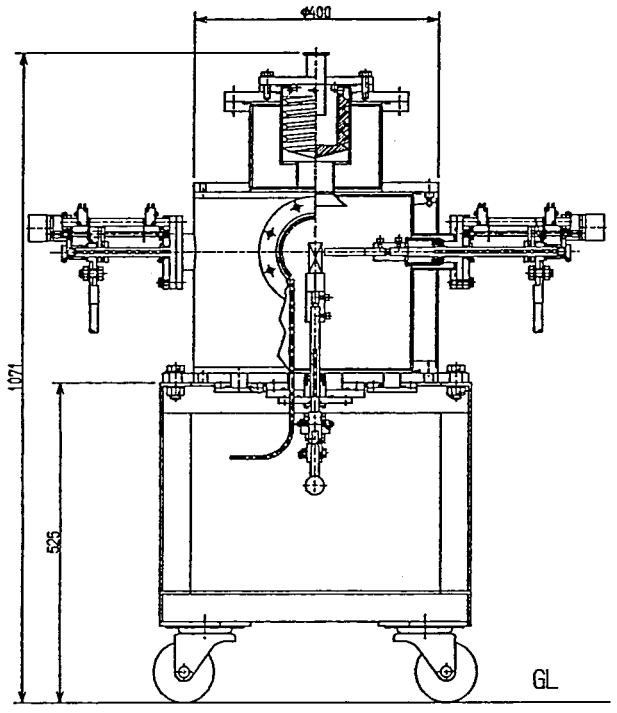

Figure 1. Newly developed fullerene generator

VIII—K Site-Selective Fluorescence Spectroscopy on Dye Molecules in Amorphous Matrices

Recently, we have developed a technique to measure the laser-induced fluorescence spectrum, including the narrow resonance fluorescence line appearing at the same wavelength as the exciting light, for localized centers with short fluorescent decay times in condensed matter. A method to obtain the fluorescence spectrum of dye molecules in a single site in disordered host matrices by the use of saturation effect of the laser-induced fluorescence has also been devised [see, J. S. AHN et al., J. Lumin. **48/49**, 405 (1991); Phys. Rev. B **48**, 9058 (1993)]. These methods give us valuable information on guest-host interactions and host dynamics.

VIII-K-1 Determination of Weighted Density of States of Vibrational Modes in Zn-substituted Myoglobin

Jeung Sun AHN, Yasuo KANEMATSU*, Makoto ENOMOTO*, and Takashi KUSHIDA* *(*Osaka Univ.)*

[*Chem. Phys. Lett.*, **215**, 336 (1993)]

Site-selective fluorescence spectroscopy has been performed for Zn-substituted myoglobin in the lowest optical absorption band at 4K. The single-site fluorescence spectrum as well as the distribution of the zero-phonon transition energy have been obtained. Furthermore, the density of states of vibrational modes of myoglobin weighted by the coupling strength between the chromophore and the polypeptide chain has been determined from the analysis of the obtained spectrum. This is the first case in which the weighted density of states of low-frequency vibrational modes has been determined in biological materials without employing any model shape functions. The results are compared with those for dye-doped polymers.

VIII-K-2 Site-Selective Fluorescence Spectroscopy of Metal Porphyrins in Noncrystalline Materials

Jeung Sun AHN, Yasuo KANEMATSU*, Yoshito NISHIKAWA*, and Takashi KUSHIDA* *(*Osaka Univ.)*

[*Synthetic Metals*, in press]

The absorption spectra and excitation-frequency dependence of the resonance fluorescence spectra have been measured and calculated for centro-symmetric metal porphyrins doped in polymer films (MgOEP-doped PS and MgOEP-doped PMMA) and naturally occurring dye-polymer system (Zn-substituted myoglobin) in the lowest optical absorption band at 4 K. In the calculation, we used the experimentally determined site-distribution function and single-site fluorescence spectrum, and assumed that the mirror-symmetry relation holds between the absorption and fluorescence spectra. The fitting curve reproduces the experimental curve quite well in ZnMb. In the case of MgOEP-doped PMMA, the difference between the fitting and experimental absorption curves is quite large and the resonance fluorescence spectra for the case of excitation at the higher-energy region of the Q(0,0) band are not reproduced well. The closed circles in Figure 1(a) denote the distribution of the integrated intensity of the difference between the calculated and measured resonance fluorescence spectra as a function of the wavenumber of the exciting

laser light. These circles reproduce the dash-dotted line quite well. Similar results were also obtained for MgOEP-doped PS. These results indicate that the observed Q(0,0) absorption bands of MgOEP-doped PMMA and MgOEP-doped PS consist of two components. A part of the excitation into the higher excited state may result in the fluorescence from the lower excited state through the fast intramolecular relaxation. The disagreement for the case of excitation at the higher-energy region of the Q(0,0) absorption band is attributed to such additional fluorescence. The splitting of the doubly degenerate excited state corresponding to the Q(0,0) absorption band is considered to be caused by the interaction between the porphyrin molecule and its environment. If so, the lifted state must be also observed in ZnMb. The broad fluorescence spectrum has been obtained at 4 K under the excitation at the high-energy region of the Q(0,0) absorption band of ZnMb. This indicates that the absorption band shown in the high-energy region of Figure 1(b) corresponds to the higher excited states.

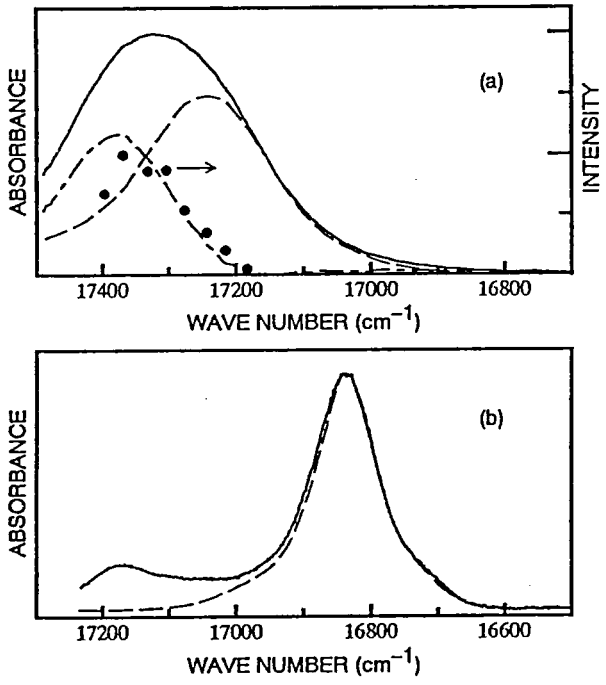

Figure 1. (a) The dash-dotted curve is the difference between the absorption spectrum (solid line) of MgOEP-doped PMMA at 4 K and a fitting curve (dashed line). (b) The absorption spectrum (solid line) of ZnMb at 4 K and a fitting curve (dashed line).

VIII-K-3 Glass Transition of Zn-substituted Myoglobin Probed by Absorption and Site-Selective Fluorescence Spectroscopies

Jeung Sun AHN, Teizo KITAGAWA, Yasuo KANEMATSU*, Yoshito NISHIKAWA*, and Takashi KUSHIDA* *(*Osaka Univ.)*

It is believed that a protein molecule has a large number of conformational substates because of its complexity and flexibility[1]. At physiological temperatures, a protein molecule fluctuates among many substates, and it is said to be fluid-like. At sufficiently low temperatures, on the other hand, each protein molecule freezes in some substates, and it becomes glass-like. To confirm this, we studied the temperature dependence of absorption and resonance fluorescence spectra of ZnMb in the temperature range between 4 and 300 K. If we employ linear approximation of the electron-phonon coupling, we can calculate the homogeneous fluorescence profile at various temperatures using the experimentally determined weighted density of states of low-frequency vibrational modes (WDOS). Furthermore, under the assumption that the mirror-symmetry relation holds between the absorption and fluorescence spectra, we can also calculate the temperature dependence of the absorption and resonance fluorescence spectra using the calculated homogeneous fluorescence profile and experimentally determined site-distribution function $G_T(\omega')$. The measured absorption and fluorescence spectra are well reproduced by the calculation below ~180 K. The electronic ground state of ZnMb is in thermal equilibrium above the glass transition temperature Tg. Thus, we calculated $G_T(\omega')$ in this temperature region assuming the Boltzmann distribution in the ground state by the use of $G_T(\omega')$ which was experimentally determined at 4 K. The dash-dotted curves in Figure 1 show the calculated $G_T(\omega')$ at each temperature for Tg=180 K. The absorption spectra observed at higher temperatures than 180 K are reproduced well by the calculation, in which we used the calculated $G_T(\omega')$ at each temperature instead of experimentally determined one at 4 K. Thus we conclude that ZnMb undergoes a liquid-glass transition around 180 K.

Reference

1) H. Frauenfelder, F. Parak and R. D. Young, *Ann. Rev. Biophys. Biophys. Chem.* **17**, 451(1988).

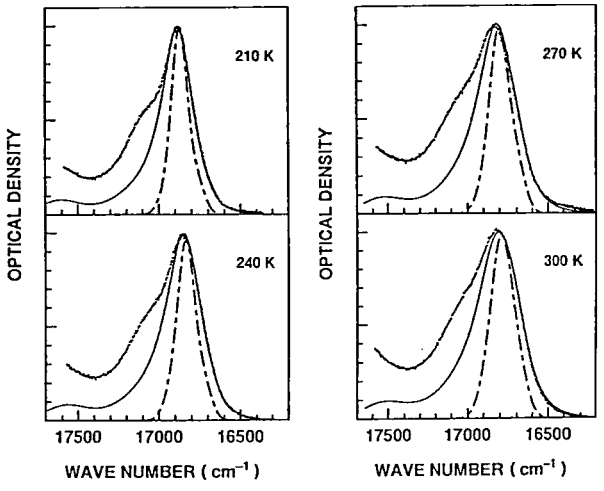

Figure 1. Absorption spectra of ZnMb in a glycerol-water (3:1) mixture at higher temperatures than 180 K. The solid lines are theoretical curves obtained from the calculated site-energy distribution function (dash-dotted line) for each temperature.

Ultraviolet Synchrotron Orbital Radiation Facility

VIII—L Development of the UVSOR Light Source

VIII-L-1 Observation of Micro-Macro Temporal Structure and Saturation Mechanism on the UVSOR-FEL

Hiroyuki HAMA, Jun-ichiro YAMAZAKI, Toshio KINOSHITA, Kazuhiko KIMURA, and Goro ISOYAMA* *(*Osaka Univ.)*

Dynamical study of a free electron laser on the UVSOR storage ring has been performed using a high resolution streak camera. It is well known phenomenon that the laser macro-temporal structure strongly depends on the detuning condition, which is one of important characteristics of the storage ring FEL dynamics. In the UVSOR-FEL, quasi-periodical pulse lasings are seen under the best synchronization between the electron bunch and the optical bunch in the cavity, and cw-like continuous lasing appears as the detuning is increased. Such two different structures have been observed on other storage rings. We recently succeeded to observe both temporal structures of laser micro- and macro-temporal structure by applying a two dimensional double-sweep technique for the streak camera. It was found out that the continuum structure is consisted of piles of many micropulse evolutions which are drifting from top to edge of the electron bunch because of the detuned condition. In this lasing case, the bunch length is a bit longer than the ordinal length and almost constant. While the best synchronized lasing, the macropulse is evolved on near the top of the bunch and the bunch length is oscillating.

To investigate the laser saturation mechanism and the bunch-heating phenomenon, the micro-macro structure was also measured with the gain-switching mode. The time dependent variation of the effective gain was calculated from the shape of the macropulse detected by a photodiode. The initial gain agreed well with the theoretical prediction as reported previous issue. The bunch length became longer as growing the laser micropulse, and after passing the maximum point of the laser power, shortening of the bunch length began due to radiation damping. Assuming the bunch length is changed by variations of the energy spread, the relative gain evolution was deduced from the peak density of electrons in the bunch and the energy spread obtained from the bunch length. As shown in Figure 1, the deduced gain evolution was in good agreement with the effective gain obtained from the shape of the macro pulse. As far as the lasing in the gain-switching mode, we can conclude that saturation mechanism of the laser power is interpreted by gain reduction due to the bunch-heating in the laser oscillation.

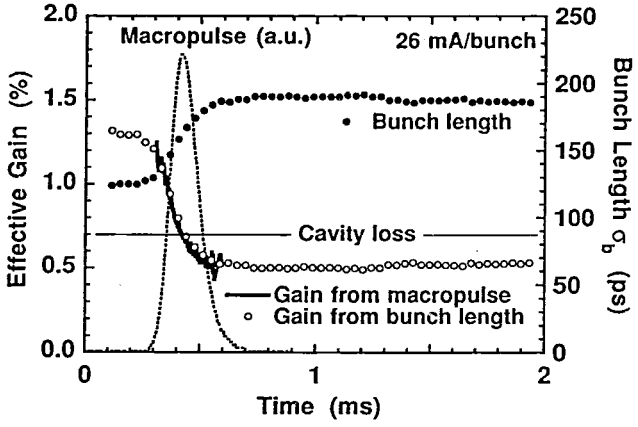

Figure 1. Evolutions of the bunch length and the effective gain in the gain-switching mode. Solid and open circles denote the bunch length and the effective gain derived from the dual-sweep spectrum of the electron bunch, respectively. Solid line shows the gain evolution derived from the laser macropulse measured by the photodiode.

VIII—M Development of Beam Lines and Equipment for UVSOR

VIII-M-1 Construction of Constant-Length Spherical Grating Monochromator

Atsunari HIRAYA, Eiken NAKAMURA, Masami HASUMOTO, Toshio KINOSHITA, Kusuo SAKAI, Eiji ISHIGURO*, and Makoto WATANABE** *(*Osaka City Univ., **RISM, Tohoku Univ., and IMS)*

A constant-length spherical grating monochromator (CL-SGM) for VUV to Soft X-ray was constructed at the bending-magnet beam line 8B1 of the UVSOR. The monochromator has a simple scanning mechanism with fixed entrance and exit slits, as well as fixed directions of incident and exit photon beams. The monochromator was designed to cover the photon energy of 31—620 eV with three interchangeable gratings. All gratings are master gratings with laminar amplitude fabricated on a synthetic quartz and coated with Au. The resolving power evaluated by ray-tracing at the lowest energy of each grating with 10 μm slit widths is ~4400 for two high energy gratings and ~7000 for a low energy grating.

In the preliminary performance check, it was found that the output spectrum of the monochromator extends from 30eV to 1 keV with intensity of $10^8 \sim 10^{10}$ photons/sec. Figure 1 shows the nitrogen K-edge absorption spectrum in the $1\sigma \rightarrow 2p\pi^*$ region of gaseous N_2 molecules measured with using the highest energy grating and 10 μm slit width. The spectrum exhibits clearly resolved vibrational structure. The resolving power at 400 eV was estimated to be ~4000, that is in good agreement with the designed value.

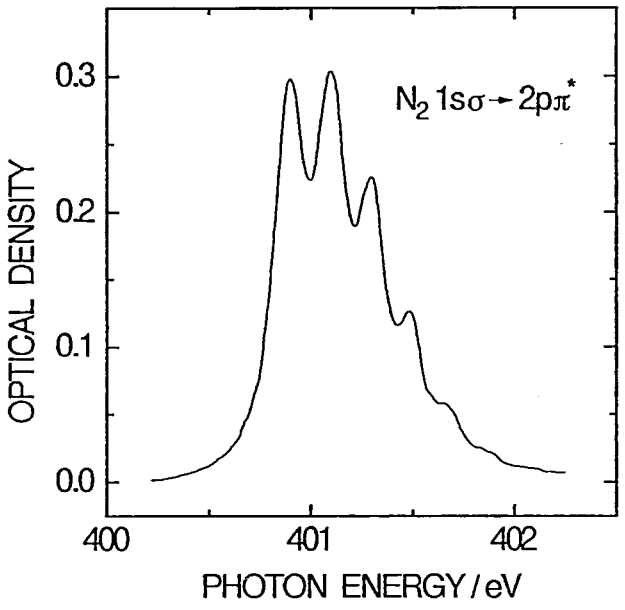

Figure 1. Nitrogen K-edge absorption spectrum in the 1sσ→2pπ* region of gaseous N_2 molecules measured with using the highest energy grating and 10 μm slits.

VIII—N Researches by the Use of UVSOR

VIII-N-1 Time Response of Photon-Stimulated Desorption of Excited-State Sodium Atoms from Sodium Halides

Sayumi HIROSE and Masao KAMADA

[*Phys. Rev. B* **48**, 17641 (1993)]

The time response of excited-state sodium desorption from NaF and NaCl has been investigated with synchrotron-radiation pulses. The decay curve of the Na D-line intensity from a desorbed excited-state sodium atom is found to consist of a fast component in the ns range and a slow component between 178 ns and 3 ms. This successful observation of the time response of excited-state alkali desorption suggests there are two types of desorption mechanism, a slow one originating from the thermal instability of surface defects and a fast one due to the lattice instability induced by an electronic transition in the surface layer.

VIII-N-2 Accumulated Photon Echoes Generated by Synchrotron Radiation

Hiroshi ITOH*, Synsuke NAKANISHI*, Masaya KAWASE*, Hitoshi FUKUDA, Hiroki NAKATSUKA**, and Masao KAMADA** *(*Kagawa Univ., **Univ. Tsukuba)*

[To be published in *Phys. Rev. A*]

We demonstrate that the accumulated photon echoes can be generated by synchrotron radiation. We believe this is the first experiment of nonlinear optical effect carried out by using radiation from an electron storage ring. A dye-doped polymer film was excited by a visible light from the storage ring and the accumulated photon echoes from the sample were observed by employing a phase modulation technique. The use of synchrotron radiation facilitates to extend the spectral range where we can observe photon echoes with ultra-high time resolution.

VIII-N-3 Observation of Surface Core-Excitons in Alkali Chlorides

Shin-ichiro TANAKA and Masao KAMADA

While the optical spectra of the alkali halides have been extensively studied, less are known about their surface property. We measured the Cl-$L_{2,3}$ absorption spectra of alkali chlorides (KCl and NaCl) via Cl-LVV Auger electron yield, and observed the surface core-exciton. The experiments are carried out by using the grasshopper monochromator and a double-pass CMA at BL2B1 of UVSOR. KCl and NaCl were evaporated on the Si(100)(2×1) surfaces. Figure 1 shows the spectra of KCl/Si(100) as a function of thickness (indicated in ML) of the film at RT. Peaks A and C (spin-pair) are ascribed to surface-excitons, while peaks B and D are ascribed to bulk-excitons [similar peaks are observed in the total-yield spectrum (dotted line)] of the KCl film. The surface core (Cl-$L_{2,3}$)-excitons are located at photon energy of 0.7 eV below the bulk core-excitons. Similar results were observe for NaCl/Si(100). The photoelectron spectra were also measured, and have shown that there were no surface core-level shifts in Cl-2p level for these systems. The AES spectra, when excited by photons whose energies corresponding to the surface excitons and the bulk excitons, were investigated in detail.

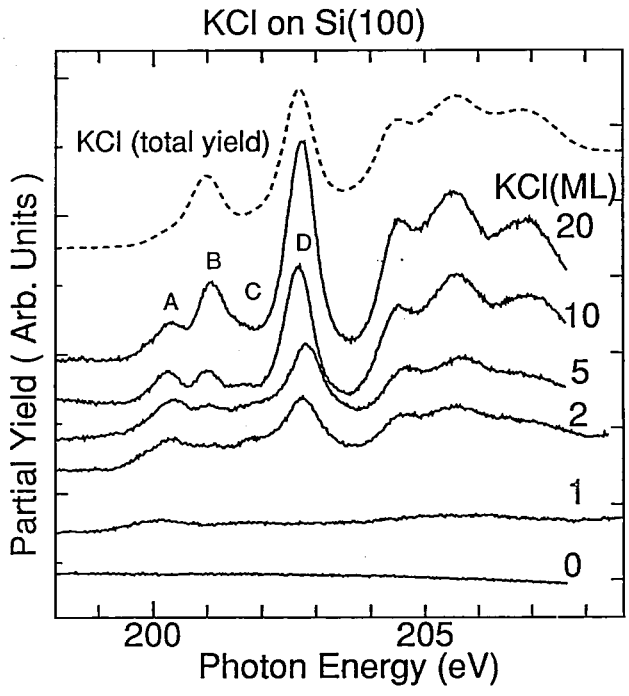

Figure 1. The Cl-$L_{2,3}$ abosrption spectra via Auger yield of KCl evaporated on the Si(100)(2×1) surface, as a function of thickness of the film. Indicated thickness (in ML; Mono Layer) were estimated using peak heights of K-LVV, Cl-LVV, and Si-LVV in AES. Total yield spectrum (dotted line) of the 20ML film are also shown.

VIII-N-4 Optical Observation of the Interaction between Low Frequency Plasma and Magnetic Field in $La_{2-x}Sr_xCuO_4$ (x=0.1)

Shin-ichi KIMURA, Mikihiko IKEZAWA*, Hironao KOJIMA, and Masashi TACHIKI*** *(*Tohoku Univ., **Yamanashi Univ.)*

Reflectivity spectra of $La_{2-x}Sr_xCuO_4$ (x=0.1) were measured with the c-axis polarization light in the wave number range between 10 and 40 cm^{-1} at 14 K under magnetic fields up to 5 tesla which was applied perpendicularly to the c-axis. It was observed for the first time that the behavior of the low energy plasma changes by magnetic field. The reflectivity below the plasma edge decreases as the magnetic field increases. The phenomenon is quantitatively consistent with the theoretical expectation. The origin is considered to be due to the vortex motion diven by the applied electric field.

RESEARCH FACILITIES

For the sake of brevity the present issue includes only the newly installed facilities and the activities since September 1993. Concerning the activities and facilities before September 1993, please refer to older IMS Annual Review issues (1978 ~ 1993).

Computer Center

The main computers at the Center are a supercomputer NEC SX-3/34R and a main-frame computer HITAC M-680. The computers are linked to international networks through Tokyo University International Science Network (TISN). About 40% of the computer time is used by the research staff at IMS, and the remaining 60% is given out as research grants to scientists outside the institute in molecular science and related field. As of March 1994, the number of project group was 187, consisting of 645 users.

In January, 1995, the HITAC M-680 is to be replaced by IBM SP2 (48 nodes) and NEC HSP (High Speed Scalor Proccessor). Total CPU performance of these system is about 4 GFLOPS, and will provide a powerful computational environment for molecular science.

The library programs of the Center amount to 805. Among them, about 200 programs can be excuted immediately. Recent additions include GAUSSIAN 92. The Quantum Chemistry Literature Database (QCLDB) has been developed by the Center in collaboration with the QCLDB group. The database CMQCA, IR2, STERIC, and QCBDB are also available at the center.

Chemical Materials Center

The Chemical Materials Center plays an important role in the synthesis and purification of chemical substances in IMS. The scientists and technical associates of this facility support other people in IMS to carry out the above works. Upon request, technicians carry out elemental and mass spectrometric analyses of new compounds prepared at IMS. They also carry out their own researches on synthesis of new interesting compounds, developments of new selective chemical transformations, elucidation of reaction mechanism, and application of new methodologies developed in IMS to the analysis of chemical substances and reactions.

Instrument Center

For the efficient use of instruments, the center is equipped with various types of instruments for general use.[1)]

Reference

1) *List of Instruments*, No.9, IMS Instrument Center (1994).

Low-Temperature Center

The main must of Low-Temperature Center is a steady supply of liquid helium and liquid nitrogen to the users in the Institute. The total amounts of liquid helium and liquid nitrogen supplied in 1993 were 37,695 *l* and 71,963 *l*, respectively.

Newly equiped machines of a dilution refrigerator (KELVINOX 36115, Oxford Instruments) and a SQUID magnetometer (MPMS 2, Quantum Design) are now available for general users.

Equipment Development Center

A number of research instruments have been designed and constructed by making use of the mechanical, electric and glass-blowing technologies at this Facility. Representative instruments developed during this fiscal year of 1993 are listed below.

Cryostat for Liquid Helium Temperature
Electron Beam Position Monitor
Secondary Electron Detector for Measuring a Metastable Atomic Beam
Liquid-Nitrogen-Cooled Discharge Metastable Atomic Beam Source
Cryostat for Optical Measurement at Liquid Helium Temperature
Variable Height Miniature Slit
Compact Z-Stage with High Load Capacity
UHV Sample Transfer System
Fullerrene Generator
Fast Rising High Voltage Pulse Generator
Deflector Voltage Controller
Powder Trap for Distilling Unit
Quartz Furnace Tube for Sublimation

Division of IMS Machines

Equipment Development Center has the division of IMS Machines. Activities of this division is described in detail in the research activities section.

Ultraviolet Synchrotron Orbital Radiation Facility

The UVSOR light source is usually operated at an electron energy of 750 MeV with an initial current of 200 mA. A higher harmonic PF system has been installed in order to suppress longitudinal coupled bunch instability with a double RF system. The instability was successfully suppressed in machine study and the system is routinely used for user experiments in multi-bunch operation. Another advantage of the double RF system is that the beam lifetime increases from 200 to 350 min. in multi-bunch operation at 200 mA because the bunch length becomes 2-3 time longer. The superconducting Wiggler with a magnetic field of 4 T is operated to provide soft x-rays up to 1.5 A. At BL8B1 a 15-m Constant Deviation Grazing Incidence monochromator has been constructed for soft x-ray spectroscopy and a high resolving power of 4,000 is achieved at 400 eV. A new monochromator named SGM-TRAIN has been designed for experiments using circulary polarized radiation with a spin resolved photoelectron spectrometer, and is now under construction at BL5A.

SPECIAL RESEARCH PROJECTS

IMS has special research projects supported by national funds. Three projects presently in progress are:

(1) Development and evaluation of molecular synergistic systems and their application to chemical energy conversion (1990–).
(2) Materials science on molecular devices (1990–).
(3) Material control in multi-reaction centers (1993–).

These projects are being carried out with close collaboration between research divisions and facilities. Collaborators from outside also make important contributions. Research fellows join these projects. The results in 1993 are reviewed in this report.

(1) Development and Evaluation of Molecular Synergistic Systems and their Application to Chemical Energy Conversion

Development of High-Sensitivity Submillimeter-Wave to Far Infrared Spectroscopic System for the Study of Transient Molecules

Shuji SAITO and Hiroyuki OZEKI

Spectroscopy in the submillimeter-wave to far infrared region has been less exploited when compared with that in other regions, because high-spectral purity and tunable radiation sources have not been available. However, recent development of radio astronomy has given much interest to this wave-length region with which warmer physical phenomena such as star-forming activity are concerned. This urges us to develop a high-sensitivity and high-resolution spectroscopic method in this region where many spectral lines of atomic fine-structure and various fundamental light molecules have not been measured.

We develop a frequency-tunable sideband far-infrared spectrometer suitable for the study of transient species. Spectroscopy of transient species needs much power so that we employ a combination of a far-infrared laser and microwave sources with a nonlinear mixer element. We installed a stable high-power CO_2 laser and an optically pumped far infrared laser which generates several fixed frequency lines between 600 to 3000 GHz. We designed and constructed a mixer mounting with non-linear element of GaAs Schottky diode, which is mounted in a Martin-Puplett diplexer separating a tunable sideband radiation from the fundamental laser beam.

Studies on Laser Cooling and Trapping of Neutral Atoms

Norio MORITA, Mitsutaka KUMAKURA, and Yoshiki MORIWAKI

We have constructed a gas-circulation system with a purification mechanism for helium atoms, and combined this system with the laser cooling/trapping apparatus so far used. This combined apparatus is mainly used for the laser cooling/trapping of ^{3}He atoms. For laser cooling/trapping of helium atom, it is unavoidable to use an atomic beam as a source of atoms to be cooled and trapped, because this atom is so light that it requires a long distance to decelerate the atomic velocity sufficiently. Although it is usual in ordinary atomic and molecular beam experiments to throw away the used gas carried in a beam, the ^{3}He gas is so expensive that we cannot discard it through vacuum pumping. This is why we need such a gas-circulation system. The system consists of a helium-tight vacuum pump and compressor, gas reservoirs, oil mist filters, active charcoal filters cooled by liquid N_2, and many valves and gauges to control the path of gas. With this system, we can get back more than 99.97% of helium gas ejected in vacuum chambers, keeping impurities within 20 ppm.

We have also made an important improvement on the metastable helium source. For laser cooling/trapping of helium atom, the atom must be excited to the triplet metastable state. Although the electron bombardment, which we have so far used, is a useful method to produce slow metastable helium atoms, its efficiency is too low to generate a sufficient number of metastable atoms. On the other hand, the dc discharge is a very efficient method, but it significantly increases the atomic temperature to make the laser cooling almost impossible in a laboratory-size cooling distance. Therefore, we have designed a new discharge cell that can suppress the temperature increase. It is in brief a liqN_2-cooled discharge cell, but is specially designed to get optimal cooling efficiency. With this metastable source, we have successfully achieved a great enhancement in the intensity of a metastable helium beam slow enough to be laser-cooled within a reasonable distance. As a result, 10^7 helium atoms have been laser-trapped at a temperature of 200μK. This number is about three orders of magnitude larger than ever achieved for helium atoms. With the above circulation system and the latter metastable source, about the same number of ^{3}He atoms have also been trapped (see II-C-1).

Mechanism of Oxygen Activation by Heme-Cupper Terminal Oxidase Superfamily

Teizo KITAGAWA, Takashi OGURA, Shun HIROTA, Denis A. PROSHLYAKOV, Shinya YOSHIKAWA *(Himeji Inst. Tech.)*, **Tatsushi MOGI** *(Tokyo Univ.)*, **Nobuhito SONE** *(Kyushu Inst. Tech.)*, **and Evan H. APPELMAN** *(Argonne Natl. Lab.)*

The terminal oxidase of respiratory chain is cytochrome *c* oxidase for aerobic organisms and quinol oxidase for *E. coli.* Both have two heme groups; one works for electron transfers and the other provides the catalytic site for dioxygen reduction. The heme iron at the catalytic site is antiferromagnetically coupled with a copper iron in the oxidized state. The dioxygen reduction is coupled with proton translocation through membrane, generating electrochemical potential which could be used for ATP synthesis. The final goal of this study is to elucidate the coupling mechanism between the electron- and proton transfers, but currently a mechanism of dioxygen reduction at the catalytic site is of spectroscopic concern. For bovine cytochrome *c* oxidase, we investigated reaction intermediates present in the time range between 0.1 and 5.4 ms following initiation of the reaction by using time-resolved resonance Raman spectroscopy combined with our original "artificial cardiovascular system for pursuit of enzymic reaction". The first intermediate gave the oxygen isotope-sensitive band at 571 cm^{-1} for $^{16}O_2$. Since the corresponding band for $^{16}O^{18}O$ split into two bands, it became confident that the binding of O_2 is of an end-on type. We succeeded in resolving the subsequent oxygen-isotope-sensitive band at 788 cm^{-1} into two components at 804 and 785 cm^{-1} by using a monochromator with higher resolution. It became clear from the experiments at lower temperatures that the 804 cm^{-1} species appears prior to the 785 cm^{-1} species. Although the appearance of the 804 cm^{-1} was of a similar rate between in H_2O and D_2O, that of the 785 cm^{-1} band was significantly slower in D_2O, suggesting that the generation of 785 cm^{-1} species from the 804 cm^{-1} species is coupled with the proton translocation. The experiments with $^{16}O^{18}O$ revealed that both bands should arise from the Fe^{IV}=O stretching but not from the O—O stretching. The reaction of oxidized enzyme with hydrogen peroxide also gave the 804 cm^{-1} band for the species called "peroxo species". Consequently, it is likely that the 785 cm^{-1} band arises from the ferryloxo species like compound II of peroxidases but the 804 cm^{-1} band arises from ferryloxo porphyrin π cation radical or corresponding oxidation state. Resonance Raman experiments were also carried out with *E. coli* cytochrome *bo* and *Bacillus* PS3 cytochrome *cao.*

Laser Raman Beat Detection of Magnetic Resonance

Tatsuhisa KATO and Michio MATSUSHITA

Laser Raman beat detection is a coherent optical- RF double resonance technique where the optical and RF field induce coherence within a three level system and a resultant Raman beat signal is detected using heterodyne detection. This technique can be applied to the study of electron paramagnetic resonance and nuclear magnetic resonance not only in the ground state of a molecule but also in the electronic excited state.

There are some causes to hide the Raman beat signal, that is, the inhomogeneity of the circumstance of the molecule, the fluctuation of the applied field, and the interference by the crystal phonon. It is the key to success in the Raman beat detection to eliminate these causes of the incoherence. Then it is needed to prepare the sophisticated single crystal sample, the highly stabilized magnetic field, and a cryostat of liquid helium. It has been completed to set up the apparatus, and the Raman beat detection is applied to the study on the triplet state of the fullerene crystal and the color center of a diamond.

Liquid Dynamics Studied by New Ultrafast Nonlinear Spectroscopies

Keisuke TOMINAGA, Yukito NAITOH, Tai Jong KANG *(Taegu Univ.),* **Gary P. KEOGH** *(Imperial College of Science, Technology, and Medicine),* **and Keitaro YOSHIHARA**

In the vibrational spectroscopies it is one of the key issues to distinguish homogeneous and inhomogeneous contributions to vibrational line broadening. Since the homogeneous and inhomogeneous contributions result from rapid perturbation to the oscillator and difference of the environment around the molecule of interest, respectively, it is possible to investigate microscopic liquid dynamics by distinguishing the two contributions. However, it is well known that frequency- or time-domain spectroscopies which are based on the third-order nonlinearlity are incapable of distinguishing the homogeneous and inhomogeneous contributions unambiguously. On the other hand, echo-type experiments, which make use of temporal two-dimentionality, have been proved to be a powerful technique to determine relative importance of inhomogeneity of dephasing process as demonstrated in magnetic resonance. We have been working on vibrational echo-type experiments on liquids in order to distinguish homogeneous and inhomogeneous contributions to the linewidths. This technique requires the application of the two excitations at different times, 0 and Δt_1, and each excitation consists of two short pulses to create vibrational coherent state by Raman transition. Vibrational coherence is detected by observing anti-Stokes Raman scattering induced by a fifth pulse at $\Delta t_1+\Delta t_2$. Two different experiments, Raman echo and five-pulse correlation experiments, have been performed to study dephasing processes of high frequency intramolecular and low frequency intermolecular vibrational modes, respectively. See Section III-B for detail.

Studies of Laser-Induced Photochemistry on Solid Surfaces

Yoshiyasu MATSUMOTO, Kyoichi SAWABE, Kazuo WATANABE, Hiroyuki KATO *(Graduate Univ. for Advanced Studies),* **and Yuri A. GRUZDKOV**

Light sources such as lasers and synchrotron radiation can be very useful for the various processes in the fabrication of microelectronics, including etching, chemical vapor deposition, atomic layer epitaxy. On the other hand, it has also been well recognized that there is an important class of catalytic reactions with the aid of photon irradiation. Although those applications of light are practically useful and important, fundamental understandings of these processes are still lacking. Therefore, this project is mainly aimed for investigating how the interaction of light and adsorbates and/or substrates promotes chemical reactions from the fundamental point of view.

We have utilized time-of-flight (TOF) spectroscopy of neutral species desorbed from the surface with sub-monolayer coverage together with the conventional techniques in surface science such as low energy electron diffraction, Auger electron spectroscopy, and temperature-programmed desorption. In this year, we have made a couple of modifications in the UHV apparatus: (1) X-ray photoelectron spectroscopy has been introduced. This reinforces our ability to clarify adsorbed states and serves to measure adsorbate coverage. (2) A closed-cycle He refrigerator is equipped with a sample manipulator. This improves our cooling capability; single crystals can be effectively cooled to ~40 K.

We have investigated photodissociation dynamics of nitrous oxide adsorbed on semiconductor surfaces and found that photodissociation dynamics depends significantly on the adsorbed state of N_2O. Furthermore, we have uncovered that methane physisorbed on Pt(111) can be effectively dissociated with the irradiation of 193 nm-photons, yielding a chemisorbed CH_3 radical and an adsorbed H atom as products. To our knowledge, this is the first observation of UV-photodissociation of methane on a well-defined surface and may open a new way to activate methane by the UV photons that can be readily obtained with a commercially available excimer laser.

Self-Organization in Chemical Reactions

Ichiro HANAZAKI, Yoshihito MORI, Noriaki OKAZAKI*, Tetsuo SEKIGUCHI*, Vladimir K. VANAG, and Gyula RÁBAI***** *(*Graduate University for Advanced Studies, **N.N.Semenov Inst. Chem. Phys. Russ. Acad. Sciences, Moscow, Russia, ***Inst. Phys. Chem., Kossuth Lajos Univ., Debrecen, Hungary)*

The self-organizing process in chemical systems is known to occur as a result of nonlinear chemical events. The temporal (oscillatory) behavior and the possibility of spatial pattern formation in such systems have been interested in relation to the understanding of living systems and also to their possible application to sensing and memory-storage devices. The response of such systems to light illumination has been studied many times but not in a systematic manner. Use of light as an external parameter is important since the feasibleness of controlling light in energy, intensity and the pulse characteristics should explore a rich variety of information on the nature of the systems. We have established the state diagram for the stationary-light illumination taking the illumination light intensity as one of the external parameters for the Belousov-Zhabotinsky system, the minimal bromate oscillator, the $Fe(CN)_6^{4-}/H_2O_2$ system, and the Briggs-Rauscher system. The wavelength dependence has also been measured to determine the cross section of photo-inhibition and -induction of oscillations. This enables us to determine the primary step caused by illumination. Now we have started to study the response of such systems to a pulsed-light illumination as a function of light intensity, pulse width and the phase in a single cycle of oscillations at which the pulsive perturbation is applied. It is particularly interesting to explore the phase relation and the nature of so called "excitability" of such systems.

Gas Phase Reaction Dynamics Studied by Crossed Beam — Ion Imaging

Toshinori SUZUKI, Kenichi TONOKURA, Nobuaki YONEKURA, and Lizla S. BONTUYAN

Two dimensional ion imaging coupled with resonance-enhanced multiphoton ionization (REMPI) makes it possible to measure differential cross sections with complete internal state selection of the products. The goal of this project is to develop a crossed molecular beam machine with an ion imaging device and to elucidate the dynamics of atmospheric and interstellar chemical reactions by measuring state-resolved differential cross sections. As the first step towards this goal, a two-dimensional (2D) ion imaging apparatus was constructed, and its performance was tested by observing photodissociation events (III-M-1, 2). Analysis programs were developed to calculate speed and angular distributions of photofragments from the 2D projection of the 3D photofragment distribution. A new slicing technique using laser sheet ionization was developed to directly observe the section of the 3D distribution containing the center-of-mass, and was compared with the reconstruction using the inverse Abel transform (III-M-2). As the second step, a pulsed hydrogen beam for the study of inelastic and reactive scattering was tested. The hydrogen beam was generated by 193 nm photolysis of H_2S or 266 nm photolysis of HI in molecular beams, and the resulting hydrogen pulse ejected at the right angle to the molecular beam was detected by [2+1] REMPI of H atom via the 2s state. The time duration of the hydrogen pulse was found to be 35 ns. Experiments involving the imaging of inelastic H atoms scattered inelastically by some molecules are being undertaken. Based on these preliminary results, a new crossed beam machine was designed for reactive scattering experiments of atoms and free radicals.

External Magnetic Field Effects upon Chemical Reactions

Ryoichi NAKAGAKI *(Kanazawa Univ. and IMS)*

In this research project, we have studied magnetic field and magnetic isotope effects upon the lifetime of biradicals derived from methylene-linked bifunctional molecules consisting of benzophenone moiety and hydrogen donors. The photoinduced intramolecular hydrogen abstraction reaction takes place on excitation of the benzophenone chromophore. Since the benzophenone moiety in the excited triplet state abstracts a hydrogen from the donor, the resultant biradical intermediate is in the triplet state. The decay time of the triplet biradical was found to be lengthened in the presence of an external magnetic field. The observed results are due to the change in the intersystem crossing rate induced by hyperfine interaction between the electronic spin and nuclear magnetic moment. On substituting the hydrogen or carbon nucleus at the particular site of the hydrogen donor with deuterium (isotopic purity of *ca.* 98%) or heavy carbon (C-13 purity of *ca.* 99%), the decay profile of biradical intermediate produced by photoexcitation of the ketone chromophore is appreciably changed on application of the magnetic fields. Deuteration lengthened

the biradical lifetime, while heavy carbon substitution shortened the biradical lifetime in comparison with that of the species composed of naturally abundant hydrogen and carbon.

The Synchrotron Radiation Excited Photochemical Process Chamber

Akitaka YOSHIGOE, Mitsuru NAGASONO, Kazuhiko MASE, and Tsuneo URISU

The reaction chamber shown in Figure 1 was constructed to study mainly the reaction mechanisms of synchrotron radiation (SR) excited photochemical processes, such as SR etching, CVD, epitaxial growth. The unique characteristic is that the samples can be transferred in the vacuum between the etching chamber and the epitaxial chamber each other. The reaction chamber consists of epitaxial chamber, etching chamber, sample storage chamber and airlock chamber. The epitaxial chamber pumped by the 500 l/s turbo molecular pump is designed as the gas source Si MBE apparatus. The base pressure is 5×10^{-10} Torr. The substrate holder is designed so that the Si wafer can be heated up to about 1200°C for cleaning by the thermal desorption of the surface oxide. The base pressure of the etching chamber is 1×10^{-9} Torr. The sample holder is designed for only room temperature experiments at present, but is going to be changed for the temperature controllable one for the range of 100—500 K. As the in situ observation method, infrared reflection absorption spectroscopy optical systems using FTIR and an RHEED system are equipped as shown in Figure 1. The samples are introduced from an air lock chamber whose base pressure is 3×10^{-9} Torr to a sample storage chamber having 1×10^{-9} Torr. 6 samples can be stored in the air lock chamber. Before introducing a sample into the reaction chamber, it is possible to do the thermal pre-treatment for samples in the sample storage chamber. This reaction chamber is connected to the SR beam line through the differential vacuum pumping systems with pressure difference of 4th order of magnitude.

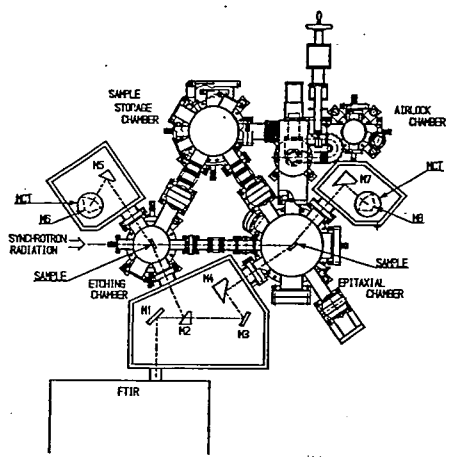

Figure 1. Reaction chambers and an IRAS system for study of SR excited surface photochemical reactions. For measurements in the etching chamber, IR beam passes through M1, M2, Sample, M5, and M6. For measurements in the epitaxial growth chamber, IR beam passes through M1, M3, M4, Sample, M7, and M8.

Development of High-Intensity Beam Source for Studies on Photoionization Mass Spectrometry and Photoelectron spectroscopy of Clusters

Koichiro MITSUKE, Hiroaki YOSHIDA, and Minoru KANNO

On the beamline BL2B2 of UVSOR we have developed two types of cluster source producing a supersonic neutral beam and a metal anion beam.

The central part of the former source is a three-stage cryogenic differential pumping system made of inner and outer cylinders and two stainless pipes blazed around each cylinder. A sample gas is expanded into the first stage from a conical nozzle of 100-μm diameter at room temperature. A molecular beam is introduced through a conical skimmer with an entrance hole of 380-μm diameter into the second stage and collimated by two slits of 2-mm diameter. The inner and outer cylinders are cooled by cold He and N_2 gases, respectively, flowing through the blazed pipes. The temperature of the wall of the inner cylinder is kept at about 30 K. We will investigate superexcited states of clusters, the number of constituent molecules of which ranges from 2 to several tens, by positive ion-negative ion coincidence spectroscopy (PINICO).

The second source has been developed for photodetachment spectroscopy of metal cluster anions to obtain information on the ground and electronically excited states of neutral clusters. Negative ions are produced at the surface of a sample metal which is placed in a xenon plasma confined by a multicusp magnetic field. The sputtered atomic ions are decelerated by collisions with flowing helium gas, and then cluster ions condensed out of the quenched vapor. Atomic and cluster ions extracted from the source are mass-separated by a magnetic mass spectrometer and allowed to intersect at 90° with the dispersed light from a VUV monochromator. The extraction voltage is set to 10—20 kV. In the first stage, we are planning to measure threshold photoelectron spectra of size-selected metal cluster anions.

(2) Materials Science on Molecular Devices

d-π Interaction in Molecular Metals

Kyuya YAKUSHI, Ilias I. KHAIRULLIN, and Toshihiro HIEJIMA

We have undertaken a systematic study on the solid molecular systems in which transition metals are embedded in a π-conjugated system from the viewpoint of the future design of the superconducting material. The highly conductive phthalocyanine salts such as $CoPc(AsF_6)_{0.5}$ and $NiPc(AsF_6)_{0.5}$ are the prototype of the one-dimensional conductors in which the d- and π-orbitals form a double-chain (two-bands) system. This year we examined the pressure dependence of the absorption spectra of these conductive phthalocyanine salts, and found a pressure-induced charge transfer from the d-band to π-band. (see IV-A-1) This phenomenon is quite unique and implies that the pressure can control the carrier concentration of these two bands, which is usually very difficult in a organic conductor. Pressure dependence (0–8 GPa) of the electrical conductivity and magnetic susceptibility of these compounds will be very important and interesting, although these experiments are technically difficult.

We have studied the preparation and characterization of 2D-polymer of CuPc to extend the d-π interacting materials, where local magnetic moments on the square lattice are embedded in a 2D Fermi sea. We systematically examined the magnetic properties of these materials by X- and Q-band ESR spectroscopy. (see IV-A-2) Since these materials are still not well-characterized, the interpretation of the magnetic properties is not straightforward. Phenomenologically, the materials prepared at lower (<500°C) temperature have a high-concentration of conduction electrons and localized electrons on Cu^{2+}. These different type species are not interacting with each other contrary to our expectation. The materials prepared at higher (>650°C) temperature shows that these two-types of signals merges into one, which means a strong interaction between the localized and delocalized electrons.

Superconducting Properties of Na-N-C_{60} Ternary Compound

Ilias I. KHAIRULLIN and Kyuya YAKUSHI

Subsequently to the last years discovery of the new superconducting Na-N-C60 compound, we have conducted a systematic study of these compounds, *i.e.* improved the preparation method by changing the chemical composition between C60 and NaN_3 and performed the X-ray diffraction experiment using the well-characterized sample. Since we still do not succeed to prepare the homogeneous superconducting material, we determined the lattice constant of the superconducting phase by comparing the X-ray diffraction patterns of superconducting and non-superconducting materials. We determined the superconducting parameters such as coherent length and penetration depth, which does not depend upon the degree of homogeneity. (see IV-B-1) This is a joint research with Dr. K. Imaeda of Inokuchi group.

Toward Comprehensive Understanding of Various Electronic Phases in Molecular Conductors

Kazushi KANODA, Kazuya MIYAGAWA, Atsushi KAWAMOTO *(Ochanomizu Univ.)*, **and Yasuhiro NAKAZAWA**

Molecular solids form a distinctive field which has large structural anisotropy due to low symmetry of molecules and softness due to loose packing of molecules. Electronic system in such an unique field is expected to show novel properties and therefore has potential as forthcoming electronic devices. Indeed, various electronic phases have been uncovered in several types of organic conductors. In the κ-phase family of BEDT-TTF charge transfer complexes, insulating, superconducting and metallic phases appear, depending on anion or pressure applied in spite of structural similarity. On the other hand, $(DMe\text{-}DCNQI)_2Cu$, a hybrid electronic system composed of π-electrons and d-electrons, exhibits metallic and insulating states, depending on partial deuteration (abbreviated by d_n with n, a number of substituted deuterium) of the methyl group in the DMe-DCNQI molecule or application of pressure to the system. There is a suggestion that these different states should be related to each other with electron correlation as a possible parameter. In order to get an unified picture of a rich variety of electronic phases, a comprehensive study to relate or compare the states is needed. However, most of the research so far were mainly devoted to problems within a specific phase. Nuclear magnetic resonance (NMR) can probe every type of electronic phase. In this project, the above two families of organic conductors have been investigated by ^{13}C- and ^{15}N-NMR. For this purpose, the central carbon sites in the BEDT-TTF molecule and one carbon and two nitrogen sites of =N-CN in the non- and partially deuterated DMe-DCNQI molecules were substituted into ^{13}C and ^{15}N isotopes. Nuclear spin lattice relaxation rate and Knight shift were measured. In the BEDT-TTF compounds, an insulator ($Cu[N(CN)_2]Cl$ salt) and superconductors ($Cu(NCS)_2$ and $Cu[N(CN)_2]Br$ salts) show strong magnetic fluctuations in a similar manner at higher temperatures. The fluctuations lead to freezing of antiferromagnetic order for the insulator but are suppressed for the superconductors at low temperatures. Thus, electron correlation is important for both phases and some mechanism of suppression of magnetic fluctuations at low temperatures seems to control the ground state. For $(DMe\text{-}DCNQI)_2Cu$ systems, an insulating phase (d_6-compound) exhibits paramagnetism of local Cu^{2+} spins and undergoes an antiferromagnetic transition at a lower temperature. In the metallic phases (d_0- and d_2-compounds), the magnetic fluctuations seen by the nuclear relaxation are considerably different from those in the insulating phase. It should be noted that the metallic state of the d_2-compound which is situated closer to the insulator shows the same magnetic behavior as the more stable metallic state of the d_0-compound, without any precursor of insulator. The mechanism of metal-insulator transition is different in these two families of materials. Now, measurements of specific heat, which characterizes

the electronic state from macroscopic viewpoint, is in progress.

Fabrication of Novel Organic Molecular Assemblies with the Use of the Molecular Beam Epitaxy Technique

Yusei MARUYAMA, Hajime HOSHI *(Tokyo Institute of Technology)*, **Keiichi KOHAMA** *(Toyota Motor Corp. and IMS)*, **and Shaoli FANG**

In order to prepare new materials which could be useful for molecular devices elements, we have started to design and fabricate ultra-thin organic multi-layered systems. In the first place, we have prepared ultra-thin single component phthalocyanine thin films to investigate epitaxial growth conditions on alkali halide single crystals. Fairly well oriented, uni-or bi-directionally, crystalline films are obtainable on the alkali halide substrates. Based on this kind of mono-film, we are going to fabricate a multi-layered system.

The SHG and/or THG of the films are investigated from the view point of the molecular structure and the epitaxy or orientation of the films.

Study on the Solid State Properties of Fullerenes

Yusei MARUYAMA, Hironori OGATA, Roger WHITEHEAD *(Durham Univ. and IMS)*, **Toshiyasu SUZUKI, Takeshi ARAI, and Atsushi SUZUKI**

In order to clarify the nature of novel molecular systems, fullerenes, we have started to measure the electronic properties of fullerene solids, mainly concerning on the transport properties of pure and/or alkali metal-doped fullerene crystals.

Charge-carrier drift mobilities of pure C_{60} single crystals were measured with the use of time-of-flight technique and the temperature dependence of the mobilities was also investigated. As for the alkali metal (K or Rb) doped C_{60} crystals, the temperature dependences of the electrical conductivities and the thermoelectric power were observed, and the "metallic" nature of these substances was revealed. Through these measurements we are going to understand the electronic nature of this novel molecular system.

NMR Studies of Novel Condensed Matter Systems

Hironori OGATA, Osamu OISHI, and Seiichi MIYAJIMA

To develop new functional materials based on molecular assemblies, synthetic and NMR studies have been conducted. In the last period our study centered on the structural, electronic, and dynamical properties of liquid crystals and low dimensional electrical conductors (reported in IV-J and IV-K, this issue). We are also developing the following new projects.

(1) Solid state NMR studies on the electronic properties of the ternary compounds of graphite and of fullerenes.

Graphite and C_{60} become metallic or superconducting when reacted with some alkali metals. If another element can be added to this binary compound, the third element has a possibility of controlling the density of states at the Fermi energy, and also of generating novel character related with guest-guest and guest-host interactions. We are conducting NMR experiments to analyze the nature of these ternary systems.

(2) Construction of a new NMR spectrometer for the measurements of anisotropic self-diffusion

For the selective measurement of translational motion of molecules, an apparatus for sharp and intense pulsed field gradient is being constructed. A rotatable quadrupole coil and a cryostat were designed to generate first rank partial derivatives, $\partial B_z/\partial q$, of the magnetic field with respective to any directions with maximum strength of 13 T m^{-1}. The spectrometer equipped also with high RF power facility, versatile pulse sequence, and a fast signal processing will be used to measure anisotropic diffusion coefficient tensor in partially ordered systems.

Exploration of New Cooperative Proton-Electron Transfer (PET) Systems

Kazuhiro NAKASUJI, Jiro TOYODA, Yasushi MORITA, Makoto TADOKORO, Tetsuji ITOH, Minoru MITSUMI, Badruz ZAMAN, Kunio HATANAKA, and Koichi TAMAKI

Search for new molecular materials based on the cooperative interactions between proton and electron has been actively continued. We are now developing a general strategy to explore new molecular materials. Cooperative proton-electron transfer (PET) in the hydrogen-bonded charge transfer (HBCT) systems might produce a molecular assembly of H-bonded neutral radicals. The solid state properties of such PET systems depend on the type and strength of the proton-electron cooperativity. Realization of a PET system under milder physical conditions can open an opportunity toward new molecular materials which possess interesting solid state properties. A molecular level stepwise consideration leads to two reasonable molecular design strategies: the exploration of new electronic systems having smaller intermolecular CT gap and an electronic modification to stabilize H-bonded neutral radical state. Our current approaches to synthesize new PET systems are as follows: (1) the donor and acceptor substituted quinhydrones, (2) the extended conjugated quinhydrones, and (3) the transition metal complexes having H-bonding networks. For example, as for the approach (1), we continue to modify the prototype benzoquinhydrone by introducing the electron donor and the acceptor substituents. As for (2), we have already reported the synthesis and solid state properties of naphtho-, bipheno-, and stilben-quinhydrone as extended conjugated quinhydrones. In these quinhydrones, we found cooperative phenomena between H-bonding and CT interaction. In order to expand the PET systems, new approach (3) are now actively performed. In the H-bonded transition metal complexes, we can utilize the additional characteristics of redox properties of the metal atoms and the intermolecular interactions between the metal atoms or between the metal atom and the ligand. As a first step, we succeeded to construct a H-bonded dimer model of the biimidazole transition metal complex. We are now concen-

trated to construct new H-bonded molecular systems of biimidazole-type and pteridine-type transition metal complexes.

Organic Conductors Based on Novel Heterocyclic Compounds

Yoshiro YAMASHITA, Shoji TANAKA, and Masaaki TOMURA

We have succeeded in preparing new electron donors giving organic conductors. 7-(1,3-Dithiol-2-ylidene)-4-methyl-4,7-dihydro[1,2,5]thiadiazolo[3.4-b]pyridines are strong electron donors and highly polarized. They gave highly conducting charge-transfer complexes with TCNQ. X-Ray analysis reveals intermolecular heteroatom contacts resulting in a unique three-dimensional network. Although planar molecules are usually used for organic conductors, butterfly-shaped bis(1,3-dithiole) donors containing a fused thiadiazole ring gave conductive cation radical salts whose composition is 1:1. The donor molecules show one-stage two-electron oxidation waves. In the crystal structures deformed donor molecules are uniformly stacked. A novel type of donor-π-acceptor system was also prepared. The molecule named BTQT has heterocyclic donor and acceptor units in one molecule. This molecule forms a novel three-dimensional crystal by interheteroatom contacts and shows a non-ohmic behavior. Heterocyclic donor-acceptor systems were used to construct narrow bandgap polymers. Other organic conductors such as transition metal complexes and functionalized polythiophene derivatives were also prepared and the properties were investigated. Details of those works are described in VIII-B section.

Electronic Structure and Reaction Dynamics of Solvated Metal Cluster Ions

Kiyokazu FUKE and Fuminori MISAIZU

Metal ions are intimately involved in chemistry and biochemistry and play a crucial role in many reactions. Although there has been extensive progress in the thermodynamic and kinetic studies of solvated metal ions, the study of microscopic aspect of solvation dynamics has been rather limited. Spectroscopic studies of the solvated metal ion clusters as a function of cluster size can provide detailed information on energetic and dynamics of solvation. The advent of mass spectrometer and metal cluster beam techniques in conjunction with laser probes now allow an attack on the problem for the solvation of metal ions and metal cluster ions through studies probing energy levels and dynamical processes occurring in solvated metal clusters.

In the present research project, we have investigated the photodissociation spectra and photoinduced hydrogen-atom elimination reaction of mass-selected $Ca^+(H_2O)_n$, using a reflectron-type TOF mass spectrometer (see VIII-C-1). Using the recently developed magnetic-bottle type photoelectron spectrometer, we have investigated the photoelectron spectra of $Cu^-(H_2O)_n$, $CuOH^-(H_2O)_n$, and $Na^-(H_2O)_n$ (see VIII-C-2, 3). We have also studied the photoionization process of solvated Rydberg radicals such as $NH_4(NH_3)_n$ and $NH_4(NH_3)_m(H_2O)_n$ in relation to the electron localization modes in clusters (see VII-D-1, 2).

(3) Material Control in Multi-Reaction Centers

Helicity *vs.* Chirality: Synthesis and Structures of Enantiomerically Pure Helical Polymers and Optically Inactive Dinuclear Complexes

Kiyoshi ISOBE, Takayoshi SUZUKI, and Hiyoshizo KOTSUKI *(Kochi Univ. and IMS)*

Enantiospecific synthesis of helicates which are polynuclear metal complexes having helical topology of the bridging ligands, is a current subject in coordination and organometallic chemistry. For this purpose, we have developed a powerful method to prepare optically active bridging ligands, 1,3-dioxolane derivatives. With this ligand or its enantiomer, enantiospecific synthesis of helicates has been performed in this study. Further, in order to understand the homo- and heterochiral molecular recognition process, preparation of a silver(I) complex with the racemic ligand has also been carried out.

A reaction of either ***R,R-L*** or its enantiomer (***S,S-L***) with AgOTf (OTf^-=$CF_3SO_3^-$) or $AgPF_6$ gives colorless crystals of $[\{Ag(\textit{R,R}\text{- or }\textit{S,S-L})\}_\infty](OTf \text{ of } PF_6)_\infty$, which have an infinite helical chain structure of a polymeric silver(I) complex. The radius of the helical chain is dependent on the co-crystallized anions because of the weak interaction between the anions and silver centers. In contrast, a reaction of AgOTf with a racemic mixture of the ligand (***rac-L***) yields an optically inactive dimeric complex, $[Ag_2(\textit{rac-L})_2](OTf)_2$, where heterochiral molecular recognition should be occurred. In the crystal the recognition may be caused by a weak hydrogen bond-like interaction between the intramolecular heterochiral ligands. In solution, however, there is no difference in ^1H, ^{13}C NMR, and other spectroscopic results when the optical activities of the ligand used in complexization change. Hence the stereospecificity found in the X-ray analyses of these compounds appears on the crystallization from the solutions. The detailed analysis of the structures of these compounds in solution and the related complexes are now in progress.

Dinulear Mixed Ligand Complexes with Tetraketonate and Polyamines

Falideh JALILEHVAND, Masako URAGAMI *(Ochanomizu Univ.)*, **Wolfgang LINERT** *(Technical Univ. Vienna)*, **and Yutaka FUKUDA** *(Ochanomizu Univ. and IMS)*

In continuing the study of dinuclear mixed ligand complexes of Cu(II) or Ni(II) with tetraketonate ligand such as 1,1,2,2-tetraacetylethanate(taet) and N-alkylated ethylene-

diamine(tmen) of diethylenetriamine(pmdt), we have synthesized some new tetraketonate ligands(L) which contain some substituent groups between two acetylacetonate moieties. The substituent groups are (o-, m- or p-)xylyl- and p-substituted benzyl-groups. We could obtain fine crystals of Cu(II), $Cu_2(L)(tmen)_2X_2$, where X=ClO_4^- or NO_3^-, which are very soluble in many organic solvent and show characteristic solvatochromism due to the donor strength of the solvent used.

Structure and nmr Behavior of Cobalt(III) Polyamine Complexes of Nitrilotris(methylenephosphonate) in Aqueous Solution

Kiyoshi SAWADA, Keiichi SATOH, and Tomohide ICHIKAWA

The complex formation of nitrilotris(methylenephosphonate)(NTMP) with cobalt(III)-polyamine complexes has been investigated by means of NMR spectroscopy. P-31 NMR spectra of the reaction mixture of Co^{III} polyamine complex with NTMP were measured at 0°C as a function of pH. The analysis of the pH dependence of P-31 NMR signals revealed the two types of complexes were formed by the reaction of cis-$[Co(en)_2Cl_2]_2^+$ with NTMP: O- monodentate complexes and O,O-bidentate complexes having an eight membered chelate ring. The protonation equilibria and P-31 NMR chemical shifts of each complex were determined and the structures of these complexes were estimated. The results of the complex formation of the NTMP complexes of cis-$[Co(en)_2(NH_3)Cl]^{2+}$ support the structure of O-monodentate complex. The reaction of fac-$[Co(dien)(H_2O)_3]^{3+}$ with NTMP forms the facial and meridional forms of O,N,O-tridentate complexes.

Study on the Interaction Between Halogen Atom of the Halogeno Complexes and the Solvent Molecules. II

Fumio KAWAIZUMI

The halogeno complexes $K_2[MX_4]$ and $K_2[MX_6]$ attract our special attention: To how much extent does the interaction of the ligand halide ion X^- with solvent molecules differ from the case for free ions in solution? Previously, we determined the partial molar volumes V_2^0 of $K_2[MX_4]$ and $K_2[MX_6]$ where M is Pt or Pd and X is Cl, Br, or SCN and found that the palladium and platinum complexes have quite similar V_2^0 values.

The solute - solvent interactions of these complexes have further been investigated from the point of compressibility of solutions. The sound velocities in solutions were measured using the precision ultrasonic velocity-meter based on the sing-around techniques. The velocity data have been combined with the density data obtained in our previous work to give the adiabatic compressibilities. The infinite dilution values of the partial molar adiabatic compressibilities K_s^0 have been determined. By subtracting the K_s^0 (K^+) values from those for the complexes, the values of K_s^0 for the halogeno complexes K_s^0 ($[MX_4]^{2-}$) and K_s^0 ($[MX_6]^{2-}$) have been determined. The values for the two thiocyanato complex ions are positive, showing that the interaction of the ligand SCN^- with the solvent water is very weak and that these complex ions have no incompressible region around them. While the volumetric behavior of the complex ions $[PtCl_6]^{2-}$ and $[PdCl_6]^{2-}$ differ only slightly, compressibility measurement has indicated that the ion $[PdCl_6]^{2-}$ interacts more strongly than $[PtCl_6]^{2-}$.

Carbon-Carbon Bond Formation in Multi-Electron Reduction of Carbon Dioxide by Homogeneous Catalysts

Koji TANAKA, Tetsunori MIZUKAWA, and Hirotaka NAGAO

Electrochemical CO_2 reduction takes place at more negative potentials than −2.0 V (vs. SCE). To reduce the high overpotential energy for the CO_2 reduction, much efforts have been paid to search for metal complexes to mediate CO_2 reduction at less negative potentials. Although a variety of metal complexes have proven to catalyze electro- and photochemical CO_2 reduction, the reduction products in those homogeneous reactions are limited to CO and HCOOH so far. From the viewpoint of Cl sources for other organic compounds, multi-electron reduction of CO_2 accompanied by carbon-carbon bond formation is much more important than two-electron reduction of CO_2. The purpose of this project is to develop new catalytic systems capable of multi-electron reduction of CO_2 accompanied by carbon-carbon bond formation. This problem may be solved by prevention of CO evolution from metal-carbonyl intermediate during the reduction of CO_2. Polypyridyl metal complexes having low energy π^* orbitals are useful candidates for the multi-electron reduction of CO_2, since electrons transferred to those complexes from electrodes and photosensitizer are expected to be accommodated into π^* orbitals of polypyridyl ligands. This may lead to reduction of the carbonyl group without fission of the metal-carbonyl bond. Along this line, we have found that $[Ru(bpy)(trpy)(CO)]^{2+}$ (bpy=bipyridine; trpy=terpyridine) can catalyze the multi-electron reduction of CO_2 in aqueous conditions at −20°C to afford not only HC(O)H and CH_3OH but also HOOCC(O)H and $HOOCCH_2OH$ through the Ru-η^1-CO_2, Ru-C(O)OH, Ru-CO, Ru-CHO, and Ru-CH_2OH intermediates.

Carbon-Carbon Bond Activation of Zirconacycles and Its Application for Selective Reactions

Tamotsu TAKAHASHI, Noriyuki SUZUKI, Koichiro AOYAGI, Ryuichiro HARA, Kayoko KASAI, Zhenfeng XI, Martin KOTORA, Toyohisa ISHIDA, and Yasushi NISHIHARA

Zirconacycles such as zirconacyclopentanes, zirconacyclopentenes and zirconacyclopentadienes are easily prepared from alkenes and/or alkynes. These compounds have very interesting properties. Their β,γ-carbon-carbon bond in the matallacycles can be cleaved. We investigated the cleavage reaction and found that replacement reaction of alkene or alkyne moiety by other unsaturated bonds such as C=C, C=N and C=O gave different type of metallacycles such as oxazirconacycles and azazirconacycles. When the

unsaturated compounds have a leaving group at β-position, elimination reaction proceeds after forming zirconacycles. This method could be used for selective allylation reaction of alkynes, preparation of allylcyclopropanes and catalytic reaction of allylic ethers with EtMgBr. This reaction was very useful since elimination proceeded only when the leaving group was in the β-position of α-substituent. For example, in the case of allylation reaction of alkynes, usual allylation using Mg, Zn, Li, B gives a mixture of regio isomers. The isomers are formed due to its mechanism involving four centered and six centered intermediates. However, the method we developed here gave only one regio isomer. Carbon-carbon bond formation occurred exclusively at γ-position of allylic ethers because of its mechanism involving a five centered intermediate. Further investigation to develop new useful synthetic methods using carbon-carbon bond activation of zirconacycles are now in progress.

OKAZAKI CONFERENCES

The Forty-seventh Okazaki Conference

Solvent Dynamic Effects on Relaxation Phenomena ***(October 5–7, 1993)***

Organizers: K. YOSHIHARA *(IMS)* **and T. OKADA** *(Osaka Univ.)*
Invited Overseas Speakers: C. B. HARRIS *(Univ. of California, U.S.A.)*, **M. A. JOHNSON** *(Yale Univ., U.S.A.)*, **K. DUPPEN** *(Univ. of Groningern, Netherlands)*, **A. NITZAN** *(Tel Aviv Univ., Israel)*, **M. MARONCELLI** *(Pennsylvania State Univ., U.S.A.)*, **and M. R. TOPP** *(Univ. of Pennsylvania, U.S.A.)*

Various kinds of relaxation phenomena including chemical reactions are closely related to the solvent dynamics. Recent progress in experiments (ultrafast laser spectroscopy, molecular beams, sensitive detection etc.) and theories (statistical and molecular dynamic methods, etc.) are improving our understandings of relaxation phenomena. The conference was organized to discuss on the following subjects (1) Molecular mechanisms of solvation dynamics and chemical reactions (2) Chemical dynamics in clusters (3) Solvent dynamic effects on molecular spectroscopy and (4) Energy relaxation and dephasing process in liquids. The conference consisted of sixteen invited talks and was attended by 50 scientists including 15 scientists of IMS. No poster session was organized and the afternoon of the middle day was used for excursion to Mikawa Bay. There were plenty of time to discuss the subjects individually. The conference was successful in exchange of vast information among specialists during the session and spare time. The experimentalists and theorists exchanged ideas very well. The understandings on solvent dynamics and relaxation phenomena have improved greatly.

The Forty-eighth Okazaki Conference

"Phthalocyanines" —Design and Application for Molecular Devices— *(January 26—28, 1994)*

Organizers: M. HATANO *(Tohoku Univ.)*, **K. YAKUSHI** *(IMS)*, **and Y. MARUYAMA** *(IMS)*
Invited Overseas Speakers: A. J. CEULEMANS *(Kathol. Univ., Belgium)*, **M. J. STILLMAN** *(Univ. Western Ontario, Canada)*, **C. C. LEZNOFF** *(York Univ., Canada)*, **D. BRAUN** *(Kathol. Univ., Belgium)*, **J. D. WRIGHT** *(Univ. Kent, U.K.)*, **and M. HANACK** *(Univ. Tubinngen, Germany)*

As a typical material for basic study of molecular functionality devices, phthalocyanines are one of the most relevant molecular materials. In the first part of this conference, the syntheses, reactions, electronic states and properties of phthalocyanine molecules, phthalocyanine complexes and assemblies of such a small number of molecules as dimers were discussed, and then to the electronic properties and applications in the solid state of these molecular aggregates the discussion was extended.

Phthalocyanine is a highly functional molecule as a building block for molecular aggregates. For example, its planar molecular shape is favarable for construction of layer structure so as to form dimer structures, liquid crystals or thin films. It can form even polymers through the bonding between center metal atoms in neighboring molecules. Substitution to the phthalocyanine-ring may control the electronic properties or steric effect of the molecules. Detailed theoretical analyses may lead to a design of novel molecules based on phthalocyanine.

From the view-points mentioned above, synthesis of new molecules, construction of new molecular assemblies and their properties were mainly discussed, and funthermore some novel aspects of phthalocynine solids including applications were discussed. Such a rather sharpe focusing of discussion in this conference was very effective to a substantial understanding on the direction for realizing molecular devices.

The Forty-ninth Okazaki Conference

The Structure and Dynamics of the Clusters Formed in Supercritical Fluids *(March 16–18, 1994)*

Organizers: O. KAJIMOTO *(Kyoto Univ.)*, **I. OHMINE** *(IMS)*, **and K. FUKE** *(IMS)*
Invited Overseas Speakers: J. TROE *(Gottingen Univ., Germany)*, **K. P. JOHNSTON** *(Univ. Texas, U.S.A)*, **F. B. BRIGHT** *(State Univ. NY, U.S.A)*, **S. HOWDLE** *(Univ. Nottingham, U.K.)*, **and J. BRENNECKE** *(Univ. Notre Dame, U.S.A)*

Supercritical fluids have recently attracted much attention because of their superior properties as solvents for extraction, separation and chemical reactions. This medium also has essential importance in the basic research of condensed phase chemical reactions because it offers an opportunity to analyze the microscopic feature of the interaction between the reactants and the environment. The clustering in supercritical solutions has been recognized as the basis of the characteristic behavior observed for the diffusion, solubility and reactivity of solute molecules in supercritical fluids. This conference was proposed for discussing the effects of clustering on various properties of supercritical solutions. We also intended in this conference to have a chance for the scientists both in basic science and chemical engineering altogether to discuss on these issues. In addition to five outstanding talks by the foreign invited speakers, fourteen Japanese scientists gave nice talks. The vivid discussions were made on the subjects such as the structure, spectroscopy and reaction dynamics of clusters in supercritical fluids, and the relation with the gas-phase clusters.

JOINT STUDIES PROGRAMS

As one of the important functions of an inter-university research institution, IMS undertakes joint studies programs for which funds are available to cover research expenses as well as travel and living expenses of individuals. The proposals from domestic scientists are reviewed and controlled by the inter-university commitee. The programs are carried out under one of five categories:

1) Joint Studies on special projects (a special project of significant relevance to the advancement of molecular science can be carried out by a team of several groups of scientists).
2) Research Symposia (on timely topics in collaboration with both outside and IMS scientists).
3) Cooperative Research (carried out in collaboration with both outside and IMS scientists).
4) Use of Facility (the Computer Center, Instrument Center and other research facilities at IMS are open to all researchers throughout the country).
5) Joint studies programs using UVSOR facilities.
   a) Special Project, b) Cooperative Research, c) Use of UVSOR Facility.
   In the fiscal year 1993, numbers of joint studies programs accepted amounted to 1, 9, 130, and 246 for categories 1)—4), respectively 2, 44 and 132 for 5a)—5c), respectively.

1) Special Projects

Synthesis and Catalysis of Oxide Clusters

Contributors: **Koji TANAKA, Kiyoshi ISOBE, Masaaki ABE, Masaru ICHIKAWA** *(Hokkaido Univ.)*, **Takafumi SIDO** *(Hokkaido Univ.)*, **Yusuke IZUMI** *(Nagoya Univ.)*, **and Kazuo URABE** *(Nagoya Univ.)*

This research project aims at synthesis of new types of oxide clusters that have active sites for chemical reactions, and at development of unique catalytic reactions for hydrocarbon transformation by using newly prepared oxide clusters.

(1) Synthesis and Reactivity of Organmetallic Oxide Clusters with Incomplete Cubic Structure and Valley Sites

Recently, we have directed our efforts primarily toward the synthesis of organmetallic oxide clusters with incomplete cubic structure and valley sites, because such clusters are expected to show unique reactivity towards organic substrates from theoretical studies and to be potential models for inorganic solid surfaces to understand the chemistry on them.

The triple cubane-type cluster, $[(RhCp^*)_4Mo_4O_{16}]$ ($Cp^* = \eta^5$-C_5Me_5), shows a novel fragmentation of cube size in the framework to form an incomplete double cubane-type methoxide cluster $[(RhCp^*)_2Mo_3O_9(OMe)_4]$. We are studying the reaction mechanism of the fragmentation and reactivities of the incomplete double cubane-type cluster.

Another oxide cluster, $[(RhCp^*)_4V_6O_{19}]$, has valley sites. We have found that the sites are able to interact with CH_3CN through the CH···O—V hydrogen bonds. This suggests that inactive C-H bonds in organic molecules are activated by the valley sites in $[(RhCp^*)_4V_6O_{19}]$. We are now developing a new reaction by using the incomplete cubic structure and valley sites in $[(RhCp^*)_2Mo_3O_9(OMe)_4]$ and $[(RhCp^*)_4V_6O_{19}]$, respectively.

(2) Characterization of Metal Oxide-Supported Organmetallic Oxide Clusters and Catalysis for Transformation of Organic Molecules

The SiO_2-supported cubane-type molybdenum oxide cluster, $[RhCp^*MoO_4]_4$, was characterized by EXAFS and IR. When the attached clusters were reduced by CO under illumination, the bridge oxygen of Mo_4O_{16} cubane framework was removed (Figure 1) and the adjacent Mo was coordinated by CO which desorbed by the evacuation at 473 K. Propene metathesis reaction proceeded on the CO photoreduced catalyst. The coordinatively unsaturated Mo site may be active for the reaction.

$[(RhCp^*)_4V_6O_{19}]$ grafted on silica was also investigated by EXAFS and IR. The gas-phase oxidation and hydration of acetonitrile proceed on silica-grafted Rh-VO cluster at 300—423 K. EXAFS and IR data suggest that changes of the framework of the Rh-VO cluster are due to decrease in V-Rh, and V-V bonding contribution occurs with appearance of new V-O bind by the thermal evacuation over 473 K (Figure 2). Transform of the framework of the V-O bonds of Rh-VO cluster was reflected in the activity change for hydration of acetonitrile.

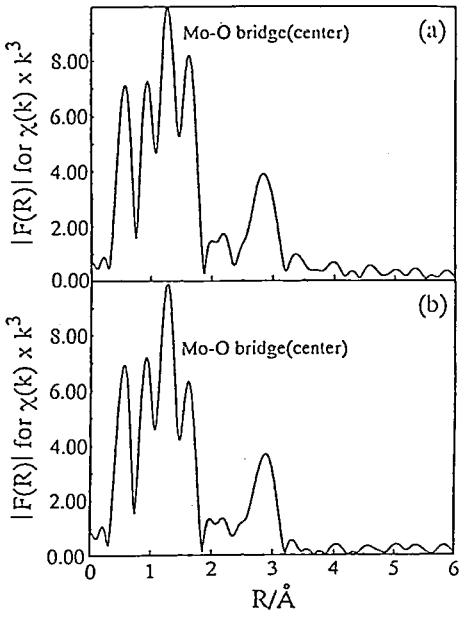

Figure 1. EXAFS spectra of $[RhCp^*MoO_4]_4$. (a): at room temperature (b): irradiation of the light (Hg-lamp) in the presence of CO.

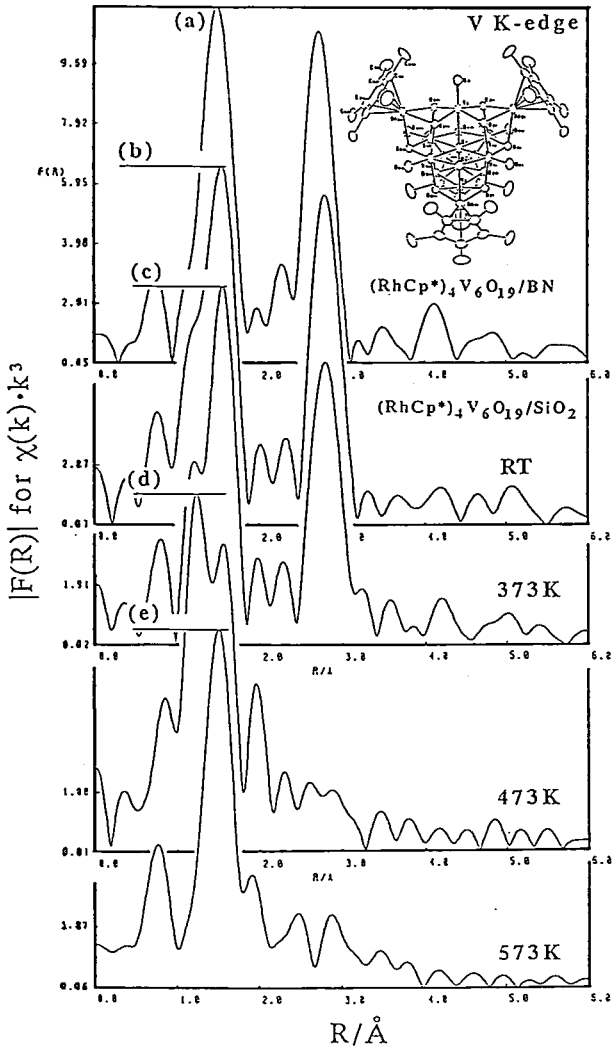

Figure 2. EXAFS characterization of SiO_2-grafted $[(RhCp^*)_4V_6O_{19}]$.

(3) Hydrogenation of Alkynes and Alkenes by Using a Coupled System of Heteropoly Oxometalates and the Wilkinson Complex

In recent years the Keggin-type heteropoly acid (abbreviated as HPA) has been actively applied as catalyst to various organic reactions, because it possesses dual catalytic function of strong acidity and oxidizing ability. We have also studied the homogeneous catalyses of HPA in order to elucidate its catalytic features at a molecular level. We think now that these interesting catalytic behaviors by HPA are undoubtedly due to the intrinsic (electronic and structural) properties of heteropoly anion, or the conjugate base of HPA. We already reported that heteropoly anion revealed an excellent modifying effect on the Wilkinson's complex.

Our attention is now paid to understanding of this modifying effect or cooperative effect of the Rh-W system by comparison with the catalytic reaction using the organometallic oxide clusters such as $[RhCp^*MoO_4]_4$, and $[(RhCp^*)_4V_6O_{19}]$.

2) Research Symposia

1. New Horison of Molecular Spectroscopy and Dissociation Dynamics by using Synchrotron Radiation
   (November 11th–13th, 1993)
   Organizer: N. Kosugi
2. Design and Control of Electronic Systems toward New Molecular Materials
   (December 9th–10th, 1993)
   Organizer: K. Nakasuji
3. Recent Progress and Future Perspective in Photo-induced Charge Transfer Process and its Related Problems
   (December 14th–15th, 1993)
   Organizer: K. Shobatake
4. Dynamics of Non-Equilibrium Material by Electronic Excitation
   (January 24th–25th, 1994)
   Organizer: Y. Shinozuka
5. Solid-State Chemistry of Fullerenes
   (February 26th, 1994)
   Organizer: K. Nasu
6. Symposium on Picosecond and Femtosecond Spectroscopy
   (March 16th–17th, 1994)
   Organizer: K. Yoshihara
7. Physics and Chemistry of Molecular Solids at High Pressure
   (July 3rd–4th, 1994)
   Organizer: K. Shiroya
8. Symposium on Physical Chemistry for Young Researchers in Molecular Science
   (July 15th, 1994)
   Organizer: Y. Nagano
9. Unified Understanding of the Motion of Finite Many-Electron System
   (July 22th–24th, 1994)
   Organizer: A. Ichimura

3) Cooperative Research

This is the most important programs IMS undertakes for conducting its own research of the common interest to both outside and IMS scientists by using the facilities at IMS. During the first half of fiscal year of 1993 ending on September 30, 60 outside scientists; and during the second half of the fiscal year, 63 outside scientists, the names and affiliations of those collaborators are found in the Research Activities.

4) Use of Facilities

The number of projects accepted for the Use of Facility Program of the Computer Center during the fiscal year of 1993 amounted to 225 (716 users) and the computer time spent for these projects is 16306 hours (converted to the HITAC M-680H time), and amounted to 76% of the total annual CPU time used.

Projects (230 users) were accepted for the Use of Facility Program of the Instrument Center during the fiscal year of 1993.

5) UVSOR

In the UVSOR Facility with the 750 MeV electron

storage ring, there are nineteen beam lines available for synchrotron radiation research (see "UVSOR ACTIVITY REPORT 1994"). The Experimental Facility of each beam line is described in the introductory pamphlet "OUTLINE OF UVSOR". The Japanese and English versions are available through UVSOR Facility. Under the following programs, a number of SR studies have been carried out by many users outside and inside IMS: a) the UVSOR Special Project, b) the UVSOR Cooperative Research Projects, c) the UVSOR Projects. Furthermore, the 10th anniversary of the UVSOR was celebrated on December 3, 1993 by many participants. The 13th UVSOR User's Symposium was held on December 3, 1993 as a satellite meeting combined with the ceremony.

5-a) UVSOR Special Project

Development of the Spin-Resolved Photoelectron Spectrometer System

Masao KAMADA, Kazumichi NAKAGAWA, Goro ISOYAMA, Atsunari HIRAYA, Shin-ichiro TANAKA, Hiroyuki HAMA, Shin-ichi KIMURA, Kusuo SAKAI, Osamu MATSUDO, Masami HASUMOTO, Eiken NAKAMURA, Yashuo FUJII,* Eiji ISHIGURO,* Kouichi ICHIKAWA, Kazuo SODA,** Kazutoshi FUKUI,*** and Sigeo OHARA****** *(*Osaka City Univ., **Univ. of Osaka Prefect., ***Fukui Univ., ****Nagoya Institute Tech.)*

The "complete" experiment, where all of the energy, the momentum, and the spin polarization of photoelectrons can be observed, has been a long desire for scientists in the world. The present project consists of following three parts: (1) The development of a spin detector which can be installed to the angle-resolved photoelectron spectrometer. An analyzing chamber with ultra-high vacuum and an electron spectrometer have already been constructed. The spin detector is a type of low-energy scattering and is now under construction. The surface analysis of a GaAs emitter is also in progress. (2) A new type monochromator (SGM-TRAIN), which covers the photon energy range of 5–250 eV, is now under construction at beam line 5A. This monochromator consists of a constant-deviation mount and a normal-incident mount. The ray-trace calculation of the SGM-TRAIN promises the good resolution and circular polarization. (3) The insertion devise which consists of periodic magnetic fields is useful to provide the circularly polarized synchrotron radiation. The calculation of the intensity and polarization from several undulator mounts has been carried out and so we have decided to apply the MPW-type undulator proposed by Prof. H. Kitamura of KEK to a 750-MeV storage ring at UVSOR.

Development of the Spectroscopic System at The Beam Line 6A1 at a Wide Energy Region

Takao NANBA,* Makoto SAKURAI,* Michihiro KOBAYASHI, Yasuhiro KONDOH,*** Masao KAMADA, Kyuya YAKUSHI, and Tsuneo URISU** *(*Kobe Univ., **Osaka Univ., ***Tohoku Univ.)*

We are planning to expand the available spectroscopic region at the beam line 6A1 from a millimeter wave to a near infrared region. For this purpose, a new interferometer covering both near infrared and middle infrared regions will be installed in addition to a Martin-Puplett interferometer in the far infrared region. The new system will cover a very wide spectroscopic range of 15000 -4 cm^{-1} and make possible following subjects,

(1) study of vibration and lattice modes in solids under high pressure up to 20 GPa,

(2) study of magnetic properties of solids under extreme conditions such as high magnetic field and high pressure, and so on.

5-b) UVSOR Cooperative Research Projects

Under this joint-study program, many synchrotron radiation experiments have been carried out with the beam lines of in-house staff in cooperation with scientists who were invited from other institutions. The total number of the projects in this category was 37 in the fiscal year of 1993.

5-c) The UVSOR Invited Research Projects

Under this joint-study program, several scientists were invited from other institutions to help for construction of new beam lines and improvement of the UVSOR storage ring and others. The total number of the projects in this category was 9 in the fiscal year of 1993.

5-d) The Use-of-UVSOR Projects

Ten out of the total of nineteen UVSOR beam lines are available for general users outside and inside IMS for their synchrotron radiation studies in the field of molecular science. The total number of the projects in this category was 123 in the fiscal year of 1993.

FOREIGN SCHOLARS

Visitors from abroad play an important role in research activities and always welcome at IMS. The following is the list of foreign scientist who visited IMS in the past year (Aug. 1993 – Jul. 1994). The sign *1 indicates an attendant to an Okazaki Conference, *2 an IMS or Japan Society for the Promotion of Science Invited Foreign Scholar, *3 an IMS councillor, *4 an IMS visiting scientist, and *5 an IMS adjunct professor or associate professor from abroad (period of stay from 9 to 12 months). Scientists who wish to visit IMS under program *2 and *5 are invited to make contact with an IMS faculty in a related field.

Prof. Sang K. Lee*2	Pusan National Univ.	(Korea)	- Aug.1993 Dec. 1993 - Feb. 1994
Prof. Jian-Min Yuan	Drexel Univ.	(U.S.A.)	Aug. 1993
Dr. A. A. Zakhidov	Uzbek Acad. Sci.	(Uzbekistan)	Aug. 1993 - Nov. 1994
Dr. V. K. Vanag*2	Semenov Inst. of Chemical Phys.	(Russia)	Sep. 1993 - Mar. 1994
Prof. M. Palma	Palermo Univ.	(Italy)	Sep. 1993
Dr. L. S. Bontuyan*4	Cornell Univ.	(Phil.)	Sep. 1993 -
Mr. J. Winkelhöfer	Embassy of the Czech Repub.	(Czech)	Sep. 1993
Mr. J. Brábnik	Embassy of the Czech Repub.	(Czech)	Sep. 1993
Dr. E. Poetsch	MERCK	(Germany)	Sep. 1993
Prof. C. Schäffer	Univ. of Copenhagen	(Danmark)	Sep. - Oct. 1993
Prof. J. Kalinowski*2	Univ. of Gdánsk	(Poland)	Sep. - Dec. 1993
Prof. J. Klafter	Tel-Aviv Univ.	(Israel)	Oct. 1993
Mr. Minhaeng Cho	Univ. of Chicago	(U.S.A.)	Oct. 1993 - Mar. 1994
Prof. V. Kamalov*1	Inst. of Chem. Phys.	(Russia)	Oct. 1993 -
Prof. C. B. Harris*1	Univ. of California, Berkeley	(U.S.A.)	Oct. 1993
Prof. M. A. Johnson*1	Yale Univ.	(U.S.A.)	Oct. 1993
Prof. A. Nitzan*1	Tel-Aviv Univ.	(Israel)	Oct. 1993
Prof. M. Maroncelli*1	Pennsylvania State Univ.	(U.S.A.)	Oct. 1993
Prof. M. R. Topp*1	Univ. of Pennsylvania	(U.S.A.)	Oct. 1993
Prof. K. Duppen*1	Univ. of Groningen	(Holland)	Oct. 1993
Mr. J. W-I Lin*1	Osaka Univ.	(U.S.A.)	Oct. 1993
Dr. H. Chosrowjan*1	Osaka Univ.	(Armenia)	Oct. 1993
Prof. R. Wortmann*1	Mainz Univ.	(German)	Oct. 1993
Mr. Y. Jia*4	Univ. of Chicago	(U.S.A.)	Oct. 1993
Dr. A. E. Johnson*1	Univ. of Rochester	(U.S.A.)	Oct. 1993
Prof. G. Rábai*5	Kossuth Lajos Univ.	(Hungray)	Oct. 1993 -
Prof. M. A. Marek	Prague Inst. of Chemical Tech.	(Czech)	Oct. 1993
Prof. K. Müllen*2	Max Plank Lab.	(Germany)	Oct. 1993
Prof. M. Herman*2	Univ. Libre de Bruxelles	(Belgium)	Oct. 1993
Dr. E. Sekreta*2	Kyoto Univ.	(U.S.A.)	Oct. 1993
Prof. M. Hanack	Tübingen Univ.	(Germany)	Oct. 1993
Dr. K. Agladze*2	Russian Acad. of Sci.	(Russia)	Nov. 1993
Prof. T. A. Miller	The Ohio State Univ.	(U.S.A.)	Nov. 1993
Prof. J. F. Hermans	Univ. of Leiden	(Holland)	Nov. 1993
Prof. V. A. Apkarian	Univ. of California, Irvine	(U.S.A.)	Nov. 1993
Prof. C. B. Moore	Univ. of California, Berkeley	(U.S.A.)	Nov. 1993
Prof. R. D. Levine*2	The Hebrew Univ. of Jerusalem	(Israel)	Nov. 1993
Dr. M. Terekhin*2	Kurchatov Inst.	(Russia)	Nov. 1993 -
Dr. N. Yu. Svechnikov*2	Kurchatov Inst.	(Russia)	Nov. 1993 -
Prof. W. Gudat*2	BESSY	(Germany)	Nov. 1993
Prof. D. Zhu*4	Inst. of Chem. Beijing	(China)	Nov. 1993
Prof. V. Saile	Louisiana State Univ.	(U.S.A.)	Nov. 1993
Prof. H. C. Wolf	Stuttgant Univ.	(Germany)	Nov. 1993
Dr. H. Helm	SRI Inst.	(U.S.A.)	Nov. 1993
Prof. G. Duxbury	Strathclyde Univ.	(U.K.)	Nov. 1993
Prof. Y. Berlin*5	Russian Acad. Sci.	(Russia)	Nov. 1993 -
Prof. Sungyul Lee	Kyunghee Univ.	(Korea)	Dec. 1993
Prof. M. Rögner	Inst. for Botany	(Germany)	Dec. 1993
Prof. Poh-Kun Tseng	Natl. Taiwan Univ.	(Taiwan)	Dec. 1993

Prof. Way-Faung Pong	Tamkang Univ.	(Taiwan)	Dec. 1993
Prof. Young S. Choi*2	Inha Univ.	(Korea)	Dec. 1993 - Feb. 1994
Mr. Taek Soo Kim	Inha Univ.	(Korea)	Dec. 1993 - Feb. 1994
Prof. Kang Young Kee*2	Chungbuk National Univ.	(Korea)	Dec. 1993 - Feb. 1994
Prof. W. Kiefer	Würzburg Univ.	(Germany)	Dec. 1993
Prof. D. G. Whitten	Univ. of Rochester	(U.S.A.)	Dec. 1993
Prof. J. Goodman	Univ. of Rochester	(U.S.A.)	Dec. 1993
Prof. G. L. McLendon	Univ. of Rochester	(U.S.A.)	Dec. 1993
Prof. A. B. Myers	Univ. of Rochester	(U.S.A.)	Dec. 1993
Prof. S. Mukamel	Univ. of Rochester	(U.S.A.)	Dec. 1993
Prof. J. M. Farrar	Univ. of Rochester	(U.S.A.)	Dec. 1993
Dr. E. Conwell	Xerox Webster Res. Center	(U.S.A.)	Dec. 1993
Dr. J. S. Facci	Xerox Corp.	(U.S.A.)	Dec. 1993
Dr. T. L. Penner	Eastman Kodak Co.	(U.S.A.)	Dec. 1993
Dr. I. Gould	Eastman Kodak Co.	(U.S.A.)	Dec. 1993
Dr. D.L. Mantell	Xerox Webster Res. Center	(U.S.A.)	Dec. 1993
Prof. M. A. El-Sayed	Univ. of California, Los Angeles	(U.S.A.)	Dec. 1993
Prof. H. D. Kasez	Univ. of California, Los Angeles	(U.S.A.)	Dec. 1993
Dr. I. Khairullin*2	Uzbek Acad. Sci.	(Uzbekistan)	- Jan. 1994
Ms. S. Tavender	Rutherford Appleton Lab.	(U.K.)	Jan. 1994
Prof. A. J. Ceulemans*1	Katholieke Univ.	(Belgium)	Jan. 1994
Prof. M. J. Stillman*1	Univ. of Western Ontario	(Canada)	Jan. 1994
Prof. C. C. Leznoff*1	York Univ.	(Canada)	Jan. 1994
Prof. D. Braun*1	Katholieke Univ.	(Belgium)	Jan. 1994
Dr. J. D. Wright*1	Univ. of Kent	(U.K.)	Jan. 1994
Prof. M. Hanack	Tübingen Univ.	(Germany)	Jan. 1994
Prof. I. H. Munro	Daresbury Lab.	(U.K.)	Jan., Feb. 1994
Dr. V. P. Suller	Daresbury Lab.	(U.K.)	Jan. 1994
Prof. Tei Jong Kang	Taegoo Univ.	(Korea)	Jan. - Feb. 1994
Prof. Yong Faung Li*4	Inst. of Chem. Academia Sinica	(China)	Jan. - Apr. 1994
Dr. Jianping Cai*4	Tokyo Chemical Industry Co. Ltd.	(China)	Feb. 1994 -
Mr. Guang-He Shi	Embassy of China	(China)	Feb. 1994
Mr. Dongxiang Li	Embassy of China	(China)	Feb. 1994
Dr. P. A. Hatherly	Univ. of Reading	(U.K.)	Feb. 1994
Prof. Yiqiu Wang	Beijing Univ.	(China)	Feb. 1994
Prof. Xiaojie Xu	Beijing Univ.	(China)	Feb. 1994
Prof. Zhongfan Liu	Beijing Univ.	(China)	Feb. 1994
Dr. D. M. P. Holland	Daresbury Lab.	(U.K.)	Feb. 1994
Dr. Y. A. Gruzdkov*2	Boreskov Inst. of Catalysis	(Russia)	Feb. 1994 -
Prof. Tong-Nyong Lee*2	Pohang Accelerator Lab.	(Korea)	Feb. 1994 -
Dr. Hwang Chanyong*4	Korean Res. Inst.	(Korea)	Feb. 1994
Dr. Park Hyungho*4	Korean Res. Inst.	(Korea)	Feb. 1994
Dr. Lee Sunwoo*4	Korean Res. Inst.	(Korea)	Feb. 1994
Mr. Cheon in-Sang*4	Korea Inst. of Sci. and Tech.	(Korea)	Feb. 1994
Mr. An ki-seok*4	Sung Kyun Kwan Univ.	(Korea)	Feb. 1994
Mr. Kim jae-min*4	Sung Kyun Kwan Univ.	(Korea)	Feb. 1994
Dr. Hwang Chisun*4	Korean Res. Inst.	(Korea)	Feb. 1994
Prof. P. Day*3	Royal Inst.	(U.K.)	Feb. 1994
Prof. D. Steinborn	Martin Luther Univ.	(Germany)	Feb. 1994
Prof. M. S. Jhon	Korea Inst. of Sci. and Tech.	(Korea)	Feb. 1994
Dr. R. J. Whitehead*2	Darham Univ.	(U.K.)	- Mar. 1994
Prof. Y. N. Molin	Russian Acad. of Sci., Novosibirsk	(Russia)	Mar. 1994
Dr. M. A. Lipton	Purdue Univ.	(U.S.A.)	Mar. 1994
Prof. J. C. Polanyi*3	Univ. of Toronto	(Canada)	Mar. 1994
Dr. H. Pal*2	Bhabha Atomic Res. Center	(India)	Mar. 1994 -
Prof. J. Troe*1	Gottingen Univ.	(Germany)	Mar. 1994
Prof. K. P. Johnston*1	Univ. of Texas	(U.S.A.)	Mar. 1994
Prof. F. V. Bright*1	State Univ. of N.Y.	(U.S.A.)	Mar. 1994
Dr. E. Sekreta*1	Kyoto Univ.	(U.K.)	Mar. 1994
Prof. S. Howdle*1	Univ. of Nottingham	(U.K.)	Mar. 1994

Prof. J. Brennecke*[1]	Univ. of Notre Dame	(U.S.A.)	Mar. 1994
Prof. K. A. Nelson	MIT	(U.S.A.)	Mar. 1994
Prof. J. Klein	Weizmann Inst. of Sci.	(Israel)	Mar. 1994
Dr. U. Hillebrecht*[2]	Düsseldorf Univ.	(Germany)	Mar. 1994
Prof. P. Knochel	Philipps Univ.	(Germany)	Mar. 1994
Ms. S. Özer	Arizona State Univ.	(Turkey)	Apr. 1994
Mr. G. Keogh	Imperial Coll.	(U.K.)	Apr. 1994 -
Prof. A. Ehrenberg*[2]	Univ. of Stockholm	(Sweden)	Apr. 1994
Prof. R. J. Whitby	Southampton Univ.	(U.K.)	Apr. 1994
Prof. K. Janda	Scripps	(U.S.A.)	Apr. 1994
Mr. M. Atiyah	Royal Society	(U.K.)	Apr. 1994
Mr. G. Allen	Royal Society	(U.K.)	Apr. 1994
Dr. R. Sowden	Sci. Council	(U.K.)	Apr. 1994
Dr. A. Mclaren	Royal Society	(U.K.)	Apr. 1994
Dr. A. H. Saleck*[2]	Köln Univ.	(Germany)	Apr. 1994 -
Prof. V. A. Ivanov*[5]	Russian Acad. of Sci., Kurnakov Inst.	(Russia)	Apr. 1994 -
Prof. B. Bagchi*[2]	Indian Inst. of Sci.	(India)	May 1994 -
Prof. P. X. Zhang	Chinese Academy of Sci.	(China)	May 1994
Prof. Tang Esheng	Inst. of High Energy Phys., Beijing	(China)	May 1994
Prof. Xian Dingchang	Inst. of High Energy Phys., Beijing	(China)	May 1994
Prof. M. Ikeda-Saito	Case Western Reserve Univ.	(U.S.A.)	May 1994
Prof. Kopin Liu	Academia Sinica	(Taiwan)	May 1994
Prof. G. Schatz	Northwestern Univ.	(U.S.A.)	May 1994
Dr. S. S. Ramamurthi*[2]	Center of Advanced Tech.	(India)	May 1994
Dr. R. Hahn*[4]	Tech. Univ. München	(Germany)	May 1994 -
Dr. L. S. Grigoryan*[4]	Armenia Acad. Sci.	(Armenia)	- Jun. 1994
Prof. Hee Kwon Chae*[2]	Hankuk Univ. of Foreign Studies	(Korea)	Jun. 1994 -
Dr. H. Chosrowjan	Osaka Univ.	(Armenia)	Jun. 1994
Dr. S. R. Meech*[4]	Univ. of East Anglia	(U.S.A.)	Jun. 1994
Prof. Chang-Guo Zhan	Central China Normal Univ.	(China)	Jun. - Aug. 1994
Prof. G. Walker	Univ. of Pittsburgh	(U.S.A.)	Jun. 1994
Prof. R. L. Christensen*[4]	Bowdoin Coll.	(U.S.A.)	Jul. 1994
Prof. Bongsoo Kim*[4]	Kyungpook National Univ.	(Korea)	Jul. 1994 -
Dr. S. H. R. Abdi*[2]	Central Salt and Marine Chem. Inst.	(India)	Jul. 1994 -
Prof. Seung C. Park*[4]	Kangwon National Univ.	(Korea)	Jul. - Aug. 1994
Prof. R. I. Hall	Univ. P et M Curie	(France)	Jul. 1994
Dr. S. R. Gandhi*[2]	MPI für Strömungsforschung	(U.S.A.)	Jul. 1994 -
Prof. Young S. Choi	Inha Univ.	(Korea)	Jul. 1994
Mr. Byung H. Kang	Kyungpook National Univ.	(Korea)	Jul. 1994
Prof. G. H. Lee*[4]	Seoul National Univ.	(Korea)	Jul. 1994
Prof. S. W. Rhee*[4]	Pohang Inst. of Sci. Tech.	(Korea)	Jul. 1994
Mr. Y. B. Park*[4]	Pohang Inst. of Sci. Tech.	(Korea)	Jul. 1994
Dr. C. G. Young*[2]	Univ. Melbourne	(Australia)	Jul. 1994
Prof. T. C. Steinle	Arizona State Univ.	(U.S.A.)	Jul. 1994

AWARDS

Professor Yoshihara's Scientific Achievements

Professor Keitaro Yoshihara was given the first DAIWA AWARD of the Daiwa Anglo-Japanese Foundation by the Lord Adrian FRS Trustee of the Foundation and Mr. Hiroshi Kitamura Ambassador of Japan in the United Kingdom on March 2, 1994 at the Royal Institution of Great Britain for his contribution to "Picosecond Laser Spectroscopy".

Many important chemical events such as various chemical reactions, intra- and intermolecular energy transfer, primary processes in vision and photosynthesis etc. occur at ultrafast time scale of picosecond (10^{-9} — 10^{-12} second). Professor Yoshihara and his coworkers established various ultrafast laser spectroscopies and studied cis-trans isomerization in solution and gas phases with stilbenes and various simple polyenes, and uncovered the great details of electronic and vibrational structures and photochemical reaction dynamics. The Award was given for a team of UK and Japanese scientists for the collaborative efforts and was received by the teams of Dr. Jeremy G. Frey of the University of Southampton with Dr. Stephen R. Meech of the Heriot-Watt University and of Professor Keitaro Yoshihara of IMS with Dr. Andrew J. Bell (from Southampton), Dr. Keisuke Tominaga, and Mr. Shigeichi Kumazaki.

Professor Akira Nakamura's Scientific Achievements

Prof. A. Nakamura of Coordiantion Chemistry Laboratories received the Award of the Chemical Society of Japan in 1994 for his contribution to "Studies on Reactive Metal Complexes with Carbon and Sulfur Ligands".

Many of the complexes coordinated by carbon ligands are reactive and some of them have been utilyzed as homogeneous catalysts. Prof. A. Nakamura has been interested in these coordination compounds for long time and synthesized many new complexes for selective homogeneous catalysis such as hydrogenation, oxygenation, polymerization, and carbenoid reaction. Later, he also investigated various model complexes for metalloenzymes especially redox-active ones and prepared many of such functional model complexes with sulfur ligands, in particular cysteine-containing oligopeptides as ligands. Some of these new complexes were found to have catalytic activity for redox reactions. His work is thus evaluated as creating fundamentally important aspects of coordination chemistry.

Associate Professor Nemoto's Scientific Achievements

Associate Professor Hisao Nemoto of Department of Applied Molecular Science received 'Progress Award in Synthetic Organic Chemistry, Japan' in 1993 for his contributions to "Synthesis of Boron Carriers for Neutron Capture Therapy and Studies of Activated Imines". Neutron capture therapy (NCT) is one of the advanced methods for the cure of cancers using the nuclear energy caused by thermal neutron absorption at the local area where boron—10 isotope is concentrated. His contribution to NCT is the design and synthesis of organoboron compounds (boron carriers) which deliver sufficient amount of boron atoms at the target tumor cells. The details are as follows.

1. Development of general methods for the synthesis of boron carriers toward treatment of cancers by NCT

He developed variety of the methods for the synthesis of boron carriers as nucleoside derivatives or amino acid analogue. Chemistry of o-carborane, an icosahedral type of boron cluster, was studied from a viewpoint of organic chemistry. He efficiently utilized transition metal catalysts for the development of new reactions.

2. Synthesis of new boron carriers having more therapeutically efficiency than the ordinary clinically used boron carriers

In vitro examinations, his designed several boron carriers are more incorporated into tumor cells than the clinically used boron carriers at present.

3. Design and preparation of new water-solubilizing moiety, polyglycerols of cascade type.

His designed new polyglycerols of cascade type, generally make the boron carriers more water-soluble and less toxic than the original corresponding molecules. Furthermore, uptake ratio of a tumor cell against a normal cell *in vitro* is increased after the boron carriers are converted to one bearing the polyglycerols.

4. Studies of "Activated Imines"

He studied the imines bearing electron withdrawing group. Analysis of an acyliminium cation at low temperature by nuclear magnetic resonance, development of transition metal-catalyzed carbon-carbon bond formation reactions, and application to the synthesis of α-amino acids were carried out. His new reagent, $ROCH(CN)_2$ as a masked formyl cyanide, played an important role for the synthesis of α-amino acids.

Associate Professor Suzuki's Scientific Achievements

Associate Professor Toshinori Suzuki of the Department of Electronic Structure received the Award of the Chemical Society of Japan for Young Chemists in 1994 for his contributions to "Reaction Dynamics via State-Selective Laser Excitation and Detection of Molecules".

Chemical reactions and energy relaxation processes are difficult to probe in real time. However, their detailed dynamics can be elucidated by measuring asymptotic properties, such as the final state distributions of products and their dependence on the initial quantum state of the reactants. Professor Suzuki has developed new laser spectroscopic methods to prepare and probe specific quantum states of molecules, which have been invaluable to the elucidation of the dynamics of intramolecular relaxation processes and bimolecular reactions. He has studied intramolecular vibrational redistribution (IVR) by stimulated emission ion dip spectroscopy, internal conversion by population labeling (hole burning) spectroscopy, and intersystem crossing by phosphorescence excitation spectroscopy. His spectroscopic studies on *trans*-stilbene revealed that the two phenyl rings have a large amplitude torsional motion (up to 50 degrees in dihedral angle), and that this motion accelerates IVR. He has also investigated photodissociation and bimolecular processes via the full characterization of product rovibrational and translational states using one-dimensional and two-dimensional (imaging) Doppler techniques. In a series of elegant experiments using one-dimensional Doppler spectroscopy and infrared diode laser spectrocopy, he has shown that the distributions for the umbrella mode of methyl radicals produced from the photodissociation of methyl iodide (CH_3I) and the reaction between oxygen (O ^3P, O ^1D) and methane (CH_4) are not inverted. These results corrected erroneous conclusions from previous studies, and clearly indicated the adiabatic nature of methyl deformation during these reactions.

LIST OF PUBLICATIONS

R. KISHI, A. NAKAJIMA, S. IWATA, and K. KAYA, "Theoretical Study of Silicon-Sodium Binary Clusters: Geometrical and Electronic Structures of Si_nNa (n=1,7)", *Chem. Phys. Lett.* **224,** 200 (1994).

A. NAKAJIMA, T. TAGUWA, K. NAKANO, K. HOSHINO, S. IWATA, and K. KAYA, "Photoelectron Spectroscopy of AlS^- Diatomic Anion", *Chem. Lett.* 1525 (1994).

Y. SONODA, S. IWATA, and Y. OSAMURA, "Molecular Orbital Study of the Ion-Molecule Reactions Producing the Hydrocarbons in Interstellar Space", *Bull. Chem. Soc. Jpn.* **66,** 3345 (1993).

H. WATANABE, M. AOKI, and S. IWATA, "Theoretical Studies of the Aluminum-Water Clusters $Al(H_2O)_n$ and Their Ions $[Al(H_2O)_n]^+$", *Bull. Chem. Soc. Jpn.* **66,** 3245 (1993).

M. HIYAMA and S. IWATA, "Theoretical Assignment of the Vibronic Bands in the Photoelectron Spectra of N_2 below 30 eV", *Chem. Phys. Lett.* **211,** 319 (1993).

T. IKEGAMI, T. KONDOW, and S. IWATA, "The Photodissociation Dynamics of Ar_3^+", *J. Chem. Phys.* **99,** 3588 (1993).

M. HIYAMA and S. IWATA, "Assignment of the Photoelectron Spectrum of HCl above 20 eV", *Chem. Phys. Lett.* **210,** 187 (1993).

T. IKEGAMI, T. KONDOW, and S. IWATA, "The Geometric and Electronic Structures of Ar_n^+(n=3–27)", *J. Chem. Phys.* **98,** 3038 (1993).

I. OHMINE, "Inherent Structure Analysis of Collective Motion and Fluctuation in Liquid Water", Atti di Connferenze, *Italian Physical Society* **43,** 7 (1993).

T. KOMATSUZAKI and I. OHMINE, "Energetics of Proton Transfer in Liquid Water I; Ab-initio Study for Origin of Manybody Interaction and Potential Energy Surface", *Chem. Phys.* **180,** 239 (1994).

M. CHO, G.R. FLEMING, S. SAITO, I. OHMINE, and R.M. STRATT, "Instantaneous Normal Mode Analysis of Liquid Water", *J. Chem. Phys.* **100,** 6672 (1994).

S. TAKADA, K. TSUDA, A. OHSAKI, and H. NAKAMURA, "Effects of Potential Energy Surface Topography and Isotope Substitution in Atom-Diatom Chemical Reactions: The Cl+H_2 and D+H_2 Systems", *Adv. in Molecular Vibrations and Collision Dynamics* **2A,** 245 (1994).

S. TAKADA and H. NAKAMURA, "Wentzel-Kramers-Brillouin Theory of Multidimensional Tunneling: General Theory for Energy Splitting", *J. Chem. Phys.* **100,** 98 (1994).

K. MORIBAYASHI, S. TAKADA, and H. NAKAMURA, "Constant Centrifugal Potential Approximation for Atom-Diatom Chemical Reaction Dynamics", *J. Chem. Phys.* **100,** 4284 (1994).

Y. TANIMURA and S. MUKAMEL, "Multistate Quantum Fokker-Planck Approach to Nonadiabatic Wave Packet Dynamics in Pump-Probe Spectroscopy", *J. Chem. Phys.* **101,** 3049 (1994).

A. ASADA, K. NISHIMOTO, and K. KITAURA, "Theoretical Study on Binding Enthalpies and Population of Isomer of $Cl^-(H_2O)_n$ Clusters at Room Temperature", *J. Phys. Chem.* **97,** 7724 (1993).

M. GOTO and S. SAITO, "Submillimeter-Wave Spectra of the PH and PD Radicals in the $^3\Sigma^-$ State", *Chem. Phys. Lett.* **211,** 443 (1993).

S.K. LEE, H. OZEKI, S. SAITO, and S. YAMAMOTO, "Submillimeter-Wave Spectrum of the SiH_3^+ Ion. J=2–1, K=0 and 1 Transitions", *Chem. Phys. Lett.* **224,** 21 (1994).

M. IZUHA, S. YAMAMOTO, and S. SAITO, "Rotational Spectrum of SiC_2 in the ν_3 Excited States", *Spectrochimica Acta* **50A,** 1371 (1994).

N. MORITA, M. KUMAKURA, T. YAMAZAKI, E. WIDMANN, H. MASUDA, I. SUGAI, R.S. HAYANO, F.E. MAAS, H.A. TORII, F.J. HARTMANN, H. DANIEL, T. von EGIDY, B. KETZER, W. MULLER, W. SCHMID, D. HORVATH, and J. EADES, "First Observation of Laser-Induced Resonant Annihilation in Metastable Antiprotonic Helium Atoms", *Phys. Rev. Lett.* **72,** 1180 (1994).

A. FUJII and N. MORITA, "Laser Spectroscopic Investigation of High Rydberg States of NO: Decay Dynamics Near the First Ionization Threshold", *Laser Chem.* **13,** 259 (1994).

Y. MIZUTANI, S. TOKUTOMI, and T. KITAGAWA, "Resonance Raman Spectra of the Photointermediates in Phytochrome Phototransformation: Deprotonation of the Chromophore in the Bleached Intermediate", *Biochemistry* **33,** 153 (1994).

S. SATO and T. KITAGAWA, "Vibrationally Hot (dd) Excited States of Ni^{II}-Porphyrin Probed by Picosecond Time-Resolved Resonance Raman Spectroscopy", *Springer Proc. Phys.* **74,** 104 (1994).

S. HIROTA, T. MOGI, T. OGURA, T. HIRANO, Y. ANRAKU, and T. KITAGAWA, "Observation of the Fe-O_2 and Fe^{IV}=O Stretching Raman Bands for Dioxygen Reduction Intermediates of Cytochrome *bo* Isolated from *Escherichia coli*", *FEBS Lett.* **352,** 67 (1994).

Y. MIZUTANI, Y. WATANABE, and T. KITAGAWA, "Resonance Raman Characterization of Iron(III) Porphyrin N-Oxide: Evidence for an Fe-O-N Bridged Structure", *J. Am. Chem. Soc.* **116,** 3439 (1994).

S. KAMINAKA, Y-X. ZHOU, A. TSUNESHIGE, T. YONETANI, and T. KITAGAWA, "Sequential Changes of the Fe-Histidine Bond upon Ligand Binding to Hemoglobins: Resonance Raman Study of $\alpha\alpha$-Crosslinked Co-Fe Hybrid Hbs", *J. Am. Chem. Soc.* **116,** 1683 (1994).

N. SONE, T. OGURA, S. NOGUCHI, and T. KITAGAWA, "Proton Pumping Activity and Visible Absorption and Resonance Raman Spectra of a cao-Type Cytochrome c Oxidase Isolated from Thermophilic Bacterium Bacillus PS3", *Biochemistry* **33,** 849 (1994).

S. OZAWA, Y. WATANABE, S. NAKASHIMA, T. KITAGAWA, and I. MORISHIMA, "Preparation and Characterization of Oxoiron(IV) Chlorin Complexes as the First Models for a Reaction Intermediate in the Catalytic Cycle of Cytochrome d", *J. Am. Chem. Soc.* **116,** 634 (1994).

K. KAMOGAWA, M. TAKAMURA, H. MATSUURA, and T. KITAGAWA, "A Multi-Reflection Raman Cell for Studying Dilute Aqueous Solutions", *Spectrochim. Acta* **50A,** 1513 (1994).

S. HIROTA, T. OGURA, K. SHINZAWA-ITOH, S. YOSHIKAWA, M. NAGAI, and T. KITAGAWA, "Vibrational Assignments of the FeCO Unit of CO-Bound Heme Proteins Revisited: Observation of a New CO-Isotope-Sensitive Raman Band Assignable to the FeCO Bending Fundamental", *J. Phys. Chem.* **98,** 6652 (1994).

T. KATO, "Absorption and Emission Spectra for C_{60} Anion", *Laser Chem.* **14,** 155 (1993).

T. SUZUKI, Y. MARUYAMA, T. KATO, K. KIKUCHI, and Y. ACHIBA, "Electrochemical Properties of La@C_{82}", *J. Am. Chem. Soc.* **115,** 11006 (1993).

T. KATO, S. SUZUKI, K. KIKUCHI, and Y. ACHIBA, "ESR Study of the Electronic Structure of Metallofullerenes: a Comparison between La@C_{82} and Sc@C_{82}", *J. Phys. Chem.* **97,** 13425 (1993).

P.B. BISHT, H. PETEK, and K. YOSHIHARA, "Exciplex Formation in van der Waals Complexes of Naphthalene-Triethylamine in a Supersonic Jet", *Chem. Phys. Lett.* **213,** 75 (1993).

V. KAMALOV, I.A. STRUGANOVA, and K. YOSHIHARA, "Time-Resolved Emission Spectra of the BIC J-Aggregate at Low Temperature", *Chem. Phys. Lett.* **213,** 559 (1993).

H. SEKIYA, M. HABU, H. UJITA, T. TSUJI, A. MORI, H. TAKESHITA, Y. NISHIMURA, H. PETEK, and K. YOSHIHARA, "Dual Fluorescence and Excited-State Intermolecular Proton Transfer in Jet-Cooled 3,4-Benzotropolone", *Chem. Phy. Lett.* **215,** 641 (1993).

H. KANDORI, R.F. BORKMAN, and K. YOSHIHARA, "Picosecond Transient Absorption of Aqueous Tryptophan", *J. Phys. Chem.* **97,** 9664 (1993).

A. AGNESI, G.C. REALI, V. KUBECEK, S. KUMAZAKI, Y. TAKAGI, and K. YOSHIHARA, "β-Barium Borate and Lithium Triborate Picosecond Parametric Oscillators Pumped by a Frequency-Tripled Passive Negative-Feedback Mode-Locked Nd: YAG Laser", *J. Opt. Soc. Am.* B **10,** 2211 (1993).

K. KEMNITZ, K. YOSHIHARA, T. SUZUMOTO, T. TANI, M. LINDRUM, J. MOLL, and D. DAEHNE, "Primary Photopysical Processes in J-Aggregates of Spectral Sensitisers", *Proc. Indian Acad. Sci.* **105,** 783 (1993).

A. DOUHAL, F. AMAT-GUERRI, A.U. ACUNA, and K. YOSHIHARA, "Picosecond Vibrational Relaxation in the Excited-State Proton-Transfer of 2-(3′-Hydroxy-2′-Naphthyl)Benzimidazole", *Chem. Phys. Lett.* **217,** 619 (1994).

V. KUBECEK, K. HAMAL, Y. TAKAGI, and K. YOSHIHARA, "Ti:Sapphire Laser Pumped by a Long Train of Pulses from Mode-Locked Nd: YAG Laser with Negative Feedback", *Czeck, J. Phys.* **44,** 115 (1994).

V. KAMALOV, I.A. STRUGANOVA, T. TANI, and K. YOSHIHARA, "Temperature Dependence of Superradiant Emission of BIC J-Aggregates", *Chem. Phys. Lett.* **220,** 257 (1994).

B. KIM and K. YOSHIHARA, "Resonance Enhanced Two Photon Ionization Spectroscopy of RbCs in a Very Cold Molecular Beam", *J. Chem. Phys.* **100,** 1849 (1994).

Y.S. CHOI, T.S. KIM, H. PETEK, K. YOSHIHARA, and R.L. CHRISTENSEN, "Evidence for Quantization of the Transition State for *cis-trans* Isomerization", *J. Chem. Phys.* **100,** 9269 (1994).

K. YOSHIHARA, Y. NAGASAWA, A. YARTSEV, S. KUMAZAKI, H. KANDORI, A.E. JOHNSON, and K. TOMINAGA, "Femtosecond Intermolecular Electron Transfer in Condensed Systems", *J. Photochem. Photobiol. A: Chem.* **80,** 169 (1994).

B. KIM, K. YOSHIHARA, and S. LEE, "Complex Resonances in the Predissociation of Cs_2", *Phys. Rev. Lett.* **73,** 418 (1994).

K. SAWABE and Y. MATSUMOTO, "Oxygen-Exchange Reaction between O_2 and NO Coadsorbed on a Pt(111) Surface: Reactivity of Molecularly Adsorbed Oxygen", *Surf. Sci. Lett.* **303,** L385 (1994).

Y.A. GURUZDKOV, K. WATANABE, K. SAWABE, and Y. MATSUMOTO, "Photochemical C-H Bond Activation of Methane on a Pt(111) Surface", *Chem. Phys. Lett.* **227,** 243 (1994).

Y. MATSUMOTO, J. LEE, H. KATO, and K. SAWABE, "Dynamics of Photochemical Processes of N_2O Adsorbed on Metal and Semiconductor Surfaces", *SPIE Proceedings* **2125,** 303 (1994).

M. TAKAYANAGI and I. HANAZAKI, "Stimulated-Emission-Pumping Laser-Induced-Fluorescence Spectroscopy of Phenol and Anisole", *Laser Chem.* **14,** 103 (1994).

J. GORECKI and I. HANAZAKI, "A Simple Phenomenological Model for Nonequilibrium Interaction between Two Reactions in a Lorentz Gas", *Chem. Phys.* **181,** 39 (1994).

Y. MORI, Y. NAKAMICHI, T. SEKIGUCHI, N. OKAZAKI, T. MATSUMURA, and I. HANAZAKI, "Photo-Induction of Chemical Oscillation in the Belousov-Zhabotinsky Reaction under the Flow Condition", *Chem. Phys. Lett.* **211,** 421 (1993).

T. KONO, M. TAKAYANAGI, and I. HANAZAKI, "Rotational Excitation of HCO Produced by the Photodissociation of Acetaldehyde", *J. Phys. Chem.* **97,** 12793 (1993).

T. GEJO, M. TAKAYANAGI, T. KONO, and I. HANAZAKI, "Hole Burning Spectrum of the Vinoxy Radical in the B(^{2}A″) State in a Supersonic Free Jet", *Chem. Lett.* **1993,** 2064 (1993).

G. RABAI and I. HANAZAKI, "Oscillatory Reaction in the System of Hydrogen Peroxide-Hydrogen Sulfite Ion-Hexacyanoferrate(II) Ion a Semibatch Reactor", *J. Phys. Chem.* **98,** 2592 (1994).

I. HANAZAKI, "Fragment Rotational Excitation due to the Parent Rotational Motion in the Dissociation of Molecules", *Chem. Phys. Lett.* **218,** 151 (1994).

T. GEJO, M. TAKAYANAGI, T. KONO, and I. HANAZAKI, "Photodissociation Dynamics of Acetaldehyde: Vibrational Energy Distribution in Photofragment HCO", *Chem. Phys. Lett.* **218,** 343 (1994).

M. TAKAYANAGI and I. HANAZAKI, "Intermolecular Vibrations and Dynamics of the Anisole · Benzene Complex Studied by the Multi-resonance Spectroscopy", *Spectrochim. Acta* **50A,** 1435 (1994).

T. SEKIGUCHI, Y. MORI, N. OKAZAKI, and I. HANAZAKI, "Photoinduction and Photoinhibition of Chemical Oscillators in the tris(2,2′-bipyridine)ruthenium(II)-Catalyzed Minimal Bromate Oscillator", *Chem. Phys. Lett.* **219,** 81 (1994).

G. RABAI, "Explanation of the Long-Lived Oscillations in the Chlorite Ion-Iodide Ion-Malonic Acid System", *J. Phys. Chem.* **98,** 5920 (1994).

H.-L. KIM, M. TAKAYANAGI, and I. HANAZAKI, "Photochemistry of $N_2O \cdot H_2O$ Complexes Produced in Supersonic Jets", *Chem. Phys. Lett.* **222,** 431 (1994).

K. TONOKURA and T. SUZUKI, "Slicing Photofragment Spatial Distribution by Laser Sheet Ionization", *Chem. Phys. Lett.* **224,** 1 (1994).

R. NAKAGAKI, N. KITAMURA, I. AOYAMA, and H. OHSHITA, "Hydrogen Bonding of Aromatic Amines in Hydroxylic Solvents 2. Absorption and Emission Spectroscopy of Substituted 7-Aminocoumarins and 7-Aminocarbostyrils", *J. Photochem. Photobiol. A: Chem.* **80,** 113 (1994).

R. NAKAGAKI, "Coment on "Photochemical Reaction of 4-Methyl-2-Quinolinecarbonitrile with Optically Active (S)- or (R)-2-Phenylpropionic Acid. The Magnetic-Field and Solvent Effects and Chiral-Symmetry Breaking", *Chem. Phys.* **185,** 405 (1994).

L.S. GRIGORYAN, K. YAKUSHI, A.V. NARLIKAR, P.K. DUTTA, and S.B. SAMANTHA, "Modification of Normal-State Superconducting Properties of High-T_c Oxides via Treatment by Metal-Phthalocyanines", *Int. J. Modern Phys. B* **8,** 615 (1993).

L.S. GRIGORYAN, K. YAKUSHI, C.-J. LIU, S. TAKANO, M. WAKATA, and H. YAMAUCHI, "Evolution of Optical Absorption and Superconductivity in Bi-2212 and 2223 Oxides Intercalated by Metal-Phthalocyanines: A Systematical Study as a Function of Intercalation Level", *Physica C* **218,** 153 (1993).

L.S. GRIGORYAN and K. YAKUSHI, "Role of Double Bi-O Layers in Flux Pinning Properties of Bi-Oxides", *Physica C* **219,** 74 (1994).

L.S. GRIGORYAN, K. YAKUSHI, A.V. NARLIKAR, and S.B. SAMANTHA, "Contribution of Interblock Coupling to T_c in High-T_c Bi-Oxides", *Mod. Phys. Lett. B* **8,** 251 (1994).

H. YAMAKADO, T. IDA, A. UGAWA, K. YAKUSHI, K. AWAGA, Y. MARUYAMA, K. IMAEDA, and H. INOKUCHI, "Structure and Solid State Properties of Stable Ring-Oxidized Conductor $CoPc(AsF_6)_{0.5}$: Interaction between Rign π-Electrons and Cobalt d-Electrons", *Synthetic Metals* **62,** 169 (1994).

I.I. KHAIRULLIN, I. SHIROTANI, and K. YAKUSHI, "X- and Q-band ESR Study of New Poly-CuPc Compounds Synthesized under High Pressure: The Possibility of Two-dimensional Sheet Polymers", *Synthetic Metals* **64,** 217 (1994).

T. ENOKI, Y. OHTSU, K. SUZUKI, K. IMAEDA, A.A. ZAKHIDOV, K. YAKUSHI, K. KIKUCHI, S. SUZUKI, and Y. ACHIBA, "Hydrogen Uptake Effects on Structures and Solid State Properties in K_3C_{60}", *Synthetic Metals* **64,** 329 (1994).

S. UJI, H. AOKI, M. TOKUMOTO, A. UGAWA, and K. YAKUSHI, "Fermi Surface and Magnetoresistance in β″-$(BEDT\text{-}TTF)_2AuBr_2$", *Physica B* **194–196,** 1307 (1994).

S. UJI, H. AOKI, M. TOKUMOTO, A. UGAWA, and K. YAKUSHI, "Fermi Surface and Magnetoresistance in an Organic Metal β″-$(BEDT\text{-}TTF)_2AuBr_2$", *Mat. Res. Soc. Symp. Proc.* **328,** 337 (1994).

Y. KOBAYASHI, T. NAKAMURA, T. TAKAHASHI, K. KANODA, B. HILTI, and J.S. ZAMBOUNIS, "Nuclear Relaxation in the Superconducting State of *(MDT-TTF)$_2$AuI$_2$*", *J. Superconductivity* **7,** 663 (1994).

T. NAKAMURA, T. NOBUTOKI, M. MIYAMOTO, Y. TSUBOKURA, R. TSUCHIYA, T. TAKAHASHI, K. KANODA, and G. SAITO, "Systematic Investigation of Electronic Structure in BEDT-TTF Based Organic Superconductors with T_c above 10K; *κ-(BEDT-TTF)$_2$X (X=Cu(NCS)$_2$, Cu[N(CN)$_2$]Br, and Cu(CN)[N(CN)$_2$])*", *J. Superconductivity* **7,** 671 (1994).

T. SUZUKI, Y. MARUYAMA, T. KATO, K. KIKUCHI, and Y. ACHIBA, "Electrochemical Properties of La@C_{82}", *J. Am. Chem. Soc.* **115,** 11006 (1993).

T. SUZUKI, Y. MARUYAMA, T. AKASAKA, W. ANDO, K. KOBAYASHI, and S. NAGASE, "Redox Properties of Organofullerenes", *J. Am. Chem. Soc.* **116,** 1359 (1994).
S. YOSHIDA, K. KOZAWA, Y. MARUYAMA, and T. UCHIDA, "Mobility of Charge Carriers in Sublimed Films of Phenothiazine Derivatives", *Bull. Chem. Soc. Jpn.* **66,** 3548 (1993).
T. NAKAMURA, T. KOMATSU, G. SAITO, T. OSADA, S. KAGOSHIMA, N. MIURA, K. KATO, Y. MARUYAMA, and T. OSHIMA, "Physical Properties and Dimensionality of κ-(BEDT-TTF)$_2$Cu(CN)[N(CN)$_2$]", *J. Phys. Soc. Jpn.* **62,** 4373 (1993).
S.L. FANG, K. KOHAMA, H. HOSHI, and Y. MARUYAMA, "Dependence of Off-Diagonal Components of $\chi^{(3)}$ on Substrate Temperature of Epitaxially Grown Vanadyl Phthalocyanine Films", *Jpn. J. Appl. Phys.* **32,** L1418 (1993).
S.L. FANG, K. KOHAMA, H. HOSHI, and Y. MARUYAMA, "Epitaxial Growth of Chloralminium Phthalocyanine and Vanadyl Phthalocyanine Double-Layer Structure by the Molecular Beam Epitaxy", *Synth. Met.* **64,** 167 (1994).
E. FRANKEVICH, Y. MARUYAMA, H. OGATA, Y. ACHIBA, and K. KIKUCHI, "Mobilities of Charge Carriers in C_{60} Orthorhombic Single Crystal", *Solid State Commun.* **88,** 177 (1993).
E. FRANKEVICH, Y. MARUYAMA, and H. OGATA, "Mobility of Charge Carriers in Vapor Phase Grown C_{60} Single Crystal", *Chem. Phys. Lett.* **214,** 39 (1993).
H. OGATA, Y. MARUYAMA, T. INABE, Y. ACHIBA, S. SUZUKI, K. KIKUCHI, and I. IKEMOTO, "Electrical Transport Properties of C_{60} Single Crystals Doped with Alkali Metals", *Mod. Phys. Lett.* **B7,** 1173 (1993).
A. SUZUKI, T. SUZUKI, R.J. WHITEHEAD, and Y. MARUYAMA, "Evidence of Spontaneous Magnetic Order in the C_{60} Complex with Tetrakis (dimethylamino)-ethylene (TDAE)", *Chem. Phys. Lett.* **223,** 517 (1994).
T. INABE, I. LUNEAU, T. MITANI, Y. MARUYAMA, and S. TAKEDA, "*N*-(2-Hydroxy-1-naphthylmethylene)-1-phenylenediamine and *N,N'*-Bis (2-hydroxy-1-naphthylmethylene)-p-phenylenediamine Crystals", *Bull. Chem. Soc. Jpn.* **67,** 612 (1994).
S.MIYAJIMA, A.F. MCDOWELL, and R.M. COTTS, "Pulsed-Field-Gradient Stimulated-Spin-Echo NMR Study of Anisotropic Self-Diffusion in Smectic Ad Liquid Crystal CBOOA", *Chem. Phys. Lett.* **212,** 277 (1993).
T. YAMAGUCHI, M. SUZUKI, and A. YOSHIDA, "Preparation and Characterizations of $CuIn_xGa_{1-x}Se_2$ Thin Films Crystallized by Annealing", *Jpn. J. Appl. Phys.* **32,** Suppl. **32–3,** 62 (1993).
A. YOSHIDA, S. IKEDA, and H. TSUCHIMOTO, "Hydrogenated Amorphous Silicon Films Prepared from Trisilane by Windowless Hydrogen Discharge Lamp", *J. Non-Cryst. Solids* **164–165,** 95 (1993).
Q.X. GUO, T. YAMAMURA, A. YOSHIDA, and N. ITOH, "Structual Properties of InN Films Grown on Sapphire Substrates by Microwave-excited Metalorganic Vapor-Phase Epitaxy", *J. Appl. Phys.* **75,** 4927 (1994).
Q.X. GUO and A. YOSHIDA, "Temperature Dependence of Band Gap Change in InN and AlN", *Jpn. J. Appl. Phys.* **33,** 2453 (1994).
Y. SAITO and A. YOSHIDA, "Defect Creation in Hydrogenated Amorphous Silicon Films Induced by Vacuum Ultraviolet Light from Synchrotron and Undulator Radiation", *Philos Mag.* **B70,** 133 (1994).
K. KANDA, S. KATSUMATA, T. NAGATA, Y. OZEKI, T. KONDOW, K. KUCHITSU, A. HIRAYA, and K. SHOBATAKE, "Photodissociation of BrCN in the Vacuum Ultraviolet Region", *Chem. Phys.* **175,** 399 (1993).
D.-C. CHE, T. KASAI, H. OHYAMA, K. KUWATA, M. KONO, K. TABAYASHI, and K. SHOBATAKE, "Fluorescence Excitation Spectra and Quantum Yield in Vacuum Ultraviolet Photodissociation of CF_3CN", *Chem. Lett.* **1994,** 133 (1994).
H. YASUMATSU, T. KONDOW, K. SUZUKI, K. TABAYASHI, and K. SHOBATAKE, "Absorption Spectra of Alkali Cyanide Vapor", *J. Phys. Chem.* **98,** 1407 (1994).
H. YOSHIKAWA and K. SHOBATAKE, "Velocity Distributions of Nascent $SiCl_n$ (n=2, 3, and 4) Products Formed from the Reaction of Si(111) with a Cl_2 Beam", *Chem. Phys. Lett.* **223,** 341 (1994).
S. HASEGAWA, T. MORI, K. IMAEDA, S. TANAKA, Y. YAMASHITA, H. INOKUCHI, H. FUJIMOTO, K. SEKI, and N. UENO, "Intermolecular Energy-Band Dispersion in Oriented Thin Films of Bis(1,2,5-thiadiazolo)-*p*-quinobis(1,3-dithiole) (BTQBT) by Angle-Resolved Photoemission", *J. Chem. Phys.* **100,** 6969 (1994).
S. HINO, K. MATSUMOTO, S. HASEGAWA, K. IWASAKI, K. YAKUSHI, T. MORIKAWA, T. TAKAHASHI, K. SEKI, K. KIKUCHI, S. SUZUKI, I. IKEMOTO, and Y. ACHIBA, "Photoelectron Spectra of a Higher Fullerene Compound C_{82} and its Potassium Complex", *Synth. Met.* **56,** 3191 (1993).
S. HINO, K. MATSUMOTO, S. HASEGAWA, K. IWASAKI, K. YAKUSHI, T. MORIKAWA, T. TAKAHASHI, K. SEKI, K. KIKUCHI, S. SUZUKI, I. IKEMOTO, and Y. ACHIBA, "Ultraviolet Photoelectron Spectra of C_{82} and K_xC_{82}", *Phys. Rev.* **B48,** 8418 (1993).
S. HINO, H. TAKAHASHI, K. IWASAKI, K. MATSUMOTO, T. MIYAZAKI, S. HASEGAWA, K. KIKUCHI, and Y. ACHIBA, "Electronic Structure of the Metallofullerene LaC_{82}: Electron Transfer from Lanthanum to C_{82}", *Phys. Rev. Lett.* **71,** 4261 (1993).
T. TAKAHASHI, T. MORIKAWA, H. KATAYAMA-YOSHIDA, S. HASEGAWA, H. INOKUCHI, K. SEKI, S. HINO, K. KIKUCHI, S. SUZUKI, I. IKEMOTO, and Y. ACHIBA, "Electronic Structure of Doped C_{60}: Strong Correlation or Lattice Distortion?", *Physica* **B186–188,** 1068 (1993).
H. MORI, I. HIRABAYASHI, S. TANAKA, T. MORI, Y. MARUYAMA, and H. INOKUCHI, "Electrical Properties and Crystal Structures of MDSe-TTF and EDSe-TTF Salts", *Solid State Commun.* **88,** 411 (1993).

Y. MISAKI, H. NISHIKAWA, K. KAWAKAMI, T. YAMABE, T. MORI, H. INOKUCHI, H. MORI, and S. TANAKA, "Eltylenedioxy Substituted 2,5-Bis(1',3'-ditiol-2'-ylidene)-1,3,4,6-tetrathiapentalenes and Their Conducting Salts", *Chem. Lett.* **1993,** 2073.

T. MORI, H. INOKUCHI, Y. MISAKI, H. NISHIKAWA, T. YAMABE, H. MORI, and S. TANAKA, "Structure and Physical Properties of $(TMEO\text{-}TTP)_2Au(CN)_2$", *Chem. Lett.* **1993,** 2085.

H. YAMOCHI, T. KOMATSU, N. MATSUKAWA, G. SAITO, T. MORI, M. KUSUNOKI, and K. SAKAGUCHI, "Structural Aspects of the Ambient-Pressure BEDT-TTF Superconductors", *J. Am. Chem. Soc.* **115,** 11319 (1993).

T. MORI, H. INOKUCHI, Y. MISAKI, T. YAMABE, H. MORI, and S. TANAKA, "Crystal Structures of Highly Conducting Iodine Complexes of TTM-TTP", *Bull. Chem. Soc. Jpn.* **67,** 661 (1993).

Y. LI, R. QIAN, K. IMAEDA, and H. INOKUCHI, "Behavior of the High Temperature Conductivity of Polypyrrole Nitrate Films", *Polymer J.* **26,** 535 (1994).

Y. LI, K. IMAEDA, and H. INOKUCHI, "pH and Temperature Effect on the Absorption Spectra of *Pseudomonas aeruginosa* Cytochrome c-551 Solution", *J. Phys. Chem.* **98,** 4726 (1994).

R. XI, B. WANG, K. ISOBE, T. NISHIOKA, K. TORIUMI, and Y. OZAWA, "Isolation and X-ray Crystal Structure of a New Octamolybdate: $[(RhCp^*)_2(\mu_2\text{-}SCH_3)_3]_4[Mo_8O_{26}] \cdot 2CH_3CN$ ($Cp^*=\eta^5\text{—}C_5Me_5$)", *Inorg. Chem.* **33,** 833 (1994).

R. XI, B. WANG, Y. OZAWA, M. ABE, and K. ISOBE, "New Linear-Type Tetranuclear Complex, $[\{RhCp^*(\mu\text{-}SCH_3)_3Mo(O)_2\}_2(\mu\text{-}O)]$ ($Cp^*=\eta^5\text{-}C_5Me_5$)", *Chem. Lett.* 323 (1994).

T. NISHIOKA, V.YU. KUKUSHIKIN, K. ISOBE, and A. VÁZQUEZ DE MIGUEL, "A Tetranuclear Rhodium Complex with μ_4-S Ligand, $[\{Rh_2Cp^*_2(\mu_2\text{-}CH_2)_2\}_2(\mu_4\text{-}S)]^{2+}$ ($Cp^*=\eta^5\text{—}C_5Me_5$), Obtained from Stepwise Abstraction of the SH^- Ligand from a Dinuclear Rhodium Dihydrosulfide Precursor by Ag^+", *Inorg. Chem.* **33,** 2501 (1994).

R. XI, B. WANG, M. ABE, Y. OZAWA, and K. ISOBE, "Fragmentation of Triple Cubane-Framework in $[(Cp^*Rh)_4Mo_4O_{16}]$ ($Cp^*=\eta^5\text{—}C_5Me_5$) by MeSH into Tetranuclear Parts in $[\{Cp^*Rh(\mu\text{-}SCH_3)_3MoO\}_2(\mu\text{-}O)_2]$ and $[\{Cp^*Rh(\mu\text{-}SCH_3)_3MoO\}_2(\mu\text{-}O)(\mu\text{-}S)]$ Providing a Novel System for Studying Stereodynamics of Thiolate Complexes", *Chem. Lett.* 1177 (1994).

S. OGO, T. SUZUKI, Y. OZAWA, and K. ISOBE, "A Heterotrimetallic Sulfide Cluster Having a Linear $Rh^{III} \cdots W^{VI} \cdots Cu^{I}$ Framework of an Octahedral-Tetrahedral-Trigonal Planar Sequence", *Chem. Lett.* 1235 (1994).

J.T. PARK, T. NISHIOKA, T. SUZUKI, and K. ISOBE, "Synthesis and Crystal Structure of $[(IrCp^*)_2(\mu\text{-}OH_3]_2(Cr_2O_7) \cdot 8H_2O$ ($Cp^*=\eta^5\text{-}C_5Me_5$). A Novel Two-Dimensional Hydrogen-Bonding Network", *Bull. Chem. Soc. Jpn.* **67,** 1968 (1994).

T. NISHIOKA and K. ISOBE, "Syntheses and Crystals Structures of Triangular Rhodium and Iridium Complexes with Triply Bridging Sulfido Ligands", *Chem. Lett.* 1661 (1994).

H. NEMOTO, J. CAI, and Y. YAMAMOTO, "Synthesis of a Water-Soluble o-Carborane Bearing Uracil Moiety via Palladium Catalyzed Reaction under Essentially Neutral Condition", *J. Chem. Soc., Chem. Commun.* 577 (1994).

H. NEMOTO, Y. KUBOTA, and Y. YAMAMOTO, "Palladium Catalyzed Addition of Masked Formyl Cyanides $ROCH(CN)_2$ to Aldehydes", *J. Chem. Soc., Chem. Commun.* 1665 (1994).

J. ADACHI and N. KOSUGI, "An *ab initio* Molecular Orbital Approach to Electronic Structure of the F Center in NaCl. Effects of Basis Set and Cluster Size", *Bull. Chem. Soc. Jpn.* **66,** 3314 (1993).

T. MIZOKAWA, A. FUJIMORI, H. NAMATAME, K. AKEYAMA, and N. KOSUGI, "Electronic Structure of the Local-singlet Insulator $NaCuO_2$", *Phys. Rev.* **B49,** 7193 (1994).

A. YAGISHITA, E. SHIGEMASA, and N. KOSUGI, "Observation of Rydberg-Valence Mixing in High-Resolution Symmetry-Resolved Oxygen K-Edge Spectra of O_2", *Phys. Rev. Lett.* **72,** 3961 (1994).

Y. ZHANG, S. SATO, H. OHSHIMA, T. HATTORI, and T. URISU, "Buried Metal Layer Enhanced Infrared Reflection Absorption Spectroscopy for Photoreactions Induced by Synchrotron Radiation on SiO_2 Surfaces", *Appl. Surf. Sci.* **79/80,** 422 (1994).

S. SATO, Y. UKISU, H. OGAWA, and Y. TAKASU, "Infrared Reflection Absorption Spectroscopy, X-Ray Photoelectron Spectroscopy and Temperature-Programmed Desorption Study on the Adsorption and Decomposition of $Fe(CO)_5$ Over Silver Surfaces", *J. Chem. Soc. Faraday Trans.* **89,** 4387 (1993).

S. SATO, Y. UKISU, H. OGAWA, and Y. TAKASU, "Surface Intermediates Formed During Photolytic Decarbonilation of Iron Pentacarbonyl Adsorbed on Silver Surfaces", *Appl. Surf. Sci.* **79/80,** 428 (1994).

K. MITSUKE, H. HATTORI, and H. YOSHIDA, "Ion-Pair Formation from Saturated Hydrocarbons through Photoexcitation of an Inner-Valence Electron", *J. Chem. Phys.* **99,** 6642 (1993).

H. YOSHIDA and K. MITSUKE, "Observation of Doubly Excited Rydberg States of N_2O by Positive Ion-Negative Ion Coincidence Spectroscopy", *J. Chem. Phys.* **100,** 8817 (1994).

H. HOSONO and H. KAWAZOE, "Radiation-Induced Coloring and Paramagnetic Centers in Synthetis SiO_2: Al Glasses", *Nucl. Instr. and Meth. in Phys. Res.* **B91,** 395 (1994).

T. HASHIMOTO, H. KAWAZOE, and H. SHIMAMURA, "Effects of Substitution of Bi with Pb in $BaBi_{1-x}Pb_xO_3$ on Crystal Structure and Conduction Behavior", *Physica* **C223,** 131 (1994).

T. OMATA, K. UEDA, N. UEDA, M. KATADA, S. FUJITSU, T. HASHIMOTO, and H. KAWAZOE, "Preparation of Oxygen Excess $SrLaFeO_{4+\delta}$ and Its Electrical and Magnetic Properties", *Solid State Commun.* **88,** 807 (1993).

T. OMATA, K. UEDA, H. HOSONO, M. KATADA, N. UEDA, and H. KAWAZOE, "Electrical and Magnetic Properties of Hole-Doped $Sr_{1+x}La_{1-x}FeO_4$", *Phys. Rev.* **B49,** 10194 (1994).

T. OMATA, K. UEDA, H. HOSONO, T. MIYAZAKI, S. HASEGAWA, N. UEDA, and H. KAWAZOE, "Electronic Structure of Hole-Doped $Sr_{1+x}La_{1-x}FeO_4$ Studied by UPS and XAS", *Phys. Rev.* **B49,** 10200 (1994).

K. YANAGAWA, Y. OHKI, T. OMATA, H. HOSONO, N. UEDA, and H. KAWAZOE, "New Oxide Phase $Cd_{2(1-x)}Y_{2x}Sb_2O_7$ Pyrochlore with a Wide Band Gap and High Electrical Conductivity", *Jpn. J. Appl. Phys.* **33,** L238 (1994).

K. YANAGAWA, Y. OHKI, N. UEDA, T. OMATA, T. HASHIMOTO, and H. KAWAZOE, "New Oxide $Cd_{1-x}Y_xSb_2O_6$ with Wide Band Gap and High Electrical Conductivity", *Appl. Phys. Lett.* **63,** 3335 (1993).

T. OMATA, N. UEDA, K. UEDA, and H. KAWAZOE, "New Ultraviolet-Transparent Electroconductive Oxide, $ZnGa_2O_4$ Spinel", *Appl. Phys. Lett.* **64,** 1077 (1994).

K. YANAGAWA, Y. OHKI, T. OMATA, H. HOSONO, N. UEDA, and H. KAWAZOE, "Preparation of $Cd_{1-x}Y_xSb_2O_6$ Thin Film on Glass Substrate by Radio Frequency Sputtering", *Appl. Phys. Lett.* **65,** 406 (1994).

H. OGAWA, S.I. GHEYAS, H. NAKAYAMA, M. NISHIO, and A. YOSHIDA, "Growth of Low-Resistivity n-Type ZnTe by Metalorganic Vapor Phase Epitaxity", *Jpn. J. Appl. Phys.* **33,** L980 (1994).

M. IKEJIRI, T. OGATA, H. OGAWA, M. NISHIO, and A. YOSHIDA, "Low Temperature Growth of ZnTe by Synchrotron Radiation Using Metalorganic Sources", *J. Vac. Sci. & Technol.* **A12,** 278 (1994).

M.C.R. COCKETT and K. KIMURA, "A Study of Anthracene-Ar_n (n=0–5) in the Ground Cationic State by Laser Threshold Photoelectron Spectroscopy: Selective Ionization of Complex Isomers Formed in the Free Jet Expansion", *J. Chem. Phys.* **100,** 3249 (1994).

K. FURUYA, K. KIMURA, Y. SAKAI, T. TAKAYANAGI, and N. YONEKURA, "Dissociation Dynamics of CH_4^+ Core Ion in the $^2A_1$ State", *J. Chem. Phys.* **101,** 2720 (1994).

K. TATSUMI, Y. INOUE, H. KAWAGUCHI, M. KOHSAKA, A. NAKAMURA, R.E. CRAMER, W. VANDOORNE, G.J. TAOGOSHI, and P.N. RICHMANN, "Structural Diversity of Sulfide Complexes Containing Half-Sandwich Cp*Ta and Cp*Nb Fragments", *Organometallics* **12,** 352 (1993).

W.-Y. SUN, N. UEYAMA, and A. NAKAMURA, "Oxidation of Benzoin to Benzil and of *p*-Substituted Benzyl Alcohol to the Corresponding Benzaldehyde Catalyzed by Iron(II) Thiolate Complexes. A Proposed Reaction Mechanism", *Tetrahedron* **49,** 1357 (1993).

W.-Y. SUN, N. UEYAMA, and A. NAKAMURA, "An Electronic Influence of a Distant Aromatic Ring in Reduced Rubredoxin Models. Iron(II) Complexes with Z-Cys-Pro-Leu-Cys-Gly-X (X=$NHCH_2C_6H_4$-*p*-F, $NHCH_2CH_2C_6H_4$-*p*-F, and Phe-OMe)", *Inorg. Chem.* **32,** 1095 (1993).

K. TATSUMI, Y. INOUE, and A. NAKAMURA, "Rigidity of the Unsymmetric Coordination Geometry of the Two Dithiolates in (C_5Me_5)Ta(norbornane-exo-2,3-dithiolate)$_2$", *J. Organomet. Chem.* **444,** C25 (1993).

M. KONDO, N. UEYAMA, K. FUKUYAMA, and A. NAKAMURA, "Synthesis, Molecular Structure, and Physical Properties of an Oxomolybdenum(IV) Complex with *p*-Chlorobenzenethiolate, $[Mo_{IV}O(p\text{-}ClC_6H_4S)_4]_2^-$, as a Model of Active Sites of Reduced Molybdo-Oxidases", *Bull. Chem. Soc. Jpn.* **66,** 1391 (1993).

K. TATSUMI, H. KAWAGUCHI, I. MATSUBARA, and A. NAKAMURA, "A Seven-Coordinate Mixed-Dithiolate Complex of Nibium(V): Synthesis and Structure of $(PPh_4)[Nb(SCH_2CH_2S)_2(SCH_2CH_2SCH_2CH_2S)]$", *Inorg. Chem.* **32,** 2604 (1993).

K. TATSUMI, H. KAWAGUCHI, Y. INOUE, and A. NAKAMURA, "$[Cp^*TaS_3\{Rh(cod)\}_2]$und$[Cp^*TaS_3\{RuH(PPh_3)_2\}_2]$-eine neue Klasse von TaM_2-Heterometallclustern", *Antew. Chem.* **105,** 791 (1993).

K. MASHIMA, Y. YAMANAKA, Y. GOHRO, and A. NAKAMURA, "Synthesis and Reaction of (η^5-Pentamethycyclopentadienyl)bis(allyl)tantalum(III)Complexes; Crystal Structure of Ta(η^5-C_5Me_5)(η^3-1-phenylallyl)$_2$", *J. Organomet. Chem.* **455,** C6 (1993).

W.-Y. SUN, N. UEYAMA, and A. NAKAMURA, "Spin-Lattice Relaxation Time and Temperature Dependence of Fluorine-19 Nuclear Magnetic Resonance Spectra of Cysteine-Containing Peptide Iron(II) Complexes", *J. Chem. Soc., Dalton Trans.* 1871 (1993).

N. UEYAMA, W.-Y. SUN, and A. NAKAMURA, "Novel Peptide Model Complexes of Reduced Rubredoxin", *Peptide Chemistry* **1992,** 491 (1993).

H. ZAIMA, N. UEYAMA, A. NAKAMURA, and S. AIMOTO, "Solution Structure of a Peptide Designed on Plastocyanin Metal Center in Trifluoroethanol and Incorporation of Cobalt(II) into the Peptide", *Chem. Lett.* 1885 (1993).

K. MASHIMA, Y. YAMANAKA, Y. GOHRO, and A. NAKAMURA, "Preparation, Characterization, and Reactions of 16-Electron Ta(η^5-C_5Me_5)(η^3-1-phenylallyl)$_2$", *J. Organomet. Chem.* **459,** 131 (1993).

K. MASHIMA, S. FUJIKAWA, and A. NAKAMURA", "Polymerization of Ethylene Catalyzed by the System Ta(η^5-C_5-Me_5)(η^4-diene)$(CH_3)_2$/MAO: An Isoelectronic Analogue for a Group 4 Metallocene Catalyst", *J. Am. Chem. Soc.* **115,** 10990 (1993).

T. OKAMURA, N. UEYAMA, A. NAKAMURA, E.W. AINSCOUGH, A.M. BRODIE, and J.M. WATERS, "The Effect of Strong NH · · · S Hydrogen Bonds in the Copper(I) Thiolate Complex, $(NEt_4)_2$[Cu(*o*-pabt)$_3$](*o*-pabt=*o*-pivaloylaminobenzenethiolato)", *J. Chem. Soc., Chem. Commun.* 1658 (1993).

Y. NAKAYAMA, K. MASHIMA, and A. NAKAMURA, "Polymerization of Monosubstituted Acetylenes Catalyzed by 2,6-Dimethylphenoxo Complexes of Group 5 and 6 Metals", *Macromolecules* **26,** 6267 (1993).

K. MASHIMA, H. NAKANO, and A. NAKAMURA, "New Synthetic Strategy for a Straight Linear Metal-Metal Bonded Tetranuclear Complex, the Pd-Mo-Mo-Pd System Supported by Four Tridentate 6-(Diphenylphosphino)-2-pyridonate Ligands", *J. Am. Chem. Soc.* **115,** 11632 (1993).

K. MASHIMA, Y. NAKAYAMA, N. KANEHISA, Y. KAI, and A. NAKAMURA, "Monocyclooctatetraenyl(thiolato)samarium(III) Complexes from the Reaction of Metallic Samarium with Cyclooctatetraene and Diaryldisulfide: Crystal Structures of $[Sm(\mu\text{-}SPh)(C_8H_8)(thf)_2]_2$ and $[\{Sm(\mu\text{-}S(2,4,6\text{-triisopropylphenyl})\}(C_8H_8)(thf)_2]$", *J. Chem. Soc., Chem. Commun.* 1847 (1993).

W.-Y. SUN, N. UEYAMA, and A. NAKAMURA, "^1H, ^2H and ^{19}F NMR Spectroscopy of a Navel Iron(II) Tetradentate Cysteine-Peptide Complex Having Only One δ Isomer. Detection of Two Isomers in Coordination of Cys-X-Y-Cys Bidentate Peptide Ligands to Iron(II) Iron", *Magnetic Resonance in Chemistry* **31,** S34 (1993).

K. SAWADA, T. KANDA, Y. NAGANUMA, and T. SUZUKI, "Formation and Protonation of Aminopolyphosphonate Complexes of Alkaline Earth and Divalent Transition Metal Ions in Aqueous Solution", *J. Chem. Soc., Dalton Trans.* 2557 (1993).

K. SAWADA, T. MIYAGAWA, T. SAKAGUCHI, and K. DOI, "Structure and Thermodynamic Properties of Aminopolyphosphonate Complexes of the Alkaline Earth Metal Ions", *J. Chem. Soc., Dalton Trans.* 3777 (1993).

K. SAWADA, S. OHGAKE, M. KOBAYASHI, and T. SUZUKI, "Preconcentration of Cadmium by Column Extraction with Trioctymethylammonium Chloride and Determination by Graphite Furnace Atomic Absorption Spectroscopy", *Bunseki Kagaku* **42,** 741 (1993).

N. KOMEDA, H. NAGAO, G. ADACHI, M. SUZUKI, A. UEHARA, and K. TANAKA, "Molecular Structure of Copper Nitrito Complexes as the Reaction Intermediate of Dissimilatory Reduction of NO_2", *Chem. Lett.* 1521 (1993).

H. NAGAO, T. MIZUKAWA, and K. TANAKA, "Carbon-Carbon Bond Formation in Electrochemical Reduction of Carbon Dioxide Catalyzed by a Ruthenium Complex", *Inorg. Chem.* 3415 (1994).

T. TAKAHASHI, K. AOYAGI, V. DENISOV, N. SUZUKI, D. CHOUEIRI, and E. NEGISHI, "Zirconium Catalyzed C-C Bond Formation Reaction of Conjugated Diynes with EtMgBr", *Tetrahedron Lett.* **34,** 8301 (1993).

T. TAKAHASHI, K. KASAI, N. SUZUKI, K. NAKAJIMA, and E. NEGISHI, "Isolation and Characterization of $(Cp_2ZrMe)_2(CH_2CH_2)$", *Organometallics* **13,** 3413 (1994).

T. TAKAHASHI, D.Y. KONDAKOV, and N. SUZUKI, "Zirconium Catalyzed or Mediated Regioselective C-C Bond Formation Reactions of Allylic Acetals", *Chem. Lett.* 259, (1994).

T. TAKAHASHI, "Development of Selective Reactions Using Zirconocene-Alkene Complexes", *J. Syn. Org. Chem. Jpn.* (in Japanese) **51,** 1145 (1993).

C. COPERET, E. NEGISHI, Z. XI, and T. TAKAHASHI, "Reaction of 3-Zircona-1-cyclopentenes and Zirconacyclopentanes with Aldehydes. A Selective and Convenient Synthesis of 4-Penten-1-ols, (Z)-5-iodo-4-penten-1-ols, and Related Alkanols", *Tetrahedron Lett.* **35,** 695 (1994).

T. TAKAHASHI, K. AOYAGI, and D.Y. KONDAKOV, "A Reagent-Dependent Highly Chemoselective Halogenation Reaction of Zirconacyclopentenes", *J. Chem. Soc., Chem. Commun.* 747 (1994).

T. TAKAHASHI, D.Y. KONDAKOV, and N. SUZUKI, "A Novel Type of Zirconium Catalyzed or -Pnomoted Cyclization Reaction", *Organometallics* **13,** 3411 (1994).

K. AOYAGI, R. HARA, D.Y. KONDAKOV, K. KASAI, N. SUZUKI, and T. TAKAHASHI, "Highly Chemoselective Functionalization of Zirconacyclopentene Compounds", *Inorg. Chim. Acta.* **220,** 319 (1994).

N. SUZUKI, K. AOYAGI, M. KOTORA, M. HASEGAWA, Y. NITTO, M. SABURI, and T. TAKAHASHI, "Regioselective Carbon-Carbon Bond Formation Reaction of Zirconocene-Alkene Complexes with Aldehydes or Ketones", *J. Organomet. Chem.* **473,** 117 (1994).

T. TAKAHASHI, M. KOTORA, K. KASAI, and N. SUZUKI, "Novel Syntheses of Eight-Five Fused Ring Compounds from Zirconacyclopentadienes", *Organometallics* **13,** 4183 (1994).

T. TAKAHASHI, M. KOTORA, K. KASAI, and N. SUZUKI, "Copper Catalyzed C-C Bond Formation Reaction of Allylzirconation Produces of Alkynes", *Tetrahedron Lett.* **35,** 5685 (1994).

E. NEGISHI, D. CHOUEIRY, T.B. NGUYEN, D.R. SWANSON, N. SUZUKI, and T. TAKAHASHI, "Nonconcerted Paths for Reactions of Alkene-Zirconocene Complexes", *J. Am. Chem. Soc.* **116,** 9751 (1994).

S. NANBU, M. GOMYO, and S. IWATA, "Potential Energy Surfaces of Some Low-Lying States of Fluoroformyl Radical FCO", *Chem. Phys.* **184,** 97 (1994).

T. KOBAYASHI, K. ONO, H. SUDA, Y. YAMASHITA, and H. KATO, "Syntheses and Spectral Properties of Norbornadiene-Fused Heterocycles: 1,3-Diphenyl-4,7-dihydro-4,7-methanobenzo[c]-thiophene, -pyrrole, and -furan", *Bull. Chem. Soc. Jpn.* **66,** 2707 (1993).

M. BONAMICO, V. FARES, A. FLAMINI, N. POLI, Y. YAMASHITA, and K. IMAEDA, "Interaction of Bis(1,2,6,7-tetracyano-3,5-dihydro-3,5-diiminopyrrolizinide) Metal Complexes with Phenazine and Derivatives. Crystal Structure of Addition Compounds of the Nickel(II) Complex with Phenazine and 5,10-Dimethyl-5,10-dihydrophenazine", *J. Chem. Soc., Dalton Trans.* 3463 (1993).

Y. YAMASHITA, K. ONO, S. TANAKA, K. IMAEDA, H. INOKUCHI, and M. SANO, "Dithio-Derivatives of p-Quinodimethanes Fused with 1,2,5-Thiadiazoles: a Novel Type of π-Donor-Acceptor System", *J. Chem. Soc., Chem. Commun.* 1803 (1993).

M. KOZAKI, S. TANAKA, and Y. YAMASHITA, "Preparation and Properties of Novel Polythiophenes Containing 1,3-Dithiol-2-ylidene Moieties", *J. Org. Chem.* **59,** 442 (1994).

S. TANAKA, M. TOMURA, and Y. YAMASHITA, "Synthesis and Characterization of Thieno[3,4-c][1,2,5]thiadiazoles", *Heterocycles* **37,** 693 (1994).

Y. YAMASHITA, K. ONO, S. TANAKA, K. IMAEDA, and H. INOKUCHI, "Nonplanar Bis(1,3-dithiole) Donors Affording Novel Cation Radical Salts", *Adv. Materials* **4,** 295 (1994).

T. SUZUKI, T. FUKUSHIMA, Y. YAMASHITA, and T. MIYASHI, "An Absolute Asymmetric Synthesis of the [2+2] Cycloadduct via Single Crystal-to-Single Crystal Transformation by Charge-Transfer Excitation of Solid-State Molecular Complexes Composed of Vinylbenzenes and Bis[1,2,5]thiadiazolotetracyanoquinodimethane", *J. Amer. Chem. Soc.* **116,** 2793 (1994).

M. TOMURA, S. TANAKA, and Y. YAMASHITA, "Synthesis, Structure, and Properties of the Novel Conducting Dithiolato-Metal Complexes Having Dicyanopyrazine Moieties", *Synth. Metal* **64,** 197 (1994).

K. ONO, S. TANAKA, K. IMAEDA, and Y. YAMASHITA, "Preparation and Properties of 7-(1,3-Dithiol-2-ylidene)-4-methyl-4,7-dihydro[1,2,5]thiadiazolo[3,4-b]pyridines: Novel Donor Molecules Containing a 1,2,5-Thiadiazole Unit", *J. Chem. Soc., Chem. Commun.* 899 (1994).

T. SUZUKI, T. SAKIMURA, S. TANAKA, Y. YAMASHITA, H. SHIOHARA, and T. MIYASHI, "2-(Thiopyran-4'-yliden)-1,3-dithioles fused with Thiophene Units: Intramolecular S—S Interaction Affecting the Redox Properties and Molecular Geometries", *J. Chem. Soc., Chem. Commun.* 1431 (1994).

C. KITAMURA, S. TANAKA, and Y. YAMASHITA, "Synthesis of New Narrow Bandgap Polymers Based on 5,7-Di(2-thienyl)thieno[3,4-b]pyrazine and Its Derivatives", *J. Chem. Soc., Chem. Commun.* 1585 (1994).

F. MISAIZU, M. SANEKATA, K. FUKE, and S. IWATA, "Photodissociation Study on $Mg^+(H_2O)_n$, n=1—5: Electronic Structure and Photoinduced Intracluster Reaction", *J. Chem. Phys.* **100,** 1161 (1994).

K. FUKE, R. TAKASU, and F. MISAIZU, "Photoionization of Hypervalent Molecular Clusters: Electronic Structure and Stability of $NH_4(NH_3)_n$", *Chem. Phys. Lett.* **229,** 597 (1994).

H. UMEMOTO, S. TSUNASHIMA, H. IKEDA, K. TAKANO, K. KUWAHARA, K. SATO, K. YOKOYAMA, F. MISAIZU, and K. FUKE, "Nascent Internal State Distributions of $ZnH(X^2\Sigma^+)$ Produced in the Reactions of $Zn(4^1P_1)$ with Some Alkane Hydrocarbons", *J. Chem. Phys.* **101,** 4803 (1994).

K. SUZUKI, T. ENOKI, and S. BANDOW, "Electronic Properties and Valence State of Sm in $(SmS)_{1.19}TaS_2$", *Phys. Rev.* **B48,** 11077 (1993).

S. BANDOW and Y. SAITO, "Encapsulation of ZrC and V_4C_3 in Graphic Nanoballs via Arc Burning of Metal Carbide/Graphite Composites", *Jpn. J. Appl. Phys.* **32,** L1677 (1993).

Y. SAITO, M. OKUDA, T. YOSHIKAWA, S. BANDOW, S. YAMAMURO, K. WAKOH, K. SUMIYAMA, and K. SUZUKI, "Synthesis of $Sc_{15}C_{19}$ Crystallites Encapsulated in Carbon Nanocapsules by Arc Evaporation of Sc-C Composite", *Jpn. J. Appl. Phys.* **33,** L186 (1994).

J.M. HOLDEN, P. ZHOU, X.X. BI, P.C. EKLUND, S. BANDOW, R.A. JISHI, K.D. CHOWDHURY, G. DRESSELHAUSE, and M.S. DRESSELHAUSE, "Raman Scattering from Nanoscale Carbons generated in a Co-Catalyzed Carbon Plasma", *Chem. Phys. Lett.* **220,** 186 (1994).

J.S. AHN, Y.KANEMATSU, M. ENOMOTO, and T. KUSHIDA, "Determination of Weighted Density of States of Vibrational Modes in Zn-Substituted Myoglobin", *Chem. Phys. Lett.* **215,** 336 (1993).

M. SUGISAKI, M. EGUCHI, O. ARIMOTO, K. NAKAMURA, and M. WATANABE, "Infrared Lattice Vibration Spectra at Low Temperature in β-ZnP_2", *J. Phys. Soc. Jpn.* **62,** 4533 (1993).

D. KIM, H.W. LEE, J.J. LEE, J.H. JE, M. SAKURAI, and M. WATANABE, "Mo-Si Multilayer as Soft X-Ray Mirrors for the Wavelengths around 20 nm Region", *J. Vac. Sci. Tech.* **A12,** 148 (1994).

S. HIROSE and M. KAMADA, "Time Response of Photon-Stimulated Desorption of Excited-State Potassium Atoms from Potassium Halides", *J. Phys. Soc. Jpn.* **63,** 1053 (1994).

M. KAMADA and S. HIROSE, "Time Response of Sputtering of Excited-State Na Atoms from Alkali Halides Irradiated with Synchrotron Radiation", *Nucl. Instrum. & Methods* **B91,** 619 (1994).

I. OUCHI, I. NAKAI, M. KAMADA, and S. TANAKA, "Core Electron Absorption Spectra of Polyester Films", *Progress Polymer Phys. Jpn.* **36,** 413 (1993).

S. HIROSE and M. KAMADA, "Time Response of Photon-Stimulated Desorption of Excited-State Sodium Atoms from Sodium Halides", *Phys. Rev. B* **48,** 17641 (1993).

K. TAMURA, T. KASUGA, M. TOBIYAMA, G. ISOYAMA, H. HAMA, and T. KINOSHITA, "Double RF System for Suppression of Longitudinal Coupled Bunch Instability on UVSOR Storage Ring", *Jpn. J. Appl. Phys.* **33,** L59 (1994).

H. HAMA, J. YAMAZAKI, and G. ISOYAMA, "FEL Experiments on the UVSOR Storage Ring", *Nucl. Instr. and Meth.* **A341,** 12 (1994).

S. KIMURA, T. NANBA, S. KUNII, and T. KASUYA, "Low-Energy Optical Excitation in Rare-Earth Hexaborides", *Phys. Rev. B* **50,** 1406 (1994).

Review Articles and Textbooks

I. OHMINE and H. TANAKA, "Fluctuation, Relaxations and Hydration in Liquid Water; Hydrogen Bond Rearrangement Dynamics", *Chem. Rev.* **93**, 2545 (1993).

Y. TANIMURA and S. MUKAMEL, "Electronic Dephasing in Femtosecond Curve Crossing Spectroscopy", Proceedings of the Fourteenth International Conference on Raman Spectroscopy, ed. by N.-T. Yu and X.-Y. Li, (John Wiley, 1994) p.23.

H. NAKAMURA, "Molecular Collisions and Chemical Reactions", *Suuri Kagaku* (in Japanese), No.360, 19 (1993).

H. SUN, K. NAKASHIMA, and H. NAKAMURA, "Characteristics of Superexcited States of Molecules and MQDT Studies of NO^+ Dissociative Recombination", Dissociative Recombination: Theory, Experiment, and Applications, ed. by B.R. Rowe, J.B.A. Mitchell, and A. Canosa (Plenum, New York), p.25 (1994).

S. LEE, M. IWAI, and H. NAKAMURA, "Characteristics and Dynamics of Doubly Excited States of Molecules", Molecules in Laser Field, ed. by A.D. Bandrauk (Marcel Dekker, New York), p.217 (1994).

S. SAITO, "Interstellar Molecules and Chemistry of Dark Clouds", in "Modern Researches on Cosmic Science", N. Kaifu Ed., JSPS Press (in Japanese), p.108–124 (1992).

R.S. HAYANO and N. MORITA, "Antiprotonic Helium Atoms", *KAGAKU* (in Japanese), **64**, 283 (1994).

S. SATO and T. KITAGAWA, "Time-Resolved Resonance Raman Study of Porphyrins and Metalloporphyrins in the Electronic Excited States", *Appl. Phys.* **B59**, 415 (1994).

K. YOSHIHARA, R. INABA, H. OKAMOTO, M. TASUMI, K. TOMINAGA, and K.A. NELSON, "Vibrational and Rotational Dynamics of Molecules in Solution Studied by Femtosecond CARS and Raman Echo", in Femtosecond Reaction Dynamics, D.A. Wiersma Ed., North Holland, Amsterdam, p.229–310 (1994).

I. HANAZAKI, H.-L. KIM, and M. TAKAYANAGI, "Photochemistry of $N_2O \cdot H_2O$ Complexes Produced in Supersonic Jets", *Laser Techniques for State-Selected and State-to-State Chemistry II, SPIE Proceedings* **2124**, 10 (1994).

I. HANAZAKI, "Nonlinear Phenomena and Self-Organization", *Kagaku* **48**, 387 (1993) (Japanese).

R. NAKAGAKI, Y. TANIMOTO, and K. MUTAI, "Magnetic Field Effects upon Photochemistry of Bifunctional Chain Molecules", *J. Phys. Org. Chem.* **6**, 381 (1993).

H. OGATA and Y. MARUYAMA, "Single Crystal" (in Japanese), *OYO BUTURI* **62**, 1036 (1993).

H. OGATA, Y. MARUYAMA, T. INABE, Y. ACHIBA, S. SUZUKI, K. KIKUCHI, and I. IKEMOTO, "Electrical Transport Properties of C_{60} Single Crystals Doped with Alkali Metals", *Mod. Phys. Lett.* **B, 7**, 1173–1192 (1993).

K. ISOBE, "New Types of Polyoxometalates: Synthesis, Structures, and Reactivities of Polyoxometalates with Organometallic Groups", *Kagakusousetu* (in Japanese), **No.20**, 65 (1993).

K. ISOBE, (a Joint Author), "Coordination Chemistry", *Koudansha-Scientific* (in Japanese), Tokyo, 1994.

Y. YAMAMOTO and N. ASAO, "Syntheses of Nitrogen Containing Compounds Using Reactive Organometallics", *J. Synth. Org. Chem. Jpn.* (in Japanese), **51**, 1005 (1993).

H. NEMOTO, "Trend Alteration from 'Synthesis of Highly Selective Single Compound' to 'Synthesis of Rational Mixtures'", *Chemistry* (in Japanese), **49**, 515 (1994).

K. TANAKA, "Electrochemical Activation of CO_2 Catalyzed by Metal Complexes" in "Redox Mechanisms and Interfacial Properties of Molecules of Biological Importance" Eds. F.A. Schultz, I. Taniguchi, p.232–236 (1994).

K. TANAKA, "Activation of Carbon Dioxide by Metal Complexes", *Organometallic News* (in Japanese), p.5–8 (1994).

K. TANAKA, "Reduction and Fixation of Carbon Dioxide by Metal Complexes", *Catalyst* (in Japanese), 35, p.492–498 (1993).

E. NEGISHI and T. TAKAHASHI, "Patterns of Stoichiometric and Catalytic Reactions of Organozirconium and Related Complexes of Synthetic Interest", *Acc. of Chem. Res.* **27**, 124 (1994).

H. KAWAZOE, "New Transparent and Electroconductive Ceramics", *Kagaku to Kogyo* (in Japanese), **47**, 660 (1994).

H. KAWAZOE, "Application of NMR Spectroscopy to the Science and Technology of Glasses and Ceramics", in "Annual Reports on NMR Spectroscopy", Vol.**28**, I. Ando and G.A. Webb Ed., Academic Press, p.1–27 (1994).

S. HASEGAWA, N. UENO, and K. SEKI, "Measurement of Intermolecular Energy-Band Dispersion on Organic Molecular Solids by ARUPS", *Molecular Electronics and Bioelectronics* (in Japanese), **5**, 93 (1994).

S. HASEGAWA, N. UENO, and K. SEKI, "Intermolecular Energy-Band Dispersion of BTQBT Thin Films", *Houshakou* (in Japanese), **7**, 119 (1994).

AUTHOR INDEX-RESEARCH ACTIVITIES AND SPECIAL RESEARCH PROJECTS

Abe, Masaaki 83, 84, 86
Achiba, Yohji 70, 71
Adachi, Gin-ya 115
Adachi, Jun-ichi 96, 97
Ahn, Jeung Sun 132, 133
Akasaka, Takeshi 67
Al-masum, Mohammad 93
Aoyagi, Koichiro 116, 117, 118, 146
Aoyagi, Mutsumi 120
Appelman, Evan H. 32
Arai, Takeshi 66, 144
Arakawa, Ichiro 102
Asao, Naoki 92, 93
Awazu, Koichi 103

Bandow, Shunji 36, 128, 129
Bi, Xiang-Xin 128, 129
Bonamico, Mario 121
Bontuyan, Lizla S. 57, 141
Borkman, Raymond F. 46

Caî, Jianping 92
Che, Dock-Chil 76
Chiba, Takehiko 69, 70
Chigira, Fumie 112
Cho, Minhaeng 19
Choi, Young S. 45
Choueiry, Danièle 116, 118
Chowdhury, K.Das 129
Cook, M. J. 68
Coperet, Christophe 116

Denisov, Victor 116
Derbyshire, F. 129
Douhal, Abderrazzak 46
Dresselhause, G. 129
Dresselhause, M.S. 129

Ebihara, Masahiro 86
Eklund, P.C. 128, 129
Endo, Kazuhiro 69
Enoki, Toshiaki 81
Enomoto, Makoto 132

Fang, Shaoli 66, 144
Fares, Vincenzo 121
Flamini, Alberto 121
Fleming, Graham R. 19
Francis, James T. 97
Fujikawa, Shinjiro 113
Fujiki, Michiya 71
Fujimori, Hiroki 69
Fujimoto, Hitoshi 70
Fujino, Masaie 71
Fuke, Kiyokazu 15, 124, 125, 126, 127, 128, 145
Fukuda, Hitoshi 135
Fukui, Hiroyuki 92
Fukushima, Takanori 122

Gejo, Tatsuo 50, 51
Gheyas, Syed Irfan 106, 107
Givens, E. 129
Gorecki, Jerzy 53
Goto, Masahiro 26, 27
Gruzdkov, Yuri A. 47, 140
Guo, Q.X. 74

Hager, G.T. 129
Hama, Hiroyuki 134
Hamano, Hideaki 109
Hanazaki, Ichiro 49, 50, 51, 52, 53, 54, 55, 56, 57, 141
Hara, Ryuichiro 117,146
Harima, Yutaka 71
Hasegawa, Maki 118
Hasegawa, Shinji 70, 71, 105
Hashimoto, Nobuhisa 57, 58
Hashimoto, Takuya 104, 105
Hasumoto, Masami 134
Hatanaka, Kunio 79, 144
Hattori, Hideo 101
Hayano, R.S. 28, 29
Hiejima, Toshihiro 61, 143
Hikida, Takumi 101
Hikosaka, Yasumasa 101
Hino, Shojun 70, 71
Hiraya, Atsunari 134
Hirayama, Takato 102
Hirose, Sayumi 135
Hirota, Shun 31, 32, 33, 139
Hirotsu, Masakazu 108
Hitchcock, Adam P. 97
Holden, J.M. 128, 129
Honda, Chikako 112
Honda, Yoshihiro 92
Hoshi, Hajime 144
Hosokawa, Takamasa 68
Hosono, Hideo 103, 105, 106

Ichikawa, Tomohide 146
Ichimura, Kenji 73
Ichimura, Mari 91
Ichimura, Satoshi 110
Ikeda, Hiroyuki 128
Ikegami, Isamu 44
Ikegami, Tsutomu 16
Ikejiri, Makoto 106, 107
Ikemoto, Isao 70
Ikezawa, Mikihiko 136
Imaeda, Kenichi 62, 70, 73, 121, 122
Imashiro, Fumio 130
Inaba, Ryoji 38
Inakuma, Masayasu 36
Inokuchi, Hiroo 62, 70, 72, 73, 121, 122
Isaka, Hiroaki 71
Ishida, Toyohisa 146
Ishiguro, Eiji 134
Ishii, Hisao 71
Isobe, Kiyoshi 81, 82, 83, 84, 85, 86, 87, 88, 89, 90, 115, 145
Isoyama, Goro 134
Ito, Koji 74
Ito, Masakatsu 20
Itoh, Hiroshi 135
Itoh, Tetsuji 79, 144
Ivanov, Valery 67
Iwai, Masahiro 23
Iwaki, Masayo 44
Iwasaki, Kentaro 70, 71
Iwata, Suehiro 15, 16, 17, 18

Jalilehvand, Falideh 145
Jewsbury, Philip 35, 36
Jishi, R.A. 129
Johnson, Alan E. 37

Kamada, Masao 135
Kamalov, Valey F. 42, 43
Kamimura, Masayasu 24
Kaminaga, Akiko 56
Kaminaka, Shoji 34
Kamogawa, Keiji 31
Kandori, Hideki 37, 44, 46
Kanematsu, Yasuo 132, 133
Kang, Tai Jong 39, 40, 140
Kanno, Minoru 102, 142
Kanoda, Kazushi 63, 64, 65, 143
Kasai, Kayoko 116, 117, 118, 146
Kasai, Toshio 76
Kashihara, Hiroko 113
Kashino, Setsuo 108
Kashiwabara, Kazuo 88, 90
Katada, Motomi 104
Kataoka, Daisuke 109
Katayama-yoshida, Hiroshi 72
Kato, Hiroyuki 47, 140
Kato, Kiyonori 64
Kato, Shinji 131
Kato, Tatsuhisa 36, 67, 140
Kawaizumi, Fumio 146
Kawakami, Kazuya 72
Kawamoto, Atsushi 63, 64, 65, 143
Kawase, Masaya 135
Kawata, Masaaki 18
Kawazoe, Hiroshi 103, 104, 105, 106
Khairullin, Ilias I. 61, 62, 73, 143

Kida, Katsuhiko 83
Kikuchi, Koichi 67, 70, 71
Kikuchi, Yoichi 111, 112
Kim, Bongsoo 41, 42
Kim, Hong-Lae 49, 51
Kimura, Kazuhiko 134
Kimura, Shin-ichi 136
Kinoshita, Toshio 134
Kishi, Reiko 16
Kitagawa, Hiroshi 79
Kitagawa, Teizo 30, 31, 32, 33, 34, 35, 36, 133, 139
Kitaura, Kazuo 24
Kobashi, Kazuhisa 69
Kobayashi, Michiko 111
Kobayashi, Takamichi 60
Kobayashi, Takao 17
Kodama, Takeshi 36
Kohama, Keiichi 66
Kojima, Hironao 136
Kojima, Masaaki 108
Kokka, Michiyo 110
Komatsuzaki, Tamiki 19, 20
Komeda, Nobutoshi 115
Kondakov, Denis Y. 116, 117
Kondow, Tamotsu 76
Konno, Shin-ichi 109
Kono, Mitsuhiko 76
Kono, Takumi 50, 51
Kosugi, Nobuhiro 96, 97
Kotora, Martin 118, 146
Kotsuki, Hiyoshizo 145
Kozaki, Masatoshi 121
Kubo, Kazuyuki 110
Kubota, Mitsuru 111
Kubota, Yasufumi 92
Kumakura, Mitsutaka 28, 30, 139
Kumashiro, Ryotaro 109
Kumazaki, Shigeichi 37, 44
Kuroda, Yasushige 108, 109
Kushi, Yoshinori 115
Kushida, Takashi 132, 133
Kuwahara, Daisuke 130
Kuwahara, Kazuya 128
Kuwata, Keiji 76

Lee, Jihwa 47
Lee, Sang K. 26
Lee, Sungyul 23, 41
Lee, W.-T. 128, 129
Li, Yongfang 73
Liu, Hong Ling 108

Maas, F.E. 28, 29
Maeda, Hironobu 109
Maruyama, Yusei 66, 67, 70, 128, 129, 144
Mase, Kazuhiko 98, 142
Mashima, Kazushi 113, 114
Masuda, Yoshio 112
Matsumoto, Kazuo 70, 71
Matsumoto, Masakazu 20
Matsumoto, Nobuo 71
Matsumoto, Yoshiyasu 47, 48, 77, 140
Matsushita, Michio 140
Meguro, Masaki 93
Mies, Frederick H. 22
Minamino, Satoshi 120
Misaizu, Fuminori 15, 124, 125, 126, 127, 128, 145
Misaki, Yohji 72, 73
Mitani, Tadaoki 79, 131
Mitsuke, Koichiro 100, 101, 102, 142
Mitsumi, Minoru 80, 144
Miyagawa, Kazuya 63, 64, 143
Miyajima, Seiichi 68, 69, 70, 144
Miyashi, Tsutomu 122, 123
Miyazaki, Akira 81
Miyazaki, Takafumi 71, 105
Miyoshi, Katsuhiko 109, 110
Mizukawa, Tetsunori 114, 115, 146
Mizuno, Yuri 108
Mizuta, Tsutomu 110
Mizutani, Yasuhisa 30, 33
Mogi, Tatsushi 33
Mori, Hatsumi 72, 73
Mori, Takehiko 70, 72, 73
Mori, Yoshihito 52, 53, 54, 56, 57, 141
Moribayashi, Kengo 21
Morikawa, Takashi 70, 72
Morimoto, Setsuo 109
Morita, Norio 28, 30, 139
Morita, Yasushi 78, 79, 144
Moriwaki, Yoshiki 139
Moriwaki, Taro 36
Moriya, Keiichi 69
Mukamel, S. 23

Nagai, Masako 33
Nagai, Toshiki 102
Nagakura, Saburo 60
Nagao, Hirotaka 114, 115, 146
Nagao, Mahiko 109
Nagasawa, Yutaka 37, 38
Nagasono, Mitsuru 98, 142
Nagata, Masaaki 131
Naitoh, Yukito 38, 39, 40, 140
Nakagaki, Ryoichi 59, 60, 141
Nakahara, Yusuke 73
Nakajima, Atsushi 16
Nakajima, Hiroshi 115
Nakajima, Kiyohiko 108, 116, 118
Nakamura, Akira 113, 114
Nakamura, Eiken 134
Nakamura, Hiroki 21, 22, 23
Nakamura, Motohiko 97
Nakanishi, Synsuke 135
Nakano, Hiroshi 114
Nakao, Yasuko 113
Nakashima, Satoru 34
Nakasuji, Kazuhiro 79, 80, 81, 82, 144
Nakatsuka, Hiroki 135
Nakayama, Hitoshi 106
Nakazawa, Hiroshi 109, 110
Nakazawa, Yasuhiro 63, 64, 65, 143
Nanbu, Shinkoh 17, 120
Narioka, Satoru 71
Naruta, Yoshinori 90, 91
Negishi, Ei-ichi 116, 118
Nelson, Keith A. 38
Nemoto, Hisao 92
Nguyen, Thinh B. 118
Nishihara, Yasushi 146
Nishii, Junji 104
Nishikawa, Hiroyuki 72
Nishikawa, Yoshito 132, 133
Nishimoto, Jyunji 94, 95
Nishio, Mitsuhiro 106, 107
Nishioka, Takanori 84, 86, 115
Nitto, Yu 118
Nomura, Sachiyo 87
Nukui, Etsuko 113

Ochoa, R. 128, 129
Ogata, Hironori 69, 70, 144
Ogata, Toshihiro 106, 107
Ogawa, Hiroshi 106, 107
Ogo, Seiji 85, 87
Ogura, Takashi 31, 32, 33, 139
Ohashi, Yuji 82
Ohgake, Satoshi 111
Ohkubo, Katsutoshi 94, 95
Ohmine, Iwao 18, 19, 20
Ohmori, Yasuharu 108
Ohsaki, Akihiko 21
Ohyama, Hiroshi 76
Oishi, Osamu 144
Okazaki, Noriaki 53, 57, 141
Okuda, Mitsumasa 129
Omata, Takahisa 104, 105, 106
Ono, Katsuhiko 121, 122
Onuki, Setsuko 92
Oonishi, Makoto 113
Ouchi, Yukio 71, 77
Ozawa, Shinji 31
Ozawa, Yoshiki 86
Ozeki, Hiroyuki 26, 27, 28, 139

Park, Joon T. 84
Petek, Hrvoje 44, 46
Poli, Nicola 121
Proshlyakov, Denis A. 32, 139

Rábai, Gyula 52, 54, 55, 56, 141
Rimo, Xi 84
Rousset, Christophe J. 118

Saburi, Masahiko 118

Saito, Gunzi 70
Saito, Kazuo 86
Saito, Shinji 19
Saito, Shuji 26, 27, 28, 139
Saito, Yahachi 129
Saito, Yoji 74
Sakai, Kusuo 134
Sakimura, Tomoo 123
Sakurai, Makoto 102
Sanekata, Masaomi 15, 124, 125, 126
Sano, Mizuka 121
Sasaki, T. 91, 110
Sasaki, Tsutomu 110
Sasayama, M. 91
Sato, Hirohiko 64
Sato, Kei 128
Sato, Shin-ichiro 34
Satoh, Keiichi 111, 112, 146
Sawabe, Kyoichi 47, 48, 140
Sawada, Kiyoshi 111, 112, 146
Sawada, Nobuyuki 90
Sei, Masaki 71
Seki, Kazuhiko 70, 71
Sekiguchi, Tetsuo 52, 53, 141
Sekiya, Hiroshi 46
Shigemasa, Eiji 96, 97
Shimamura, Harunari 104
Shimomura, Hiroshi 86, 87
Shintani, Noriko 113
Shinzawa-itoh, Kyoko 31, 32, 33
Shiohara, Hiroaki 123
Shirakura, Yasuhiro 112
Shirotani, Ichimin 61
Shobatake, Kosuke 75, 76
Sohara, Tsuyoshi 112
Someda, Kiyohiko 22
Sone, Kozo 113
Sonoda, Yoko 17
Sumiyama, Kenji 129
Suzuki, Atsushi 66, 144
Suzuki, Kenji 129
Suzuki, Masatatsu 115
Suzuki, Masayoshi 74
Suzuki, Noriyuki 116, 117, 118, 146
Suzuki, Shinzo 70
Suzuki, Takanori 122, 123
Suzuki, Takayoshi 84, 85, 87, 88, 89, 90, 145
Suzuki, Toshinori 57, 58, 141
Suzuki, Toshio 111, 112
Suzuki, Toshiya 69
Suzuki, Toshiyasu 66, 67, 144
Swanson, Douglas R. 118

Tabayashi, Kiyohiko 76
Tachiki, Masashi 136
Tadokoro, Makoto 79, 81, 82, 90, 144
Takada, Shoji 21
Takahashi, Hiroaki 71
Takahashi, Takashi 70, 72
Takahashi, Tamotsu 116, 117, 118, 146
Takami, Toshiya 120
Takamura, M. 31
Takano, Kazuto 128
Takano, Shuro 27
Takasu, Ryozo 126, 127
Takata, Yasutaka 97
Takayanagi, Masao 49, 50, 51
Tamaki, Koichi 79, 144
Tanaka, Hideki 19
Tanaka, Koji 114, 115, 146
Tanaka, Shin-ichiro 135
Tanaka, Shoji 70, 72, 73, 121, 122, 123, 145
Tang, Jian 27
Tani, Fumito 91
Taniguchi, Hiromi 64
Tanimura, Yoshitaka 23, 24
Tanner, David B. 63
Tasaka, Motoyuki 108
Taylor, R. E. 69
Ten-no, Seiichiro 16, 18
Terao, Takehiko 130
Terui, Toshifumi 66
Tokutomi, Satoru 30
Tominaga, Keisuke 37, 38, 39, 40, 41, 140
Tomita, Norikazu 24
Tomura, Masaaki 123, 145
Tonokura, Kenichi 57, 58, 141
Torii, H.A. 28, 29
Toyoda, Jiro 78, 79, 80, 81, 82, 144
Toyohara, Kiyotuna 114
Tsuda, Kenichiro 21
Tsukamoto, Keizo 125, 126
Tsunashima, Shigeru 128

Uchiyama, Koichi 131
Ueda, Kazushige 104, 105, 106
Ueda, Naoyuki 104, 105, 106
Uehara, Akira 115
Uekusa, Hidehiro 82
Ugawa, Akito 62, 63
Umemoto, Hironobu 128
Uragami, Masako 145
Urisu, Tsuneo 98, 142
Usui, Satoshi 94, 95
Uzu, Tomoko 113

Vanag, Vladimir K. 52, 53, 141

Wakoh, Kimio 129
Watanabe, Hidekazu 15
Watanabe, Kazuo 47, 140
Watanabe, Makoto 134
Weibel, Daniel E. 102
Whitehead, Roger J. 66, 144
Widmann, E. 28
Xi, Zhenfeng 116, 146

Yagishita, Akira 96, 97
Yakushi, Kyuya 61, 62, 63, 70, 73, 143
Yamabe, Tokio 72, 73
Yamaguchi, Toshiyuki 74
Yamaguchi, Yoshitaka 110
Yamamoto, Satoshi 28
Yamamoto, Shigeyoshi 35
Yamamoto, Yoshinori 92, 93
Yamamuro, Noriko 68
Yamamuro, Saeki 129
Yamasaki, Tomoaki 110
Yamashita, Kazuo 71
Yamashita, Yoshiro 70, 121, 122, 123, 145
Yamazaki, Jun-ichiro 134
Yamazaki, T. 28
Yanagawa, Kazuhiko 105, 106
Yano, Shinichi 69
Yartsev, Arkadiy 37, 38
Yasumatsu, Hisato 76
Yonekura, Nobuaki 141
Yoshida, Akira 74, 106
Yoshida, Hiroaki 100, 142
Yoshigoe, Akitaka 98, 142
Yoshihara, Keitaro 37, 38, 39, 40, 41, 42, 43, 44, 46, 140
Yoshii, Toshihito 108
Yoshikawa, Hiroshi 74, 75
Yoshikawa, Shinya 139
Yoshikawa, Tadanobu 129
Yoshikawa, Yuzo 108, 109
Yoshimura, Daisuke 71
Yoshinobu, Jun 48
Yumoto, Masatoshi 92
Yuto, Koji 108
Yuyama, Akira 71

Zaman, Badruz 78, 144
Zhan, Chang-Guo 15
Zhang, Yanping 98
Zhou, Ping 129
Zhu, Chaoyuan 22, 23

Institute for Molecular Science, Myodaiji, Okazaki 444, Japan